N/P-based Sterically Demanding Ligands: Synthesis, Reactivity and Catalysis

Roberto Nolla Saltiel, MRes

Thesis submitted to the University of Nottingham for the degree of

Doctor of Philosophy

February 2019

Declaration

The work described in this thesis was carried out at the University of Nottingham in the laboratory B46 between January 2016 and January 2019, under the supervision of Dr Deborah L. Kays. All the work is my own unless stated the contrary, and has not previously been submitted for any degrees at this or any other university.

Roberto Nolla Saltiel

Abstract

Herein, the synthesis of two new families of carbazole-based, imino pincer proligands is presented. The first one, relies in the double substitution of a carbazole core, to form symmetric tridentate *N*-based pincers, employing highly sterically demanding substituents (**5** [Ar*] and **6** [Naph]). While for the second one, a methodology has been developed that allows selective mono substitution of a carbazole derivative (1,2,3,4-tetrahydrocarbazole), from which bidentate *N*-chelates could be synthesised (**9** [Ar*] and **10** [Dipp]).

The Group 1 salts of these ligands, have been accessed *via* direct deprotonation/organoelimination reactions. In the case of the symmetric proligands **5** and **6**, alkali metal complexes have been prepared by reaction with readily available ^{t}BuLi (**11** and **12**), NaH (**13**) and KH (**14**). While in the case of the asymmetric proligand **9**, similar compounds have been prepared *via* transamination with Li[N(SiMe$_3$)$_2$] (**15**), Na[N(SiMe$_3$)$_2$] (**16**) and K[N(SiMe$_3$)$_2$] (**17**). NMR determinations of the Group 1 salts **12**-**14** and **15**-**17**, demonstrate a change in chemical shift, attributable to the size of the alkali metal coordinated. Additionally, **12**-**14** were found active in dehydrogenation reactions of Me$_2$NH·BH$_3$, following recent interest in the development of catalysts based on Group 1 metals. From these experiments, it was possible to determine contrasting reactivity, dependant of the cation and solvent employed; with the reactivity observed following a pattern consistent with the relative position of the metals in the group. This allowed, in some cases, selective and preferential formation of dehydrocoupling/dehydrogenation products.

Following synthesis of the Group 1 salts, a range of homoleptic and heteroleptic complexes could be accessed *via* a variety of methodologies, which include direct metathesis reaction between a Group 1 salt or organoelimination reactions with the free ligand. A wide variety of metal-compounds have been prepared, extending this work, quite prolifically in the particular case of the naphthyl-substituted tridentate proligand **6**; to include examples of Group 2 (**24**-**25**), first row transition-metals (**26**-**34**), Group 12 (**35**-**37**), Group 13 (**38**-**40**) and Group 14 (**41**-**43**). Similar work, performed with the asymmetric proligand **9**; from which Group 2 (**44**) and Group 14 (**45**) complexes could be characterised.

Two metal complexes (**24** and **27**), were thoroughly studied in the context of space availability around the metal centre, for their eventual use in catalytic processes. From these, five-coordinate complexes could be prepared, relying on the presence of electron rich nitrogen/oxygen functionalities, to bind to the metal centre. From which characterisation of two families of compounds (**24b**-**e** and **27a**-**d**), could be achieved.

Similarly, first row metal complexes **26**-**30** were found to be adequate precatalysts for the hydrophosphination of activated alkenes. The reaction was optimised, finding the cobalt(I)-carbonyl complex **29** to be the most active/selective; reactivity which was extended to a range of activated olefins (**46**-**56**). For the first time for a procedure of such nature, the employment of a cobalt(I) species was exemplified. A reaction mechanism has been proposed, based on stoichiometric reactions, and the reactivity observed for the catalysts employed.

In parallel to the study of complexes derived from a carbazole scaffold, studies on the coordination ability of several, hemilabile *N/P*-based, phosphino(di)carboxamides (**L-57**–**59** [PCAs] and **L-60**–**61** [PDCAs]) to $[(p\text{-cym})RuCl_2]_2$ were carried out. In all cases, the product obtained was found to be coordinated *via* the phosphorus of the PCA/PDCA, with a pseudo-octahedral geometry, in a classical piano-stool arrangement (**57**-**61**). Attempts at forming four- and six-membered metallacycles *via* deprotonation/halide scavenging, of the amido-hydrogen and a chloride, respectively; followed by intramolecular attack, evidenced that compounds derived from PCAs (**57**-**59**), to be too sterically hindered to allow cyclisation. While analogous PDCA-substituted derivatives (**60**-**61**), subjected to such treatment enabled formation of six-membered metallacycles (**62**-**63**). In both cases, this methodology accesses a mixture of two positional isomers (**62a**/**b** and **63a**/**b**). Geometry optimisation calculations were carried out for the cyclised products (**62a'**/**b'**-**63a'**/**b'**) and are in full agreement with their spectroscopic characterisation.

Acknowledgments

First and foremost, I would like to thank my supervisor Dr Deborah L. Kays for giving me the opportunity of joining her research group, and express my sincere gratitude for all her guidance, support and understanding, throughout the last four years. I would also like to thank Prof. Neil Champness for monthly progress meetings and supervision, during the first six months of my PhD; and Dr Graham Newton for assessment of my first year report.

My most sincere gratitude goes to Dr Ana M. Geer, for all her influential advice, unrelenting support and friendship. I am very fortunate to have worked with somebody as constructive, supportive and passionate. Your unwavering guidance and aid throughout, have been crucial during my time in the UK, and for that I am very grateful.

To past and present members of the Kays and Champness group and to my friends and colleagues; Dr Alexander Ried, Dr Allie Gower, Amy South, Andrew Valentine, Charlotte Gidman, Gareth Ashworth, Glen Murray, Dr Helen Sharpe, Dr Katherine Shaw, Dr Kevan Grant, Dr Steve Skowron, Dr Toby Blundell, Yu "Archie" Liu, Olivia Churchill, Dr Katharina Kastner, for all their support, friendship and all the memories, both in the lab and out of it. I would also like to thank my project students, Tom Linford-Wood, William Watkinson and Ashleigh James, for all their hard work.

Special thanks to Dr William Lewis, for all his patience teaching me crystallography, and all the bouldering t(r)ips, to Dr Huw Williams, Mr Shazad Aslam and Mr Kevin Butler for NMR discussions and experiments set up, Dr Mick Cooper, Mr Graham Coxhill, Mr Ben Pointer-Gleadhill and the EPSRC NMSF (Swansea) for MS determinations, Dr E. Stephen Davies for CV measurements, Dr Laurence Taylor for mechanistic discussions, Dr Tong Liu and Mr Stephen Boyer (London Metropolitan University) for elemental analyses.

Thanks also go to administrative staff and the University of Nottingham-Immigration support team and to Ms Maggie Mallory for all the help, ensuring a smooth transition into living/studying in the UK. Technical support and stores staff, in particular Mr Mark Guyler for helping to look after the lab, Mr Clive Dixon and Mr Conor Howell-Bennett for repairing my broken NMR tubes/glassware and Sue for the friendly chats every day, and all the tea.

To my parents and my brother, for their constant encouragement and for always supporting my endeavours. To my family in Mexico, but especially to Andrea, Lydia, Niko and Naty, for continuously inspiring me to be better.

To the Mexican Council for Science and Technology (CONACYT) [CVU 600474], and the University of Nottingham (School of Chemistry) for funding my studies.

"Cuando mi cuerpo falle, mi espíritu dominará".

Publications

- Roberto Nolla-Saltiel, Ana M. Geer, William Lewis, Alexander J. Blake and Deborah L. Kays. "Dehydrogenation of Dimethylamine-borane Mediated by Group 1 Pincer Complexes" *Chem. Commun*., **2018**, *54*, 1825-1828.

- Roberto Nolla-Saltiel, Ana M. Geer, William Lewis, Alexander J. Blake, E. Stephen Davies and Deborah L. Kays. "Hydrophosphination of Activated Alkenes by a Cobalt(I) Pincer Complex" *Manuscript in preparation*.

- Roberto Nolla-Saltiel, Ana M. Geer, Helen R. Sharpe, Laurence J. Taylor, Thomas G. Linford-Wood, Ashleigh James, Jamie Allen, William Lewis, Alexander J. Blake, Jonathan McMaster and Deborah L. Kays. "Organoruthenium Complexes Containing Phosphinodicarboxamide Ligands" *Manuscript in preparation*.

- Roberto Nolla-Saltiel, Ana M. Geer, William Lewis, Alexander J. Blake and Deborah L. Kays. "Synthesis and Reactivity of Group 12-14 Pincer Complexes Supported by a Carbazole Scaffold" *Manuscript in preparation*.

Table of Contents

Chapter I. General Introduction 14

1.1 Introduction 15

1.2 Basic Concepts of Coordination Chemistry: Chelates, Chelation and Denticity . 16

1.3 Pincer Ligands 18

1.4 N-based Heterocyclic Ligands 20

1.5 Carbazole-based Chelates 21

1.6 Synthesis of 1,8- and 1,3,6,8-tetrasubstituted Carbazoles 23

1.7 Metal-Nitrogen Bond Formation (Synthetic methodologies) 24

1.7.1 Metathesis Reactions 24

1.7.2 Organoelimination 26

1.7.3 Transamination 26

1.8 Homoleptic and Heteroleptic Complexes 27

1.9 Asymmetric Ligands Based on Tetrahydrocarbazole 28

1.10 Aims and Objectives 30

Chapter II. Ligands Synthesis 31

2.1 Results and Discussion 32

2.2 Ligand Design: How Much Steric Hindrance is Required? 33

2.2.1 Symmetric Carbazole [Ar_2*carbH] 33

2.2.2 Symmetric Carbazole [$Naph_2$carbH] 36

2.2.3 Asymmetric Tetrahydrocarbazole [Ar*THCarbH] 38

2.2.4 Asymmetric Tetrahydrocarbazole [DippTHCarbH] 42

2.3 Conclusions 42

2.4 Experimental Section 43

2.4.1 Synthesis and Characterisation 43

..... Chapter III. Group 1 Salts and Catalytic Dehydrogenation of Dimethylamine-borane 52

3.1 Introduction to Group 1 Chemistry 53

3.2 Dehydrogenation of Amine-Boranes 53

3.3 Aims and Objectives 54

3.4 Results and Discussion 55
3.4.1 Synthesis of Group 1 Salts 55
3.4.2 Group 1 Salts and Catalytic Dehydrogenation of Dimethylamine-borane .. 73
3.5 Conclusions 83
3.6 Experimental Section 84
3.6.1 Synthesis and Characterisation 84
Chapter IV. Synthesis of Homoleptic and Heteroleptic Carbazolido Complexes 91
4.1 Introduction to Homoleptic and Heteroleptic Carbazolido Complexes 92
4.2 Aims and Objectives 94
4.3 Results and Discussion 95
4.4 Low-coordinate Metal Centres Employing [Ar_2*carbH] 95
4.4.1 Metathesis Reactions with Group 2 Metal(II) Salts 95
4.5 Low-coordinate Metal Centres Employing [$Naph_2$carbH] 97
4.5.1 Metathesis/Organoelimination Reactions with Group 2 Metal(II) Salts 97
4.5.2 Metathesis Reactions with First Row Transition-Metal(II) Salts 102
4.5.3 Metathesis Reactions with Group 12 Metal(II) Salts 124
4.5.4 Metathesis Reactions with Group 13 Metal(III) Salts 132
4.5.5 Metathesis Reactions with Group 14 Metal(II) Salts 139
4.6 Low-coordinate Metal Centres Employing [Ar*THCarbH] 159
4.6.1 Organoelimination Reactions with Group 2 Compounds 159
4.6.2 Organoelimination Reactions with Group 12 Compounds 162
4.7 "Probing the Coordination Sphere"-Initial Studies Towards Catalysis Employing [$Naph_2$carbH] as Ligand 164
4.7.1 Coordination Studies Employing Closed and Open-shell Complexes 164
4.8 Conclusions 177
4.9 Experimental Section 180
4.9.1 Synthesis and Characterisation 180
Chapter V. Heteroleptic First-Row Transition Metal Complexes and Hydrophosphination of Activated Alkenes 203
5.1 Introduction 204

5.2 Aims and Objectives 206
5.3 Results and Discussion 207
5.3.1 Catalytic Hydrophosphination of Olefins 207
5.3.2 Catalytic Studies 209
5.3.3 Reaction Scope 210
5.3.4 Towards a Reaction Mechanism 215
5.3.5 Proposed Reaction Mechanism 216
5.4 Conclusions 218
5.5 Experimental Section 219
5.5.1 Synthesis and Characterisation 219
Chapter VI. Organoruthenium Complexes Based on Hemilabile N/P-Ligands. 227
6.1 Introduction to Hemilabile N/P-based Ligands 228
6.2 Introduction to Ruthenium-Metallocene Chemistry 229
6.3 Aims and Objectives 230
6.4 Results and Discussion 231
6.4.1 Synthesis of Coordination Compounds [Ru(p-cym){$PPh_2C(=O)N(H)R$}Cl_2] (R = ^{i}Pr, Ph, p-tol) 231
6.4.2 Synthesis of Coordination Compounds [Ru(p-cym){$PPh_2C(=O)N(R)C(=O)N(H)R$}Cl_2] (R = Ph, p-tol) 233
6.4.3 Synthesis of Metallacycles [Ru(p-cym){κ^2-P,N-$PPh_2C(=O)N(R)C(=O)NR$}Cl] (R = Ph, p-tol) 236
6.5 Conclusions 244
6.6 Experimental Section 245
6.6.1 Synthesis and Characterisation 245
Chapter VII. Global Conclusions 252
General Experimental Procedures 255
8.1 Inert Atmosphere Techniques 256
8.2 Solvents Employed 256
8.3 Starting Materials and Reagents 256
8.4 NMR Spectroscopy 257
8.5 DOSY NMR and Hydrodynamic Radii Calculations 257

8.6 Evans Method 258
8.7 Mass Spectrometry 258
8.8 Elemental Analysis 258
8.9 Infrared Spectroscopy 259
8.10 UV/vis Absorption Spectroscopy 259
8.11 Cyclic Voltammetry 259
8.12 DFT Methodologies 259
8.13 Crystallographic Methods 260

Crystallographic Data

DFT-Geometry Optimisation Structures

References

Compounds List

Abbreviations

Ar	Aryl
Ar*	2,6-bis(diphenylmethyl)-4-methylphenyl
Ar*NH_2	2,6-bis(diphenylmethyl)-4-methylaniline
[Ar_2*carbH]	1,8-di(Ar*)imino-3,6-di(*tert*-butyl)-9*H*-carbazole
[Ar*THCarbH]	8-(Ar*)imino-1,2,3,4-Tetrahydro-9*H*-carbazole
ASAP	Atmospheric Solids Analysis Probe
ATR	Attenuated Total Reflectance
Å	Angstrom (10^{-10} m)
bs	broad singlet (NMR)
^{n}Bu	*n*-butyl
^{t}Bu	*tert*-butyl
$CDCl_3$	deuterated chloroform
CD_2Cl_2	deuterated dichloromethane
C_6D_6	deuterated benzene
COSY	Correlated Spectroscopy (NMR)
CV	Cyclic Voltammetry
δ	NMR chemical shift (ppm)
DFT	Density Functional Theory
[DippTHCarbH]	8-(Dipp)imino-1,2,3,4-Tetrahydro-9*H*-carbazole
Dipp	2,6-diisoprophyl-phenyl
DOSY	Diffusion Ordered Spectroscopy (NMR)
$\Delta\nu_{1/2}$	Half-height peak width
d	doublet (NMR)
dd	double doublet (NMR)
DCM	dichloromethane, CH_2Cl_2
DMF	dimethylformamide
η	*eta*, hapticity
ESI	Electrospray Ionisation
EI	Electron Ionisation
Fc^+/Fc	Ferrocene/Ferrocenium pair (CV)
g	Gas
I	Nuclear spin
IR	Infrared
J	Coupling constant (NMR)
i	*ipso*
h	Hour(s)
HMBC	Heteronuclear Multiple Bond Correlation (NMR)
HMDS	Hexamethyldisilazide anion, bis(trimethylsilyl)amide
HOMO	Highest Occupied Molecular Orbital
HSQC	Heteronuclear Single Quantum Coherence Spectroscopy (NMR)
Hz	Frequency (NMR)
λ	Wavelength
LDA	Lithium Diisopropylamide
LUMO	Lowest Unoccupied Molecular Orbital
[M]	Molecular peak
m	multiplet (NMR)
m	*meta*
m	medium signal (IR)
Me	Methyl
μ_{eff}	Effective magnetic moment
Mes	Mesityl
m/z	Mass to charge ratio
MS	Mass Spectrometry
Naph	1-Naphthyl

[Naph$_2$carbH]	1,8-dinaphthylimino-3,6-di(*tert*-butyl)-9*H*-carbazole
NHC	*N*-heterocyclic carbene
NMR	Nuclear Magnetic Resonance
NOESY	Nuclear Overhauser Effect Spectroscopy (NMR)
o	*ortho*
π	Pi (orbital symmetry)
p	*para*
p-cym	*para*-cymene, 1-Methyl-4-(propan-2-yl)benzene
p-tol	*para*-tolyl
pK_a	acid dissociation constant
Ph	Phenyl
ppm	Parts per million
PPSE	Polyphosphoric Acid Trimethylsilyl Ester
^{i}Pr	Isopropyl
q	quartet (NMR)
r.t.	room temperature
σ	Sigma (orbital symmetry)
s	singlet (NMR)
s	strong signal (IR)
τ_4	Geometry index (four-coordinate)
τ_5	Geometry index (five-coordinate)
t	triplet (NMR)
THF	tetrahydrofuran
td	triple doublet (NMR)
TLC	Thin Layer Chromatography
TMEDA	*N,N,N'N'*-tetramethylethylenediamine
tt	triple triplet (NMR)
UV/Vis	Ultraviolet/visible
v	vibrational frequency
w	weak signal (IR)
WCA	Weakly Coordinating Anion
XRD	X-ray Diffraction
Xyl	Xylyl

Chapter I. General Introduction

It is the aim of this chapter to familiarise the reader with key concepts of coordination chemistry, targeted to the formation of low-coordinate metal complexes, stabilised by *N*-based ligands, with significant focus on carbazole-based systems. The synthesis of ligands containing these moieties is first targeted, giving a detailed explanation of how differing synthetic pathways that allow modifications to the central carbazole core, in turn allow the formation of stable low-coordinate metal centres.

1.1 Introduction

A continuing challenge in modern coordination and organometallic chemistry is the formation and stabilisation of complexes featuring highly unsaturated transition metal centres. Such compounds have been of interest not only from a fundamental structure/bonding perspective, but also from a viewpoint of applied reactivity, finding use in small molecule activation and catalysis as well as magnetism. The use of sterically demanding ligands is a recurring theme throughout the field which allows the stabilisation of novel and otherwise inaccessible metal environments.

The quest for systems with such characteristics, has been revitalised in the last decade by the discovery of the first room temperature stable metal-metal quintuple bond.[1] Along these, some recent examples in this area that denote the interest in the synthesis of previously unexplored bonding motives include the first crystallographically characterised calcium-transition-metal bond.[2] While *N*-based systems, such as the β-diketiminate, Nacnac, have been used to stabilise a rare example of a complex with an unsupported magnesium-iron bond[3] and the first example of a dimeric magnesium(I)-magnesium(I) complex (Figure 1.1.1).[4]

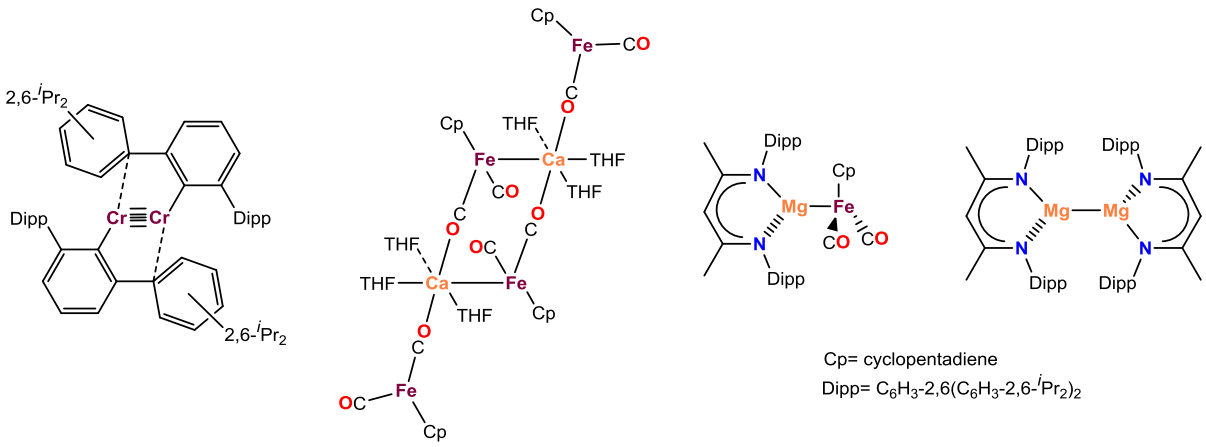


Figure 1.1.1 A dimeric quintuple bonded chromium(I) species (left), first example of a calcium/transition-metal bond (centre-left), an unsupported magnesium-iron bond (centre-right) and the first example of a dimeric magnesium(I) complex (right).

These findings highlight that with the use of appropriate ligand frameworks and new synthetic methodologies, previously inexistent systems are feasible. Having these compounds now available in the literature should facilitate further reactivity studies of the rapidly expanding type of polar metal-metal bond systems.

1.2 Basic Concepts of Coordination Chemistry: Chelates, Chelation and Denticity

Within the field of coordination chemistry, the coordination number for a specific atom in a complex, equals to the number of σ-bonds between the ligands employed and the central atom. Therefore, in the case in which a given ligand has more than one donating site towards a metallic centre, the formation of cyclic structures called chelate rings, takes place. The term chelate derived from the great claw or "χηλη" (chele) of the lobster and other crustaceans, was coined in 1920 by Morgan and Drew, to describe a series of compounds derived from the reaction of acetylacetone with metals, metalloids and non-metals.[5] Therefore and structurally speaking, the ligand employed requires at least two potential binding states, in order to form a chelate (Figure 1.2.1).[6]

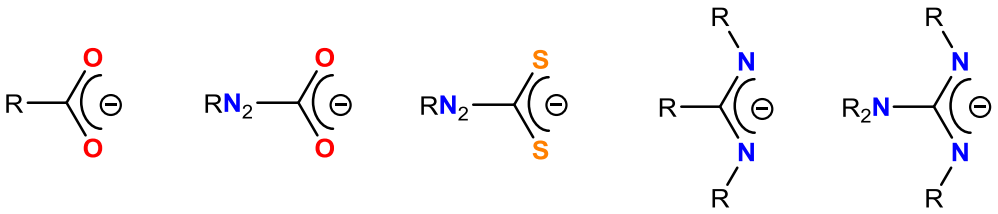


Figure 1.2.1 Selected examples of commonly used chelates. [From left to right] carboxylate, carbamate, dithiocarbamate, amidinate and guanidinate.

The process of coordination of the donor atoms from the ligand towards a central atom is called chelation.[6,7] Chelation involves the coordination of more than one non-contiguous, σ-electron pair donor atom from a given ligand, to the same central atom. The number of such ligating atoms in a single chelating ligand to the same central atom is called denticity, and is typically indicated by the adjectives bidentate (2), tridentate (3), tetradentate (4), *etc.* (Figure 1.2.2).

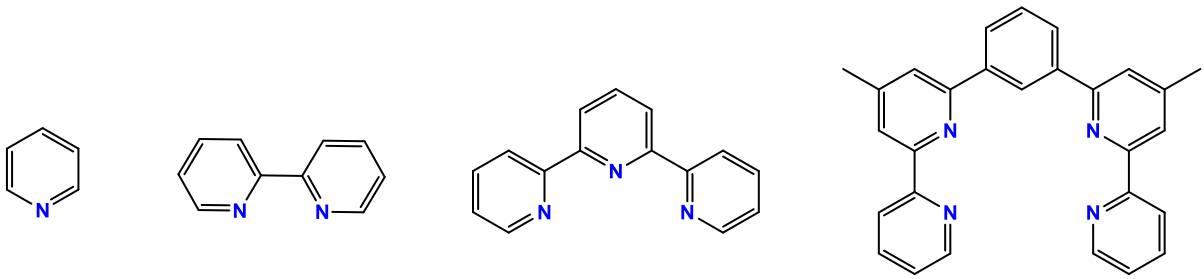


Figure 1.2.2 Examples of N-based ligands with increasing denticity. [From left to right] pyridine (monodentate), bipyridine (bidentate), terpyridine (tridentate) and quaterpyridine (tetradentate).

In comparison to their monodentate analogues, chelate complexes exhibit enhanced thermodynamic and kinetic stability, which is commonly referred to as the chelate effect.[8] One way to reason this significant increase in stability, is realising that an optimum metal-donor interaction contributes to an enthalpy gain, favoured by the formation of cyclic arrangements.[9] In addition, an entropic factor that dictates the likelihood of an intermolecular attack happening is drastically reduced. Once that a polydentate ligand is bound to the metal centre, further stabilisation is achieved when the chelate rings are part of a larger preformed macrocyclic arrangement (Figure 1.2.3). This contributes to the saturation of the metal centre concealing it, and as a consequence, making the resulting complex more stable.[10]

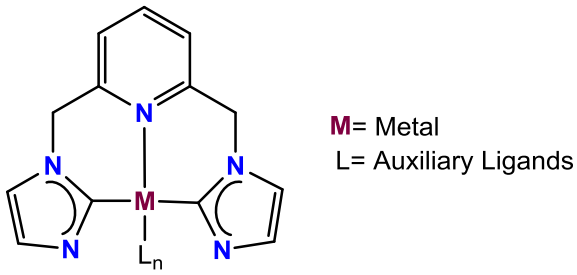


Figure 1.2.3 Example of a CNC tridentate metal complex.

1.3 Pincer Ligands

Also notable are pincer ligands, which are commonly defined as chelators that bind to three adjacent coplanar sites on the metal centre, and constitute a niche of ligand frameworks due to their suitable balance between stability and reactivity.[11] A multitude of differing scaffold systems have been described, which incorporate the ability to chelate metal centres. However, pincer ligands have emerged as an independent class of ligand systems, with their own special characteristics.[12,13] Systems based on this architecture were initially developed relying on motives that would allow at least one metal-carbon *σ* bond;[14,15] typically bilaterally symmetrical and commonly using terdentate pincer ligands, which normally result in the formation of two five-membered metallacyclic rings, but have since included examples of asymmetric ligands too (Figure 1.3.1).

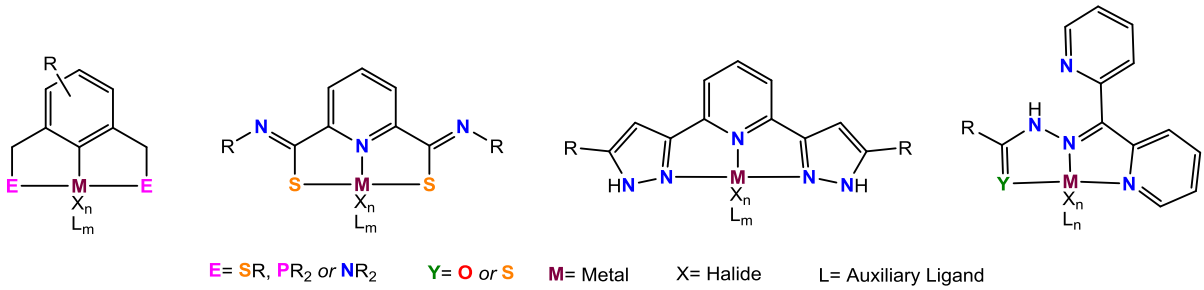
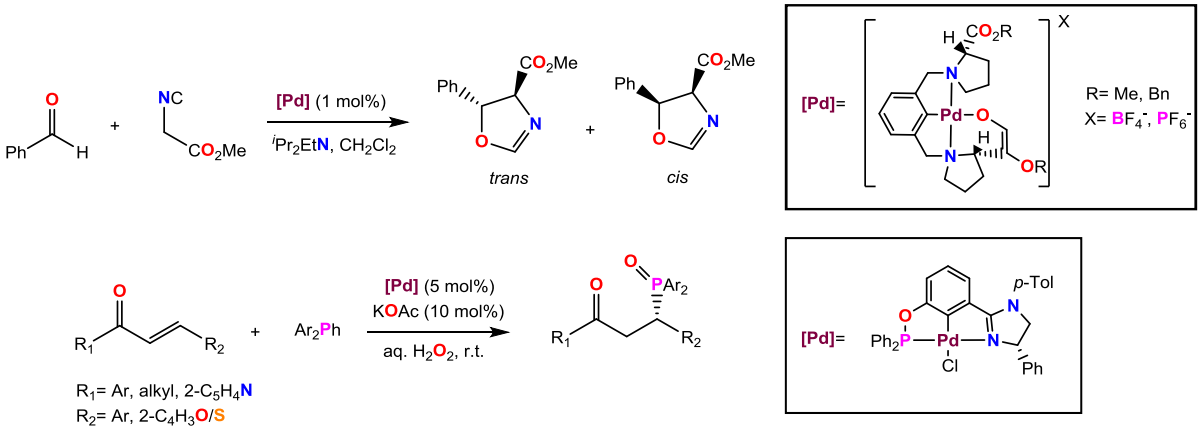


Figure 1.3.1 Selected examples of pincer-type ligands. [From left to right] ECE type, SNS type, NNN type and NNO/S type.

The aforementioned metallacyclic rings, and the overall rigid tridentate framework, imparts the necessary thermal stability to the system, while also allowing modification of the flanking groups, which in turn can be used to tailor the steric and electronic properties of the resulting compound. Their relative ease of preparation, has allowed for an explotion of different binding motives and coordination modes, to systems that include and are not limited to, *ONS*,[16] *CNS*,[17] *NNN*,[18] *NNS*,[19] *NNO*,[20] *PNP*,[21] *CNC*,[22] *SNS*[23] and *SeNSe* [24] (Figure 1.3.1).

The rich array of pincer-type ligands and the vast number of possible funciontal and auxiliary groups, combine strong electron donating properties, along with their steric and electronic tunability. As a consequence, wide variations in structure and therefore in electronic properties, can be achieved. These characteristics combined with their ability to stabilise the metal centre, while also allowing interaction with other substrates defines an essential feature of pincer ligands, necessary for small molecule activation and catalysis.[25]

Exemplifying this, Gosiewska *et al.* have presented preliminary studies of palladium *NCN*-pincer complexes, which catalyse the aldol condenstation of benzaldehyde and methyl α-isocyanoacetate, with low catalyst loadings (1 mol%), good conversions (60-80%), with modest enantoselectivities, and with preference for the *trans*-oxazoline product.[26] While Yang *et al.* have made use of palladium(II) *PCN* complexes, in an efficient enantioselective catalyst, targeting the hydrophosphination of enones (Scheme 1.3.1).[27] Further research targeting the optimisation of this and other pincer complexes, based on their ligands systems would potentially enrich and enchance their overall performance and selectivities.



Scheme 1.3.1 Stereoselective formation of oxazolines (above), and enantioselective hydrophosphination of enones (below), catalysed by palladium pincer complexes.

1.4 N-based Heterocyclic Ligands

Bidentate N-based ligands such as the β-diimines and their monoanionic derivatives the *β*-diketiminates (Figure 1.4.1), have been used since the 1970s by virtue of their strong affinity to metals, their high adaptability for the stabilisation of numerous elements, their ease with which they can be further substituted, and finally their diversity of bonding modes.[28] Having these characteristics grants them an important role as spectator ligands. As a consequence of this, they are often able to stabilise complexes in unusually low metal oxidation states, as cations, and other containing multiply bonded (to metal) co-ligands.[29–31]



Figure 1.4.1 A β-diimine and the corresponding monoanionic β-diketiminate.

Similarly, and making use of the enormous range of nitrogen-containing heterocyclic systems available; a great number of heterocyclic-based systems, have been used in coordination chemistry. Selected examples reported in the literature making use of these motives include, a self-assemblying copper(II) complexes with multidentate Schiff-base ligands incorporating imidazole groups,[32] a titanium(III)-pyrazolate complex with a Ti_2N_4 framework,[33] benzoxazole-NHC-platinum complexes, catalytically active in the hydrosilylation of styrenes,[34] π-π stacked/stabilised silver bipyridine complexes[35] and a chromium(I) tricarbonyl complexes stabilised by a pyrrolyl substituent (Figure 1.4.2).[36]

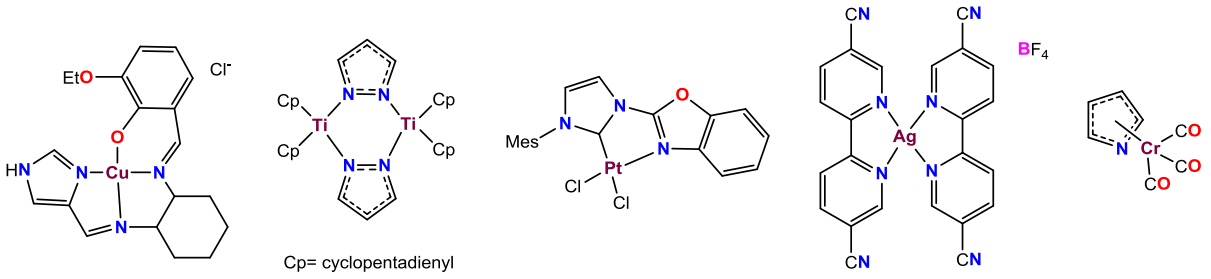


Figure 1.4.2 Selected examples of N-based heterocyclic complexes. Note the variety of N-heterocyclic ligands employed. [From left to right] imidazole, pyrazole, imidazole/benzoxazole, bipyridine and pyrrole.

1.5 Carbazole-based Chelates

One example of a very versatile and potentially sterically demanding *N*-based proligand is carbazole and its derivatives (Figure 1.5.1). Carbazole is a planar symmetric aromatic heterocyclic organic compound similar to indole. It was first isolated from coal tar in 1872 by Graebe and Glazer.[37] The molecule presents three coplanar rings in resonance and can be interpreted as a double substituted pyrrole, making it symmetric.

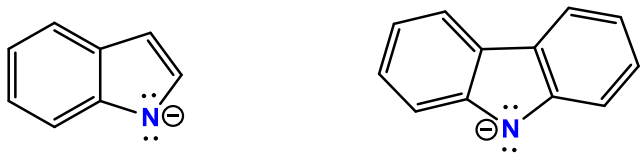


Figure 1.5.1 Conjugated bases of indole and carbazole.

Shortly after, several synthetic methodologies were developed targeting the synthesis of carbazole and functionalised derivatives, later recognised to exhibit important photo-physical and biological properties, an area of research which has become of particular interest in recent years.[38] Molecules containing this motif are in vogue as it is exemplified by recent advances in asymmetric substitution towards the formation of chiral quaternary carbon bonds, as well as further understanding of the importance of biologically active carbazole alkaloids and their derivatives in nature (Figure 1.5.2).[39]

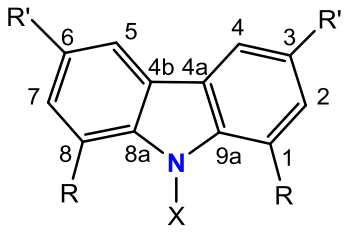


Figure 1.5.2 General numbering scheme of carbazol-9-yl compounds.

The central carbazolido-nitrogen offers a strong *σ*-donor functionality, a feature that has been primarily exploited in the form of 1,8-electron-rich disubstituted carbazolyl scaffolds. Tuneable protection can be obtained through the selection of the flanking substituents, which have shown to be essential to form unsaturated metal centres. Selected examples that rely on the carbazole backbone are iridium *PNP* pincer complexes employed in the catalytic hydrogenation of olefins ***A***,[40] *CNC* pincer complexes functionalised with lateral donor *N*-Heterocyclic carbenes ***B***,[41] *NNN* phosphinimine complexes capable of supporting

rare-earth ions ***C***[42] and iminic *NNN* complexes based on 1,8-bis(imino)carbazoles employed in the stabilisation of a wide range of transition-metals ***D*** (Figure 1.5.3).[43,44]

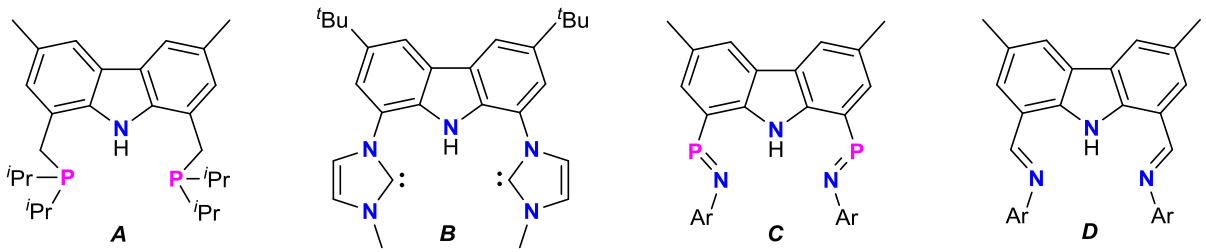


Figure 1.5.3 Selected examples of pincer complexes based on a carbazole scaffold.

In the particular case of 1,8-bis(imino) derived carbazoles, these have not been as widely explored, with few examples reported in the literature[45–48] and only a handful of structures crystallographically authenticated.[44,49–52] While in parallel, some recent notable examples of transition metal carbazolyl complexes based on this scaffold include a Cu(II) triazole complex which works as a highly sensitive fluorescent probe for the detection of cyanide,[53] a terminal carbonyl Rh(I) complex active in the carbonylation of methanol,[44] an Fe(III) compound capable of enantioselectivelly generating asymmetric epoxides from alkenes,[50] a *bis*-phosphine Rh(I) complex active in the dehydrogenation of alkanes and alkenes[54] and a chiral Cr(III) complex supported by a C_2-symmetrical bis(oxazolinyl)-carbazolyl ligand, which has proven effective for the asymmetric catalysis of Nozaki-Hiyama allylation reactions (Figure 1.5.4).[55] [*For further examples of carbazolido-based complexes, see the introduction to Chapter IV*].

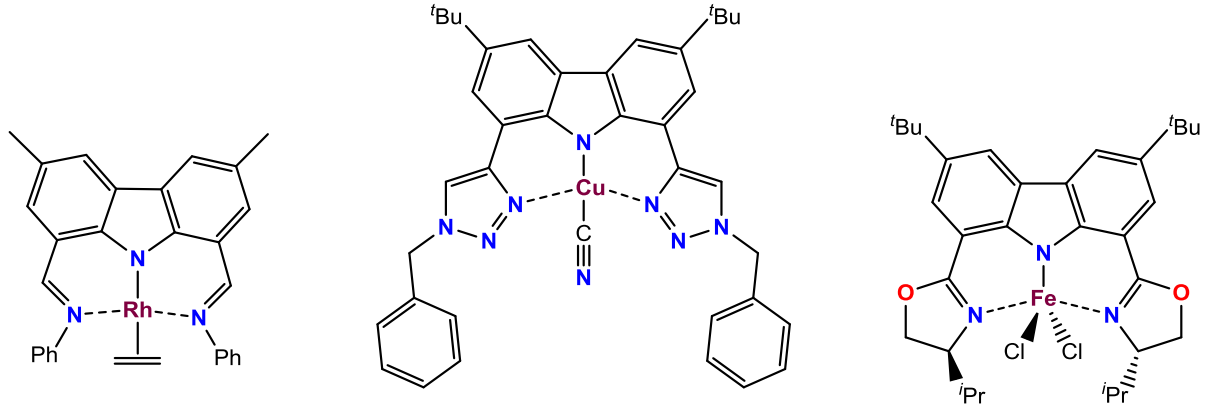
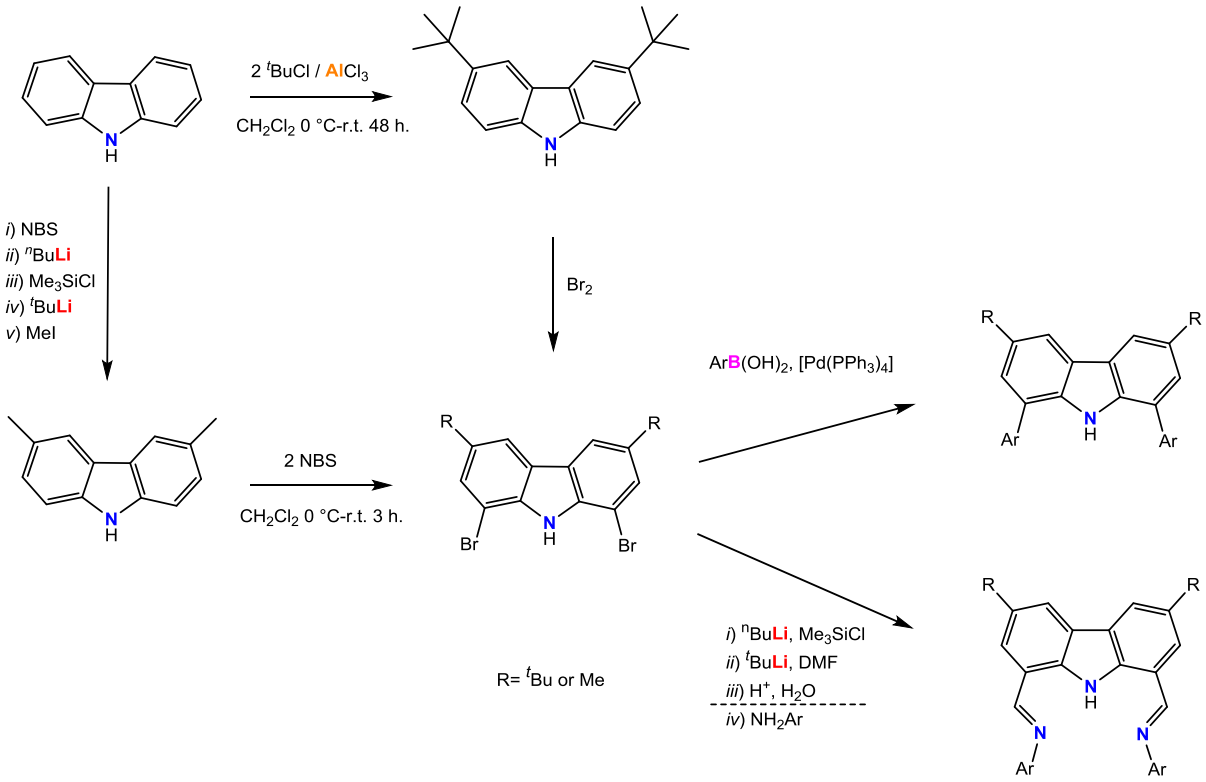


Figure 1.5.4 Selected examples of carbazolido pincer metal complexes.

1.6 Synthesis of 1,8- and 1,3,6,8-tetrasubstituted Carbazoles



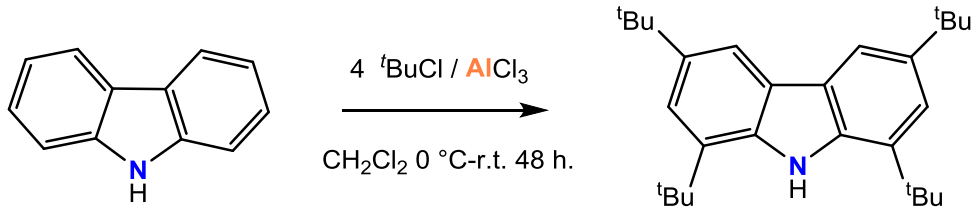
Scheme 1.6.1 Synthesis of 1,8-diaryl substituted carbazolyl ligands and 1,8-bis(imino)carbazoles.

In order to achieve the desired protection over the carbazole scaffold, typically two main methods of substitution on the 1- and 8-positions are used (Scheme 1.6.1).[51] Initially, both methodologies rely on the propensity of carbazole itself to undergo substitution reactions at the 3- and 6- positions. Reported methodologies make use of an initial double Friedel-Crafts reaction or a double bromination with *N*-bromosuccinimide, followed by alkylation. This is usually done to protect and subsequently direct the substitution towards the flanking 1- and 8-positions with bromines. Once this is achieved, two divergent pathways become accessible. In the first case the formation of 1,8-diaryl substituted carbazolyl ligands is targeted by formation of a carbon-carbon bond by means of a palladium catalyst and a suitable arylboronic acid in a Suzuki/Miyaura coupling reaction.[56]

In contrast, the second methodology relies on the ease of conversion of the 1,8-dibromo derivative to the 1,8-diformylcarbazole using DMF as source of the carbonyl flanking

groups. Once formed, the 1,8-diformylcarbazole derivative can undergo a double Schiff-base condensation with different aryl amines to afford 1,8-bis(imino)carbazoles.[44,51,52,57]

Although less explored, one additional protocol relies on the susceptibility of carbazole to undergo four consecutive substitutions through a Friedel-Crafts alkylation mechanism. As an example 1,3,6,8-tetra-*tert*-butylcarbazole has been synthesised using this methodology (Scheme 1.6.2).[58]



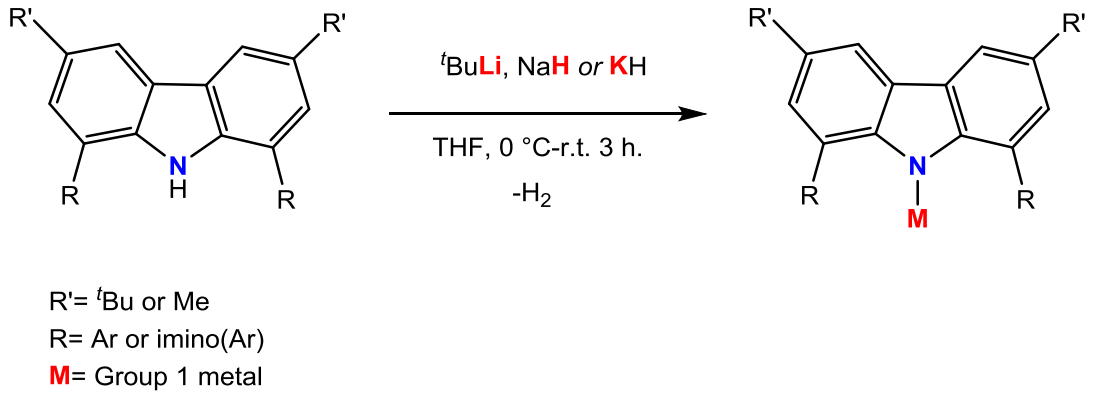
Scheme 1.6.2 Synthesis of 1,3,6,8-tetra-tert-butylcarbazole.

In all three cases, the ease of selective substitution in the desired positions, the variation of the substituents in the 1- and 8-positions of carbazole and consequently the ability to tune their steric hindrance around the nitrogen, makes them good candidates as proligands for the extremely challenging task of stabilising low-coordinate metal centres.

1.7 Metal-Nitrogen Bond Formation (Synthetic methodologies)

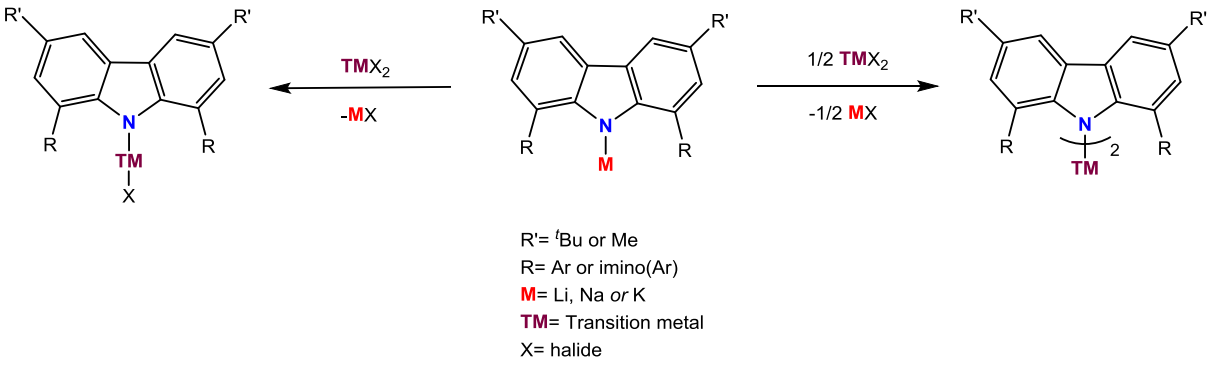
1.7.1 Metathesis Reactions

Regardless from which of the previously described ligand systems has been chosen to work with, the next step towards the formation of metallic complexes typically involves the formation of a Group 1 species (Scheme 1.7.1). As such, several readily available reagents such as ^{n}BuLi, ^{t}BuLi, NaH and KH can be reacted with the free carbazole, yielding the corresponding Group 1 salt.[46–48,56]



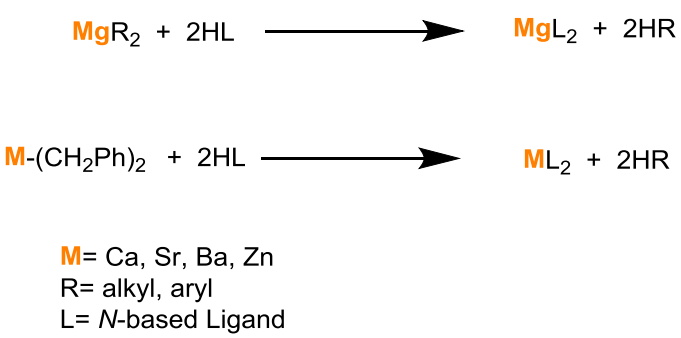
Scheme 1.7.1 Formation of Group 1 salts.

Once formed, the Group 1 complex serves as a useful starting material from which a wide range of compounds can be accessed *via* metathetical reactions. This methodology involves the reaction between a suitable carbazolido-Group 1 salt and a metal halide, aided by the formation and precipitation of the Group 1 metal halide out of the organic solvent, which provides a strong driving force, favoured by high lattice energy and insolubility in most organic solvents. By modifying the stoichiometry of the reaction it is possible to synthesise homoleptic or heteroleptic species (Scheme 1.7.2).[7] Although a variety of factors such as the solvent, the metal halide, the stoichiometry, the alkali metal and the ligand can pose an issue; this is the most common way of synthesising transition metal complexes. Noticeably and despite its popularity, there are reports acknowledging the risk that smaller alkali metals may become incorporated into the structure forming hetero-bimetallic species.[59]



Scheme 1.7.2 Formation of homoleptic and heteroleptic transition-metal complexes via metathesis reactions.

1.7.2 Organoelimination



Scheme 1.7.3 Metal-nitrogen bond formation via an organoelimination reaction.

Commercially available organozinc and organomagnesium reagents such as $ZnMe_2$, $^nBu_2Mg$, MeMgI, and easily prepared Me_2Mg[60] are commonly used in this methodology, making it a synthetic pathway widely used for the synthesis of *N*-based magnesium complexes (Hauser bases) and zinc analogues.[61,62] However, analogous methodologies to access the elusive heavier Group 2 analogues were not applicable until quite recently, due to the limited supply of equivalent precursors, due to their associated decomposition mechanisms (Scheme 1.7.3) [*See Chapter IV for additional details on Group 2 decomposition pathways*]. In the case of calcium in particular, there are now a few examples of organoelimination reactions using dibenzylcalcium.[63]

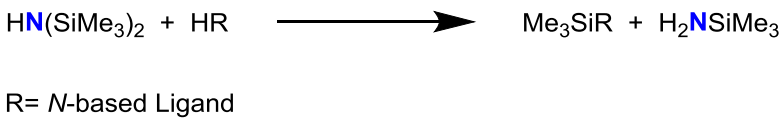
Both methods previously described are particularly attractive owing to the strong thermodynamic drive towards the formation of the hydrocarbons, and as a consequence its elimination from the reaction mixture that usually works as the driving force of the reaction. Nevertheless, great care must be applied to choose the appropriate reactions conditions as heavier alkaline earth metal metalorganic complexes are excellent nucleophiles and deprotonating agents, and will readily promote ether cleavage.[64]

1.7.3 Transamination



Scheme 1.7.4 Formation of a metal-nitrogen bond, via transamination.

The simple preparation of Group 1[65] and 2[66] amides, and their good solubility in a variety of solvents from which the $HN(SiMe_3)_2$ by-product can be easily removed, has made transamination an attractive synthetic pathway (Scheme 1.7.4). Still, a limiting factor in this reaction is the pK_a of the hydrocarbon or *N*-based ligand source. In this case, only those with a higher acidity than $HN(SiMe_3)_2$ can be utilised. If the pK_a is not within this range, a competing side reaction is promoted (Scheme 1.7.5).[67] This side mechanism involves the protonation of the liberated secondary amine and formation of the corresponding silane.



Scheme 1.7.5 Competing side-reaction in synthesis via transamination.

1.8 Homoleptic and Heteroleptic Complexes

Following a metathesis reaction between a Group 1 salt and a metal halide, the resulting product can be either a homoleptic or heteroleptic species (Figure 1.8.1). Metal centres that are substituted by two non-equivalent groups are examples of heteroleptic species. In contrast, a homoleptic compound exhibits only one type of ligand. It should be kept in mind that if the formation of a heteroleptic species it is to occur, the ligand used should grant sufficient steric hindrance to the metal centre which must out-compete the stabilisation awarded by a fully saturated homoleptic metallic centre.[68] As such it is common to find that less hindered ligands afford the formation of homoleptic products.

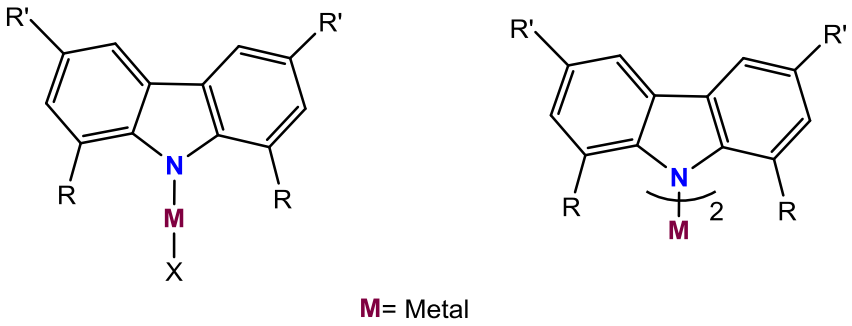


Figure 1.8.1 A heteroleptic metal(II) 1,3,6,8-substituted carbazole (left) and an analogous homoleptic metal(II) compound (right).

1.9 Asymmetric Ligands Based on Tetrahydrocarbazole

In a similar way to their symmetric 1,8-bis(imino) counterparts, there are limited studies of the formation of bidentate *N*-based ligands based on an asymmetric carbazole, with a negligible study of their synthesis and use in inorganic chemistry. One particular example of a family bearing such scaffold is 1,2,3,4-tetrahydrocarbazole (Figure 1.9.1). Similar to carbazole, this compound conains three contiguous rings. With the noticeable difference that one of the flanking rings has been reduced and as a consequence the molecule is no longer planar nor symmetric.

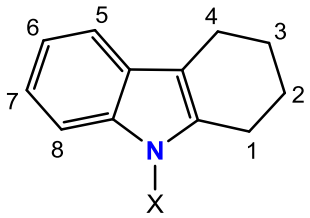
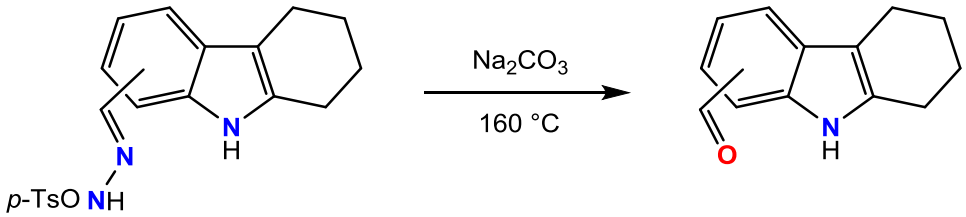


Figure 1.9.1 General numbering scheme of 1,2,3,4-tetrahydrocarbazoles.

Previous work in this area in the 1960s by Tomlinson *et al*. highlight the interest in forming formyl derivatives, from which further synthetic modifications can be carried out. This was primarily done by decomposition of the corresponding *p*-toluene-sulfonylhydrazide, at high temperature in the presence of anhydrous sodium carbonate (Scheme 1.9.1). By doing so, the four corresponding aldehydes, substituted in the aromatic ring, could be prepared with varying degrees of success.[69]

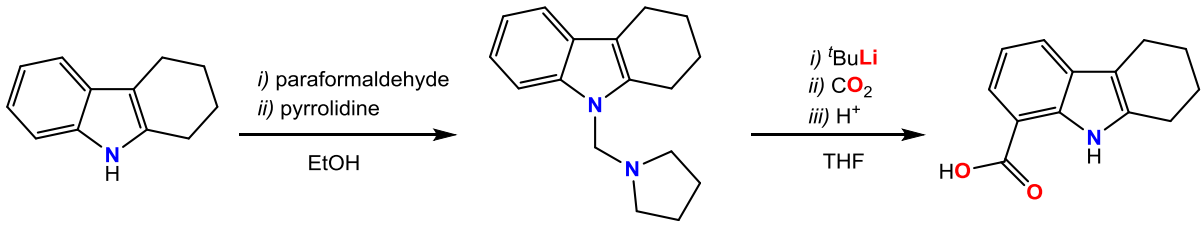


p-TsO = *p*-Toluenesulfonyl

Scheme 1.9.1 Formation of formyl derivatives of 1,2,3,4,-tetrahydrocarbazole.

Complementing this, there is the report of a methodology developed in the late 1980s, which can be applied in the synthesis of both symmetric and asymmetric carbazoles. The procedure involves reacting carbazole or 1,2,3,4-tetrahydrocarbazole with formaldehyde and an amine in ethanol to form the corresponding aminal (Mannich Base), formally

protecting the central nitrogen moiety (Scheme 1.9.2).[70] Most importantly, upon reaction with ^{t}BuLi, the newly formed aminal works as a lithio-directing functionality. This is of particular interest since both substrates previously mentioned have been found to have differing but equally rich substitution patterns. Under these conditions, carbazole undergoes lithiation at the 1-position. While, 1,2,3,4-tetrahydrocarbazole undergoes lithiation at the 8-position, and good yields of electrophilic addition products have been reported, regardless of the size of the electrophile. Following the synthesis, removal of the nitrogen-protecting function is readily achieved by mild acid-catalysed hydrolysis, enabling a clean synthetic approach for a family of substituted carbazole cores.



Scheme 1.9.2 Formation of an 8-substituted tetrahydrocarbazole derivative, employing CO_2 as electrophile.

Literature searches following a potential synthetic route taking advantage of the previously aforementioned methodologies, in the form of either formyl or imino derivatives, yield no results (SciFinder, as of January 2019), which highlights this as a previously unexplored synthetic route.[71] These syntheses could be explored, aiming towards the formation of previously unexplored asymmetric *N*-based bidentate ligands.

1.10 Aims and Objectives

There is a wide range of *N*-based pincer complexes employed in the literature, some of these have been found to have the right geometry/electronic properties, for stabilising low-coordinate metal centres, which in turn have allowed the isolation and characterisation of previously unexplored oxidation sates/reactivities.

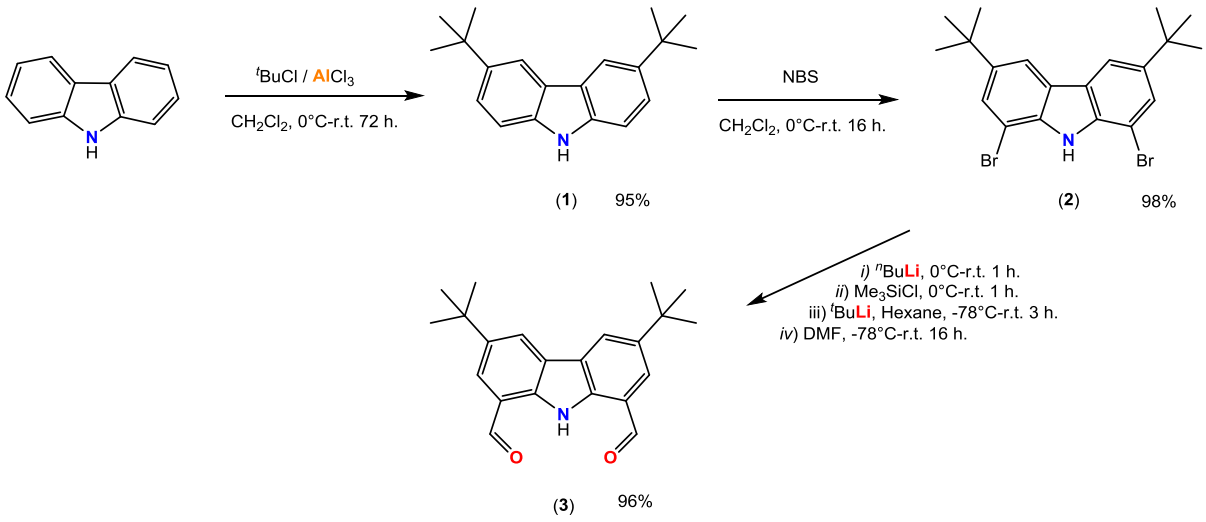
In line with this and as mentioned in the introduction, the use of nitrogen based symmetric 1,8-bis(imino)carbazoles, and their asymmetric analogues 8-imino-1,2,3,4-tetrahydrocarbazoles has been comparatively neglected or remains unexplored. As such, it is a primary objective of this project to synthesise novel highly hindered carbazole based ligands.

In following chapters, the synthesis and characterisation of a new family of symmetric/asymmetric imino carbazoles is targeted, with their ability to stabilise low-coordinate metal centres attempted later on; all of this with the eventual goal of using these highly reactive centres in catalysis and small molecule activation.

Chapter II. Ligands Synthesis

2.1 Results and Discussion

The synthesis of novel low-coordinate transition-metal centres was initially targeted by means of the synthesis of **1** [3,6-di-*tert*-butyl-9*H*-carbazole] (Scheme 2.1.1). As such, carbazole was reacted with two equivalents of ^{t}BuCl in the presence of $AlCl_3$, following reports by Gibson *et al*.[51] The formation of the desired product was confirmed by the emergence of new alkyl peaks, as noted by ^{1}H and $^{13}C\{^{1}H\}$ NMR spectra. Once formed, the 3,6-di-*tert*-butyl-9*H*-carbazole (**1**) was treated with two equivalents of *N*-bromosuccinimide, resulting in the formation of **2** [1,8-dibromo-3,6-di-*tert*-butyl-9*H*-carbazole] in quantitative yield.



*Scheme 2.1.1 Sequential synthesis of the 1,8-diformyl carbazole **3**.*

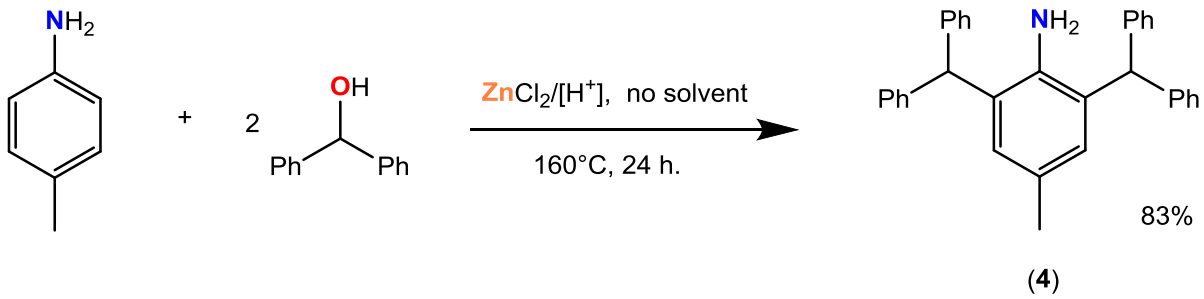
Consequently, the synthesis of a 1,8-diformyl derivative, was approached following a one pot methodology. In a first step, the 1,8-dibromo-3,6-di-*tert*-butyl-9*H*-carbazole (**2**) synthesised in a previous reaction, was deprotonated at low temperature with ^{n}BuLi. The *in situ* generated lithium salt was quenched with chlorotrimethylsilane, formally protecting the nitrogen in the carbazole scaffold with a trimethylsilyl group. Following this, the reaction of ^{t}BuLi with the protected carbazole, enabled a lithium-halogen exchange to take place; which was readily reacted with DMF to form the dialdehyde **3** [1,8-diformyl-3,6-di-*tert*-butyl-9*H*-carbazole] in good yield. The NMR spectra for **3** closely agreed with the reported literature.[51]

Having synthesised **3**, the next step involved the double substitution of the flanking formyl groups with a suitable amine to form imines (Schiff bases).

2.2 Ligand Design: How Much Steric Hindrance is Required?

Since one of the main objectives of this project involves the use of sterically encumbering *N*-based ligands as flanking groups, and with the eventual goal of forming imino derivatives *via* condensation reactions. A very important question arises; how sterically encumbering should our flanking amine be, in order to stabilise low-coordinate metal centres?

Having considered this, and acknowledging numerous reports recognising a remarkable ability to stabilise a wide variety of elements.[72–76] The tetraphenyl aniline Ar*NH_2 (Ar* = 2,6-bis(diphenyl)-4-methylphenyl) (**4**) was prepared following the report by Berthon *et al.* (Scheme 2.2.1).[77] This substituent was originally envisaged in the synthesis of novel NHC carbenes, but has since been used in a wide range of coordinatively unsaturated systems.[78] The preparation of this aniline is described in Scheme 2.2.1, where diphenylmethanol was reacted with *p*-toluidine at 160 °C to obtain the symmetric disubstitution on the aromatic ring in high yield, requiring no further purification.

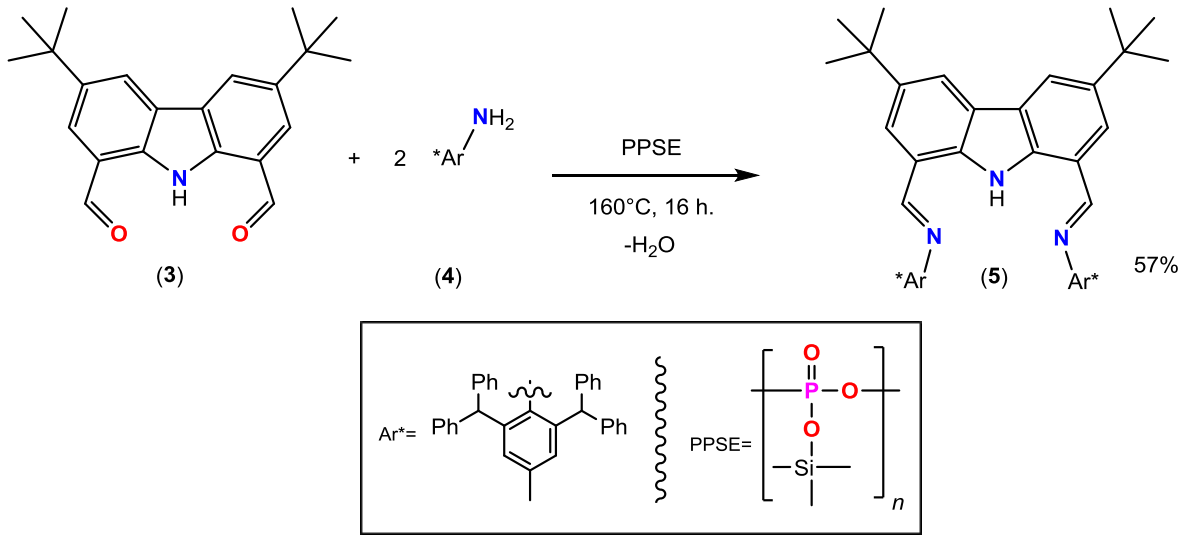


Scheme 2.2.1 Synthesis of ArNH_2 (**4**).*

2.2.1 Symmetric Carbazole [Ar_2*carbH]

Initial attempts to form a 1,8-bis(imino)carbazole by reacting the dialdehyde **3** and the amine **4**, through an acid-catalysed double Schiff base condensation under reflux in toluene, afforded negligible amounts of the monosubstituted aldimine derivative. Looking towards the formation of the disubstituted product [Ar_2*carbH] (**5**), the reaction was repeated using a Dean-Stark apparatus *via* azeotropic removal of the water formed as by-product of the condensation reaction using HCl as catalyst. However, no evidence of the formation of the desired product could be obtained through this method. Finally, it was envisioned that the use of methodology previously employed in the closely related formation of amidines in the presence of PPSE (polyphosphoric acid trimethylsilyl ester)

could afford the desired product (Scheme 2.2.2).[79] Accordingly, the dialdehyde **3** and the highly hindered aniline **4**, were reacted using the *in situ* generated PPSE as solvent at a temperature of 160 °C.



Scheme 2.2.2 Double Schiff-base condensation in the presence of PPSE.

The ^{1}H NMR spectrum of the light-brown solid obtained, showed full disappearance of the singlet at 10.25 ppm (indicative of the formyl substituent) exhibiting a newly formed singlet at 8.18 ppm in accordance with formation of an imino (–C*H*=N-Ar*) functional group (**5**). Accordingly, the broad signal at 11.48 ppm, associated to the N*H* of the 1,8-diformyl complex **3**, disappeared granting a new signal at 12.40 ppm, in accordance with a newly formed compound. Crystals of **5**, suitable for X-ray diffraction were obtained from slow evaporation of a hexane/dichloromethane solution at room temperature.

The solid state structure of **5** revealed half of the molecule occupying the asymmetric unit with the central rings of the Ar* moieties lying parallel to each other (Figure 2.2.1). The eight remaining flanking phenyl groups were found to be in an interlocked arrangement, most likely a consequence of the high hindrance of the close flanking groups.

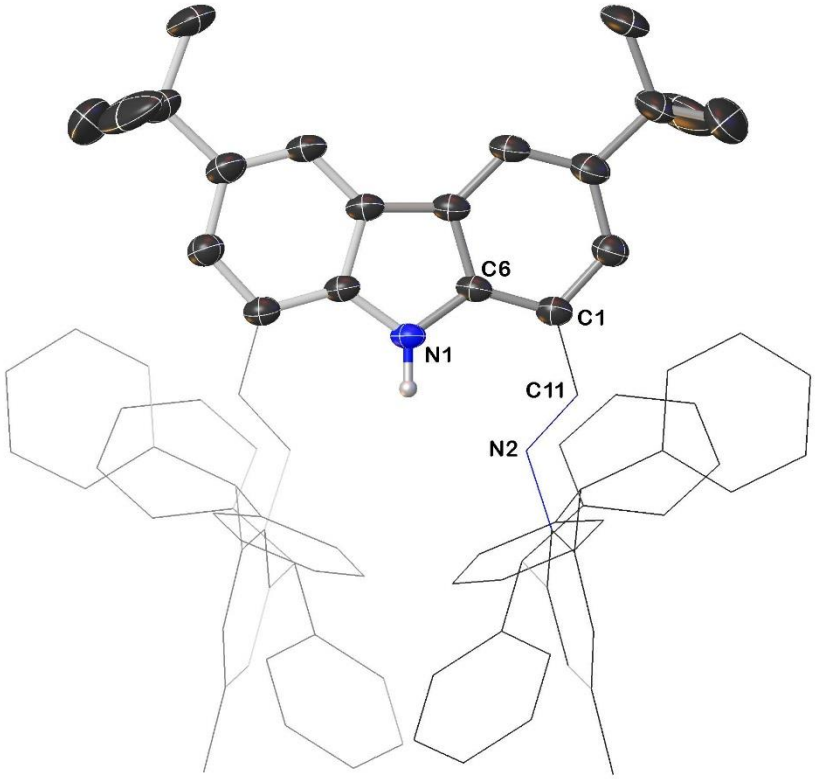


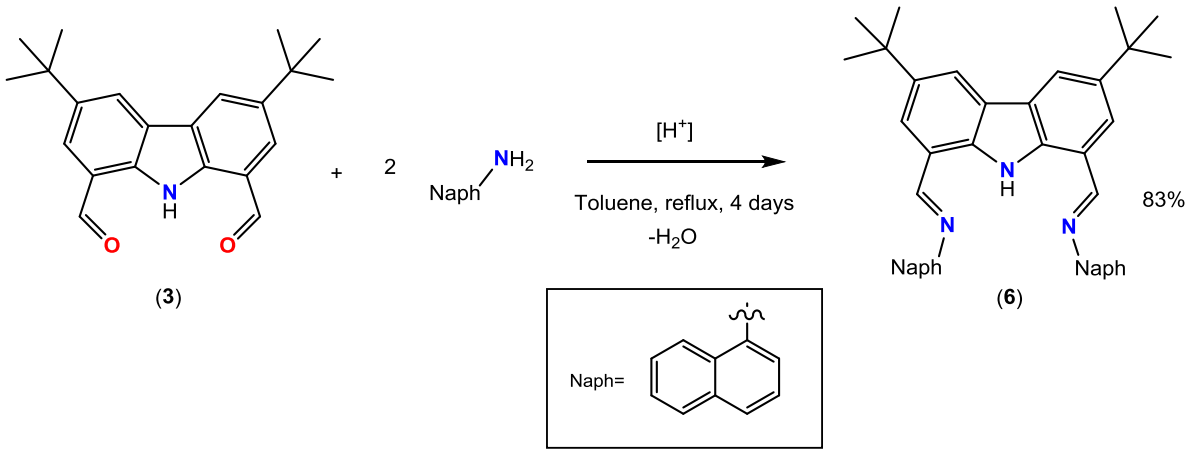
*Figure 2.2.1 Molecular structure of the symmetric unit of **5**, with displacement ellipsoids set at 50% probability level, hydrogen atoms with the exception of H1 (white sphere) have been omitted, with flanking –CH=N-Ar* moieties in wireframe form for clarity.*

Bond Length (Å)		Bond Angle (°)	
N2–C11	1.276(4)	N1–C6–C1	128.8(3)
		N2–C11–C1	122.0(3)

*Table 2.2.1 Selected bond lengths and angles for **5**.*

2.2.2 *Symmetric Carbazole [Naph$_2$carbH]*

Using a similar approach, the use of 1-naphthylamine was tested as a potential flanking group. Following previous reports, the condensation reaction was first attempted using SiO_2 as dehydrating agent at toluene reflux for 16 hours under acidic conditions (Scheme 2.2.3).[80,81] A ^{1}H NMR spectrum showed evidence of the formation of the desired disubstituted product. However, it was evident by the high amount of unreacted 1-naphthylamine present in the sample that the reaction needed longer reaction times and potentially, higher temperatures. With this in mind, the reaction was repeated using analogous conditions to the ones previously described while increasing the reaction time to 4 days at a temperature of 120 °C. By doing so, the desired 1,8-dinaphthylimino-3,6-di-*tert*-butyl-9*H*-carbazole ([Naph$_2$carbH] **6**) could be synthesised in good yield.[82]



*Scheme 2.2.3 Formation of **6**.*

Following the synthesis and organic work-up, crystals of **6** were grown from slow evaporation of a hexane/ethyl acetate solution.

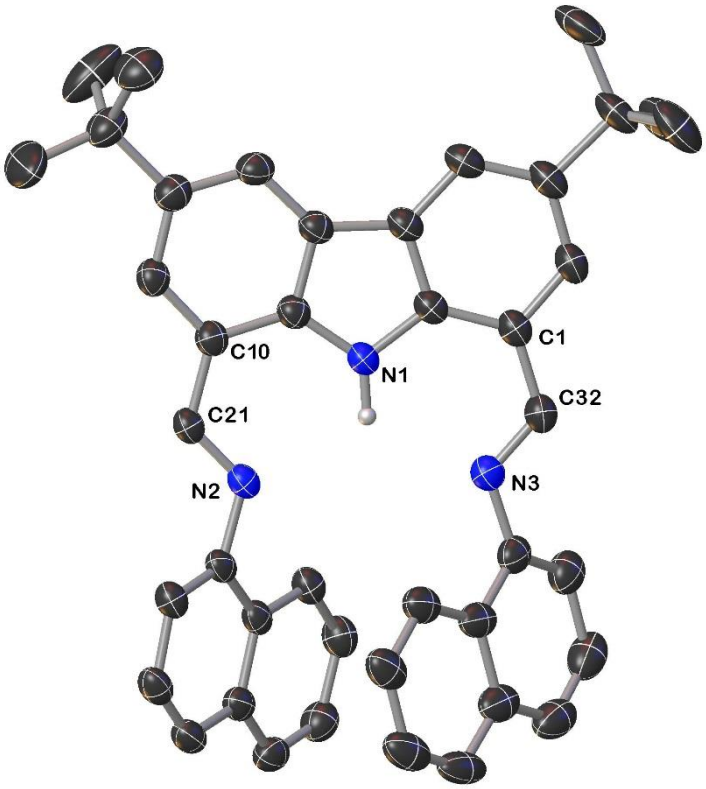


*Figure 2.2.2 Molecular structure of **6**, with displacement ellipsoids set at 50% probability level, hydrogen atoms with the exception of H1 (white sphere) have been omitted for clarity.*

The solid state structure of **6**, crystallised in the $P2_1/c$ space group, with one molecule occupying the asymmetric unit (Figure 2.2.2). The double condensation of the formyl flanking groups is evident, with the presence of two naphthyl imine substituents. The flanking naphthyl groups lie parallel to each other in an *anti*-fashion and in close proximity to each other [3.703(12) Å]; most likely a consequence of π-π stacking.[82,83]

Bond Length (Å)		Bond Angle (°)	
C21–N2	1.282(3)	N2–C21–C10	120.87(17)
C32–N3	1.286(3)	N3–C32–C1	121.35(18)

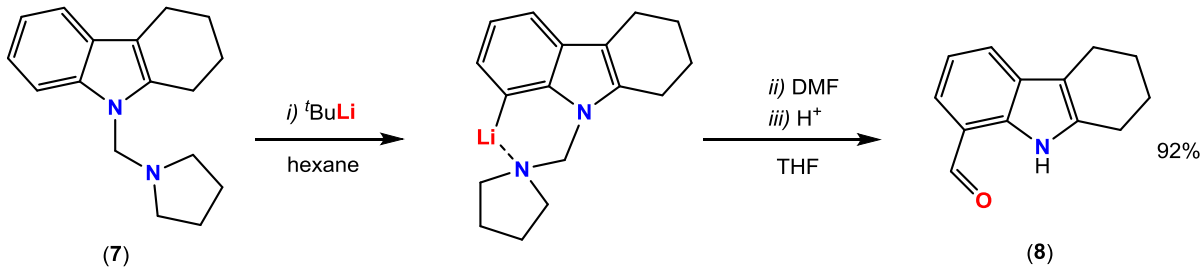
*Table 2.2.2 Selected bond lengths and angles for **6**.*

2.2.3 Asymmetric Tetrahydrocarbazole [Ar*THCarbH]

As mentioned in Chapter 1, there are limited reports regarding the synthesis of asymmetric derivatives based on the 1,2,3,4-tetrahydrocarbazole skeleton. In analogy with the synthesis of symmetric *N*-based tridentate carbazole ligands, extending these systems to asymmetric bidentate tetrahydrocarbazole systems is of great interest, due to their potential use in the stabilisation of low-coordinate metal centres, while also sufficing adequate space for their use in catalysis and small molecule activation.[84]

As such, and in a first approach, efforts were focused on the methodologies reported by Katrizky *et al*., from which a wide range of electrophiles can be substituted in the 8-position of the asymmetric carbazole.[70] In line with this, and despite not being mentioned in said report, it was extrapolated that upon lithiation, 1,2,3,4-tetrahydrocarbazole could be reacted with DMF as electrophile, following a procedure reminiscent of the formation of 1,8-diformyl-carbazole,[51] by which an asymmetric 8-formyl-1,2,3,4,-tetrahydrocarbazole could be synthesised.

With this as an aim, 1,2,3,4-tetrahydrocarbazole was converted into the corresponding aminal **7** (Mannich base), by reaction with one equivalent of paraformaldehyde and pyrrolidine in ethanolic solution [as described in the General Introduction] (Scheme 2.2.4). Full conversion to the desired product could be corroborated by the appearance of a singlet at high field (^{1}H NMR spectroscopy), characteristic of the newly formed *N*-methylene substituted derivative (-N–C*H*$_2$-N-), in excellent yield, which was in line with previously reported data.[70]



*Scheme 2.2.4 Formation of 8-formyl-1,2,3,4-tetrahydrocarbazole (**8**).*

The isolated product (**7**) was later reacted, at 80 °C, with a slight excess of ^{t}BuLi in hexane. By doing so, to the *in situ* generated lithium salt was added a stoichiometric amount of dry DMF (Scheme 2.2.4). Closely followed by quenching/deprotection of the central carbazolido nitrogen by acid catalysed hydrolysis (**8** [CHO-THCarbH]). Full NMR analysis of the resulting dark brown semisolid (**8**) in $CDCl_3$, evidenced the presence of a formyl moiety in the molecule as corroborated by the presence of a new signal at 9.9 ppm (^{1}H

NMR spectrum) and 194 ppm ($^{13}C\{^{1}H\}$ NMR spectrum), respectively. Crystals of **8**, suitable for X-ray structural determination, were grown from concentrated solutions in a mixture of hexane and dichloromethane.

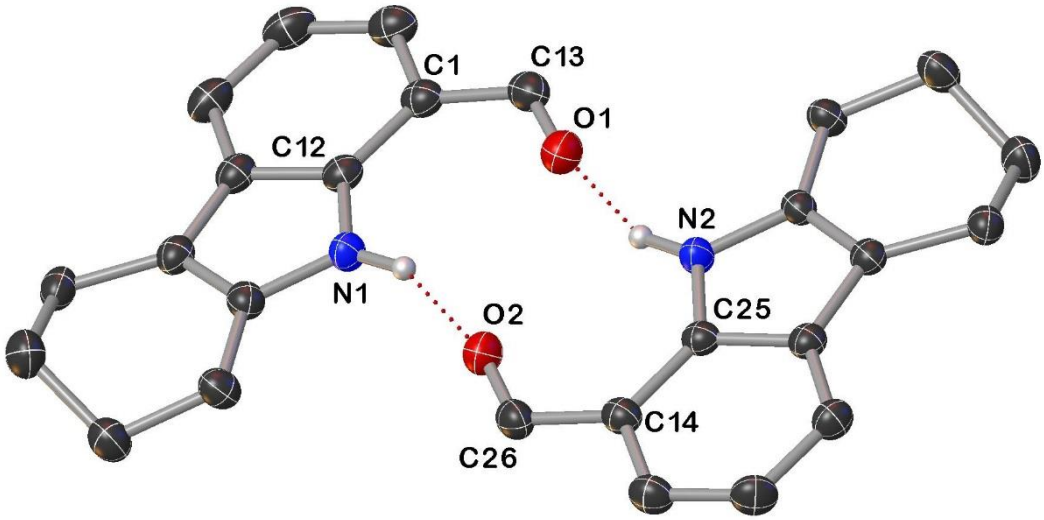


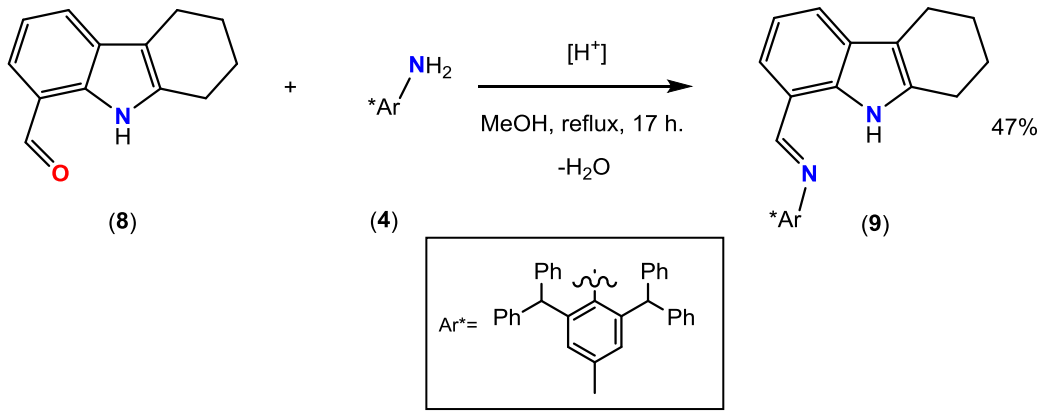
*Figure 2.2.3 Molecular structure of **8**, showing the two crystallographically independent molecules, with displacement ellipsoids set at 50% probability level, hydrogen atoms with the exception of H1/H2 (white spheres; H1 attached to N1, H2 attached to N2) have been omitted for clarity.*

The solid state structure of **8** contains two crystallographically independent molecules occupying the asymmetric unit (Figure 2.2.3). The asymmetry of the carbazole core is evident from the flanking ring being non-coplanar with the rest of the indole moiety. More so, the two molecules occupying the asymmetric unit, are engaged in the formation of hydrogen bonded pairs, arising from the mutualistic interactions between the carbazole *N*-proton and the oxygen of the formyl group, substituted on the aromatic ring of the tetrahydrocarbazole molecule [O1–H2 = 2.1809(12) Å, O2–H1 = 2.1243(11) Å; O1–N2 = 2.972(2) Å, O2–N1 = 2.914(2) Å; N2–H2–O1 = 152.69(9)°, N1–H1–O2 = 152.37(9)°].

Bond Length (Å)		Bond Angle (°)	
C1–C13	1.451(2)	C1–C13–O1	124.73(15)
C13–O1	1.217(2)	N1–C12–C1	130.16(15)
C14–C26	1.450(2)	C14–C26–O2	124.24(14)
C26–O2	1.221(2)	N2–C25–C14	130.31(14)

*Table 2.2.3 Selected bond lengths and angles for **8**.*

Initial attempts to form an asymmetric 8-imino substituted carbazole were met, following an acid catalysed condensation reaction between the formyl derivative **8** and the highly sterically encumbered aniline **4**, prepared in a previous step (Scheme 2.2.5). Similar to the synthesis of the symmetric analogue **5**, reactions carried out in methanol at room temperature overnight, afforded negligible formation of the substituted product. Heating the reaction mixture for 17 hours at reflux, was required in order to afford the formation of the asymmetric Ar*-substituted aldimine **9** (Schiff base) [Ar*THCarbH]. Following purification of the crude mixture, the pure product could be isolated in good yield.



*Scheme 2.2.5 Synthesis of **9**.*

In a similar way to the formation of **5** and **6**, upon condensation, the formyl moiety undergoes a change in chemical shift from 194 to 165 ppm, as observed in the $^{13}C\{^{1}H\}$ NMR spectrum, with a similar change observed in the ^{1}H NMR spectrum. The highly encumbered, asymmetric aldimine **9** was isolated in good yield and crystals suitable for X-ray diffraction were grown from the slow evaporation of concentrated hexane/dichloromethane extracts.

In the solid state, **9** is monomeric and crystallises in the *P*-1 space group, with only one molecule occupying the asymmetric unit (Figure 2.2.4). Formal replacement of the aldehyde for the –C*H*=N-Ar* substituent, is visible, in line with a successful condensation reaction. Although the central ring of the Ar* moiety lies within the best mean plane generated by the central ring of the carbazole (pyrrole), the substituent does not lie coplanar with the carbazole ring [plane twist angle 129.84(6)°]. With the remaining four phenyl groups residing almost perpendicular to each other on both sides of the central *p*-toluidine ring.

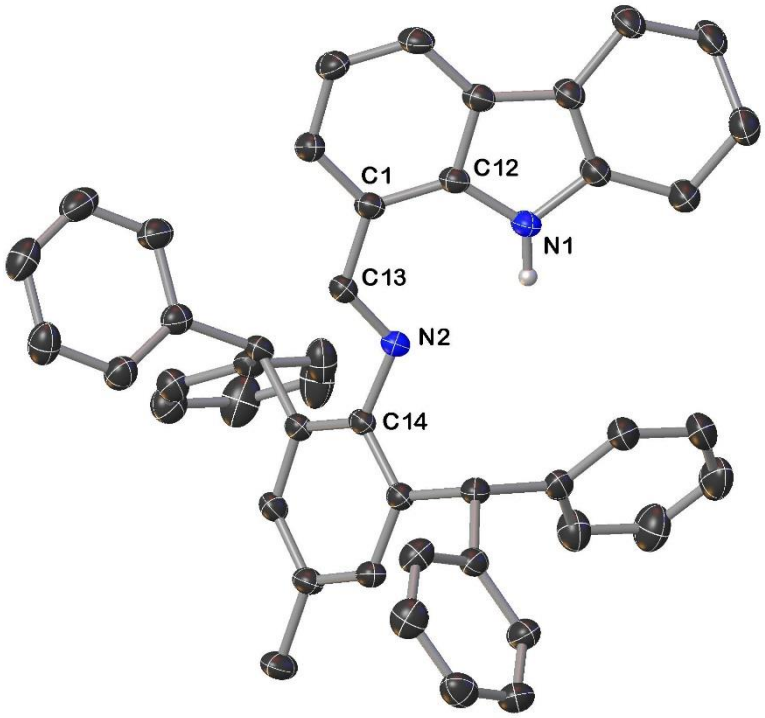


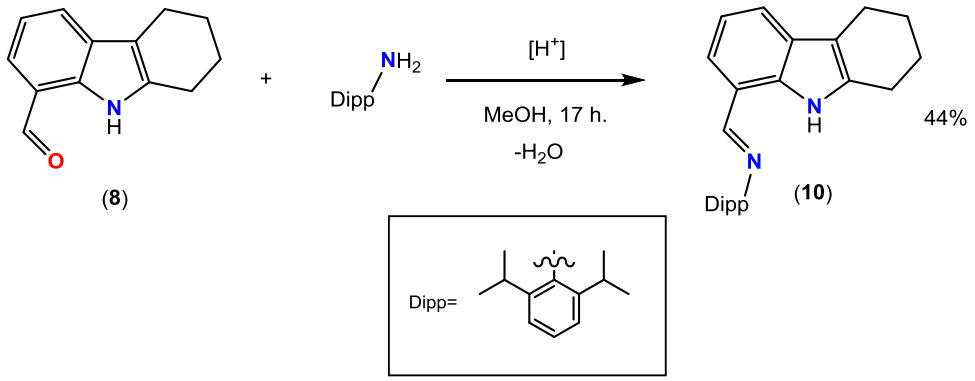
*Figure 2.2.4 Molecular structure of **9**, with displacement ellipsoids set at 50% probability level, hydrogen atoms with the exception of H1 (white sphere) have been omitted for clarity.*

Bond Length (Å)		Bond Angle (°)	
C1–C13	1.452(2)	C1–C13–N2	122.71(14)
C13–N2	1.283(2)	N1–C12–C1	108.91(12)
C14–N2	1.4219(19)	C13–N2–C14	117.92(13)

*Table 2.2.4 Selected bond lengths and angles for **9**.*

2.2.4 Asymmetric Tetrahydrocarbazole [DippTHCarbH]

Employing a similar approach, a condensation reaction with 2,6-diisopropylaniline was tested. Comparatively smaller, this aniline proved to be easier to substitute, requiring only mild conditions (room temperature overnight) *via* an acid catalysed Schiff condensation reaction (Scheme 2.2.6). Although growing crystals suitable for single crystal diffraction was attempted, to no effect, full NMR characterisation, gave clear evidence of complete conversion to the substituted asymmetric carbazole [DippTHCarbH] (**10**) in moderate yield. With similar behaviours in both ^{1}H and $^{13}C\{^{1}H\}$ NMR spectra to the ones mentioned above for aldimines **5**-**6** and **9**.



*Scheme 2.2.6 Synthesis of **10**.*

2.3 Conclusions

The synthesis of novel *N*-based carbazolido proligands has been achieved. This has been accomplished in the basis of the formation of two families of proligands *via* condensation reactions to form imines (Schiff bases) [**5** and **6**]. To this effect, a variety of methods have been attempted. From this it has been possible to observe an increasing degree of complexity in the synthesis of such compounds on the basis of the steric hindrance of the substituent employed. The synthesis of two symmetric *NNN* carbazolido pincer proligands, based on carbazole, with varying degree of steric bulk, was achieved. While a new methodology has been developed in order to synthesise comparatively hindering, flanking groups in asymmetric systems based on 1,2,3,4-tetrahydrocarbazole, to form bidentate 8-substitued *NN*-pincer chelates (**9** and **10**). Following this methodology, the formation of two asymmetric imines has been accomplished, while at the same time demonstrating the potential usefulness of this synthetic route, for the incorporation of other functional groups.

2.4 Experimental Section

2.4.1 Synthesis and Characterisation

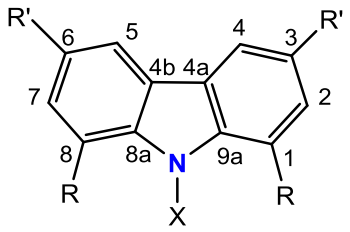


Figure 2.4.1 General numbering scheme for carbazole based compounds.

3,6-di(*tert*-butyl)-9*H*-carbazole (**1**):[51]

[^{t}Bu$_2$carbazole]

To a mixture of carbazole (15 g, 89 mmol) and aluminium chloride (13 g, 98 mmol, 1.1 eq.) in dichloromethane (120 mL) at 0 °C was added a solution of ^{t}Butyl chloride (19 mL, 179 mmol, 2 eq.) over 30 minutes. The resulting mixture was allowed to warm to room temperature and stirred at this temperature for 72 hours. After this time, 150 mL of water were added and the organic layer was separated and dried over magnesium sulphate. Volatiles were removed *in vacuo* yielding a light brown powder (24 g, 95%). Data is consistent with the reported literature.[51] Crystals of **1** suitable for X-ray diffraction were grown at room temperature, *via* evaporation of a saturated solution in dichloromethane.

^{1}H NMR (300 MHz, $CDCl_3$, 25 °C) δ(ppm): 8.10 (d, 2H, *J* = 2 Hz, H4 +H5), 7.76 (br s, 1H, N*H*), 7.46 (dd, 2H, *J* = 8.4 and 2 Hz, H2 + H7), 7.31 (dd, 2H, *J* = 8.3 and 0.5 Hz, H1 and H8), 1.47 (s, 18H, C(CH_3)$_3$).

^{13}C{^{1}H} NMR (75 MHz, $CDCl_3$, 25 °C) δ(ppm): 142.20 (C3 + C6), 138.00 (C8a + C9a), 123.49 (C4 + C5), 123.27 (C4a + C4b), 116.14 (C2 + C7), 110.00 (C1 + C8), 34.67 (*C*(CH$_3$)$_3$), 32.02 (C(*C*H$_3$)$_3$).

HRMS/ESI+ *m/z*: [M+H] calculated 280.2060, found 280.2064; formula $C_{20}H_{26}N$.

1,8-dibromo-3,6-di(*tert*-butyl)-9*H*-carbazole (**2**):[51]

[^{t}Bu$_2$Br$_2$carbazole]

To a solution of **1** (20 g, 72 mmol) in dichloromethane (1 L) kept at 0 °C , was added *N*-bromosuccinimide (26 g, 150 mmol, 2.1 eq.) over a period of 1 hour. The resulting mixture was allowed to reach room temperature and kept stirring for additional 3 hours. After this time, the reaction mixture was washed with water and the organic phase separated and dried over magnesium sulphate. Volatiles were removed under vacuum affording the titled product as a light brown powder (29 g, 99%). Data is consistent with the reported literature.[51] Crystals of **2** suitable for X-ray diffraction were grown at room temperature, *via* evaporation of a saturated solution in dichloromethane.

^{1}H NMR (300 MHz, $CDCl_3$, 25 °C) δ (ppm): 8.15 (br s, 1H, N*H*), 7.99 (d, 2H, *J* = 1.36 Hz, H4 + H5), 7.65 (d, 2H, *J* = 1.58 Hz, H2 + H7), 1.45 (s, 18H, C(C*H*$_3$)$_3$).

^{13}C{^{1}H} NMR (75 MHz, $CDCl_3$, 25 °C) δ (ppm): 144.78 (C3 + C6), 136.33 (C8a + C9a), 126.65 (C4 + C5), 124.83 (C4a + C4b), 115.97 (C2 + C7), 104.02 (C1 + C8), 34.94 (*C*(CH$_3$)$_3$), 31.93 (C(*C*H$_3$)$_3$).

HRMS/ESI- *m/z*: [M-H] calculated 434.0124, found 434.0118; formula $C_{20}H_{22}Br_2N$.

1,8-diformyl-3,6-di(*tert*-butyl)-9*H*-carbazole (**3**):[51]

[^{t}Bu$_2$CHO$_2$carbazole]

A solution of ^{n}BuLi (2.5 M, 8 mL, 20 mmol, 1.1 eq.) was added slowly to a solution of **2** (8 g, 18 mmol) in diethyl ether (*ca.* 100 mL) at 0 °C. The resulting mixture was stirred at this temperature for 1 hour. Subsequently, the mixture was kept at 0 °C and clorotrimethyl silane (2.5 mL, 20 mmol, 1.1 eq.) was added slowly. After the addition was finished, the reaction mixture was allowed to reach room temperature and kept stirring for additional 1 hour. After this time, the mixture was cooled down to –78 °C and a solution of ^{t}BuLi (5 g, 78 mmol, 4.3 eq.) in hexane (40 mL) was added dropwise over a period of 30 minutes. The resulting mixture was warmed up to 0 °C and stirred at the mentioned temperature for 3 hours. The reaction was cooled down to –78 °C once again and dimethylformamide (7.8 mL, 100 mmol, 5.5 eq.) was added slowly. The mixture was allowed to reach room temperature and kept stirring for 16 hours. The crude of the reaction was cooled down to 0 °C and quenched with HCl (1 M, 75 mL) and furtherly extracted with dichloromethane (50 mL x 3). Removal of volatiles under vacuum afforded a bright red powder (2.96 g, 96%). Data is consistent with the reported literature.[51] Crystals of **3** suitable for X-ray diffraction were grown at room temperature, from a saturated solution in acetone/$CDCl_3$.

^{1}H NMR (300 MHz, $CDCl_3$, 25 °C) δ (ppm): 11.48 (br s, 1H, N*H*), 10.25 (s, 2H, (O=C*H)*), 2.64 (d, 2H, *J* = 1.6 Hz, H4 + H5), 7.96 (d, 2H, *J* = 2 Hz, H2 + H7), 1.54 (s, 18H, C(CH_3)$_3$).

^{13}C{^{1}H} NMR (75 MHz, $CDCl_3$, 25 °C) δ (ppm): 192.92 (O=*C*H), 143.12 (C3 + C6), 136.93 (C8a + C9a), 129.42 (C4 + C5), 123.41 (C4a + C4b), 119.93 (C1 + C8), 34.79 (*C*(CH$_3$)$_3$), 31.86 (C(*C*H$_3$)$_3$).

IR ν/cm^{-1} (ATR): 3435 (N*H*) m, 2959 m, 2863 w, 1676 (HC=O) s, 1589 s, 1483 s.

HRMS/ESI- *m/z*: [M+Na] calculated 358.1777, found 358.1782; formula $C_{22}H_{25}NNaO_2$.

2,6-bis(diphenylmethyl)-4-methylaniline (**4**):[77]

[Ar*NH$_2$]

Diphenylmethanol (30 g, 162 mmol, 2 eq.) and *p*-toluidine (8.7 g, 81 mmol) were placed in a 250 mL round bottom flask equipped with a stirring bar. The reaction mixture was heated to a temperature of 50 °C. Shortly after, a solution of $ZnCl_2$ (5.5 g, 41 mmol, 0.5 eq.) in concentrated HCl (36%, 6.8 mL, 81 mmol) was added to the resulting yellow liquid. A condenser was adapted to the system, the temperature was increased (150 °C) and left stirring for 24 hours, affording a brown solid. This solid was extracted into dichloromethane and washed sequentially with NH_4Cl (2 x 50 mL) and brine (2 x 50 mL). The combined organic layers were dried over magnesium sulphate and filtered. The removal of solvent *in vacuo* afforded a white powder (30 g, 83%). Data is consistent with the reported literature.[77] Crystals of **4** suitable for X-ray diffraction were grown from a concentrated solution in hexane, at −30 °C.

^{1}H NMR (300 MHz, $CDCl_3$, 25 °C) δ (ppm): 7.33-7.20 (m, 12H, Ph), 7.13-7.10 (m, 8H, Ph), 6.40 (s, 2H, Ar*H*), 5.47 (s, 2H, -C*H*Ph$_2$), 3.28 (br s, 2H, N*H*$_2$), 2.04 (s, 3H, C*H*$_3$).

^{13}C{^{1}H} NMR (75 MHz, $CDCl_3$, 25 °C) δ (ppm): 142.74, 139.58, 129.51, 129.23, 129.01, 128.44, 126.64, 126.55 (Ar-*C*), 52.35 (Ph$_2$*C*H), 20.97 (Ar*C*H$_3$).

1,8-di(Ar*)imino-3,6-di(*tert*-butyl)-9*H*-carbazole (**5**):

[Ar$_2$*carbH]

Under a flow of N_2, a Schlenk flask was charged with P_2O_5 (1.3 g, 8.7 mmol, 4.2 eq.), hexamethyldisiloxane (4.2 g, 26 mmol, 12.5 eq.) and dichloromethane (10 mL). The reaction mixture was heated to reflux for 1 hour affording a colourless syrup. After this

time, the reaction vessel was cooled down to room temperature and volatiles were removed under vacuum. Following this, the system was heated to 130 °C through an oil bath, to which a neat mixture of **4** (1.8 g, 4.2 mmol, 2 eq.) and **3** (0.7 g, 2.1 mmol, 1 eq.) was added. The resulting mixture was heated up to 160 °C, and left stirring for 16 hours. The crude of the reaction was basified with NaOH (1 M, 20 mL) and extracted with $CHCl_3$. Volatiles were removed under vacuum affording a brown powder, which was furtherly purified by dissolution in hot hexane/methanol and filtered affording a brown microcrystalline powder (1.4 g, 57%). Crystals of **5** suitable for X-ray diffraction were grown from concentrated solutions in MeOH/hexane/dichloromethane at room temperature, *via* solvent evaporation.

^{1}H NMR (300 MHz, $CDCl_3$, 25 °C) δ(ppm): 12.40 (s, 1H, N*H*), 8.18 (s, 2H, (N=C*H*)), 7.34-7.12 (m, 44H, Ph), 5.73 (s, 4H, -C*H*Ph_2), 5.49 (s, 4H, -C*H*Ph_2), 2.32 (s, 3H, *ArCH*$_3$), 2.06 (s, 3H, ArC*H*$_3$), 1.40 (s, 18H, C(C*H*$_3$)$_3$).

^{13}C{^{1}H} NMR (75 MHz, $CDCl_3$, 25 °C) δ (ppm): 167.28 (N=*C*H), 149.36 (N-C), 142.74, 139.62, 134.59, 131.97, 129.74, 129.51, 129.32, 129.22, 129.02, 128.44, 128.16, 128.00, 126.55 (Ar-*C* + carbazole-C), 52.73 (Ph_2CH), 52.36 (Ph_2*C*H), 34.50 (*C*(CH$_3$)$_3$), 31.86 (C(*C*H$_3$)$_3$), 21.54 (ArCH$_3$), 20.97 (ArCH$_3$).

IR ν/cm^{-1} (ATR): 3381 (N*H*) m, 3058 m, 3026 m, 2957 m, 1597 (N=CH) s, 1492 s, 1238 m.

Anal. Calcd for $C_{88}H_{79}N_3$: C 89.68, H 6.76, N 3.57; Found C 85.24, H 6.76, N 3.40.

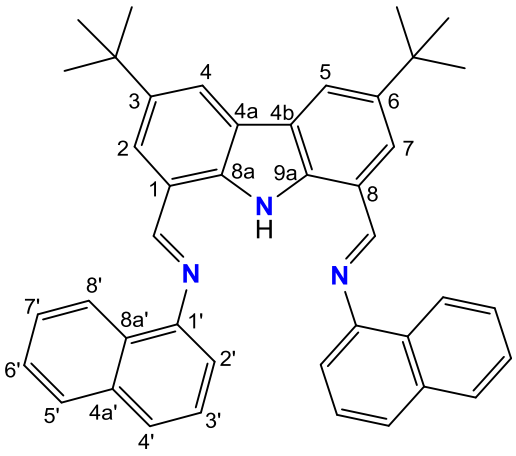


*Figure 2.4.2 Numbering scheme for **6**.*

1,8-dinaphthylimino-3,6-di(*tert*-butyl)-9*H*-carbazole (**6**):[82]

[$Naph_2carbH$]

1,8-diformyl-3,6-di-*tert*-butyl-9*H*-carbazole (**3**) (2 g, 5.9 mmol), 1-naphthylamine (1.7 g, 11.9 mmol, 2 eq.) and SiO_2 (*cat.*) were charged in a 500 mL round bottom flask to which 150 mL of toluene and a few drops of glacial acetic acid were added. A condenser was set up, and the reaction mixture set to reflux for 4 days open to air. The crude of the reaction was filtered while hot and the filtrate washed with diethyl ether (2 x 50 mL). Removal of volatiles *in vacuo* yielded a dark brown powder which was recrystallised from acetone, affording the desired product as bright yellow needles (2.75 g, 79%). Crystals of **6** suitable for X-ray diffraction were grown at room temperature, from acetone *via* solvent evaporation.

^{1}H NMR (400 MHz, $CDCl_3$, 25 °C) δ (ppm): 13.02 (s, 1H, N*H*), 8.94 (s, 2H, (N=C*H*)), 8.40 (d, 2H, *J* = 1.7 Hz, H4 + H5), 8.17 (d, *J* = 8.9 Hz, 2H, Naph *H*8'), 7.86 (d, 2H, *J* = 1.8 Hz, H2 + H7), 7.56 (d, 2H, *J*= 8.2 Hz, Naph *H*4'), 7.46-7.41 (m, 4H, Naph *H*3' and *H*5'), 7.17 (dd, 2H, *J* = 7.2 and 1.0 Hz, Naph *H*2'), 6.95 (ddd, 2H, *J* = 8.1, 6.9 and 1.0 Hz Naph *H*6'), 6.38 (ddd, 2H, *J*= 8.1, 6.9 and 1.0 Hz Naph *H*7'), 1.59 (s, 18H, C(CH_3)$_3$).

^{13}C{^{1}H} NMR (100 MHz, $CDCl_3$, 25 °C) δ (ppm): 160.97 (N=*C*H), 149.59 (N-*C*1'), 142.51 (C3 + C6), 137.14 (C8a + C9a), 133.64 (quatern-Naph *C*4a'), 128.75 (quatern-Naph *C*8a'), 127.80 (C2 + C7), 126.72 (Naph *C*5'), 125.69 (Naph *C*4' and *C*6'), 125.58 (Naph *C*3'), 124.97 (Naph *C*7'), 123.80 (Naph *C*8'), 123.70 (C1 + C8), 120.21 (C4 + C5), 119.56 (4a + 4b), 112.62 (Naph *C*2'), 34.98 (*C*(CH_3)$_3$), 32.23 (C(*C*H_3)$_3$).

HRMS/ESI- *m/z*: [M+H] calculated 586.3217, found 586.3215; formula $C_{42}H_{40}N_3$.

IR *v*/cm^{-1} (ATR): 3349 (N*H*) w, 3044 w, 2952 s, 2901 s, 1591 (N=CH) s, 1567 s, 1482 s.

Anal. Calcd for $C_{42}H_{39}N_3$: C 85.82, H 7.03, N 7.15; Found C 83.07, H 6.61, N 6.98.

UV/vis (THF, c = 1.0 x 10^{-5} mol dm^{-3}): λ_{max}/nm (ε x 10^4 / dm^{3}mol^{-1}cm^{-1}) 393 (2.78).

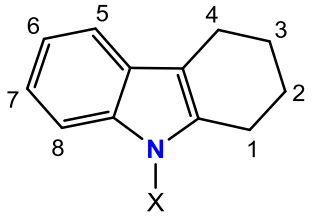


Figure 2.4.3 General numbering scheme for 1,2,3,4-tetrahydrocarbazoles based systems.

9-(1-Pyrrolidinomethyl)-1,2,3,4,-tetrahydrocarbazole (**7**):[70]

In a 250 mL round bottom flask, 1,2,3,4-tetrahydrocarbazole (15 g, 87.6 mmol, 1 eq.) and paraformaldehyde (3.0 g, 101 mmol, 1.2 eq.). The resulting mixture was eluted with ethanol (60 mL) and shortly after the pyrrolidine (8.18 mL, 98.1 mmol, 1.2 eq.) was added. A water condenser was fitted and the temperature was set at 80 °C, affording shortly after a light-yellow solution. The reaction was heated at reflux for 24 hours, after which the solvent was evaporated under vacuum, affording a light yellow oil. This oil was extracted with ethyl acetate (2 x 50 mL) and washed with deionised water (2 x 100 mL). To the combined organic layers was added 0.1 M HCl (2 x 100 mL) and furtherly washed with ethyl acetate (2 x 50 mL), with the latter phase being discarded. The aqueous phase was washed once more with ethyl acetate (100 mL) and later basified with aqueous ammonia solution (*ca.* 200 mL of 35% NH_3). Finally, the resulting aqueous solution was extracted with hexanes and the solvent was evaporated, affording the desired product as a light yellow oil which became a yellow solid shortly after (20.45 g, 92%). Data is consistent with reported literature.[70]

^{1}H NMR (300 MHz, d_6-DMSO, 25 °C) δ(ppm): 7.44 (d, 1H, *J* = 8.0 Hz, Ar-*H*), 7.34 (d, 1H, *J* = 8.0 Hz, Ar-*H*), 7.07-7.01 (m, 1H, Ar-*H*), 6.96 (td, 1H, *J* = 7.4 and 1.1 Hz, Ar-*H*), 4.83 (s, 2H, N-C*H*$_2$-N), 2.76 (t, 2H, *J* = 5.8 Hz, C*H*$_2$), 2.63 (t, 2H, *J* = 5.8 Hz, C*H*$_2$), 2.56-2.50 (m, 4H, C*H*$_2$), 1.90-1.75 (m, 4H, C*H*$_2$), 1.66-1.62 (m, 4H, C*H*$_2$).

^{13}C{^{1}H} NMR (75 MHz, d_6-DMSO, 25 °C) δ (ppm): 136.82 (quaternary), 135.77 (quaternary), 126.88 (quaternary), 120.22 (Ar-*C*), 118.40 (Ar-*C*), 117.12 (Ar-*C*), 109.63 (Ar-*C*), 108.57 (quaternary), 60.69 (N-*C*H$_2$-N), 50.93 (*C*H$_2$-N), 23.01 (CH$_2$ pyrrolidine), 22.83 (*C*H$_2$), 22.73 (*C*H$_2$), 21.71 (*C*H$_2$), 20.64 (*C*H$_2$).

HRMS/ESI+ *m/z*: [M+H] calculated 254.1783, found 255.1863; formula $C_{17}H_{23}N_2$.

IR *v*/cm^{-1} (ATR): 3052 w, 2931 s, 2829 w, 2806 w, 1461 s, 1323 s.

Anal. Calcd for $C_{17}H_{22}N_2$: C 80.27, H 8.72, N 11.01; Found C 80.13, H 8.91, N 10.97.

8-Formyl-1,2,3,4-Tetrahydro-9*H*-carbazole (**8**):

[CHO-THCarbH]

In two separate Schlenk flasks, the aminal **7** (3.0 g, 11.8 mmol, 1 eq.) and ^{t}BuLi (1.1 g, 17.7 mmol, 1.5 eq.) were dissolved in dry hexane (60 mL). The solution containing the aminal, was cooled down to –80 °C in an acetone/dry ice bath, and the ^{t}BuLi solution was drop-wise added over a 30 min period. Upon addition of ^{t}BuLi, the once homogeneous

colourless solution turned into a yellow heterogeneous mixture. The resulting mixture was left stirring for 16 hours, allowing it to reach room temperature slowly. Subsequently, 20 mL of dry THF was added affording an orange solution; this was cooled down to –80 °C with subsequent addition of DMF (1.4 mL, 17.7 mmol, 1.5 eq.). Following this addition, the mixture was warmed slowly to room temperature and left stirring for additional 24 hours. After this time, the reaction vessel was opened to air and 1M HCl was added (120 mL). The crude of the reaction mixture was then heated to reflux for 2 hours, after which the system was cooled to room temperature and extracted with ethyl acetate (3 x 200 mL). The combined organic phases were washed with brine (3 x 100 mL) and volatiles were removed under vacuum. The title compound was obtained as a dark yellow-brown semi-solid (2.81 g, 54%). Crystals of **8** suitable for X-ray diffraction were grown at room temperature, from a concentrated solution in hexane/dichloromethane, *via* solvent evaporation.

^{1}H NMR (300 MHz, C_6D_6, 25 °C) δ(ppm): 9.99 (s, 1H, (O=C*H)*), 7.66 (d, 1H, *J* = 7.7 Hz, Ar-*H*), 7.46 (dd, *J* = 7.4 and 1.1 Hz, Ar-*H*), 7.10 (t, 1H, *J* = 7.6 Hz, Ar-*H*), 2.71-2.56 (m, 4H, CH_2), 1.89-1.74 (m, 4H, CH_2).

^{13}C{^{1}H} NMR (75 MHz, C_6D_6, 25 °C) δ(ppm): 193.88 (H*C*=O), 127.68 (Ar-*C*), 125.14 (Ar-*C*), 121.06 (quaternary), 119.68 (quaternary), 119.17 (quaternary), 118.68 (Ar-*C*), 117.80 (quaternary), 110.41 (quaternary), 23.35 (*C*H_2), 23.25 (*C*H_2), 23.12 (*C*H_2), 20.82 (*C*H_2).

HRMS/ESI- *m/z*: $[M-H]^-$ calculated 198.0924, found 198.0915; formula $C_{13}H_{12}NO$.

IR *v*/cm^{-1} (ATR): 3054 (N*H*) s, 2925 s, 1666 (HC=O) s, 1569 s, 1468 s.

Anal. Calcd for $C_{13}H_{13}NO$: C 78.36, H 6.58, N 7.03; Found C 74.18, H 6.52, N 6.74

8-(Ar*)imino-1,2,3,4-Tetrahydro-9*H*-carbazole (**9**):

[Ar*THCarbH]

Aldehyde **8** (0.65 g, 3.3 mmol, 1 eq.) and **4** (1.4 g, 3.3 mmol, 1 eq.) were dissolved in a mixture of CH_2Cl_2 (30 mL) and MeOH (20 mL), affording a yellow homogeneous solution. To this solution, formic acid (15 drops) was added and the mixture was heated to reflux for 16 hours. The reaction mixture was cooled down and volatiles were removed under vacuum. The crude product was then extracted with hot methanol (3 x 20 mL), affording the desired compound as a light brown oil (0.95 g, 47%). Crystals of **9** suitable for X-ray

diffraction were grown from the slow evaporation of a concentrated solution in hexane/dichloromethane at room temperature.

^{1}H NMR (400 MHz, $CDCl_3$, 25 °C) δ(ppm): 9.49 (s, 1H, N*H*), 7.62 (d, 1H, *J* = 7.7 Hz, Ar-*H*), 7.50 (s, 1H, (N=C*H*)), 7.31-7.24 (m, 10H, Ph), 7.17 (d, 2H, *J*= 8.4 Hz, Ph), 7.08-7.06 (m, 10H, Ph), 6.74 (s, 2H, -C*H*Ph_2), 6.67 (d, 1H, Ar-*H*), 5.53 (s, 2H, Ar-*H*), 2.81 (t, 2H, *J* = 5.1 Hz, C*H*$_2$), 2.67 (t, 2H, *J* = 5.1 Hz, C*H*$_2$), 2.25 (s, 3H, Ar-C*H*$_3$), 2.02-1.91 (m, 4H, CH_2).

^{13}C{^{1}H} NMR (100 MHz, $CDCl_3$, 25 °C) δ(ppm): 165.84 (N=*C*H), 148.82 (Ar*C-N), 143.97 (quaternary), 142.91 (quaternary), 135.35 (quaternary), 133.73 (quaternary), 133.50 (quaternary), 132.43 (quaternary), 129.90, 129.68, 129.38, 129.17, 128.90, 128.61, 128.24, 126.72, 126.22, 125.72, 121.47 (Ar-*C*), 118.20, 109.64 (quaternary), 52.25, 23.60 (*C*H_2), 23.43 (*C*H_2), 23.36 (*C*H_2), 21.55 (Ar-*C*H_3), 21.02 (*C*H_2).

HRMS/ASAP *m/z*: [M+H] calculated 621.3270, found 621.3268; formula $C_{46}H_{41}N_2$.

IR *v*/cm^{-1} (ATR): 3388 (N*H*) s, 3025 w, 2931 w, 1628 (N=CH) s, 1572 s, 1492 s, 1463 s, 1325 s.

Anal. Calcd for $C_{46}H_{40}N_2$: C 88.99, H 6.49, N 4.51; Found C 86.57, H 6.33, N 4.02

8-(Dipp)imino-1,2,3,4-Tetrahydro-9*H*-carbazole (**10**):

[DippTHCarbH]

Aldehyde **8** (0.1 g, 0.5 mmol, 1 eq.) and 2,6-diisopropylaniline (0.09 g, 0.5 mmol, 1 eq.) were dissolved in methanol (30 mL) affording a yellow solution. Formic acid was then added (5 drops) and the resulting mixture was stirred at room temperature for 17 hours. Volatiles were then removed under vacuum affording a brown oil. A low pressure, trap to trap system was set up, and the pressure in the whole system was reduced, with gentle heating of the crude mixture, removing unreacted aniline. By doing so, the title compound could be isolated as a dark yellow, microcrystalline solid (0.08 g, 44%).

^{1}H NMR (300 MHz, $CDCl_3$, 25 °C) δ(ppm): 10.34 (s, 1H, N*H*), 8.41 (s, 1H, (N=C*H*)), 7.68 (d, 1H, *J* = 7.8 Hz, Ar-*H*), 7.34 (dd, 1H, *J* = 7.4 and 1.1 Hz, Ar-*H*), 7.24-7.15 (m, 4H, Ar-*H*/Ar), 3.08 (sept, 2H, *J* = 6.8 Hz, -C*H*$^{i\text{Pr}}$), 2.85-2.79 (m, 4H, C*H*$_2$), 2.02-1.86 (m, 4H, C*H*$_2$), 1.19 (d, 12H, *J* = 6.8 Hz, -C*H*$_3^{i\text{Pr}}$).

HRMS/ESI$^+$ *m/z*: [M+H] calculated 358.2409, found 359.2481; formula $C_{25}H_{31}N_2$.

IR $\tilde{\nu}$/cm^{-1} (ATR): 3401 (N*H*) s, 2957 s, 1626 (N=CH) s, 1607 s, 1575 s, 1461 s, 1438 s, 1326 w.

Chapter III. Group 1 Salts and Catalytic Dehydrogenation of Dimethylamine-borane

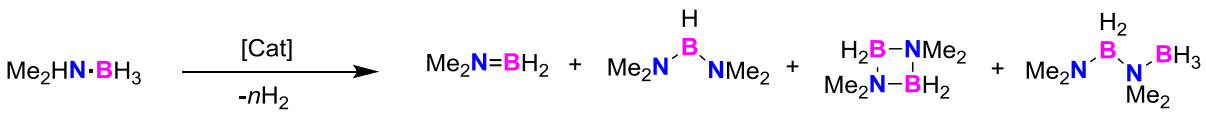
3.1 Introduction to Group 1 Chemistry

The chemistry of Group 1 containing compounds has been primarily used in stoichiometric reactions in the form of organic salts in which a proton has been replaced by a Group 1 metal. As such, alkali metal containing reagents such as lithium diisopropylamide (LDA) and *n*-butyllithium (^{n}BuLi) are commonly used in the selective abstraction of acidic protons[88–90] or as source of insoluble salts, in metathesis reactions, by anchoring the reaction towards the desired products with concomitant precipitation of a Group 1 halide.

In terms of the use of Group 1 metals in catalysis, the high natural abundance of the top three lighter congeners of the group and their relative stability, under the right conditions, makes them ideal candidates for catalytic studies. Despite this, Group 1 salts are still largely unexplored in catalytic processes. Recent examples in this area include the use of alkali metal amides, which have been used as catalysts for the cross-dehydrogenative coupling of hydrosilanes with amines[91] and the dehydrocoupling of boranes, amines and amine-borane adducts.[92,93]

3.2 Dehydrogenation of Amine-Boranes

Dehydrogenation/dehydrocoupling reactions, are those involving the formation of monomeric and polymeric element-element bonds, in which gaseous hydrogen is liberated as by-product (Scheme 3.2.1).[94] In the particular case of the aforementioned dehydrocoupling of ammonia borane ($H_3N{\cdot}BH_3$) and related amine-boranes, catalytic processes involving such molecules have gained considerable significance due their potential application as hydrogen storage materials,[95–98] hydrogen transfer reagents[99,100] and BN-based ceramics and polymers;[101–103] derived from its high weight percentage of hydrogen (19.6 wt %), and their potential use in the so-called "hydrogen economy".



Scheme 3.2.1 Dehydrogenation of dimethylamine-borane and some of the known products.

An important aspect of metal-catalysed dehydrogenation of amine-boranes, appears to be directly linked to the Lewis character of the metal employed. As such, these transformations have been explored through the use of s-block,[104–108] p-block,[109–113] precious metals,[114–117] rare earth,[118] and frustrated Lewis pair,[119] based catalysts. Further

exploring this, the use of Group 1 containing precatalysts has recently started to be explored, due to their high natural abundance and strongly Lewis acidic nature.[82,92,120,121]

3.3 Aims and Objectives

Continuing the study of low-coordinate metal centres, and as a first step, it is the main objective of this chapter to make use of the symmetric/asymmetric carbazole based proligands generated in the previous chapter (**5**-**6** and **9**-**10**). In order to access Group 1 derivatives, a variety of different methodologies including direct deprotonation with readily available starting materials, will be attempted.

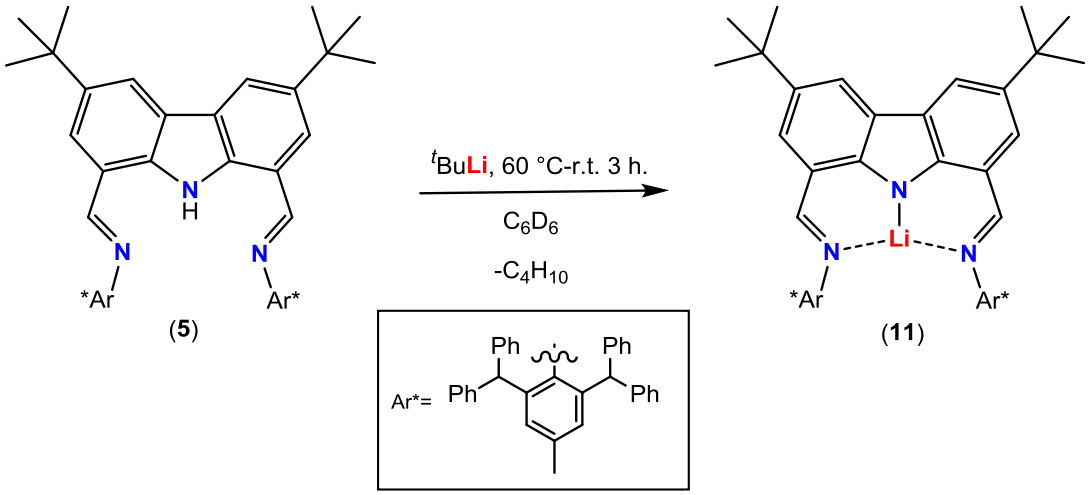
Secondly, and following thorough characterisation of the Group 1 compounds generated, it is desirable to carry out a study on their capability to work as precatalysts in the dehydrocoupling/dehydrogenation of amine-boranes and other suitable heterodehydrocoupling substrates.

3.4 Results and Discussion

3.4.1 Synthesis of Group 1 Salts

3.4.1.1 Synthesis of [Ar_2*carbLi]

The formation of Group 1 salts of the symmetric/asymmetric proligands **5**-**6** and **9**-**10**, was attempted, starting with **5**. In this case, the ligand was initially reacted with ^{n}BuLi at 0 °C. Upon warming to room temperature, the reaction mixture displayed a bright green colouration, similar to previous observations described by Gibson *et al*.[51,52] ^{1}H and ^{7}Li{^{1}H} NMR spectra of the crude mixture, however, showed no noticeable conversion of the product to the corresponding lithium salt. It was pressumed that the incredibly high steric hindrance of the ligand system might have limited the availability of the base to react with the carbazole. This was not surprising, considering the high steric bulk that the Ar* flanking groups provide around the central N*H*.



*Scheme 3.4.1 Attempted formation of the lithium salt **11**.*

As such, the reaction was repeated in an NMR tube using ^{t}BuLi as base and C_6D_6 as the solvent (Scheme 3.4.1 and Figure 3.4.1). By doing this, the progress of the reaction could be constantly monitored by NMR. Upon addition of the base, no significant indication of the formation of the lithium salt was observed. The NMR sample was subsequently warmed up in an oil bath to a temperature of 60 °C for one hour. After this, a ^{1}H NMR spectrum evidenced the presence of a new set of signals at lower field in a 1:1 ratio. Further heating of the NMR sample at 60°C afforded full conversion to a new product as noted by the ^{1}H, ^{13}C{^{1}H} and ^{7}Li{^{1}H} NMR spectra ([Ar$_2$*carbLi] **11**). Shortly after reaching completion and cooling down to room temperature, crystals suitable for X-ray diffraction were obtained.

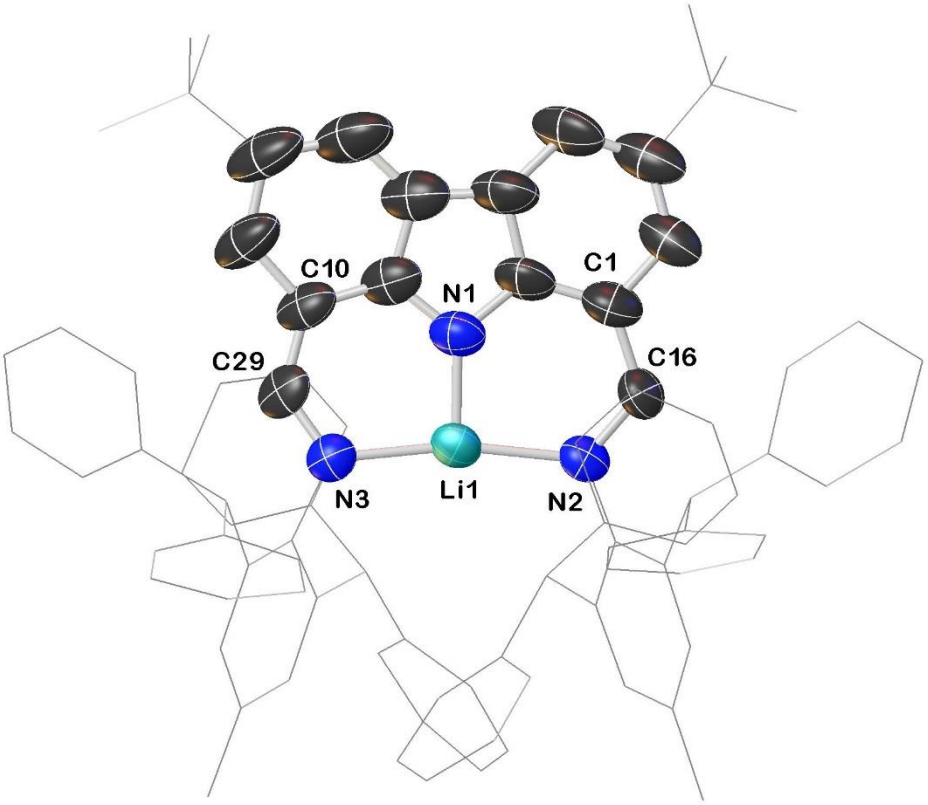


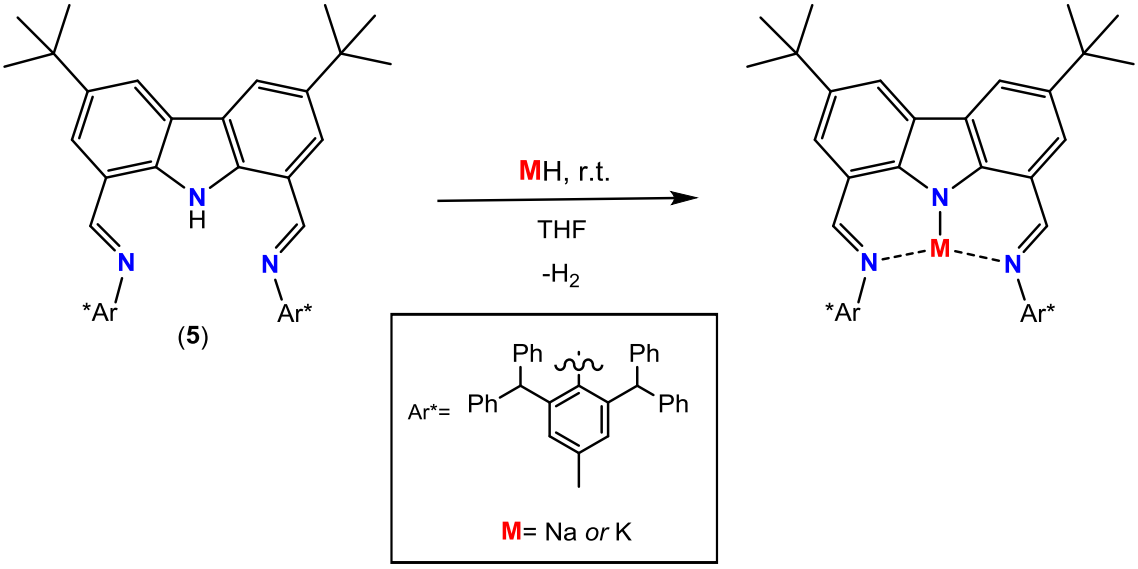
*Figure 3.4.1 Molecular formula for **11**, with displacement ellipsoids set at 50% probability level, hydrogen atoms have been omitted, with flanking –Ar* moieties in wireframe form for clarity.*

In the solid state, **11** is monomeric (Figure 3.4.1). The coordination sphere for Li1 is completed primarily by the bond with N1 [Li1–N1 = 1.75(2) Å] with additional coordination of the flanking iminic nitrogen atoms [N2 and N3]. The lithium atom Li1 is surrounded by the flanking phenyl groups locked in place, residing on the best mean plane generated by the carbazole backbone.

Bond Length (Å)		Bond Angle (°)	
Li1–N2	1.97(6)	N3–C29–C10	130(3)
Li1–N3	2.05(6)	N2–C16–C1	120(2)
N2–C16	1.32(3)		
N3–C29	1.35(3)		

*Table 3.4.1 Selected bond lengths and angles for **11**.*

Upon successful formation of the lithium salt **11**, further efforts to form the corresponding sodium and potassium salts were attempted (Scheme 3.4.2).



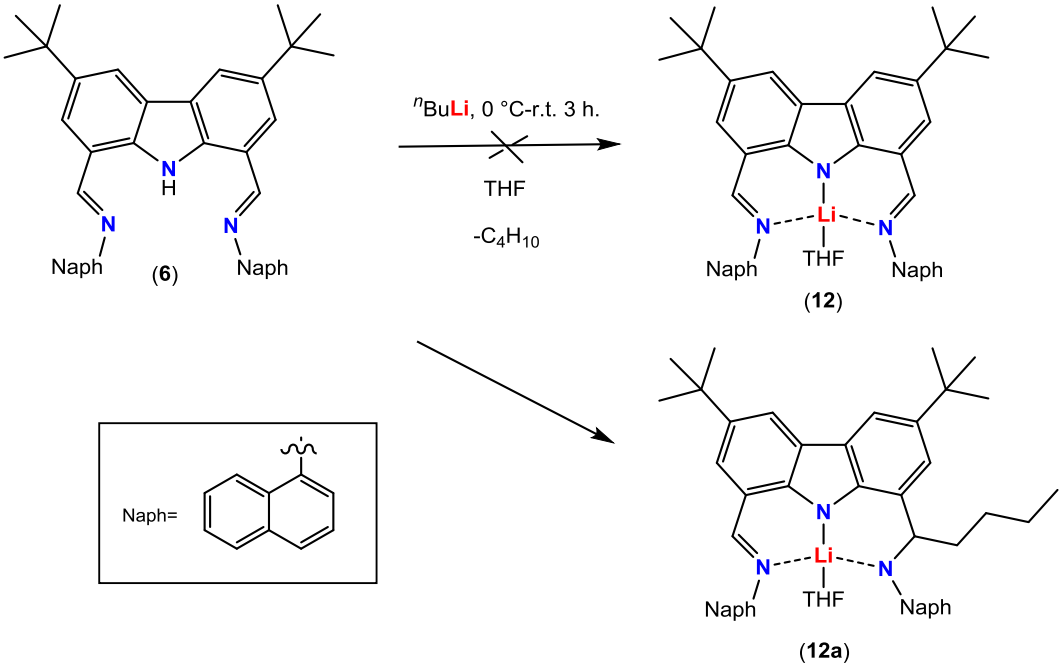
*Scheme 3.4.2 Attempted synthesis of the Na and K salts of **5**.*

Thus, **5** was reacted into two parallel methodologies, the first one using NaH and the second one using KH with THF as a solvent at room temperature. Similar to the formation of the lithium salt (**11**), a characteristic bright green colouration was observed. In the case of KH, the reaction was stopped after 24 hours. In contrast, the experiment where NaH was used was kept stirring at room temperature for additional 6 days. However, a ^{1}H NMR spectrum of the reaction mixture showed no evidence of the formation of the desired Group 1 salt, as noted by the presence of the N*H* signal at 12.99 ppm in these experiments. Both crude mixtures were individually extracted into hexane. However, only the presence of free ligand **5**, and decomposition products (Ar*NH$_2$) could be characterised (NMR

spectroscopy and X-ray diffraction measurements). It is hypothesised that although the reaction conditions were relatively mild, the presence of the NaH or KH facilitates the decomposition of the previously formed Schiff base **5**. The apparent instability of the Ar* flanking group, can be explained on the basis of its similarity to the triarylmethyl (trityl) radical[122] and the non-innocent character of *N*-based ligands containing this motif.[123,124]

3.4.1.2 Towards the Synthesis of [Naph$_2$carbLi]

Deprotonation of **6** at low temperature using ^{n}BuLi in THF afforded a bright orange solution upon reaching room temperature (Scheme 3.4.3). The ^{1}H, ^{7}Li{^{1}H} and ^{13}C{^{1}H} NMR spectra, confirmed full conversion of the starting material and a notable shifting towards low field indicative of an anionic species. Additionally, the presence of at least two equivalents of THF subsequent to drying the product under vacuum overnight, suggested metallation of the ligand system (^{1}H NMR).[82]



*Scheme 3.4.3 Formation of the alkylated lithium salt **12a**.*

Orange crystals suitable for X-ray diffraction analysis evidenced that although the ligand system was successfully deprotonated; the product had undergone alkylation of a flanking aldiminic group was obtained as well, exhibiting a butyl chain as substituent (**12a**).

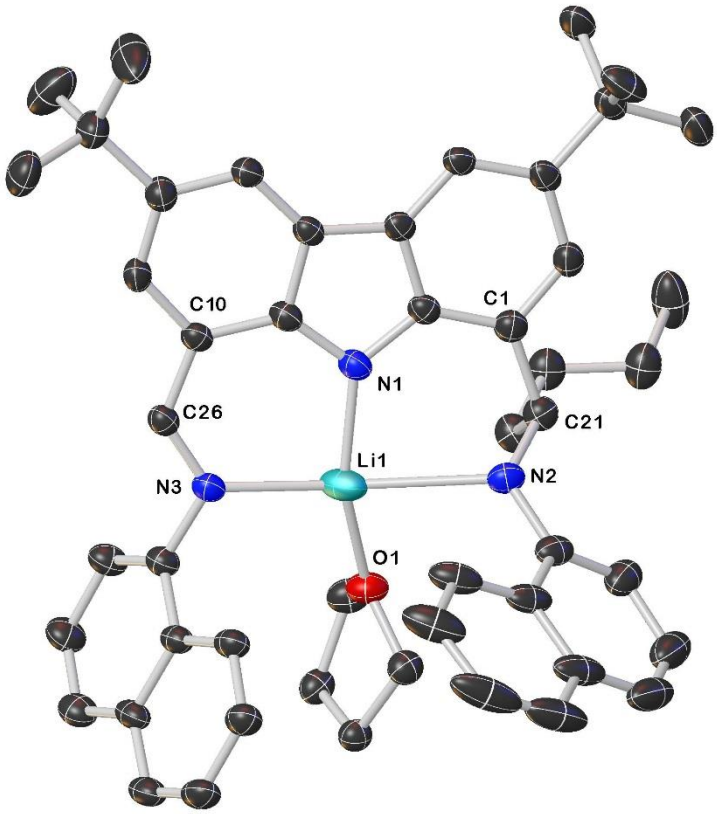


*Figure 3.4.2 Molecular structure of the alkylated lithium salt **12a**, with displacement ellipsoids set at 50% probability level, hydrogen atoms have been omitted for clarity.*

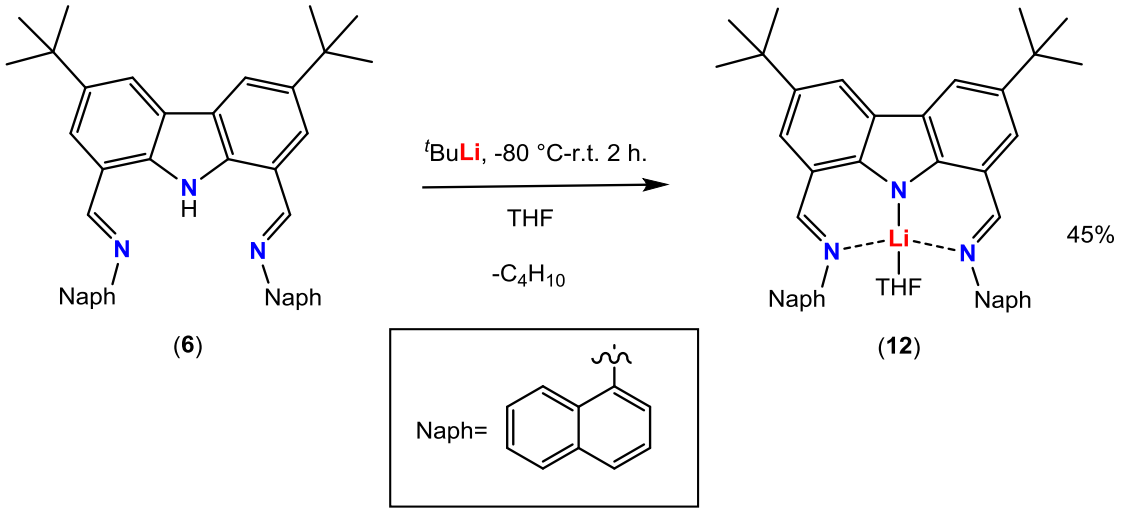
The solid state determination of **12a**, revealed a monomeric structure (Figure 3.4.2). Similar to **11**, the coordination sphere for Li1 is completed by the bond with the central carbazolido nitrogen, and the flanking iminic nitrogens N2 and N3 [Li1–N2 = 2.644(4) Å and Li1–N3 = 2.117(4) Å, respectively). The difference between these two distances, is consequence of the butyl chain substitution on N2, with a change in hybridisation in C21 (sp^2 to sp^3). This can clearly be seen in the bond lengths and angles, when comparing C21 [C21–N2 = 1.4895(19) Å, N2–C21–C1 = 108.10(12)°] and C26 (C26–N3 = 1.292(2) Å, N3–C26–C10 = 125.68(16)°]. Finally, the coordination sphere of Li1 is completed by one THF molecule.

	Bond Length (Å)		Bond Angle (°)
Li1–N1	1.933(3)	N3–Li1–N2	160.2(2)
Li1–N2	2.644(4)	N2–C21–C1	108.1(1)
Li1–N3	2.117(4)	N3–C26–C10	125.7(2)
Li1–O1	1.914(3)		
C26–N3	1.292(2)		
C21–N2	1.489(2)		

*Table 3.4.2 Selected bond lengths and angles for **12a**.*

3.4.1.3 Synthesis of [Naph$_2$carbLi(thf)]

It was determined that in order to avoid alkylation of the flanking aldiminic groups, a less nucleophilic base should be used (Scheme 3.4.4). As such, the reaction was repeated using ^{t}BuLi as deprotonating agent. By doing so at –80 °C, using similar conditions to those previously described, a bright orange powder, corresponding to the Group 1 salt [Naph$_2$carbLi(thf)] (**12**) could be obtained, in good yield.[82]



*Scheme 3.4.4 Formation of lithium salt **12.***

Crystals suitable for X-ray diffraction of **12**, were grown from a saturated hexane solution at room temperature.

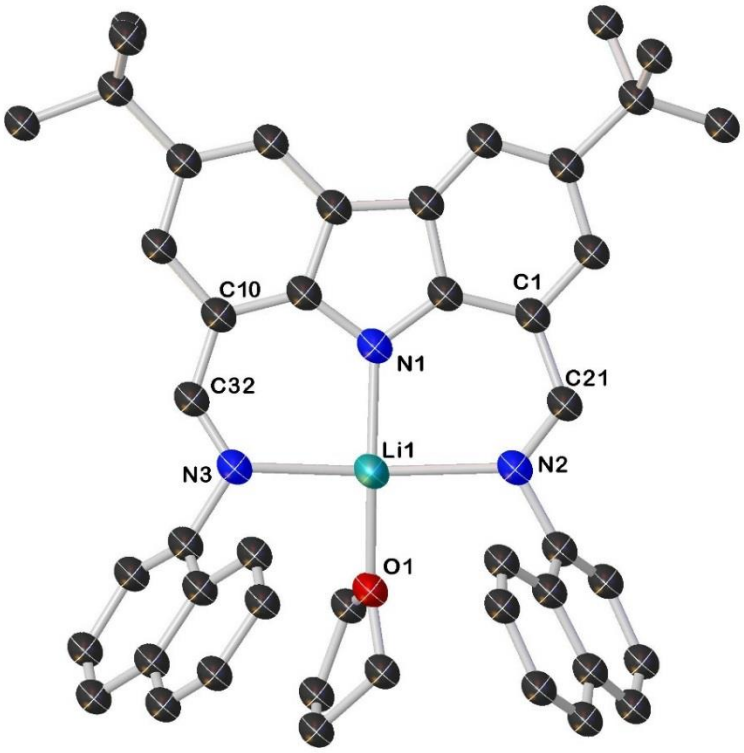


*Figure 3.4.3 Molecular structure for **12**, with displacement ellipsoids set at 50% probability level, hydrogen atoms have been omitted for clarity.*

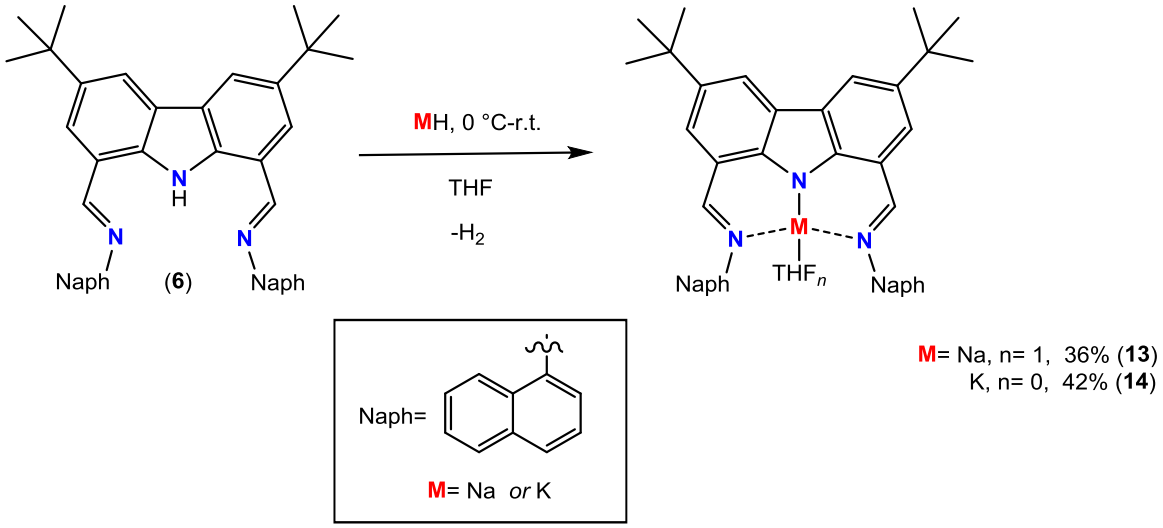
In the solid state, **12** is monomeric (Figure 3.4.3). Noticeably, no substitution of the flanking iminic groups is present. The coordination sphere of the lithium centre is completed by the tridentate carbazole and one molecule of THF, with the flanking naphthyl groups locked in position in a *syn* conformation. The distance L1–N1 in **12** [1.97(4) Å], is similar to the equivalent bonds found in **12a** and **11** [1.9333(3) Å and 1.97(6) Å, respectively].

Bond Length (Å)		Bond Angle (°)	
Li1–N1	1.97(4)	N3–Li1–N2	167(3)
Li1–N2	2.25(5)	C10–C32–N3	130(3)
Li1–N3	2.17(5)	C1–C21–N2	123(3)
Li1–O1	1.91(4)		
C32–N3	1.28(2)		
C21–N2	1.31(2)		

*Table 3.4.3 Selected bond lengths and angles for **12**.*

3.4.1.4 *Synthesis of [Naph$_2$carbNa(thf)] and [Naph$_2$carbK]$_2$*

In parallel, **6** was reacted with NaH and KH at low temperature, using THF as the solvent (Scheme 3.4.5). The reaction mixture afforded a bright orange-red solution upon reaching room temperature. As with the reaction with ^{t}BuLi, the NMR spectra showed full conversion to the corresponding Group 1 salts {[Naph$_2$carbNa(thf)] (**13**) and [Naph$_2$carbK]$_2$ (**14**)}. Following this procedure, moderate yields of isolated crystalline material could be obtained (**13**, 36%; **14**, 42%).[82]



*Scheme 3.4.5 Formation of Group 1 salts **13** and **14**.*

Similar to the lighter Group 1 metal salt **12**, crystals of **13** suitable for single crystal diffraction were grown from saturated hexane solutions, following extraction from the reaction vessel.

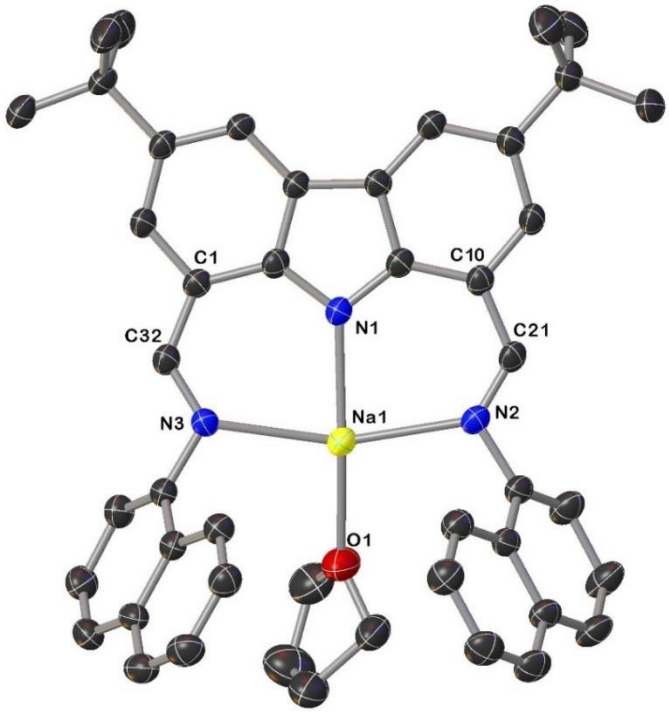


*Figure 3.4.4 Molecular structure for **13**, with displacement ellipsoids set at 50% probability level, hydrogen atoms have been omitted for clarity.*

Complex **13**, is monomeric in the solid state (Figure 3.4.4). Similar to **12**, the coordination sphere of the metal centre is filled by the tridentate ligand and finally by one molecule of THF, with the flanking naphthyl groups locked in position mirroring each other.[82] The distances Na1–N1 [2.287(3) Å], Na1–N2 [2.398(3) Å] and Na1–N3 [2.408(3) Å] observed in the determination of **13**, are very similar to the equivalent bond lengths found in the sodium salt of 1,8-(4′,4′-dimethyloxazolin-2′-yl)-3,6-^{t}Bu-carbazole [Na1–N1 = 2.278(2) Å, Na1-N2 = 2.414(2) Å and Na1-N3 = 2.407(2) Å].[125]

Bond Length (Å)		Bond Angle (°)	
Na1–N1	2.287(3)	N1–Na1–O1	164.2(2)
Na1–N2	2.398(3)	N3–Na1–N2	158.09(1)
Na1–N3	2.408(3)	N2–C21–C10	126.7(3)
C21–N2	1.275(4)	N3–C32–C1	126.0(3)
C32–N3	1.296(4)		
Na1–O1	2.294(3)		

*Table 3.4.4 Selected bond lengths and angles for **13**.*

In comparison, **14** adopts a bimetallic, dimeric structure in the solid state, in which half of the molecule lies in the asymmetric unit (Figure 3.4.5 and Figure 3.4.6). Additionally to the coordination of the metal to the tridentate ligand, the higher hapticity of the ligand-metal binding is supported by an η^6 interaction between the potassium and an additional carbazolyl arene ring (K1–C23$_{plane}$ = 2.986(4) Å). Finally, the coordination sphere of the metal is completed by an η^3 interaction (K1–C12 = 3.476(10) Å and K1–C20 = 3.455(9) Å), with a flanking naphthyl moiety (Figure 3.4.6).[82] Although, this is a coordination motif that has been previously reported, there are few structurally authenticated examples of a potassium cation bound to a carbazole ring in an η^6 conformation.[48] Normally, structures depicting such binding mode are part of a heterobimetallic structure.[126,127] Multi-hapto binding motifs are also found in the potassium complexes [(1,8-Xyl$_2$-3,6-^{t}Bu$_2$carb)K(thf)],[48] (η^6, Xyl = 2,6-Me$_2$C$_6$H$_3$) and [(1,8-Ph$_2$-3,6-Me$_2$carb)K][128] (η^2).

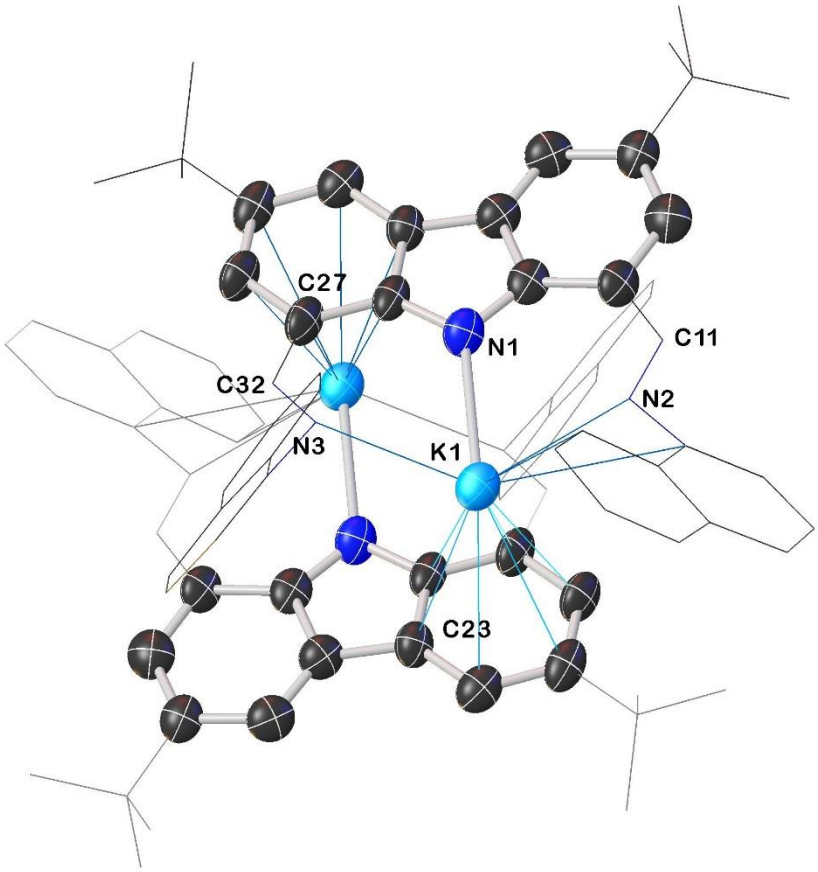


*Figure 3.4.5 Molecular structure of the symmetric unit of **14** (left) and asymmetric unit (right), with displacement ellipsoids set at 50% probability level, hydrogen atoms have been omitted, with flanking substituents presented on wireframe from for clarity.*

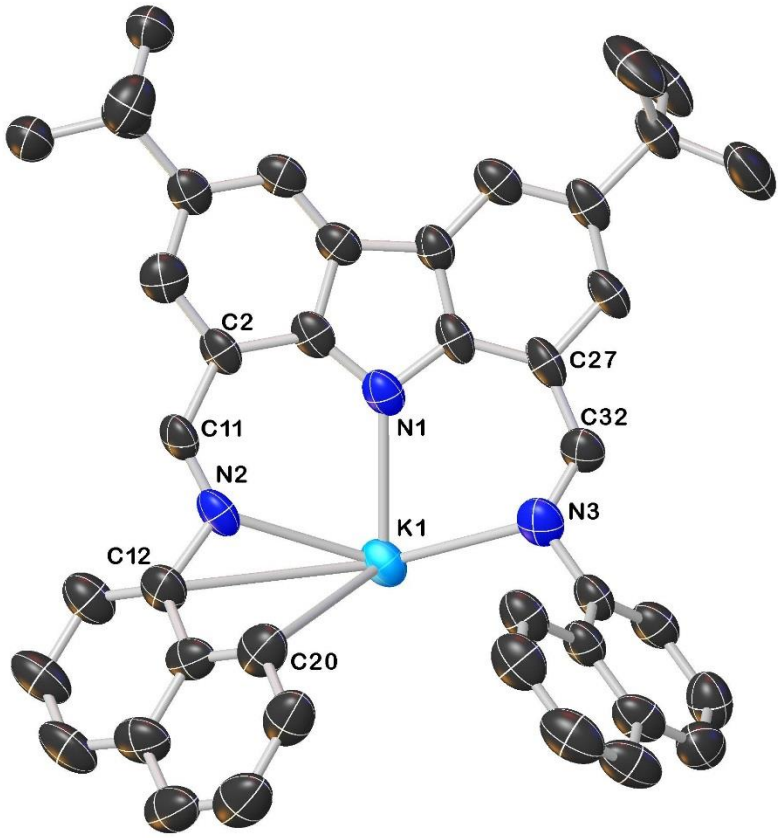


*Figure 3.4.6 Molecular structure of **14**, showing one of the sub-units (asymmetric unit) with additional interactions to the naphthyl ring, with displacement ellipsoids set at 50% probability level, hydrogen atoms have been omitted for clarity.*

Bond Length (Å)		Bond Angle (°)	
K1–N1	2.680(8)	N3–K1–N2	158.09(12)
K1–N2	2.747(8)	N2–C11–C2	127.1(8)
K1–N3	2.762(9)	N3–C32–C27	127.1(9)

*Table 3.4.5 Selected bond lengths and angles for **14**.*

Compounds **12**-**14** are readily soluble in solvents such as toluene and benzene, and ^{1}H NMR spectroscopic measurements, including DOSY NMR experiments, indicate only one species in solution. The increase in ionic radii can be followed using the most distal protons on the naphthyl substituents in **12**-**14** in the ^{1}H NMR spectrum (Figure 3.4.7). Asymmetry is also observed in the aforementioned resonances (*H*6'–*H*8' of the naphthyl group) for **14**, and suggests a greater degree of interaction between the metal centre and one of the

flanking groups; following the increasing alkali metal ionic radius favouring the adoption of a higher hapticity binding motif.[129] This has been found to be true in cases in which the flanking groups are bulky and have little to no possibility of accommodating the metal centre, where the classical σ-bond conformation gets replaced by a multi-hapto π-bonded mode.[48,130,131]

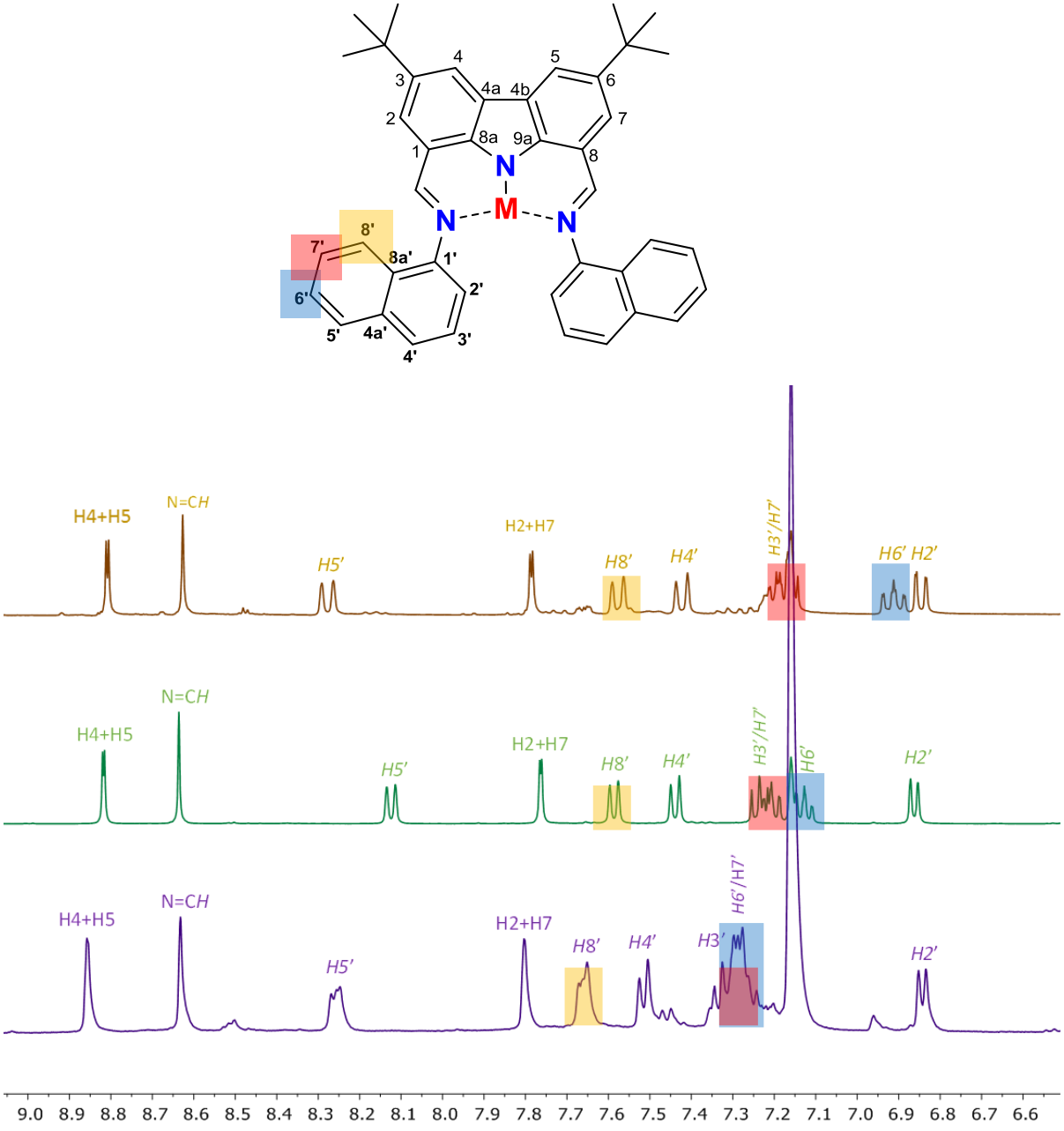
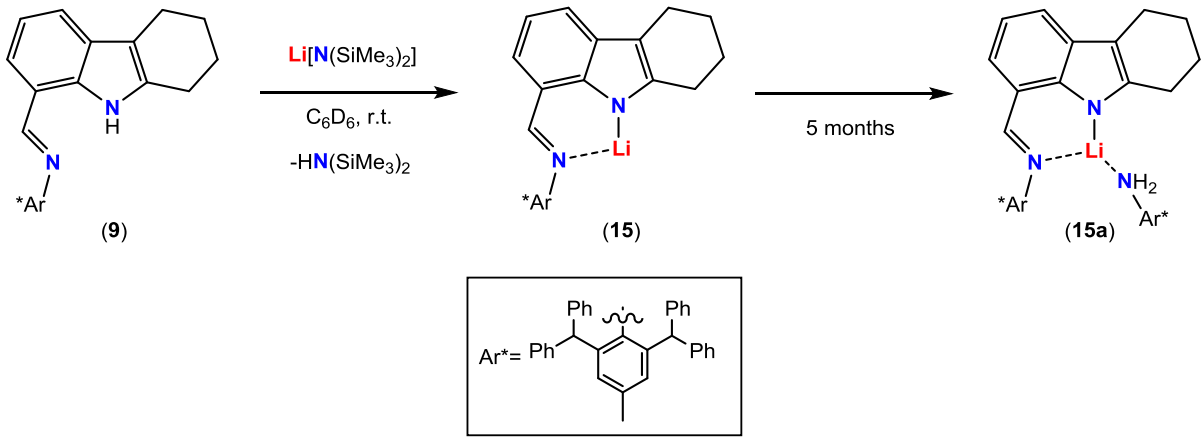


*Figure 3.4.7 Selected region of the ^{1}H NMR spectra of complex **12** (yellow), **13** (green) and **14** (purple) in C_6D_6.*

3.4.1.5 Synthesis of [Ar*THCarbLi]

Continuing with the formation of the Group 1 salts of the asymmetric ligand, [Ar*THCarbH] (**9**). It was decided to approach this synthesis by means of a transamination/deprotonation methodology. As such, the free ligand was reacted with one equivalent of Li[N(SiMe$_3$)$_2$] in C_6D_6 (Scheme 3.4.6). Upon addition of the base, the yellow solution containing the ligand turned bright orange, not dissimilar from the behaviour observed upon formation of the symmetric Group 1 salts **12**-**14**. ^{1}H and ^{13}C{^{1}H} NMR spectra of the resulting compound showed confirmation of full conversion to a new species. While a ^{7}Li{^{1}H} NMR spectrum exhibited only a sole resonance peak at -0.75 ppm ([Ar*THCarbLi] **15**). Several crystallisation attempts for said compound were pursued, only managing to procure a sample of sufficient quality several months after synthesis. From the solid state determination it was possible to observe formation of the intended lithium salt. However, the apparent long-term instability of the Ar* group observed in the synthesis of the sodium and potassium salts of **5**, is also evident here (*vide supra*); as additional coordination to the metal centre is observed in the form of Ar*-NH$_2$. It is suspected that the presence of an excess of the base employed for deprotonation is responsible of the eventual decomposition of **9**/**15** to form **15a**.[122]



*Scheme 3.4.6 Synthesis of **15** and further decomposition to form **15a**.*

Crystals suitable for single crystal diffraction of **15a**, were grown from a C_6D_6 concentrated solution, with hexane vapour diffusion.

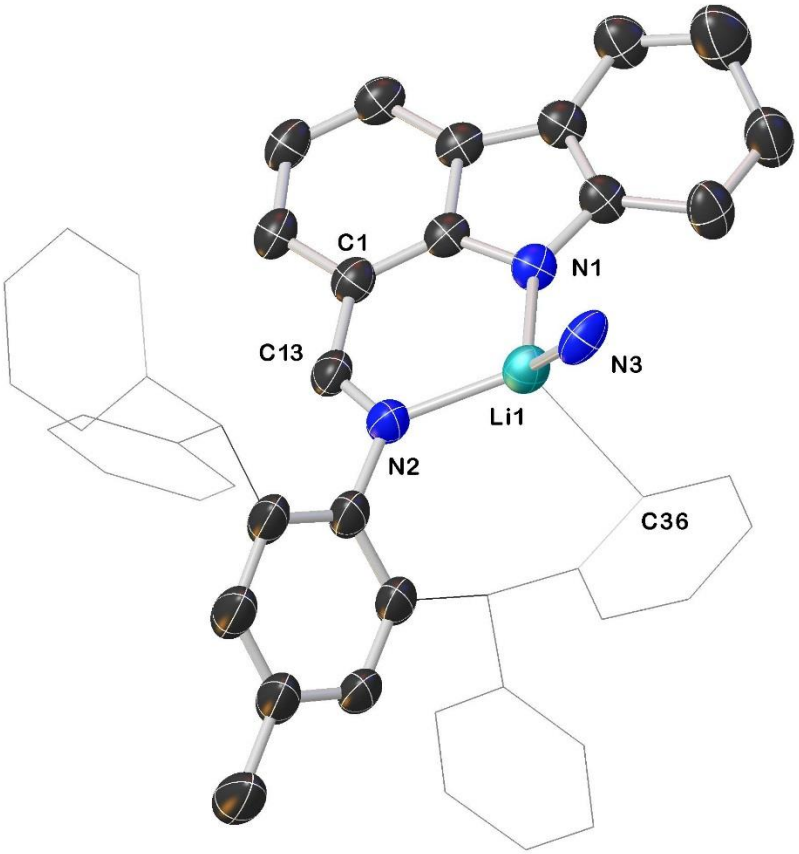


*Figure 3.4.8 Molecular structure for **15a**, with displacement ellipsoids set at 50% probability level. The –Ar* substituent attached to N3 and the hydrogen atoms have been omitted, with the –$CHPh_2$ substituents presented in wireframe form for clarity.*

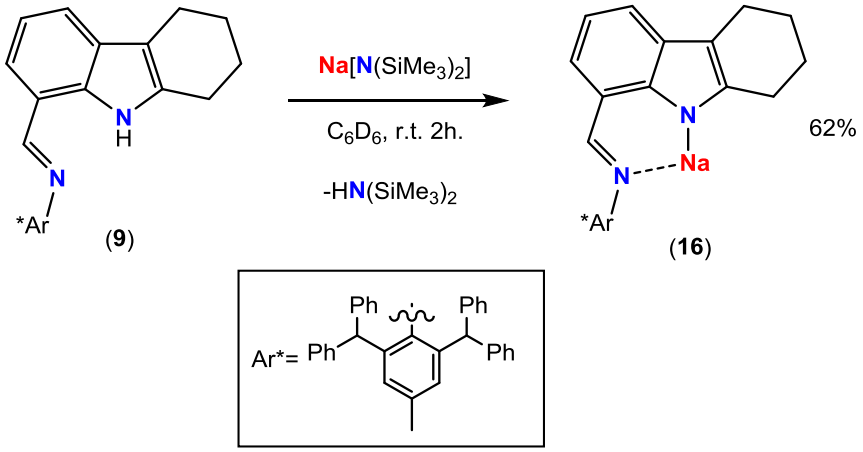
The solid state determination of **15a**, revealed a monomeric structure (Figure 3.4.8). As observed by ^{1}H NMR characterisation, deprotonation of the central carbazolido ring was achieved forming a bidentate chelate in which Li1 is coordinated to both N1 and N2. Additionally, an η^1-interaction with an adjacent flanking phenyl group is also observed [Li1–C36= 2.534(5) Å].

	Bond Length (Å)		Bond Angle (°)
Li1–N1	1.943(6)	N3–Li1–N2	125.5(3)
Li1–N2	2.052(7)	N1–Li1–N2	99.3(3)
Li1–N3	2.116(7)		
C13–N2	1.292(4)		

*Table 3.4.6 Selected bond lengths and angles for **15a**.*

3.4.1.6 Synthesis of [Ar*THCarbNa]

Following an analogous procedure, formation of the sodium salt was carried out, employing $Na[N(SiMe_3)_2]$ as deprotonating agent (Scheme 3.4.7). Similar changes in colouration upon deprotonation to that of **15** were observed. A ^1H NMR spectrum of the resulting reaction mixture evidenced almost full disappearance of the starting material after 1 hour at room temperature ([Ar*THCarbNa] **16**). It is worth noting the comparatively lower solubility of this compound in C_6D_6. This is similar to the behaviour previously noted in the characterisation of the Group 1 salts **12**-**14**, in which the increase in ionic radii of the Group 1 metal, drastically reduces the solubility of said salt.[82] Despite this, full conversion to **16** could be achieved, shortly followed by isolation of the resulting bright orange-red crystals of the title compound in good yield.



*Scheme 3.4.7 Synthesis of **16**.*

Crystals of **16** suitable for single crystal diffraction, were grown from a C_6D_6 concentrated solution, with hexane vapour diffusion.

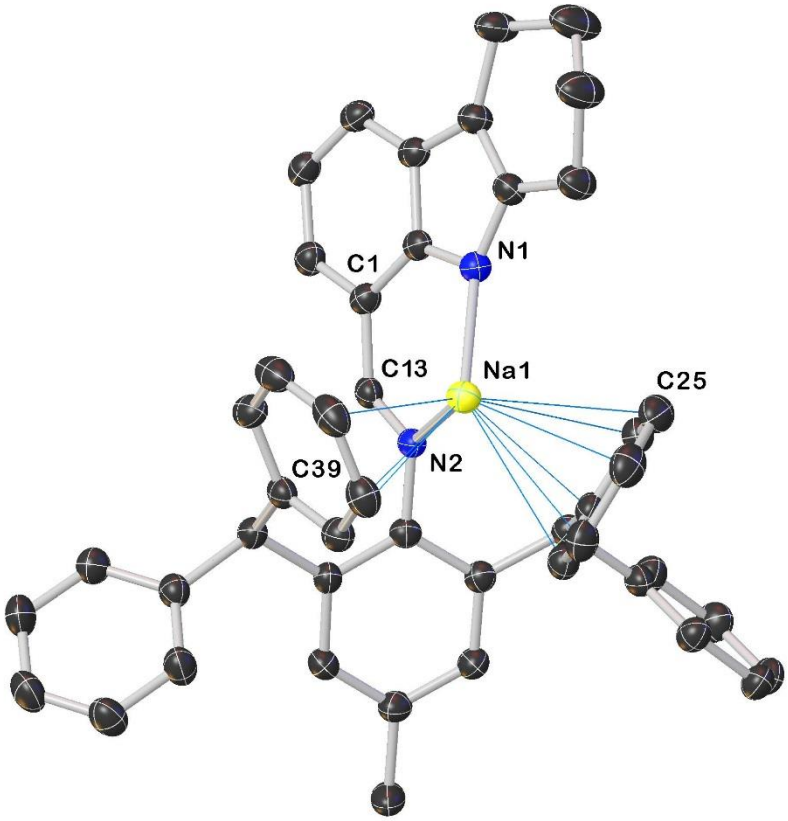


*Figure 3.4.9 Molecular structure for **16**, with displacement ellipsoids set at 50% probability level, hydrogen atoms have been omitted for clarity.*

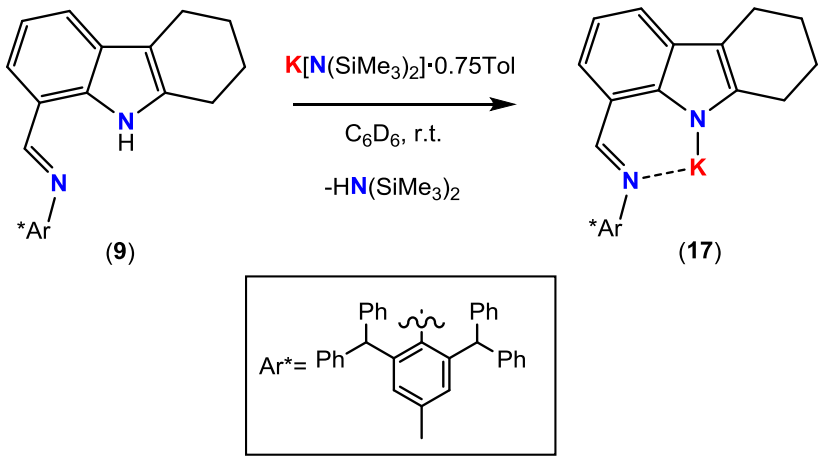
In the solid state, **16** is monomeric, with only one molecule occupying the asymmetric unit (Figure 3.4.9). The coordination sphere around the metal centre is supported by the bidentate asymmetric ligand, taking two coordination sites. Similar to the lithium analogue **15**, additional interactions with the adjacent flanking aryl rings [Na1–$C25_{plane}$ (η^6) = 2.6574(11) Å, Na1–$C39_{plane}$ (η^3) = 2.745(2) Å], from the Ar*-N=C moiety, are also observed. In line with similar multi-hapto π-bonded systems previously mentioned,[48,130,131] the sodium atom, does not lie directly in line with the best mean plane generated by the bidentate ligand, but slightly above it [Na1–$N1_{plane}$ = 0.791(3) Å].

Bond Length (Å)		Bond Angle (°)	
Na1–N1	2.287(3)	N1–Na1–N2	83.29(7)
Na1–N2	2.398(3)	N2–C13–C1	127.0(2)
Na1–C25$_{plane}$	2.6574(2)		
Na1–C39	2.8097(14)		
C13–N2	1.286(3)		

*Table 3.4.7 Selected bond lengths and angles for **16**.*

3.4.1.7 Synthesis of [Ar*THCarbK]

Finally, the synthesis of the potassium salt of **9** was attempted. In line with the lighter Group 1 analogues, the ligand was reacted with K[N(SiMe$_3$)$_2$] (Scheme 3.4.8). By doing so, an instant change in colouration was observed, yielding a red solution ([Ar*THCarbK] **17**); which shortly after became heterogeneous and subsequently, a red solid. Due to the lack of solubility, NMR spectroscopic characterisation was limited, even when to the isolated material was added ca. 2mL of THF. The insoluble nature of the potassium salt formed, is most likely a consequence of the rapid formation of polymeric chains, with several examples that include [KN(Ph)Me]$_\infty$, [{(thf)KN(Ph)^{i}Pr}$_5$]$_\infty$, [{(thf)KN(Ph)^{i}Pr}$_2$·2KN(Ph)^{i}Pr], and [(dme)$_{0.25}$KN-(Ph)^{i}Pr]$_\infty$ (dme = 1,2-dimethoxyethane).[59,132,133]



*Scheme 3.4.8 Attempted synthesis of **17**.*

Further work aiming towards the characterisation and crystallographic elucidation of this compound is still on-going. It is expected that using a polar solvent, such as THF or diethyl ether or stoichiometric additives such as TMEDA, during the synthesis, might limit the formation of polymeric aggregates. Increasing the solubility of the resulting solvated salt, an essential feature required for full NMR characterisation.

Despite these limitations in solubility, comparison of the three asymmetric Group 1 salts synthesised (**15**-**17**) by ^{1}H NMR was carried out. From which it was possible to observe a similar behaviour to the one found in the ^{1}H NMR spectra of the symmetric, naphthyl substituted, Group 1 salts **11**-**14**; this is particularly evident in the signal characteristic for the imino group (*H*C=N-Ar*), in which an increment in the size of the metal, subjects the ligand to a consistent change in chemical shift towards low-field (Figure 3.4.10). Suggesting increasing deshielding of the ligand as a consequence of a greater interaction between the metal and the bidentate ligand system.

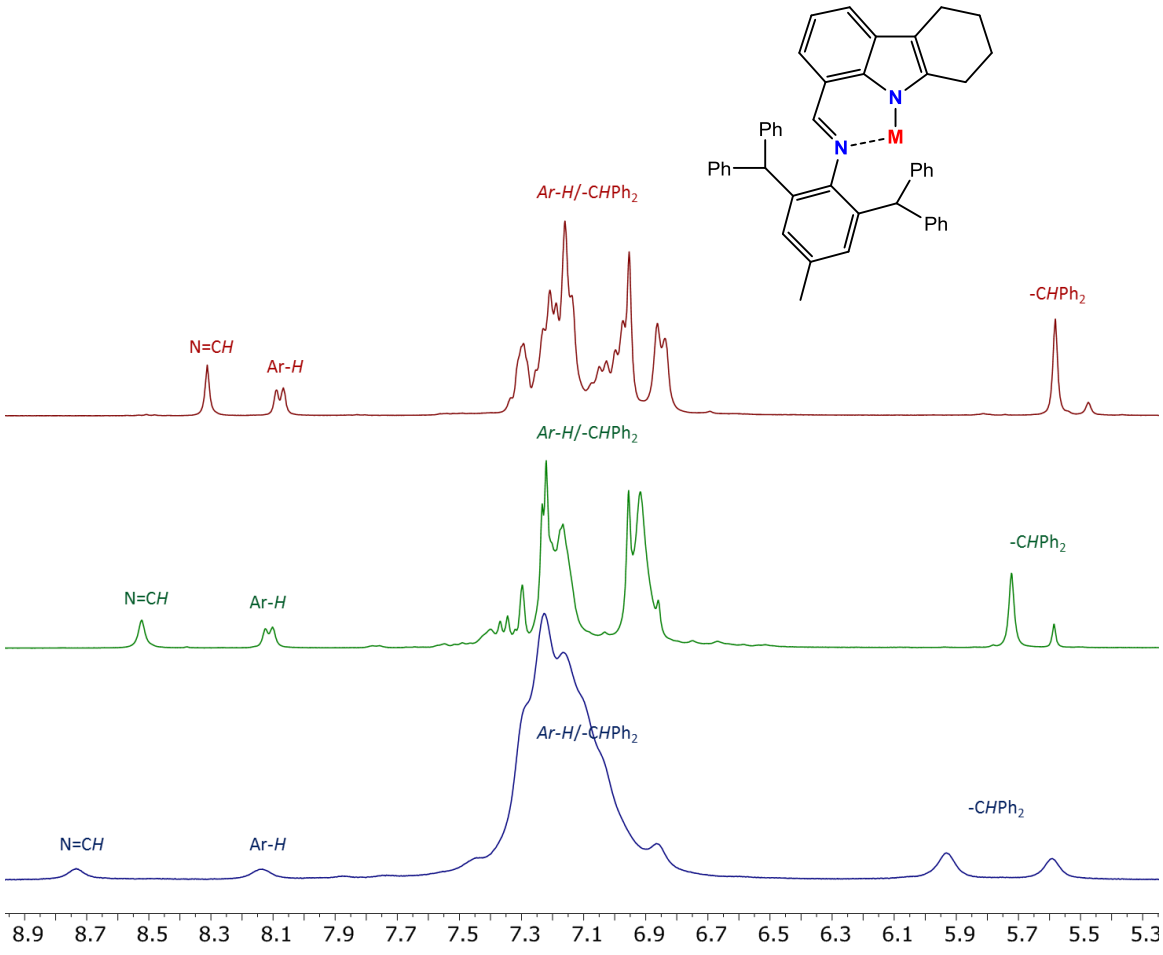


*Figure 3.4.10 Selected region of the ^{1}H NMR spectra of **15** (red), **16** (green) and **17** (blue) in C_6D_6.*

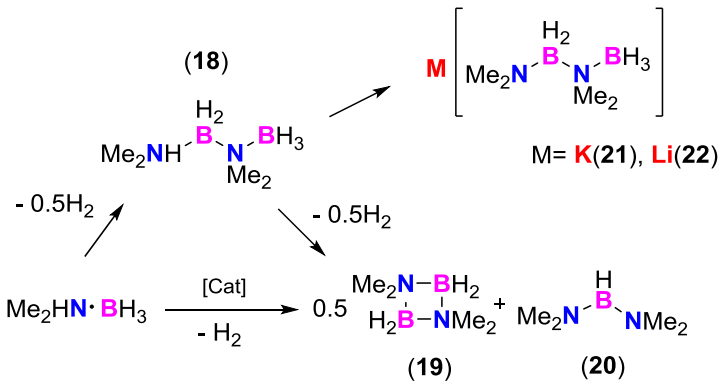
3.4.2 Group 1 Salts and Catalytic Dehydrogenation of Dimethylamine-borane

Having structurally authenticated a number of Group 1 salts, efforts were focused on the use of these compounds, in reactions with amine-borane derivatives.

The catalytic dehydrocoupling/dehydrogenation of ammonia borane ($H_3N{\cdot}BH_3$) and related amine-boranes is the subject of increasing research interest[94,134] due to the use of these processes in applications such as hydrogen storage,[95–98] hydrogen transfer reagents[99,100] and BN-based ceramics and polymers.[101–103] While it is possible to effect thermal release of hydrogen from ammonia borane or amine-boranes using high temperatures, the electronegativity difference between nitrogen and boron also permits the release of hydrogen mediated by a catalyst (Scheme 3.4.9). Although there are a number of main group stoichiometric or catalytic dehydrogenation reactions using complexes featuring the Group 2[104–107] or p-block[109–113] elements, precatalysts based on Group 1 complexes remain largely unexplored in this,[120,135] or other related catalysis.[92,136] The high natural abundance of the three lightest congeners of the Group (Li, Na, K) and their lack of participation in Schlenk-type equilibria,[135] makes them ideal candidates for use as well defined precatalysts for dehydrogenation reactions.

However, an issue with the use of Group 1 precatalysts for amine-borane dehydrogenation has been recently highlighted by the groups of Hill and Mulvey, where the active catalysts can form insoluble metal hydride aggregates which in turn can hinder catalytic processes.[120,135] Pincer ligands are attractive for the design of robust and effective catalysts, as they provide increased thermal stability through tridentate coordination and rigid steric protection, preventing aggregation at the metal centre whilst allowing the approach of small molecules for reaction.[137]

Taking this in consideration and following full spectroscopic and crystallographic authentication of the Group 1 salts **12**-**14**, a study of their reactivity towards amino-borane adducts, was attempted.



*Scheme 3.4.9 Dehydrogenation of $Me_2NH{\cdot}BH_3$ using **12-14**.*

An initial assessment of the catalytic activity for dehydrogenation of $Me_2NH{\cdot}BH_3$ (Figure 3.4.11) was tested *via* the reaction of the amine-borane in C_6D_6 or THF with 5 mol% of **12** at room temperature, revealing only minor formation of dehydrogenation products and $LiBH_4$ (entries 2 and 3, Table 3.4.8).

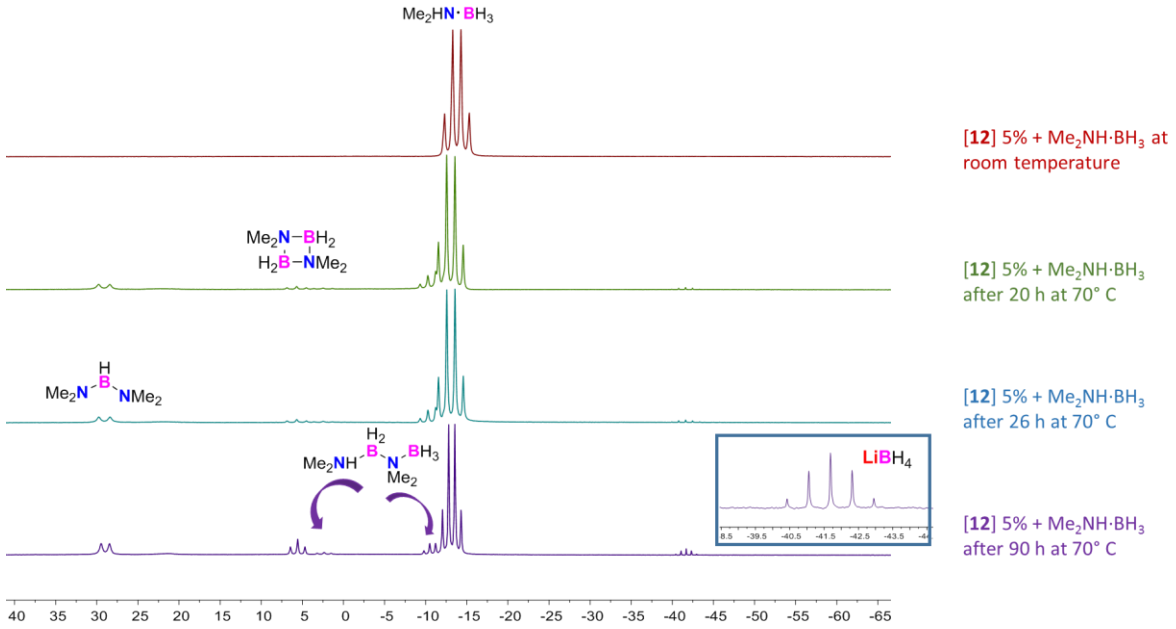


*Figure 3.4.11 Monitoring by ^{11}B NMR spectroscopy of the reaction between complex **12** (5 mol%) and $Me_2NH{\cdot}BH_3$ in C_6D_6.*

Under stoichiometric conditions, no initial conversion at room temperature of $Me_2NH{\cdot}BH_3$ was observed, and heating at 70 °C for 67 hours in C_6D_6 afforded diaminoborane **20** (62%) as the main product, oligomers/polymers (20%) and the salt $Li[NMe_2BH_2NMe_2BH_3]$ (**22**)(4%). Noticeably, a $^{7}Li\{^{1}H\}$ NMR spectrum of the resulting reaction mixture exhibited only one resonance at 0.66 ppm, upfield from the original 3.33 ppm found in **12**, suggesting a transformation in the lithium species during the reaction. When the sodium complex **13** was used as precatalyst in C_6D_6 at 70 °C, a colour change from bright orange to colourless was observed and the ^{11}B NMR spectrum showed the formation of dehydrogenation products; with a conversion of 53% after 1.5 hours (entry 5, Table 3.4.8).

*Table 3.4.8 Dehydrogenation of $Me_2NH{\cdot}BH_3$ with **12-14**.*[a)]

Entry	Catalyst (mol%)	Solvent	T (°C)	t (h)	Conversion (%)[b)]	Product Ratio[c)] **18**/**19**/**20**
1	**-**	C_6D_6	70	24	0	-
2	**12** (5)	C_6D_6	70	17	9	<1/6/2[d)]
3	**12** (5)	THF	70	20	7	1/1/5[d)]
4	**12** (5)	Pyridine	70	18	99	1/1/97
5	**13** (5)	C_6D_6	70	1.5	53	3/36/14
6	**13** (10)	C_6D_6	70	1	72	4/47/21
7	**13** (5)	THF	70	4	6	<1/<1/5
8	**13** (5)	Pyridine	70	1.5	23	3/1/19
9	**13** (5)	Pyridine	70	18	98	3/0/95
10	**14** (5)	C_6D_6	70	24	24	1/12/11
11	**14** (5)	THF	70	4	4	<1/1/2[e)]
12	**14** (5)	Pyridine	70	18	99	<1/2/98
13	**-**	Pyridine	70	18	9[f)]	-

[a)] Reaction conditions: 5.8 mg, 8.48 $x10^{-3}$ mmol of **12**-**14**, 0.6 mL of solvent. Samples were heated in an oil bath, progress was monitored by NMR spectroscopy. [b)] Determined by ^{11}B NMR spectroscopy. [c)] Ratio by ^{11}B NMR spectroscopy. [d)] Small amounts of $LiBH_4$ (<1%) were detected. [e)] Selective formation of **21**. [f)] Formation of $Py{\cdot}BH_3$.[92]

Increasing the precatalyst loading to 10 mol% led to higher conversions, 72% after 1 h (entry 6, Table 3.4.8). When using THF as a solvent almost no reaction was observed, which further supports an initial exchange/coordination mechanism involving THF and $Me_2NH{\cdot}BH_3$ (entry 7, Table 3.4.8). To further understand this, the stoichiometric reaction between **13** and $Me_2NH{\cdot}BH_3$ was performed; after 20 hours at 70 °C most of the amine-borane had decomposed to the diaminoborane $[HB(NMe_2)_2]$(**20**) (63%). The formation of a small amounts of $NaBH_4$ were detected at early stages and during the catalytic process. It has been reported that sodium containing salts such as $Na[H_3B{-}NMe_2{-}BH_3]$, decompose in THF solution[138,139] forming $NaBH_4$ and the cyclic borazane $[Me_2NBH_2]_2$ (**19**). No change was observed by ^{11}B NMR spectroscopy when monitoring the reaction between **13** and $Me_2NH{\cdot}BH_3$ at room temperature, but the ^1H NMR spectrum displayed a difference in chemical shift from **13**, mainly on the pendant flanking groups, which is probably a consequence of the $Me_2NH{\cdot}BH_3$ exchanging with the THF on the metal centre.

Similar behaviour was observed when the non-active substrate $Me_3N{\cdot}BH_3$ was employed (Figure 3.4.12).

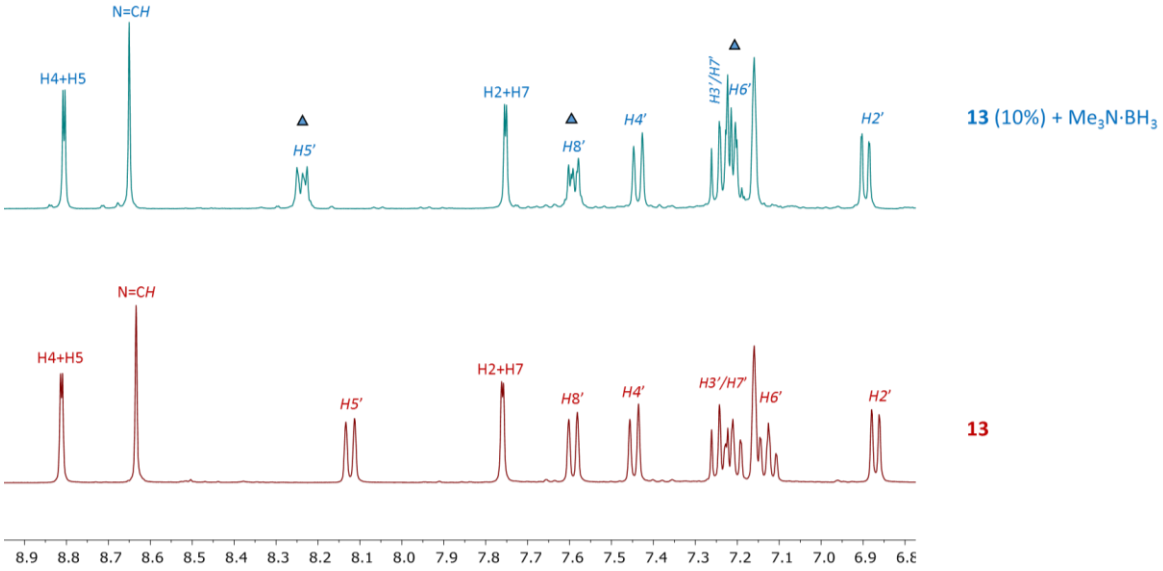


*Figure 3.4.12 Monitoring by ^1H NMR spectroscopy of the reaction between complex **13** (10 mol%) and $Me_3N{\cdot}BH_3$ in C_6D_6.*

When the potassium salt **14** (5 mol%) was employed as the precatalyst in C_6D_6 solution, modest conversions were obtained (entry 10, Table 3.4.8). Changing the solvent to THF (using 5 mol% of **14**) at 70 °C yielded limited conversion, with the potassium salt **21** as the main product (entry 11, Table 3.4.8). To further understand the lower catalytic activity of the potassium species, stoichiometric reactions at room temperature were carried out in C_6D_6 (2 : 1 ratio of $Me_2NH{\cdot}BH_3$: **14**); small conversions of $Me_2NH{\cdot}BH_3$ and to the linear dimer $Me_2NH{-}BH_2{-}NMe_2{-}BH_3$ (**18**) were observed (2%). After an additional 90 hours, only low conversion of the starting material was observed (*ca*. 23%). From this reaction, crystals suitable for X-ray diffraction were grown from hexane vapour diffusion yielding $K[BH_3NMe_2BH_3]$ (**21a**), most likely obtained from the thermal decomposition of **21** (Figure 3.4.13).[138] When analogous stoichiometric reactions were performed in THF, even at room temperature, full conversion of $Me_2NH{\cdot}BH_3$ was observed, yielding **20** (10%) and $[NMe_2BH_2NMe_2BH_3]$(**21**) (90%).[120] This suggest that the limited reactivity of **14** in THF is most likely a consequence of the stability of **21**.

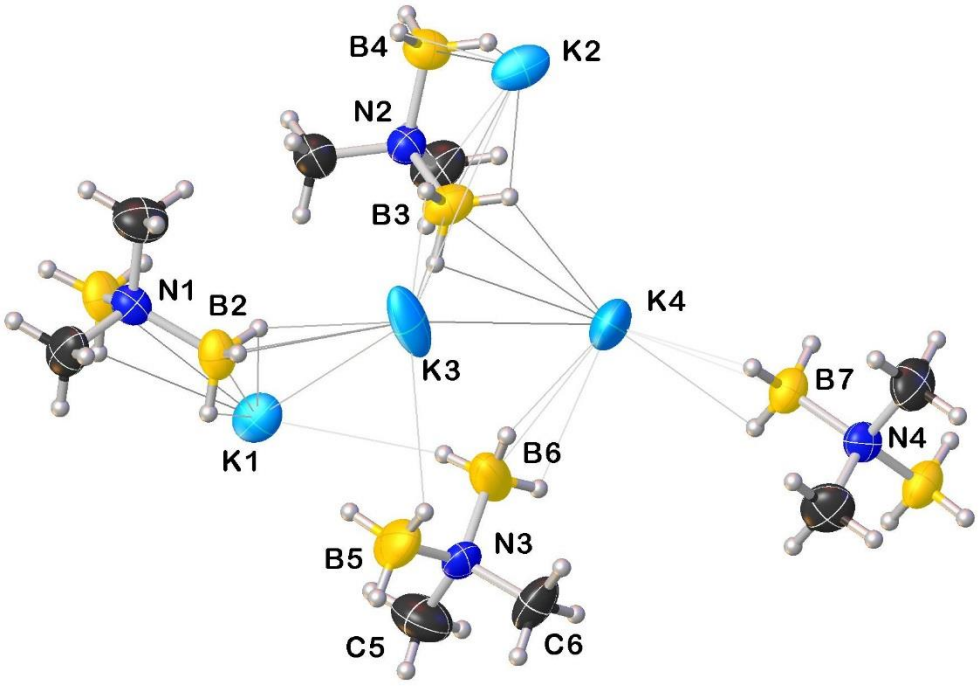


*Figure 3.4.13 Molecular structures of **21a**, with displacement ellipsoids set at the 50% probability level.*

Bond Length (Å)		Bond Angle (°)	
C6–N3	1.4668(8)	C5–N3–C6	107.79(9)
N3–N5	1.547(10)	C6–N3–B6	109.0(8)
N3–B6	1.569(10)	B5–N3–B6	112.2(10)
N3–C5	1.495(10)	C6–N3–B5	109.4(10)

*Table 3.4.9 Selected bond lengths and angles for **21a**.*

3.4.2.1 Reaction Monitoring; Open system and NMR Monitoring

Furthermore, performing the reaction in an open system set-up, with **13** as the precatalyst, allowed the monitoring of the liberation of H_2 occurring in parallel to the formation of the dehydrogenation products. The liberation of H_2 observed through this method was consistent with the conversion observed by ^{11}B NMR spectrum (Figure 3.4.14) and the reaction was scaled up successfully to use 100 mg of $Me_2NH{\cdot}BH_3$, where very similar ratios of products were formed in analogous reaction times.

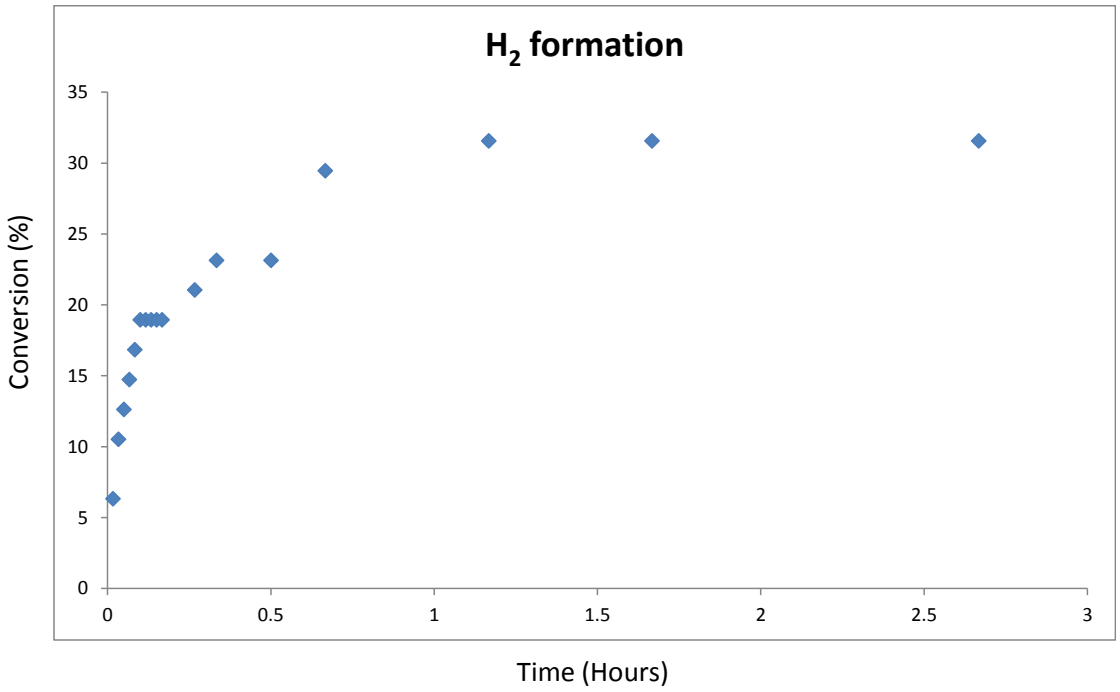


Figure 3.4.14 Graph representing the formation of H_2 in an open system.

3.4.2.2 Solvent Dependence

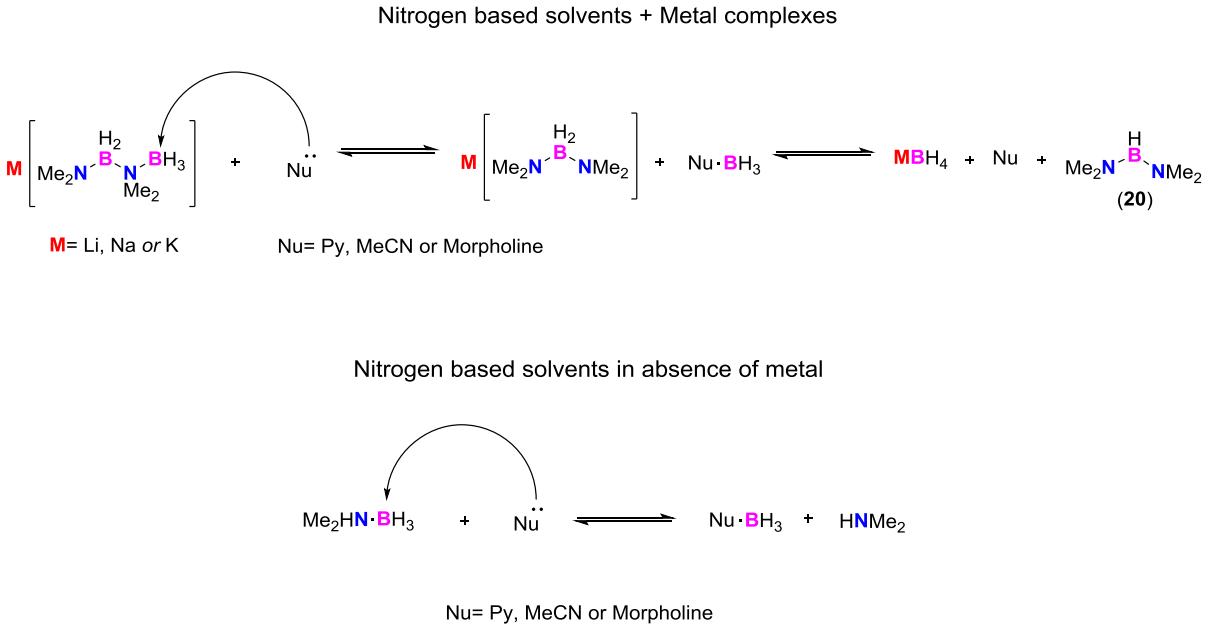
Performing the catalysis in pyridine with 5 mol% of **12**–**14** at 70 °C for 18 hours, allowed selective formation of **20** (entries 4, 9 and 12, Table 3.4.8). While a reaction in absence of pre-catalysts confirms that formation of diaminoborane **20** does not occur, only formation of $Py{\cdot}BH_3$ was observed (entry 13, Table 3.4.8).[140] Previous reports highlight the use of polar solvents to promote or limit the interconversion of some of the dehydrogenation products.[141,142] This observation, together with the previous results in pyridine, encouraged a detailed study while varying the solvent, with the aim of investigating the effects of polarity and nucleophilicity on the catalysis (Table 3.4.10).

*Table 3.4.10 Comparative study in different solvents, employing **13** as catalyst.*

Entry	Catalyst (mol%)	Solvent	T (°C)	t (h)	Conv. (%)[b]	Product Ratio[c] **18**/**19**/**20**
1	**13** (5)	C_6D_6	70	1.5	53	3/36/14
2	**13** (5)	THF	70	4	6	<1/<1/5
3	**13** (5)	Pyridine	70	18	98	3/0/95
4	**13** (5)	MeCN	70	18	13	0/0/4/9[d]
5	**13** (5)	Morpholine	70	18	-[e]	-[e]
6	**13** (5)	$F_3CC_6H_5$	70	18	17	3/9/5

[a] Reaction conditions: 5.8 mg, 8.48 x10^{-3} mmol of **13**, 0.6 mL of solvent. Samples were heated in an oil bath, progress was monitored by NMR spectroscopy. [b] Determined by ^{11}B NMR spectroscopy. [c] Ratio by ^{11}B NMR spectroscopy. [d] MeCN·BH_3 ratio. [e] Could not be integrated due to overlapping peaks.

Experiments employing MeCN and morpholine as solvents showed formation of the corresponding borane adducts (MeCN·BH_3/morpholine·BH_3, respectively) and **20** (entries 4 and 5, Table 3.4.10) [Scheme 3.4.10].[140] While additionally giving some insight into the metal catalysed mechanism, involving initial formation of [Me_2N-BH_2-NMe_2-BH_3]/[Me_2N-BH_2-NMe_2] salts, to the corresponding metal borohydride and **20**.



*Scheme 3.4.10 Proposed mechanistic pathway for the formation of borane adducts and **20**.*

Increasing the polarity of the solvent from C_6D_6 to $F_3CC_6H_5$ led to a decrease in reaction rate (entries 1 and 6, Table 3.4.10). Selective and quantitative formation of **20** was only achieved in pyridine which may be due to the nucleophilicity of the pyridine together with the thermal instability of $Py{\cdot}BH_3$ which drives the reaction to **20** (Figure 3.4.15), similar to that reported by Mulvey *et al*.[140,143]

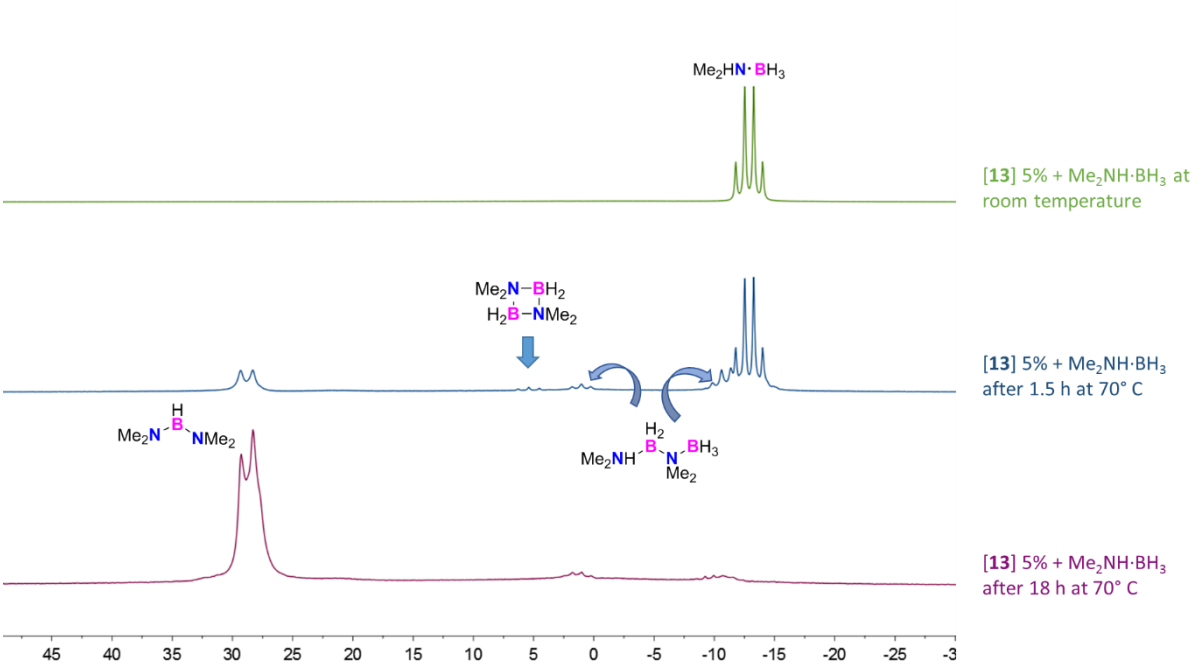


*Figure 3.4.15 Monitoring by ^{11}B NMR spectroscopy of the reaction between complex **13** (5 mol%) and and $Me_3N{\cdot}BH_3$ in pyridine.*

3.4.2.3 Reactivity with H_2

It has been postulated that the diminished conversion of the $Me_2NH{\cdot}BH_3$ in dehydrogenation reactions occurs due to concomitant formation of insoluble hydrides.[121] With this in mind, a solution of **13** in C_6D_6 was exposed to H_2, and a slow but certain decomposition of the precatalyst to the parent carbazole **6** was observed (Figure 3.4.16). It seems that upon initial coordination at room temperature and further activation by increase in the temperature, the initial products of dehydrogenation, and more importantly the affiliated liberation of H_2, readily converts the Group 1 metal complex into a neutral-ligand/soluble-hydride complex, forming a neutral chelate-adduct which can react further. Similar mechanisms have been reported for transition-metal[144,145] and actinide complexes,[146] in which a hydride-substituted metal is the catalytic species. Although these experiments have shown the potential for the associated H_2 to reduce **13** back to the parent proligand, such decomposition has not been observed under the reaction conditions employed during catalysis. Additionally, and looking to understand the nature of the catalytic species at latter stages in the process, it was envisioned that the higher degree of asymmetry observed in the ^1H NMR spectra is a consequence of the presence of high number of amine-borane salts as by-products of the reactions. Such salts could work as nucleophiles towards the flanking imines, as shown with the substitution of a butyl chain to form **12a** (Figure 3.4.2). Also, some of the by-products of dehydrogenation are known to reduce unsaturated groups such as imines.[139,147,148]

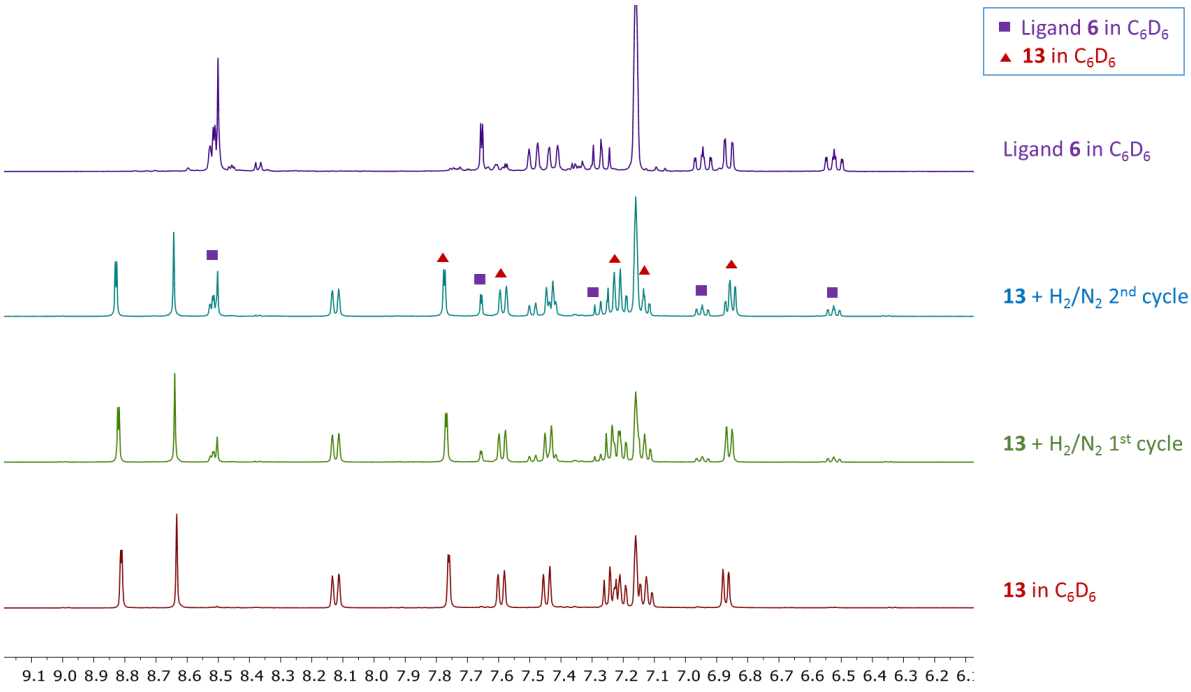


*Figure 3.4.16 Monitoring by ^1H NMR spectroscopy of the reaction between complex **13** and $H_2(g)$ in C_6D_6.*

3.4.2.4 DOSY NMR Spectroscopic Studies

The coordination between alkali metals and $Me_2NH{\cdot}BH_3$ and/or their dehydrogenation products is well documented and typically relies on hydrogen bond-stabilised interactions with the highly polarised $-NR_2–BH_3$ moieties.[120,138,149] Having taken this in consideration and looking to get better insight on the nature of the catalytic process DOSY NMR experiments were carried out, suggesting that **13** is monomeric in solution (Table 3.4.11). Additional experiments evidenced only small changes in the diffusion coefficient during the catalytic process, ruling out the formation of aggregates or dimers in solution.

Table 3.4.11 Diffusion coefficients obtained from DOSY NMR (21 °C).

Substrate	Diffusion Coefficient (m^2/s)	Hydrodynamic Radius (m)
13	$5.34x10^{-10}$	$5.49x10^{-10}$
13 + $Me_2NH{\cdot}BH_3$ at room temperature[a)]	$5.45x10^{-10}$	$5.38x10^{-10}$
13 + $Me_2NH{\cdot}BH_3$ after heating at 70 °C for 0.5 hour[a)]	$6.28x10^{-10}$	$4.67x10^{-10}$
13 + $Me_2NH{\cdot}BH_3$ after heating at 70 °C for 0.5 hour[b)]	$5.89x10^{-10}$	$4.98x10^{-10}$

[a)] Ratio **13**:$Me_2NH{\cdot}BH_3$ 1:1, Concentration [0.017M]; [b)] Ratio **13**:$Me_2NH{\cdot}BH_3$ 1:20, Concentration [0.014M]

3.5 Conclusions

The formation of Group 1 salts *via* organoelimination reactions has allowed the synthesis and characterisation of the incredibly hindered lithium salt **11**. In parallel, a new family of symmetric naphthyl substituted carbazoles, has proved sufficiently shielding to allow the synthesis and stabilisation of the first three Group 1 metals [lithium (**12**), sodium (**13**) and potassium (**14**)] of the group.

Similarly, the asymmetric 1,8-bisimino(Ar*)-substituted ligand **9**, has been successfully deprotonated employing a transamination mechanism. Following this methodology, three Group 1 metal salts [lithium (**15**), sodium (**16**) and potassium (**17**)], have been synthesised and structurally authenticated.

NMR characterisation of these salts (**12**-**14** and **15**-**17**), has allowed determination of similar electronic environments upon salt formation, with the ability to show a change in chemical shift as a direct consequence of the size of the metal employed.

Full characterisation of the Group 1 salts featuring an iminonaphthyl carbazolido *NNN*-pincer ligand (**12**-**14**) facilitated a study in which said salts work as precatalysts in the dehydrogenation of $Me_2NH{\cdot}BH_3$, where the cation and solvent employed plays a vital role in the outcome of the reaction and the products observed. The reactivity of the three Group 1 salts tested follows a pattern consistent with their relative positions among their group. As such, **12** is relatively unreactive, **14** readily reacts with $Me_2NH{\cdot}BH_3$ forming very stable salts that do not participate in the catalytic cycle, while **13** exhibits an intermediate behaviour. The observed reactivity differs from previous work reported in the literature for Group 1 bis(trimethylsilyl)amides; this trend in reactivity seems to be directly linked to the size of the cation (the smaller/more polarisable, the more reactive), with sodium (**13**) demonstrating the optimum reactivity for this catalysis.

3.6 Experimental Section

3.6.1 Synthesis and Characterisation

1,8-di(Ar*)imino-3,6-di(*tert*-butyl)-9-lithium-carbazole (**11**):

[Ar_2*carbLi]

A mixture of **5** (40 mg, 0.03 mmol) and ^{t}BuLi (6 mg, 0.09 mmol, 3 eq) were dissolved in C_6D_6 (1 mL) and the reaction monitored by NMR spectroscopy. No initial reaction was observed (^{1}H NMR spectroscopy). After further heating of the reaction mixture at 60 °C in an oil bath for 3 hours, full conversion of the starting material was observed. Crystals of **11** suitable for X-ray diffraction were grown at room temperature, from a concentrated solution in C_6D_6.

^{1}H NMR (300 MHz, C_6D_6, 25 °C) δ (ppm): 8.61 (s, 2H, (N=C*H*)), 7.56 (s, 4H, Ar), 7.09-6.68 (m, 40H, Ph), 5.94 (s, 4H, -C*H*Ph$_2$), 5.68 (s, 4H, -C*H*Ph$_2$) 2.06 (s, 6H, ArC*H*$_3$), 1.43 (s, 18H, C(C*H*$_3$)$_3$).

^{7}Li{^{1}H} NMR (117 MHz, C_6D_6, 25 °C) δ (ppm): 4.86, 1.58, 0.06, -1.21, -2.14, -2.65, -2.77 (m).

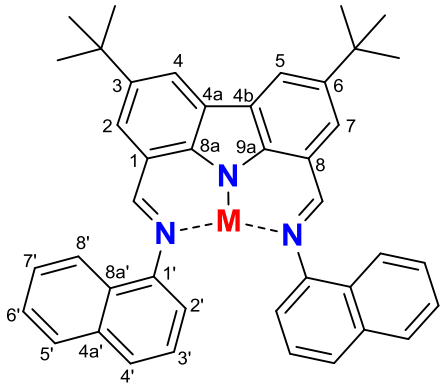


Figure 3.6.1 Numbering scheme for [Naph$_2$carb]$^-$ based Group 1 salts.

1,8-dinaphthylimino-3,6-di(*tert*-butyl)-9-lithium-carbazole(THF) (**12**):[82]

[Naph$_2$carbLi(thf)]

To a mixture of **6** (150 mg, 0.25 mmol) and ^{t}BuLi (17 mg, 0.25 mmol) at –78 °C, THF (30 mL) was slowly added, affording a bright orange mixture. The resulting solution was allowed to warm slowly to room temperature and left stirring at this temperature for an

additional hour. Volatiles were removed under vacuum affording a bright orange solid (75 mg, 45%). Crystals of **12** suitable for X-ray diffraction were grown from a concentrated hexane solution at room temperature.

^{1}H NMR (300 MHz, C_6D_6, 25 °C) δ (ppm): 8.81 (d, 1.9H, *J* = 1.5 Hz, H4 + H5), 8.63 (s, 2H, (N=C*H*)), 8.28 (d, 2H, *J* = 8.4 Hz, Naph *H*5'), 7.78 (d, 2H, *J* = 1.9 Hz, H2 + H7), 7.58 (d, 2H, *J* = 8.2 Hz, Naph *H*8'), 7.42 (d, 2H, *J* = 8.3 Hz, Naph *H*4'), 7.23-7.18 (m, 4H, Naph *H*3' and *H*7'), 6.91 (ddd, 2H, *J* = 8.2, 6.9 and 1.2 Hz, Naph *H*6'), 6.85 (dd, 2H, *J* = 7.2 and 1 Hz, Naph *H*2'), 1.60 (s, 18H, C(CH_3)$_3$).

^{7}Li{^{1}H} NMR (117 MHz, C_6D_6/C_4D_8O, 25 °C) δ (ppm): 3.02, 2.31 (s).

^{13}C{^{1}H} NMR (100 MHz, C_6D_6, 25 °C) δ (ppm): 167.81 (N=*C*H), 152.27 (N-*C*1'), 151.04 (C3 + C6), 138.26 (C8a + C9a), 134.77 (C4a + C4b), 129.65 (C2 + C7), 129.17 (quatern-Naph *C*8a'), 128.27 (quatern-Naph *C*4a'), 127.92 (Naph *C*8'), 127.0 (Naph *C*6'), 126.71 (Naph *C*3'), 126.41 (Naph *C*7'), 123.46 (Naph *C*4'), 122.78 (Naph *C*5'), 120.76 (C4 + C5), 120.35 (C1 + C8), 115.94 (Naph *C*2'), 35.19 (*C*(CH$_3$)$_3$), 32.92 (C(*C*H$_3$)$_3$).

HRMS/EI *m/z*: [M-C_4H_8O]$^{+}$ calculated 590.3211, found 590.3215; formula $C_{42}H_{38}N_3Li$.

IR *v*/cm^{-1} (Nujol): 2930 s, 2726 s, 1629 w, 1594 w, 1462 s, 1304 w.

UV/vis (THF, c = 1.0 x 10^{-5} mol dm^{-3}): λ_{max}/nm (ε x10^4 / dm^{3}mol^{-1}cm^{-1}) 396 (2.48).

1,8-dinaphthylimino-3,6-di(*tert*-butyl)-9-sodium-carbazole(THF) (**13**):[82]

[Naph$_2$carbNa(thf)]

To a mixture of **6** (200 mg, 0.34 mmol) and NaH (16.4 mg, 0.68 mmol, 2 eq.) in a Schlenk flask at 0 °C, THF (30 mL) was slowly added. The resulting suspension was stirred at 0 °C for 30 min. After this time, the vessel was allowed to reach room temperature and stirred for 16 hours. The resulting dark red suspension was filtered to remove unreacted NaH and the volatiles were removed under vacuum yielding an orange powder (82 mg, 36%). Crystals suitable of **13** suitable for X-ray diffraction were grown from a concentrated hexane solution at room temperature.

^{1}H NMR (400 MHz, C_6D_6, 25 °C) δ (ppm): 8.82 (d, 2H, *J* = 1.9 Hz, H4 + H5), 8.64 (s, 2H, (N=C*H*)), 8.12 (d, 2H, *J* = 8.3 Hz, Naph *H*5'), 7.76 (d, 2H, *J* = 1.9 Hz, H2 + H7), 7.59 (d, 2H, *J* = 8.1 Hz, Naph *H*8'), 7.44 (d, 2H, *J* = 8.3 Hz, Naph *H*4') 7.24 (t, 2H, *J*= 7.51 Hz, Naph *H*3'), 7.21 (ddd, 2H, *J* = 14.87, 8.17 and 1.09 Hz, Naph *H*7'), 7.13 (ddd, 2H, *J* =

15.17, 8.05 and 1.13 Hz, Naph *H*6'), 6.86 (d, 2H, *J* = 6.7 Hz, Naph *H*2'), 1.60 (s, 18H, C(C*H*$_3$)$_3$).

^{13}C{^{1}H} NMR (100 MHz, C_6D_6, 25 °C) δ (ppm): 169.09 (N=*C*H), 152.17 (N-*C*1'), 151.46 (C3 + C6), 137.0 (C8a + C9a), 134.36 (quatern-Naph *C*8a'), 131.48 (C2 + C7), 129.02 (quatern-Naph *C*4a'), 128.42 (Naph *C*8'), 127.94 (C4a + C4b), 126.80 (Naph *C*6'), 126.60 (Naph *C*3'), 126.49 (Naph *C*7'), 124.84 (Naph *C*4'), 122.78 (Naph *C*5'), 121.98 (C4 + C5), 120.74 (C1 + C8), 115.27 (Naph *C*2'), 34.69 (*C*(CH$_3$)$_3$), 32.52 (C(*C*H$_3$)$_3$).

HRMS/EI *m/z*: [M-C$_4$H$_8$O]$^+$ calculated 607.2958, found 607.2955; formula $C_{42}H_{38}N_3Na$.

IR *v*/cm^{-1} (Nujol): 3052 w, 2922 s, 2853 s, 2726 w, 1625 s, 1599 s, 1561 s.

UV/vis (THF, c = 1.0 x 10^{-5} mol dm^{-3}): λ_{max}/nm (ε x10^4 / dm^{3}mol^{-1}cm^{-1}) 395 (7.63).

1,8-dinaphthylimino-3,6-di(*tert*-butyl)-9-potassium-carbazole (**14**):[82]

[Naph$_2$carbK]$_2$

To a mixture of **6** (200 mg, 0.34 mmol) and KH (27 mg, 0.68 mmol, 2 eq.) in a Schlenk flask at 0 °C, THF (30 mL) was slowly added. The resulting suspension was warmed slowly to room temperature and left stirring for additional 3 hours. The resulting dark red suspension was filtered to remove unreacted hydride, and volatiles were removed under vacuum yielding the product as a dark orange-red powder (110 mg, 42%). Crystals of **14** suitable for X-ray diffraction were grown from a concentrated hexane solution at room temperature.

^{1}H NMR (400 MHz, C_6D_6, 25 °C) δ (ppm): 8.86 (d, 2H, *J* = 1.07 Hz, H4 + H5), 8.63 (s, 2H, (N=C*H*)), 8.27-8.25 (m, 2H, Naph *H*5'), 7.80 (d, 2H, *J* = 1.1 Hz, H2 + H7), 7.67-7.65 (m, 2H, Naph *H*8'), 7.52 (d, 2H, *J* = 8.2 Hz, Naph *H*4'), 7.33 (d, 2H, *J* = 7.4 Hz, Naph *H*3'), 7.30-7.28 (m, 4H, Naph *H*6' + *H*7'), 6.84 (d, 2H, *J* = 7.1 Hz, Naph *H*2'), 1.60 (s, 18H, C(C*H*$_3$)$_3$).

^{13}C{^{1}H} NMR (100 MHz, C_6D_6, 25 °C) δ (ppm): 168.28 (N=*C*H), 152.30 (N-*C*1'), 152.20 (C3 + C6), 136.38 (C8a + C9a), 134.66 (quatern-Naph *C*8a'), 132.14 (C2+C7), 128.32 (Naph *C*8'), 128.83 (quatern-Naph *C*4a'), 127.39 (C4a+ C4b), 126.88 (Naph *C*3'), 126.85 (Naph *C*6'), 126.78 (Naph *C*7'), 124.74 (Naph *C*4'), 123.55 (Naph *C*5'), 121.71 (C4 + C5), 121.51 (C1 + C8), 114.67 (Naph *C*2'), 34.63 (*C*(CH$_3$)$_3$), 32.55 (C(*C*H$_3$)$_3$).

HRMS/ASAP *m/z*: [M+H]$^+$ calculated 624.2781, found 624.2797; formula $C_{42}H_{39}N_3K$.

IR ν/cm^{-1} (Nujol): 3052 s, 2968 s, 2726 s, 2853 s, 1623 w, 1603 w, 1571 s.

UV/vis (THF, c = 5.0 x 10^{-6} mol dm^{-3}): λ_{max}/nm (ε x10^4 / dm^{3}mol^{-1}cm^{-1}) 389 (9.73).

8-(Ar*)imino-1,2,3,4-Tetrahydro-9-lithium-carbazole (**15**):

[Ar*THCarbLi]

To a solution of **9** (40 mg, 0.07 mmol, 1 eq.) in C_6D_6 (0.4 mL) was added a solution of Li[N(SiMe$_3$)$_2$] (11 mg, 0.07 mmol, 1 eq.) dropwise with stirring stirring, an intense orange colouration was formed in the solution upon addition. Crystals of **15a** suitable for X-ray diffraction were grown from C_6D_6 solutions, *via* hexane vapour diffusion, at room temperature.

[Characterisation of **15** following synthesis]:

^{1}H NMR (300 MHz, C_6D_6, 25 °C) δ (ppm): 8.31 (s, 1H, (N=C*H*)), 8.08 (d, 1H, *J* = 6.4 Hz, Ar-*H*), 7.33-6.84 (m, 24H, Ar-*H*/-C*H*Ph$_2$), 5.58 (s, 2H, Ar-*H*/-C*H*Ph$_2$), 3.32-3.17 (m, 2H, C*H*$_2$), 2.91-2.76 (m, 2H, C*H*$_2$), 2.34-2.15 (m, 4H, C*H*$_2$), 2.03 (s, 3H, Ar-C*H*$_3$).

^{7}Li{^{1}H} NMR (117 MHz, C_6D_6, 25 °C) δ (ppm): -0.75 (s).

^{13}C{^{1}H} NMR (75 MHz, C_6D_6, 25 °C) δ (ppm): 168.82 (N=*C*H), 148.74 (quaternary), 147.11 (quaternary), 144.47 (quaternary), 144.21 (quaternary), 142.30 (quaternary), 136.84 (quaternary), 133.65 (quaternary), 130.27, 130.06, 129.45, 129.06, 128.97, 128.84, 128.77, 127.50, 126.91, 123.64 (Ar-*C*), 118.15 (quaternary), 114.03 (Ar-*C*), 108.11 (quaternary), 53.27 (Ar-*C*/-*C*HPh$_2$), 28.05 (*C*H$_2$), 25.55 (*C*H$_2$), 25.29 (*C*H$_2$), 22.73 (*C*H$_2$), 21.21 (Ar-*C*H$_3$).

8-(Ar*)imino-1,2,3,4-Tetrahydro-9-sodium-carbazole (**16**):

[Ar*THCarbNa]

A mixture of **9** (40 mg, 0.07 mmol, 1 eq.) and Na[N(SiMe$_3$)$_2$] (12 mg, 0.07 mmol, 1 eq.) were dissolved in C_6D_6 (0.6 mL), whereupon an instant colour change from light yellow to bright orange was observed. Dark orange crystals of **16** suitable for X-ray diffraction were grown from C_6D_6 solutions *via* hexane vapour diffusion (25.3 mg, 62%), at room temperature.

^{1}H NMR (300 MHz, C_6D_6, 25 °C) δ (ppm): 8.46 (s, 1H, (N=C*H*)), 8.05 (d, 1H, *J* = 7.1 Hz, Ar-*H*), 7.42-6.98 (m, 12H, Ar-*H*), 6.96-6.69 (m, 12H, Ar-*H*), 5.66 (s, 2H, Ar-*H*/-C*H*Ph_2), 3.29-3.13 (m, 2H, C*H*$_2$), 2.84-2.69 (m, 2H, C*H*$_2$), 2.33-2.10 (m, 4H, C*H*$_2$), 1.99 (s, 3H, Ar-C*H*$_3$).

^{13}C{^{1}H} NMR (75 MHz, C_6D_6, 25 °C) δ (ppm): 170.22 (N=*C*H), 150.21 (quaternary), 147.65 (quaternary), 145.53 (quaternary), 143.47 (quaternary), 142.17 (quaternary), 136.57 (quaternary), 132.70 (quaternary), 130.35, 130.26, 130.02, 129.65, 128.77, 126.84, 125.57, 122.87 (Ar-*C*), 113.52 (Ar-*C*) 107.09, 53.08 (Ar-*C*/-*C*HPh_2), 28.34 (*C*H$_2$), 25.80 (*C*H$_2$), 25.52 (*C*H$_2$), 22.92 (*C*H$_2$), 21.20 (Ar-*C*H$_3$).

HRMS/EI *m/z*: $[M]^+$ calculated 642.3005, found 642.3007; formula $C_{46}H_{39}N_2Na$.

8-(Ar*)imino-1,2,3,4-Tetrahydro-9-potassium-carbazole (**17**):

[Ar*THCarbK]

A mixture of **9** (40 mg, 0.07 mmol, 1 eq.) and K[N(SiMe$_3$)$_2$]·0.75toluene (17 mg, 0.07 mmol, 1 eq.) was dissolved in C_6D_6 (0.6 mL), whereupon an instant colour change from light yellow to bright orange was observed, with concomitant formation of an insoluble dark orange solid. Following the synthesis, to the product were added 2 mL of THF with no noticeable effect in the solubility.

All signals observed as broad singlets (br s).

^{1}H NMR (300 MHz, C_6D_6/C_4D_8O, 25 °C) δ (ppm): 8.73 (br s, 1H, (N=C*H*)), 8.13 (br s, 1H, Ar-*H*), 7.58-6.86 (m, 24H, Ar-*H*), 5.93 (br s, 2H, Ar-*H*), 5.59 (br s, 2H, Ar-*H*/-C*H*Ph_2), 3.30 (br s, 2H, C*H*$_2$), 2.86 (br s, 2H, C*H*$_2$), 2.26 (br s, 3H, Ar-CH$_3$), 2.06 (br s, 2H, C*H*$_2$).

Group 1 salts **12**-**14** and dehydrogenation of dimethylamine-borane:[82]

Typical dehydrogenation procedure using catalytic amounts of the group 1 salts and $Me_2NH{\cdot}BH_3$:

13 (5.76 mg, 8.48 x10^{-3} mmol) and $Me_2NH{\cdot}BH_3$ (10 mg, 0.16 mmol, 20 eq.) were dissolved in 0.6 mL of either C_6D_6 or THF (with a C_6D_6 insert) and transferred to a J. Young's tap modified borosilicate glass NMR tube. The resulting NMR sample was transferred to an oil bath set up to the desired temperature (Table 3.4.8) and monitored until the resonances

attributed to the starting material disappeared (*via* ^{11}B NMR spectroscopy) or when no significant further reaction progress was observed.

Open system experiments:

13 (5.76 mg, 8.48 x10^{-3} mmol) and $Me_2NH{\cdot}BH_3$ (10 mg, 0.16 mmol, 20 eq.) were dissolved in 0.6 mL of toluene and transferred to a J. Young's tap modified borosilicate glass NMR tube containing a magnetic stirrer (the magnetic stirrer was removed following the catalytic run, in a glovebox, prior to NMR determinations). The resulting NMR sample was adapted to a system constituted by a glass adapter, a three-way tap (attached to a Schlenk line) and an inverted burette filled with paraffin oil. An oil bath was warmed up to 70 °C and after careful deoxygenation of the whole system, the NMR sample was warmed up. Opening of the three-way tap to the burette allowed the liberation of H_2 to be measured over time by displacement of the paraffin oil. The volume of H_2 determined using this methodology closely correlated with similar conversion determined by ^{11}B NMR spectroscopy (Entry 5, Table 3.4.8,).

This system was scaled up according to the following procure; **13** (57.6 mg, 0.0848 mmol) and $Me_2NH{\cdot}BH_3$ (100 mg, 1.69 mmol, 20 eq.) were dissolved in 6 mL of toluene and in a Schlenk tube containing a magnetic stirrer. The resulting bright orange solution was adapted under N_2 flow, to a system constituted by a glass adapter, a three-way tap (attached to a Schlenk line) and an inverted burette filled with paraffin oil. An oil bath was warmed up to 70 °C and after careful deoxygenation of the whole system, the system was warmed up. The three-way tap was then opened to the burette, allowing the liberation of H_2 to be measured over time by displacement of the paraffin oil. The volume of H_2 determined using this methodology closely correlated with that determined by ^{11}B NMR spectroscopy.

Table 3.6.1 ^{11}B NMR chemical shifts of relevant compounds observed in $Me_2NH{\cdot}BH_3$ dehydrocoupling reactions.

Compound	^{11}B NMR Chemical Shift (δ)	Reference
$Me_2NH{\cdot}BH_3$	-12.3 (*q*)	*Chem. Eur. J.*, **2011**, *17*, 4099-4103.
$Me_3N{\cdot}BH_3$	-7.70 (*q*)	*Chem. Ber.* **1966**, *99*, 1049-1067.
$Me_2N{=}BH_2$	37.9 (*t*)	*J. Organomet. Chem*., **2016**, *821*, 154-162.
$HB(NMe_2)_2$	29 (*d*)	*Chem. Eur. J.*, **2010**, *16*, 8508-8515.
$B(NMe_2)_3$	-21 (*br*)	*J. Organomet. Chem.,* **2016**, *821*, 154-162.
$[Me_2N{-}BH_2]_2$	5.5 (*t*)	*J. Am. Chem. Soc*., **2003**, *125*, 9424-9434.
$Me_2HN{-}BH_2{-}NMe_2{-}BH_3$	2.3 (*t*), -13.1 (*q*)	*Chem. Eur. J.,* **2011**, *17*, 4099-4103.
$Li[Me_2NBH_2NMe_2BH_3]$	3.5 (*t*), -14.7 (*q*)	*Dalton Trans.,* **2015**, *44*, 12078-12081.
$Na[Me_2NBH_2NMe_2BH_3]$	1.9 (*t*), -14.7 (*q*)	*Dalton Trans.,* **2015**, *44*, 12078-12081.
$K[NMe_2BH_2NMe_2BH_3]$	2.6 (*t*), -12.3 (*q*)	*Dalton Trans.,* **2015**, *44*, 12078-12081.
$Na[H_3BNMe_2BH_2NMe_2BH_3]$	28 (*br*)	*Inorg. Chem.,* **2013**, *52*, 10690-10697.
$Na[H_3B{-}NMe_2{-}BH_3]$	29.7 (*br*)	*Eur. J. Inorg. Chem.,* **1999**, 1373-1379.
Oligo/polymers	26-36 (*br*)	*J. Am. Chem. Soc.,* **2003**, *125*, 9424-9434.
$LiBH_4$	-41.5 (*quint*)	*J. Phys. Chem. C.,* **2014***,* 6596-6603.
$NaBH_4$	-42.4 (*quint*)	*Eur. J. Phys. Chem.,* **1959**, *63*, 1533-1535.
KBH_4	-38.7 (*quint*)	*J. Phys. Chem. C.,* **2014***,* 6596-6603.
Pyridine$\cdot BH_3$	-11.6 (*q*)	*RSC Adv.,* **2014**, *4*, 26207-26210.
Morpholine$\cdot BH_3$	-14.8 (*q*)	*RSC Adv.,* **2014**, *4*, 26207-26210.

Chapter IV. Synthesis of Homoleptic and Heteroleptic Carbazolido Complexes

4.1 Introduction to Homoleptic and Heteroleptic Carbazolido Complexes

As mentioned in Chapter I, pincer complexes assembled around a carbazolido core, allow for the synthesis and stabilisation of a wide range of coordination metal complexes. Buried volume calculations (% V_{Bur}) have been used to quantify the steric demands of 1,8-diaryl-carbazolyls, from which it has been possible to identify these motives as ideal substituents, offering a superior degree of steric protection to that found on similar bulky ligands, such as *m*-terphenyls (Figure 4.1.1).[78,128]

Exemplifying this and highlighting the ability of the scaffold to adapt to the metal centre employed, include experiments by Aldridge *et al*. from which it has been found that 1,8-dimesityl-3,6-dimethylcarbazolido ligands afford sufficient steric congestion around the central carbazolido-nitrogen, enabling the stabilisation of the first monomeric three-coordinate amidogallium dihalide complex. The fact that this compound restricts the formation of halide-bridged dimers in the solid state, furtherly proves that the flanking aryl rings on the carbazolyl framework offer a greater steric support in the vicinity of the metal centre ***A***.[128]

Using analogous systems, Gibson *et al*. reported the synthesis of elusive heteroleptic aluminium complexes, of the form 1,8-diphenyl-3,6-dimethylcarbazole-dialkyl-aluminium, *via* metathesis reaction of the corresponding lithium salt and aluminium compounds (R_2AlCl), yielding suspected three-coordinate alkylated-aluminium centres. Additionally, these dialkylaluminium carbazolyl products, could be converted to cationic species following reaction with $[H(OEt_2)_2[B(Ar^F)_4]$. Species derived from these experiments showed low activities for the oligomerisation of ethylene, while selectively affording low molecular weight (C_4-C_{10}) olefinic products ***B***.[56]

Similarly, the use of 1,8-diphenyl-3,6-dimethylcarbazole has yielded the formation of formally two-coordinate homoleptic transition-metal complexes with near-linear N–M–N geometry of chromium, manganese, iron and cobalt; where the two metal-substituted carbazolido moieties are near perpendicular to each other, and the metal centres are free from coordinating solvent, due to the high steric hindrance of the flanking phenyl rings ***C***.[45]

Carbazole moieties have also been used as means of linking two macrocyclic metallo-bisporphyrin arrangements, in which the porphyrin macrocylces substituents are cofacial to each other, with the three nitrogen atoms of the carbazole bridge also providing flexibility to chelate metals, allowing the formation of three-metal systems, useful in optoelectronics and dyad systems ***D***.[43]

Furthermore Kays *et al*. prepared a family of 1,8-diaryl and 1,3,6,8-tetra-(*tert*-butyl)-carbazol-9-yl proligands which proved useful in the formation of highly unstable heteroleptic magnesium species (Hauser bases). On one hand ligands with *tert*-butyl substituents in the 1- and 8- positions afford π-type compounds, in which the carbazolyl ligand acts more as a multihapto donor, while 1,8-diaryl substituted ligands yield σ-type compounds. These findings highlight significant differences in the coordination motifs, which depend heavily on the nature of the 1- and 8- substituents, essential for the stabilisation of low-coordinate magnesium complexes ***E*** (Figure 4.1.1).[48,150]

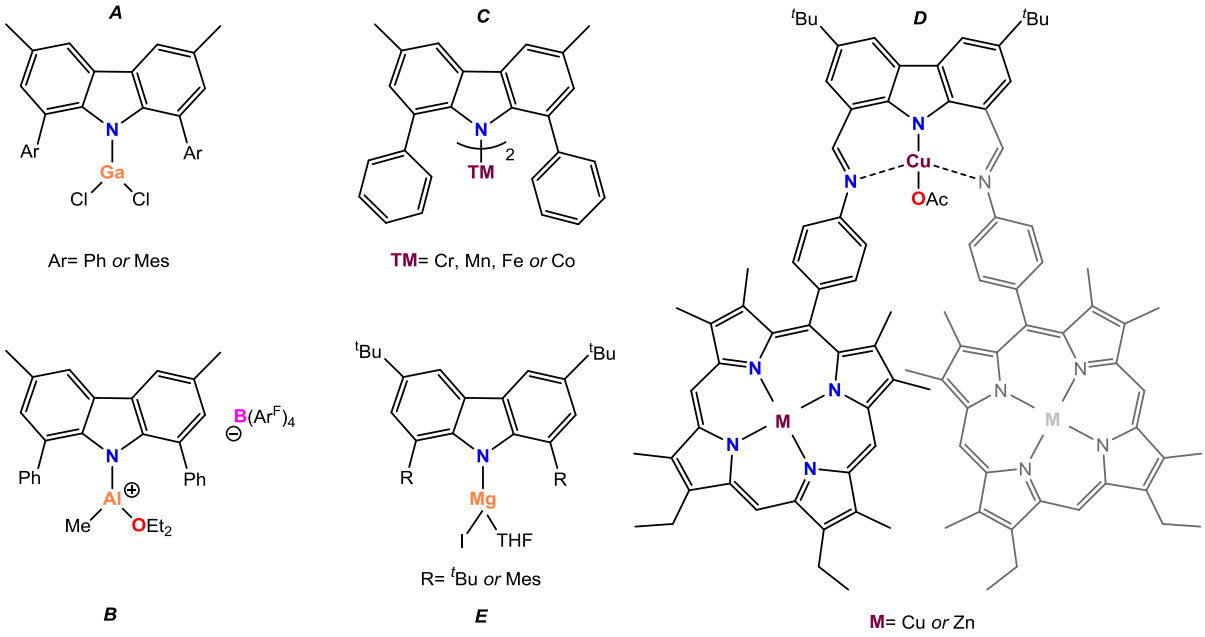


Figure 4.1.1 Selected examples of low-coordinate metal complexes formed using carbazolido-ligands.

4.2 Aims and Objectives

Making use of the *N*-based ligand systems generated/described in the previous section, it is the main objective of this chapter to generate metal-carbazolido complexes. This objective will be targeted primarily, aiming towards the formation of heteroleptic complexes. The different flanking groups employed, might in turn allowed to study differences in the coordination environments of the metal centres upon complexation, arising from the differing steric hindrance provided by the flanking groups, in both the symmetric and asymmetric carbazole ligands (**5**-**6** and **9**-**10**).

Simiarly, and since the aim is to prepare a series of low-coordinate complexes, it would be desirable to study differences among different metals employed (both against their corresponding group and period), while keeping the auxiliary proligand constant. Such approach would in turn allow a systematic study of the library of coordination compounds generated, to be used in catalysis and small molecule activation; a key feature that could be extended to optimisation of catalytic processes and similar organic transformations.

4.3 Results and Discussion

4.4 Low-coordinate Metal Centres Employing [Ar_2*carbH]

4.4.1 Metathesis Reactions with Group 2 Metal(II) Salts

4.4.1.1 Towards the Synthesis of [Ar_2*carbMgI]

Acknowledging the limited space available for substitution in the heavily crowded lithium salt **11** (Figure 4.4.1), it was envisaged that a smaller metal(II) halide would have adequate size to fit in the highly constrainted pocket, provided by the carbazolido proligand, following a metathesis reaction.

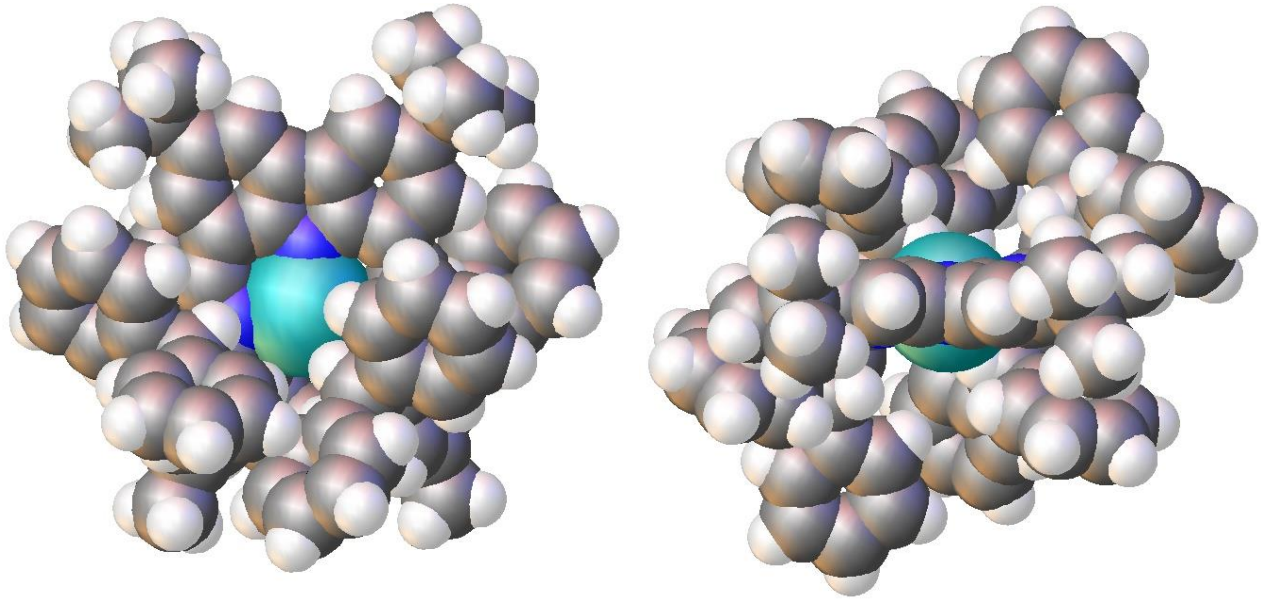
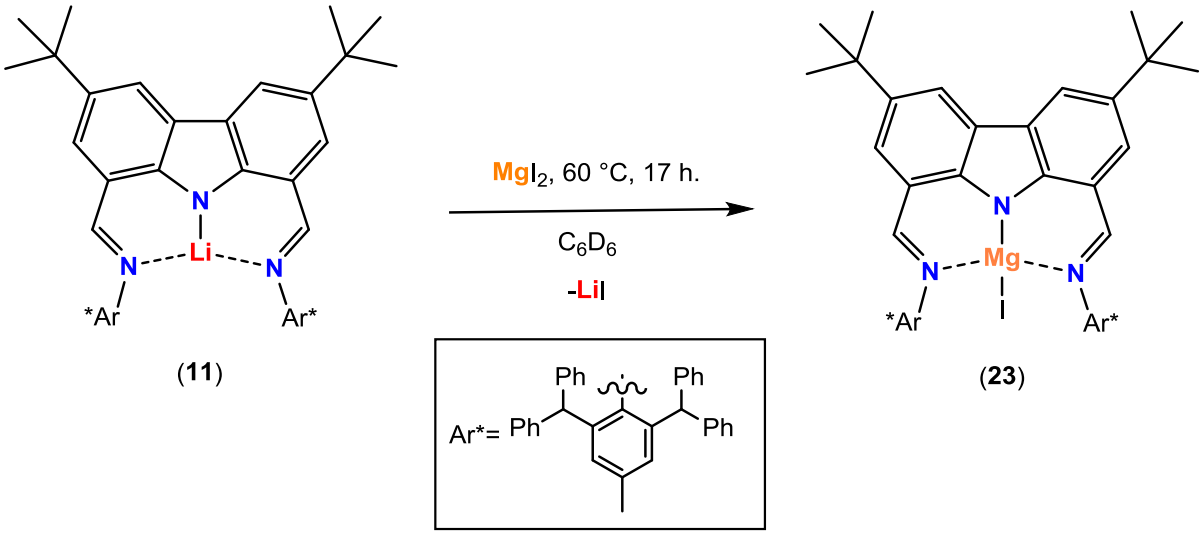


*Figure 4.4.1 Space filling diagram of the lithium salt **11**, normal to the carbazolido core (left) and upper view along the carbazolido axis (right).*



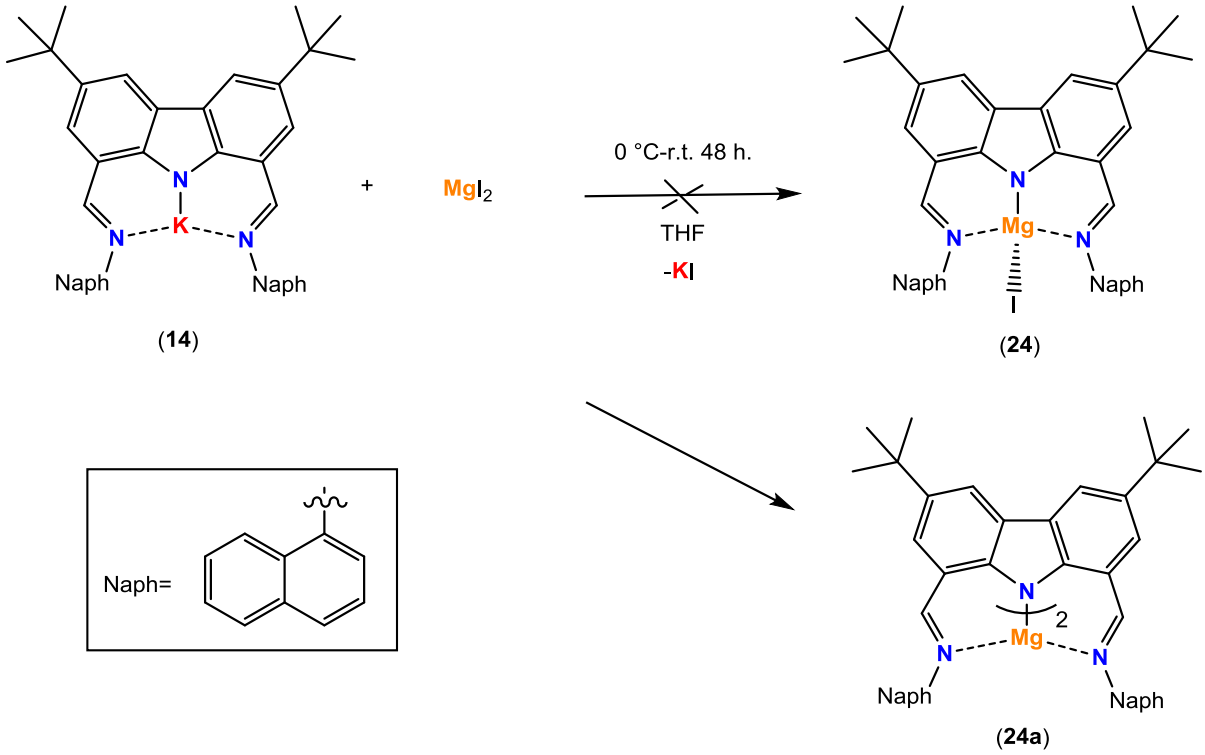
*Scheme 4.4.1 Formation of a Group 2 complex via a metathesis reaction between **11** and MgI_2.*

Initially the lithium salt **11** was synthesised following an identical procedure to the one discussed previously (*vide supra*). Following deprotonation, the *in situ* generated lithium salt **11** was reacted with MgI_2 in C_6D_6 (Scheme 4.4.1). No reaction occurred under these conditions. The sample was then heated in an oil bath at 60 °C for 17 hours, after which the ^1H NMR spectrum evidenced initial disappearance of the signals which are characteristic to the lithium salt, while at the same time a new set of signals at higher field grew in. Additionally, the absence of the characteristic N*H* and lack of overlap with the signals of the free ligand, suggested the formation of a new species ([Ar_2*carbMgI] **23**). Despite several attempts at growing crystals adequate for single crystal diffraction, it has not been possible to corroborate the structure of **23**. However, it has been inferred that the resulting structure is the intended heteroleptic complex, in agreement with the stoichiometry employed, and the lack of available space around the metal centre to accommodate a second tridentate ligand.

4.5 Low-coordinate Metal Centres Employing [Naph$_2$carbH]

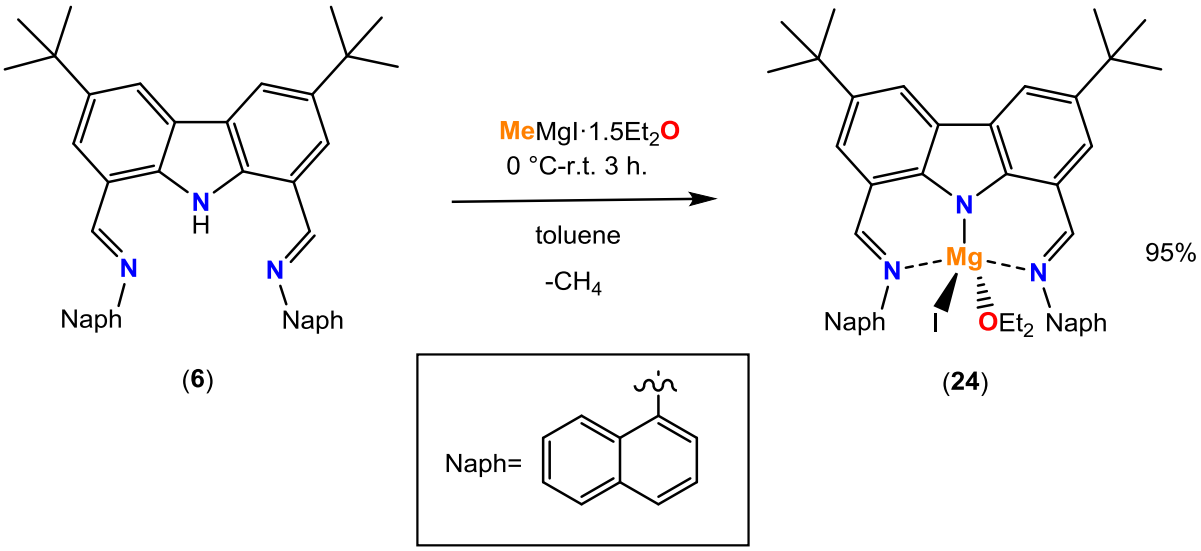
4.5.1 Metathesis/Organoelimination Reactions with Group 2 Metal(II) Salts

4.5.1.1 Synthesis of [Naph$_2$carbMg(OEt$_2$)I] and [(Naph$_2$carb)$_2$Mg]



*Scheme 4.5.1 Attempted synthesis of Hauser Base **24**.*

Initial attempts to extend the formation of heteroleptic Hauser bases to the symmetric naphthyl substituted ligand **6**, were attempted by means of a metathesis reaction. With this in mind, **6** was deprotonated in THF solution, employing KH as base. As such, the *in situ* generated potassium salt **14**, was reacted at low temperature with an excess of MgI_2 (Scheme 4.5.1). Previous results in the Kays group, have used a similar methodology to successfully synthesise Hauser bases, such as 1,8-Ar$_2$-3,6-^{t}Bu$_2$carbMgI(THF) [Ar = Xyl or Mes; Xyl = 3,5-Me$_2$C$_6$H$_3$; Mes = 2,4,6-Me$_3$C$_6$H$_2$] and 1,3,6,8-^{t}Bu$_4$carbMgI(THF)$_2$.[48] Under these conditions, a dark-orange powder was isolated, which characterisation *via* NMR spectroscopy in C_6D_6 showed conversion to a new product, and ruled out the presence of free ligand or the potassium salt **14**. Further characterisation *via* X-ray diffraction allowed corroboration towards the synthesis of a homoleptic complex ([(Naph$_2$carb)$_2$Mg] **24a**) instead of the targeted heteroleptic complex (**24**).



*Scheme 4.5.2 Synthesis of **24** via organoelimination.*

It was envisaged that the synthesis of the heteroleptic Hauser base complex would be possible *via* an organoelimination reaction, with concomitant liberation of methane (Scheme 4.5.2). A similar methodology has been employed in the synthesis of mononuclear *β*-diketiminate based three-coordinate magnesium complex [^{Ar*}LMgBr(OEt$_2$); ^{Ar*}L= (Ar*NCMe)$_2$CH].[151] In such circumstances, the proligand **6** was directly reacted with readily available Grignard reagent, MeMgI·1.5Et$_2$O, from which an orange solid could be isolated. A ^{1}H NMR spectrum of this solid, corroborated that deprotonation of the central carbazole nitrogen had occurred, with full conversion to a new product ([Naph$_2$carbMg(OEt$_2$)I] **24**). NMR characterisation of the isolated product was conclusive of the formation of an heteroleptic magnesium complex, with additional coordination of diethyl ether, as evidenced by characteristic signals in both ^{1}H and ^{13}C{^{1}H} NMR, which did not disappear even after prolonged exposure to vacuum. Crystals of **24**, suitable for X-ray diffraction were grown from a concentrated C$_6$D$_6$ solution at room temperature.

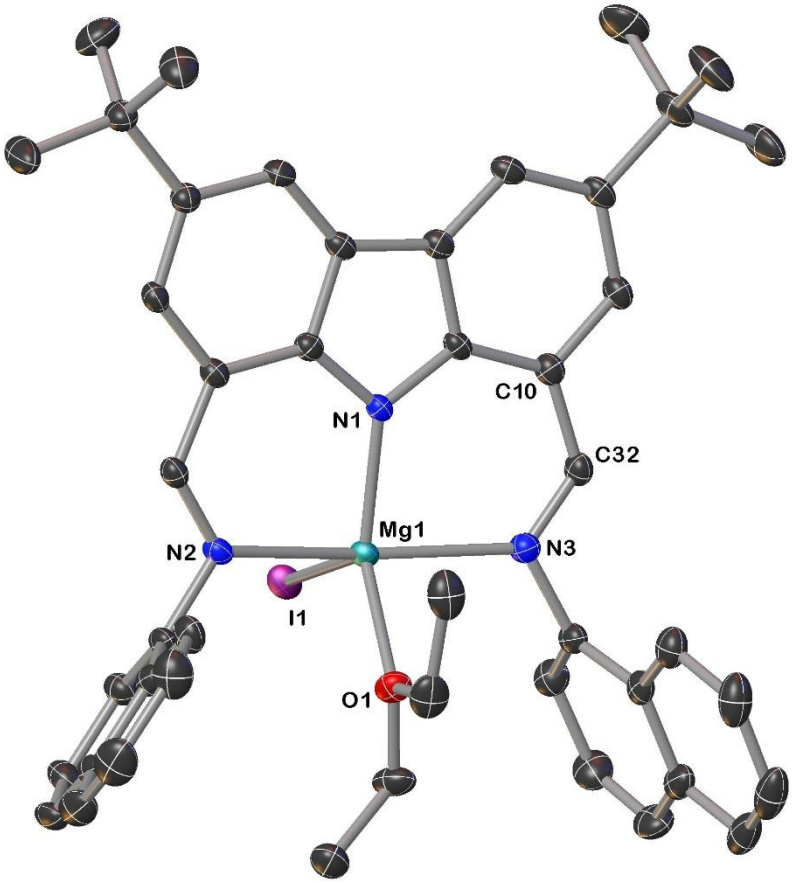


*Figure 4.5.1 Molecular structure for one of the crystallographically independent molecules of **24**, with displacement ellipsoids set at 50% probability level, hydrogen atoms have been omitted for clarity.*

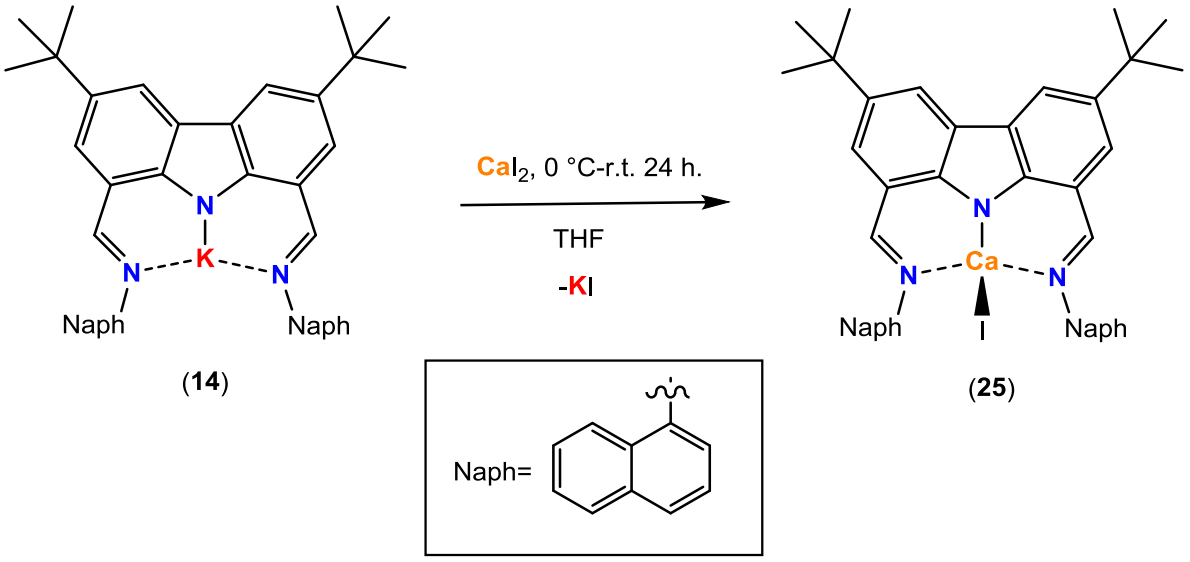
In the solid state, **24** is monomeric, with two crystallographically independent heteroleptic molecules in the asymmetric unit (Figure 4.5.1). The coordination sphere around the five-coordinate magnesium centre is close to trigonal bipyrimidal (τ_5 = 0.53),[152] and is occupied by the tridentate ligand in three coplanar positions, an iodide, with additional coordination of a solvation molecule (Et_2O) introduced in the reaction *via* the magnesium salt employed MeMgI·1.5Et_2O. The flanking naphthyl groups adopt a *syn* conformation. The metal lies in close proximity to the best mean plane generated by the carbazolido moiety (0.215(2) Å). The distance Mg1-N1 found in **24** (2.0373(19) Å) is similar to the equivalent determination for the carbazolido-magnesium complexes, 1,3,6,8-^{t}Bu$_4$carbMgI(THF)$_2$ and 1,8-Mes$_2$-3,6-^{t}Bu$_2$-carbMgI(THF) [2.101(5) Å and 2.009(6) Å, respectively].[48]

Bond Length (Å)		Bond Angle (°)	
Mg1– N1	2.037(2)	N2–Mg1–N3	166.86(7)
Mg1–N2	2.254(2)	N2–Mg1–N1	87.08(7)
Mg1–N3	2.251(2)	N1–Mg1–I1	113.23(5)
Mg1–I1	2.7718(7)	N1–Mg1–O1	134.91(7)
Mg1–O1	2.061(2)		

*Table 4.5.1 Selected bond lengths and angles for **24**.*

4.5.1.2 Synthesis of [Naph$_2$carbCaI]

In order to access a heavier Group 2 analogue, and due to the limitation of the availability of suitable starting materials as source of calcium (*vide infra*);[64,153,154] a metathesis reaction was tested employing CaI_2 (Scheme 4.5.3) to synthesise a calcium complex. Initial NMR scale experiments between the potassium salt **14** and CaI_2 in C_6D_6 afforded no new products. Acknowledging the limited solubility of the calcium salt in said solvent, small amounts of d_8-THF were added to the reaction mixture, followed by sonication at room temperature. Under these conditions, initial conversion to a new product could be observed, as evidenced by a ^{1}H NMR spectrum. Further heating at 60 °C for 16 hours resulted in full disappearance of the starting material.



*Scheme 4.5.3 Synthesis of **25** via metathesis reaction.*

Encouraged by these results, the reaction was repeated in a larger scale, from the *in situ* generated potassium salt **14** at low temperature and slow, dropwise addition of the resulting bright red solution to a solution containing an excess of CaI_2, in THF. Further stirring at room temperature for 24 hours, followed by removal of volatiles *in vacuo* yielded a dark yellow solid ([$Naph_2$carbCaI] **25**); which presented identical ^{1}H and $^{13}C\{^{1}H\}$ NMR spectra to the ones observed under the initial NMR scale reaction conditions.

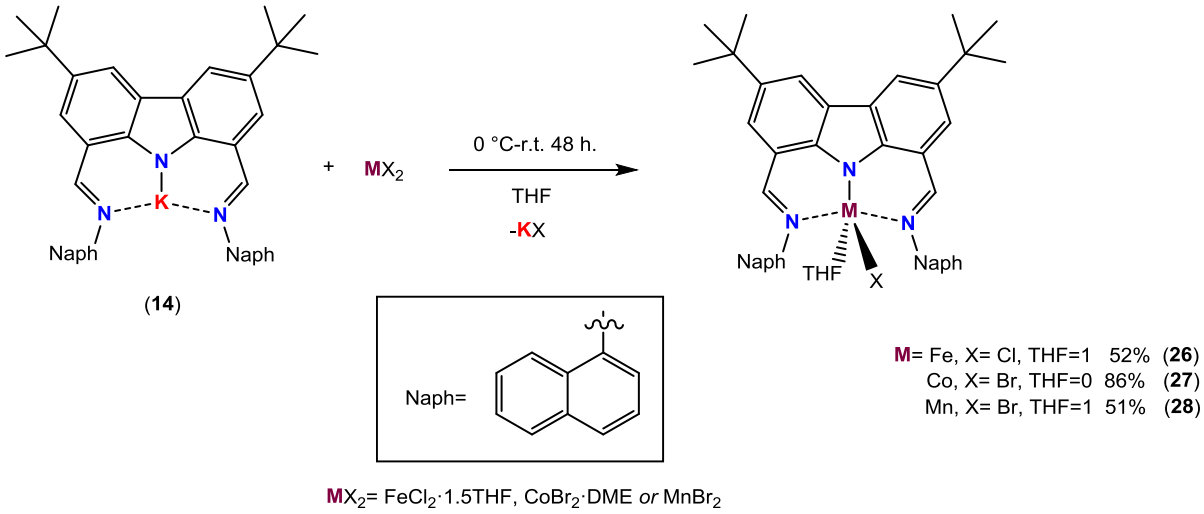
Attempts at growing crystals for this product were carried out by extracting the crude yellow solid into hexane, at room temperature, from which a yellow-green solution could be obtained. However, X-ray diffraction analysis of the resulting light yellow crystals revealed complete degradation of the Group 2 compound to the corresponding carbazole **6** only.

It is suspected that although a calcium-containing compound could be prepared following these procedures, the high propensity of compounds bearing this metal to rearrange/decompose, due to their higher propensity to undergo Schlenk-like solution redistribution reactions,[155] and their increased oxophilic character, which often leads to ether-cleavage reactions,[154] limits their characterisation and long-term stability. The decomposition pathways for heavier Group 2 compounds are very well documented, furtherly highlighting the difficulty in their synthesis and characterisation.[61,153]

4.5.2 Metathesis Reactions with First Row Transition-Metal(II) Salts

4.5.2.1 Heteroleptic Complexes

4.5.2.2 Synthesis of [Naph$_2$carbFe(thf)Cl], [Naph$_2$carbCoBr] and [Naph$_2$carbMn(thf)Br]



*Scheme 4.5.4 Formation of heteroleptic 1,8-bis(imino)carbazolido complexes **26**-**28**.*

The ease of preparation/short reaction time, the cleanliness of the product obtained *via* this method and the previous work portraying the ability of the ligand to stabilise low-coordinate, Group 1 metal centres **12**-**14**, prompted us to attempt salt metathesis reactions involving three first-row transition metal salts (Scheme 4.5.4).[82] Thus, the *in situ* generated potassium salt was reacted with two equivalents of $FeCl_2$·1.5THF, $CoBr_2$·DME and $MnBr_2$ in THF, affording [Naph$_2$carbMX(THF)] {MX = FeCl (**26**), MnBr (**28**)} or Naph$_2$carbCoBr (**27**), respectively. Pure samples of **26**-**28** were readily isolated, following toluene extraction from the crude reaction mixtures at room temperature in moderate to good yields of isolated crystalline material (**26**, 52%; **27**, 86%; **28**, 51%), which have been fully characterised.

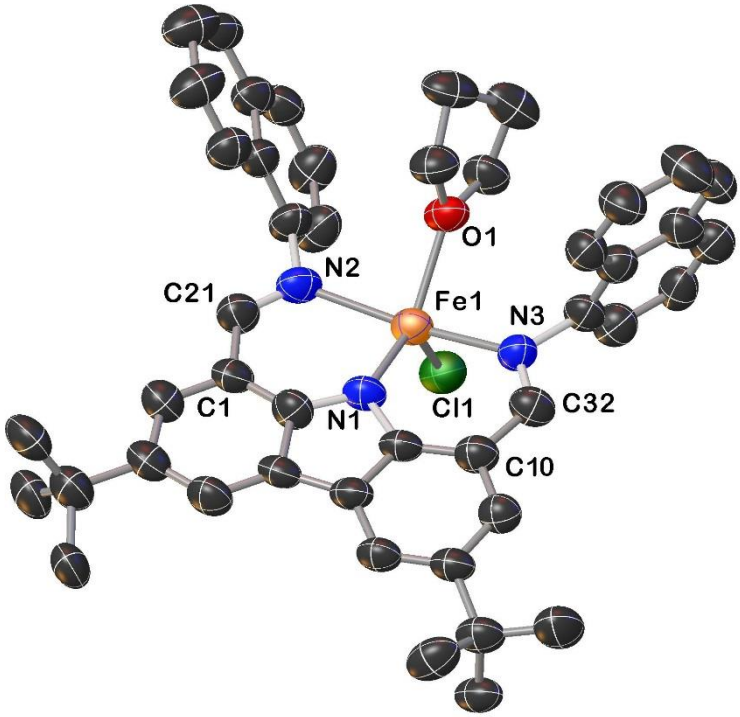


*Figure 4.5.2 Molecular structure for **26**, with displacement ellipsoids set at 50% probability level, hydrogen atoms have been omitted for clarity.*

The solid state structure determination of **26**, denotes a monomeric heteroleptic complex with one molecule occupying the asymmetric unit (Figure 4.5.2). The coordination geometry of the central metal ion displays a distorted trigonal bipyramidal geometry (τ_5 = 0.49),[152] where three of the coordination positions are taken by the tridentate carbazolido ligand with a chloride and a molecule of THF taking the remaining equatorial positions. The geometries observed for the metal centre are consistent with similar five-coordinate, iron-carbazolido complexes. With the distance Fe1–N1 [2.001(8) Å] determined for **26**, found to be within range of the equivalent lengths found in the closely related complexes (1,8-Ph_2-3,6-Me_2-carbazolide)$FeCl_2$,[51] [1,8-(4′-^{i}Pr-oxazolin-2′-yl)$_2$-3,6-Ph_2-carbazolide]$FeCl_2$[50] and (1,8-Ph_2-3,6-Me_2-carbazolide)$_2$Fe[45] (1.959(3) Å, 1.967(4) Å, and 1.972(2) Å, respectively).

Bond Length (Å)		Bond Angle (°)	
Fe1–N1	2.001(8)	N2–C21–C1	124.5(11)
Fe1–N2	2.245(10)	N3–C32–C10	123.1(11)
Fe1–N3	2.207(9)	N2–Fe1–N3	164.1(4)
Fe1–Cl1	2.288(4)	N1–Fe1–N2	86.1(3)
Fe1–O1	2.152(7)	Cl1–Fe1–O1	107.6(3)
C21–N2	1.294(14)	N1–Fe1–O1	134.3(3)
C32–N3	1.307(12)	N1–Fe1–Cl1	118.5(3)

*Table 4.5.2 Selected bond lengths and angles for **26**.*

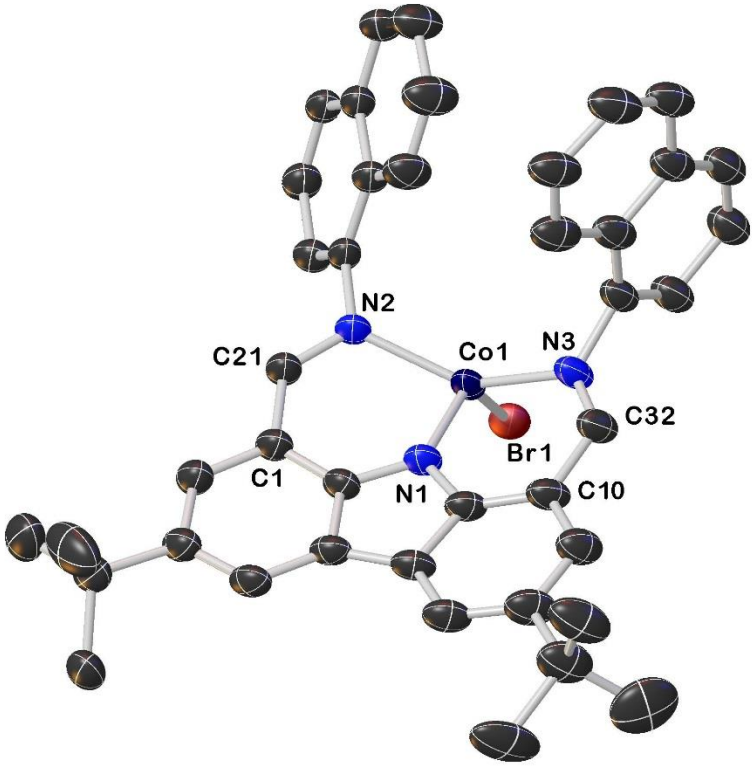


*Figure 4.5.3 Molecular structure for one of the crystallographically independent molecules of **27**, with displacement ellipsoids set at 50% probability level, hydrogen atoms have been omitted for clarity.*

Comparatively, in the case of **27**, two crystallographically independent molecules occupy the asymmetric unit, with the metal centre being four-coordinate and presenting a seesaw geometry (τ_4' = 0.61) (Figure 4.5.3).[156] Three of the coordination positions are occupied by the tridentate carbazolido ligand while the last one is taken by the bromide. Contrary to the potassium salt **17**, the flanking naphthyl groups are not in a periplanar conformation. The previously stated and the absence of additional coordinated THF to the metal, is likely a consequence of the bulkier halide. This type of conformation for a Co(II) centre is rare, only been reported once before, using a similar *NNN* carbazolido pincer ligand [(1,8-(Mes-imino)$_2$-3,6-Me$_2$-carbazolide]CoCl].[52] The distances Co1–N1 [1.906(2) Å], Co1–N2 [2.063(2) Å] and Co1–N3 [2.046(2) Å] found in **27**, are consistent with the analogous measurements in the aforementioned Co(II) complex [Co1–N1 = 1.912(4) Å, Co1–N2 = 2.067(5) Å and Co1–N3 = 2.072(5) Å], with minimum variations between the two structures arising from the differing halide [Co1–Br1 = 2.3675(4) Å / N1–Co1–Br1 = 124.86(6)° *vs.* Co1–Cl1 = 2.2.66(2) Å / N1–Co1–Cl1 = 124.98(13)°].[52]

Bond Length (Å)		Bond Angle (°)	
Co1–N1	1.906(2)	N1–Co1–Br1	124.86(6)
Co1–N2	2.063(2)	N2–Co1–N3	140.54(8)
Co1–N3	2.046(2)	N2–C21–C1	127.0(2)
Co1–Br1	2.3675(4)	N3–C32–C10	126.2(2)
C21–N2	1.307(3)		
C32–N3	1.307(3)		

*Table 4.5.3 Selected bond lengths and angles for **27**.*

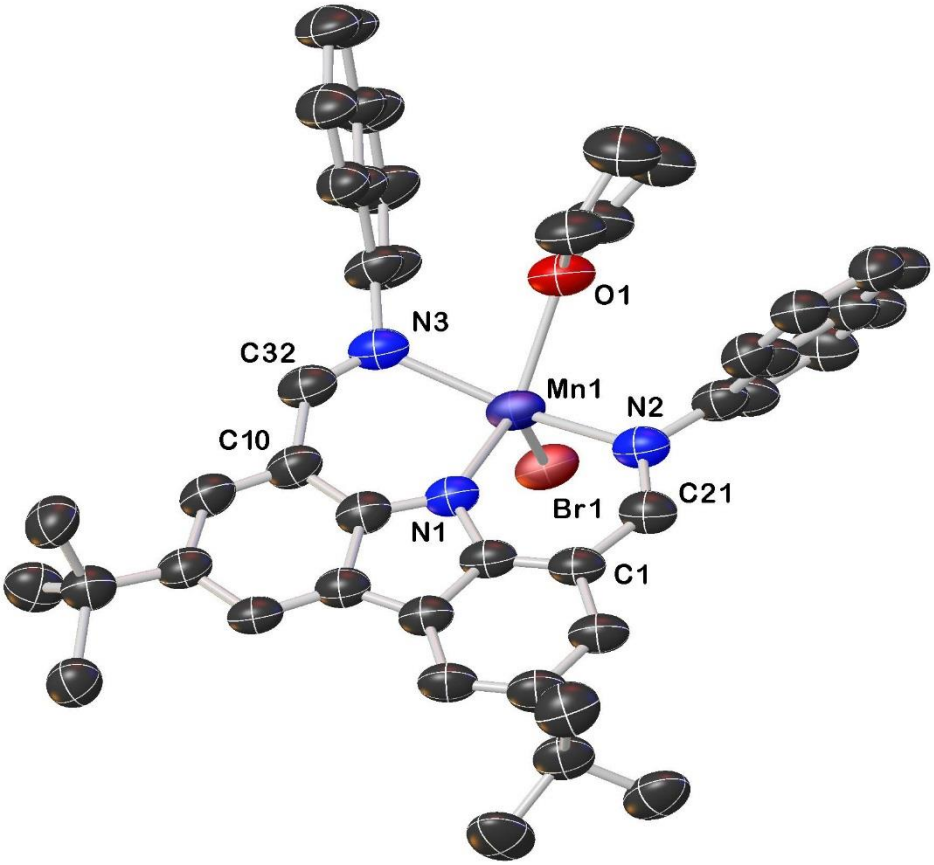


*Figure 4.5.4 Molecular structure for **28**, with displacement ellipsoids set at 30% probability level, hydrogen atoms have been omitted for clarity.*

In the solid state, **28** is monomeric, with one heteroleptic molecule in the asymmetric unit (Figure 4.5.4). The coordination sphere of the metal centre is filled by one molecule of the tridentate carbazolido ligand, a bromide and a molecule of THF. As a consequence, the metal centre exhibits distorted trigonal bipyramidal geometry (τ_5 = 0.39)[152]. This coordination motif for Mn(II) is rare, with the solid state determination of **28** being the first example of a monomeric heteroleptic carbazolido complex. Similarly, only three Mn(II)-homoleptic carbazolido complexes have been crystallographically authenticated, including [(Carbazol-9-yl)$_2$-Mn-(THF)$_3$],[157] and [(1,8-Ph$_2$-3,6-Me$_2$-carbazolide)$_2$Mn].[45] The distance Mn1–N1 [2.064(7) Å] in **28**, is within range of those found in the aforementioned Mn(II)-carbazolido complexes [2.080(2) Å and 2.0442(15) Å, respectively].[45,157]

	Bond Length (Å)		Bond Angle (°)
Mn1–N1	2.064(7)	N1–Mn1–Br1	116.2(2)
Mn1–N2	2.303(9)	N2–Mn1–N3	157.1(3)
Mn1–N3	2.296(10)	N1–Mn1–O1	133.6(3)
Mn1–Br1	2.51(2)	N3–C32–C10	128.1(11)
Mn1–O1	2.168(7)		
N3–C32	1.25(1)		

*Table 4.5.4 Selected bond lengths and angles for **28**.*

4.5.2.2.1 Structural Comparison of the Heteroleptic First Row Transition-Metal Complexes

Although similar, the solid state determinations of **26**-**28**, allow for important structural comparisons. A noticeable change in coordination geometry, can be observed when moving from left to right of this period, going from five-coordinate in the Mn(II) and Fe(II) complexes **28** and **26**, to four-coordinate in the Co(II) complex **27**. The distance between the metal centres and their corresponding carbazolido nitrogen [M1–N1, M = Mn (**28**) 2.064(7) Å, Fe (**26**) 2.001(8) Å and Co (**27**) 1.9062(17) Å], diminishes in length. This is most likely a consequence of the decrease in ionic radii, as a consequence of the effective nuclear charge increasing across the period. As such, the net positive charge on an electron on the atom would increase, as a consequence of the increasing number of protons in the nucleus.[158] Similarly, the decrease in ionic radius is particularly noticeable, when the distances between the metal centre and the flanking iminic groups (N2 and N3) are compared [M1–N2, M = Mn (**28**) 2.303(9) Å, Fe (**26**) 2.245(10) Å and Co (**27**) 2.063(2) Å] *vs.* [M1–N3, M = Mn (**28**) 2.296(10) Å, Fe (**26**) 2.207(9) Å and Co (**27**) 2.046(2) Å]. Additionally, the angle N1–M1–X1 increases following a similar trend [N1–M1–X1, M = Mn (**28**) 116.2(2)°, Fe (**26**) 118.5(3)° and Co (**27**) 124.86(6)°], even when considering the differences in coordination environment, and the dissimilar halide employed.

	M = Mn X = Br (**28**)	Fe Cl (**26**)	Co Br (**27**)
M1–N1	2.064(7)	2.001(8)	1.906(2)
M1–N2	2.303(9)	2.245(10)	2.063(2)
M1–N3	2.296(10)	2.207(9)	2.046(2)
M1–X1	2.51(2)	2.288(4)	2.368(4)
M1–O1	2.168(7)	2.152(7)	-
N1–M1–X1	116.2(2)	118.5(3)	124.86(6)
N2–M1–N3	157.1(3)	164.1(4)	140.54(8)
N1–M1–O1	133.6(3)	134.3(3)	-

*Table 4.5.5 Selected bond lengths (Å) and angles (°) for **26**, **27** and **28**.*

4.5.2.2.2 Electrochemical Characterisation

Electrochemical characterisation for compounds **26**-**28** has been carried out (Figure 4.5.5). From these it was possible to determine that compounds **26** and **28** show no redox activity in the potential range between 0 and –2 V *vs.* Fc^+/Fc. At more negative potentials compounds **26** and **28** show a series of reduction processes, the first of which, at E_p^c –2.14 and –2.21 V, respectively show a small return wave, at E_p^a -1.96 and -2.09 V, respectively, at faster scan rates (0.3 Vs^{-1}) that may indicate some limited stability of the primary product of electron transfer. In **28** a clearly defined second reduction is noted at E_p^c –2.38 V. Both **26** and **28** show oxidation processes at potentials above 0 V that result in a broad reduction wave at *ca.* –0.5 V *vs.* Fc^+/Fc. Compound **27** appears easier to reduce than **26** and **28** and shows a reduction process at E_p^c –1.81 V with an associated re-oxidation wave at E_p^a –1.28 V. At positive potentials compound **27** shows a series of oxidation processes, at E_p^a 0.32, 0.52 and 0.64 V *vs.* Fc^+/Fc, with the latter two processes resulting in a series of reductions noted in the return cycle.

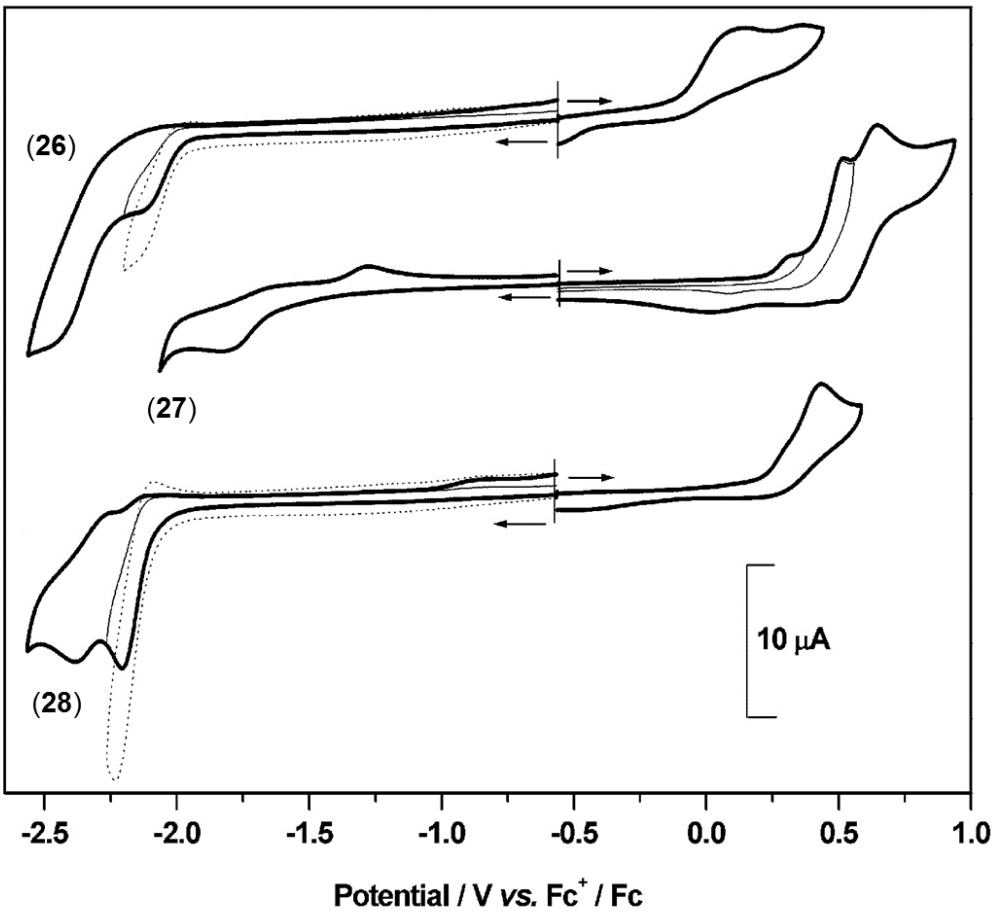
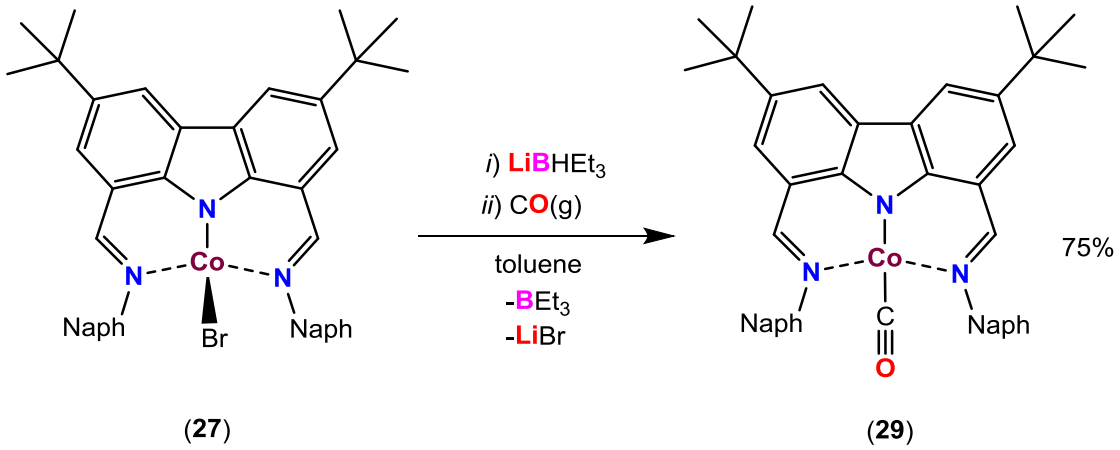


*Figure 4.5.5 Cyclic voltammetry for **26** (top), **27** (middle) and **28** (bottom) as 1 mM solutions in THF containing [NBu_4][BF_4] (0.5 M) as supporting electrolyte. Data recorded at ambient temperature and 0.1 Vs^{-1} scan rate. Dotted lines show data recorded at 0.3 Vs^{-1} scan rate.*

4.5.2.2.3 Synthesis of Metal(I)-carbonyl Complexes via Reductive Carbonylation

4.5.2.2.3.1 Synthesis of [Naph$_2$carbCo(CO)]



*Scheme 4.5.5 Formation of **29** via reductive carbonylation.*

Having synthesised and characterised transition metal(II) complexes **26**-**28**, and inspired by recent advances in CO activation,[159–162] a solution of **27** in C_6D_6, was exposed to an atmosphere of CO. Although paramagnetic in nature, the ^{1}H NMR spectrum of the resulting mixture showed no significant differences to the resonances observed for **27**. Following this and pursuing the activation of our metal centre *via* removal/exchange of the halide, one equivalent of LiBHEt$_3$ was added (Scheme 4.5.5), leading to an immediate colour change from bright purple to black. A ^{1}H NMR spectrum of the resulting compound revealed the formation of a new paramagnetic compound, most probably the hydride substituted analogue of **27** [Naph$_2$carbCoH]$_n$ (*n* = 1 or 2, **27-H**).[159,163] In line with this and previous experiments, it was anticipated to access carbon monoxide activation, following the exposure of the *in situ* generated hydride complex with CO, in the form of (C=O)H_n derivatives.[164,165] Surprisingly, X-ray diffraction studies of black crystals obtained through this methodology revealed the formal replacement of the halide/hydride moiety by CO, affording [Naph$_2$carbCo(CO)] (**29**) (Scheme 4.5.5). Similar transformations have been reported starting from the heteroleptic metal-halide *via* reduction with Na/Hg amalgam with further exposure to CO.[159,166]

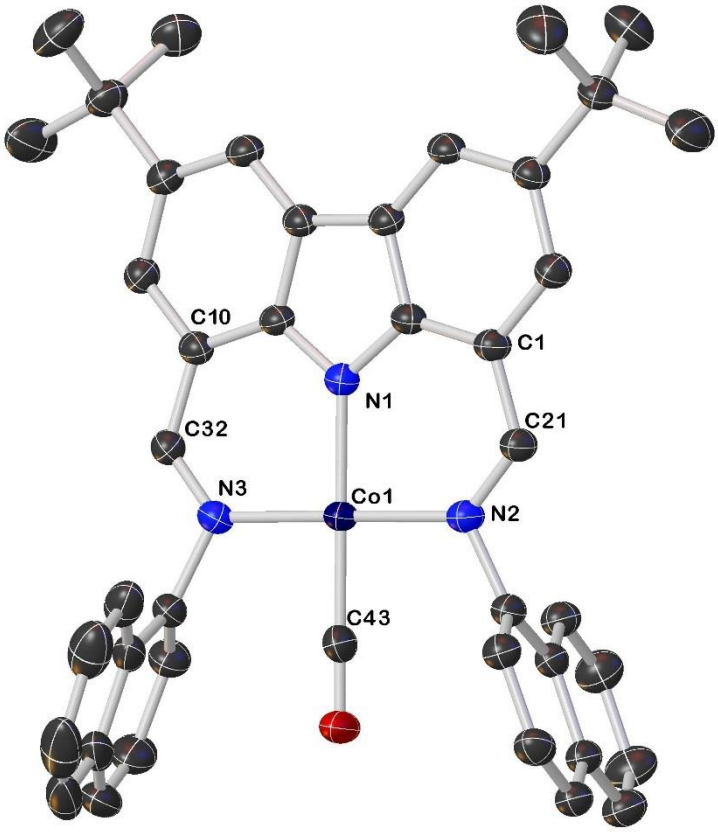


*Figure 4.5.6 Molecular structure for **29**, with displacement ellipsoids set at 50% probability level, hydrogen atoms have been omitted for clarity.*

	Bond Length (Å)		Bond Angle (°)
Co1–C43	1.762(2)	N3–Co1–N2	179.47(7)
Co1–N1	1.887(2)	N3–Co1–N1	90.12(7)
Co1–N2	1.937(2)	N2–Co1–N1	90.40(7)
Co1–N3	1.947(2)	N1–Co1–C43	179.22(11)
C32–N3	1.308(3)		

*Table 4.5.6 Selected bond lengths and angles for **29**.*

The coordination sphere of the metal complex **29**, shows a square planar geometry (τ_4' = 0.006),[156] in which three positions are occupied by the tridentate carbazolido ligand and one molecule of CO, with the flanking naphthyl groups in an *anti* conformation from each other (Figure 4.5.6). In addition to the new coordination sphere around the metal centre, there has been a change of oxidation state from cobalt(II) in **27** to cobalt(I) in **29**. The distance Co1–N1 [1.887(2) Å] in **29** is shorter than the equivalent found in **27** [1.906(2) Å], indicative of a metal centre more strongly bound to the ligand, upon change of oxidation state. With a similar behavour also observed between the flanking aldiminic nitrogens (N2/N3) and the metal, [Co1–N2 = 1.9368(18) Å, Co1-N3 = 1.947(2) Å; for **29** / Co1–N2 = 2.063(2) Å, Co1–N3 = 2.046(2) Å; for **27**]. Moreover, there are substantial changes in the bond angles associated [N1–Co1–Br = 124.86(6)° and N2–Co1–N3 = 140.54(8) for **27** *vs.* N1–Co1–CO = 179.22(11)° and N2–Co–N3 = 179.47(7)° for **29**].

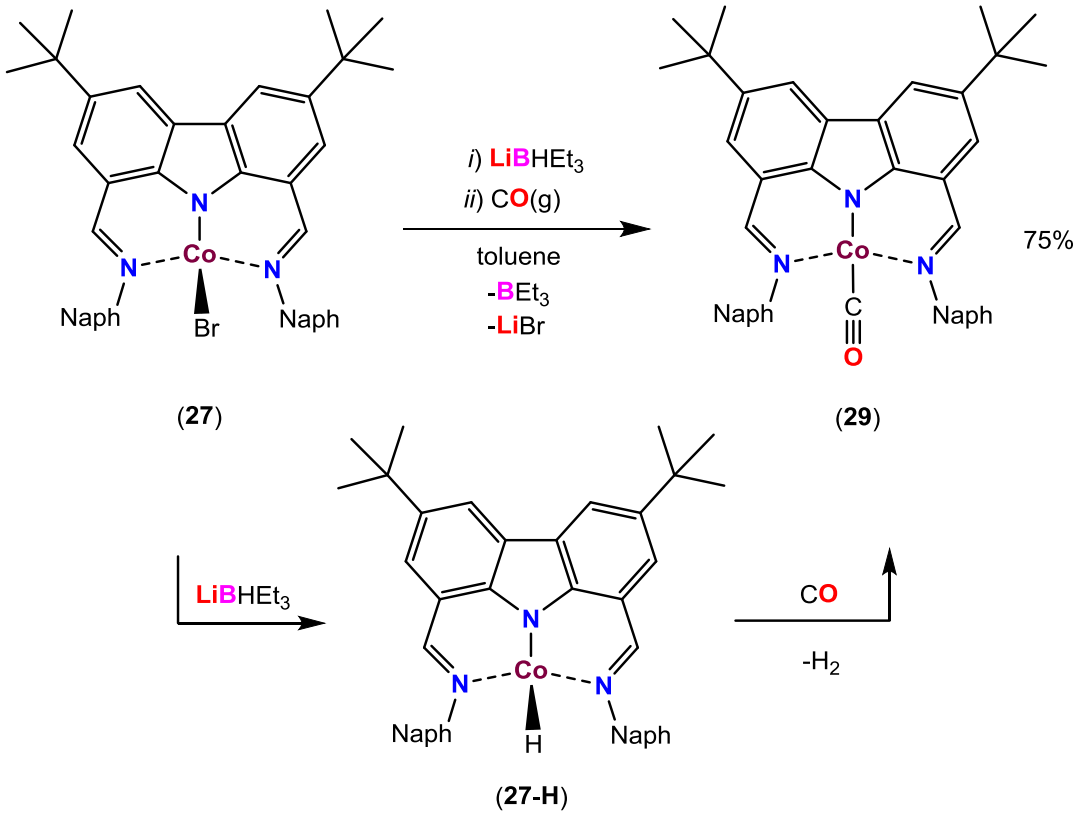
M=	Co	Co
X =	Br	CO
	(**27**)	(**29**)
M1–N1	1.906(2)	1.887(2)
M1–N2	2.063(2)	1.937(2)
M1–N3	2.046(2)	1.947(2)
M1–X	2.368(4)	1.762(2)
N1–M1–X1	124.86(6)	179.22(11)
N2–M1–N3	140.54(8)	179.47(7)

*Table 4.5.7 Selected bond lengths (Å) and angles (°) for **27** and **29**.*

There are limited reports of pincer cobalt(I)-carbonyl complexes bearing only one CO ligand, that do not dissociate CO under mild vacuum, which include (^{t}BuPOCOP)Co(CO) (POCOP = κ^3-C_6H_3-1,3-[OP^{t}Bu$_2$]$_2$ and [(TIMEN^{Xyl})Co(CO)]Cl {TIMEN = tris[2- (3-arylimidazol-2-ylidene)ethyl]amine)}.[159,166–170] The distance Co1–C43 [1.762(2) Å] found in **29**, corresponding to the metal-CO bond, is similar to the equivalent distance measured for Co(I)-complexes, such as, (^{t}BuPOCOP)Co(CO) [1.727(2) Å][159] and (κ^2-^{i}PrPNP)Co(CO)$_2$H) [1.752(2) Å] (^{i}PrPNP = MeN[CH$_2$CH$_2$(P^{i}Pr$_2$)]$_2$),[170] and significantly shorter than the one found in [(TIMEN^{Xyl})Co(CO)]Cl [1.846(2) Å].[168] In addition, the IR spectrum of **29**, shows an intense stretching band at (ν_{CO}) 1908 cm^{-1}, which is in range of terminal carbonyls bound to Co(I) [*e.g.* (^{t}BuPOCOP)Co(CO); 1899 cm^{-1}], indicating strong backbonding character from the metal to the carbonyl ligand.[159] Similar observations in

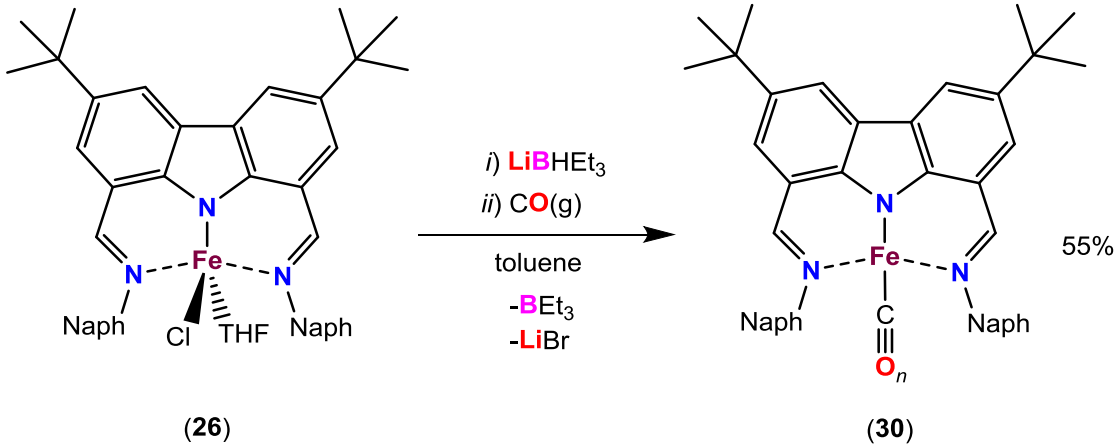
square planar Co(I)-carbonyl complexes, have attributed this behaviour to a better orbital overlap between the ion and the carbonyl ligand, in line with a decrease in the electronegativity of the metal centre, upon change in oxidation state.[159,167]

A plausible mechanism for this transformation would involve initial replacement of the halide by $LiBHEt_3$ to form an elusive cobalt(II)-hydride intermediate (**27-H**) (Scheme 4.5.6); similar transformations have been reported involving a bimolecular pathway in which a hydride-bridged dimer[163] can easily liberate one equivalent of H_2 upon exposure/coordination to CO.[163,171]



*Scheme 4.5.6 Proposed reaction mechanism for the formation of **29**, via reductive carbonylation.*

4.5.2.2.3.2 Synthesis of [Naph$_2$carbFe(CO)]



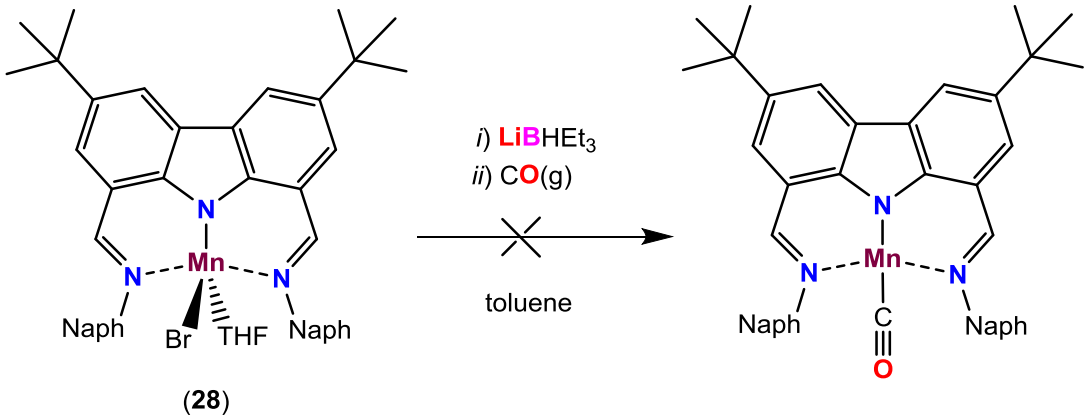
*Scheme 4.5.7 Preparation of **30**.*

Looking to access a reduced version of **26**, analogous reactions monitored by IR spectroscopy showed strong evidence of peaks ranging from 2020-1909 cm^{-1}, attributable to the formation of an iron(I) carbonyl complex ([Naph$_2$carbFe(CO)] **30**); with a major peak at 1909 cm^{-1}, which is at lower energy than the equivalent absorbtions reported for similar iron based terminal-carbonyl complexes, such as [2,6-(^{i}Pr$_2$PO)$_2$C$_6$H$_3$]Fe(H)(PMe$_3$)(CO)] (1928 cm^{-1}) and [C$_5$H$_5$Fe(CO)(COCH$_3$){P(C$_6$H$_5$)$_3$}] (1920 cm^{-1}), indicative of strong back-donation from the metal centre to the carbonyl ligand in **30**.[172–174] Unfortunatelly, and although several attempts at growing crystals suitable for single X-ray diffraction, were attempted. It has not been possible to determine precisely the structure of **30** in the solid state. Despite this, multinuclear structures relying on bridging carbonyls have been ruled out, due to absence of characteristic signals at lower wavenumber (1800-1500 cm^{-1}). Following synthesis, this compound could be isolated, as a dark brown powder, in good yield (55%) (Scheme 4.5.7).

4.5.2.2.3.3 Synthesis of [Naph$_2$carbMn(CO)]

When a similar transformation (*reductive carbonylation*) was tested with **28** as starting material, no evidence of formation of a carbonyl complex could be observed (Scheme 4.5.8). Although manganese(I)-carbonyl complexes are reported in the literature,[175] they are known to readily liberate CO upon exposure to low power visible light. A feature that has been used for medical purposes, due to their ability to selectively release CO, as a response of photoirradiation, with a recent example including [Mn(CO)$_3$(CH$_3$CN)(tryptophan)], which has been demonstrated to be cytotoxic to *E. coli* cells following irradiation.[176] This has been rationalised as a consequence of the carbonyl moiety being on the same plane as the ligand [bipyridine and related *N*-based ligands (L)],

that renders the CO more labile and prone to photolysis, in complexes of the type $[MnL(CO)_3]$.[177,178]



(**28**)

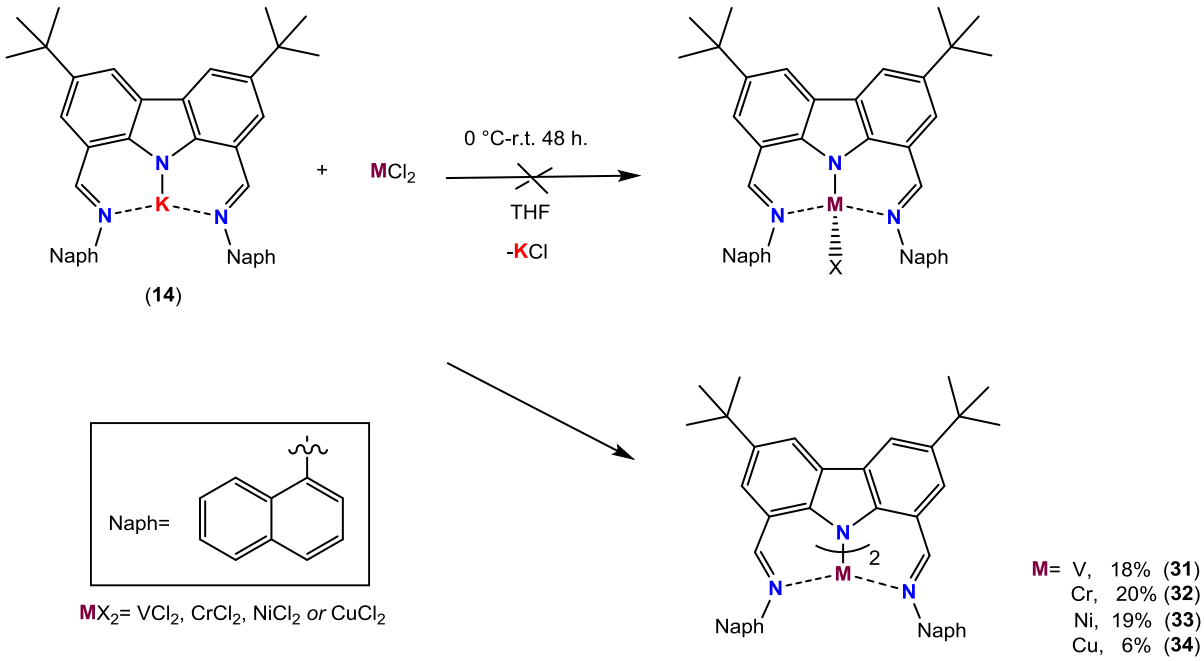
Scheme 4.5.8 Attempted synthesis of a Mn(I)-carbonyl complex.

4.5.2.3 Homoleptic Complexes

4.5.2.4 Synthesis of [(Naph$_2$carb)$_2$V], [(Naph$_2$carb)$_2$Cr], [(Naph$_2$carb)$_2$Ni] and [(Naph$_2$carb)$_2$Cu]

Encouraged by the successful synthesis of complexes **24**-**28**, it was decided to extend the formation of heteroleptic complexes with this ligand system to a range of first-row transition-metals (Scheme 4.5.9). The method employed was identical to the one described previously for the synthesis of first row transition-metals **26**-**28**, using for this purpose an excess of VCl_2, $CrCl_2$, $NiCl_2$ or $CuCl_2{\cdot}THF_{0.8}$ for the metathesis reaction. Although, the stoichiometry was kept the same as in all the previous experiments, solid state determinations resolved that the compounds generated throughout this methodology, afforded primarily homoleptic complexes with general formula [{(*tert*-butyl-bis(imino)naphthylcarbazole)$_2$M}, [(Naph$_2$carb)$_2$V] (**31**), [(Naph$_2$carb)$_2$Cr] (**32**), [(Naph$_2$carb)$_2$Ni] (**33**) or [(Naph$_2$carb)$_2$Cu] (**34**)].

Isolated low yields of crystalline material were obtained, in all cases, from samples employed for X-ray diffraction, from concentrated hexane extracts following completion of the reaction; 18% (**31**), 20% (**32**), 19% (**33**) and 6% (**34**), respectively.



*Scheme 4.5.9 Metathesis reactions attempted targeting the formation of heteroleptic carbazolido complexes **31-34**.*

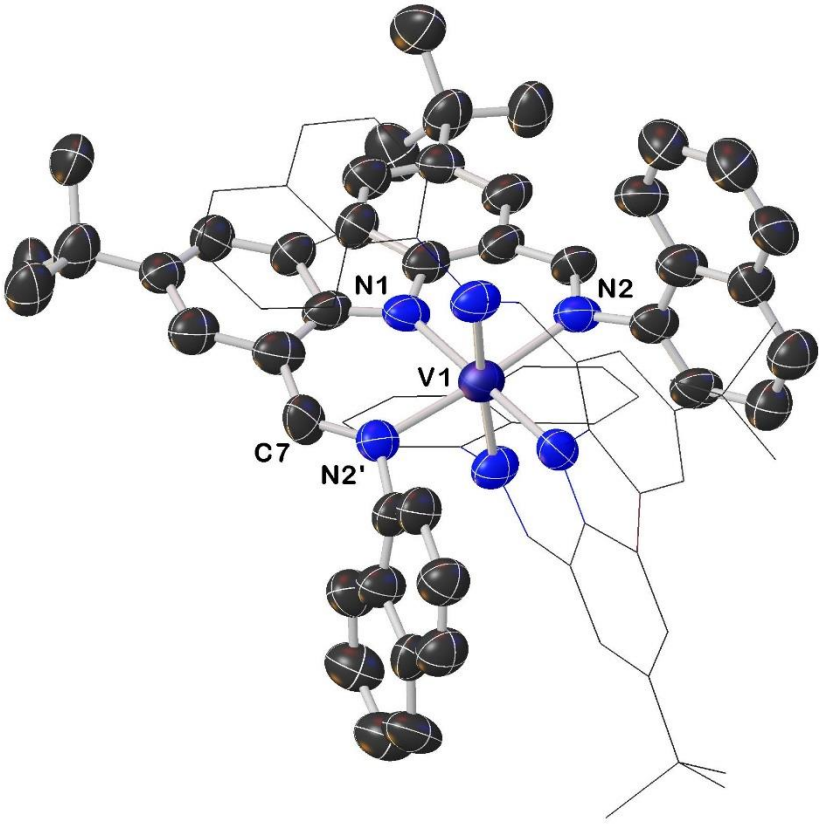


*Figure 4.5.7 Molecular structure for the symmetric unit of **31**, with displacement ellipsoids set at 50% probability level. Hydrogen atoms have been omitted, with a second carbazolido ligand presented in wireframe form for clarity.*

The solid state structure of **31** crystallised in the *P*2/*n* space group, revealing a monomeric structure with two half molecules occupying the asymmetric unit (Figure 4.5.7), with a mirror plane through the V1–N1 bond. The coordination sphere of V1 is saturated by two ligand moieties, almost perpendicular to each other, exhibiting an octahedral geometry; the plane twist angle between the best mean plane generated by the two central pyrrolido rings, on the two ligands, is 93.5(10)°. Most noticeably, the flanking naphthyl groups are in an *anti*-conformation, interlocking with and adjacent ligand in a motif that resembles a paddle-wheel. In addition, the aforementioned flanking groups, reside above and below the carbazole core plane. The distance between said moieties is within range of π-π stacking interactions.[83] This conformation is very similar to the one found in closely related Group 12, naphthyl-substituted, *m*-terphenyl homoleptic complexes.[179] The distance V1–N1 in **31** [2.070(15) Å] is longer than the equivalent measurement found in the heteroleptic V(II)-carbazolido complex, [V(carbazole)$_2$(NMe$_2$)$_2$] (1.930(10) Å), previously reported by Vendier *et al.*, used in the catalytic hydroamination of alkynes.[180]

Bond Length (Å)		Bond Angle (°)	
V1–N1	2.07(2)	N1–V1–N2	87.3(3)
V1–N2	2.16(2)	N2–V1–N2′	174.6(6)
V1–N2′	2.16(2)	N1–V1–N1′	180.0(8)
C7–N2′	1.30(2)		

*Table 4.5.8 Selected bond lengths and angles for **31**.*

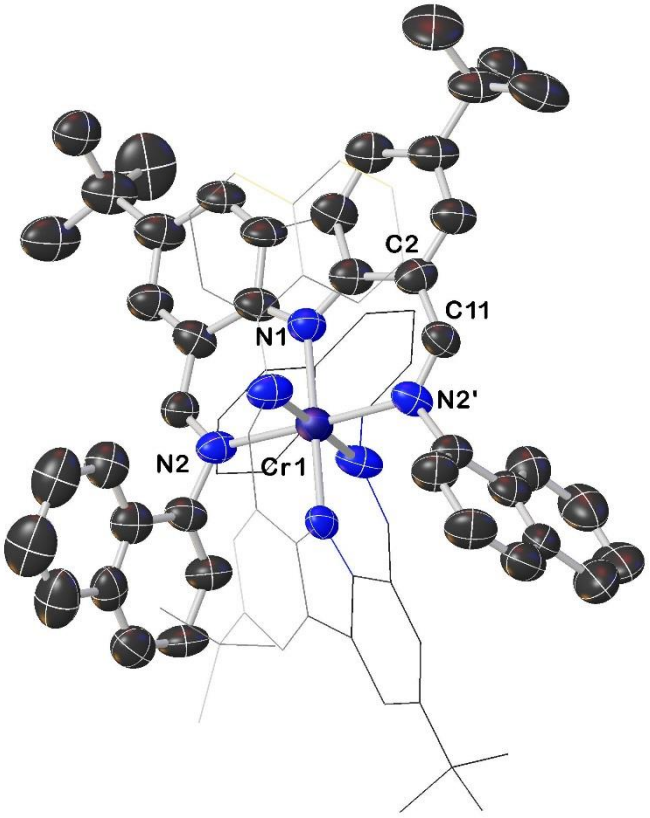


*Figure 4.5.8 Molecular structure for the symmetric unit of **32**, with displacement ellipsoids set at 50% probability level. Hydrogen atoms have been omitted, with a second carbazolido ligand presented in wireframe form for clarity.*

Bond Length (Å)		Bond Angle (°)	
Cr1–N1	2.007(2)	N1–Cr1–N2	89.1(3)
Cr1–N2	2.08(2)	N2–Cr1–N2’	178.3(7)
Cr1–N2’	2.08(2)	N1–Cr1–N1’	180.0(2)
C11–N2	1.27(2)	C2–C11–N2’	127.6(13)

*Table 4.5.9 Selected bond lengths and angles for **32**.*

The solid state structures of Cr(II) and Ni(II) complexes **32** and **33** are isomorphous and isostructural to **31** (Figure 4.5.8 and Figure 4.5.9), forming six-coordinate, octahedral metal centres. The plane twist angle between the best mean plane generated by the two carbazolido ligands is 92.2(9)° in **32**, with an equivalent angle of 94.09(11)° in **33**.

The Cr1–N1 distance in **32** [2.0066(17) Å], is shorter than the analogous distance found in *N*-pyrrolidinyl substituted, cyclopentadienylchromium(III) complexes [(cyclo-C_4H_8N-C_2H_4-C_5H_4)$CrCl_2$], reported by Verhovnik *et al*. [2.125(3) Å, 2.175(2) Å and 2.175(4) Å], that have been found to be catalytically active in the polymerisation of alkenes,[181] while the analogous distance Ni1–N1 [1.980(2) Å] in **33**, is longer than the one found in heteroleptic Ni(II)-carbazolido complexes, like [Cp^NNiL] (Cp^N = [2-(N,N-dimethylamino)eth-1-yl]cyclopentadienyl; L = carbazolato) [N1–N1 = 1.898(5) Å].[182,183]

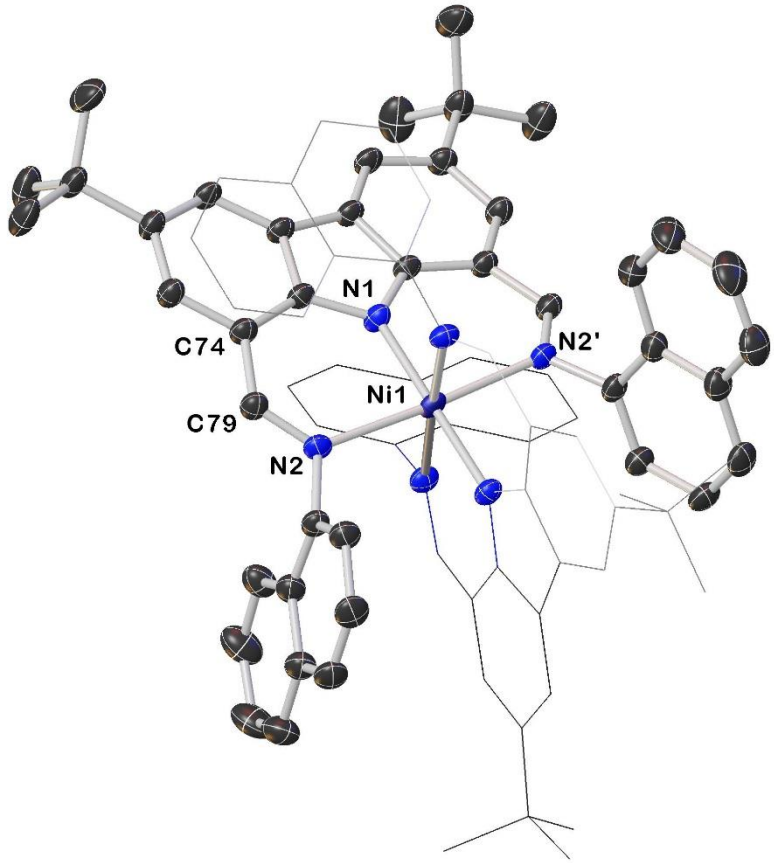


*Figure 4.5.9 Molecular structure for the symmetric unit of **33**, with displacement ellipsoids set at 50% probability level. Hydrogen atoms have been omitted, with a second carbazolido ligand presented in wireframe form for clarity.*

	Bond Length (Å)		Bond Angle (°)
Ni1–N1	1.980(2)	N1–Ni1–N2	88.27(4)
Ni1–N2	2.217(2)	N2–Ni1–N2’	176.53(9)
Ni1–N2’	2.217(2)	N1–Ni1–N1’	180.0(12)
C79–N2	1.292(2)	C74–C79–N2	125.1(2)

*Table 4.5.10 Selected bond lengths and angles for **33**.*

Similarly, and although alike in structure to **31**-**33**, in the solid state, **34** crystallises in the $P2_1/c$ space group (Figure 4.5.10). Contrary to the lighter analogues (**31**-**33**), this homoleptic complex does not reside in a special position. As a consequence, one whole molecule occupies the asymmetric unit. In accordance with the previous structures, the complex describes a six-coordinate homoleptic copper centre, with two interlocked ligands. Additionally, the plane twist angle between the best mean plane generated by the two ligands (70.268(7)°), is comparatively smaller than the equivalent angle found in **31**-**33** (*ca.* 90°). The distance Cu1–N1 in **34** [1.919(8) Å], is shorter than the analogous distance found in Cu(II)-porphyrin systems (1.992(5) Å–2.053(5) Å].[184]

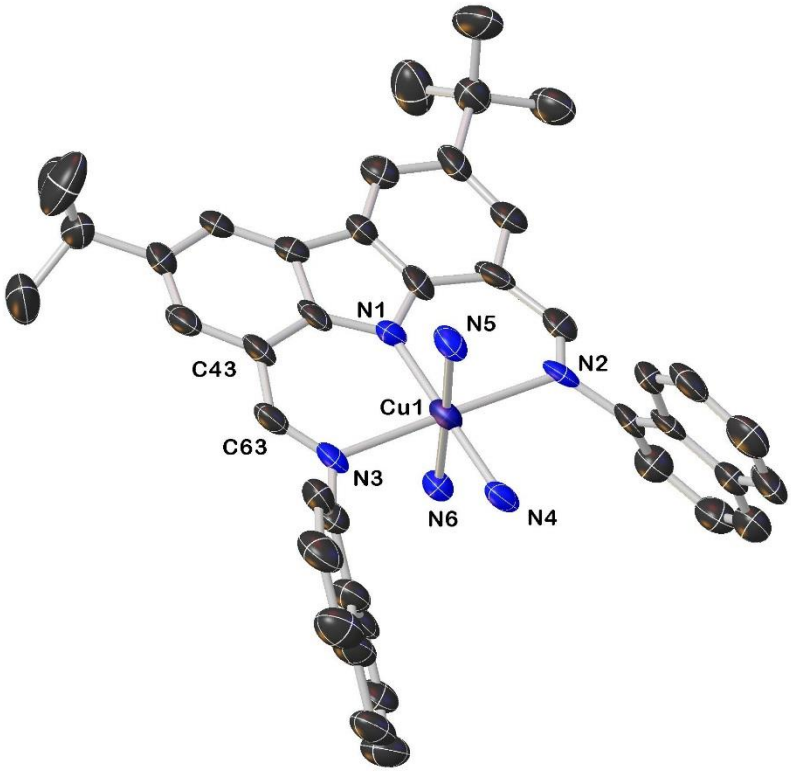


*Figure 4.5.10 Molecular structure of **34**, with displacement ellipsoids set at 50% probability level. Hydrogen atoms have been omitted, with the second carbazolido ligand connected via N4-N5-N6 also omitted for clarity.*

The carbazolido-nitrogen distances Cu1–N1 and Cu1–N4 in **34**, are similar [1.919(8) Å and 1.906(8) Å, respectively], with analogous measurements of the bond lengths arising from the flanking aldimines to the metal centre (N2-N3 and N5-N6), evidencing dissimilar coordination environments [Cu1–N2 = 2.360(9) Å / Cu1–N3 = 2.321(8) Å / Cu1–N5 = 2.346(7) Å / Cu1–N6 = 2.328(7) Å]. The equivalent measurements in **31**-**33** remain constant with the corresponding opposing ligand, due to symmetry operations; a characteristic that **34** does not posses. It is conceivable that these differences are merely a consequence of crystal packing. However, there are examples in which similar variations have been observed in octahedral d^9 Cu(II)-species. In such cases, the disparity in binding distances on equivalent ligands, has been attributed to the required distortion of the system to remove the orbital degeneracy present in such six-coordinate centres (Jahn-Teller distortion), with similar observations noted in octahedral Cu(II)-complexes coordinated by bipyridine, 1,10-phenanthroline and pyridine-*N*-oxides.[185,186]

	Bond Length (Å)		Bond Angle (°)
Cu1–N1	1.919(8)	N1–Cu1–N2	91.1(3)
Cu1–N2	2.360(9)	N2–Cu1–N3	178.4(3)
Cu1–N3	2.321(8)	N1–Cu1–N4	179.0(4)
C63–N3	1.28(2)	N5–Cu1–N6	178.8(3)
Cu1–N4	1.906(8)	C43–C63–N3	127.1(10)
Cu1–N5	2.346(7)		
Cu1–N6	2.328(7)		

*Table 4.5.11 Selected bond lengths and angles for **34**.*

4.5.2.4.1 Structural Comparison of the Homoleptic First Row Transition-Metal Complexes

Unlike the heteroleptic complexes **26**-**28**, which present different coordination environments and structures (*vida supra*), the solid state determinations of the homoleptic complexes **31**-**34** present almost identical motives. Three of these compounds (**31**-**33**) crystalise in the same space group (*P*2/n), with very similar unit cells; with the noticeable exception of the crystal structure of **34** ($P2_1/c$). Similarly, it would appear to be a consistent shortening of the bond, between the central carbazolido-nitrogen and the metal centre, alike of **26**-**28**, when going from left to right in the period [M1–N1, M = V (**31**) 2.070(15) Å, Cr (**32**) 2.007(2) Å, Ni (**33**) 1.980(2) Å]; with the exception of the Cu(II)-

complex **34**, with equivalent distances of 1.919(8) Å and 1.906(8) Å. However, this trend is not respected when comparing the distance between the metal centre and the flanking iminic-nitrogens [M1–N2, M = V (**31**) 2.158(13) Å, Cr (**32**) 2.083(10) Å, Ni (**33**) 2.217(2) Å, Cu (**34**) 2.360(9) and 2.321(8) Å]. Additionally, and as a consequence of the symmetry of these structures, the plane twist angles generated by the two opposing carbazolido rings, only drastically varies from close to ortogonality in the structure of **34** [$N1_{plane}$–N'_{plane}. = 93.5(10)° (**31**) ≈ 92.2(9)° (**32**) ≈ 94.09(11)° (**33**) > 70.268(7)° (**34**)]. In all cases, the metal centre occupies the best mean plane generated by the two carbazolido ligands.

M=	V (**31**)	Cr (**32**)	Ni (**33**)	Cu (**34**)
M1–N_{carb}	2.070(15)	2.007(2)	1.980(2)	1.919(18)/1.906(8)
M1–N_{imine}	2.158(13)	2.083(10)	2.217(2)	2.360(9)/2.321(8) 2.346(7)/2.328(7)
N_{carb}–M–N_{carb}	180.0(8)	180.0(2)	180.0(12)	179.0(4)
N_{imine}–M–N_{imine}	174.6(6)	178.3(7)	176.53(9)	178.4(3)/178.8(3)
N_{plane}–N_{plane}	93.5(10)	92.2(9)	94.09(11)	70.268(7)

*Table 4.5.12 Selected bond lengths (Å) and angles (°) for **31**-**34**. [N_{carb} = carbazolido nitrogen; N_{imine} = opposing flanking iminic nitrogen(s); N_{plane}–N_{plane} = plane twist angle between the two carbazolido ligands].*

4.5.2.4.2 First Row Transition-Metal Complexes -Homoleptic vs. Heteroleptic-

As noticed so far in this chapter, it has been our aim to preferentially and selectively form heteroleptic complexes using proligand **6**. To this effect, several precautions were taken during the synthesis. In all cases, the first row transition-metal(II) halides employed were used in a stoichiometric excess with respect to the ligand employed, using a soluble salt of the metal of interest, and by slow drop-wise addition of the deprotonated ligand to the solution of the metal halide. With this considered, it was postulated that there would be an excess of metal-halide to proligand at all times, ensuring selective formation of a heteroleptic complex. Noticeably, and as described above (*vida supra*), it was only possible to authenticate the formation of three heteroleptic complexes following this methodology (**26**-**28**). These metals reside almost in the middle of their period, bisecting on both ends with elements that yielded solely homoleptic systems (**31**-**34**).

It is difficult to unequivocally determine the apparent preference of the early- and late-transition-metals for this series, to form six-coordinate compounds, or the apparent greater stability of the middle transition-metals, to only be substituted once.[187] This could be dependant on the differing electrophilicity of the metal(II) centres,[158] their size,[188] or the energy required to break the metal-halide bond *vs.* the stability of the resulting product.[189] In terms of the latter, and strictly speaking, it would be interesting to see if noticeable differences could be observed, by only varying the metal centre, which would strictly involve the use of metal(II)-salts with the same halide for synthesis, in all cases.

4.5.2.4.3 Magnetic Moment Determinations

Having crystallographically authenticated the solid state structures of compounds **26**-**33**. It was of interest to determine the magnetic moment of these compounds in solution. To this effect, the Evans Method was employed, and the values obtained for compounds **26**-**33** are presented below (Table 4.5.13).[382]

Table 4.5.13 Magnetic moments obtained via the Evans Method.

Compound	Magnetic Moment (μ_B)[a)]
26	3.33
27	2.92
28	3.64
29	1.58
30	2.77
31	1.96
32	3.15
33	2.09

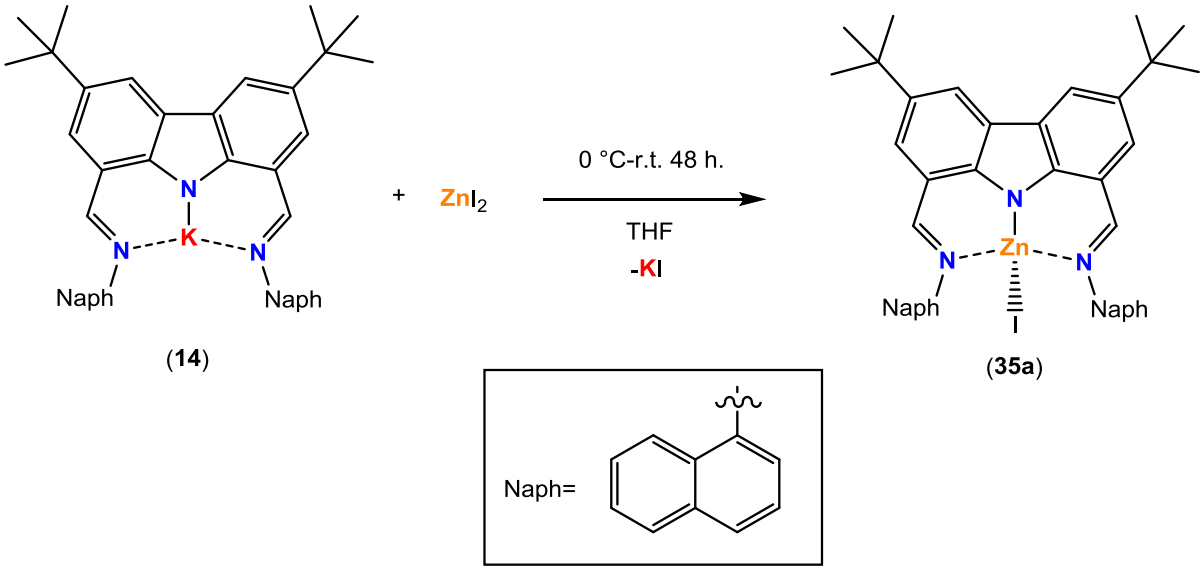
[a)] Calculated at 25 °C, *via* the Evans Method.[382]

The magnetic moment values obtained, differ from those expected, for the idealised geometries described in the crystal structures. As such, certain considerations should be mentioned, regarding the way these values have been determined. These include, that the averaged values hereby described, are the consequence of at least three determinations

per compound. In all cases, samples of known concentration were prepared in C_6D_6, procuring not to saturate the solution (heterogeneous samples). Additionally, these measurements rely heavily on the crystallographic determinations, both for the value related to the accurate mass of the compound of interest, and in terms of the molecular orbital diagram as a consequence of the geometry of the metal centre (in addition to preferences between high spin *vs.* low spin). Since the Evans method is a determination that occurs in solution, there is a chance that these values do not directly correlate with similar determinations in the solid state. As such, the values depicted in Table 4.5.13, should only be considered as an initial step in the characterisation of the magnetic moment of these compounds. Additional corroboration of these magnitudes by SQUID measurements should be carried out, in case of requiring a more thorough study of the magnetic properties of compounds **26**-**33**.

4.5.3 Metathesis Reactions with Group 12 Metal(II) Salts

4.5.3.1 Synthesis of [Naph$_2$carbZnI] and [(Naph$_2$carb)$_2$Zn]

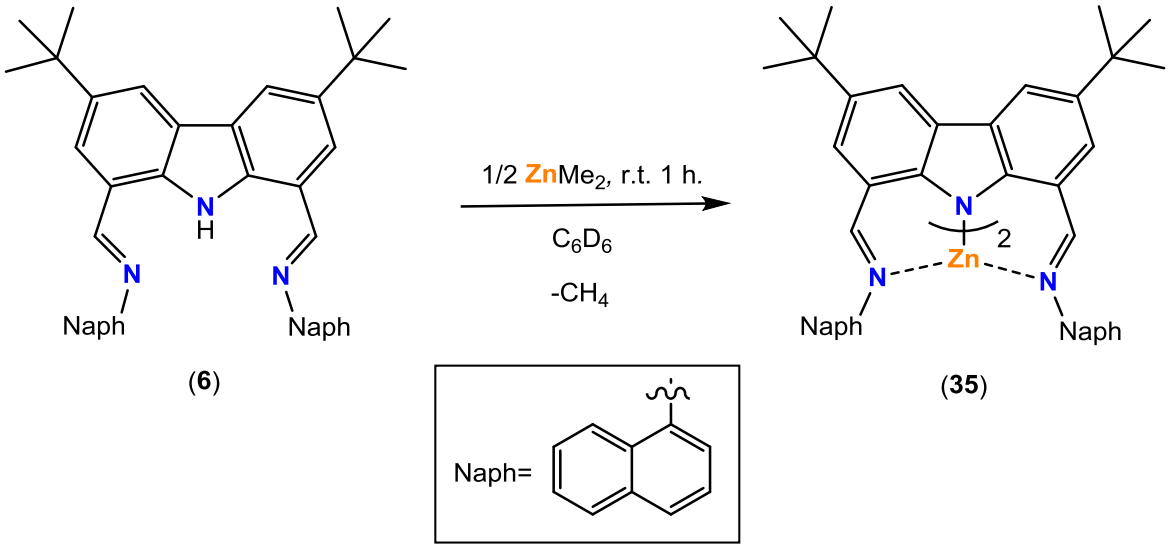


*Scheme 4.5.10 Attempted synthesis of **35a**.*

Attempts towards the formation of group 12 complexes with proligand **6**, relied initially in the *in situ* generation of the corresponding potassium salt **14**, with an excess of KH, using THF as the solvent. Starting with the formation of a heteroleptic zinc complex *via* salt

metathesis with ZnI_2 at low temperature allowed the formation of an orange suspension ([$Naph_2carbZnI$] **35a**) (Scheme 4.5.10). Removal of volatiles *in vacuo* and extraction into hexane allowed purification of the resulting bright orange-red powder. ^{1}H and $^{13}C\{^{1}H\}$ NMR spectra of the product formed through this method, denoted full conversion of the potassium salt (**14**) to a single compound without any evidence of the presence of remaining proligand (**6**). Several attempts at growing crystals of the suspected heteroleptic complex, however, were encumbered by the recurring presence of a black film forming on the walls of the Schlenk flask upon extraction into hexane. It is speculated to correspond with a decomposition pathway in which the metal centre becomes reduced to zinc metal (Schlenk equilibrium).[190,191]

Despite this, attempts at generating a zinc-bearing compound with this ligand were followed in accordance with an organoelimination reaction ([$(Naph_2carb)_2Zn$] **35**) (Scheme 4.5.11), resembling a synthetic procedure, employed in the comparative formation of Group 2 compounds **24** and **24a**.



*Scheme 4.5.11 Synthesis of **35**.*

As such, the proligand **6** was reacted with half an equivalent of $ZnMe_2$, at room temperature employing C_6D_6 as solvent. Previous reports in this area, have used a similar methodology to access polymetallic, guanidinate-based complexes, such as $[Zn\{Me_2NC(N^iPr)_2\}Me]_2$.[192] Upon doing this, instantaneous change in colouration from the characteristic bright yellow of **6** to an intense orange, was observed. Characterisation of the resulting reaction mixture by ^{1}H and $^{13}C\{^{1}H\}$ NMR spectroscopy revealed full

disappearance of the signals attributed to **6**. Additionally, the presence of any remaining, unreacted $ZnMe_2$ could be ruled out by means of the characteristic signals for the substituted methyl groups. The data suggested a double substitution on the metal centre had taken place, according with the stoichiometry employed (**35**). Shortly after reaching completion, orange crystals of **35**, suitable for X-ray diffraction were observed growing upon exposure to hexane vapours.

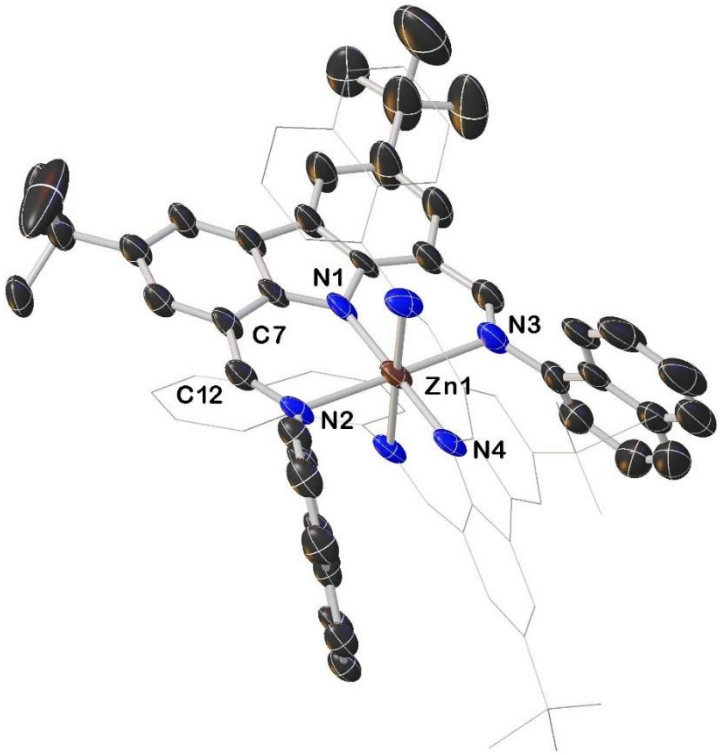


*Figure 4.5.11 Molecular structure of the symmetric unit of **35**, with displacement ellipsoids set at 50% probability level. Hydrogen atoms have been omitted, with a second carbazolido ligand presented in wireframe form for clarity.*

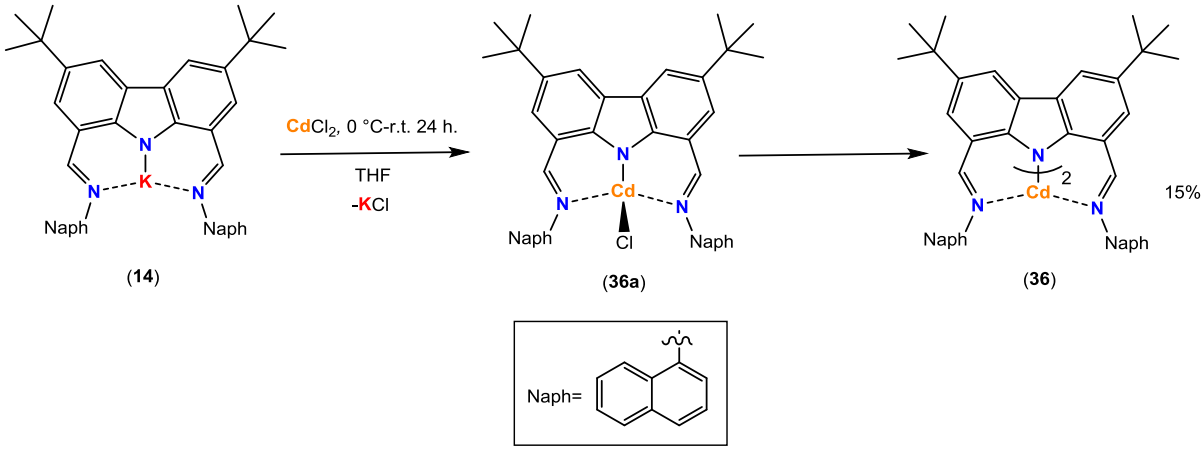
Consistent with the stoichiometry utilised, the solid state determination of **35**, evidenced the formation of a six-coordinate homoleptic complex; with half a molecule occupying the asymmetric unit (Figure 4.5.11). The coordination around the metal centre is equivalent to the structures of first row transition–metal complexes **31**-**34**. With the plane twist angle between the best mean plane generated by the two ligands in **35**, being closely related to the comparatively smaller angle found in the analogous copper compound **34**, (77.1(7)°). The distance Zn1-N1 [1.941(8) Å] in **35**, is similar to the one found in closely related nitrogen-substituted zinc complexes $[Zn\{(Me_3Si)_2NC(NCy)\}_2]$ and $[Zn\{Me_2NC(N^iPr)_2\}Me]_2$ [2.011(2) Å–2.201(3) Å],[192] while also longer than the equivalent measurement found in the homoleptic carbazolido complex $[(^tBu_4carbazole)_2Zn]$ [1.867(3) Å–1.887(3) Å].[46]

	Bond Length (Å)		Bond Angle (°)
Zn1–N1	1.941(8)	N1–Zn1–N2	88.8(3)
Zn1–N2	2.364(8)	N2–Zn1–N3	178.4(3)
Zn1–N3	2.343(9)	N1–Zn1–N4	179.7(6)
C12–N2	1.304(11)	C7–C12–N2	123.5(9)

*Table 4.5.14 Selected bond lengths and angles for **35**.*

4.5.3.2 Synthesis of [Naph$_2$carbCdCl] and [(Naph$_2$carb)$_2$Cd]

Following a metathetical pathway, and looking to access the heavier Group 12 congeners, this protocol was repeated by reacting the potassium salt **14** with $CdCl_2$ in THF. By doing this, a dark yellow-orange solid could be isolated (Scheme 4.5.12). Spectroscopic characterisation of the isolated product in C_6D_6 confirmed the formation of a new diamagnetic product by ^{1}H and $^{13}C\{^{1}H\}$ NMR spectroscopies. However, a $^{113}Cd\{^{1}H\}$ NMR resolved two main signals, one intense peak found at 655 ppm, with a comparatively less intense signal found at 509 ppm. The aforementioned signals observed in the $^{113}Cd\{^{1}H\}$ spectrum have been assigned to correspond to a mixture of homoleptic (**36**) and heteroleptic (**36a**) species, with the homoleptic component being in greater proportion. These assignments follow similar reports in this area, from which a consistent change in chemical shift towards downfield has been observed upon increase in the coordination number.[193,194]



*Scheme 4.5.12 Formation of complex **36a**, and further conversion to **36**.*

Exemplyfing this are the $^{113}Cd\{^{1}H\}$ NMR chemical shifts of several crystallographically authenticated Cd(II) centres. Formally two-coordinate [(tetra-*tert*-butyl-carbazole)$_2$Cd],[46]

presents a peak in the $^{113}Cd\{^{1}H\}$ NMR spectrum at 76 ppm, with monomeric two coordinate species $Cd[N(SiMe_3)]_2$ and $Cd[N(SiPhMe_2)_2]_2$ exhibiting resonance peaks at 294 ppm and 264 ppm, respectively.[193] While studies on the cadmium-metalloporphyrin Cd(TPP) [TPP = $\alpha\beta\gamma\delta$-tetraphenylporphyrin] have found analogous values at 413 ppm (four-coordinate) and 429 ppm (six-coordinate), upon additional coordination of dioxane on axial positions.[194] As such, it is expected that the difference between the two signals observed for **36** and **36a**, directly follows their dissimilar coordination geometries [four-coordinate **36a** (509 ppm) *vs.* six-coordinate **36** (655 ppm)] (Scheme 4.5.12). Following synthesis, crystals suitable for X-ray diffraction were grown from a concentrated hexane extract.

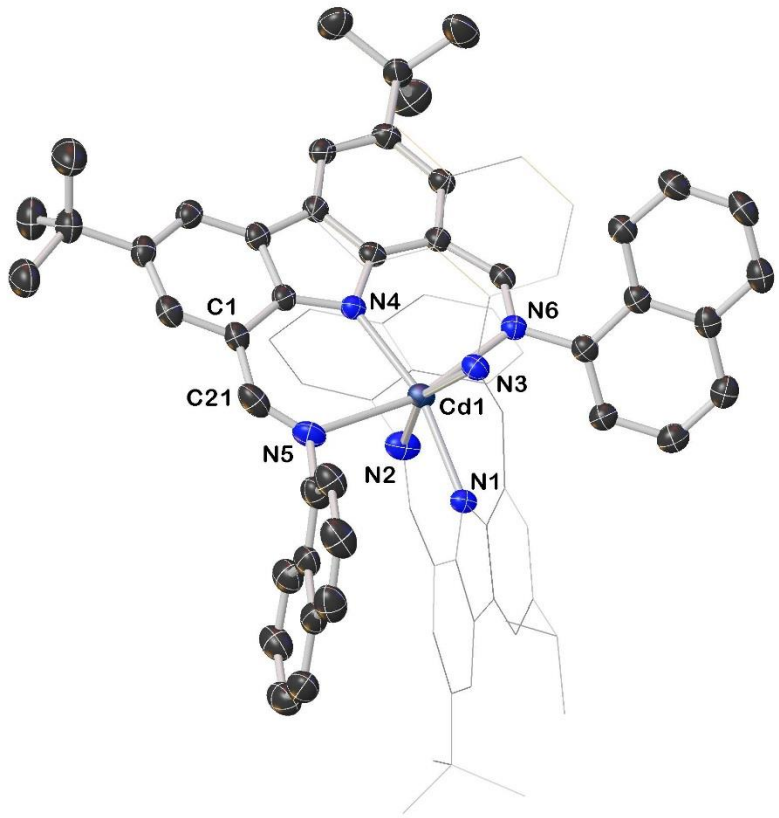


*Figure 4.5.12 Molecular structure for the symmetric unit of **36**, with displacement ellipsoids set at 50% probability level. Hydrogen atoms have been omitted, with a second carbazolido ligand presented in wireframe form for clarity.*

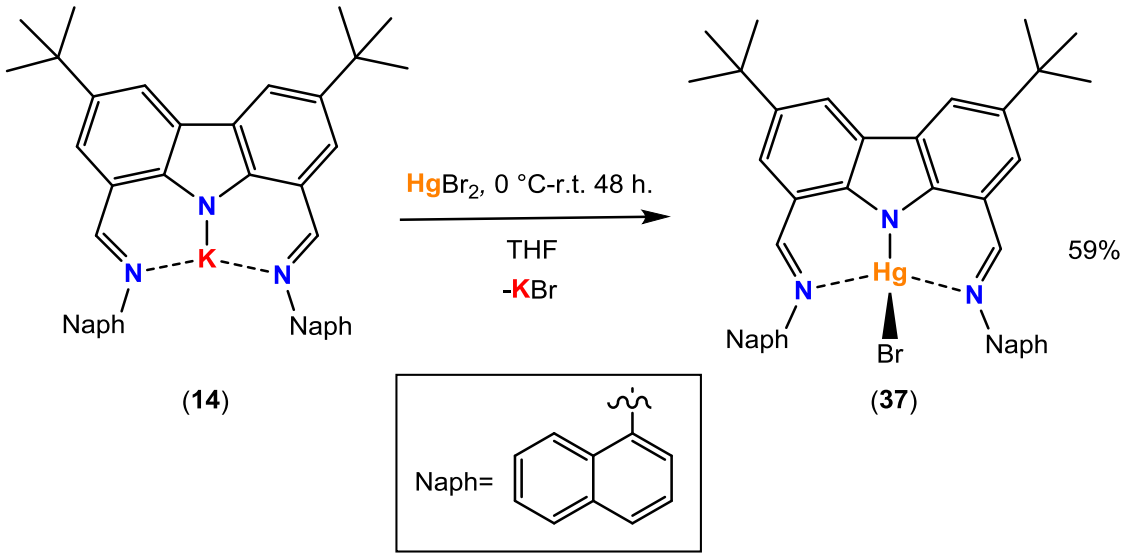
	Bond Length (Å)		Bond Angle (°)
Cd1–N1	2.216(3)	N1–Cd1–N2	82.04(10)
Cd1–N2	2.466(3)	N2–Cd1–N3	161.31(10)
Cd1–N3	2.459(3)	N1–Cd1–N4	163.57(9)
Cd1–N4	2.221(3)	N1–Cd1–N3	83.75(9)
Cd1–N5	2.537(3)	N5–Cd1–N6	164.08(9)
Cd1–N6	2.418(3)	N4–Cd1–N3	108.32(9)
C21–N5	1.238(5)	C1–C21–N5	127.6(3)

*Table 4.5.15 Selected bond lengths and angles for **36**.*

In line with our determinations by $^{113}Cd\{^{1}H\}$ NMR spectroscopy, the solid state structure evidenced the formation of a six-coordinate homoleptic complex; with a molecule occupying the asymmetric unit ([(Naph$_2$carb)$_2$Cd] **36**) (Figure 4.5.12). The coordination around the metal centre is consistent with the structures of homoleptic compounds **31**-**34**. With a comparable plane twist angle between the best mean plane generated by the two ligands in **36** [95.01(13)°], found to be closely related to ones found in the analogous complexes **31**-**33**,. Differentiating from other homoleptic complexes, such as **35**, synthesised employing this ligand, the two carbazolido ligands are not periplanar to each other; formally describing the cadmium centre as a distorted octahedron [*e.g.* N1–Cd1–N4 = 163.57(9)° and N2–Cd1–N3 = 161.31(10)°]. This is most likely a consequence of the presence of a bigger metal centre being coordinated. The distances Cd1–N1 [2.216(3) Å] and Cd1–N4 [2.221(3) Å], are longer than the ones found in closely related homoleptic complexes such as (^{t}Bu$_4$carbazole)$_2$Cd [2.107(4) Å and 2.117(4) Å], and metalloporphyrine complex [Cd(TPP)·2Dioxane] [TPP = *αβγδ*-tetraphenylporphyrin] [2.10(1) Å to 2.18(1) Å].[46,194]

Further NMR characterisation of isolated crystals of **36**, evidenced further changes in the $^{113}Cd\{^{1}H\}$ NMR, consistent with the disappearance of the peak at 509 ppm, which suggests decomposition/conversion of **36a** to its homoleptic counterpart **36** (six-coordinate compound, with a change in chemical shift moving downfield). As such, it is presumed that under the metathesis reaction conditions described above (excess of $CdCl_2$), the formation of a heteroleptic complex is first accomplished (**36a**). Studies seeking to determine the stability of **36a** in solution found that this species is not long lived, furtherly converting to **36** in the span of two weeks, most likely a consequence of Schlenk equilibrium.

4.5.3.3 Synthesis of [Naph$_2$carbHgBr]



*Scheme 4.5.13 Synthesis of heteroleptic, mercury compound **37**.*

Aiming to extend the study to a mercury bearing compound, a metathesis reaction was attempted employing $HgBr_2$ (Scheme 4.5.13). The dark red solution of the *in situ* generated potassium salt **14**, was reacted at 0 °C with a colourless solution of $HgBr_2$ in THF. By doing so, the immediate precipitation of a dark yellow solid was observed ([Naph$_2$carbHgBr] **37**). Full NMR characterisation of the isolated dark yellow-brown solid obtained from the reaction indicated the formation of a new compound. In parallel, a $^{199}Hg\{^1H\}$ NMR spectrum of **37**, demonstrated a peak at –1353.45 ppm. The sole resonance peak found for **37**, is similar to those reported for amine-mercuric chloride(II) complexes such as $[(CH_3(CH_2)_3NH_2]_2HgCl_2$, $[(CH_3)_3CNH_2]_2HgCl_2$, $[(CH_3)_2NH]HgCl_2$ and $[Ph(CH_2)NH(CH_3(CH_2)_3)]HgCl_2$, with values of –1242 ppm, –1252 ppm, –1301 ppm and –1341 ppm, respectively.[195,196]

Following this methodology, **37** could be isolated in good yield (59%) and crystals suitable for solid state determinations were grown from a saturated hexane solution, at room temperature.

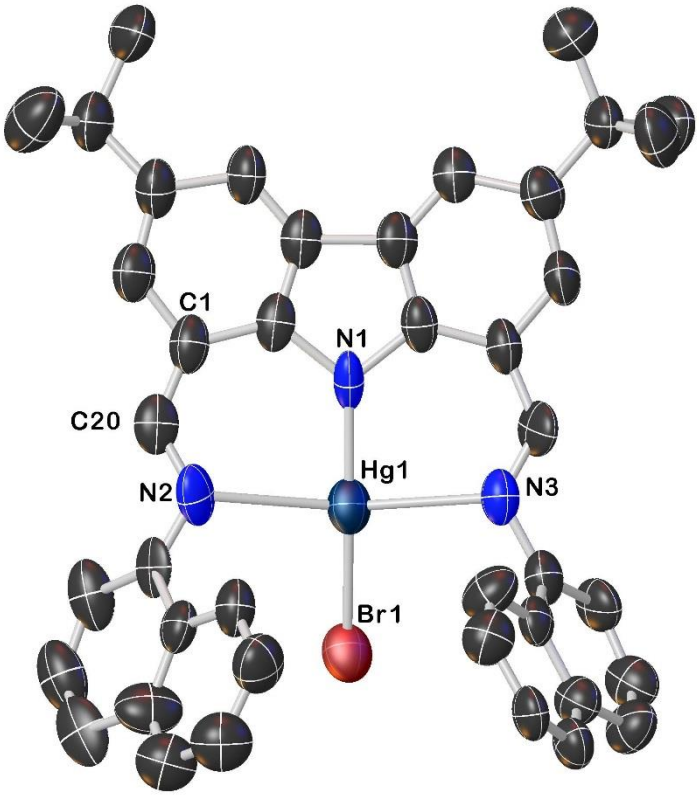


*Figure 4.5.13 Molecular structure for one of the crystallographically independent molecules of **37**, with displacement ellipsoids set at 50% probability level; hydrogen atoms have been omitted for clarity.*

In the solid state, **37** is monomeric, with two crystallographically independent heteroleptic molecules in the asymmetric unit, lying on an inversion centre (Figure 4.5.13). The coordination sphere of the metal centre is completed by one molecule of the tridentate carbazolido ligand and a bromide. The compound exhibits the flanking naphthyl groups in a *syn* conformation; with the metal centre presenting a distorted square planar geometry (τ_4' = 0.21).[156] The distances Hg1–N1 [2.08(2) Å] and Hg1–Br1 [2.423(3) Å], are shorther than the equivalent lengths measured for Hg(II)-quinquedentate complexes, supported by macrocyclic Schiff base ligands, such as $[HgL(Br)]_2[Hg_2Br_6]$ (L = 2,6-diacetylpyridine(imine)-4,7-diazadecane-1,10-diamine) {Hg1–Br1 = 2.565(5) Å and Hg1–N1 = 2.44(3) Å}.[197]

Bond Length (Å)		Bond Angle (°)	
Hg1-N1	2.08(2)	N1-Hg1-Br1	172.1(6)
Hg1-N2	2.51(2)	N2-Hg1-N3	143.0(6)
Hg1-N3	2.62(2)	N2-C20-C1	126(2)
Hg1-Br1	2.423(3)		
C20-N2	1.30(2)		

*Table 4.5.16 Selected bond lengths and angles for **37**.*

4.5.4 Metathesis Reactions with Group 13 Metal(III) Salts

4.5.4.1 Introduction to Hypervalency

So far in this Chapter, it has been the main objective to synthesise and stabilise low-coordinate metal complexes, with the eventual use of these highly reactive centres in catalysis and small molecule activation. However, this approach is not the only path that enables the exploration of these kind of reactivities. A parallel area of research, from which a great number of pincer complexes have been used is hypervalency. Hypervalent compounds can be seen as S_N2 transition states, and are defined as main group metal element (s and p block; Group 1, 2 and 13-18) compounds that contain a formally assignable number of electrons (*N*), greater than the octet in the valence shell, directly associated with an atom (*M*), that is directly coordinated/bound to a number (*L*) of ligands.[198] The nomenclature employed, [*N*-*M*-*L*], allows the designation and classification of hypervalent structures, from which trigonal bipyramidal, square pyramidal and octahedral are the most typical arrangements found.[199] This increasing interest in hypervalent/hypercoordinated compounds is derived initially on their structural peculiarities, but it has also been expanded on the basis of their reactivity, from which numerous organic reactions are known to involve intermediates of greater coordination number.[200,201]

In the particular case of hypervalent Group 13 compounds, the first crystallographically characterised, example to feature boron was reported by Akiba *et al*., and made use of the sterically rigid, oxygen-based ligand 1,8-dimethoxy-9-anthracene (Figure 4.5.14).[202] Since then, a handful of additional hypervalent boron compounds have been reported, all of which have incorporated pincer-type ligands.[203–208] In recent years, further efforts have

been extended to the use of nitrogen-donor systems, which have included flanking primary amines, pyrimidine and pyridine; all of which have allowed structural authentication of the formation of hypervalent boron centres.[207,208]

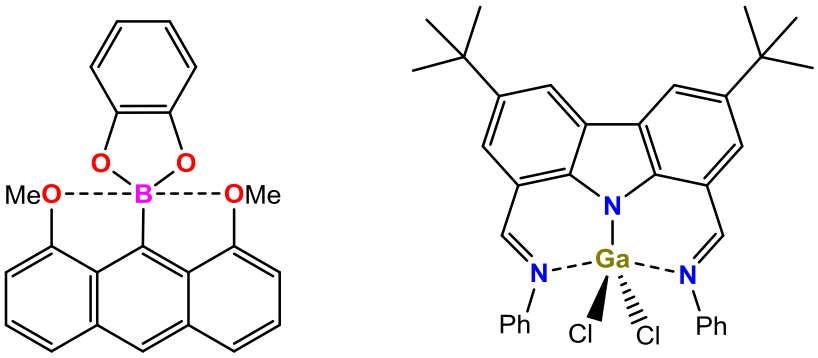
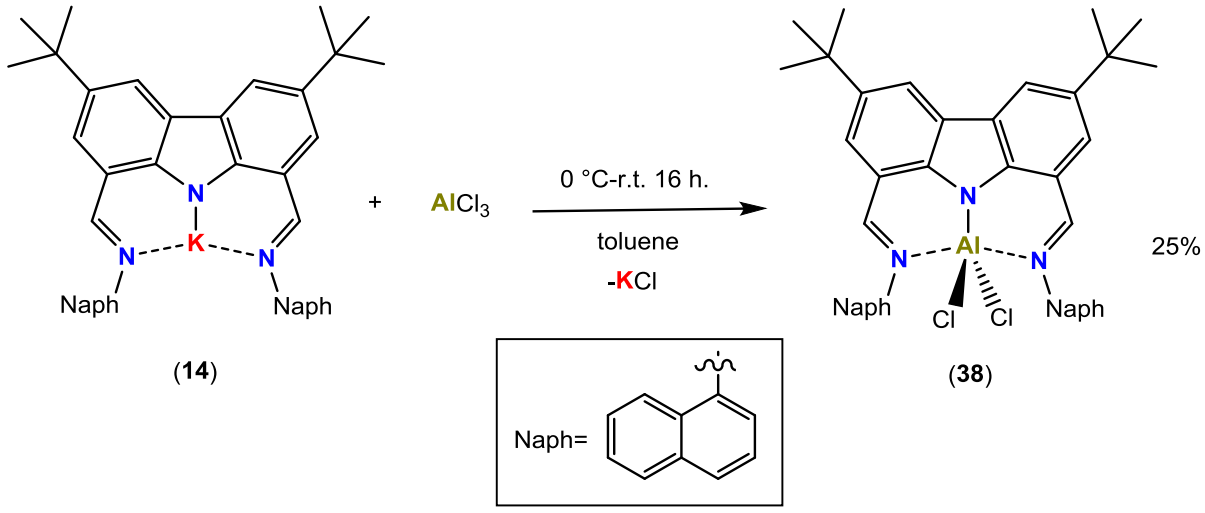


Figure 4.5.14 Structure of the first authenticated hypervalent boron [10-B-5] complex (left) and previous work in the Kays group, on the first hypervalent carbazolyl gallium complex [10-Ga-5] (right).

Previous work in the Kays group,[81] has taken notice of the similarities between Gibson's trigonal bipyramidal carbazolyl complex [1,8-Diphenylimino-3,6-dimethylcarbazolide]$FeCl_2$,[51] and the geometry adopted by reported hypervalent Group 13 compounds, from which it has been possible to synthesise and structurally characterise the first example of a hypervalent five-coordinate carbazolyl gallium complex, supported by a 1,8-bis(imino)carbazolyl ligand (Figure 4.5.14).[81] Following these results, this section seeks to extend this study towards the formation of a new family of hypervalent Group 13, carbazolyl complexes.

4.5.4.2 *Synthesis of [Naph$_2$carbAlCl$_2$]*

Although examples of hypervalent boron compounds are reported in the literature, there is still a limited number of examples in which similar structures have been authenticated for the heavier congeners of the group. In the particular case of aluminium, there is only a small number of structures deposited in the CCDC (23 results representing five/six-coordinate aluminium(III); December 2018),[209] corresponding to hypervalent aluminium(III) species, with the majority of these relying on multiple *N*-based, primary/secondary amine donors.[210–212] Typical synthetic approaches rely either on coordination with a chelate, or by directly deprotonating a suitable *N*-based ligand with an organoaluminium compound such as $AlMe_3$, obtaining methyl-substituted aluminium compounds. In cases where the metal-halide substituted compounds are required, further substitution can be performed by reacting the methyl-bound compound with molecular iodine, with concomitant liberation of MeI.[213–215]



*Scheme 4.5.14 Synthesis of **38**.*

Aiming towards this, the formation of heteroleptic complexes bearing a Group 13(III) centre were initiated using $AlCl_3$ in a metathetical approach (Scheme 4.5.14). Thus, a metathesis reaction between the potassium salt **14** and the metal halide, at low temperature in a non-coordinating solvent such as toluene, yielded a bright orange-yellow suspension of [Naph$_2$carbAlCl$_2$] (**38**). Purification of the resulting dark brown-orange solid, isolated after removal of volatiles under vacuum, by dissolution in hexane, allowed full characterisation of the title compound. From a similar concentrated extract, it was possible to grow light yellow crystals of **38**, suitable for X-ray diffraction.

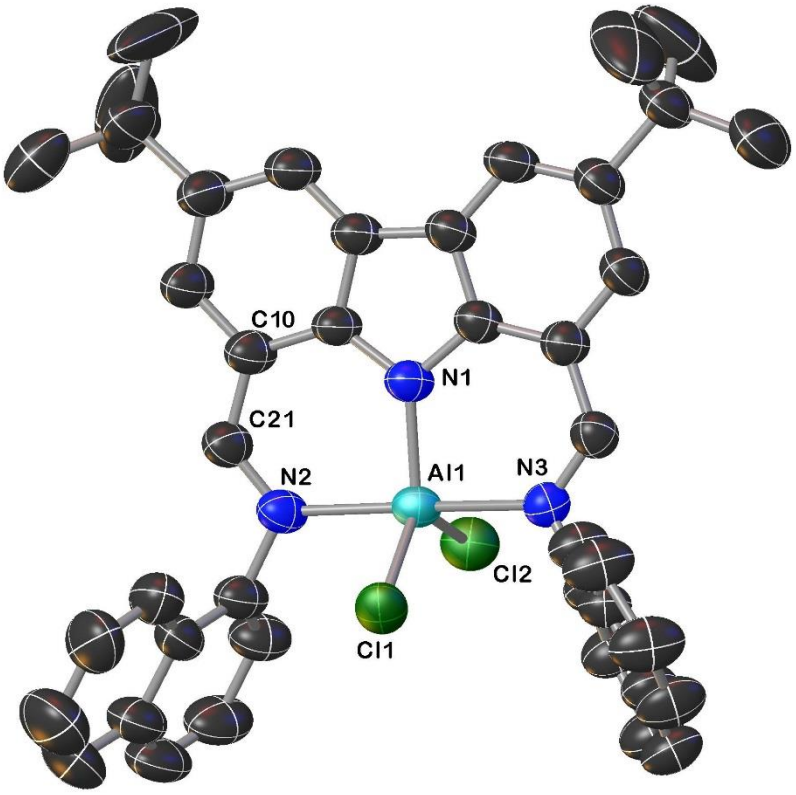


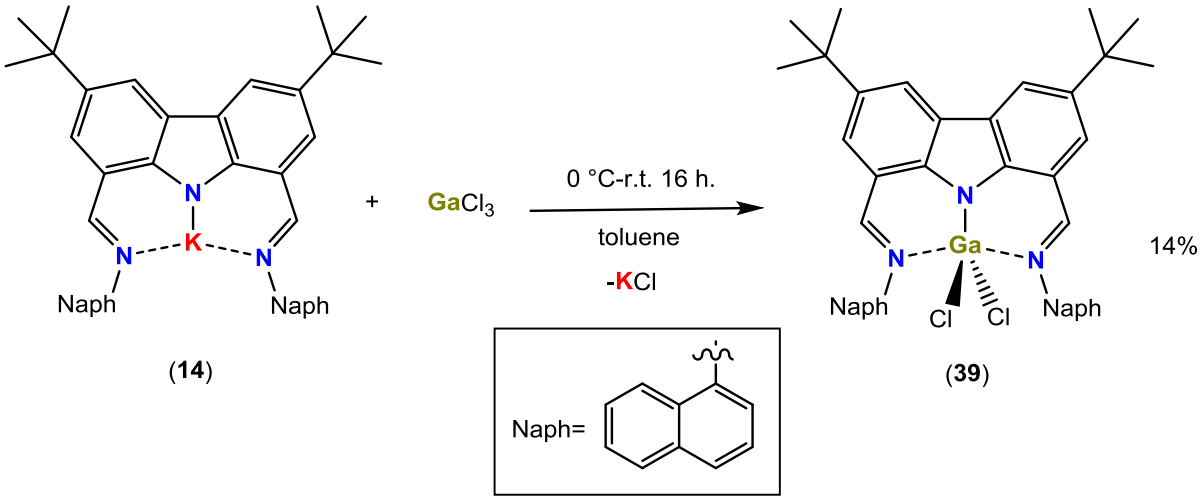
*Figure 4.5.15 Molecular structure for **38** [10-Al-5], with displacement ellipsoids set at 50% probability level, hydrogen atoms have been omitted for clarity.*

In the solid state **38**, crystallises in the $P2_1/c$ space group, with one molecule occupying the asymmetric unit (Figure 4.5.15). The coordination motif around the metal centre is five-coordinate (τ_5 = 0.78),[152] with three coplanar positions occupied by the tridentate ligand with two additional chlorides coordinated. Following the nomenclature described above, **38** is the first crystallographically authenticated hypervalent aluminium carbazolyl complex [10-Al-5]. The distance N1–Al1 [1.873(4) Å] in **38**, is within the range of analogous nitrogen bound, hypervalent aluminium centres, such as {[(^{i}PrNHCH$_2$CH$_2$)(^{i}PrNCH$_2$CH$_2$)N^{i}Pr]AlCl$_2$} [1.819(3) Å, 2.040(3) Å and 2.130(3) Å] and [Cl$_2$Al-C$_8$H$_{20}$N$_4$][Al(C$_4$H$_9$)$_2$] [1.953(3) Å, 2.032(3) Å, 2.018(3) Å and 1.954(3) Å], with the additional coordination of the two axial iminic-nitrogens (N2 and N3), also in agreement [N2–Al1 = 2.105 Å and N3–Al1 = 2.095(4) Å]. Comparatively, the distances Al1–Cl1 [2.1650(15) Å] and Al1–Cl2 [2.1726(16) Å], are shorter than those found in {[(^{i}PrNHCH$_2$CH$_2$)(^{i}PrNCH$_2$CH$_2$)N^{i}Pr]AlCl$_2$} [2.206(4) Å / 2.2548(4) Å] and [Cl$_2$Al-C$_8$H$_{20}$N$_4$][Al(C$_4$H$_9$)$_2$] [2.408(1) Å / 2.351(1) Å], indicative of a stronger metal-halogen bond in **38**.[210,212]

Bond Length (Å)		Bond Angle (°)	
Al1–Cl1	2.165(2)	N1–Al1–Cl1	127.5(2)
Al1–Cl2	2.173(2)	N1–Al1–Cl2	111.1(2)
Al1–N1	1.873(4)	N2–Al1–N3	174.4(2)
Al1–N2	2.105(4)	C10–C21–N2	124.6(4)
Al1–N3	2.095(4)		
C21–N2	1.284(6)		

*Table 4.5.17 Selected bond lengths and angles for **38**.*

4.5.4.3 Synthesis of [Naph$_2$carbGaCl$_2$]



*Scheme 4.5.15 Synthesis of **39**.*

Following the successful formation of a hypervalent aluminium centre (**38**), an analogous reaction was attempted with $GaCl_3$ (Scheme 4.5.15). As mentioned in the introduction to this section, previous work in the Kays group, has allowed the isolation of a five-coordinate 1,8-diphenylimino-3,6-di(*tert*-butyl)carbazolylgallium dichloride,[81] while comparable examples such as BPI-$GaCl_2$ [BPI= 1,3-bis(2-pyridylimino)isoindoline][216] (five-coordinate) and [1,8-Mes$_2$-3,6-Me$_2$carbazolyl)$GaCl_2$][128] (three-coordinate) are also known.

Similarly, the metathesis reaction between the potassium salt **14** and $GaCl_3$ was carried out at low temperature employing toluene, as the solvent. By doing so it was attempted to eliminate the possibility of the solvent competing for coordination sites, around the

metal centre. The resulting yellow-orange solid afforded from the crude reaction mixture, was extracted into hexane at room temperature; from which yellow-orange crystals could be isolated ([Naph$_2$carbGaCl$_2$] **39**). Crystals isolated from this extract allowed for characterisation of **39** in the solid state, with a yield of 14%.

In the solid state **39**, is isostructural and isomorphic to **38**, with one molecule occupying the asymmetric unit (Figure 4.5.16). The coordination geometry around the metal centre is five coordinate (τ_5 = 0.74),[152] with three coplanar positions occupied by the tridentate ligand with coordination of two additional chloride anions. Similar to the lighter congener, **39** can be described as [10-Ga-5], exhibiting very similar bond lengths/angles to those found in previously reported five-coordinate gallium compounds, such as BPI-GaCl$_2$ [BPI= 1,3-bis(2-pyridylimino)isoindoline]. The distances Ga1–N1 [1.915(3) Å], Ga1–N2 [2.164(3) Å] and Ga1–N3 [2.162(3) Å] in **39**, are similar to the equivalent distances found in BPI-GaCl$_2$ [1.9094(15) Å, 2.1083(15) Å and 2.1193(15) Å], and in the closely related [1,8-diphenylimino-3,6-di(*tert*-butyl)carbazolylgallium dichloride] [1.915(3) Å, 2.193(3) Å and 2.156(3) Å].[81,216]

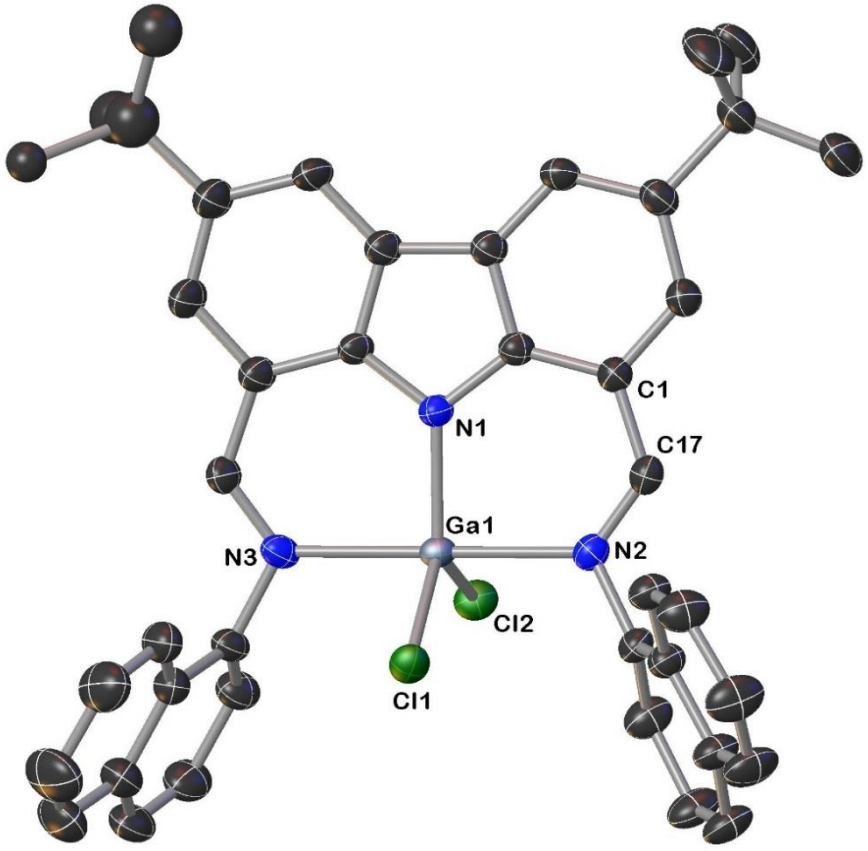
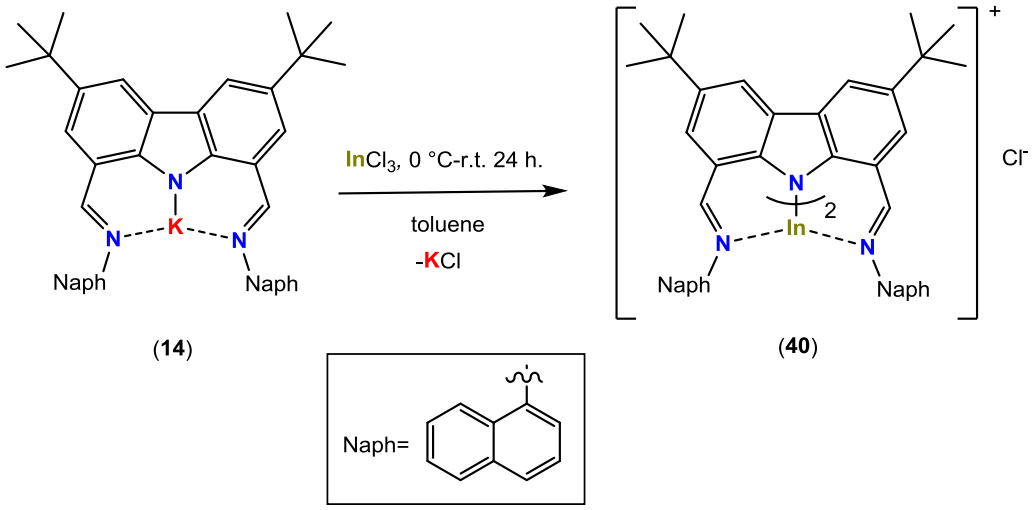


*Figure 4.5.16 Molecular structure for **39** [10-Ga-5], with displacement ellipsoids set at 50% probability level, hydrogen atoms have been omitted for clarity.*

	Bond Length (Å)		Bond Angle (°)
Ga1–Cl1	2.1982(10)	N1–Ga1–Cl1	128.77(11)
Ga1–Cl2	2.2034(10)	N1–Ga1–Cl2	111.78(10)
Ga1–N1	1.915(3)	N2–Ga1–N3	173.46(13)
Ga1–N2	2.164(3)	C1–C17–N2	125.2(4)
Ga1–N3	2.162(3)		
C17–N2	1.292(5)		

*Table 4.5.18 Selected bond lengths and angles for **39**.*

4.5.4.4 Synthesis of [(Naph$_2$carb)$_2$In]Cl



*Scheme 4.5.16 Synthesis of homoleptic complex **40**.*

Continuing with a heavier Group 13 element, the same reaction was performed employing $InCl_3$ as reagent, in a metathesis reaction (Scheme 4.5.16), taking inspiration from similar procedures reported in the literature, which targeted the formation of indium complexes of 1,3-diphenyltrizene.[217] As such, reaction of the *in situ* generated potassium salt **14** and $InCl_3$, at 0°C, in toluene exhibited no initial change in colour. Further stirring at room temperature afforded a fluorescent orange solution (**40**). From this solution and after removal of volatiles, a light yellow powder could be isolated. Following extraction into toluene and further removal of solvent under vacuum, allowed the isolation of an In(III) complex. This affirmation was corroborated by HRMS (ASAP), from which a molecular ion corresponding to 1319.4937 m/z could be observed, the acquired data matches a compound of formula $C_{84}H_{77}N_6InCl$ consistent with the formation of a homoleptic In(III)-

complex, rather than the intended heteroleptic species (Scheme 4.5.16). This contrasting/atypical reactivity has been previously noted for In(III), where one particular example comes from the reaction between $InCl_3$ and either 1 or 2 equivalents of the monoanionic diphenyltriazenide, from which it was expected to form $[InCl_2(dpt)]$ and $[InCl(dpt)_2]$ (dpt = 1,3-diphenyltrizene), respectively. Instead the ionic complex $[NHEt_3][InCl_2(dpt)_2]$, could be obtained preferentially and in near quantitative yield.[217]

4.5.5 *Metathesis Reactions with Group 14 Metal(II) Salts*

Tetrylenes, are Group 14 compounds of general formula R_2M, where M is an electron-deficient metal centre, with only six electrons in the valence shell (Figure 4.5.17). The lightest example of this is a carbene, a compound in which the carbon atom is in a formal divalent state.[218,219] First described by Arduengo *et al*., in 1991,[220] *N*-heterocyclic carbenes (NHCs) are electrically neutral species of general formula $(R_2N)_2C$: [where R = alkyl or aryl groups], where the central carbon atom is divalent, with a six-electron valence shell.[221] Heavier NHC analogues, silylenes (NHSi),[222] germylenes (NHGe),[223] stannylenes (NHSn)[224] and plumbylenes (NHPb),[225] are also known and in some cases even predate the chemistry of stable carbenes.[226,227]

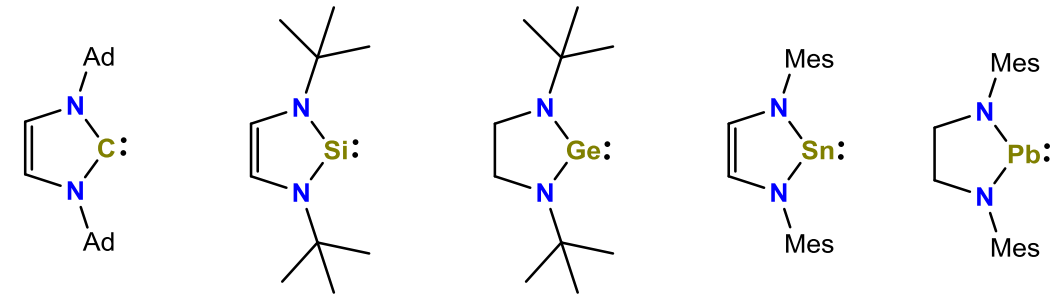


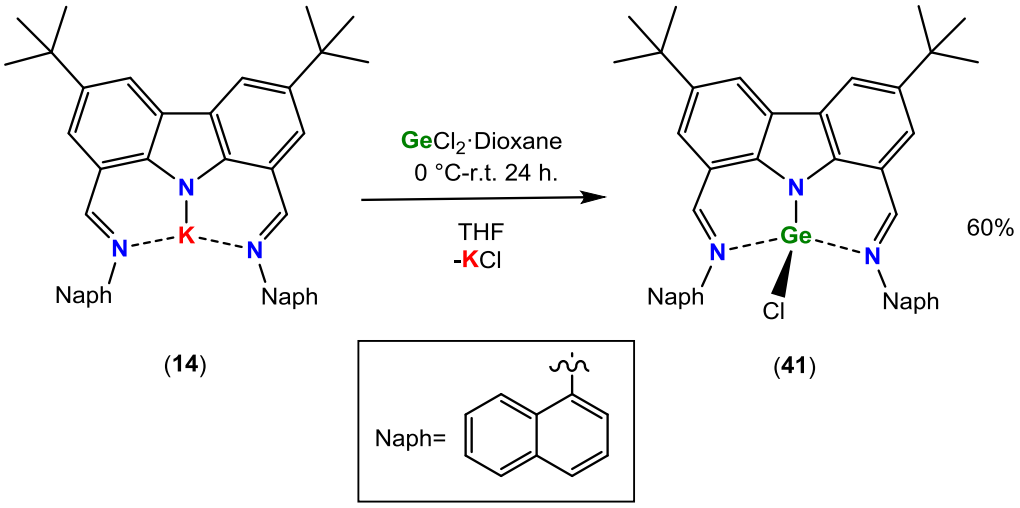
Figure 4.5.17 Examples of crystallographically authenticated tetrylenes.

The first stannylene was reported by Veith in 1975,[228] and the first isolable acyclic diamido tetrylenes reported in 1974, independently, by Lappert[229] and Zuckerman.[230] The key stabilising effect in these compounds arises from the extra electron density provided by the adjacent/flanking nitrogen atoms to the empty p_z-orbital of the metal, while the nitrogen atoms also withdraw electron density from the Group 14 element, increasing its thermodynamic stability. Typically, tetrylenes present a bent geometry at the Group 14

element, and exclusively exist in the singlet ground state. In this geometry, the σ-orbital contains two electrons, while the p_z-orbital remains vacant, a characteristic that has been exploited in a rich range of ambiphilic reactions with nucleophiles and electrophiles alike.[215,231–234]

Taking this into account, it remains of interest to generate and study low-valent Group 14 compounds supported by the symmetric bis(imino)naphthyl carbazolido proligand **6**.

4.5.5.1 Synthesis of [Naph$_2$carbGeCl]



*Scheme 4.5.17 Synthesis of **41**.*

In a first approach, GeCl$_2$·dioxane was used in a metathesis reaction with the potassium salt (**14**) in THF (Scheme 4.5.17). Under these conditions, and following completion of the reaction towards the formation of a new product ([Naph$_2$carbGeCl] **41**), dark orange-red crystals, suitable for solid state determinations, could be grown from a concentrated hexane solution at room temperature.

The X-ray crystal structure of **41** revealed a monomeric heteroleptic complex (Figure 4.5.18). The coordination sphere around the metal centre is formally four coordinate (τ_4' = 0.45);[156] with three positions occupied by the tridentate carbazolido ligand and a chloride. The metal centre occupies the space defined by the tridentate ligand and closely intersects the best mean plane generated (0.2107(16) Å). The angle between the metal centre and the chloride N1–Ge1–Cl1 [96.94(7)°] is close to being orthogonal due to the presence of a stereochemically active lone pair of electrons on the metal centre, and is in close agreement with similar, crystallographically characterised Ge(II) metal centres, such

as chlorogermanium-1,9-dimethyl-5-phenyldipyrrin and [Ge(C_{NHC}^N_{amido})Cl] {C_{NHC}^N_{amido} = 1-Mesityl-3-(2-(mesitylamino)ethyl)-1H-imidazol-3-ium}, with similar values of 94.66(55)° and 99.07(7)°, respectively.[81,235] The distances Ge1–N1 [2.001(2) Å], Ge1–N2 [2.272(2) Å] and Ge1–N3 [2.373(2) Å] found in **41**, are longer than the equivalent distances found in chlorogermanium-1,9-dimethyl-5-phenyldipyrrin [1.9758(16) Å / 1.9761(16) Å] and [Ge(C_{NHC}^N_{amido})Cl] [1.891(2) Å].[81,235]

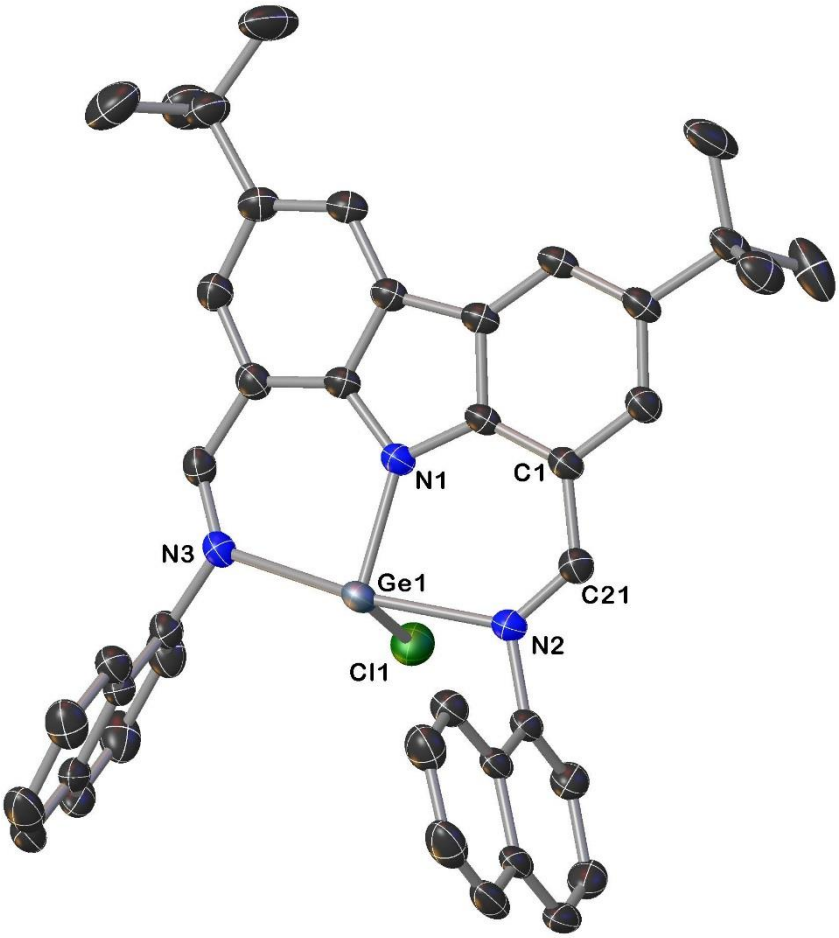
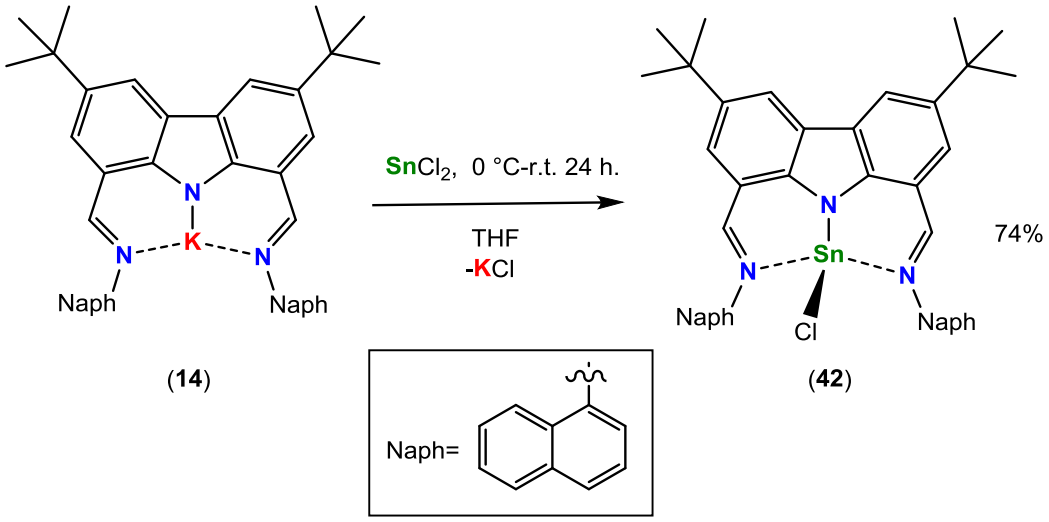


*Figure 4.5.18 Molecular structure for **41**, with displacement ellipsoids set at 50% probability level, hydrogen atoms have been omitted for clarity.*

Bond Length (Å)		Bond Angle (°)	
Ge1–N1	2.001(2)	N1–Ge1–Cl1	96.94(7)
Ge1–N2	2.272(2)	N2–Ge1–N3	167.94(8)
Ge1–N3	2.373(2)	C1–C21–N2	123.3(2)
Ge1–Cl1	2.2982(8)		
C21–N2	1.270(4)		

*Table 4.5.19 Selected bond lengths and angles for **41**.*

4.5.5.2 Synthesis of [Naph$_2$carbSnCl]



*Scheme 4.5.18 Synthesis of **42**.*

Following the successful synthesis of **41**, a parallel reaction was tested, employing $SnCl_2$ as metal source. Metathesis reaction between the potassium salt **14**, and $SnCl_2$ in THF at low temperature, followed by NMR analyses, were in close agreement with full consumption of the starting material and further conversion to a new product ([Naph$_2$carbSnCl] **42**) (Scheme 4.5.18). In the $^{119}Sn\{^1H\}$ spectrum, it was possible to determine a clear dependence of the chemical shift for the metal centre, with the solvent employed for characterisation. As such, a wide range $^{119}Sn\{^1H\}$ NMR spectrum in $CDCl_3$ presented a single resonance at 25.9 ppm, with a similar determination in C_6D_6, exhibiting an equivalent peak at −123.2 ppm. This value is not dissimilar from the resonance peaks observable in heteroleptic β-diketiminato-tin(II)-halide complexes, such as [Sn({N(SiMe$_3$)C(Ph)}$_2$CH)Cl], [Sn{N(SiMe$_3$)C(Ph)CHC(^{t}Bu)N(SiMe$_3$)}Cl] and [Sn{N(SiMe$_3$)C(Ph)CHC(^{t}Bu)N(H)}Cl]. With comparable chemical shifts in C_6D_6 of −118.2 ppm, −118.0 ppm and −166.5 ppm, respectively.[236] The change in chemical shift behaviour upon exchange of the solvent, has been previously described and rationalised on the basis of weak interactions/binding between the metal centre and the solvent employed.[231,237] Also supporting of this is numerous examples in which the metal centre shows a preferential coordination towards benzene and other neutral arenes.[238,239] Dark yellow, crystalline material of **42**, suitable for X-ray analysis was obtained from a hexane extract, at room temperature.

In the solid state, **42** is monomeric, clearly depicting a heteroleptic metal centre (Figure 4.5.19). Similar to the behaviour observed in between the Group 13 analogues **38** and **39**, **42** is isostructural/isomorphous to its lighter congener **41**. In line with this, the coordination sphere around the metal centre is formally four coordinate (τ_4' = 0.54)[156] with three of the positions occupied by the tridentate carbazolido ligand, with the flanking naphthyl groups in a *syn*-conformation and a chloride. There is clear evidence of the presence of a lone pair of electrons occupying an additional position around the metal centre in **42**, as noted in the generated angle between N1–Sn1–Cl1 [94.96(7)°], similar to the analogous angles found in [Ge(C_{NHC}^N_{amido})Cl] {C_{NHC}^N_{amido} = 1-Mesityl-3-(2-(mesitylamino)ethyl)-1H-imidazol-3-ium} and [Sn(Cl)[{κ^2-N,N($SiMe_3$)}$_2$$C_{10}H_6$-1,8]SnCl [96.51(8)° and 97.10(10)° / 95.84(9)°, respectively];[235,240] while the distance Sn1–N1 in **42** [2.191(2) Å] is within range of the analogous distances found for [Ge(C_{NHC}^N_{amido})Cl] [2.088(2) Å], [Sn(Cl)[{κ^2-N,N($SiMe_3$)}$_2$$C_{10}H_6$-1,8]SnCl [2.262(3) Å], and other related halide substituted Group 14(II) metal centres.[231,232,235]

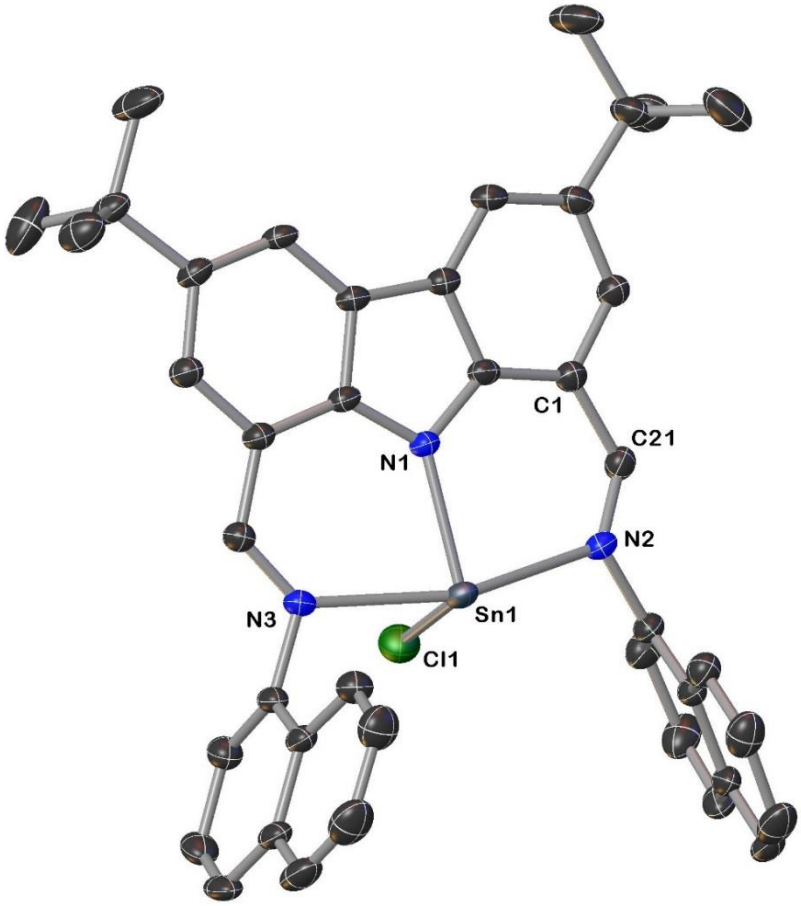
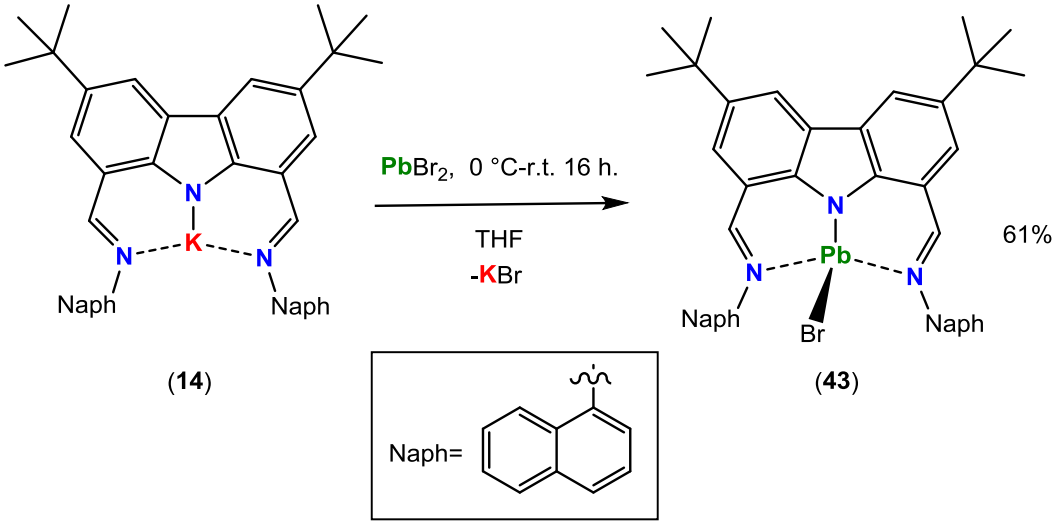


*Figure 4.5.19 Molecular structure for **42**, with displacement ellipsoids set at 50% probability level, hydrogen atoms have been omitted for clarity.*

Bond Length (Å)		Bond Angle (°)	
Sn1–N1	2.191(2)	N1–Sn1–Cl1	94.96(7)
Sn1–N2	2.463(2)	N2–Sn1–N3	159.89(8)
Sn1–N3	2.408(2)	C1–C21–N2	123.6(3)
Sn1–Cl1	2.4600(8)		
C21–N2	1.279(4)		

*Table 4.5.20 Selected bond lengths and angles for **42**.*

4.5.5.3 Synthesis of [Naph$_2$carbPbBr]



*Scheme 4.5.19 Synthesis of **43**.*

Finally, the synthesis of a lead-bearing heteroleptic complex was targeted. As such, the *in situ* generated potassium salt **14**, formed from low temperature deprotonation of the ligand **6**, was slowly added to a suspension of $PbBr_2$ in THF (Scheme 4.5.19). Initial NMR characterisation of the product in C_6D_6, yielded low quality/broad spectra, which is most likely a consequence of the low solubility of the compound in apolar solvents. $CDCl_3$ proved an adequate solvent for NMR characterisation. The compound presents bilateral symmetry in both ^{1}H and $^{13}C\{^{1}H\}$ NMR spectra, although characterisation by $^{207}Pb\{^{1}H\}$ NMR was attempted, using a wide range of chemical shifts (2800 ppm to 1200 ppm and –400 ppm to –3400 pm), this was met with no success. These regions were scanned following reports on the chemical shifts of three- and four-coordinate heteroleptic lead(II)-halide complexes

supported by *N*-based ligands, from which selected examples include, [{N^N$^{i\text{Pr}}$}PbCl] [N^N^{i}Pr = C_6H_4(1-*N*{2,6-$^{i}Pr_2C_6H_3$})(2-CH-*N*(2,6-$^{i}Pr_2C_6H_3$)] (1317 ppm),[241] [{BDI$^{i\text{Pr}}$}PbCl] {BDI = $HC(CMeNAr)_2$; Ar = 2,6-$^{i}Pr_2C_6H_3$)} (1413 ppm),[242] [{BDI$^{\text{Ph}}$}PbCl] [BDI$^{\text{Ph}}$ = {$N(C_6H_5)C(Me)\}_2CH$] (1227 ppm),[243] [{BDI^{DMP}}PbCl] {BDI^{DMP} = [N{(2,6-$Me_2C_6H_3$)C(Me)}$_2$CH] (1388 ppm)[243] and [{(2-Me_2NCH_2)C_6H_4N($SiMe_3$)}Pb(μ-Cl)]$_2$ (1816 ppm).[244] Difficulties associated with the determination of ^{207}Pb{^{1}H} NMR spectra have been previously reported,[73] and include formation of polymeric structures, extreme senstivitity to subtle molecular (*e.g*. solvent coordination) and physical changes (*e.g*. temperature),[245] and in particular cases it has been presumed that the fast relaxation of the lead nucleus is responsible for the limited observations.[246,247] Despite this, the resulting product was isolated from the concomitant salt formed, by extraction into toluene ([Naph$_2$carbPbBr] **43**). Upon doing so, dark orange crystals suitable for X-ray diffraction could be grown at room temperature, and subsequently isolated in good yield (61%).

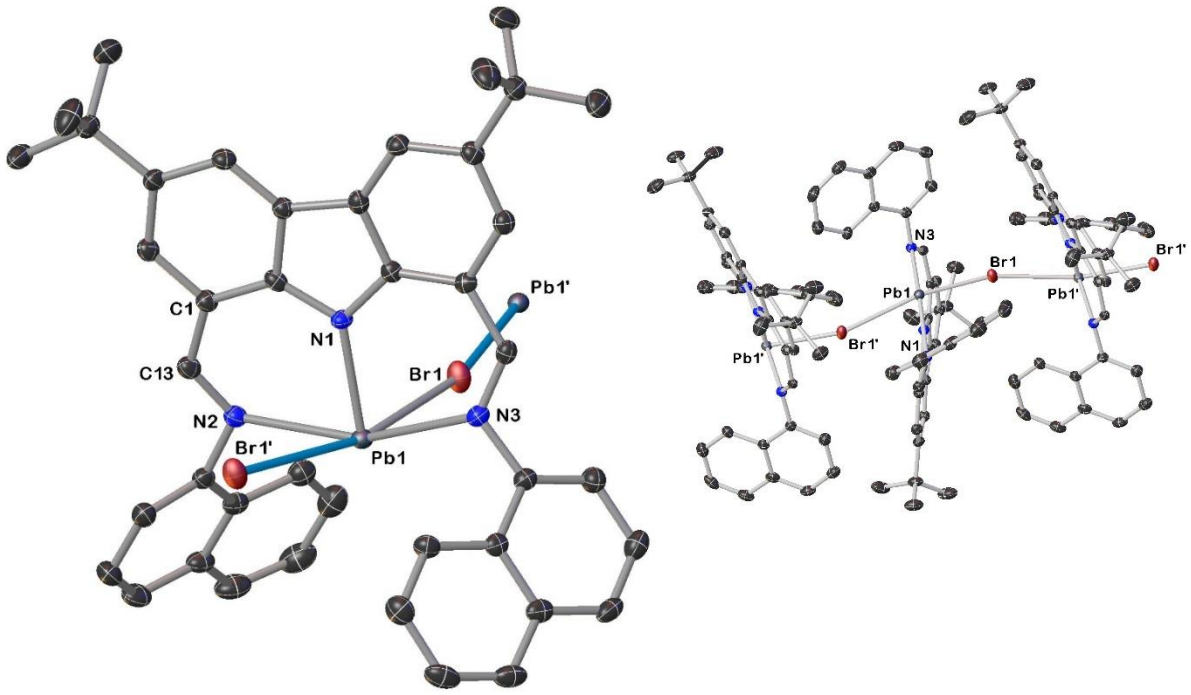


*Figure 4.5.20 Molecular structure for the first polymorph of **43** (left), depicting the 1D Pb-Br-Pb…∞ coordination motif (right), with displacement ellipsoids set at 50% probability level, with hydrogen atoms and carbazolido ligand for Pb1' (left) omitted for clarity.*

Solid state determinations for **43** allowed the elucidation of two different polymorphs. In the first one, crystallising with one molecule per asymmetric in the *P*2$_1$/n space group, with a coordination sphere not dissimilar to the previously discussed Group 14 heteroleptic complexes **41** and **42**, with one molecule occupying the asymmetric unit (Figure 4.5.20),

and the coordination sphere being completed by the *NNN*-pincer ligand on three positions and a bromide ion. However, additional coordination can be observed in the form of a repetitive Pb–Br···Pb…∞ motif along one main axis, forming a one dimensional coordination polymer (τ_5 = 0.12).[152] Comparable lead-containing coordination motifs have been previously reported and, directly correlated this behaviour to the comparatively greater radius of the metal centre and/or the halide employed [*e.g.* Pb(L)I_2 , L = 2,2'-bipyridine-1,10-phenanthroline and {Pb(MPOAc)$_2$(H_2O)}$_n$, MPOAC = mono phenyl acetate].[248–250] Additionally, and explained on the basis of the increasing ionic radius, the naphthyl substituents are in an *anti*-conformation, with the adjacent imine moieties, twisting in opposing directions from the plane generated by the carbazolido ring.

Bond Length (Å)		Bond Angle (°)	
Pb1–N1	2.297(3)	N1–Pb1–Br1	86.41(8)
Pb1–N2	2.578(3)	N2–Pb1–N3	159.75(9)
Pb1–N3	2.259(3)	C1–C13–N2	126.4(3)
Pb1–Br1	2.8591(4)	Br1'–Pb1–Br1	167.251(4)
C13–N2	1.288(5)		

*Table 4.5.21 Selected bond lengths and angles for **43** (polymorph 1).*

The second polymorph of **43**, however, crystallises in the *I*2/*m* space group (Figure 4.5.21), with a molecule cut in half by a mirror plane along the carbazole N1–Pb1 axis. Differing from the polymorph previously described, no coordination to adjacent metal centres can be observed (τ_4' = 0.55).[156] However, a close contact interaction can be seen between the lone pair of the Pb(II) metal centre and a C_6D_6 molecule. The bonding interaction (Pb1–$C28_{plane}$ = 3.62422(2) Å) is longer than the one found in the comparable interaction between a lead(II) centre and a benzene molecule in [(η^6-C_6D_6)Pb($AlCl_4$)$_2$]·C_6H_6 (*ca.* 3.11 Å).[239] There are literature examples in which even longer lengths in lead-arene interactions (*ca.* 3.83 Å) stabilise dimeric structures [*e.g.* {Pb-κ^2-*N,N*-DippN(CH_2)$_3$N(Dipp)}$_2$, Dipp = 2,6-diisopropylphenyl].[225,238,251] Hence, although the interaction between the benzene ring and **43** is in alignment, this is only suggestive of a weak interaction. Finally, the sterically encumbering naphthyl substituents were found to be in a *syn*-conformation.

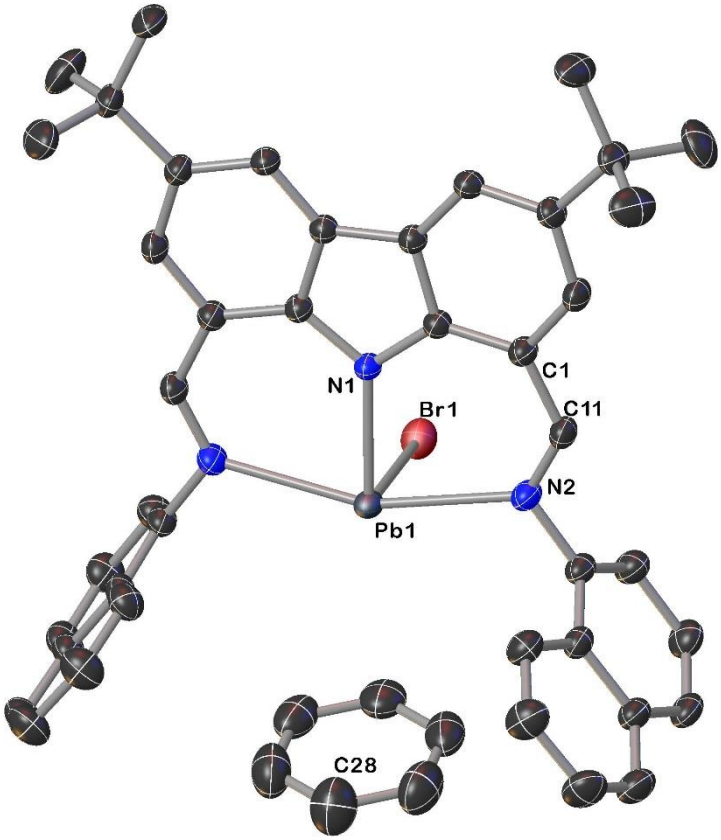


*Figure 4.5.21 Molecular structure for the second polymorph of **43**, with displacement ellipsoids set at 50% probability level, hydrogen atoms have been omitted for clarity.*

	Bond Length (Å)		Bond Angle (°)
Pb1–N1	2.309(2)	N1–Pb1–Br1	90.71(5)
Pb1–N2	2.555(2)	N2–Pb1–N3	160.43(7)
Pb1–N3	2.555(2)	C1–C11–N2	126.5(2)
Pb1–Br1	2.7140(3)		
C11–N2	1.279(3)		
$Pb1–C28_{plane}$	3.62422(2)		

*Table 4.5.22 Selected bond lengths and angles for **43** (polymorph 2).*

Similar to the behaviour found for the Group 1 salts **12**-**14** in ^{1}H NMR (Figure 4.5.22). In benzene solution, compounds **41**-**43** present a direct change in chemical shift (downfield) attributable to the increase in ionic radius. However, this behaviour is not only observable in the most distal protons of the naphthyl rings, as in the aforementioned Group 1 salts, but in almost all the signals observable, suggesting a greater degree of interaction between the metal centre, the ligand and/or the lone pair of electrons.

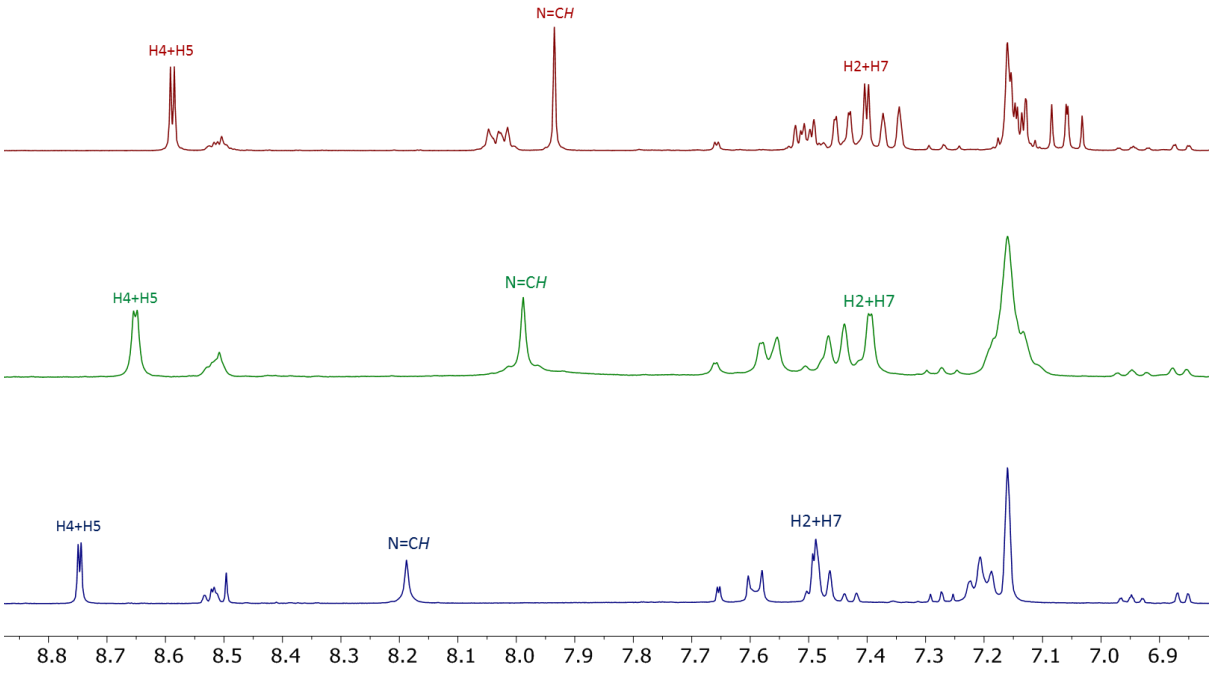


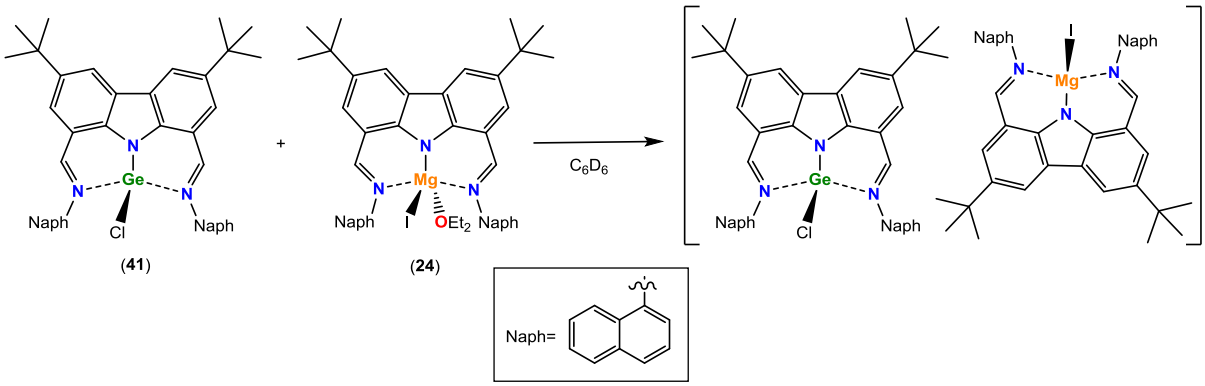
*Figure 4.5.22 Comparative ^{1}H NMR spectra of **41** (top), **42** (centre) and **43** (bottom), in C_6D_6.*

4.5.5.3.1 Reactivity and Halide Replacement Reactions

4.5.5.3.1.1 Reaction of [Naph$_2$carbGeCl] with [Naph$_2$carbMg(OEt$_2$)I]

As evidenced by the solid state determinations of the heteroleptic Group 14(II) complexes generated *via* metathesis reaction, in all three cases (**41**-**43**) the metal centre is bearing a lone pair of electrons. There are reports in the literature in which the ambiphilic character of the lone pair has been used in reactivity.[74,231,235] With this in mind, and acknowledging the Lewis Acid character of the analogous Mg(II) complex **24**; it was envisaged that upon reaction, these two compounds could be useful towards the formation of heterobimetallic complexes, or perhaps even, a frustrated Lewis pair (FLP) complex (Scheme 4.5.20).[252] FLP chemistry is an area of research that has rapidly expanded in recent years, finding

application in small molecule activation and catalysis, due to atypical non-classical reactivity.[252,253]



Scheme 4.5.20 Attempted synthesis of a heterobimetallic compound.

With this aim, an equimolar amount of **41** and **24** were reacted in C_6D_6. By doing so, the reaction could be monitored by ^1H NMR spectra. Upon reaction, full conversion to two new products could be determined on the basis of the full disappearance of the characteristic signals for both starting materials.

Despite this, X-ray diffraction determinations of the crystals obtained following reaction, yielded only the formation of **41a** [Naph$_2$carbGeI], from which a halide replacement is apparent, obtaining the iodide substituted germanium complex. The bond lengths and angles found for this compound, do not differ significantly from the ones found in **41**. With the only differences arising from the comparatively bigger iodide present on the coordination sphere of the metal centre (τ_4' = 0.41) (Figure 4.5.23).[156]

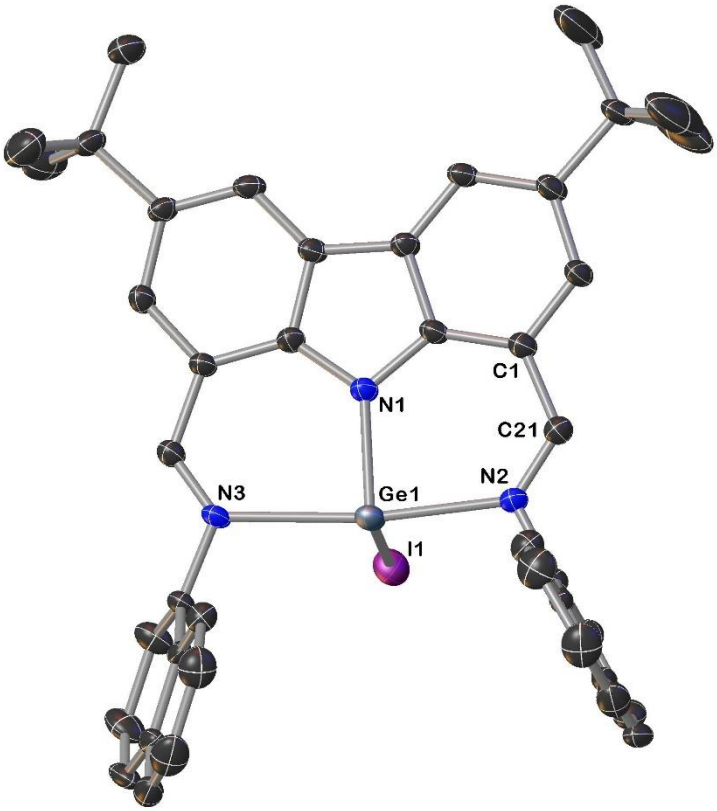
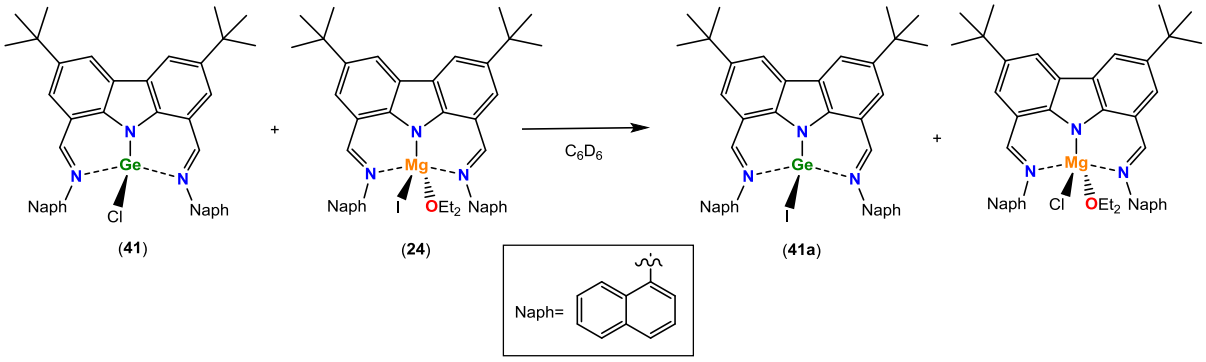


*Figure 4.5.23 Molecular structure for **41a**, with displacement ellipsoids set at 50% probability level, hydrogen atoms have been omitted for clarity.*

Bond Length (Å)		Bond Angle (°)	
Ge1–N1	1.998(3)	N1–Ge1–I1	95.09(10)
Ge1–N2	2.231(3)	N2–Ge1–N3	172.20(11)
Ge1–N3	2.384(3)	C1–C21–N2	123.5(4)
Ge1–I1	2.7366(6)		
C21–N2	1.271(5)		

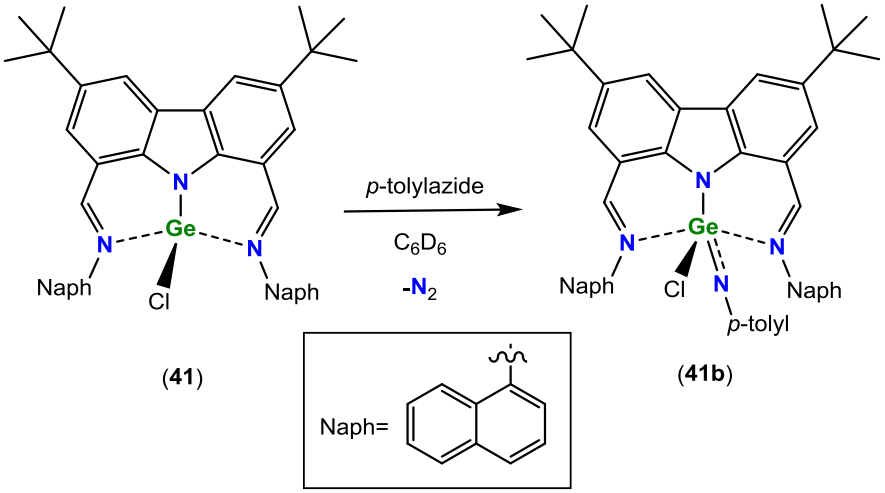
*Table 4.5.23 Selected bond lengths and angles for **41a**.*

This behaviour can be explained on the basis of the hard-soft metal-halide interaction, in which a rearrangement for a better suited/better orbital overlap, drives the interchange of anions (Scheme 4.5.21).[254–256]



*Scheme 4.5.21 Formation of **41a** via halide exchange.*

4.5.5.3.1.2 Reaction of [Naph$_2$carbGeCl] with p-tolylazide



*Scheme 4.5.22 Attempted synthesis of the germanium-imino compound **41b**.*

Looking to study the potential reactivity of the lone pair of electrons present in the Group 14 tetrylene complexes, one equivalent of **41** was reacted with one equivalent of *p*-tolylazide, in C_6D_6 (Scheme 4.5.22). Similar reactions have been reported in the literature, affording in most cases metal-imino substituted products, such as μ^2-azine-bridged dimers and metalo-tetrazolines.[257,258] It is postulated that these transformations occur *via* initial

conversion to an imino-tetrylene intermediate, with concomitant liberation of gaseous dinitrogen, which acts as driving force for the reaction.

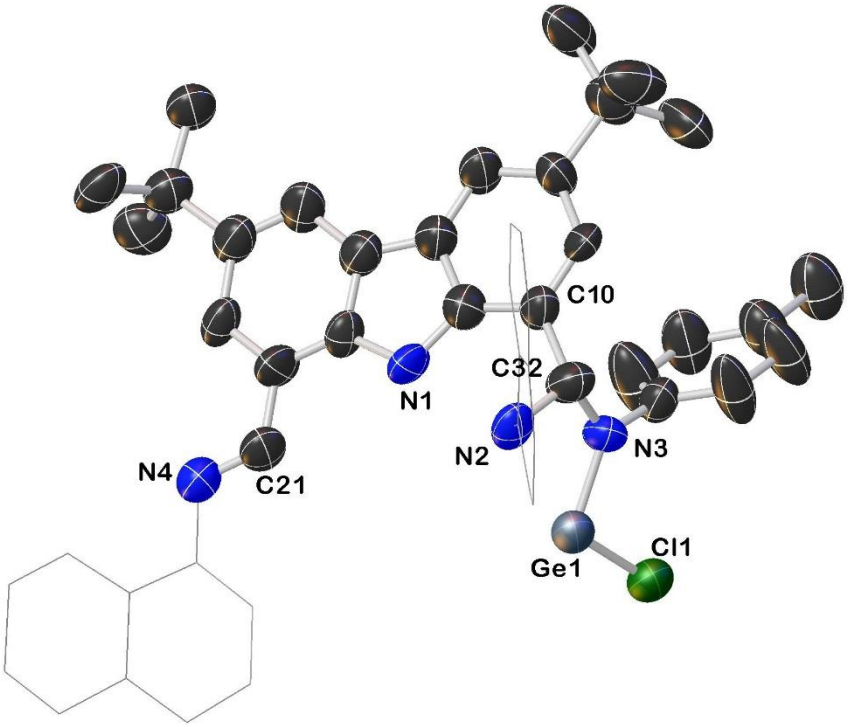


*Figure 4.5.24 Molecular structure for the monomeric form of **41c** (asymmetric unit) with displacement ellipsoids set at 50% probability level. Hydrogen atoms have been omitted, and –naphthyl substituents are presented in wireframe form for clarity.*

As such, and upon reaction, a ^{1}H NMR spectrum of the resulting reaction mixture, evidenced a myriad of peaks; with full disappearance of **41**, suggesting formation of either a mixture of products or an asymmetric product. Despite this, shortly after reaching completion, crystals suitable for X-ray analysis could be grown *via* hexane vapour diffusion ([Naph$_2$-*p*-tolylcarbGeCl]$_2$ **41c**) (Figure 4.5.24).

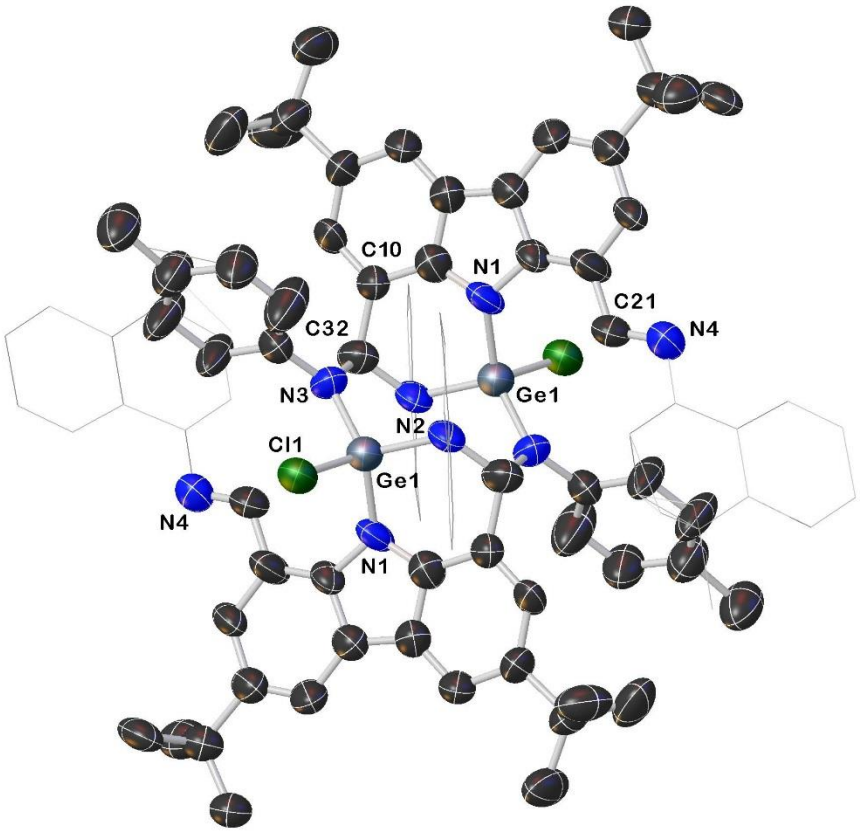
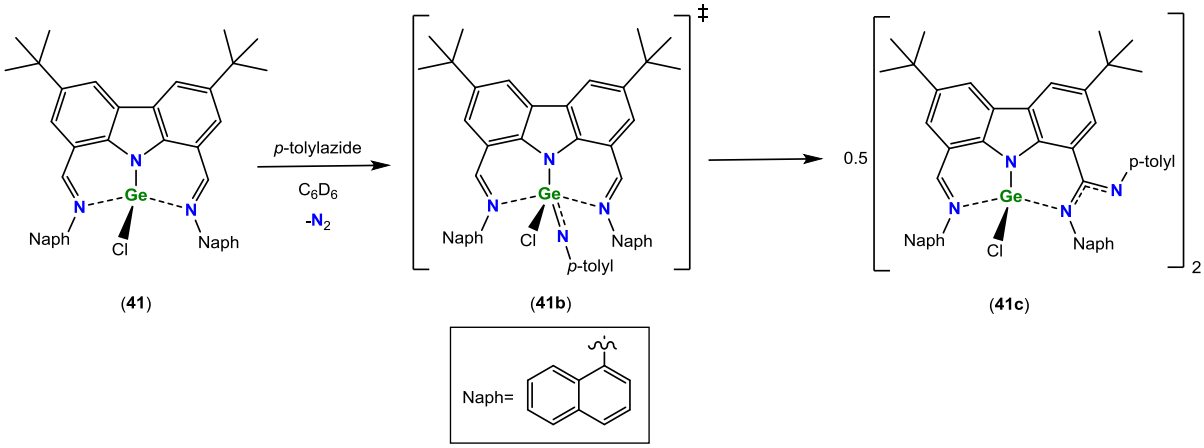


*Figure 4.5.25 Molecular structure of **41c** (symmetric unit) with displacement ellipsoids set at 50% probability level. Hydrogen atoms have been omitted, and –naphthyl substituents are presented in wireframe form for clarity.*

	Bond Length (Å)		Bond Angle (°)
Ge1-N1	1.99(2)	N1-Ge1-Cl1	104.8(6)
Ge1-N2	1.85(2)	N2-Ge1-Cl1	109.7(9)
Ge1-N3	1.81(2)	N1-Ge1-N2	104.2(7)
Ge1-Cl1	2.131(8)	N1-Ge1-N3	122.2(10)
C32-N2	1.45(3)	N2-C32-N3	109(2)
C32-N3	1.50(3)		

*Table 4.5.24 Selected bond lengths and angles for **41c**.*

In the solid state, **41c** crystallises in the *P*-1 space group as a dimeric structure (Figure 4.5.25). The coordination sphere around the metal centre is constituted by the central carbazolido nitrogen [N1], a chloride and one of the flanking naphthyl substituents [N2] and a *p*-toluidine fragment from an adjacent germanium monomer [N3] (τ_4' = 0.85).[156] However, the carbon holding the imine moiety N2 has been substituted by a *p*-toluidine/imino fragment N3, suggesting that an intramolecular nucleophilic attack from the *in situ* generated iminogermylene complex has taken place. This behaviour is not dissimilar from the reactivity observed to form the *n*-butyl substituted compound **12a**; highlighting the propensity of the ligand (**6**), to be substituted by nucleophiles (Scheme 4.5.23).



*Scheme 4.5.23 Intramolecular rearrangement to from **41c**.*

From the crystal structure, it can be postulated that upon initial formation of an elusive germanium-imino compound **41b**, this readily reacts in an intramolecular fashion, substituting an adjacent flanking naphthyl imine, yielding **41c** (Scheme 4.5.23). Additionally, two further features can be noticed in the solid state structure. The first one, includes formation of an eight-membered metallacycle, with a second molecule of **41c**, constituted by the former naphthyl imine flanking groups N2/C32 and the imino fragments N3. The arrangement adopted by the heterometallacycle is similar to a chair-conformation (C), as evidenced by the torsion angles and symmetry of the ring [109.7(9)°, 112.7(9)°, 118.8(13)° and 109(2)° *vs.* 119.9°] (Figure 4.5.26).[259]

	Bond Length (Å)		Bond Angle (°)
Ge1–N3	1.81(2)	N2–Ge1–Cl1	109.7(9)
Ge1–N2	1.85(2)	N2–Ge1–N3	112.7(9)
N3–C32	1.50(3)	Ge1–N3–C32	118.8(13)
C32–N2	1.45(3)	N3–C32–N2	109(2)
Ge1–Cl1	2.131(8)		

*Table 4.5.25 Selected bond lengths and angles for **41c**.*

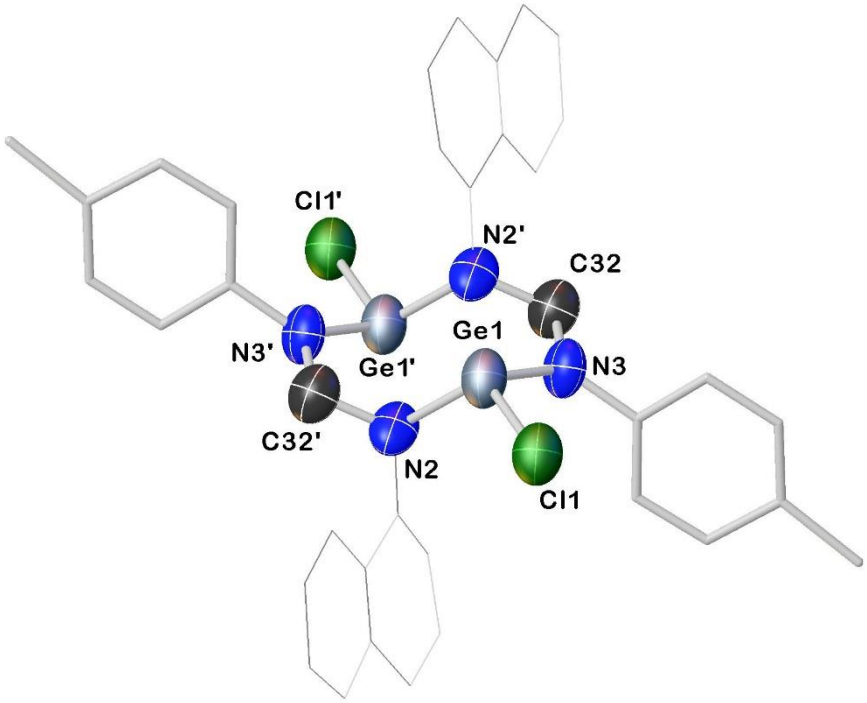


*Figure 4.5.26 Fragment of the molecular structure of **41c**, depicting the central eight-memberd metallacycle, with displacement ellipsoids set at 50% probability level. Hydrogen atoms have been omitted, and –naphthyl substituents are presented in wireframe form for clarity.*

While the second, corresponds to the formation of an additional six-membered metallacycle formed by the carbazolido nitrogen N1, the metal centre and a substituted flanking imino-naphthyl group N2/C32, with no additional coordination of the remaining unreacted flanking imine (Figure 4.5.27).

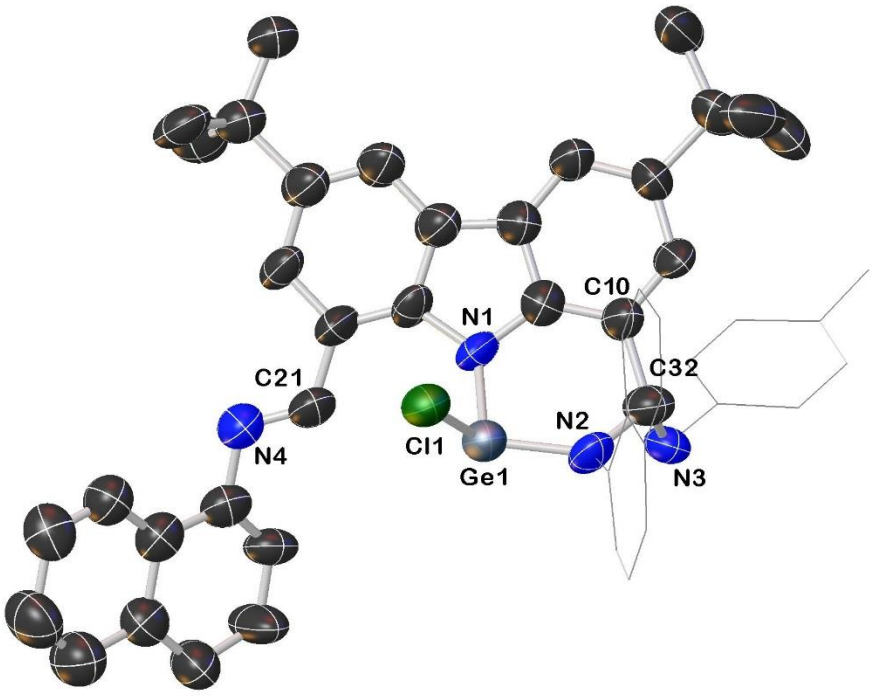
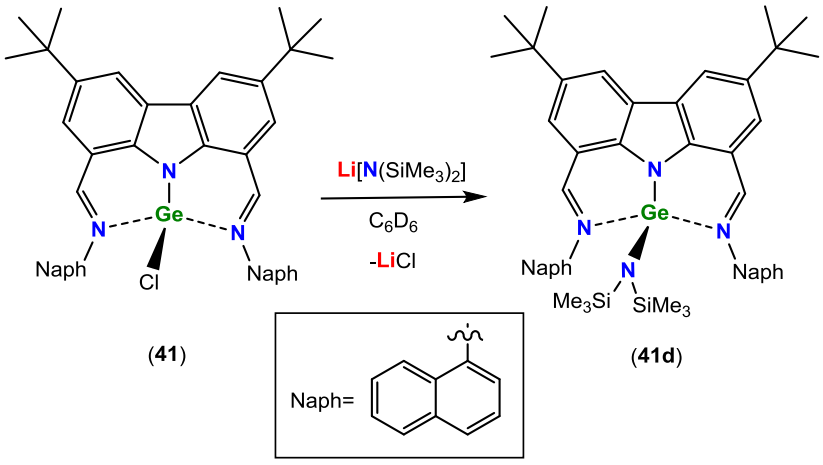


*Figure 4.5.27 Fragment of the molecular structure for the monomeric form of **41c**, with displacement ellipsoids set at 50% probability level. Hydrogen atoms have been omitted, and –naphthyl/–p-toluidyl substituents are presented in wireframe form for clarity.*

4.5.5.3.1.3 Formation of [Naph$_2$carbGeHMDS]



*Scheme 4.5.24 Halide replacement reaction to form **41d**.*

Continuing the reactivity studies on this germanium compound, a halide replacement reaction was attempted. With this aim, **41** was reacted with one equivalent of Li[N(SiMe$_3$)$_2$] in C_6D_6, with concomitant formation of LiCl (Scheme 4.5.24). Upon reacting, the characteristic orange colour of **41** was replaced with the formation of a bright red solution ([Naph$_2$carbGeHMDS] **41d**). ^{1}H and ^{13}C{^{1}H} NMR spectra corroborated full conversion to a new product, while a ^{29}Si{^{1}H} NMR spectrum (–1.12 ppm) and a ^{7}Li{^{1}H} NMR spectrum (–0.44 ppm), evidenced creation of a new silylated compound and formation of LiCl, respectively. Following this, bright orange crystals of **41d** could be grown from a saturated solution in C_6D_6.

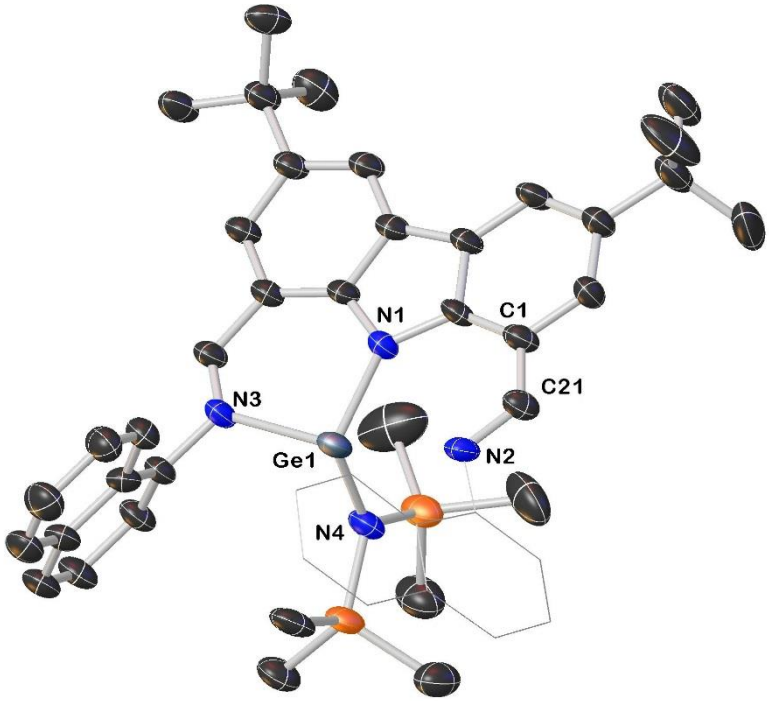


*Figure 4.5.28 Molecular structure for **41d**, with displacement ellipsoids set at 50% probability level. Hydrogen atoms have been omitted, with a –naphthyl substituent presented in wireframe form for clarity.*

In the solid state **41d** is monomeric and crystallises in the $P2_1/n$ space group (Figure 4.5.28). Similar to the parent compound, the coordination sphere around the central germanium centre is completed by the tridentate carbazolido ligand, with the halide being replaced by a $[N(SiMe_3)_2]^-$ anion (HMDS) (τ_4' = 0.36).[156] The bond lengths Ge1–N2 and Ge1–N(3) are different from each other (2.066(5) *vs.* 2.54568(17) Å, respectively), most likely a consequence of steric hindrance/solid state packing and/or the presence of the comparatively bigger anion. The rotation around the Ge1–N4 axis in **41d**, is obstructed by the two naphthyl substituents in *syn*-conformation.; with the distance between the two aforementioned atoms [Ge1–N4 = 1.935(6) Å], being slightly longer than the equivalent

found in previously reported HMDS-substituted germanium centres, such as [Au{GeCl(HMDS)$_2$}(THT)] and [Au{GeCl(HMDS)$_2$}{Ge(HMDS)$_2$}] (THT = tetrahydrotiophene), with equivalent distances ranging from 1.86(1) Å to 1.882(4) Å.[260,261] The limited availability of space around said moiety and the aforementioned asymmetry in the chelate, are responsible for the two distinctive signals attributable to the trimethylsilyl-substituents. This is observed in the ^{1}H and ^{13}C{^{1}H} NMR spectra, which make these substituents magnetically inequivalent [0.10 and –0.41 ppm (^{1}H NMR) / 2.60 and 4.99 ppm (^{13}C{^{1}H} NMR)].

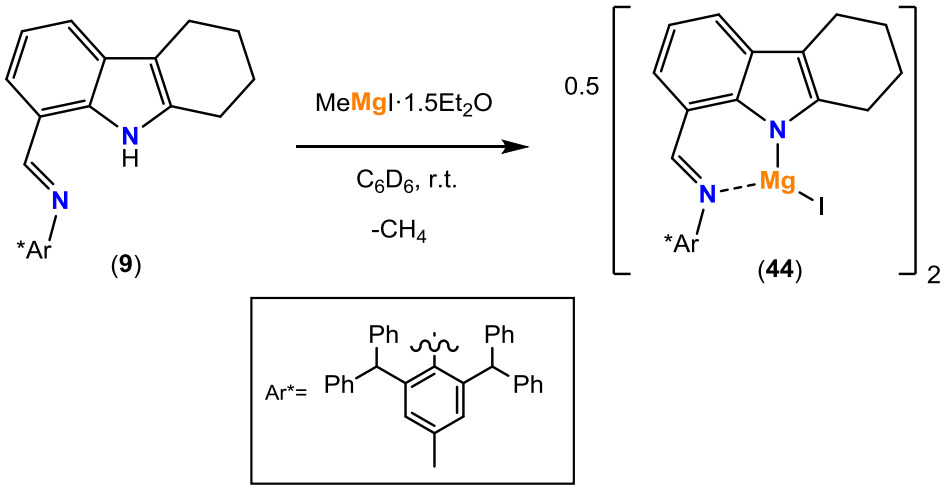
	Bond Length (Å)		Bond Angle (°)
Ge1–N1	2.066(5)	N1–Ge1–N4	101.1(2)
Ge1–N2	2.5457(2)	N2–Ge1–N3	174.5189(7)
Ge1–N3	2.330(6)	C1–C21–N2	126.1(7)
Ge1–N4	1.935(6)		
C21–N2	1.280(8)		

*Table 4.5.26 Selected bond lengths and angles for **41d**.*

4.6 Low-coordinate Metal Centres Employing [Ar*THCarbH]

4.6.1 Organoelimination Reactions with Group 2 Compounds

4.6.1.1 Synthesis of [Ar*THCarbMgI]$_2$



*Scheme 4.6.1 Formation of **44** via organoelimination.*

Encouraged by the synthesis and authentication of **24** and looking to extend the formation of low coordinate Group 2 complexes to the asymmetric proligand [Ar*THCarbH] (**9**) based on a tetrahydrocarbazole core, an organoelimination reaction was carried out. As such, an equimolar amount of **9** was reacted with MeMgI·1.5Et$_2$O, in C$_6$D$_6$. Upon addition of the Grignard reagent to the proligand, an immediate change in colouration could be observed, affording a bright orange solution ([Ar*THCarbMgI]$_2$ **44**) (Scheme 4.6.1). With the resulting ^{1}H and ^{13}C{^{1}H} NMR spectra, exhibiting consistent disappearance of the starting material to form a new product. Additionally, this was particularly obvious in the signals characteristic to the imino (Ar*-N=C) fragment in the ^{13}C{^{1}H} NMR spectrum, with downfield shifting on the newly formed product (167 ppm in **9** *vs.* 178 ppm in **44**)

Following synthesis and characterisation, crystals of **44** suitable for X-ray diffraction were grown from C$_6$D$_6$, at room temperature.

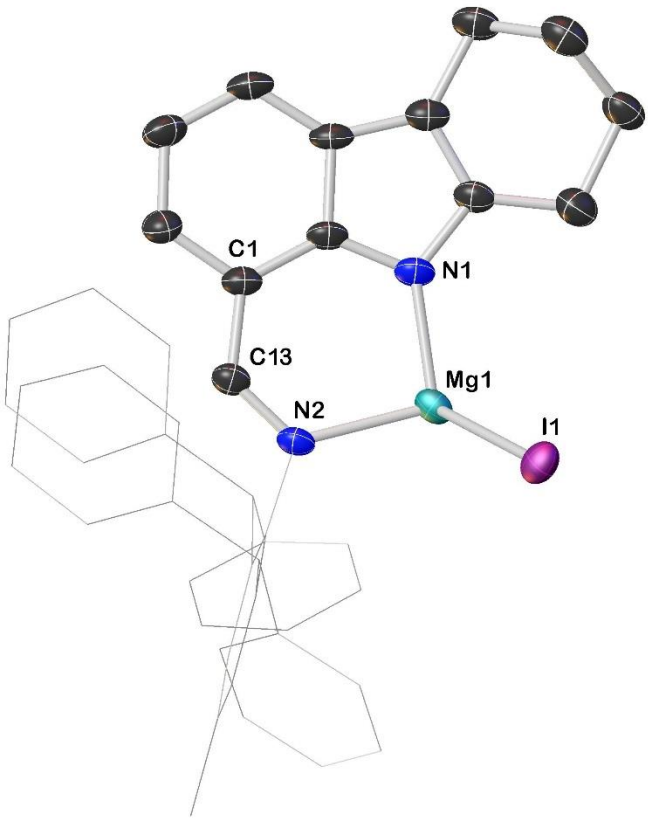


*Figure 4.6.1 Molecular structure of **44**, depicting the monomeric fragment (asymmetric unit), with displacement ellipsoids set at 50% probability level. Hydrogen atoms have been omitted, with the –Ar* substituent presented in wireframe form for clarity.*

In the solid state, **44** is a dimer (Figure 4.6.1 and Figure 4.6.2). The coordination around the metal centre is completed by the bidentate asymmetric ligand and an iodide bridge. With a second monomer related by a centre of inversion, forming a halide-bridged dimer (τ_4' = 0.89) (Figure 4.6.2).[156] The best mean plane generated by the tetrahydrocarbazole moieties is almost perpendicular to the plane generated by the Mg1–I1 bridge [89.622(5)°]. With the flanking Ar*-N=C substituent residing in coplanar/mirrored positions rotated 180° with respect to each other. The distance Mg1–Mg1 in **44** is shorter [3.49889(15) Å] than the equivalent distances found in previously reported Mg(II)-iodide bridged dimers (*ca*. 4 Å).[262,263] Which include the starting material employed in the synthesis of the first stable magnesium(I) compound, exhibiting a Mg–Mg bond [*e.g.* (Priso)Mg(μ-I)$_2$Mg(OEt$_2$)(Priso); Priso = {(Ar)NC(NR'$_2$)N(Ar)}, Ar = 2,6-diisopropylphenyl and R' = isopropyl].[4]

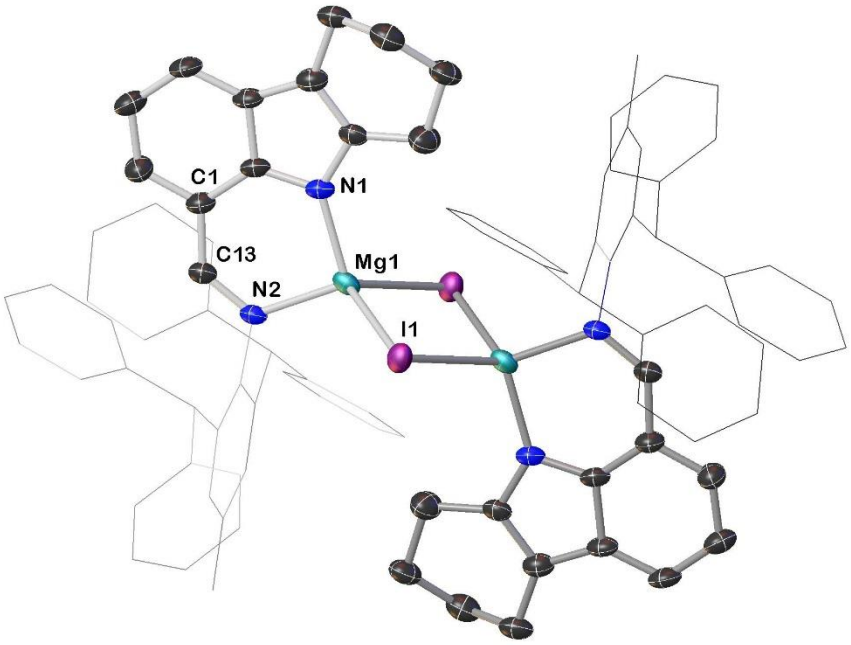


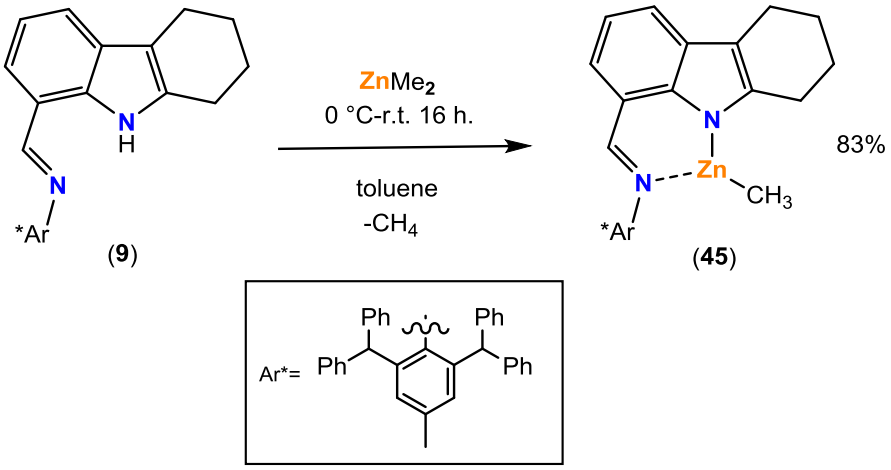
*Figure 4.6.2 Molecular structure for the dimeric arrangement of **44** (symmetric unit), with displacement ellipsoids set at 50% probability level. Hydrogen atoms have been omitted, with –Ar* substituents presented in wireframe form for clarity.*

	Bond Length (Å)		Bond Angle (°)
Mg1–N1	1.981(11)	N1–Mg1–N2	96.5(5)
Mg1–N2	2.062(12)	N1–Mg1–I1	117.8(4)
Mg1–I1	2.727(4)	N2–Mg1–I1	115.3(3)

*Table 4.6.1 Selected bond lengths and angles for **44**.*

4.6.2 Organoelimination Reactions with Group 12 Compounds

4.6.2.1 Synthesis of [Ar*THCarbZnMe]



*Scheme 4.6.2 Synthesis of **45**.*

In an analogous process to the Group 2 complex **44** previously described, it was envisaged that low coordinate zinc complexes could also be synthesised by deprotonation of **9** by a suitable organozinc complex *via* organoelimination. Towards this aim, **9** was reacted at 0 °C, in toluene solution, with a slight excess of $ZnMe_2$. Noticeably, and in contrast with the synthesis of **44**, no immediate change in colouration was observed. The resulting dark yellow solid obtained after removal of volatiles, showed full conversion to a new product ([Ar*THCarbZnMe] **45**) (Scheme 4.6.2). The clear presence of a characteristic methyl group in the NMR spectra (CH_3 substituent [–0.68 ppm; ^{1}H NMR] and [–6.61 ppm; $^{13}C\{^{1}H\}$ NMR]), suggested the formation of a heteroleptic complex, with a pendant methyl group still attached to the metal.

Following full NMR characterisation, the product was extracted into warm hexane, from which dark yellow crystals could be grown at room temperature.

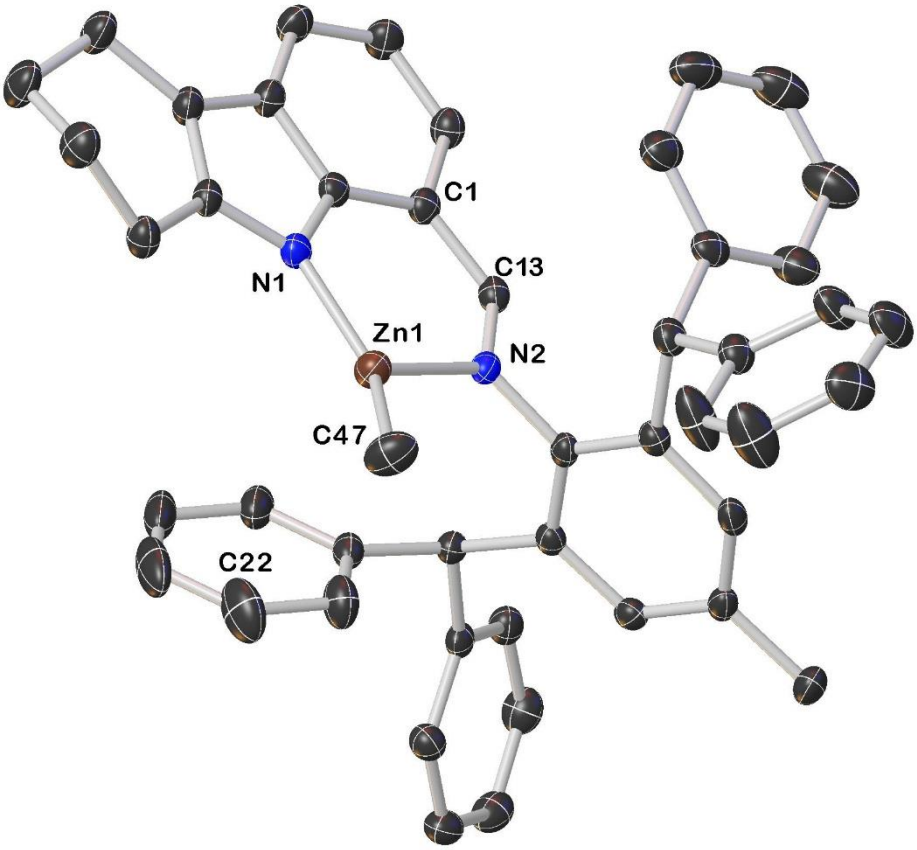


*Figure 4.6.3 Molecular structure for **45**, with displacement ellipsoids set at 50% probability level, hydrogen atoms have been omitted for clarity.*

In the solid state **45** crystallised in the *P*-1 space group, with one molecule occupying the asymmetric unit (Figure 4.6.3). The coordination sphere of metal centre is completed by the asymmetric bidentate ligand and a methyl group arising from the parent $ZnMe_2$ reagent, which lies in close proximity to the best mean plane of the tetrahydrocarbazole core [0.277(3) Å]. The distance Zn1–C47 [1.954(2) Å] is within range of the equivalent measurements found in analogous methyl-substituted zinc centres, such as $[ZnMe(DAD)]^+[MeB(C_6F_5)_3]^-$ and $[\{^tBuC(NDipp)_2\}ZnMe(^tBuPy)]$ [DAD = $(MeC{=}NC_6H_3{}^iPr_2\text{-}2,6)_2$; Dipp = 2,6-diisopropyltoluene], with values of 1.914(4) Å and 1.9710(15) Å, respectively.[264–266] Additionally, there is an interaction with one of the flanking groups pending from the Ar* moiety [$Zn1–C22_{plane}$ = 3.377(2) Å], this extra coordination to arenes, has also been previously observed, arising from comparable low-coordinate metal environments.[265]

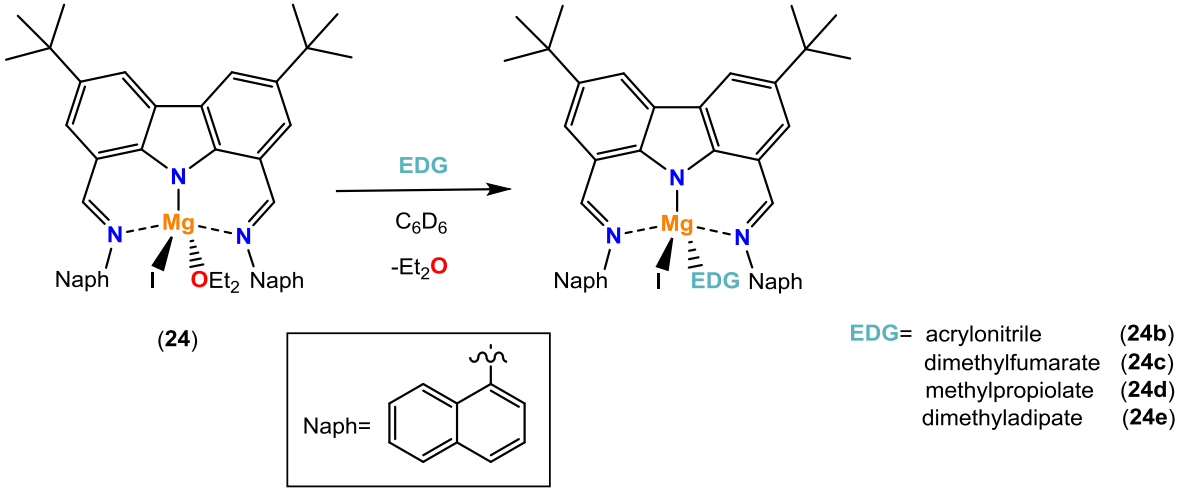
	Bond Length (Å)		Bond Angle (°)
Zn1–N1	1.9280(18)	N1–Zn1–N2	93.41(7)
Zn1–N2	2.0840(18)	N1–Zn1–C47	142.81(10)
Zn1–C47	1.954(2)	N2–Zn1–C47	122.07(10)
C13–N2	1.295(3)	C1–C13–N2	125.2(2)

*Table 4.6.2 Selected bond lengths and angles for **45**.*

4.7 "Probing the Coordination Sphere"-Initial Studies Towards Catalysis Employing [Naph$_2$carbH] as Ligand

4.7.1 Coordination Studies Employing Closed and Open-shell Complexes

4.7.1.1 Synthesis of Complexes of the Form [Naph$_2$carbMgI]-substrate



*Scheme 4.7.1 Synthesis of coordination compounds **24b-24e**.*

As mentioned previously in this chapter, it has been possible to synthesise, structurally authenticate and fully characterise the heteroleptic magnesium complex **24** (Hauser base). The presence of a molecule of Et_2O coordinated to the magnesium centre, suggests space available for coordination/reactivity, while also denoting the Lewis acidic character of the central metal ion. With this in mind, and with the eventual goal of employing compound

24 for catalysis, a systematic study of the space available/adequate functional groups towards coordination was attempted.

As such, a wide range of unsaturated groups were tested. ^{1}H NMR spectra of the resulting reaction mixtures between **24** and one equivalent of the targeted substrate, showed specific preference for electron rich, nitrogen or oxygen-based donating groups (EDG), found in aldehydes/ketones, esters and aromatic amines (**24b**-**e**) (Scheme 4.7.1). As determined by ^{1}H NMR spectroscopy, isocyanates, azides, pyridine-oxides and other electron deficient groups were not capable of replacing the coordinated Et_2O, in line with a Lewis acid/base replacement mechanism. Additionally, it could be observed that upon successful coordination/replacement of the Et_2O, the signals of said solvent would be readily resolved. In all the cases in which replacement of Et_2O with an electron rich substrate could be corroborated by ^{1}H NMR characterisation, crystals could be readily obtained from the mother liquor and the solid state determinations of such examples are presented below.

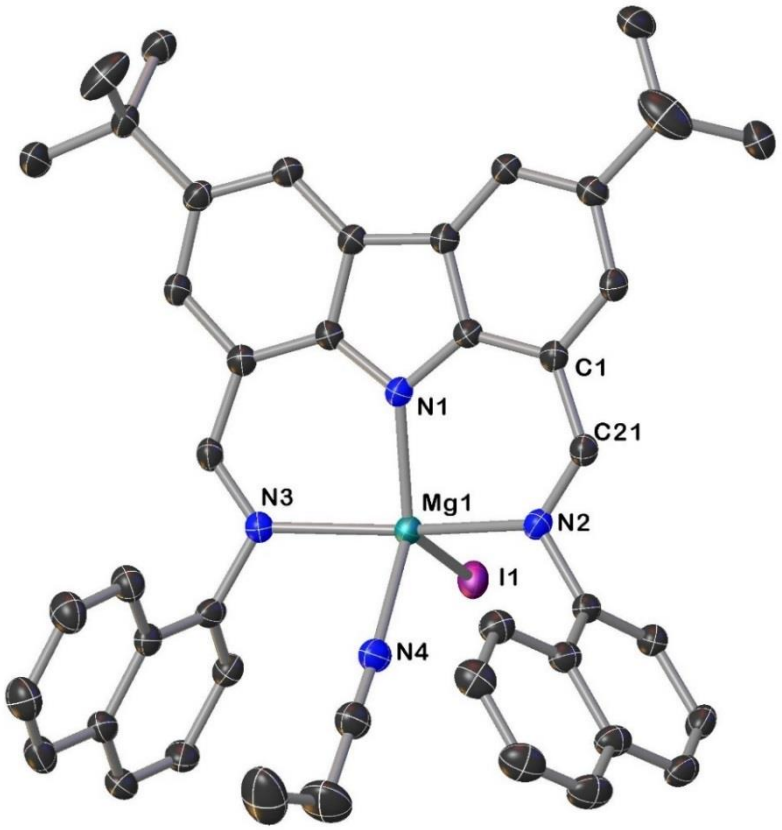


*Figure 4.7.1 Molecular structure for **24b**, with displacement ellipsoids set at 50% probability level, hydrogen atoms have been omitted for clarity.*

In the solid state, **24b** crystallises in the *P*-1 space group and a monomeric, heteroleptic complex (Figure 4.7.1), with only one molecule occupying the asymmetric unit. The coordination sphere around the five-coordinate metal centre Mg(1) is not dissimilar from the one found in the parent compound **24** (τ_5 = 0.35),[152] with the exception that the coordinated solvent (Et_2O) has been replaced by a molecule of acrylonitrile, coordinated *via* the cyano nitrogen [Mg1–N4 = 2.152(3) Å].

Bond Length (Å)		Bond Angle (°)	
Mg1–N1	2.034(2)	N2–Mg1–N3	159.58(10)
Mg1–N2	2.233(2)	N2–Mg1–N1	86.41(9)
Mg1–N3	2.214(2)	N1–Mg1–I1	114.27(8)
Mg1–I1	2.7323(9)	N1–Mg1–N4	138.45(11)
Mg1–N4	2.152(3)	C1–C21–N2	126.3(3)
C21–N2	1.297(4)	N3–Mg1–N1	86.97(9)

*Table 4.7.1 Selected bond lengths and angles for **24b**.*

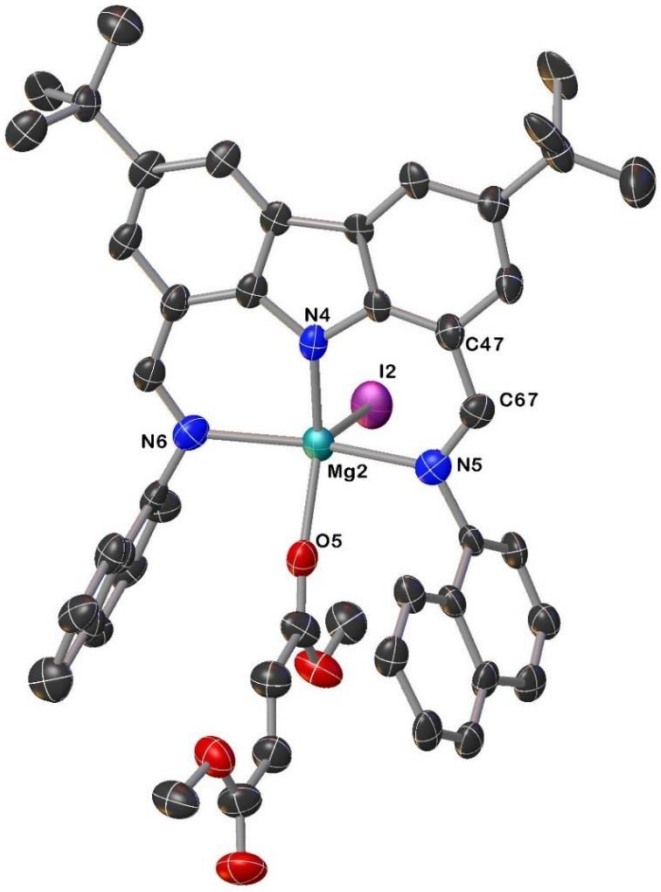


*Figure 4.7.2 Molecular structure for one of the crystallographically independent molecules for **24c**, with displacement ellipsoids set at 50% probability level, hydrogen atoms have been omitted for clarity.*

In the solid state, **24c** crystallises with two crystallographically independent molecules occupying the asymmetric unit (Figure 4.7.2). Similar to **24b**, the coordination sphere around the magnesium centre is completed by the tridentate carbazolido ligand, an iodide and a molecule of dimethylfumarate coordinated *via* the carbonylic oxygen of one of the esters (τ_5 = 0.20).[152]

Bond Length (Å)		Bond Angle (°)	
Mg2–N4	2.061(16)	N5–Mg2–N6	158.5(7)
Mg2–N5	2.260(17)	N4–Mg2–I2	107.0(5)
Mg2–N6	2.222(2)	N4–Mg2–O5	146.5(7)
Mg2–I2	2.736(6)	C47–C67–N5	124.7(18)
Mg2–O5	2.03(2)		
C67–N5	1.30(3)		

*Table 4.7.2 Selected bond lengths and angles for **24c**.*

In the solid state, **24d** is monomeric (Figure 4.7.3). The coordination sphere around the metal centre is completed by the tridentate *NNN*-pincer ligand, the iodide and a molecule of methylpropiolate, coordinated *via* the carbonilic oxygen of the propiolate [Mg1–O1 =

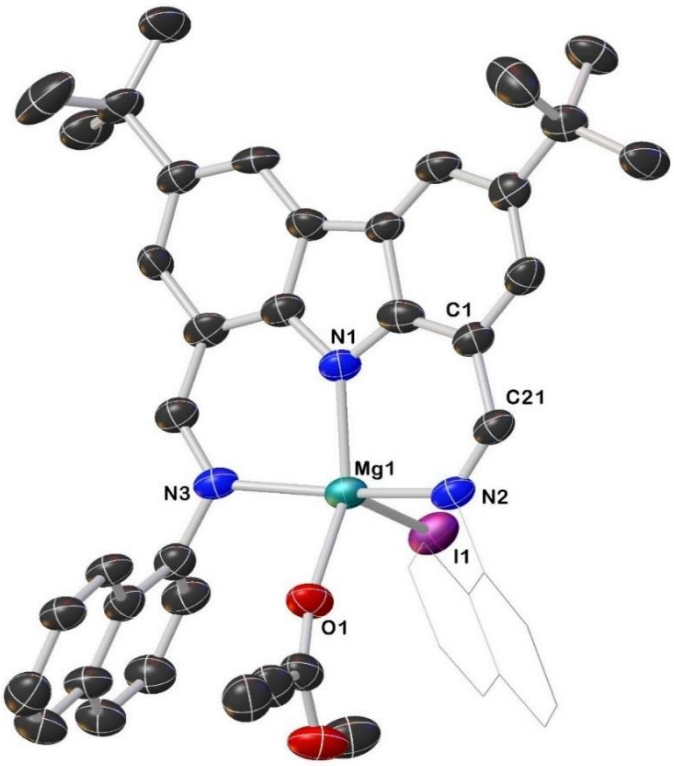


*Figure 4.7.3 Molecular structure for **24d**, with displacement ellipsoids set at 50% probability level. Hydrogen atoms have been omitted with a flanking –naphthyl subtituent being presented in wireframe form for clarity.*

2.045(6) Å] (τ_5 = 0.37).[152] The bond lengths and angles are in close agreement with those found in **24c**.

Bond Length (Å)		Bond Angle (°)	
Mg1–N1	2.032(7)	N2–Mg1–N3	161.1(3)
Mg1–N2	2.191(8)	N1–Mg1–I1	111.2(2)
Mg1–N3	2.213(8)	N1–Mg1–O1	138.9(3)
Mg1–I1	2.730(3)	C1–C21–N2	126.7(8)
Mg1–O1	2.045(6)		
C21–N2	1.292(12)		

*Table 4.7.3 Selected bond lengths and angles for **24d**.*

In the solid state, **24e** is monomeric, crystallising in the $P2_1$ space group, with one molecule occupying the asymmetric unit (Figure 4.7.4). The coordination sphere around the metal centre is completed by the symmetric carbazolido ligand, taking three coplanar coordination positions, with an iodide and a molecule of dimethyladipate, coordinated *via* the carbonilic oxygen of one of the two available esters (τ_5 = 0.31).[152]

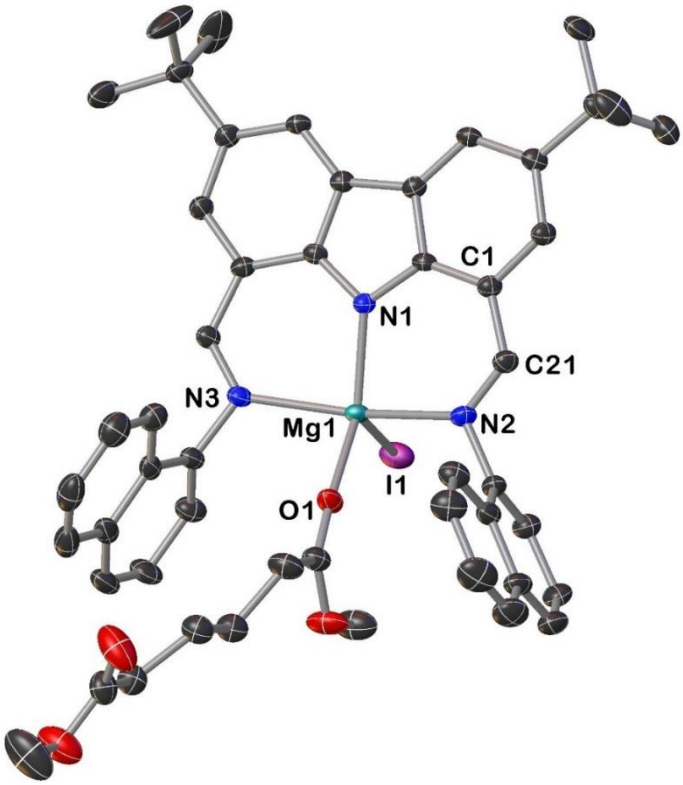


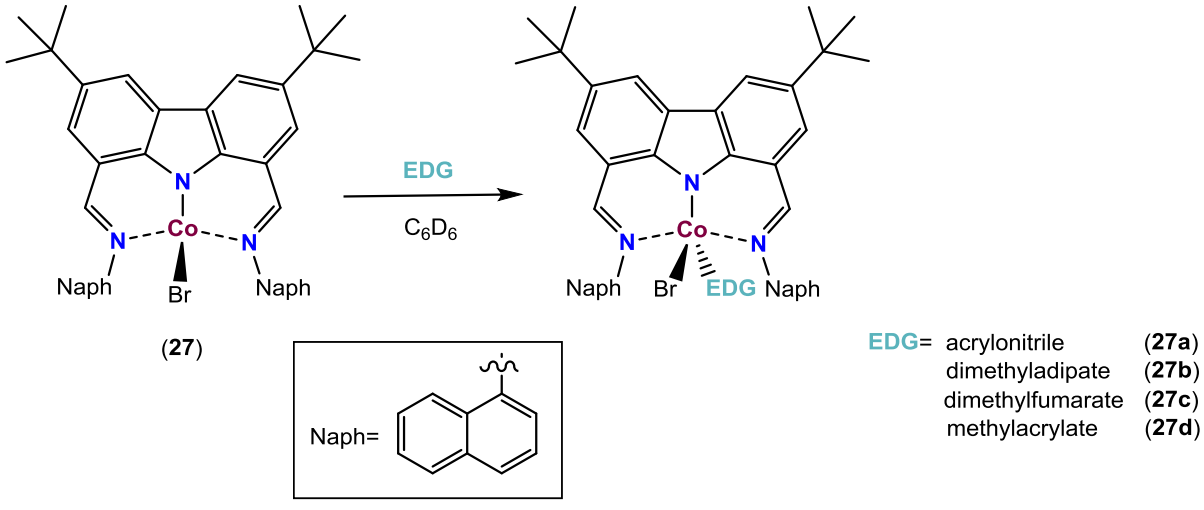
*Figure 4.7.4 Molecular structure for **24e**, with displacement ellipsoids set at 50% probability level, hydrogen atoms have been omitted for clarity.*

Bond Length (Å)		Bond Angle (°)	
Mg1–N1	2.03274(3)	N2–Mg1–N3	160.3215(4)
Mg1–N2	2.20536(3)	N1–Mg1–I1	107.2856(12)
Mg1–N3	2.20598(3)	N1–Mg1–O1	141.6997(4)
Mg1–I1	2.75397(4)	C1–C21–N2	125.9931(7)
Mg1–O1	2.03264(3)		
C21–N2	1.292(12)		

*Table 4.7.4 Selected bond lengths and angles for **24e**.*

4.7.1.1.1 Synthesis of Complexes of the Form [Naph$_2$carbCoBr]-substrate

In parallel, it was envisaged that a systematic study of the coordination/space availability around the four-coordinate metal centre in the analogous cobalt(II) bromide complex **27** could be fruitful, in the eventual task of determining a suitable family of substrates/processes catalysed by a cobalt centre. Although featuring a paramagnetic metal centre, similar behaviour to that observed for **24** with a variety of substrates (*vide supra*), the ^{1}H NMR spectra of the resulting reaction mixtures between **27** and N/O-based electron donating groups (EDG), evidencing the analogous Lewis-acidic character of **27**, and formation of new compound (**27a**-**d**) (Scheme 4.7.2).



*Scheme 4.7.2 Synthesis of coordination compounds **27a**-**27d**.*

In one case in particular, when dimethyladipate (**27b**) was employed the stoichiometry of the reaction was purposely modified to allow the formation of both a single and a double substituted compound. This has been rationalised by comparison with a similar test employing dimethylfumarate (**27c**), that the successful double substitution is directly correlated with the length of the chain employed. It was reasoned that the comparatively longer dimethyladipate presented the minimum length necessary to be able to achieve this [distances measured between the two carbazolido oxygens, dimethylfumarate 5.166(2) Å *vs.* dimethyladipate 8.382(5) Å].

Following synthesis and characterisation of the five coordinate compounds (**27a**-**d**), crystals suitable for X-ray diffraction were grown from concentrated C_6D_6 solution, upon exposure to hexane vapours, in the glovebox.

In the solid state, **27a** is monomeric, with one molecule occupying the asymmetric unit (Figure 4.7.5). Similar to the magnesium analogue **24b**, the coordination sphere around the metal centre is completed by the tridentate carbazolido ligand, occupying three coplanar positions, with a bromide and one molecule of acrylonitrile coordinated *via* the ciano nitrogen [Co1–N4 = 2.0755(16) Å] (τ_5 = 0.47).[152]

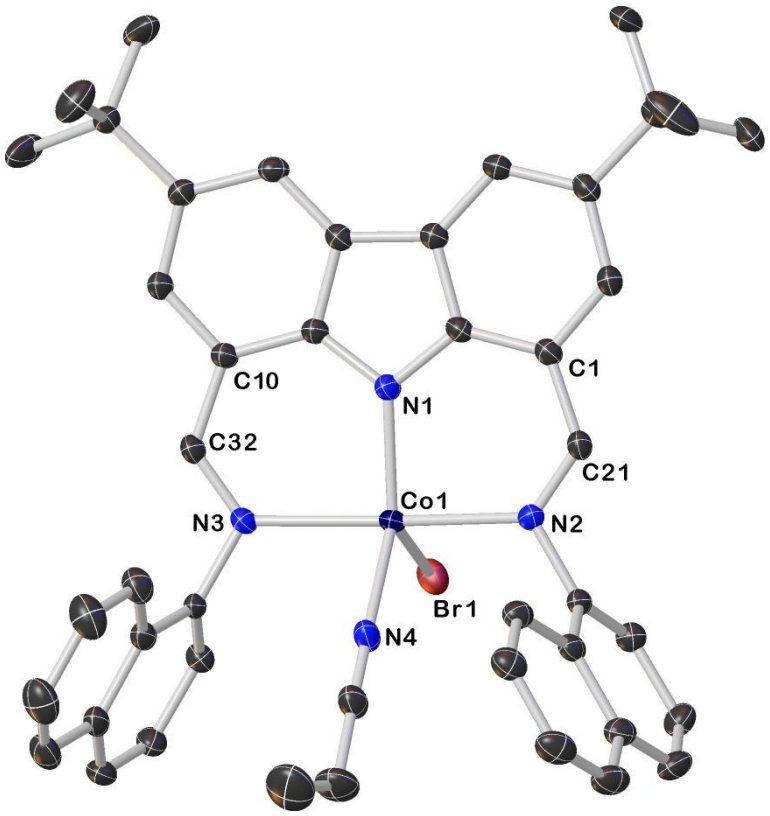


*Figure 4.7.5 Molecular structure for **27a**, with displacement ellipsoids set at 50% probability level, hydrogen atoms have been omitted for clarity.*

Bond Length (Å)		Bond Angle (°)	
Co1–N1	1.968(2)	N1–Co1–Br1	116.44(5)
Co1–N2	2.201(2)	N2–Co1–N3	165.50(6)
Co1–N3	2.199(2)	N2–C21–C1	125.4(2)
Co1–Br1	2.4306(4)	N3–C32–C10	125.4(2)
Co1–N4	2.076(2)	N1–Co1–N4	137.20(7)
C21–N2	1.289(2)		
C32–N3	1.290(2)		

*Table 4.7.5 Selected bond lengths and angles for **27a**.*

In the solid state, **27b** crystallises in the *I*2/*a* space group, with half a molecule occupying the asymmetric unit (Figure 4.7.6). The coordination sphere around the metal centre is completed by the carbazolido ligand, occupying three equatorial positions, a bromide and one molecule of dimethyladipate coordinated *via* the carbonylic oxygen of one of the esters (τ_5 = 0.65);[152] while the second ester is bound to another heteroleptic cobalt centre. The two cobalt complexes are coplanar, occupying opposing mirror image conformations, with respect to each other.

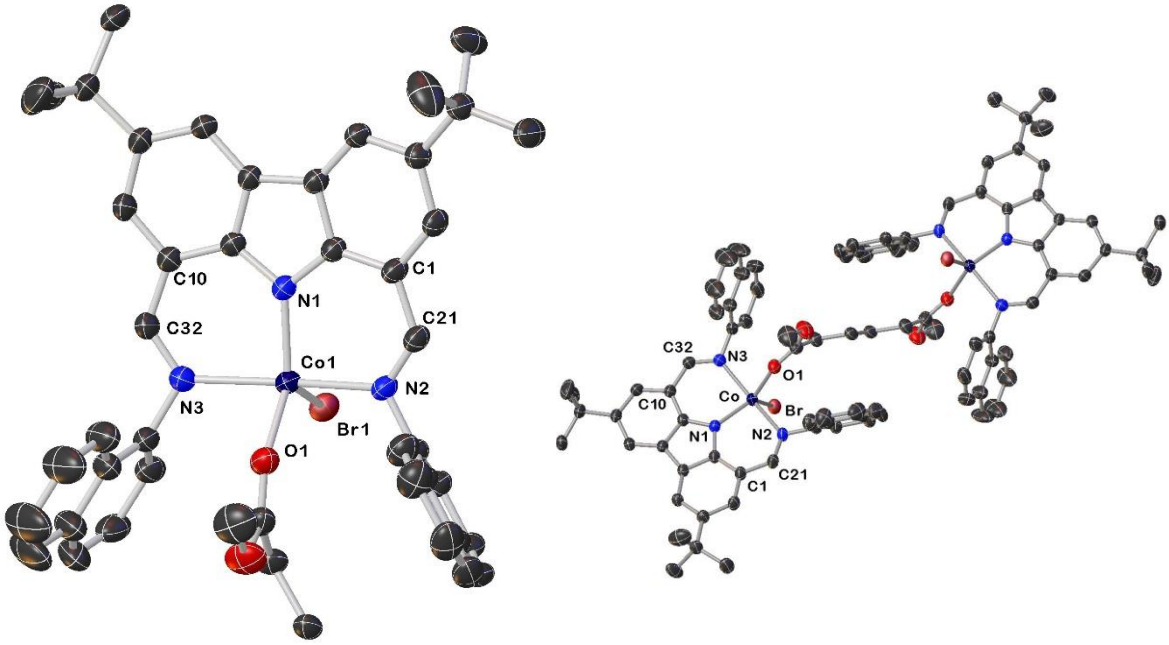


*Figure 4.7.6 Molecular structure for **27b**, showing the asymmetric unit (left) and the symmetric unit (right), with displacement ellipsoids set at 50% probability level, hydrogen atoms have been omitted for clarity.*

Bond Length (Å)		Bond Angle (°)	
Co1–N1	1.953(2)	N1–Co1–Br1	115.07(5)
Co1–N2	2.164(2)	N2–Co1–N3	166.34(7)
Co1–N3	2.174(2)	N2–C21–C1	125.91(19)
Co1–Br1	2.4463(4)	N3–C32–C10	126.0(2)
Co1–O1	2.075(2)	N1–Co1–O1	127.03(7)
C21–N2	1.293(3)		
C32–N3	1.288(3)		

*Table 4.7.6 Selected bond lengths and angles for **27b**.*

In the solid state, **27c** is monomeric, with one molecule occupying the asymmetric unit (Figure 4.7.7). Similar to the magnesium analogue **24c** (dimethylfumarate), the coordination sphere around the metal centre is completed by the tridentate carbazolido ligand, occupying three coplanar positions, with a bromide and one molecule of dimethylfumarate coordinated *via* the carbonylic oxygen of one of the esters [Co1–O1 = 2.1076(13) Å] (τ_5 = 0.54).[152]

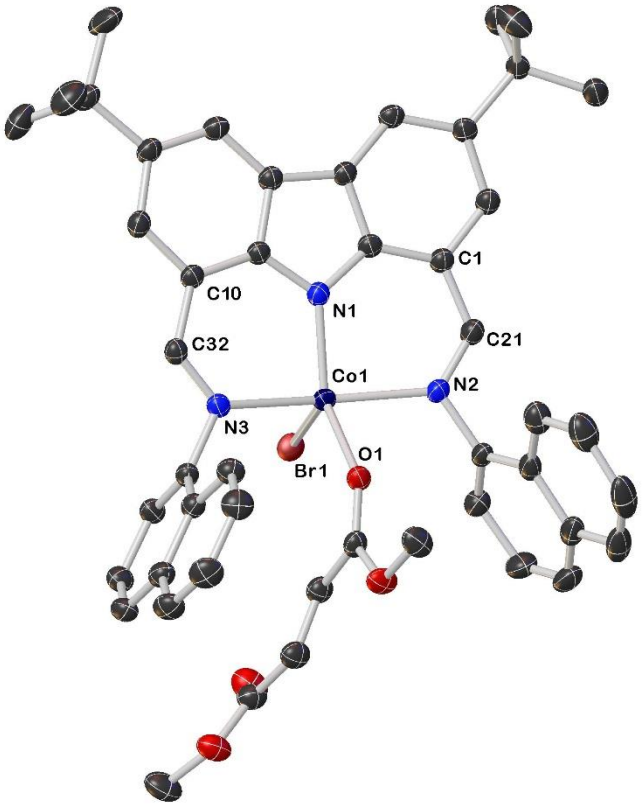


*Figure 4.7.7 Molecular structure for **27c**, with displacement ellipsoids set at 50% probability level, hydrogen atoms have been omitted for clarity.*

Bond Length (Å)		Bond Angle (°)	
Co1–N1	1.9611(16)	N1–Co1–Br1	112.43(5)
Co1–N2	2.152(2)	N2–Co1–N3	165.88(6)
Co1–N3	2.177(2)	N2–C21–C1	125.9(2)
Co1–Br1	2.4396(3)	N3–C32–C10	126.1(2)
Co1–O1	2.1076(13)	N1–Co1–O1	132.91(6)
C21–N2	1.285(3)		
C32–N3	1.291(2)		

*Table 4.7.7 Selected bond lengths and angles for **27c**.*

In the solid state, **27d** is monomeric, with one molecule occupying the asymmetric unit (Figure 4.7.8). Similar to **27b**-**c**, the coordination sphere around the metal centre is completed by the tridentate carbazolido ligand, occupying three coplanar positions, with a bromide and one molecule of methylacrylate coordinated *via* the carbonylic oxygen of one of the esters [Co1–O1 = 2.0796(11) Å] (τ_5 = 0.71).[152]

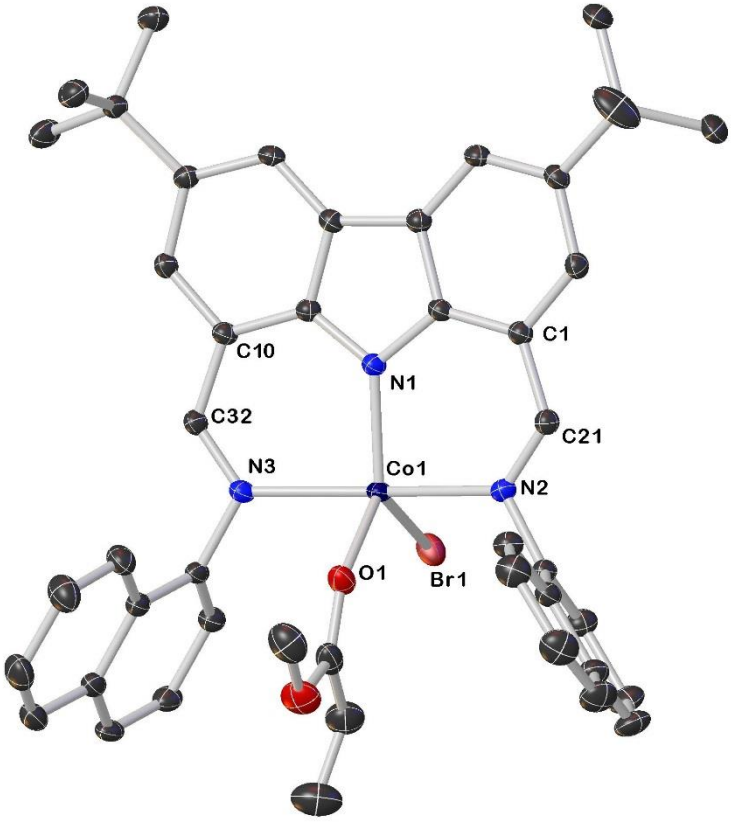


*Figure 4.7.8 Molecular structure for **27d**, with displacement ellipsoids set at 50% probability level, hydrogen atoms have been omitted for clarity.*

Bond Length (Å)		Bond Angle (°)	
Co1–N1	1.9554(12)	N1–Co1–Br1	116.87(4)
Co1–N2	2.1716(12)	N2–Co1–N3	167.67(5)
Co1–N3	2.1905(12)	N2–C21–C1	125.56(13)
Co1–Br1	2.4434(3)	N3–C32–C10	125.90(13)
Co1–O1	2.0796(11)	N1–Co1–O1	125.17(5)
C21–N2	1.291(2)		
C32–N3	1.292(2)		

*Table 4.7.8 Selected bond lengths and angles for **27d**.*

4.7.1.2 Coordination Differences Between Compounds Derived from [Naph$_2$carbMg(OEt$_2$)I] and [Naph$_2$carbCoBr]

Taking a closer look at the arrangements of the five-coordinate compounds (**24b**-**e** and **27a**-**d**) obtained, it is evident from the crystal structure determinations that very similar geometries and substitution patterns are present. However, some additional conclusions can be drawn. It would appear that there is a preferential structure adopted, particularly when a long-chain substituent was used. In such cases, this substituent would preferentially reside/adopt a defined area around the metal-halide bond. In the case of the coordination compounds derived from the heteroleptic magnesium complex **24** (**24b**-**e**), this area seems to be delimited by the symmetric flanking naphthyl groups and the iodide, with the substitution of the organic substrates pointing away from the metal-halide bond (Figure 4.7.9).

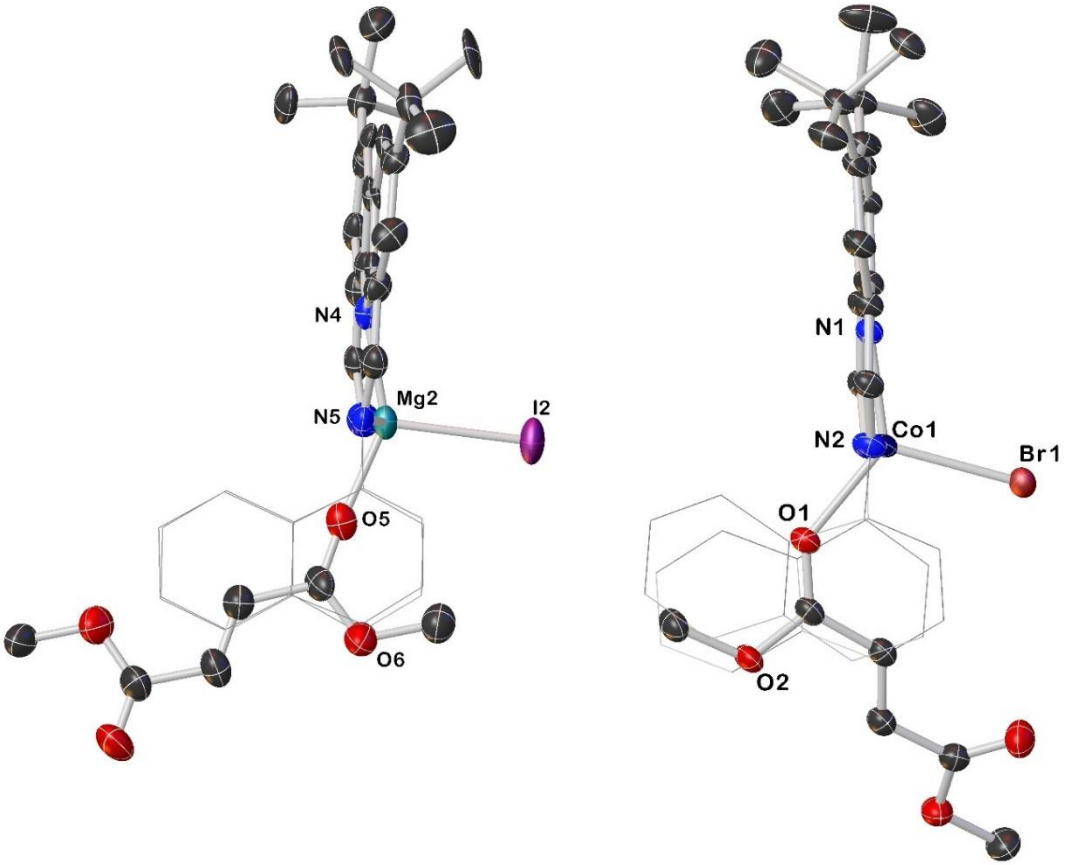


*Figure 4.7.9 Comparative side view, along the carbazolido core plane, for the molecular structures of **24c** (left) and **27c** (right), demonstrating dissimilar environments despite coordination of the same substituent (dimethylfumarate). Flanking –naphthyl groups presented in wireframe form for clarity.*

While a similar conformation is also found in the cobalt compounds derived from **27** (**27a**-**d**), the substituting organic molecules point in the same direction as the metal-bromide bond, occupying the space directly underneath said bond. This differing behaviour is difficult to justify unequivocally to only one mechanism and is most likely a consequence of multiple factors taking place simultaneously. In a first approach, it could be argued that is likely the consequence of crystal packing. However, it is notorious that directly comparing the solid state determinations of some of the similarly substituted compounds [**24b** *vs*. **27a** (acrylonitrile), **24c** *vs*. **27c** (dimethylfumarate) and **24e** *vs.* **27b** (dimethyladipate)], draws attention to only minimal differences in terms of connectivity for the whole compound with the notorious exception of the coordinated substrate. With each couple of metal complexes being found to crystallise in the same space group and same number of molecules per asymmetric unit. Despite these similarities, an important factor to consider is the size difference between the two differing halides employed (iodide *vs.* bromide). However, variation arising from the differing open/closed-shell

conformations of the metals employed, as well as the interaction of the metal against the unsaturated substrates employed, could also be a determining factor in the adoption of said conformers in the solid state.

Having said this, it would be desirable to carry out a comparative study between the differing structures observed for substituted-**24**/**27** compounds in solution (NMR spectroscopy), in order to determine rotational barriers or differing behaviours in solution. However, these determinations are hampered by the inherit paramagnetism of the cobalt(II) metal centre (**27**). Despite this, the differing geometry observed in the solid state determinations of the compounds generated *via* these methodologies, could enable the study of comparative/complementing catalytic mechanisms, based on regioselective substitution, in which abundant and non-toxic metals are employed.

4.8 Conclusions

The experiments described in this chapter show the remarkable ability of pincer ligands to stabilise and enable unusual coordination motives, while also making special emphasis on the use of adequate flanking groups, as key components in these formulations. It has been noticed that using extremely bulky substituents on the formation of the sterically encumbering proligand **5**, has yielded limited results. From this it has been possible to assess that such bulky systems although synthetically feasible, further limit coordination towards metal centres. Comparatively, great attention has been put in the formation and stabilisation of a wide range of metal complexes, employing the less sterically demanding, naphthyl substituted proligand **6**:

- Experiments with this proligand have been carried out accessing Group 2 metal complexes *via* salt metathesis with MgI_2 (**24a**) and CaI_2 (**25**). While in parallel, the formation of a five-coordinate heteroleptic magnesium complex was done and crystallographically authenticated, following organoelimination between the naphthyl ligand and MeMgI (**24**).
- Numerous attempts at the formation of first-row transition metal(II) complexes, *via* metathesis, enabled the formation of heteroleptic, four- and five-coordinate metal complexes of iron (**26**), cobalt (**27**) and manganese (**28**). While, also yielding six-coordinate homoleptic complexes of vanadium (**31**), chromium (**32**), nickel (**33**) and copper (**34**).
- Following the synthesis of the heteroleptic first-row transition metal(II) complexes **26**-**28**, and looking to study the reactivity of these compounds with $CO_{(g)}$. A novel methodology could be identified (reductive carbonylation), from which reduced iron(I) (**30**) and cobalt(I)-carbonyl (**29**) compounds could be prepared.
- Preparation of Group 12 complexes was effected *via* metathesis and organoelimination reactions, affording zinc compounds **35** and **35a**. With heavier congeners of this group also accessible *via* metathesis reactions (**36**-**37**). From these experiments, it has been possible to observe the apparent instability of the Group 12 compounds supported by this ligand system. In the case of the zinc compounds previously mentioned, experiments aiming towards the formation of heteroleptic complex **35a**, exhibited formation of a thin metallic film and full decomposition of the formed complex. In line with this, synthesis of a heteroleptic cadmium complex (**36a**) is suspected to exhibit a similar behaviour, evidenced in $^{113}Cd\{^1H\}$ NMR determinations. As such, and shortly after successful synthesis of **36a**, full decomposition in solution to the homoleptic complex **36**, was observed. While analogous reactions, employing $HgBr_2$, had allowed the synthesis and crystallographic characterisation of a four-coordinate mercury compound (**37**).

- In parallel to the formation of low-coordinate metal complexes, hypervalent Group 13 metal complexes of aluminium (**38**) and gallium (**39**) were prepared, presenting a five-coordinate metal centre ([10-Al-5] and [10-Ga-5]); with **38** being the first crystallographically characterised hypervalent aluminium complex supported on a carbazolido ligand. Analogous reactions with $InCl_3$, showed a dissimilar behaviour from that of the lighter elements of the group in metathesis reactions, yielding the homoleptic In(III) complex **40**, in agreement with similar examples reported in the literature.
- Heteroleptic Group 14 complexes could be prepared, *via* the metathesis reaction of the *in situ* generated potassium salt **14** and metal(II)-halides. As such, $GeCl_2$·Dioxane, $SnCl_2$ and $PbBr_2$ were used in the synthesis of four-coordinate tetrylenes **41**-**43**. The solid state structures of the three complexes were determined, denoting presence of a stereochemically active lone pair of electrons, with isomorphous/isostructural arrangements for the germanium (**41**) and tin (**42**) complexes. Concluding that the lead complex (**43**) could be found in two different polymorphs in the solid state. One presenting a 1D coordination polymer, based on a repetitive Pb-Br-Pb…$_\infty$ pattern. With the second polymorph, showing a formally four-coordinate monomer, with additional interaction to C_6D_6. An initial study of the reactivity of these compounds was done, starting with the heteroleptic germanium compound **41**. From this and founded on reports acknowledging the ambiphilic character of the lone pair of electrons of the germylene, formation of an imino-germylene was attempted by reaction with *p*-tolylazide (**41b**). Crystal structure determinations allowed characterisation of a suspected derivative arising from the formation of a compound of this kind (**41c**), and a mechanism for the formation of **41c** has been proposed. Additionally, it was envisaged that reaction of **41** with the previously mentioned Hauser base **24**, would result in the formation of a heterobimetallic compound or frustrated Lewis paired complex (FLP), founded in their opposing Lewis character. However, from these experiments only halide replacement complex **41a** could be isolated, and its preparation has been rationalised as a consequence of hard-soft metal/halide preferences. Finally, a hexamethyldisilazide-substituted germanium complex (**41d**), could be prepared from the metathesis reaction between **41** and $Li[N(SiMe_3)_2]$.
- With the eventual goal of their use in catalysis, the coordination ability and the space available around the metal centres in **24** and **27** has been studied, by addition of electron rich functional groups. Solution NMR determinations of the five-coordinate complexes generated (**24b**-**e** and **27a**-**d**), in conjunction with solid state determinations has allowed to resolve clear preference for nitrogen and oxygen-based substrates. Small molecules containing electron-donating groups,

employed in these studies include nitriles, aldehydes, ketones and esters. Direct comparison of compounds coordinating the same substrate, has allowed determination of two differing structures in the solid state. In the case of the magnesium centre (**24**), five-coordinate structures derived from these experiments present a preference for accommodating the O/N-based substrate away from the metal-halide bond, while the opposite is true for the analogous cobalt centre (**27**). It is expected that these determinations will shed some light on differing mechanistic pathways, in catalysis.

Finalising these studies, and looking to extend the formation of low-coordinate metal complexes to the novel asymmetric ligand based on 1,2,3,4-tetrahydrocarbazole (**9**). The formation of a Hauser Base, has been achieved by means of an organoelimination reaction between **9** and MeMgI, affording a halide-bridged dimeric structure (**44**), consistent with a less sterically bulky ligand. Whereas initial work on the synthesis of Group 12 metal centres has been carried *via* organoelimination with $ZnMe_2$ (**45**), yielding a terminal, methyl substituted metal centre.

The vast library of compounds prepared using these carbazolido-based ligands, furtherly encourages and supports a comparative study of the catalytic activities of these low-coordinate metal centres, from which reaction optimisation studies and differing reactivities could be pursued.

4.9 Experimental Section

4.9.1 Synthesis and Characterisation

1,8-di(Ar*)imino-3,6-di(*tert*-butyl)-9-magnesium-iodide-carbazole (**23**):

[Ar_2*carbMgI]

A mixture of **5** (40 mg, 0.03 mmol, 1 eq.) and ^{t}BuLi (6 mg, 0.09 mmol, 3 eq.) was dissolved in C_6D_6 (1 mL) in a J. Young´s tap NMR tube. No initial reaction was observed (^{1}H NMR spectroscopy). After heating the reaction mixture to 60 °C for 17 hours, MgI_2 (9.4 mg, 0.03 mmol, 1 eq.) was added to the sample. No initial reaction was observed at room temperature (^{1}H NMR spectroscopy), heating at 60 °C in an oil bath for 16 hours gave evidence of full disappearance of the starting material.

^{1}H NMR (300 MHz, C_6D_6, 25 °C) δ (ppm): 8.50 (d, 2H, *J* = 1.9 Hz), 7.70 (d, 6H, *J* = 5.4 Hz), 7.12-6.70 (m, 42H, Ph), 6.37 (d, 2H, *J* = 1.8 Hz, -C*H*Ph_2), 6.00 (s, 2H, -C*H*Ph_2), 1.89 (s, 6H, ArC*H*$_3$), 1.42 (s, 18H, C(C*H*$_3$)$_3$).

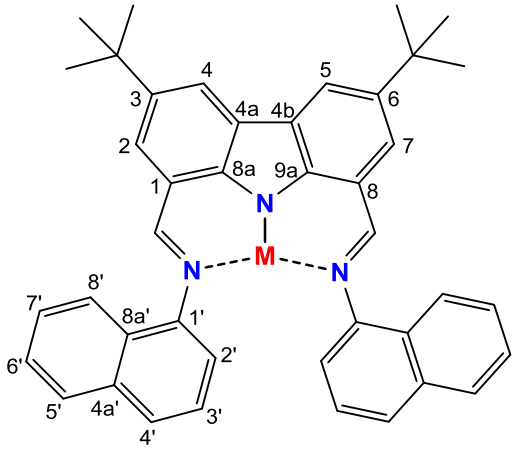


*Figure 4.9.1 General numbering scheme for compounds derived from **6**.*

1,8-dinaphthylimino-3,6-di(*tert*-butyl)carbazolido-9-magnesium-iodide-carbazole(OEt_2) (**24**):

[$Naph_2$carbMg(OEt_2)I]

To a mixture of **6** (475 mg, 0.8 mmol, 1 eq.) and MeMgI·1.5Et_2O (267 mg, 0.9 mmol, 1.2 eq.) at 0 °C was slowly added toluene (100 mL) affording a bright orange suspension. Shortly after this, the mixture was allowed to warm slowly to room temperature and stirred for 3 hours. The solvent was then removed under vacuum affording an orange-yellow

solid, which was dried for 17 hours (740 mg, 95%). Despite thorough removal of volatiles, *ca.* 1 eq. of toluene could not be removed from the product and was considered for the final yield, and all further reactions. Crystals suitable for X-ray diffraction were grown from a saturated C_6D_6 solution, at room temperature.

^{1}H NMR (400 MHz, C_6D_6, 25 °C) δ (ppm): 8.65 (d, 2H, *J* = 1.8 Hz, H4 + H5), 8.21 (s, 2H, (N=C*H*)), 7.55 (d, 2H, *J* = 8.2 Hz, Naph *H*5'), 7.43 (d, 2H, *J* = 8.3 Hz, Naph *H*2'/*H*4'), 7.39 (d, 2H, *J* = 1.3 Hz, H2 + H7), 7.33-7.25 (m, 2H, Naph *H*3'), 7.15-7.11 (m, 4H, Naph *H*6'/*H*4'/*H*2'), 7.07-7.01 (m, 2H, Naph *H*8'), 6.95-6.84 (m, 2H, Naph *H*7'), 1.46 (s, 18H, C(C*H*$_3$)$_3$).

^{13}C{^{1}H} NMR (100 MHz, C_6D_6, 25 °C) δ (ppm): 173.33 (N=*C*H), 148.55 (C8a + C9a), 140.28 (C3 + C6), 137.90 (quatern-Naph), 134.74 (quatern-Naph), 130.99 (C2 + C7), 129.34 (Naph *C*8'), 128.93 (Naph *C*5'), 126.26 (Naph *C*3'/*C*4'/*C*2'), 125.98 (Naph C2'/*C*4'/*C*6'), 125.70 (Naph *C*7') , 123.64 (C4 + C5), 122.48 (C4a + C4b), 118.00 (C1 + C8), 34.74 (*C*(CH$_3$)$_3$), 32.22 (C(*C*H$_3$)$_3$).

HRMS/EI *m/z*: [M-Et$_2$O-I]$^+$ calculated 608.2911, found 608.2913; formula $C_{42}H_{38}N_3Mg$.

IR *v*/cm^{-1} (Nujol): 2921 s, 2854 s, 2782 w, 1633 s, 1594 s, 1584 s, 1569 s, 1506 s, 1464 s, 1393 s.

[1,8-dinaphthylimino-3,6-di(*tert*-butyl)-carbazole]$_2$-9-magnesium (**24a**):

[(Naph$_2$carb)$_2$Mg]

To a mixture of **6** (100 mg, 0.17 mmol, 1 eq.) and KH (14 mg, 0.34 mmol, 2 eq.) at 0 °C, dry THF (30 mL) was slowly added. The resulting mixture was stirred at this temperature for 1 hour, and after this time, the solution was stirred at room temperature for additional 2 hours, affording a dark red solution. In a separate schlenk, MgI_2 (47 mg, 0.18 mmol, 1.2 eq.) was weighed, and dry THF (30 mL) was added. The reaction mixture was cooled down to 0 °C, and the dark-red solution containing **14** was filtered/dropwise added to the MgI_2 suspension over 30 minutes. The resulting mixture was left stirring at the temperature described and allowed to reach room temperature over the course of 16 hours, with further stirring for additional 24 hours, affording a light orange suspension. After this time, the solvent was removed under vacuum, yielding a dark orange powder. This powder was then extracted into hexane (3 x 30 mL) affording an orange solution. Further evaporation of volatiles allowed the isolation of a dark orange solid. Crystals were grown from a concentrated solution in hexane at room temperature. The quality of the X-ray data was low but allowed corroboration for the formation of the homoleptic complex.

^{1}H NMR (300 MHz, C_6D_6, 25 °C) δ (ppm): 9.04 (d, 2H, *J* = 6.5 Hz, Naph), 8.66 (d, 2H, *J* = 1.9 Hz H4 + H5), 8.22 (s, 2H, (N=C*H*)), 7.54 (d, 2H, *J* = 8.3 Hz, Naph), 7.49 (d, 2H, *J* = 8.1 Hz, Naph), 7.41-7.33 (m, 4H, Naph/H2+H7), 7.29 (t, 2H, *J* = 7.5 Hz, Naph), 7.12-7.04 (m, 2H, Naph), 6.97-6.85 (m, 2H, Naph), 1.46 (s, 18H, C(C*H*$_3$)$_3$).

^{13}C{^{1}H} NMR (100 MHz, C_6D_6, 25 °C) δ (ppm): 173.92 (N=*C*H), 149.18 (quaternary), 148.56 (quaternary), 139.77 (quaternary), 134.35 (quaternary), 130.53 (C2 + C7), 125.77, 125.47, 125.26, 123.19 (C4 + C5), 122.75, 121.86, 120.99 (quaternary), 117.67 (quaternary), 34.34 (*C*(CH$_3$)$_3$), 31.84 (C(*C*H$_3$)$_3$).

1,8-dinaphthylimino-3,6-di(*tert*-butyl)-9-magnesium-iodide-carbazole(acrylonitrile) (**24b**):

[Naph$_2$carbMg(acrylonitrile)I]

In a J. Young's NMR tube, **24** (20 mg, 0.022 mmol, 1 eq.) was suspended in 0.6 mL of C_6D_6, acrylonitrile (1.5 µL, 0.033 mmol, 1.5 eq.) was added, affording a pale orange-yellow solution. Crystals suitable for X-ray diffraction were grown from a concentrated solution in C_6D_6, exposed to hexane vapours, at room temperature.

^{1}H NMR (300 MHz, C_6D_6, 25 °C) δ (ppm): [signals for acrylonitrile diffuse, with one equivalent of Et_2O liberated] 8.65 (d, 2H, *J* = 1.9 Hz, H4 + H5), 8.20 (s, 2H, (N=C*H*)), 7.62 (d, 2H, *J* = 8.3 Hz, Naph), 7.51-7.32 (m, 8H, Naph/H2 + H7), 7.12 (d, 2H, *J* = 7.5 Hz, Naph), 7.08-6.97 (m, 4H, Naph), 6.90 (t, 2H, *J* = 7.4 Hz, Naph), 1.46 (s, 18H, C(C*H*$_3$)$_3$).

1,8-dinaphthylimino-3,6-di(*tert*-butyl)-9-magnesium-iodide-carbazole(dimethylfumarate) (**24c**):

[Naph$_2$carbMg(dimethylfumarate)I]

In a J. Young's NMR tube, **24** (15 mg, 0.016 mmol, 1 eq.) was suspended in 0.6 mL of C_6D_6, dimethylfumarate (8 mg, 0.05 mmol, 3 eq.) was added, affording a pale orange-yellow solution. Crystals suitable for X-ray diffraction were grown from a concentrated solution in C_6D_6, exposed to hexane vapours, at room temperature.

^{1}H NMR (300 MHz, C_6D_6, 25 °C) δ (ppm): [signals for dimethylfumarate diffuse, with one equivalent of Et_2O liberated] 8.67 (d, 2H, *J* = 1.8 Hz, H4 + H5), 8.50 (d, 2H, *J* = 6.4 Hz, Naph), 8.14 (s, 2H, (N=C*H*)), 7.47 (d, 2H, *J* = 7.9 Hz, Naph), 7.43 (d, 2H, *J* = 1.8 Hz, H2

+ H7), 7.39 (d, 2H, *J* = 7.9 Hz, Naph), 7.28-7.18 (m, 4H, Naph), 7.13-6.86 (m, 2H, Naph), 6.82-6.53 (br s, 2H, Naph), 1.48 (s, 18H, C(C*H*$_3$)$_3$).

1,8-dinaphthylimino-3,6-di(*tert*-butyl)-9-magnesium-iodide-carbazole(methylpropiolate) (**24d**):

[Naph$_2$carbMg(methylpropiolate)I]

In a J. Young's NMR tube, **24** (20 mg, 0.03 mmol, 1 eq.) was suspended in 0.6 mL of C_6D_6, and methylpropiolate (2.15 µL, 0.03 mmol, 1 eq.) was added, affording a pale orange-yellow solution. Crystals suitable for X-ray diffraction were grown from a concentrated solution in C_6D_6, exposed to hexane vapours, at room temperature.

^{1}H NMR (300 MHz, C_6D_6, 25 °C) δ (ppm): [signals for methylpropiolate diffuse, with one equivalent of Et_2O liberated] 8.65 (d, 2H, *J* = 1.8 Hz, H4 + H5), 8.18 (s, 2H, (N=C*H*)), 7.63-7.52 (m, 2H, Naph), 7.46 (d, 2H, *J* = 7.7 Hz, Naph), 7.41 (d, 2H, *J* = 1.7 Hz, H2 + H7), 7.35 (d, 2H, *J* = 7.8 Hz, Naph), 7.32-7.19 (m, 2H, Naph), 7.14-6.98 (m, 4H, Naph), 6.95-6.82 (m, 2H, Naph), 1.47 (s, 18H, C(C*H*$_3$)$_3$).

1,8-dinaphthylimino-3,6-di(*tert*-butyl)-9-magnesium-iodide-carbazole(dimethyladipate) (**24e**):

[Naph$_2$carbMg(dimethyladipate)I]

In a J. Young's NMR tube, **24** (15 mg, 0.02 mmol, 1 eq.) was suspended in 0.6 mL of C_6D_6, and dimethyladipate (15 mg, 0.08 mmol, 4 eq.) was added, affording a pale orange-yellow solution. Crystals suitable for X-ray diffraction were grown from a concentrated solution in C_6D_6, exposed to hexane vapours, at room temperature.

^{1}H NMR (400 MHz, C_6D_6, 25 °C) δ (ppm): [signals for dimethyladipate diffuse, with one equivalent of Et_2O liberated] 8.66 (br s, 2H, H4 + H5), 8.60 (d, 2H, *J* = 7.2 Hz, Naph), 8.16 (s, 2H, (N=C*H*)), 7.52 (d, 2H, *J* = 8.6 Hz, Naph), 7.48 (d, 2H, *J* = 8.3 Hz, Naph), 7.45-7.37 (m, 4H, Naph/ H2 + H7), 7.29 (t, 2H, *J* = 7.5 Hz, Naph), 7.12 (d, 1H, *J* = 7.3 Hz, Naph), 7.06 (t, 2H, *J* = 7.2 Hz, Naph), 7.01 (d, 1H, *J* = 7.6 Hz, Naph), 6.89 (t, 2H, *J* = 8.0 Hz, Naph), 1.47 (s, 18H, C(C*H*$_3$)$_3$).

1,8-dinaphthylimino-3,6-di(*tert*-butyl)-9-calcium-iodide-carbazole (**25**):

[Naph$_2$carbCaI]

A mixture of **6** (100 mg, 0.17 mmol, 1 eq.) and KH (14 mg, 0.34 mmol, 2 eq.) at 0 °C in THF (30 mL) was stirred for 1 hour. After this time, the reaction mixture was allowed to warm slowly to room temperature and stirred for an additional 2 hours, affording a dark red solution. This mixture was added dropwise to a suspension of CaI_2 (100 mg, 0.34 mmol, 2 eq.) in THF (30 mL) at 0 °C over 30 minutes. This mixture was allowed to reach room temperature for 48 hours, affording a bright yellow suspension. After this time, the solvent was removed under vacuum, yielding a dark yellow powder, which was extracted into hexane (3 x 30 mL) from which upon removal of volatiles afforded a dark yellow solid.

^{1}H NMR (300 MHz, C_6D_6, 25 °C) δ (ppm): 8.89 (d, 2H, *J* = 2.0 Hz, H4 + H5), 8.64-8.59 (m, 2H, Naph), 8.51 (s, 2H, (N=C*H*)), 8.02-7.84 (m, 2H, Naph), 7.77 (d, 3H, *J* = 1.7 Hz, Naph/H2 + H7) 7.61-7.50 (m, 3H, Naph), 7.44-7.31 (m, 3H, Naph), 7.08-7.03 (m, 1H, Naph), 6.97 (dd, 1H, *J* = 7.3 and 1.1 Hz), 6.63 (ddd, 1H, *J* = 8.3, 6.8 and 1.3 Hz), 1.58 (s, 18H, C(C*H*$_3$)$_3$).

1,8-dinaphthylimino-3,6-di(*tert*-butyl)-9-iron-chloride-carbazole(THF) (**26**):

[Naph$_2$carbFe(thf)Cl]

In a Schlenk flask, a mixture of **6** (200 mg, 0.34 mmol, 1 eq.) and KH (28 mg, 0.70 mmol, 2 eq.) were allowed to react in THF (30 mL) at 0 °C for 1 hour, and after this time, the reaction mixture was warmed to room temperature and stirred for an additional 2 hours, affording a dark red solution. This mixture was added dropwise to a Schlenk containing a suspension of $FeCl_2{\cdot}THF_{1.5}$ (87 mg, 0.70 mmol, 2 eq.) in THF (30 mL) at 0 °C over a period of 10 minutes. The resulting mixture was allowed to reach room temperature and stirred for 48 hours. After this time, the solvent was removed under vacuum, yielding a brown-red powder, which was extracted into warm toluene (3 x 30 mL) from which the title compound was obtained following evaporation of volatiles under vacuum (131 mg, 52%). Crystals suitable for X-ray diffraction were grown from a concentrated hexane solution at room temperature.

^{1}H NMR (400 MHz, C_6D_6, 25 °C) δ (ppm): [all peaks appear as broad singlets] 57.28 ($\Delta\nu_{1/2}$= 350 Hz), 20.48 ($\Delta\nu_{1/2}$= 365 Hz), 10.83 ($\Delta\nu_{1/2}$= 225 Hz), 8.52 ($\Delta\nu_{1/2}$= 75 Hz), 6.10 ($\Delta\nu_{1/2}$= 118 Hz), 2.12 ($\Delta\nu_{1/2}$= 47 Hz), 1.47 ($\Delta\nu_{1/2}$= 80 Hz), 0.31 ($\Delta\nu_{1/2}$= 50 Hz), –2.60 ($\Delta\nu_{1/2}$= 226 Hz), –3.73 ($\Delta\nu_{1/2}$= 197 Hz), –16.13 ($\Delta\nu_{1/2}$= 273 Hz), –25.54 ($\Delta\nu_{1/2}$= 427 Hz).

μ_{eff} (Evans' NMR Method, C_6D_6, 25 °C)= 3.33 μ_B.

HRMS/ASAP *m/z*: $[M\text{-}Cl\text{-}C_4H_8O]^+$ calculated 638.2462; found 638.2460 formula $C_{42}H_{38}N_3Fe$.

IR ν/cm^{-1} (Nujol): 2958 s, 2855 s, 1666 w, 1570 s, 1554 w, 1507 s, 1461 s.

UV/vis (toluene, c = 2.67 x 10^{-5} mol dm^{-3}): λ_{max}/nm (ε x10^3 / dm^{3}mol^{-1}cm^{-1}) 386 (9.29).

1,8-dinaphthylimino-3,6-di(*tert*-butyl)-9-cobalt-bromide-carbazole (**27**):

[Naph$_2$carbCoBr]

In a Schlenk flask, a mixture of **6** (500 mg, 0.9 mmol, 1 eq.) and KH (68 mg, 1.7 mmol, 2 eq.), were allowed to react in THF (30 mL) at 0 °C for 1 hour, and then stirred at room temperature for an additional 2 hours, affording a dark red solution. This mixture was added dropwise to a solution of $CoBr_2$·DME (527 mg, 1.7 mmol, 2 eq.) in THF (30 mL), at 0 °C, and allowed to warm slowly to room temperature with further stirring for additional 48 hours, affording a light-brown solution. Volatiles were removed under vacuum, and the resulting brown powder was extracted into warm toluene (3 x 30 mL), yielding a dark brown-purple solution. Removal of volatiles under vacuum afforded the title compound was obtained as a bright purple powder (530 mg, 86%). Crystals suitable for X-ray diffraction were grown from a concentrated hexane solution at room temperature.

^{1}H NMR (400 MHz, C_6D_6, 25 °C) δ (ppm): [all peaks appear as broad singlets] 46.94 ($\Delta\nu_{1/2}$= 160 Hz), 22.06 ($\Delta\nu_{1/2}$= 206 Hz), 4.74 ($\Delta\nu_{1/2}$= 111 Hz), 2.13 ($\Delta\nu_{1/2}$= 89 Hz), 1.37 ($\Delta\nu_{1/2}$= 141 Hz), 1.02 ($\Delta\nu_{1/2}$= 62 Hz), 0.32 ($\Delta\nu_{1/2}$= 83 Hz), –0.38 ($\Delta\nu_{1/2}$= 137 Hz), –2.76 ($\Delta\nu_{1/2}$= 121 Hz) ($\Delta\nu_{1/2}$= 104 Hz), –15.69 ($\Delta\nu_{1/2}$= 130 Hz), –18.25 ($\Delta\nu_{1/2}$= 239 Hz), –64.21 ($\Delta\nu_{1/2}$= 2179 Hz).

μ_{eff} (Evans' NMR Method, C_6D_6, 25 °C)= 2.92 μ_B.

HRMS/ASAP *m/z*: $[M]^+$ calculated 722.1581; found 722.1597 formula $C_{42}H_{38}N_3BrCo$.

IR ν/cm^{-1} (Nujol): 2956 s, 2921 s, 2854 s, 1545 s, 1461 s.

UV/vis (toluene, c = 1.38 x 10^{-5} mol dm^{-3}): λ_{max}/nm (ε x10^3 / dm^{3}mol^{-1}cm^{-1}) 386 (9.91).

1,8-dinaphthylimino-3,6-di(*tert*-butyl)-9-cobalt-bromide-carbazole(acrylonitrile) (**27a**):

[Naph$_2$carbCo(acrylonitrile)Br]

In a J. Young's NMR tube, **27** (40 mg, 0.05 mmol, 1 eq.) was dissolved in 0.6 mL of C_6D_6, affording a dark purple solution, to which, acrylonitrile (4 µL, 0.06 mmol, 1.1 eq.) was added. This sample was sonicated at room temperature for 5 minutes. A paramagnetic ^{1}H NMR spectrum, confirmed full disappearance of **27**, and formation of a new product.

Crystals suitable for X-ray diffraction were grown from a concentrated C_6D_6 solution, exposed to hexane vapours, at room temperature.

^{1}H NMR (400 MHz, C_6D_6, 25 °C) δ (ppm): [all peaks appear as broad singlets] 56.02 ($\Delta\nu_{1/2}$= 1460 Hz), 18.63 ($\Delta\nu_{1/2}$= 390 Hz), 13.57 ($\Delta\nu_{1/2}$= 114 Hz), 10.72 ($\Delta\nu_{1/2}$= 526 Hz), 5.25 ($\Delta\nu_{1/2}$= 50 Hz), 4.03 ($\Delta\nu_{1/2}$= 114 Hz), 3.67 ($\Delta\nu_{1/2}$= 50 Hz), 2.10 ($\Delta\nu_{1/2}$= 47 Hz), 1.49 ($\Delta\nu_{1/2}$= 150 Hz), 0.28 ($\Delta\nu_{1/2}$= 56 Hz), –8.86 ($\Delta\nu_{1/2}$= 280 Hz), –24.61 ($\Delta\nu_{1/2}$= 1460 Hz), –41.27 ($\Delta\nu_{1/2}$= 1426 Hz).

HRMS/ASAP *m/z*: $[M\text{-}C_3H_3N]^+$ calculated 722.1581; found 722.1567 formula $C_{42}H_{38}N_3CoBr$.

1,8-dinaphthylimino-3,6-di(*tert*-butyl)-9-cobalt-bromide-carbazole(dimethyladipate) (**27b**):

By controlling the stoichiometry of the reaction, it was possible to synthesise both the mono and the double-metallated product:

[Naph$_2$carbCo(dimethyladipate)Br]

For the mono-metallated product: A sample of **27** (10 mg, 0.013 mmol, 1 eq.) was dissolved in 0.6 mL of C_6D_6 in a J. Young's NMR tube, and dimethyladipate (11.3 µL, 0.06 mmol, 5 eq.) was added. A ^{1}H NMR spectrum of the solution confirmed full disappearance of **27**, and formation of a new product. Crystals suitable for X-ray diffraction were grown from a concentrated C_6D_6 solution, exposed to hexane vapours, at room temperature.

^{1}H NMR (400 MHz, C_6D_6, 25 °C) δ (ppm): [all peaks appear as broad singlets/single coordinated product] 54.59 ($\Delta\nu_{1/2}$= 259 Hz), 20.01 ($\Delta\nu_{1/2}$= 267 Hz), 14.55 ($\Delta\nu_{1/2}$= 194 Hz), 4.99 ($\Delta\nu_{1/2}$= 61 Hz), 3.77 ($\Delta\nu_{1/2}$= 74 Hz), 3.28, 2.11 ($\Delta\nu_{1/2}$= 35 Hz), 0.30 ($\Delta\nu_{1/2}$= 116 Hz), –11.05 ($\Delta\nu_{1/2}$= 187 Hz), –12.04 ($\Delta\nu_{1/2}$= 121 Hz), –47.37 ($\Delta\nu_{1/2}$= 1509 Hz).

HRMS/EI *m/z*: $[M\text{-}C_8H_{14}O_4]^+$ calculated 722.1576; found 722.1576 formula $C_{42}H_{38}N_3CoBr$.

[Naph$_2$carbCoBr]-dimethyladipate-[Naph$_2$carbCoBr]

For the double-metallated product: A sample of **27** (15 mg, 0.02 mmol, 1 eq.) was dissolved in 0.6 mL of C_6D_6 in a J. Young's tap NMR tube, and dimethyladipate (1.7 µL, 0.01 mmol, 0.5 eq.) was added. A ^{1}H NMR spectrum confirmed full disappearance of **27**,

and formation of a new product. Crystals suitable for X-ray diffraction were grown from a concentrated C_6D_6 solution, exposed to hexane vapours, at room temperature.

^{1}H NMR (400 MHz, C_6D_6, 25 °C) δ (ppm): [all peaks appear as broad singlets/double coordinated product] 48.63 ($\Delta\nu_{1/2}$= 195 Hz), 21.38 ($\Delta\nu_{1/2}$= 244 Hz), 20.30 ($\Delta\nu_{1/2}$= 165 Hz), 4.77 ($\Delta\nu_{1/2}$= 122 Hz), 2.12 ($\Delta\nu_{1/2}$= 87 Hz), 1.39 ($\Delta\nu_{1/2}$= 121 Hz), 0.33 ($\Delta\nu_{1/2}$= 117 Hz), –2.07 ($\Delta\nu_{1/2}$= 123 Hz), –14.78 ($\Delta\nu_{1/2}$= 158 Hz), –16.59 ($\Delta\nu_{1/2}$= 262 Hz), –60.41.

HRMS/ASAP *m/z*: $[M\text{-}C_{50}H_{52}BrCoN_3O_4]^+$ calculated 722.1581; found 722.1648 formula $C_{42}H_{38}N_3CoBr$.

1,8-dinaphthylimino-3,6-di(*tert*-butyl)-9-cobalt-bromide-carbazole(dimethylfumarate) (**27c**):

[Naph$_2$carbCo(dimethylfumarate)Br]

A mixture of **27** (15 mg, 0.02 mmol, 1 eq.) and dimethylfumarate (9 mg, 0.06 mmol, 3 eq.) was dissolved in 0.6 mL of C_6D_6 in a J. Young's tap NMR tube. After sonication at room temperature for 10 minutes a ^{1}H NMR spectrum was performed, which confirmed full disappearance of **27**, and the formation of a new product. Crystals suitable for X-ray diffraction were grown from a concentrated C_6D_6 solution exposed to hexane vapours, at room temperature.

^{1}H NMR (400 MHz, C_6D_6, 25 °C) δ (ppm): [all peaks appear as broad singlets] 52.06 ($\Delta\nu_{1/2}$= 287 Hz), 21.48 ($\Delta\nu_{1/2}$= 300 Hz), 17.99 ($\Delta\nu_{1/2}$= 220 Hz), 11.05 ($\Delta\nu_{1/2}$= 577 Hz), 4.97 ($\Delta\nu_{1/2}$= 167 Hz), 4.28 ($\Delta\nu_{1/2}$= 192 Hz), 2.11 ($\Delta\nu_{1/2}$= 160 Hz), 1.03 ($\Delta\nu_{1/2}$= 192 Hz), –1.45 ($\Delta\nu_{1/2}$= 160 Hz), –13.70 ($\Delta\nu_{1/2}$= 185 Hz), –14.69 ($\Delta\nu_{1/2}$= 230 Hz), –55.98 ($\Delta\nu_{1/2}$= 2149 Hz).

HRMS/ASAP *m/z*: $[M\text{-}C_6H_8O_4]^+$ calculated 722.1581; found 722.1567 formula $C_{42}H_{38}N_3CoBr$.

1,8-dinaphthylimino-3,6-di(*tert*-butyl)-9-cobalt-bromide-carbazole(methylacrylate) (**27d**):

[Naph$_2$carbCo(methylacrylate)Br]

A sample of **27** (15 mg, 0.02 mmol, 1 eq.) was dissolved in 0.6 mL of C_6D_6 in a J. Young's tap NMR tube, and methylacrylate (18 µL, 0.2 mmol, 10 eq.) was added. A ^{1}H NMR spectrum confirmed full disappearance of **27**, and formation of a new product. Crystals

suitable for X-ray diffraction were grown from a concentrated C_6D_6 solution, exposed to hexane vapours, at room temperature.

^{1}H NMR (400 MHz, C_6D_6, 25 °C) δ (ppm): [all peaks appear as broad singlets] 57.23 ($\Delta\nu_{1/2}$= 431 Hz), 20.84 ($\Delta\nu_{1/2}$= 455 Hz), 12.92 ($\Delta\nu_{1/2}$= 455 Hz), 4.32, 3.52 ($\Delta\nu_{1/2}$= 623 Hz), 1.68 ($\Delta\nu_{1/2}$= 500 Hz), –10.29 ($\Delta\nu_{1/2}$= 323 Hz), –11.52 ($\Delta\nu_{1/2}$= 290 Hz), –43.95 ($\Delta\nu_{1/2}$= 1056 Hz).

HRMS/ASAP *m/z*: $[M\text{-}Br\text{-}C_4H_6O_2]^+$ calculated 643.2398; found 643.2396 formula $C_{42}H_{38}N_3Co$.

1,8-dinaphthylimino-3,6-di(*tert*-butyl)-9-manganese-bromide-carbazole(THF) (**28**):

[$Naph_2carbMn(thf)Br$]

In a Schlenk flask, **6** (200 mg, 0.4 mmol, 1 eq.) and KH (28 mg, 0.7 mmol, 2 eq.), were cooled down to 0 °C, dry THF (30 mL) was slowly added and the resulting mixture was stirred at this temperature for 1 hour. After this time, the reaction mixture was stirred at room temperature for additional 2 hours, affording a dark red solution. This was added dropwise to a suspension of $MnBr_2$ (147 mg, 0.7 mmol, 2 eq.) in THF (30 mL) at 0 °C. The resulting mixture was allowed to reach room temperature, stirring for 48 hours, affording an orange-red suspension. Volatiles were removed under vacuum, yielding a yellow-orange powder, which was extracted into hot toluene and filtered to separate from metal salts, affording a dark pink-orange solution. Removal of volatiles yielded a dark pink-orange powder (135 mg, 51%). Crystals suitable for X-ray diffraction were grown from a concentrated solution in hexane at room temperature.

^{1}H NMR (400 MHz, C_6D_6, 25 °C) δ (ppm): [all peaks appear as broad singlets] 22.08 ($\Delta\nu_{1/2}$= 1437 Hz), 13.40 ($\Delta\nu_{1/2}$= 25 Hz), 8.51 ($\Delta\nu_{1/2}$= 27 Hz), 6.52 ($\Delta\nu_{1/2}$= 27 Hz), 2.11 ($\Delta\nu_{1/2}$= 61 Hz), 1.49 ($\Delta\nu_{1/2}$= 29 Hz), 0.30 ($\Delta\nu_{1/2}$= 27 Hz), -8.95 ($\Delta\nu_{1/2}$= 808 Hz).

μ_{eff} (Evans' NMR Method, C_6D_6, 25 °C)= 3.64 μ_B.

MS/ASAP *m/z*: $[M\text{-}C_4H_8O\text{-}Br]^+$ calculated 639.2446; found 639.2454 formula $C_{42}H_{38}N_3Mn$.

IR ν/cm^{-1} (Nujol): 2955 s, 2926 s, 2854 s, 1631 s, 1599 s, 1571 s, 1482 s, 1461 s.

UV/vis (toluene, c = 2.53 x 10^{-5} mol dm^{-3}): λ_{max}/nm (ε x10^3 / dm^{3}mol^{-1}cm^{-1}) 386 (14.48).

1,8-dinaphthylimino-3,6-di(*tert*-butyl)-9-cobalt- carbonyl-carbazole (**29**):

[$Naph_2carbCo(CO)$]

In a Schlenk flask, **27** (50 mg, 0.07 mmol, 1 eq.) was dissolved in toluene (15 mL), affording a dark brown solution. $Li[BHEt_3]$ (1M, 69 µL, 0.07 mmol) was added, rendering the solution black. The atmosphere in the Schlenk was replaced with CO(g) *via* three freeze-thaw cycles (x 3). Left stirring at room temperature for 22 hours, followed by emoval of volatiles allowed isolation of **29** as a black powder (34.8 mg, 75%). Crystals suitable for X-ray diffraction, were grown from a saturated C_6D_6 solution *via* hexane vapour diffusion, at room temperature.

^1H NMR (400 MHz, C_6D_6, 25 °C) δ (ppm): [all peaks appear as broad singlets] 56.04 ($\Delta\nu_{1/2}$= 198 Hz), 22.53 ($\Delta\nu_{1/2}$= 209 Hz), 15.55 ($\Delta\nu_{1/2}$= 178 Hz), 8.94 ($\Delta\nu_{1/2}$= 93 Hz), 8.44 ($\Delta\nu_{1/2}$= 94 Hz), 5.67 ($\Delta\nu_{1/2}$= 140 Hz), 4.07 ($\Delta\nu_{1/2}$= 129 Hz), 1.66 ($\Delta\nu_{1/2}$= 106 Hz), 0.96 ($\Delta\nu_{1/2}$= 130 Hz), 0.30 ($\Delta\nu_{1/2}$= 84 Hz), –12.38 ($\Delta\nu_{1/2}$= 160 Hz), –13.96 ($\Delta\nu_{1/2}$= 177 Hz), –52.6 ($\Delta\nu_{1/2}$= 944 Hz).

μ_{eff} (Evans' NMR Method, C_6D_6, 25 °C)= 1.58 μ_B.

HRMS/ASAP *m/z*: $[M\text{-}CO]^+$ calculated 643.2398; found 643.2402 formula $C_{42}H_{38}N_3Co$.

IR ν/cm^{-1} (toluene): 3649 w, 3439 w, 2012 w, 1908 (C≡O), 1834 w, 1753 w.

1,8-dinaphthylimino-3,6-di(*tert*-butyl)-9-iron-carbonyl-carbazole (**30**):

[$Naph_2carbFe(CO)$]

In a Schlenk flask, **26** (30 mg, 0.04 mmol, 1 eq.) was dissolved in toluene (15 mL), affording a dark brown solution. To this solution, $Li[BHEt_3]$ (1M, 40 µL, 0.04 mmol, 1 eq.) was added, affording a black solution. The schlenk was adapted to a schlenk line running on CO(g). The atmosphere in the Schlenk was replaced with CO(g) *via* three freeze-thaw cycles (x 3). Left stirring at room temperature for 22 hour, followed by removal of volatiles allowed isolation of **30** as a brown powder (14.8 mg, 55%).

^1H NMR (400 MHz, C_6D_6, 25 °C) δ (ppm): [all peaks appear as broad singlets] 45.41 ($\Delta\nu_{1/2}$= 452 Hz), 3.66 ($\Delta\nu_{1/2}$= 124 Hz), 2.12 ($\Delta\nu_{1/2}$= 72 Hz), 1.46 ($\Delta\nu_{1/2}$= 89 Hz), 1.12 ($\Delta\nu_{1/2}$= 41 Hz), 0.95 ($\Delta\nu_{1/2}$= 354 Hz), 0.29 ($\Delta\nu_{1/2}$= 51 Hz), –23.11 ($\Delta\nu_{1/2}$= 193 Hz).

μ_{eff} (Evans' NMR Method, C_6D_6, 25 °C)= 2.77 μ_B.

MS/ASAP *m/z*: $[M\text{-}CO]^+$ calculated 640.2415; found 640.2 formula $C_{42}H_{38}N_3Fe$.

IR ν/cm^{-1} (toluene): 2020 s, 1999 s, 1976 s, 1909 (C≡O) s.

[1,8-dinaphthylimino-3,6-di(*tert*-butyl)-carbazole]$_2$-9-vanadium (**31**):

[(Naph$_2$carb)$_2$V]

In a Schlenk flask, **6** (100 mg, 0.17 mmol, 1 eq.) and KH (14 mg, 0.35 mmol, 2 eq.), were cooled down to 0 °C, and dry THF (15 mL) was slowly added. The resulting mixture was left stirring at this temperature for 1 hour. After this time, the reaction mixture was allowed to warm slowly to room temperature and left stirring for 2 hours, affording a dark red solution. This mixture was added dropwise to a suspension of VCl_2 (22 mg, 0.2 mmol, 1.5 eq.) in THF (15 mL) at 0 °C. The resulting mixture was left stirring at 0 °C, and allowed to reach room temperature slowly, stirring for 48 hours, obtaining a dark orange-brown suspension. Volatiles were removed under vacuum, ensuring full disappearance of solvent, employing a warm water bath, and yielding a yellow-orange powder. This powder was extracted into warm hexane to separate from unreacted metal salts/KCl, affording a dark brown-red solution. Removal of volatiles yielded a dark purple powder (37 mg, 18%). Crystals suitable for X-ray diffraction were grown from a concentrated solution in hexane at room temperature.

^{1}H NMR (400 MHz, C_6D_6, 25 °C) δ(ppm): 13.40 ($\Delta\nu_{1/2}$= 13 Hz), 8.50 ($\Delta\nu_{1/2}$= 16 Hz), 7.65 ($\Delta\nu_{1/2}$= 7 Hz), 7.50 ($\Delta\nu_{1/2}$= 14 Hz), 7.48 ($\Delta\nu_{1/2}$= 6 Hz), 7.44 ($\Delta\nu_{1/2}$= 6 Hz), 7.42 ($\Delta\nu_{1/2}$= 7 Hz), 6.96 ($\Delta\nu_{1/2}$= 18 Hz), 6.87 ($\Delta\nu_{1/2}$= 6 Hz), 6.85 ($\Delta\nu_{1/2}$= 6 Hz), 6.52 ($\Delta\nu_{1/2}$= 21 Hz), 3.79 ($\Delta\nu_{1/2}$= 106 Hz), 1.49 ($\Delta\nu_{1/2}$= 22 Hz), 1.41 ($\Delta\nu_{1/2}$= 29 Hz).

μ_{eff} (Evans' NMR Method, C_6D_6, 25 °C)= 1.96 μ_B.

HRMS/ASAP *m/z*: $[M]^+$ calculated 1219.5571; found 1219.5581 formula $C_{84}H_{76}N_6V$.

[1,8-dinaphthylimino-3,6-di(*tert*-butyl)-carbazole]$_2$-9-chromium (**32**):

[(Naph$_2$carb)$_2$Cr]

In a Schlenk flask, **6** (100 mg, 0.17 mmol, 1 eq.) and KH (14 mg, 0.35 mmol, 2 eq.), were cooled down to 0 °C, and dry THF (15 mL) was slowly added. The resulting mixture was left stirring at this temperature for 1 hour. After this time, the ice bath was removed and left stirring at room temperature for additional 2 hours, affording a dark red solution. This mixture was added dropwise to a suspension of $CrCl_2$ (22 mg, 0.2 mmol, 1.5 eq.) in THF (15 mL) at 0 °C. The resulting mixture was left stirring at 0 °C, and allowed to reach room temperature, and stirred for 48 hours, obtaining a dark yellow-brown suspension. Volatiles

were removed under vacuum, yielding a dark yellow-brown powder. This powder was extracted into warm hexane to separate from unreacted metal salts/KCl, affording a dark brown-red solution. Removal of volatiles yielded a dark red-brown powder (40 mg, 20%). Crystals suitable for X-ray diffraction were grown from a concentrated solution in hexane at room temperature.

^{1}H NMR (400 MHz, C_6D_6, 25 °C) δ (ppm): 8.51 ($\Delta\nu_{1/2}$= 22 Hz), 3.71 ($\Delta\nu_{1/2}$= 108 Hz), 1.77 ($\Delta\nu_{1/2}$= 132 Hz), 1.49 ($\Delta\nu_{1/2}$= 76 Hz), 1.43 ($\Delta\nu_{1/2}$= 12 Hz), 0.39 ($\Delta\nu_{1/2}$= 13 Hz), 0.30 ($\Delta\nu_{1/2}$= 11 Hz), −17.98 ($\Delta\nu_{1/2}$= 2179 Hz).

μ_{eff} (Evans' NMR Method, C_6D_6, 25 °C)= 3.15 μ_B.

HRMS/ASAP *m/z*: $[M]^+$ calculated 1220.5537; found 1220.5532 formula $C_{84}H_{76}N_6Cr$.

[1,8-dinaphthylimino-3,6-di(*tert*-butyl)-carbazole]$_2$-9-nickel (**33**):

[(Naph$_2$carb)$_2$Ni]

In a Schlenk flask, **6** (100 mg, 0.17 mmol, 1 eq.) and KH (14 mg, 0.35 mmol, 2 eq.), were cooled down to 0 °C, and dry THF (15 mL) was slowly added. The resulting mixture was left stirring at this temperature for 1 hour. After this time, the ice bath was removed and left stirring at room temperature for additional 2 hours, affording a dark red solution. This mixture was added dropwise to a suspension of $NiCl_2$ (24 mg, 0.2 mmol, 1.5 eq.) in THF (15 mL) at 0 °C. The resulting mixture was left stirring at 0 °C, and stirred for 48 hours, obtaining a dark yellow-brown suspension. Volatiles were removed under vacuum, yielding a dark yellow-brown powder. This powder was extracted into warm hexane to separate from unreacted metal salts/KCl, affording a dark brown-red solution. Removal of volatiles yielded a dark pink-red powder (39 mg, 19%). Crystals suitable for X-ray diffraction were grown from a concentrated solution in hexane/THF at room temperature.

^{1}H NMR (400 MHz, C_6D_6, 25 °C) δ (ppm): 22.24, 9.67 ($\Delta\nu_{1/2}$= 319 Hz), 5.76 ($\Delta\nu_{1/2}$= 393 Hz), 2.12, 1.48, 0.41, −9.49 ($\Delta\nu_{1/2}$= 1119 Hz).

μ_{eff} (Evans' NMR Method, C_6D_6, 25 °C)= 2.09 μ_B.

MS/ASAP *m/z*: $[M]^+$ calculated 1226.5481; found 1226.5 formula $C_{84}H_{76}N_6Ni$.

[1,8-dinaphthylimino-3,6-di(*tert*-butyl)-carbazole]$_2$-9-copper (**34**):

[(Naph$_2$carb)$_2$Cu]

In a Schlenk flask, **6** (100 mg, 0.17 mmol, 1 eq.) and KH (14 mg, 0.35 mmol, 2 eq.) were cooled down to 0 °C, and dry THF (15 mL) was slowly added. The resulting mixture was left stirring at this temperature for 1 hour. After this time, the resulting solution was dropwise added to a solution of $CuCl_2 \cdot THF_{0.8}$ (34 mg, 0.2 mmol, 1.5 eq.) in THF (15 mL) at 0 °C. The resulting mixture was left stirring at 0 °C, and stirred for 48 hours, obtaining a dark orange-brown suspension. Volatiles were removed under vacuum, yielding a dark yellow-brown powder. This powder was extracted into warm hexane to separate from unreacted metal salts/KCl, affording a brown-green solution. Removal of volatiles yielded a gold-yellow powder (13 mg, 6%). Crystals suitable for X-ray diffraction were grown from a concentrated solution in hexane at room temperature.

^{1}H NMR (400 MHz, C_6D_6, 25 °C) δ (ppm): [NMR sample of very low concentration] 8.51, 7.67, 7.48, 7.36, 7.26, 7.24, 7.21, 7.13, 6.96, 6.41, 3.57, 3.31, 1.42, 1.25, 1.18, 0.30.

HRMS/ASAP *m/z*: $[M-H]^+$ calculated 1230.5439; found 1230.5291 formula $C_{84}H_{75}N_6{}^{63}Cu$.

[1,8-dinaphthylimino-3,6-di(*tert*-butyl)-carbazole]$_2$-9-zinc (**35**):

$[(Naph_2carb)_2Zn]$

In the J. Young's NMR tube, **6** (40 mg, 0.07 mmol, 1 eq.) was dissolved in 0.6 mL of C_6D_6, and $ZnMe_2$ (1.2M, 28 µL, 0.035 mmol, 0.5 eq.) was added, affording an orange solution. ^{1}H NMR characterisation of the resulting solution, confirmed full disappearance of the starting material, and conversion to a new product. Crystals suitable for X-ray diffraction were grown from a concentrated solution in C_6D_6 exposed to hexane vapours, at room temperature.

^{1}H NMR (300 MHz, C_6D_6, 25 °C) δ (ppm): 8.63 (d, 4H, *J* = 1.9 Hz, H4 + H5), 8.22 (d, 4H, *J* = 8.4 and 1.1 Hz, Naph), 8.17 (s, 4H, (N=C*H*)), 7.54 (d, 4H, *J* = 8.2 Hz, Naph), 7.48 (d, 4H, *J* = 1.9 Hz, H2 + H7), 7.42 (d, 4H, *J* = 8.3 Hz, Naph), 7.15-6.98 (m, 12H, Naph), 6.77 (ddd, 4H, *J*= 8.2, 6.9, and 1.2 Hz, Naph), 1.51 (s, 36H, C(CH_3)$_3$).

^{13}C{^{1}H} NMR (75 MHz, C_6D_6, 25 °C) δ (ppm): 167.28 (N=*C*H), 149.11 (N-*C*1'), 148.14 (C3 + C6), 140.66 (quaternary), 137.89 (quaternary), 134.44 (quaternary), 129.87 (C2 + C7), 129.34, 128.57, 126.77, 126.62, 126.32, 126.20, 125.97, 125.70, 123.19, 122.51 (C4 + C5), 119.118 (quaternary), 117.80, 34.82 (*C*$(CH_3)_3$), 32.27 (C(*C*H_3)$_3$).

HRMS/ASAP *m/z*: $[M+H]^+$ calculated 1233.5501; found 1233.5493 formula $C_{84}H_{77}N_6Zn$.

1,8-dinaphthylimino-3,6-di(*tert*-butyl)-9-zinc-iodide-carbazole (**35a**):

[$Naph_2carbZnI$]

In a Schlenk flask, **6** (100 mg, 0.17 mmol, 1 eq.) and KH (14 mg, 0.34 mmol, 2 eq.) were cooled to 0 °C, and THF (20 mL) was slowly added. The resulting mixture was left stirring at this temperature for 1 hour, affording a dark red-orange solution, with further stirring at room temperature for 2 hours. This mixture was added dropwise to a suspension of ZnI_2 (54 mg, 0.17 mmol, 1 eq.) in THF (20 mL) at 0 °C over a period of 20 minutes. The resulting bright orange, murky suspension was left stirring for 16 hours at room temperature. Subsequently, volatiles were removed under vacuum affording a bright orange-red powder, which was extracted into warm hexane (3 x 20 mL), affording an orange solution. The solvent was then removed isolating a bright orange powder.

^{1}H NMR (300 MHz, C_6D_6, 25 °C) δ (ppm): 8.69 (d, 2H, *J* = 1.7 Hz, Naph), 8.20 (s, 2H, (N=C*H*)), 8.04 (d, 2H, *J* = 7.4 Hz, Naph), 7.77-7.59 (m, 2H, Naph), 7.54-7.48 (m, 2H, Naph), 7.40-7.30 (m, 2H, Naph), 7.21 (d, 4H, *J* = 8.1 Hz, Naph), 6.69-6.59 (m, 4H, Naph), 1.57 (s, 18H, C(CH_3)$_3$).

1,8-dinaphthylimino-3,6-di(*tert*-butyl)-9-cadmium-chloride-carbazole (**36a**):

[$Naph_2carbCdCl$]

In a Schlenk flask, **6** (100 mg, 0.17 mmol, 1 eq.) and KH (14 mg, 0.34 mmol, 2 eq.) were cooled down to 0 °C, and dry THF (20 mL) was slowly added. The resulting mixture was left stirring at this temperature for 1 hour, affording a dark red-orange solution; with further stirring at room temperature for an additional hour. This solution was added dropwise to a suspension of $CdCl_2$ (62 mg, 0.34 mmol, 2 eq.) in THF (20 mL). The resulting bright yellow suspension was left stirring for 16 hours and allowed to reach room temperature on its own. The next morning, volatiles were removed under vacuum affording a dark yellow powder; which was extracted into warm hexane (3 x 20 mL), obtaining a yellow solution. The solvent was then removed isolating a bright yellow-orange powder.

^{1}H NMR (400 MHz, C_6D_6, 25 °C) δ (ppm): 8.67 (d, 2H, *J* = 2.0 Hz, H4 + H5), 8.20 (s, 2H, (N=C*H*)), 7.86-7.70 (m, 2H, Naph), 7.64-7.53 (m, 2H, Naph), 7.46-7.31 (m, 2H, Naph), 7.30-7.18 (m, 2H, Naph), 7.13-6.98 (m, 4H, Naph), 6.93 (d, 1H, *J* = 8.0 Hz, Naph), 6.88 (t, 1H, *J*= 7.3 Hz, Naph), 6.53 (dd, 2H, *J* = 8.2 and 7.2 Hz, Naph), 1.46 (s, 18H, C(CH_3)$_3$).

^{113}Cd{^{1}H} NMR (89 MHz, C_6D_6, 25 °C) δ (ppm): 655.57.

HRMS/ASAP *m/z*: $[M\text{-}Cl]^+$ calculated 694.2096; found 694.2096 formula $C_{42}H_{38}N_3Cd$.

[1,8-dinaphthylimino-3,6-di(*tert*-butyl)-carbazole]$_2$-9-cadmium (**36**):

[(Naph$_2$carb)$_2$Cd]

Concentrated solutions of **36a** were used for growing crystals from which samples of **36** could be isolated, as dark yellow-orange crystals (33 mg, 16%). Crystals suitable for X-ray diffraction were grown from a concentrated extract in hexane, at room temperature.

^{1}H NMR (300 MHz, C_6D_6, 25 °C) δ (ppm): 8.27-8.05 (m, 8H, (N=C*H*)/Naph), 7.57-7.35 (m, 6H, Naph), 7.27 (d, 6H, *J* = 8.1 Hz, Naph), 7.10-6.97 (m, 4H, Naph), 6.93 (d, 4H, *J* = 8.0 Hz, Naph), 6.88 (t, 4H, *J* = 7.2 Hz, Naph), 6.52 (t, 4H, *J* = 7.8 Hz, Naph), 6.41-6.36 (m, 4H, Naph), 1.46 (s, 36H, C(C*H*$_3$)$_3$).

^{13}C{^{1}H} NMR (75 MHz, C_6D_6, 25 °C) δ (ppm): 171.85, 170.42 (N=*C*H), 150.32 (N-*C*1'), 149.63 (N-*C*1'), 148.48, 137.83 (quaternary), 133.77 (quaternary), 131.13 (Naph-*C*), 127.21, 127.14, 126.64, 124.98, 124.68, 124.60, 124.34, 123.62, 120.91, 118.19, 118.03, 34.13 (*C*(CH$_3$)$_3$), 32.03 (C(*C*H$_3$)$_3$).

^{113}Cd{^{1}H} NMR (89 MHz, C_6D_6, 25 °C) δ (ppm): 509.01.

1,8-dinaphthylimino-3,6-di(*tert*-butyl)-9-mercury-bromide-carbazole (**37**):

[Naph$_2$carbHgBr]

In a Schlenk flask, **6** (100 mg, 0.17 mmol, 1 eq.) and KH (14 mg, 0.34 mmol, 2 eq.) were cooled down to 0 °C, and dry THF (20 mL) was slowly added. The resulting mixture was left stirring at this temperature for 1 hour, after which the ice bath was removed and left stirring at room temperature for an additional hour, affording a dark red solution. This solution was added dropwise to a solution of $HgBr_2$ (61 mg, 0.17 mmol, 1 eq.) in THF (15 mL). The resulting solution was left stirring for 48 hours. After this time, the reaction mixture turned dark yellow. Volatiles were removed under vacuum, affording a dark yellow-brown powder. The crude of the reaction was extracted into warm hexane affording a dark yellow clear solution. Further removal of volatiles allowed isolation of a dark yellow-brown powder (86 mg, 59%). Crystals suitable for X-ray diffraction were grown from a concentrated solution in hexane, at room temperature.

^{1}H NMR (400 MHz, C_6D_6, 25 °C) δ (ppm): 8.60 (d, 2H, *J* = 1.9 Hz, H4 + H5), 8.38 (dd, 2H, *J* = 8.4 and 1.1 Hz, Naph *H*5'), 8.29 (s, 2H, (N=C*H*)), 7.59 (d, 2H, *J* = 8.2 Hz, Naph *H*8'), 7.52-7.47 (m, 4H, H2 + H7/Naph *H*4'), 7.23 (t, 2H, *J* = 8.1 Hz, Naph *H*3'), 7.23 (ddd, 2H, *J* = 8.2, 6.8 and 1.2 Hz, Naph *H*7'), 7.10 (ddd, 2H, *J* = 8.2, 6.8 and 1.2 Hz, Naph *H*6'), 6.93 (dd, 2H, *J* = 7.2 and 1.0 Hz, Naph *H*2'), 1.49 (s, 18H, C(C*H*$_3$)$_3$).

^{13}C{^{1}H} NMR (100 MHz, C_6D_6, 25 °C) δ (ppm): 166.68 (N=*C*H), 148.09 (N-*C*1'), 145.80 (C3 + C6), 142.02 (C8a + C9a), 134.41 (quatern-Naph *C*8a'), 132.01 (C2 + C7), 128.83 (quatern-Naph *C*4a'), 126.81 (C4a + C4b), 126.64 (Naph *C*3'), 126.62 (Naph *C*7'), 126.44 (Naph *C*4'), 125.98 (Naph *C*6'), 123.56 (Naph *C*5'), 121.10 (C4 + C5), 120.48 (C1 + C8), 116.59 (Naph *C*2'), 34.72 (*C*(CH$_3$)$_3$), 32.10 (C(*C*H$_3$)$_3$).

^{199}Hg{^{1}H} NMR (72 MHz, C_6D_6, 25 °C) δ (ppm): -1353.45.

HRMS/ASAP *m/z*: [M-Br]$^{+}$ calculated 782.2733; found 782.2714 formula $C_{42}H_{38}N_3Hg$.

1,8-dinaphthylimino-3,6-di(*tert*-butyl)-9-aluminium-dichloride-carbazole (**38**):

[Naph$_2$carbAlCl$_2$]

In a Schlenk flask, **6** (100 mg, 0.17 mmol, 1 eq.) and KH (14 mg, 0.34 mmol, 2 eq.) were cooled down to 0 °C, and dry toluene (20 mL) was slowly added. The ice bath was removed after 1 hour, and left stirring at room temperature for an additional hour. This solution was added dropwise to a suspension of $AlCl_3$ (23 mg, 0.17 mmol, 1 eq.) was in toluene (20 mL). Following this, a bright orange-yellow suspension could be obtained, that was left stirring for 16 hours, allowing it to reach room temperature slowly. After this time, the reaction mixture turned dark orange-brown. Volatiles were removed under vacuum affording a light brown-orange solid. This solid was extracted in warm hexane (20 mL x 3) affording a bright orange solution. Removal of the solvent under vacuum, allowed isolation of a dark yellow-orange powder (29 mg, 25%). Crystals suitable for X-ray diffraction were grown from a concentrated hexane solution, at room temperature.

^{1}H NMR (300 MHz, C_6D_6, 25 °C) δ (ppm): [exceeds expected integration] 8.56-8.45 (m, 2H), 8.37 (d, 1H, *J* = 8.3 Hz), 7.96 (d, 1H, *J* = 8.5 Hz), 7.85 (s, 2H), 7.66 (d, 2H, *J* = 1.9 Hz), 7.60 (d, 2H, *J* = 8.7 Hz), 7.54 (d, 2H, *J* = 7.5 Hz), 7.48 (t, 2H, *J* = 7.5 Hz), 7.44-7.41 (m, 2H), 7.27 (dd, 2H, *J* = 8.2 and 7.2 Hz), 7.12 (d, 2H, *J* = 8.7 Hz), 7.05-7.00 (m, 2H), 6.95 (ddd, 1H, *J* = 8.1, 6.8 and 1.2 Hz), 6.86 (dd, 1H, *J* = 7.3 and 1.1 Hz), 6.52 (d, 1H, *J* = 8.7 Hz), 1.36 (s, 18H, C(C*H*$_3$)$_3$).

HRMS/ASAP *m/z*: [M+H]$^{+}$ calculated 682.2336; found 682.2334 formula $C_{42}H_{39}N_3AlCl_2$.

1,8-dinaphthylimino-3,6-di(*tert*-butyl)-9-gallium-dichloride-carbazole (**39**):

[$Naph_2carbGaCl_2$]

In a Schlenk flask, **6** (100 mg, 0.17 mmol, 1 eq.) and KH (14 mg, 0.34 mmol, 2 eq.) were cooled down to 0 °C, and dry toluene (20 mL) was slowly added. The ice bath was removed after 1 hour, and left stirrint at room temperature for an additional hour. This solution was added dropwise to a suspension of $GaCl_3$ (30 mg, 0.17 mmol, 1 eq.) in toluene (20 mL). Following this, an orange-brown suspension could be obtained, that was left stirring for 16 hours, allowing it to reach room temperature slowly. After this time, the reaction mixture turned dark orange-brown. Volatiles were removed under vacuum affording a yellow-orange solid. This solid was extracted in warm hexane (20 mL x 3) affording a bright orange solution. Removal of the solvent under vacuum, allowed isolation of a yellow-orange powder (17mg, 14%). Crystals suitable for X-ray diffraction were grown from a concentrated hexane solution, at room temperature.

^{1}H NMR (300 MHz, C_6D_6, 25 °C) δ (ppm): [exceeds expected integration] 8.54-8.47 (m, 2H), 8.32-8.23 (m, 2H), 8.07 (d, 1H, *J* = 8.6 Hz), 7.89 (d, 2H, *J* = 8.4 Hz), 7.80 (s, 2H), 7.66 (d, 2H, *J* = 1.8 Hz), 7.61-7.41 (m, 4H), 7.27 (dd, 2H, *J* = 8.3 and 7.2 Hz), 7.12 (d, 1H, *J* = 7.5 Hz), 6.95 (ddd, 2H, *J* = 8.2, 6.8 and 1.2 Hz), 6.86 (dd, 1H, *J* = 7.3 and 1.1 Hz), 6.52 (ddd, 1H, *J* = 8.3, 6.8 and 1.3 Hz), 1.36 (s, 18H, C(C*H*$_3$)$_3$).

HRMS/ASAP *m/z*: $[M+H]^+$ calculated 724.1777; found 724.1767 formula $C_{42}H_{39}N_3GaCl_2$.

{[1,8-dinaphthylimino-3,6-di(*tert*-butyl)-carbazole]$_2$-9-indium}chloride (**40**):

[$(Naph_2carb)_2In$]Cl

In a Schlenk flask, **6** (100 mg, 0.17 mmol, 1 eq.) and KH (14 mg, 0.34 mmol, 2 eq.) were cooled down to 0 °C, and subsequently dry toluene (20 mL) was slowly added. The reaction was left stirring at this temperature for 1 hour and for an additional hour, at room temperature. The resulting solution was added dropwise to a suspension of $InCl_3$ (76 mg, 0.34 mmol, 2 eq.) in toluene (20 mL). The reaction mixture was left stirring at this temperature and allowed to reach room temperature for 24 hours. Following this, volatiles were removed under vacuum, obtaining a yellow powder which was extracted into warm toluene (20 mL x 3). A dark orange solid could be isolated following removal of volatiles under vacuum. Crystals suitable for X-ray diffraction were grown from a concentrated solution, in toluene at -30 °C. The quality of the X-ray data was low, but allowed corroboration for the formation of the homoleptic complex.

^{1}H NMR (300 MHz, C_6D_6, 25 °C) δ (ppm): 8.57-8.46 (m, 12H), 7.66 (s, 4H), 7.49 (d, 4H, *J* = 8.4 Hz), 7.43 (d, 4H, *J* = 8.2 Hz), 7.27 (t, 4H, *J* = 7.7 Hz), 6.95 (t, 4H, *J* = 7.3 Hz), 6.86 (d, 4H, *J* = 7.2 Hz), 6.53 (t, 4H, *J* = 7.7 Hz), 1.49 (s, 36H, C(C*H*$_3$)$_3$).

HRMS/ASAP *m/z*: $[M+H]^+$ calculated 1319.4937; found 1319.4937 formula $C_{84}H_{77}N_6InCl$.

1,8-dinaphthylimino-3,6-di(*tert*-butyl)-9-germanium-chloride-carbazole (**41**):

[Naph$_2$carbGeCl]

In a Schlenk flask, **6** (200 mg, 0.34 mmol, 1 eq.) and KH (28 mg, 0.68 mmol, 2 eq.) were cooled down to 0 °C, and THF (50 mL) was slowly added. The resulting mixture was left stirring at this temperature for 1 hour, yielding a dark red solution of **14**, which was left stirring at room temperature for an additional hour. The resulting solution was added dropwise to a solution of $GeCl_2$·Dioxane (158 mg, 0.68 mmol, 2 eq.) in THF (50 mL). The reaction mixture was left stirring with the ice bath, allowing it to reach room temperature for 24 hours. Following this, the solvent was removed under vacuum, affording a dark orange solid. The reaction crude was extracted into warm hexane (30 mL x 3) from which a dark orange solution could be obtained. Further evaporation of volatiles allowed isolation of a dark orange-red powder (160 mg, 60%). Despite thorough removal of volatiles, *ca.* 1 eq. of toluene could not be removed from the product and was considered for the final yield, and all further reactions. Crystals suitable for X-ray diffraction were grown from a concentrated solution in hexane, at room temperature.

^{1}H NMR (400 MHz, $CDCl_3$, 25 °C) δ (ppm): 8.64 (s, 2H, (N=C*H*)), 8.50 (d, 2H, *J* = 2.0 Hz, H4 + H5), 8.01 (d, 2H, *J* = 8.0 Hz, Naph *H*8'), 7.81 (d, 2H, *J* = 7.6 Hz, Naph *H*2'), 7.74-7.68 (m, 4H, Naph *H*4'/H2 + H7), 7.48-7.36 (m, 8H, Naph *H*3'/*H*5'/*H*6'/*H*7'), 1.53 (s, 18H, C(C*H*$_3$)$_3$).

^{13}C{^{1}H} NMR (100 MHz, $CDCl_3$, 25 °C) δ (ppm): 165.62 (N=*C*H), 145.38 (N-*C*1'), 142.41 (C3 + C6), 140.98 (C8a + C9a), 138.03 (quaternary), 134.37 (quatern-Naph C4a'), 130.77 (C2 + C7), 129.19 (quaternary), 128.38 (quaternary), 128.10 (Naph *C*2'), 127.97 (quaternary), 126.86 (Naph *C*4'), 126.61 (quaternary), 126.40 (quaternary), 126.32 (quaternary), 125.84 (Naph *C*3'/*C*6'), 125.45 (quaternary), 123.93 (Naph *C*8'), 123.26 (C4 + C5), 119.68 (Naph *C*5'/*C*7'), 119.33 (quatern-Naph C8a'), 34.74 (*C*(CH$_3$)$_3$), 32.01 (C(*C*H$_3$)$_3$).

HRMS/ASAP *m/z*: $[M+H]^+$ calculated 690.2075; found 690.2075 formula $C_{42}H_{39}N_3GeCl$.

IR ν/cm^{-1} (Nujol): 2955 s, 2923 s, 2854 s, 1636 s, 1617 s, 1574 s, 1463 s, 1393 w.

1,8-dinaphthylimino-3,6-di(*tert*-butyl)-9-germanium-iodide-carbazole (**41a**):

[$Naph_2$carbGeI]

In the glovebox, **24** (6 mg, 6.65 μmol, 1 eq.) and **41** (5 mg, 6.65 μmol, 1 eq.) were suspended in C_6D_6 (0.6 mL). The resulting suspension was transferred to a J. Young's tap NMR tube and agitated via sonication at room temperature for 5 minutes. A ^{1}H NMR spectrum, evidenced full disappearance of both starting materials. Crystals suitable for X-ray diffraction were grown from this solution upon exposure to hexane vapours, in the glovebox, at room temperature.

^{1}H NMR (400 MHz, C_6D_6, 25 °C) δ (ppm): 8.56 (d, 2H, *J* = 2.0 Hz, H4 + H5), 8.08-8.02 (m, 2H, Naph), 7.98 (s, 2H, (N=C*H*)), 7.53 (dd, 2H, *J* = 7.2 and 1.1 Hz, Naph), 7.50-7.46 (m, 2H, Naph), 7.44 (d, 2H, *J* = 2.0 Hz, H2 + H7), 7.33 (d, 2H, *J* = 8.3 Hz, Naph), 7.13 (dd, 2H, *J* = 7.1 and 5.5 Hz, Naph), 7.09-6.98 (m, 4H, Naph), 1.41 (s, 18H, C(C*H*$_3$)$_3$).

1-naphthylimino-3,6-di(*tert*-butyl)-8-naphthyl-p-tolyl-amidine-9-germanium-chloride-carbazole (**41c**):

[$Naph_2$-*p*-tolylcarbGeCl]$_2$

In a Schlenk flask, **41** (30 mg, 0.04 mmol, 1 eq.) was dissolved in dry toluene (10 mL), and *p*-tolylazide (6.1 μL, 0.05 mmol, 1.2 eq.) was added. The resulting reaction mixture was left stirring at room temperature for 20 hours. After this time, a ^{1}H NMR spectrum of an aliquote, evidence presence of remaining unreacted starting materials, reason by which the reaction mixture was heated at 60 °C, in an oil bath. After this time, volatiles were removed under vacuum, isolating a red powder (11.2 mg, 37%). NMR characterisation of this product exhibited full consumption of the starting materials, while also yielding an increasingly complicated/broad spectrum, with a myriad of peaks ranging from 10 to 5 ppm (^{1}H NMR). Crystals suitable for X-ray diffraction were grown from a concentrated solution in C_6D_6, upon exposure to hexane vapours, at room temperature.

HRMS/ASAP *m/z*: $[M-H]^+$ calculated 797.2474; found 797.2370 formula $C_{49}H_{44}N_4GeCl$.

1,8-dinaphthylimino-3,6-di(*tert*-butyl)-9-germanium-hexamethyldisilazide-carbazole (**41d**):

[$Naph_2$carbGeHMDS]

In a Schlenk flask, a solution of Li[N($SiMe_3$)$_2$] (14 mg, 0.08 mmol, 2 eq.) in toluene (10 mL), was added dropwise to a solution of **41** (30 mg, 0.04 mmol, 1 eq.) in toluene (10

mL). The reaction mixture was left stirring at room temperature for 16 hours. Volatiles were removed under vacuum, and the resulting orange solid was extracted with hot hexane (20 mL x 3), affording an orange solution. Further removal of solvent allowed isolation of a red solid (14 mg, 41%). Crystals suitable for X-ray diffraction were grown from a concentrated solution in C_6D_6, exposed to hexane vapours, at room temperature.

^{1}H NMR (400 MHz, C_6D_6, 25 °C) δ (ppm): 8.61 (d, 2H, *J* = 2.1 Hz, H4 + H5), 8.42 (s, 2H, (N=C*H*)), 8.41 (d, 2H, *J* = 9.0 Hz, Naph), 7.86 (d, 2H, *J* = 8.2 Hz, H2 + H7), 7.61 (d, 2H, *J* = 7.9 Hz, Naph), 7.51 (d, 2H, *J* = 8.2 Hz, Naph), 7.31 (ddd, 2H, *J* = 8.4, 6.8 and 1.4 Hz, Naph), 7.25 (dd, 2H, *J* = 14.9 and 1.1 Hz, Naph), 7.22 (t, 2H, *J* = 7.2 Hz, Naph), 7.14-7.11 (m, 2H, Naph), 1.45 (s, 18H, C(C*H*$_3$)$_3$), 0.10 (s, 9H, (N-Si(C*H*$_3$)$_3$)), -0.41 (br s, 9H, (N-Si(C*H*$_3$)$_3$)).

^{13}C{^{1}H} NMR (100 MHz, C_6D_6, 25 °C) δ (ppm): 164.74 (N=*C*H), 148.02 (N-*C*1'), 143.47 (C8a + C9a), 141.57 (C3 + C6), 134.73 (quatern-Naph *C*4a'), 129.82 (C2 + C7), 129.33, 128.98 (quatern-Naph *C*8a'), 128.57 (C4a + C4b), 127.40, 126.84, 126.26, 126.09, 125.70, 125.16, 122.59 (C4 + C5), 121.18 (C1 + C8), 118.10, 34.65 (*C*(CH$_3$)$_3$), 32.00 (C(*C*H$_3$)$_3$), 4.99 (N-Si(*C*H$_3$)$_3$), 2.67 (N-Si(*C*H$_3$)$_3$).

^{29}Si{^{1}H} NMR (80 MHz, C_6D_6, 25 °C) δ (ppm): –1.12.

HRMS/ASAP *m/z*: $[M+H]^+$ calculated 815.3364; found 815.3353 formula $C_{48}H_{57}N_4GeSi$.

1,8-dinaphthylimino-3,6-di(*tert*-butyl)-9-tin-chloride-carbazole (**42**):

[Naph$_2$carbSnCl]

In a Schlenk flask, **6** (100 mg, 0.17 mmol, 1 eq.) and KH (14 mg, 0.34 mmol, 1 eq.) were cooled to 0 °C, and THF (30 mL) was slowly added. This mixture was left stirring 0 °C for 1 hour, and at room temperature for an additional hour. The resulting solution was added dropwise to a solution of $SnCl_2$ (65 mg, 0.34 mmol, 2 eq.) in THF (30 mL). The reaction mixture was left stirring at this temperature for 24 hours and allowed to reach room temperature slowly. Following this, the reaction had turned yellow, volatiles were removed under vacuum, affording a yellow solid. The crude of the reaction was extracted into warm hexane (30 mL x 3). A dark orange solid could be isolated after removal of solvent under vacuum (92.3 mg, 74%). Crystals suitable for X-ray diffraction were grown from a concentrated solution in hexane, at room temperature.

^{1}H NMR (400 MHz, $CDCl_3$, 25 °C) δ (ppm): 8.65 (s, 2H, (N=C*H*)), 8.53 (d, 2H, *J* = 2.0 Hz, H4 + H5), 8.37 (d, 2H, *J* = 1.7 Hz), 8.15 (d, 2H, *J* = 8.4 Hz, Naph), 7.84 (dd, 2H, *J* = 7.0

and 1.8 Hz, Naph), 7.74-7.70 (m, 2H, Naph), 7.72 (d, 2H, *J* = 2.3 Hz, H2 + H7), 7.50-7.40 (m, 6H, Naph), 1.53 (s, 18H, C(C*H*$_3$)$_3$).

^{13}C{^{1}H} NMR (100 MHz, $CDCl_3$, 25 °C) δ (ppm): 167.40 (N=*C*H), 160.98 (quaternary), 149.62 (quaternary), 145.52 (quaternary), 141.71 (quaternary), 137.16 (quaternary), 134.40 (quaternary), 133.66 (quaternary), 132.02 (C2 + C7), 128.77, 128.24, 127.81, 126.93, 126.74, 126.56, 125.70, 125.60, 124.99, 123.37 (C4 + C5), 120.24, 119.62, 119.48, 112.63, 34.68 (*C*(CH$_3$)$_3$), 32.02 (C(*C*H$_3$)$_3$).

^{119}Sn{^{1}H} NMR (149 MHz, $CDCl_3$, 25 °C) δ (ppm): 25.9.

^{119}Sn{^{1}H} NMR (149 MHz, C_6D_6, 25 °C) δ (ppm): -123.2.

HRMS/ASAP *m/z*: $[M]^+$ calculated 735.1772; found 735.1797 formula $C_{42}H_{38}N_3SnCl$.

IR *v*/cm^{-1} (Nujol): 2955 s, 2924 s, 2854 s, 1631 w, 1614 w, 1592 w, 1463 s, 1391 w.

1,8-dinaphthylimino-3,6-di(*tert*-butyl)-9-lead-bromide-carbazole (**43**):

[Naph$_2$carbPbBr]

In a Schlenk flask, **6** (100 mg, 0.17 mmol, 1 eq.) and KH (14 mg, 0.34 mmol, 2 eq.) were cooled to 0 °C, and THF (30 mL) was slowly added. This mixture was left stirring 0 °C for 1 hour, and at room temperature for an additional hour. The resulting solution was added dropwise to a solution of $PbBr_2$ (125 mg, 0.34 mmol, 2 eq.) in THF (30 mL). The reaction mixture was left stirring at this temperature for 16 hours and allowed to reach room temperature slowly. The next morning the reaction had turned bright yellow, volatiles were removed under vacuum, affording a yellow solid. The crude of the reaction was extracted into warm toluene (30 mL x 3). A dark yellow solid could be isolated after removal of volatiles under vacuum (90.4 mg, 61%). Crystals suitable for X-ray diffraction, revealing two different polymorphs, were grown from concentrated solutions in toluene, at room temperature.

^{1}H NMR (400 MHz, $CDCl_3$, 25 °C) δ (ppm): 8.76 (s, 2H, (N=C*H*)), 8.59 (d, 2H, *J* = 2.1 Hz, H4 + H5), 7.81 (d, 2H, *J* = 7.2 Hz, Naph), 7.74 (d, 2H, *J* = 2.0 Hz, H2 + H7), 7.69 (d, 2H, *J* = 8.3 Hz, Naph), 7.49-7.38 (m, 6H, Naph), 7.22 (d, *J* = 7.8 Hz, 2H, Naph), 7.15 (d, 2H, *J* = 8.0 Hz, Naph), 1.51 (s, 18H, C(C*H*$_3$)$_3$).

^{13}C{^{1}H} NMR (100 MHz, $CDCl_3$, 25 °C) δ (ppm): 167.28 (N=*C*H), 160.97 (quaternary), 149.59 (quaternary), 146.49 (quaternary), 144.10 (quaternary), 142.50 (quaternary),

141.19 (C3 + C6), 137.99 (quaternary), 137.15 (quaternary), 134.28 (quaternary), 132.72 (C2 + C7), 129.16 (Naph), 128.43 (Naph), 128.35 (Naph), 127.64 (C4a + C4b), 127.57, 126.92 (Naph), 126.77, 126.15, 125.43, 123.60 (C4 + C5), 122.02 (C1 + C8), 120.23, 118.69 (Naph), 112.62 (Naph), 34.60 ($C(CH_3)_3$), 32.07 ($C(CH_3)_3$).

HRMS/ASAP *m/z*: $[M+H]^+$ calculated 868.2058; found 868.2062 formula $C_{42}H_{39}N_3PbBr$.

IR ν/cm^{-1} (Nujol): 2928 s, 2854 s, 1629 w, 1611 w, 1564 w, 1462 s, 1392 w, 1377 w, 1364 w.

8-(Ar*)imino-1,2,3,4-Tetrahydro-9-magnesium-iodide-carbazole (**44**):

$[Ar^*THCarbMgI]_2$

In the glovebox, **9** (40 mg, 0.07 mmol, 1 eq.) and $MeMgI{\cdot}1.5Et_2O$ (20 mg, 0.07 mmol, 1.1 eq.) were dissolved in C_6D_6 (1 mL), affording a bright orange solution. Crystals suitable for X-ray diffraction were seen growing shortly after synthesis in C_6D_6, at room temperature.

^1H NMR (300 MHz, C_6D_6, 25 °C) δ (ppm): 7.87 (d, 1H, *J* = 7.2 Hz, Ar-*H*), 7.72-7.38 (m, 4H, Ar-*H*/Ph), 7.32-7.18 (m, 6H, Ph), 7.14-7.07 (m, 4H, Ph), 7.04-6.91 (m, 10H, Ph), 6.87 (s, 1H, (N=C*H*)), 6.15 (d, 2H, *J* = 7.4 Hz, Ar-*H*), 3.42-3.20 (m, 2H, CH_2), 3.06-2.94 (m, 2H, CH_2), 2.10-1.94 (m, 7H, CH_2/Ar-CH_3).

$^{13}C\{^1H\}$ NMR (75 MHz, C_6D_6, 25 °C) δ (ppm): 178.31 (N=*C*H), 146.28 (quaternary), 146.04 (quaternary), 143.86 (quaternary), 143.59 (quaternary), 143.20 (quaternary), 135.96 (quaternary), 133.01 (quaternary), 130.53, 130.19, 129.41, 129.11, 128.73, 128.56, 126.89, 126.82, 125.06, 115.75, 115.70, 119.09 (quaternary), 52.66 (Ar-*C*/-*C*HPh_2), 27.27 (*C*H_2), 24.62 (*C*H_2), 24.42 (*C*H_2), 22.12 (*C*H_2), 21.23 (Ar-*C*H_3).

HRMS/ASAP *m/z*: $[M+H]^+$ calculated 771.2087; found 771.2095 formula $C_{46}H_{40}N_2MgI$.

8-(Ar*)imino-1,2,3,4-Tetrahydro-9-zinc-methyl-carbazole (**45**):

[Ar*THCarbZnMe]

In a schlenk, to a solution of **9** (40 mg, 0.07 mmol, 1 eq.) in toluene (20 mL), was added $ZnMe_2$ (1.2M, 69 µL, 0.08 mmol, 1.1 eq.), at 0 °C. The resulting solution was left stirring at this temperature and allowed to reach room temperature for 16 hours. The next morning the solution was light orange. Volatiles were removed under vacuum obtaining a

dark yellow solid (38 mg, 83%). Crystals suitable for X-ray diffraction were grown from a concentrated hexane solution.

^{1}H NMR (300 MHz, C_6D_6, 25 °C) δ (ppm): 7.81 (dd, 1H, *J* = 7.5 and 1.0 Hz, Ar-*H*), 7.59 (s, 1H, (N=C*H*)), 7.17-6.84 (m, 22H, Ar-*H*/Ph), 6.73-6.67 (m, 2H, Ar-*H*/Ph), 5.51 (s, 2H, -C*H*Ph_2), 3.01-2.81 (m, 4H, C*H*$_2$), 1.97-1.83 (m, 7H, C*H*$_2$/Ar-C*H*$_3$), -0.68 (s, 3H, -CH_3).

^{13}C{^{1}H} NMR (75 MHz, C_6D_6, 25 °C) δ (ppm): 172.08 (N=C*H*), 146.48 (quaternary), 146.12 (quaternary), 143.44 (quaternary), 142.83 (quaternary), 142.31 (quaternary), 141.89 (quaternary), 137.88 (quaternary), 137.66 (quaternary), 135.53 (quaternary), 135.52 (quaternary), 130.22, 130.20, 130.02, 129.34, 129.08, 128.78, 128.73, 128.57, 127.11, 126.77, 125.70, 125.11, 116.61, 115.73, 110.75, 53.55 (-*C*HPh_2), 26.43 (*C*H$_2$), 24.48 (*C*H$_2$), 21.99 (*C*H$_2$), 21.44 (Ar-*C*H$_3$), 21.26 (*C*H$_2$), -6.61 (-*C*H$_3$).

HRMS/ASAP *m/z*: $[M+H]^+$ calculated 699.2718; found 699.2711 formula $C_{47}H_{43}N_2Zn$.

Chapter V. Heteroleptic First-Row Transition Metal Complexes and Hydrophosphination of Activated Alkenes

5.1 Introduction

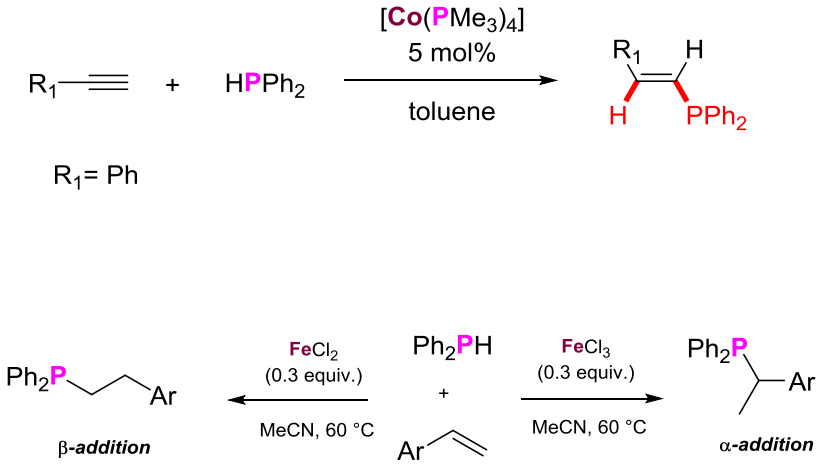
Phosphorus-containing compounds are a precious commodity, finding use in numerous areas such as, for example, organo-catalysis[267], bulk and fine chemical production[268] and the pharmaceutical industry.[269] Aiming to access new synthetic routes for their preparation, these industries have stimulated the development of more effective, atom-economical routes and viable strategies for their preparation. However, a continuing challenge in this area is the ability to selectively and cleanly access a compound of interest.

In particular of this work and following a previous report from our research group, involving the hydrophosphination of isocyanates employing a low-coordinate iron(II) metal complex,[270] it is of interest to extend these studies to further unsaturated substrates. Thus, the hydrophosphination of olefins and alkynes, has received much attention in the last two decades.[271–277] The potential for regio- and stereoselectivity in catalytic hydrophosphination has in turn, driven the development of metal-catalysed hydrophosphination processes; which have been revitalised by the development of tailored catalyst design, a core area for regioselective metal-catalysed hydrophosphination. Similarly, diminishing supplies of noble metals will eventually limit their accessibility for catalysis. This is a significant reason by which, the quest for cheaper, earth-abundant, non-toxic catalysts, for hydrophosphination and other hetero-atom insertion processes, involving iron,[271,272,275,278–287] cobalt[166,288–292] and manganese,[293] has found reinvigorated interest and further growth (Scheme 5.1.1).

There is a wide array of examples in which a cobalt catalyst has been used in order to aid H-heteroatom bond formation/C-H functionalisation. Notable examples of cobalt(II)-metal centres capable of carrying such transformations are [$Co(acac)_2$] catalysed hydrophosphination of internal alkynes,[289] *Z*-selective hydrosilylation of terminal alkynes[290], [*NNN*-$CoCl_2$] pincer-complexes active in regio- and enantioselective hydrosilylation/hydrogenation of terminal alkynes,[291], $CoCl_2$ catalysed hydroamination of buta-1,3-dienes[294] and a functionalised cobalt-salen complex active in the regioselective hydrothiolation of unactivated alkenes (Scheme 5.1.1).[295]

Comparatively, some examples of catalytically active cobalt(I)-metal centres are orthoalkenylation of an azobenzene derivative with diphenylacetylene[296] and isomerisation-hydroboration of alkenes using [$Co(H)(N_2)(PPh_3)_3$],[297] piano-stool compounds [$Cp^*Co(CH_2{=}CHSiMe_3)_2$], active in the inter- and intramolecular hydroacylation of olefins with aromatic[298] and aliphatic aldehydes.[299] As well as, synthesis of enamines *via* intramolecular hydrogen transfer[300] and chemoselective hydroboration of alkenes and nitriles employing a [*CCC*-CoN_2] pincer complex,[301] to mention but a few.

Although the hydrophosphination of alkynes catalysed by cobalt-containing compounds is known,[288,289,302] to the best of my knowledge, there are no examples in the literature, as of yet, in which a cobalt catalyst has been employed in a similar transformation employing, the comparatively less reactive, olefins as substrate.



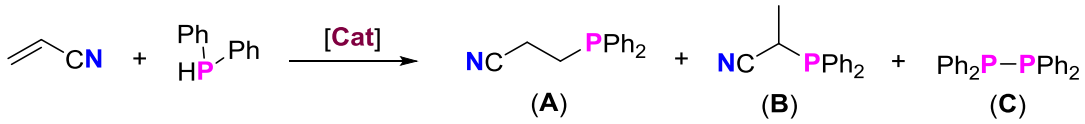
Scheme 5.1.1 Examples of selective trans-hydrophosphination of alkynes catalysed by a cobalt complex (above) and hydrophosphination of alkenes catalysed by iron salts (below).

5.2 Aims and Objectives

As mentioned in the introduction, there is a number of examples in the literature, in which a metal complex has been used to aid/direct the formation of new heteroatom-carbon bonds in hydroelementation reactions. The use of complexes containing iron, cobalt and manganese had been widely studied; but challenges arising from less activated unsaturated substrates and, selectivity of the catalysts employed remain to be addressed. It is because of this and following the work reported in Chapter 4, in terms of additional coordination to the first-row transition metal complexes (**27a-d**), that it is of interest to study the reactivity of complexes **26**-**30** in the hydrophosphination of activated alkenes. Particular emphasis will be placed on the use of cobalt(II) and cobalt(I) carbazolido complexes (**27**/**29**) for this reactivity.

5.3 Results and Discussion

5.3.1 Catalytic Hydrophosphination of Olefins



Scheme 5.3.1 Hydrophosphination of acrylonitrile with diphenylphosphine [Cat] = ***26-30****.*

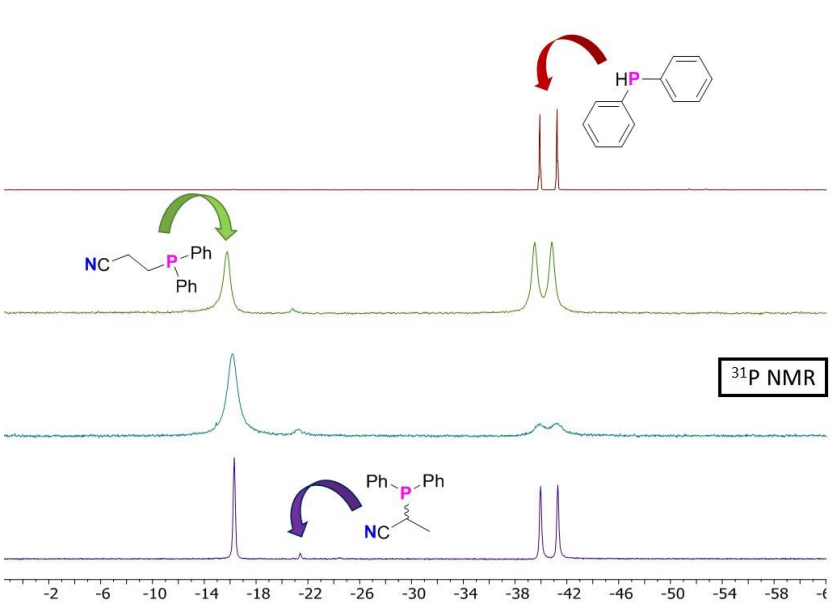
An initial assessment of the catalytic activity for the hydrophosphination of alkenes using the heteroleptic metal complexes **26**-**30** (Scheme 5.3.1) was tested *via* the reaction of acrylonitrile with diphenylphosphine ($PHPh_2$) in C_6D_6 using 5 mol% of **26**, (Entry 3, Table 5.3.1) with no initial formation of hydrophosphination products at room temperature. Upon heating at 60 °C for 22 hours, selective formation of the linear isomer (**A**/**46**) was observed (20%).

Table 5.3.1 Catalyst screening and reaction optimisation for the hydrophosphination of acrylonitrile

Entry	Catalyst (mol%)	Solvent	T (°C)	*t* (h)	Conv. (%)[d]	Product Ratio[d] **A**/**B**/**C**	Yield (%)[e]
1	-	C_6D_6	60	18	2	2/0/0	-
2	-[b]	C_6D_6	60	18	1	1/0/0	-
3	**26** (5)	C_6D_6	60	22	20	20/0/0	-
4	**26** (5)[b]	C_6D_6	60	22	11	11/0/0	-
5	**27** (5)	C_6D_6	60	17	40	39/0/1	-
6	**27** (5)[b]	C_6D_6	60	18	61	58/3/0	-
7	**28** (5)[b]	C_6D_6	60	18	13	12/1/0	-
8	**27** (5)[b]	Toluene	80	18	88	74/3/11	63
9	**27**-**H** (5)[c]	Toluene	80	22	70	68/2/0	-
10	**29** (5)	Toluene	80	1.5	100	100/0/0	89
11	**30** (5)	Toluene	80	17	59	37/7/15	27

[a] Reaction conditions: 5.0 mg of metal catalyst, 0.6 mL of solvent, 20 equiv. of acrylonitrile/$PHPh_2$. Samples were heated in an oil bath, progress was monitored by ^{31}P NMR spectroscopy. [b] 20 equiv. of NEt_3 added; [M]: NEt_3, 20 to 1. [c] 1 equiv. of $Li[BHEt_3]$ added; [M]: $Li[BHEt_3]$, 1 to 1. [d] Determined by ^{31}P NMR spectroscopy, **A** = Anti-markovnikov product, **B** = Markovnikov product, **C** = $Ph_2P–PPh_2$. [e] Isolated as the phosphine oxide, following oxidation with H_2O_2.

Further heating for four days, yielded close to 50% conversion of the starting $PHPh_2$, with the linear isomer **A**, as the main product (49% *vs*. branched isomer **B** 2%). When using complex **26** (5 mol%) as the catalyst, addition of NEt_3 lead to lower conversions (11% of the linear isomer, Entry 4, Table 5.3.1). The cobalt complex **27**, shows a higher activity than **26** when NEt_3 was used as an additive (Entry 6, Table 5.3.1), after 18 hours, 61% conversion was achieved, giving a mixture of linear and branched isomers, with **A** obtained in a 58%. Using the manganese complex **28**, under identical reaction conditions; however, only enabled a 13% conversion after 18 hours, with the anti-Markovnikov isomer in a 12% (Entry 7, Table 5.3.1). Increasing the temperature to 80 °C, our system reached 88% conversion of the starting material with a 74% formation of linear product (Entry 8, Table 5.3.1). Similarly we expected that the formal replacement of the bromide in **27** with a hydride would increase the catalytic activity of our metal complex (Entry 9, Table 5.3.1).[291] However, the *in situ* generated hydride complex **27-H** exhibited a decreased reactivity when compared with **27** under similar conditions; 70% conversion after 22 hours. Much to our surprise, when the *in situ* generated cobalt(I)-carbonyl complex **29** was tested using toluene as solvent, high conversion and selectivity was achieved in under two hours at 80 °C (Entry 10, Table 5.3.1) (quantitative conversion, only linear isomer obtained) (Figure 5.3.1).



Catalyst / Solvent	T (°C) / t (h)	Conversion (%)
-	-	-
26 / C_6D_6	60 / 68	38
27 / C_6D_6	60 / 72	82
28 / C_6D_6	60 / 72	41

*Figure 5.3.1 Comparative ^{31}P NMR spectra of $PHPh_2$ (red); and in situ monitoring of the hydrophosphination of acrylonitrile using **26** (green), **27** (blue) and **28** (purple) in C_6D_6 at similar times.*

In parallel, the analogous iron(I)-carbonyl complex **30**, only yields a 59% conversion after 17 hours, with significant proportion of the branched isomer **B** and the dehydrocoupling product **C** (Entry 11, Table 5.3.1). It is worth mentioning that although the hydrophosphination of alkenes catalysed by first-row transition metals is known,[278,280,293] this is the first example in which a cobalt complex has been used in this transformation, with the analogous insertion in the more reactive alkynes being well documented for both hydrophosphination[288,289] and hydrosylilation.[166,291,292,303]

5.3.2 Catalytic Studies

Following these determinations, the conditions described in (Entry 10, Table 5.3.1) were further used, due to their fast reaction times and high selectivity. In order to distinguish the true nature of the catalytic process, selective poisoning experiments with Hg[279,304] and CS_2,[270,305] were performed (Table 5.3.2). No changes were observed in either the reaction rate or catalyst selectivity, suggesting that the reaction most likely occurs through a homogenous mechanism. Moreover, the reaction does not appear to be catalysed by radicals since the presence of cumene[270,278,306,307] and 1,4-cyclohexadiene,[308,309] does not affect the rate of the reaction, thus providing good indication that the catalytic process is homogeneous in nature. Experiments following these conditions, were monitored by ^{31}P NMR spectroscopy, and the conversion rate/reaction time, was identical to those experiments carried out in absence of additive (Figure 5.3.2).

Table 5.3.2 Catalytic studies

Additive	**29** : Additive Ratio[a)]	Conversion observed
-	0:0	2
-	1:0	100
Hg drop	Excess of Hg	100
CS_2	1:10	95
Cumene	1:5	100
1,4-cyclohexadiene	1:5	100

[a)] Reaction conditions: **29** (5 mg, 6.92 x10^{-3} mmol), acrylonitrile (9.06 µL, 0.138 mmol, 20 eq.), $PHPh_2$ (24 µL, 0.138 mmol, 20 eq.) and an additive. Selective formation of (**46**); followed by ^{31}P NMR spectroscopy.

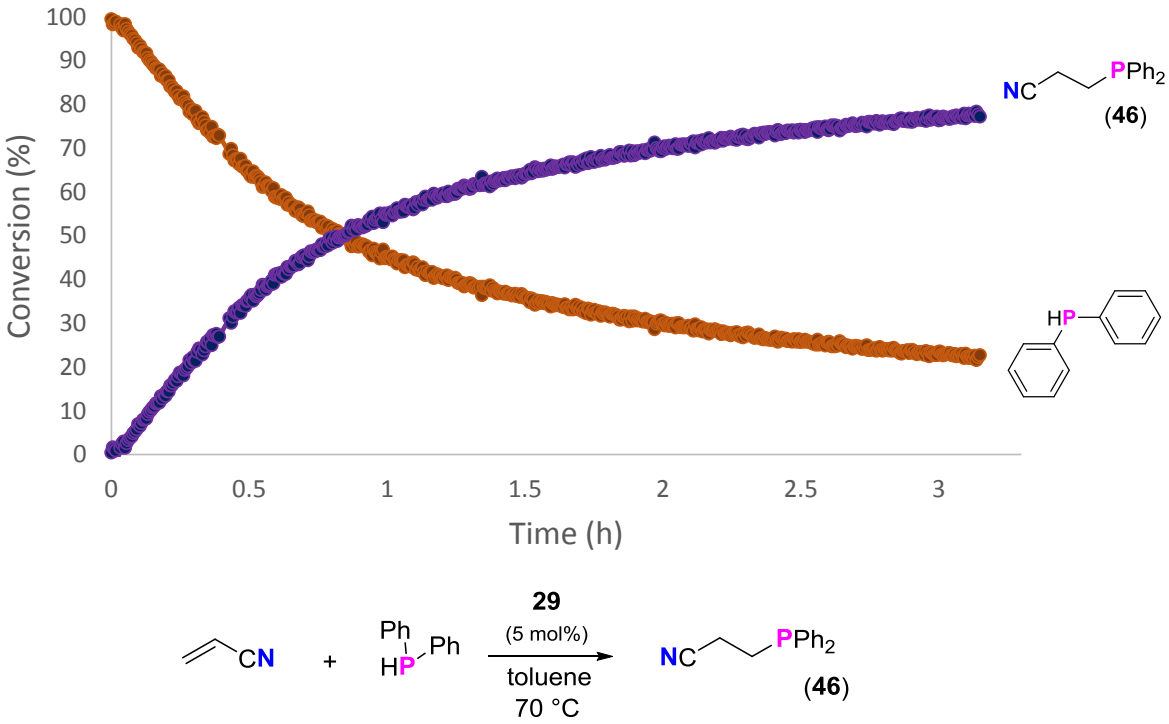


*Figure 5.3.2 Graph of conversion (%) vs. time (h). Showing production of **46** and consumption of $PHPh_2$, with **29** (5 mol%) as catalyst as determined by $^{31}P\{^1H\}$ NMR spectroscopy.*

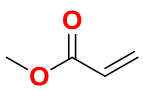
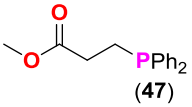
5.3.3 Reaction Scope

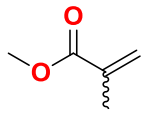
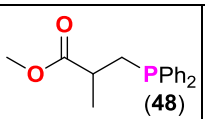
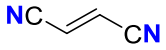
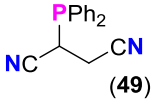
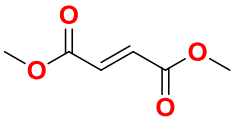
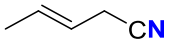
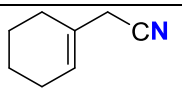
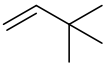
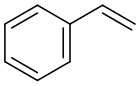
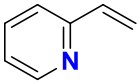
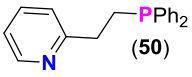
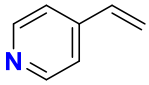
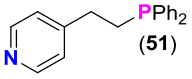
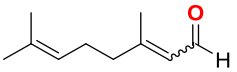
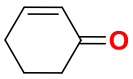
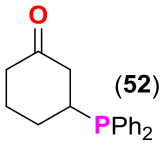
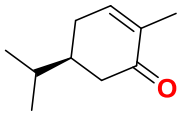
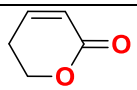
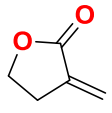
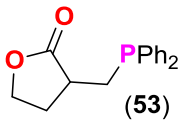
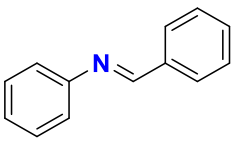
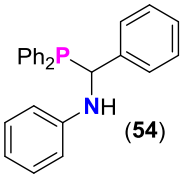
Having established complex **29** as the most selective/active metal catalyst, the optimised reaction conditions were then examined using a variety of activated unsaturated substrates. Results of the hydrophosphination reactions catalysed by cobalt(I) are shown in Table 5.3.3. Using α-carbonyl unsaturated substrates such as methylacrylate, reach full conversion to the linear product **47** in 5 hours (Entry 1, Table 5.3.3). In parallel, when the double bond is substituted with a methyl group, only 26% conversion of the starting material was achieved, despite prolonged reaction times (Entry 2, Table 5.3.3), most likely a consequence of steric hindrance limiting substitution (**48**). Activated non-terminal alkenes were tested for this transformation (Entries 3 and 4, Table 5.3.3); despite their similarities, only the less sterically hindered, fumaronitrile was susceptible to substitution, showing full conversion to **49**, in one hour. When the double bond is moved to the β-position, even when activating functional groups are present (Entries 5 and 6, Table 5.3.3), no evidence of hydrophosphination was observed.

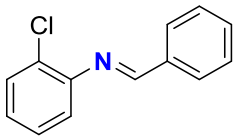
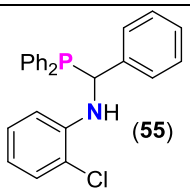
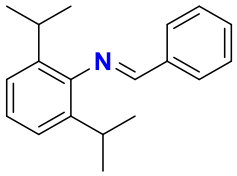
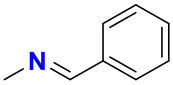
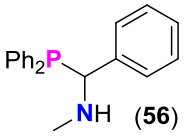
It was however noticeable, that in all cases in which coordination is not possible (Entries 7 and 8, Table 5.3.3), the dehydrocoupling product $Ph_2P–PPh_2$ (**C**) is obtained as the only product. This suggests that in substrates inactive for this transformation, an alternative pathway is enabled, in which the only possible reaction is the stoichiometric transformation of $PHPh_2$ to $Ph_2P–PPh_2$ (**C**) (Entries 5-8, 11, 13, 14 and 18, Table 5.3.3). When vinylpyridines were used (Entries 9 and 10, Table 5.3.3), full conversion to the linear isomers, **50** and **51**, was achieved in 20 and 40 hours, respectively. The terpenoid, citral was employed under analogous conditions, no evidence of hydrophosphination could be observed (Entry 11, Table 5.3.3). In contrast, α-unsaturated ketones, showed to be suitable substrates, giving selective substitution in the β-position, with respect to the carbonyl, in up to 81% conversion (Entry 12, Table 5.3.3). In line with Entries 1 and 2, the presence of a methyl group on the unsaturation completely inhibits hydrophosphination of the double bond (Entry 13, Table 5.3.3) in cyclohexanone derivatives.

The isomeric lactones described in Entries 14 and 15, highlight the preference of this process for activated terminal alkenes, only yielding the anti-Markovnikov product **53**, in 4 hours. Aromatic imines with different *ortho*-substituents (Entries 16-18, Table 5.3.3) are capable of carrying out this process with moderate conversions (Entries 16 and 17) in under 6 hours. However, when *iso*-propyl groups are used as substituents (Entry 18, Table 5.3.3), no insertion was observed. This would be expected due to the high hindrance of the substituents, however this groups are not in close proximity to the double bond. Directly comparing the Lewis acidity of the iminic protons of these substrates (by ^{1}H NMR spectroscopy) suggests that it is the comparatively more basic nature of the imine in Entry 18 that limits the availability of the insertion process. This is in line with a similar behaviour observed between Entries 12 and 14. Considerably more acidic aliphatic imine employed in Entry 19, behaves similar to its aromatic congeners, affording a modest conversion of 38% after 5 hours, affording **56**.

*Table 5.3.3 Screening of substrates for the hydrophosphination of alkenes catalysed by **29**.*

Entry	Substrate[a)]	*t* (h)	Conv. (%)[b)]	Product Ratio[b)] **A**/**B**/**C**	Reaction Product	Yield (%)[c)]
1		5	100	99/0/1	 (**47**)	83

2		72	26	23/0/3	 (**48**)	13
3		1	100	-/100/0	 (**49**)	74
4		70	2	- /0/2	-	-
5		20	2	0/0/2	-	-
6		24	5	0/0/5	-	-
7		22	7	0/0/7	-	-
8		71	3	0/0/3	-	-
9		40	94	92/0/2	 (**50**)	81
10		20	95	95/0/0	 (**51**)	90
11		20	3	0/0/3	-	- *d)*
12		24	81	79/0/2	 (**52**)	52*e)*
13		24	4	0/0/4	-	-
14		24	3	0/0/3	-	-
15		4	86	86/0/0	 (**53**)	77
16		6	71	-/69/2	 (**54**)	58

17		6	76	-/75/2	 (**55**)	65
18		6	2	-/-/2	-	-
19		5	38	-/36/2	 (**56**)	38[f]

[a] Reaction conditions: 5.0 mg, 6.92 x10^{-3} mmol of **29** (5 mol%), 0.6 mL of toluene, 20 equiv. of alkene/$PHPh_2$. Samples were heated in an oil bath at 80 °C, progress was monitored by NMR spectroscopy. [b] Determined by ^{31}P NMR spectroscopy **A**= Anti-markovnikov product, **B**= Markovnikov product, **C**=Ph_2P-PPh_2. [c] Isolated as the phosphine oxide, following oxidation with H_2O_2. [d] No substitution. [e] β-substituted product. [f] Decomposes upon oxidation, giving the α-hydroxy phosphine oxide **56a**.

In all cases in which hydrophosphination of the substrate was observed, and following either completion or no significant changes in the proportion of products. The resulting product was purposely oxidised in the presence of H_2O_2, allowing isolation of the resulting phosphine oxide (**46a**-**56a**).[281] In the case of the insertion product derived from the *N*-benzylidenemethyl amine (Entry 19, Table 5.3.3). The ^{1}H and $^{13}C\{^{1}H\}$ NMR spectra did not match the expected structure following the oxidation of **56**. Thus, crystals of this compound, suitable for X-ray diffraction, were grown at room temperature, from a concentrated solution in diethyl ether, and the structure is presented below (Figure 5.3.3).

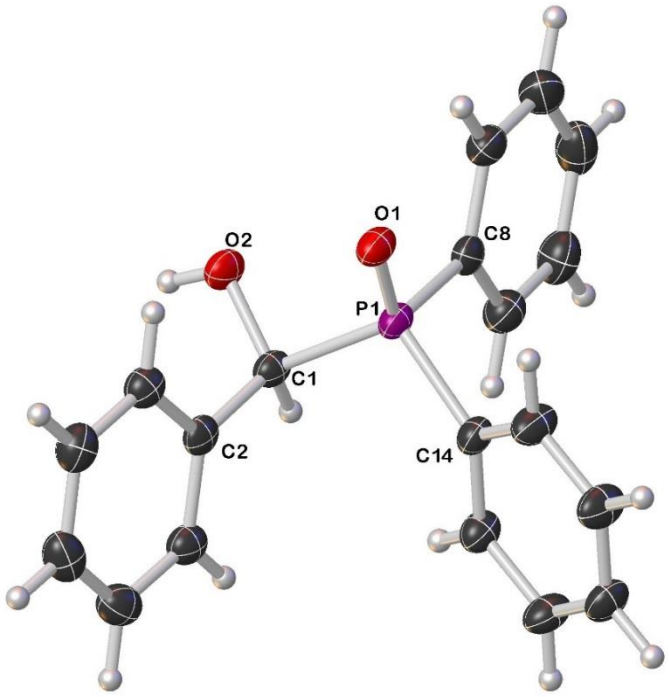


*Figure 5.3.3 Molecular structure of the decomposition product **56a**; L-enantiomer vs. R-enantiomer ratio within the crystal lattice (95:5), with displacement ellipsoids set at the 50% probability level.*

Rather than obtaining the amino-phosphine oxide derived from oxidation of **56**, the solid state determination of the resulting product, evidenced formation of an α-hydroxy phosphine oxide (**56a**) (Figure 5.3.3). The mechanism of formation of this product has been rationalised as a direct consequence of the comparatively unstable aliphatic amino-phosphine oxide, formed in the presence of H_2O_2. With similar observations been previously reported in reactions between aminophosphines/amino-*bis*(phospines) and aldehydes/ketones.[310,311]

Bond Length (Å)		Bond Angle (°)	
P1–O1	1.495(2)	O1–P1–C8	111.53(10)
P1–C1	1.835(2)	O1–P1–C14	111.81(9)
P1–C8	1.806(2)	O1–P1–C1	113.41(8)
P1–C14	1.807(8)	O2–C1–C2	113.16(12)
C1–O2	1.427(2)	O2–C1–P1	100.59(10)
C1–C2	1.511(2)	C1–P1–C8	104.23(8)

*Table 5.3.4 Selected bond lengths and angles for **56a**.*

5.3.4 Towards a Reaction Mechanism

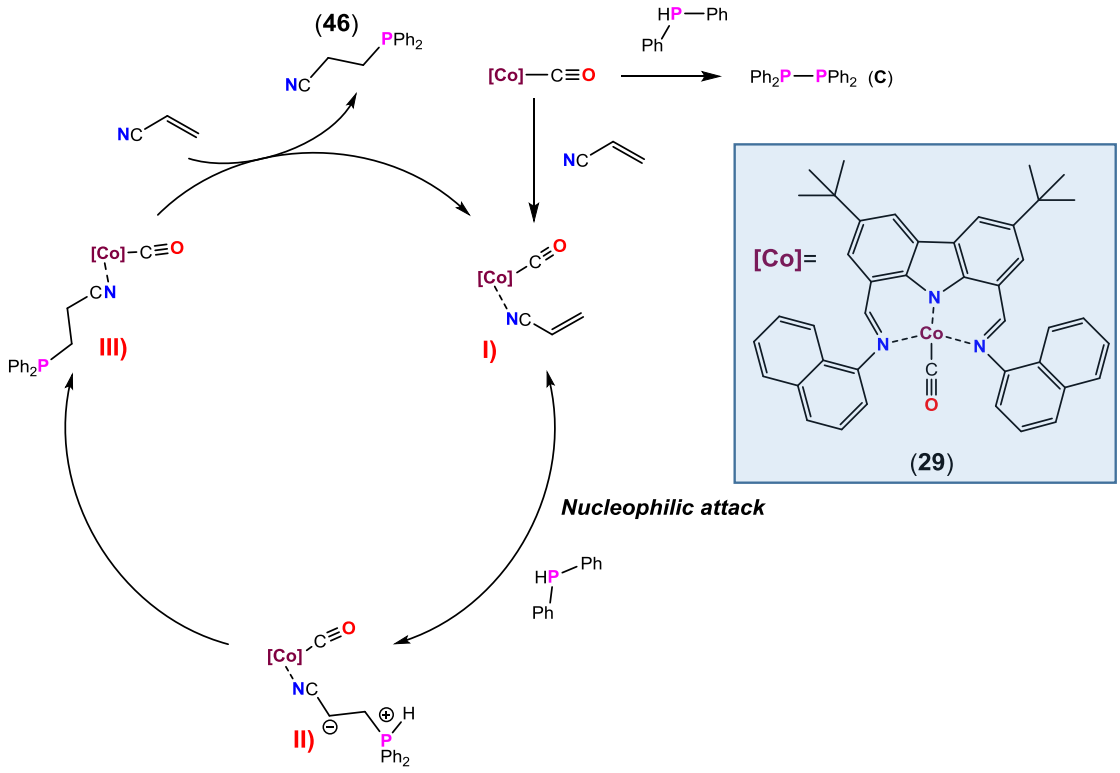
In terms of how this transformation is taking place, there are reports in the literature detailing two possible initial steps proposed for transition metal complexes in hydrophosphination reactions; the first one involves initial coordination of the secondary phosphine to the metal centre, which yields a metal-phosphide complex, which is known to be prominent in systems catalysed by platinum,[312–317] lanthanide metals[318–321] and in some cases even iron.[271,281] Although less common, an alternative mechanism, involves the formation of a metal-olefin complex.[322] This intermediate has been most commonly reported for late first-row transition metals[275,323] and in limited cases by noble metals.[323–325]

Following this, and as a subsequent step, it has been demonstrated in the analogous hydroamination of alkenes, that contrary to popular belief, the η^2-olefin is not directly activated upon coordination by the metal centre. The activation occurs on going from η^2 to η^1 coordination. This slippage by the alkene displacement of the coordinated olefin localizes the LUMO of the Ligand-M-[alkene] complex on the most distant carbon atom, enhancing the interaction with the incoming nucleophilic phosphine, a key feature in the reaction mechanism that explains selective formation of anti-Markovnikov substitution product.[325–327]

Several attempts of forming a metal-phosphide complex between $PHPh_2$ and **27**/**29** were carried out, showing no evidence supporting the formation of a compound of such nature, even when stoichiometric amounts of NEt_3 or $K[NSi(Me_3)_2]$ were added, as determined by ^1H and ^{31}P NMR spectroscopy. Nevertheless, it has been possible to synthesise, characterise and crystallographically authenticate several examples of metal-substrate-coordination complexes using **27** and unsaturated substrates; these have been described in detail in Chapter 4 (**27a**-**d**). These examples highlight the space available for coordination/reactivity around the low-coordinate metal centre. Additionally, all examples isolated are coordinated *via* an electron rich nitrogen or oxygen atom, rather than the olefinic moiety. With the aforementioned catalytic experiments showing that in cases in which a metal-olefin complex cannot be formed the main outcome of the reaction is the stoichiometric formation of dehydrocoupling product $Ph_2P–PPh_2$, this observation has also been previously reported by Webster *et al.*, in a similar process catalysed by an iron metal complex.[271,286]

5.3.5 Proposed Reaction Mechanism

The mechanism depicted in Scheme 5.3.2, looks to reconcile all the observations previously stated, however it does not attempt to give unequivocal identity of all the components of the reaction mixture.



*Scheme 5.3.2 Proposed reaction mechanism for the hydrophosphination of acrylonitrile, catalysed by **29**.*

Initially, **29** coordinates the unsaturated substrate, forming the coordinated complex (**I**), similar to complexes **27a-d** (Scheme 5.3.2). Initial loss of carbon monoxide from the parent metal complex *via* an initial hydroformylation/carbonylation mechanism, has been ruled out following NMR (^{1}H and ^{13}C{^{1}H} NMR spectra show no formation of carbonylic products) and MS determinations (absence of molecular ions consistent with CO homologation into the substrate), suggesting **29** as the catalytically active species. If the unsaturated substrate is too sterically hindered or if inactive (*e.g.* styrene), and alternative pathway allows the stoichiometric dehydrocoupling reaction to take place, giving Ph_2P–PPh_2. Intermediate **I** can then undergo nucleophilic substitution by the secondary phosphine. Kinetic determinations previously reported using an isostructural (four coordinate/square planar) and isolectronic (d^8), Ni(II) complex to **29**, [Ni(κ^3-Pigiphos)($NCMeCCH_2$)]$^{2+}$, have shown this initial step is reversible, due to low energy

barriers for a phosphine nucleophilic attack and elimination, respectively.[322] This step affords intermediate **II**, in a regioselective manner; with subsequent proton transfer to yield **III**. It should be mentioned that several attempts to isolate and crystallographically characterise intermediate **III**, or analogues, were carried out with no success, suggesting rapid decomposition of **III** to give product **46** and the cobalt(I) catalyst (**29**), which coordinates an additional molecule of acrylonitrile, completing the catalytic cycle.

5.4 Conclusions

Heteroleptic metal(I)/(II) complexes **26**-**30** are active catalysts for the hydrophosphination of activated olefins. The method has been extended to a range of substrates, employing for the first time a cobalt(I)-carbonyl complex in hydrophosphination of alkenes, yielding selectively the anti-Markovnikov phosphine. Attempts at characterising the mechanism by which the reaction takes places has allowed us to draw similarities with analogous heteroatom insertion reactions, founded in crystallographically authenticated intermediates. From controlled poisoning experiments, it has been possible to determine that the nature of the catalytic systems is most likely homogeneous and not radical based. However, further research is needed to ascertain the catalyst resting state and the exact nature of the reaction mixture in catalysis.

5.5 Experimental Section

5.5.1 Synthesis and Characterisation

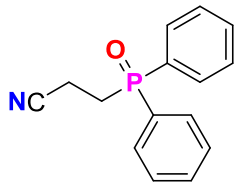
Typical procedure for the hydrophosphination of activated alkenes:

To the isolated or *in situ* generated **29** (5 mg, 6.92 x10^{-3} mmol) in solution, acrylonitrile (9.06 µL, 0.138 mmol, 20 eq.) and then $PHPh_2$ (24 µL, 0.138 mmol, 20 eq.) were added. The resulting NMR sample was transferred to an oil bath set up to the desired temperature (Table 5.3.1 and Table 5.3.3) and monitored until the resonances attributed to the starting material disappeared (^{31}P NMR spectroscopy) or when no significant reaction progress was observed (**46**).

In order to isolate the hydrophosphination products, the reaction mixtures were purposely oxidised (**46a**),[281] in all cases the crude mixture was opened to air and eluted through a silica gel plug (petroleum ether 40-60) removing the unreacted $PHPh_2$. The column was then washed with Et_2O, this fraction was exposed to H_2O_2 (30% w/w, 5 mL) and stirred at room temperature for 10 min. The reaction mixture was quenched with deionised water and the organic phase was separated, dried and evaporated.

In the particular case of products **51a** and **52a**, the crude after oxidation had to be extracted with dichloromethane due to the increased solubility of the products in H_2O.

Characterisation for the hydrophosphination products as oxides (unless otherwise stated):



3-(diphenylphosphinyl)-propanenitrile (**46a**):[328]

^1H NMR (400 MHz, $CDCl_3$, 25 °C) δ (ppm): 7.76-7.71 (m, 4H, ^{o}Ph), 7.60-7.50 (m, 6H, ^{m}Ph/^{p}Ph), 2.64 (s, 4H, 2x-C$\underline{H}_2$-).

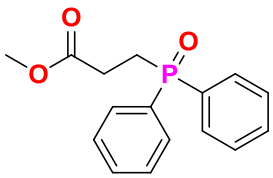
$^{13}C\{^1H\}$ NMR (100 MHz, $CDCl_3$, 25 °C) δ (ppm): 132.73 (d, J = 2.78 Hz, ^{p}Ph), 130.87 (d, J = 9.47 Hz, ^{o}Ph), 129.20 (d, J = 12.12 Hz, ^{m}Ph), 125.63 (s, -$\underline{C}$≡N), 118.66 (d, J = 18.40 Hz, ^{i}Ph), 26.37 (d, J = 70 Hz, –$\underline{C}H_2$-P(O)Ph_2), 10.54 (s, N≡C-$\underline{C}H_2$-).

^{31}P NMR (162 MHz, 25 °C) δ (ppm): –15.7 (as free phosphine, toluene with C_6D_6 insert), 32.54 (as oxide, $CDCl_3$).

HRMS/ESI+ *m/z*: [M+H] calculated 256.0886; found 256.0880 formula $C_{15}H_{15}NOP$.

IR *v*/cm^{-1} (ATR): 2957 w, 2923 w, 2258 (C≡N) w, 1436 s, 1180 (P=O) s.

Yellow oil (31.4 mg, 89%).



3-(diphenylphosphinyl)-propanoic acid-methyl ester (**47a**):[329]

^{1}H NMR (400 MHz, C_6D_6, 25 °C) δ (ppm): 7.40-7.31 (m, 5H, Ph), 7.08-6.98 (m, 5H, Ph), 3.27 (s, 3H, -O-C*H*$_3$), 2.30 (s, 4H, 2x-C*H*$_2$-).

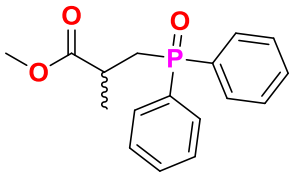
^{13}C{^{1}H} NMR (100 MHz, C_6D_6, 25 °C) δ (ppm): 172.85 (s, -*C*=O), 133.10 (d, *J*= 19.0 Hz, Ph), 128.82 (Ph), 128.77 (Ph), 51.19 (-O-*C*H$_3$), 30.77 (d, *J*= 19.9 Hz, -*C*H$_2$-P(O)Ph$_2$), 23.57 (d, *J* = 12.5 Hz, CH$_3$O(C=O)-*C*H$_2$-).

^{31}P NMR (162 MHz, 25 °C) δ (ppm): –15.35 (as free phosphine, toluene with C_6D_6 insert), 32.51 (as oxide, $CDCl_3$).

HRMS/ESI+ *m/z*: [M+H] calculated 289.0988; found 289.1001 formula $C_{16}H_{18}O_3P$.

IR *v*/cm^{-1} (ATR): 2955 w, 1735 (C=O) s, 1436 s, 1173 (P=O) s.

Yellow oil (32.3 mg, 83%).



3-(diphenylphosphinyl)-2-methyl, propanoic acid-methyl ester (**48a**):[307,330,331]

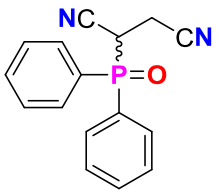
^{1}H NMR (400 MHz, $CDCl_3$, 25 °C) δ (ppm): 7.77-7.62 (m, 4H, ^{o}Ph), 7.45-7.36 (m, 2H, ^{p}Ph), 7.36-7.28 (m, 4H, ^{m}Ph), 3.5 (s, 3H, -O-C*H*$_3$), 1.43 (m, 3H, -C*H*$_2$-/-C*H*-), 0.86 (s, 3H, -C*H*$_3$).

^{31}P NMR (162 MHz, 25 °C) δ (ppm): –19.58 (as free phosphine, toluene with C_6D_6 insert), 31.20 (as oxide, $CDCl_3$).

HRMS/ESI+ *m/z*: [M+Na] calculated 325.0964; found 325.0959 formula $C_{17}H_{19}NaO_3P$.

IR *v*/cm^{-1} (ATR): 2958 w, 2926 w, 2866 w, 1694 (C=O) s, 1463 s, 1127 (P=O) s.

Yellow oil (5.3 mg, 13%).



2-(diphenylphosphinyl)-butanedinitrile (**49a**):

^{1}H NMR (400 MHz, $CDCl_3$, 25 °C) δ (ppm): 8.02-7.94 (m, 2H, Ph), 7.93-7.84 (m, 2H, Ph), 7.73-7.68 (m, 2H, Ph), 7.66-7.57 (m, 4H, Ph), 3.82-3.68 (m, 1H, -C*H*-P(O)Ph$_2$), 3.17-3.07 (m, 1H, -C*H*$_2$- *anti* to CH), 2.85-2.72 (m, 1H, -C*H*$_2$- *syn* to CH).

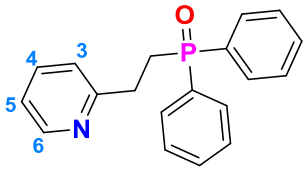
^{13}C{^{1}H} NMR (100 MHz, $CDCl_3$, 25 °C) δ (ppm): 134.12 (dd, *J* = 12.6, 2.2 Hz, Ph), 132.33 (d, *J* = 9.3 Hz, Ph), 131.34 (d, *J* = 10 Hz, Ph), 129.58 (t, *J* = 13.2 Hz, Ph), 30.33 (s, -*C*H-P(O)Ph$_2$), 15.91 (s, -C*H*$_2$-).

^{31}P NMR (162 MHz, 25 °C) δ (ppm): –2.53 (as free phosphine, toluene with C_6D_6 insert), 26.52 (as oxide, $CDCl_3$).

HRMS/ESI+ *m/z*: [M+H] calculated 281.0838; found 281.0840 formula $C_{16}H_{14}N_2OP$.

IR *v*/cm^{-1} (ATR): 3058 w, 2960 w, 2924 w, 2871 w, 2243 (C≡N) w, 1438 s, 1193 (P=O) s.

Dark yellow oil (28.6 mg, 74%).



2-[2-(diphenylphosphinyl)ethyl]-pyridine (**50a**):[332,333]

^{1}H NMR (400 MHz, $CDCl_3$, 25 °C) δ (ppm): 8.49 (d, J = 3.6 Hz 1H, ^{4}Py), 7.80-7.76 (m, 4H, ^{o}Ph), 7.55-7.43 (m, 7H, $^{m\&p}$Ph + ^{5}Py), 7.14 (d, J = 7.7 Hz, 1H, ^{3}Py), 7.09-7.07 (m, 1H, ^{6}Py), 3.15-3.09 (m, 2H, Py-C$\underline{H_2}$), 2.82-2.75 (m, 2H, –C$\underline{H_2}$-P(O)Ph_2).

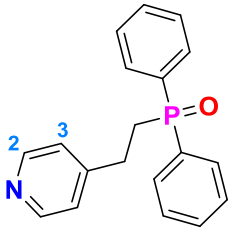
^{13}C{^{1}H} NMR (100 MHz, $CDCl_3$, 25 °C) δ (ppm): 160.23 (s, ^{i}Py), 149.32 (s, ^{4}Py), 136.73 (s, ^{5}Py), 131.88 (d, J = 2.81 Hz, ^{m}Ph), 130.97 (d, J = 9.3 Hz, ^{o}Ph), 128.81 (d, J = 11.7 Hz, ^{p}Ph), 123.28 (s, ^{3}Py), 121.67 (s, ^{6}Py), 29.69 (s, Py-$\underline{C}H_2$), 28.98 (s, –$\underline{C}H_2$-P(O)Ph_2).

^{31}P NMR (162 MHz, 25 °C) δ (ppm): –15.60 (as free phosphine, toluene with C_6D_6 insert), 32.32 (as oxide, $CDCl_3$).

HRMS/ESI+ *m/z*: [M+Na] calculated 330.1018; found 330.1027 formula $C_{19}H_{18}NaNOP$.

IR ν/cm^{-1} (ATR): 3056 w, 2960 w, 2913 w, 1437 s, 1162 (P=O) s.

Yellow oil (34.6 mg, 82%).



4-[2-(diphenylphosphinyl)ethyl]-pyridine (**51a**):[333]

^{1}H NMR (400 MHz, $CDCl_3$, 25 °C) δ (ppm): 8.46 (s, 2H, ^{2}Py), 7.76-7.71 (m, 5H, Ph), 7.54-7.44 (m, 5H, Ph), 7.10 (d, J = 4.9 Hz, 2H, ^{3}Py), 2.95-2.88 (m, 2H, Py-C$\underline{H_2}$), 2.59-2.52 (m, 2H, –C$\underline{H_2}$-P(O)Ph_2).

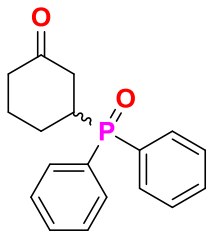
^{13}C{^{1}H} NMR (100 MHz, $CDCl_3$, 25 °C) δ (ppm): 150.54 (d, J = 14.8 Hz, ^{i}Py), 149.48 (s, ^{2}Py), 132.18 (d, J = 2.7 Hz, Ph), 130.81 (d, J = 9.4 Hz, Ph), 128.93 (d, J = 11.7 Hz, Ph), 128.41 (d, J = 10.9 Hz, ^{i}Ph), 123.81 (s, ^{3}Py), 30.61 (d, J = 70.4 Hz, –$\underline{C}H_2$-P(O)Ph_2), 27.08 (d, J = 2.9 Hz, Py-$\underline{C}H_2$).

^{31}P NMR (162 MHz, 25 °C) δ (ppm): –15.81 (as free phosphine, toluene with C_6D_6 insert), 31.49 (as oxide, $CDCl_3$).

HRMS/ESI+ *m/z*: [M+H] calculated 308.1199; found 308.1191 formula $C_{19}H_{19}NOP$.

IR ν/cm^{-1} (ATR): 3056 w, 2916 w, 1437 s, 1167 (P=O) s.

Colourless oil (37.8 mg, 90%).



3-(diphenylphosphinyl)-cyclohexanone (**52a**):[332,334]

^{1}H NMR (400 MHz, $CDCl_3$, 25 °C) δ (ppm): 7.97-7.93 (m, 1H, Ph), 7.80-7.71 (m, 4H, Ph), 7.52-7.30 (m, 7H, Ph), 2.72-2.57 (m, 1H, –C*H*-P(O)Ph_2), 2.46-2.32 (m, 1H, C*H*), 2.46-2.22 (m, 1H, C*H*), 2.22-2.10 (m, 1H, C*H*), 2.07-1.88 (m, 1H, C*H*), 1.88-1.76 (m, 1H, C*H*), 1.75-1.55 (m, 1H, C*H*), 1.45 (s, 1H, CH), 1.41 (s, 1H, CH).

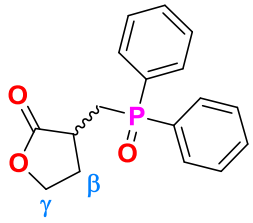
^{13}C{^{1}H} NMR (100 MHz, $CDCl_3$, 25 °C) δ (ppm): 209.81 (d, *J* = 14.3 Hz, -*C*=O), 132.56 (d, *J* = 8.5 Hz, Ph), 132.22, 131.80, 131.01 (dd, *J* = 9.0, 1.9 Hz, Ph), 129.05 (dd, *J* = 11.6, 2.5 Hz, Ph), 128.51, 41.22, 39.45 (d, *J* = 3.1 Hz, *C*H), 37.94 (d, *J* = 71.5 Hz, –*C*H-P(O)Ph_2), 26.53 (d, *J* = 15.7 Hz, *C*H), 25.27 (d, *J* = 7.6 Hz, *C*H), 23.44 (d, *J* = 2.8 Hz, *C*H).

^{31}P NMR (162 MHz, 25 °C) δ (ppm): –3.74 (as free phosphine, toluene with C_6D_6 insert), 33.12 (as oxide, $CDCl_3$).

HRMS/ESI+ *m/z*: [M+Na] calculated 321.1015; found 321.1034 formula $C_{18}H_{19}NaO_2P$.

IR ν/cm^{-1} (ATR): 3091 w, 3057 w, 2942 w, 2864 w, 1709 (C=O) s, 1437 s, 1173 s, 1117 (P=O) s.

Yellow oil (21.4 mg, 52%).



3-((diphenylphosphoryl)methyl)dihydrofuran-2(3H)-one (**53a**):

^{1}H NMR (400 MHz, $CDCl_3$, 25 °C) δ (ppm): 7.78-7.74 (m, 4H, ^{o}Ph), 7.57-7.45 (m, 6H, $^{m\&p}$Ph), 4.32 (t, J = 8.6, 1H, γ), 4.10 (q, J = 9.7, 1H, γ'), 3.19-3.01 (m, 1H, –C$\underline{H}_2$-P(O)Ph_2 *anti* to CH), 2.80 (quint, J = 9.37 Hz, 1H, C$\underline{H}$), 2.58-2.45 (m, 1H, β-C$\underline{H}_2$-*anti* to C*H*), 2.25 (q, J = 11.9 Hz, 1H, –C$\underline{H}_2$-P(O)Ph_2 *syn* to CH), 2.01 (quint, J = 8.35 Hz, 1H, β'-C$\underline{H}_2$- *syn* to CH).

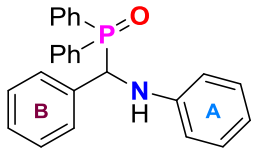
^{13}C{^{1}H} NMR (100 MHz, $CDCl_3$, 25 °C) δ (ppm): 178.75 (d, J = 18.0 Hz, -$\underline{C}$=O), 132.39 (d, J = 67.9 Hz, ^{i}Ph), 132.32 (d, J = 9.7 Hz, ^{p}Ph), 130.87 (dd, J = 28.1, 9.9 Hz, ^{o}Ph), 129.06 (dd, J = 16.6, 11.6 Hz, ^{m}Ph), 67.11 (s, γ), 34.57 (s, $\underline{C}$H), 32.19 (s, –$\underline{C}H_2$-P(O)Ph_2), 30.16 (s, β).

^{31}P NMR (162 MHz, 25 °C) δ (ppm): –18.74 (as free phosphine, toluene with C_6D_6 insert), 30.60 (as oxide, $CDCl_3$).

HRMS/ESI+ *m/z*: [M+Na] calculated 323.0808; found 323.0812 formula $C_{17}H_{17}NaO_3P$.

IR ν/cm^{-1} (ATR): 3056 w, 2873 w, 1762 (C=O) s, 1437 s, 1175 (P=O) s.

Yellow oil (32.3 mg, 77%).



α-(diphenylphosphinyl)-*N*-phenyl-benzenemethanamine (**54a**):[335]

^{1}H NMR (400 MHz, $CDCl_3$, 25 °C) δ (ppm): 7.89-7.84 (m, 2H, ^{Bo}Ph), 7.57 (td, J = 7.4, 1.3 Hz, 1H, ^{Bp}Ph), 7.49 (td, J = 7.4, 3.0 Hz, 2H, ^{Bm}Ph), 7.42-7.36 (m, 3H, ^{p}Ph), 7.29 (d, J = 3.1 Hz, 1H, ^{m}Ph), 7.13 (s, 5H, ^{o}Ph), 7.11-7.06 (m, 2H, ^{Am}Ph), 6.67 (t, J = 7.3 Hz, 1H, ^{Ap}Ph), 6.60 (d, J = 7.7 Hz, 2H, ^{Ao}Ph), 5.21-5.15 (m, 2H, –C$\underline{H}$-P(O)Ph_2).

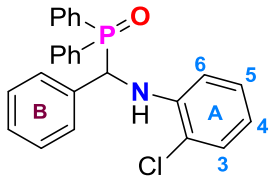
$^{13}C\{^{1}H\}$ NMR (100 MHz, $CDCl_3$, 25 °C) δ (ppm): 146.21 (d, *J* = 12.0 Hz, ^{Ai}Ph), 135.20 (d, *J* = 2.0 Hz, ^{Bi}Ph), 132.44 (d, *J* = 2.8 Hz, ^{Bp}Ph), 132.08 (d, *J* = 2.9 Hz, ^{p}Ph), 131.81 (d, *J* = 9.0 Hz, ^{Bo}Ph), 131.11 (d, *J* = 66.2 Hz, ^{i}Ph), 130.13 (d, *J* = 70.2 Hz, ^{i}Ph), 129.34 (s, ^{Am}Ph), 128.94 (d, *J* = 11.6 Hz, ^{Bm}Ph), 128.50 (d, *J* = 4.5 Hz, ^{o}Ph), 128.31 (m, ^{m}Ph), 118.52 (s, ^{Ap}Ph), 114.07 (s, ^{Ao}Ph), 57.49 (d, *J* = 75.0 Hz, –CH-P(O)Ph_2).

^{31}P NMR (162 MHz, 25 °C) δ (ppm): 5.26 (as free phosphine, toluene with C_6D_6 insert), 33.12 (as oxide, $CDCl_3$).

HRMS/ESI+ *m/z*: [M+H] calculated 384.1512; found 384.1411 formula $C_{25}H_{23}NOP$.

IR ν/cm^{-1} (ATR): 3388 (N*H*) m, 3059 w, 3046 w, 2895 w, 1600 s, 1503 s, 1122 (P=O) s.

Colourless solid (29.7 mg, 58%).



α-(diphenylphosphinyl)-*N*-(2-chloro-phenyl)-benzenemethanamine (**55a**):

^{1}H NMR (400 MHz, $CDCl_3$, 25 °C) δ (ppm): 7.82-7.77 (m, 2H, Ph), 7.61-7.56 (m, 3H, Ph), 7.52-7.45 (m, 3H, Ph), 7.34 (td, *J*= 7.6, 3.0 Hz, 2H, Ph), 7.21 (dd, *J*= 7.9, 1.4 Hz, 1H, ^{A}*6*), 7.18-7.14 (m, 5H, Ph), 6.97 (m, 1H, ^{A}*4*), 6.62 (td, *J*= 7.7, 1.3 Hz, 1H, ^{A}*5*), 6.54 (dd, *J*= 8.2, 0.9 Hz, 1H, ^{A}*3*), 5.54 (t, *J*= 8.7 Hz, 1H, N*H*), 5.23 (td, *J*= 13.3, 8.8 Hz, 1H, –C*H*-P(O)Ph_2).

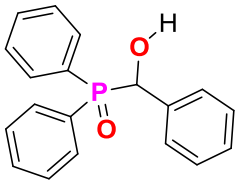
$^{13}C\{^{1}H\}$ NMR (100 MHz, $CDCl_3$, 25 °C) δ (ppm): 142.18 (d, *J*= 11.9 Hz, ^{Ai}Cl-Ph), 134.58 (d, *J*= 2.1 Hz, ^{i}Ph), 132.43 (dd, *J*= 31.6, 2.8 Hz, ^{i}Ph), 132.03 (d, *J*= 9 Hz, Ph), 131.85 (d, *J*= 9.0 Hz, Ph), 130.72 (d, *J*= 16.9 Hz, ^{i}Ph), 129.41 (s, ^{A}*6*), 128.87 (d, *J*= 11.6 Hz, Ph), 128.45 (d, *J*= 15.0 Hz, ^{i}Ph), 128.40 (s, Ph), 128.31 (d, *J*= 4.2 Hz, Ph), 127.98 (d, *J*= 2.7 Hz, ^{i}Ph), 127.78 (s, ^{A}*4*), 120.52 (s, ^{Ai}Ph), 118.74 (s, ^{A}*5*), 112.94 (s, ^{A}*3*), 57.69 (d, *J*= 74.3 Hz, –CH-P(O)Ph_2).

^{31}P NMR (162 MHz, 25 °C) δ (ppm): 7.60 (as free phosphine, toluene with C_6D_6 insert), 31.59 (as oxide, $CDCl_3$).

HRMS/ESI+ *m/z*: [M+H] calculated 418.1122, found 418.1131 formula $C_{25}H_{22}ClNOP$.

IR ν/cm^{-1} (ATR): 3386 (N*H*) w, 3056 w, 3028 w, 2920 w, 1594 s, 1499 s, 1436 s, 1174 (P=O) s.

Pink solid (37.2 mg, 65%).



<u>α-(diphenylphosphinyl)-benzenemethanol</u> (**56a**):[336,337]

^{1}H NMR (400 MHz, $CDCl_3$, 25 °C) δ (ppm): 7.86-7.71 (m, 2H), 7.67-7.32 (m, 9H), 7.24-7.13 (m, 5H), 5.51 (broad, 1H, –C<u>*H*</u>-P(O)Ph$_2$).

^{31}P NMR (162 MHz, 25 °C) δ (ppm): –0.71 (as free phosphine, toluene with C_6D_6 insert), 31.08 (after oxidation/decomposition product, $CDCl_3$).

HRMS/ESI+ *m/z*: [M+H] calculated 309.1044; found 309.1021 formula $C_{19}H_{17}O_2P$.

IR ν/cm^{-1} (ATR): 3197 (O*H*) s, 2961 w, 2901 w, 1435 s, 1161 w, 1143 (P=O) w.

Light-yellow solid (15 mg, 38%).

Chapter VI. Organoruthenium Complexes Based on Hemilabile N/P-Ligands

In addition to ligand systems based on the carbazole moiety, there is increasing interest in exploring ligand systems that have more than one donating group (N/P), capable of substituting/chelating a metal centre, and that can be prepared following atom-economical routes.[317,338–341] Previous work in this area in our research group, directly followed the publication of the first transition-metal catalysed hydrophosphination of isocyanates; from which monoinsertion products (phosphinocarboxamides $PH_2C(=O)N(H)R$) and unprecedented double insertion products (phosphinodicarboxamides $PH_2C(=O)N(R)C(=O)N(H)R$) could be formed.[270] Later investigations, led to initial studies of the coordination chemistry of these compounds with $[Ru(p\text{-cym})Cl_2]_2$ (*p*-cym = *para*-cymene), with limited characterisation.[342] Due to this, the present chapter seeks to extend the existent library of compounds employing bidentate hemilabile ligands based on phosphino(di)carboxamide substituents, while also looking to complete the existent characterisation, from which observations of the structural and electronic properties of these compounds could be made.

6.1 Introduction to Hemilabile N/P-based Ligands

Modern coordination and organometallic chemistry relies on the choice of ligands capable of forming and stabilising discrete metal centres. One particular family of ligands capable of such feat, incorporate phosphine donors, from which in recent years hemilabile ligands incorporating hard and soft donor atoms have attracted particular attention,[343] with applications in coordination chemistry,[343–345] biomedicine,[346,347] enantioselective catalysis[348,349] and supramolecular and self-assembled arrays.[350]

Recently, Kays *et al*. reported the hydrophosphination of isocyanates which leads to formation of functionalised phosphinocarboxamides (PCAs) and an unprecedented family of phosphinodicarboxamides (PDCAs),[270] where the combination of hard (N or O) and soft (P) donors on the molecule results in hybrid and potentially hemilabile donors, enabling binding to a wide range of metals in diverse coordination modes.[351] Somewhat surprisingly, however, the use of PCAs as ligands is limited,[343–345,352] while the use of PDCAs as ligands has not previously been reported. With a close analogue found in the unique diinsertion of phenyl isocyanates into an amine bond, reported using lanthanide metal centres, to form complexes of general formula $Cp_2Ln[\eta^2{:}\eta^1\text{-PyNCON(Ph)CON}H\text{Ph}]$ (Ln = Yb, Er, Y, Dy and Gd; Py = 2-pyridyl), from which substituted ureas can be prepared.[353]

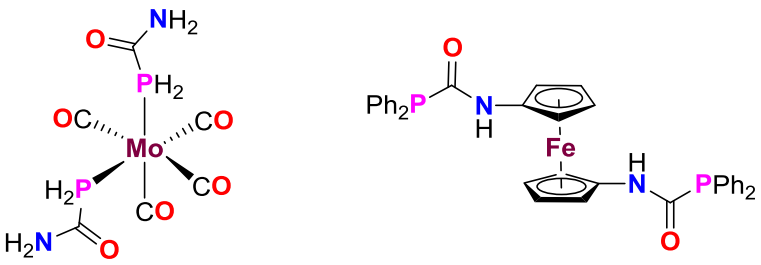
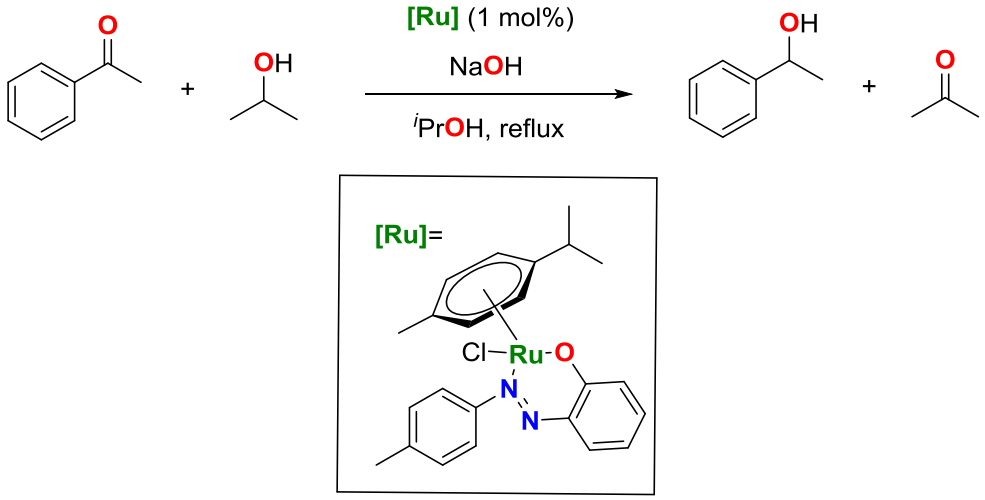


Figure 6.1.1 Examples of metal centres substituted by PCAs.

Examples in which primary PCAs have been used in the synthesis of metal complexes, include *cis*-$Mo(CO)_4(PH_2C(=O)NH_2)_2$[352] and $[Ru(p\text{-cym})\{PH_2C(=O)N(H)Cy\}Cl_2$; Cy = cyclohexyl ; *p*-cym = *para*-cymene][344] while Nakazawa's work on the reaction between a ferrocene derivative bearing a PCA moiety, $Fe(\eta^5\text{-}C_5H_4N(H)C(=O)PPh_2)_2$ with $PtX_2(PPh_3)_2$ (X = Cl, Br), has allowed for the unprecedented selective synthesis of M_4L_6 cage complexes, facilitated by hydrogen bonding interactions between the PCA moiety and the halide ion (Figure 6.1.1).[354]

6.2 Introduction to Ruthenium-Metallocene Chemistry



Scheme 6.2.1 A transfer hydrogenation process, catalysed by a ruthenium-arene complex.

In parallel, the chemistry of half-sandwich ruthenium complexes has been widely studied due to their potential use in catalysis, an area which has found noticeable development,[355–364] and the ease of interconversion to other Ru(0) and Ru(II) complexes.[358] In particular, ruthenium(II) complexes of the type $[(\eta^6\text{-arene})RuCl_2(PR_3)]$ (R = aryl or alkyl) are of

interest owing to their role as effective precursors for a variety of catalytic and stoichiometric organic transformations.[359,365] Noticeable examples of processes catalysed by hemilabile *p*-cymene-ruthenium(II) derived centres[351] include the transfer hydrogenation of ketones and benzaldehydes (Scheme 6.2.1),[356,357,366] the isomerisation of olefins such as allylbenzene and 1-octene[355] and a wide range of nucleophilic attack dominated, heteroatom insertion reactions towards allenylidene and cumulenylidene complexes.[362]

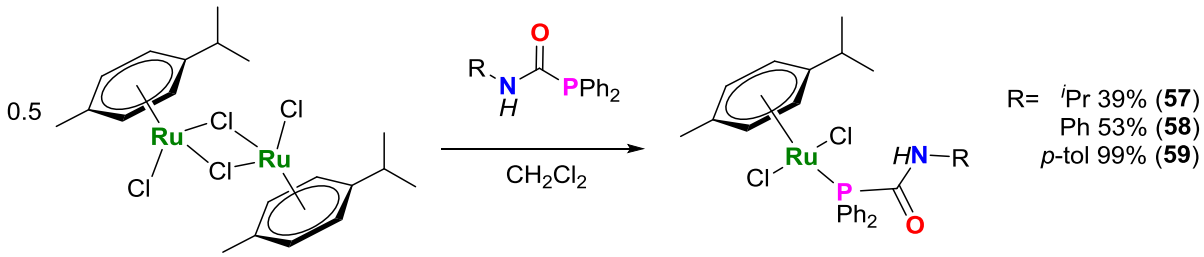
6.3 Aims and Objectives

Following initial experiments in our group, derived from the coordination of PCAs/PDCAs with $[Ru(p\text{-cym})Cl_2]_2$, which had allowed to structurally authenticate two complexes; $[Ru(p\text{-cym})\{Ph_2PC(=O)N(H)^iPr\}Cl_2]$ (**57**) and $[Ru(p\text{-cym})\{PH_2C(=O)N(R)C(=O)N(H)p\text{-tolyl}\}Cl_2]$ (**61**).[342] It is the main objective of this chapter to obtain full characterisation of these compounds. While at the same time, extending the number of coordination compounds derived from PCAs/PDCAs. Additionally, it has been postulated, based on the presence of an aminic proton in these moieties, that upon deprotonation, four- and six-membered ruthenium-metallacycles could be synthesised. As such, the library of compounds obtained from the coordination tests between PCAs/PDCAs and $[Ru(p\text{-cym})Cl_2]_2$ would allow to investigate said hypothesis.

6.4 Results and Discussion

6.4.1 Synthesis of Coordination Compounds [Ru(p-cym){$PPh_2C(=O)N(H)R$}Cl_2] (R = ^{i}Pr, Ph, p-tol)

Encouraged by recent reports in the formation/coordination of metal centres employing PCAs [$PH_2PC(=O)NH_2$ and $PH_2C(=O)N(H)Cy$],[344,352] the Lewis base character of these ligands towards coordination of [Ru(*p*-cym)Cl_2]$_2$ was investigated.[270] A solution of [Ru(*p*-cym)Cl_2]$_2$ and **L-57** ($PH_2C(=O)N(H)^iPr$) in a 1:2 ratio in dichloromethane was stirred at room temperature for 16 hours, which after removal of solvent, and extraction into toluene resulted in the precipitation of **57** as a dark red solid (Scheme 6.4.1),[342] with subsequent experiments showing a comparable conversion to the desired compound, even when coordinating solvents such as THF were used.



*Scheme 6.4.1 Synthesis and structure of ruthenium complexes (**57**-**59**); free PCAs (**L-57**–**L-58**).*

The $^{31}P\{^1H\}$ NMR spectrum for **57** in C_6D_6 revealed a singlet resonance peak at 29.8 ppm, and the ^1H NMR spectrum showed characteristic, shifted signals for the PCA ligand, noticeably is the significant downfield shift of the N*H* proton upon coordination (8.63 *vs.* 5.35 ppm). In contrast, the carbonyl group is shifted slightly upfield in the $^{13}C\{^1H\}$ NMR spectra, with respect to **L-57**, indicative of a change in the multiple bond character of the carbonyl after coordination to the metal centre (Table 1).[367–369] The use of phosphinocarboxamides with nitrogen-substituted aromatic groups (**L-58** and **L-59**) affords analogous compounds of general formula [Ru(*p*-cym){$Ph_2PC(=O)N(H)R$}Cl_2; R= Ph (**58**) and *p*-tolyl (**59**)[342]] (Scheme 6.4.1).

Pure samples of **57**-**59** were readily isolated from their respective reaction mixtures, in good to excellent yields (**57**, 39%; **58**, 53%; **59**, 99%), upon removal of volatiles as air-stable bright-red solids. Crystals suitable for single-crystal X-ray diffraction for **57**-**59** were grown from concentrated toluene extracts, at room temperature.

In the solid state, **57-59** feature a pseudo-octahedral geometry in a classical piano-stool arrangement, in which the coordination sphere consists of an η^6-bound *p*-cymene, two chlorides, and the phosphorus atom from the PCA (Figure 6.4.1). The Ru–Cl and Ru–P bond lengths for **57-59** are within the sum of the Van der Waals radii between the two elements [**57**: Ru1–Cl1 2.4115(5) Å, Ru1–P1 2.3476(5) Å; **58**: Ru1–Cl1 2.4142(6) Å, Ru1–P1 2.3448(6) Å; **59**: Ru1–Cl1 2.4171(4) Å, Ru1–P1 2.3517(4) Å][370] and are similar to closely related compounds,[344,356,357,365,366,371] which include [Ru(*p*-cym){PH_2(CO)N*H*Cy}Cl_2].[344] In addition, intramolecular hydrogen bonding between the amide fragment and one of the chlorides, is also observed. [H1(H2)–Cl1(Cl2); **57**: 2.53(2) Å; **58**: 2.3455(6) Å; **59**: 2.277(16) Å; **60**: 2.3703(3) Å ; **61**: 2.44(5) Å] & [N1(N2)–Cl1(Cl2); **57**: 3.1243(18) Å; **58**: 3.197(2) Å; **59**: 3.1310(15) Å; **60**: 3.248(2) Å; **61**: 3.296(4) Å].

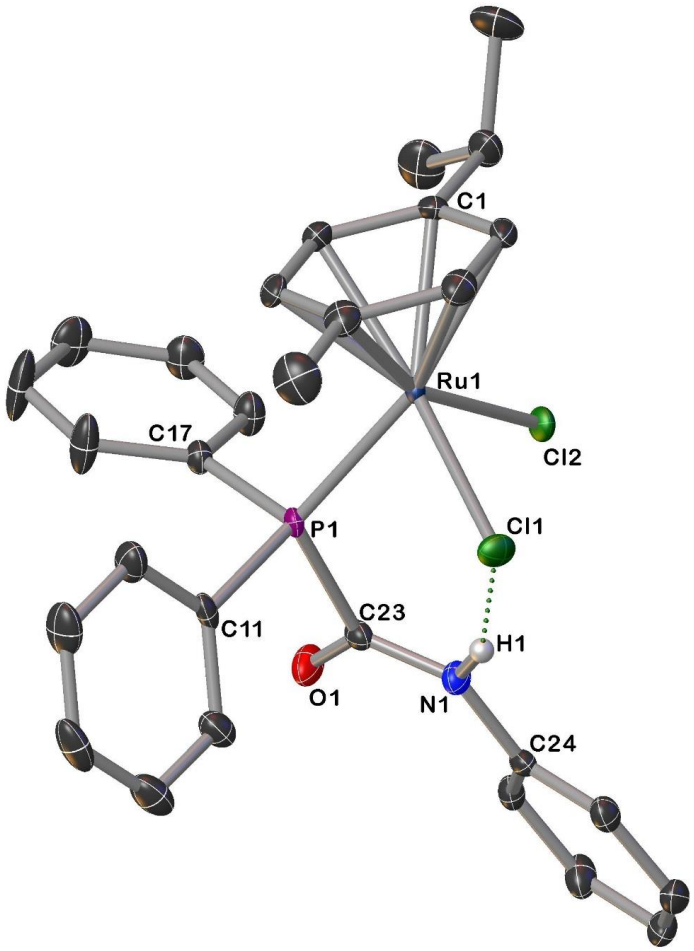


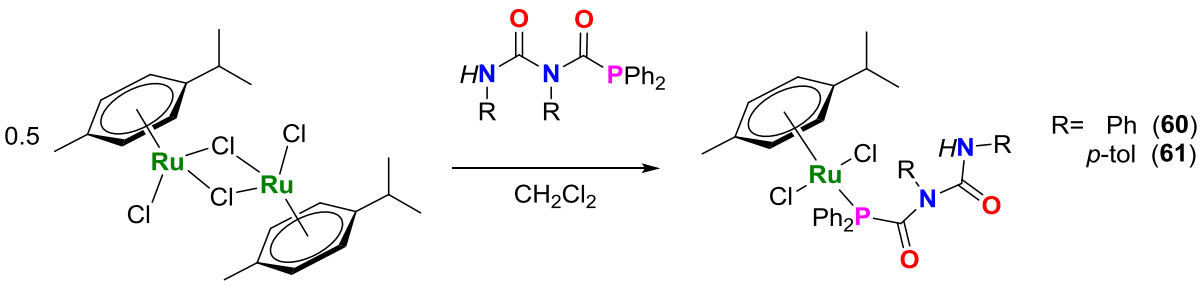
*Figure 6.4.1 Molecular structure for **58**, with displacement ellipsoids set at the 50% probability level. Crystallisation solvent and hydrogen atoms, with the exception of H1 (white sphere), have been omitted for clarity.*

Bond Length (Å)		Bond Angle (°)	
$C1_{plane}$–Ru1	1.700608(13)	Cl1–Ru1–Cl2	88.95(2)
Ru1–Cl1	2.4142(6)	Cl1–Ru1–P1	85.17(2)
Ru1–Cl2	2.4151(6)	Cl2–Ru1–P1	86.87(2)
Ru1–P1	2.3448(6)	Ru1–P1–C11	118.55(8)
P1–C17	1.819(2)	Ru1–P1–C17	111.89(8)
P1–C11	1.837(2)	Ru1–P1–C23	118.02(7)
P1–C23	1.901(2)		

*Table 6.4.1 Selected bond lengths and angles for **58**.*

6.4.2 Synthesis of Coordination Compounds [Ru(p-cym){$PPh_2C(=O)N(R)C(=O)N(H)R$}Cl_2] (R = Ph, p-tol)

In parallel, the phosphinodicarboxamides $PH_2C(=O)NPhC(=O)NHR$ (R = Ph **L-60**, *p*-tolyl **L-61**] were reacted with [Ru(*p*-cym)Cl_2]$_2$ (Scheme 6.4.2) under similar conditions, obtaining in all cases, compounds of the form [Ru(*p*-cym){$PH_2C(=O)N(R)C(=O)N(H)R$}Cl_2]; {R= Ph (**60**) and *p*-tolyl (**61**) }.[342]



*Scheme 6.4.2 Synthesis and structure of ruthenium complexes (**60**-**61**); free PDCAs (**L-60**–**L-61**).*

Crystals of **60** and **61**[342] suitable for single-crystal X-ray diffraction were grown from concentrated toluene solutions at room temperature (Figure 6.4.2). In the solid state, **60** and **61** feature an 18 electron, ruthenium metal centre which is bound to two chloride ions, the phosphorus atom from the PDCA and an additional η^6-interaction with the *p*-cymene moiety, in a similar structure to **57**-**59** (Figure 2). Complexes **60** and **61** exhibit intramolecular hydrogen bonding interactions between the amido moiety and one of the

metal-bound chloride ligands. The core of the PDCA ligands is twisted compared to the free ligand (**L-60** and **L-61**),[270] most likely arising from $\pi\cdots\pi$ stacking interactions between the phosphorus aryl groups and the phenyl moiety [$C17_{plane}$–$C24_{plane}$ = 3.635(3) Å], which highlights the flexibility of the PDCA ligand.

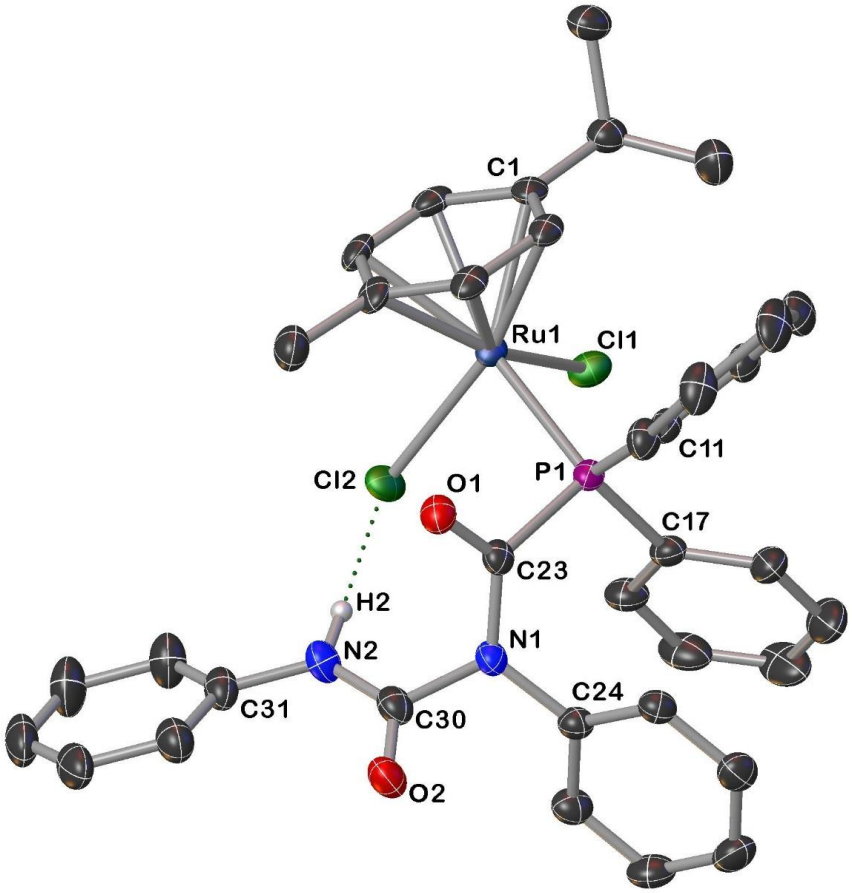


*Figure 6.4.2 Molecular structure for **60**, with displacement ellipsoids set at the 50% probability level. Crystallisation solvent and hydrogen atoms, with the exception of H2 (white sphere), have been omitted for clarity.*

Bond Length (Å)		Bond Angle (°)	
$C1_{plane}$–Ru1	1.70081(4)	Cl1–Ru1–Cl2	88.27(2)
Ru1–Cl1	2.3943(6)	Cl1–Ru1–P1	89.34(2)
Ru1–Cl2	2.4295(5)	Cl2–Ru1–P1	87.45(2)
Ru1–P1	2.3677(6)	Ru1–P1–C11	112.45(7)
P1–C11	1.830(2)	Ru1–P1–C17	117.91(8)
P1–C17	1.814(2)	Ru1–P1–C23	105.82(7)
P1–C23	1.886(2)		

*Table 6.4.2 Selected bond lengths and angles for **60**.*

6.4.2.1 NMR Studies and Behaviour in Solution

In contrast to compounds **57**-**59**, which are readily soluble in solvents such as $CD_3C_6D_5$ and C_6D_6, the solubility of compounds **60** and **61** is negligible in low polarity hydrocarbons. However, adequate solubility in CD_2Cl_2, allowed for full characterisation, and NMR measurements including DOSY NMR determinations (*vide infra*), indicate only one species in solution (Table 6.4.3 and Table 6.4.4).

The chemical shifts of the phosphorus-bound PCA/PDCA complexes **57-61**, have been found, in all cases to be downfield shifted with respect to their corresponding free ligand (**L-57**/**L-61**),[270] as observed for other transition metal phosphinocarboxamide complexes.[352] A similar effect can be observed in the chemical shifts for the amide N*H* protons, which are also shifted downfield, most likely a consequence of intramolecular hydrogen bonding, with clearly demarked chemical shift regions for the aliphatic PCA (**57**), the aromatic PCAs (**58**-**59**) and the aromatic PDCAs (**60**-**61**). In contrast, an upfield shift is observed for the $^{13}C\{^1H\}$ NMR.

*Table 6.4.3 Selected NMR spectroscopic data δ (ppm) for complexes **57-63**.*

Compound	^{31}P Free ligand[a)]	^{31}P PCA/PDCA complex[b)]	$^{13}C_{PCO}$ PCA/PDCA complex[b)]	$^{1}H_{NH}$ PCA/PDCA complex[b)]
57	−4.0	29.8[a)]	167.4	8.6
58	−0.2	37.2	167.6	10.1
59	−0.9	36.6	167.5	10.0
60	8.3	33.5	178.2/177.7[c)]	9.2
61	8.0	33.8	177.9/177.5[c)]	9.2
62	-	52.6	-[d)]	-
63	-	52.3	170.9 / 162.1[c)]	-

[a)] PDA/PDCA chemical shifts reported in ppm in C_6D_6.[270,342] [b)] Chemical shifts reported in ppm in CD_2Cl_2. [c)] Chemical shifts for $Ph_2P(C{=}O)$ and $N(C{=}O)$ in ppm in CD_2Cl_2. [d)] Signal not observed.

Additionally, compounds **57**-**61** present bilateral symmetry in the *p*-cymene fragment as shown by ^1H and $^{13}C\{^1H\}$ NMR spectra. There is clear evidence of scalar spin-spin coupling between the *p*-cymene moiety and the phosphorus of the PCA/PDCA.[372] This is particularly evident in the $^{13}C\{^1H\}$ NMR spectra, due to additional multiplicity in the non-quaternary aromatic carbons (^{i}Pr-C_6H_4-Me), as two distinctive doublets (d, $^2J_{CP}$= 4 and 6 Hz, respectively) [Figure 6.4.3].

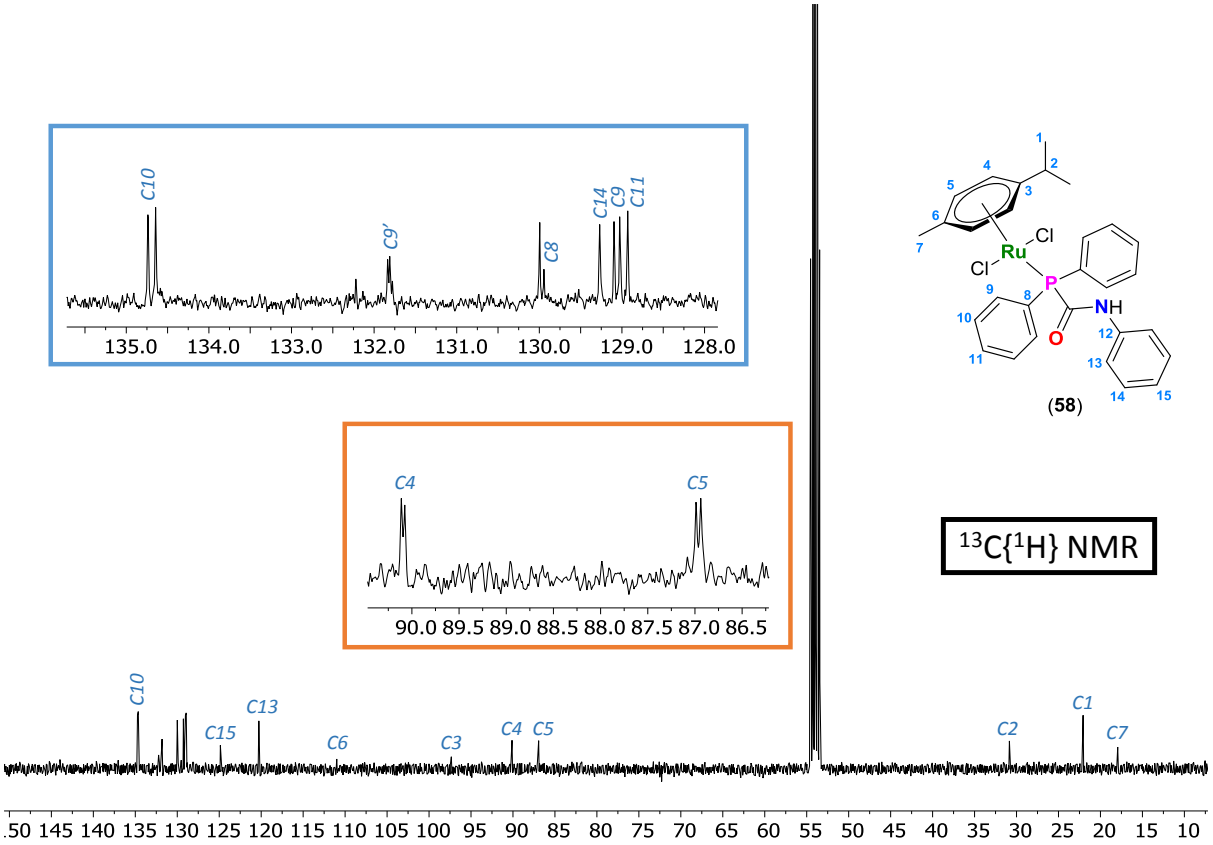
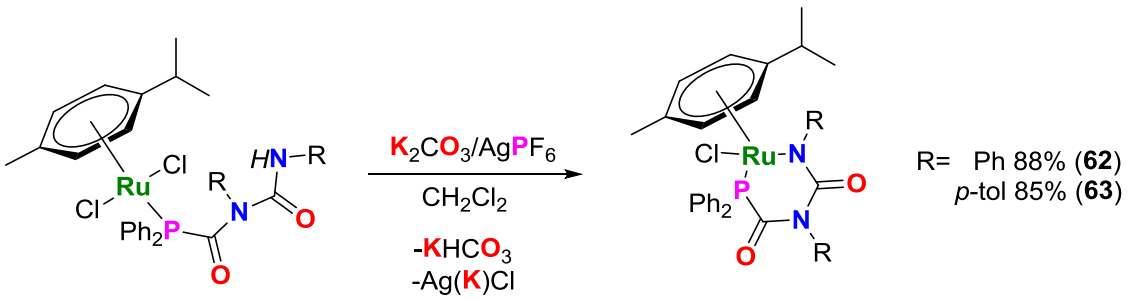


*Figure 6.4.3 $^{13}C\{^{1}H\}$ NMR spectra of **58** in CD_2Cl_2. Note the additional multiplicity in C4 and C5 (orange rectangle).*

6.4.3 Synthesis of Metallacycles [Ru(p-cym){κ²-P,N-PPh₂C(=O)N(R)C(=O)NR}Cl] (R = Ph, p-tol)

Deprotonation reactions, with the aim of forming five- and six-membered metallacycles were attempted (Scheme 6.4.3). As such, **60** and **61** were reacted with K_2CO_3 in CD_2Cl_2 at room temperature. Under these conditions, it was possible to observe initial consumption of the coordinated compound (*via* ^{31}P NMR spectroscopy) and formation of a new single resonance peak around 52 ppm for the PDCA-substituted ruthenium centres (Table 6.4.3). Heating of the sample in an oil bath (50 °C) however, afforded only increasingly complicated spectra, without complete consumption of starting material. Looking to aid a consecutive deprotonation/cyclisation mechanism, an analogous reaction with addition of a stoichiometric amount of $AgPF_6$ as a halide scavenging agent was investigated.



*Scheme 6.4.3 Formation of six-membered metallacycles (**62**-**63**).*

In the presence of both K_2CO_3 and $AgPF_6$, full disappearance of **60** and **61** was observed leading to the formation of six-membered metallacycles **62** and **63**. In contrast, an analogous reaction with **58** showed no evidence for the formation of a five-membered metallacycle, which is likely a consequence of the higher ring strain resulting from the shorter PCA.

In the ^{31}P NMR spectra the resonances for the metallacycles **62** and **63** are shifted downfield with respect to **L-60** and **L-61** (Table 6.4.3), which is in line with that reported for *N,P*-chelates[367–369] that form six-membered metallacycles from which a downfield shift is seen upon metal-phosphorus bond formation. A full spectroscopic study as well as DFT calculations on **62** agree with the formulation depicted in Scheme 6.4.3. Halide replacement by $[PF_6]^-$ has been ruled out by means of NMR spectroscopy and MS analyses (ion trap). Although only a single resonance is observed in the ^{31}P NMR spectra (Table 6.4.3), the formation of two distinct isomers [**62a** (symmetric) and **62b** (asymmetric)] can be observed by ^1H NMR and DOSY NMR spectroscopy, (Table 6.4.4 and Figure 6.4.4). The *para* substituents correlate with the ratio of isomers, this is a 60:40 mixture for **62** and 87:13 for **63**. In both cases, the major product stands out due to the complete loss of symmetry (as observed by ^1H and $^{13}C\{^1H\}$ NMR spectra), on the *p*-cymene fragment (Figure 6.4.4), with the minor product remaining bilaterally symmetrical.

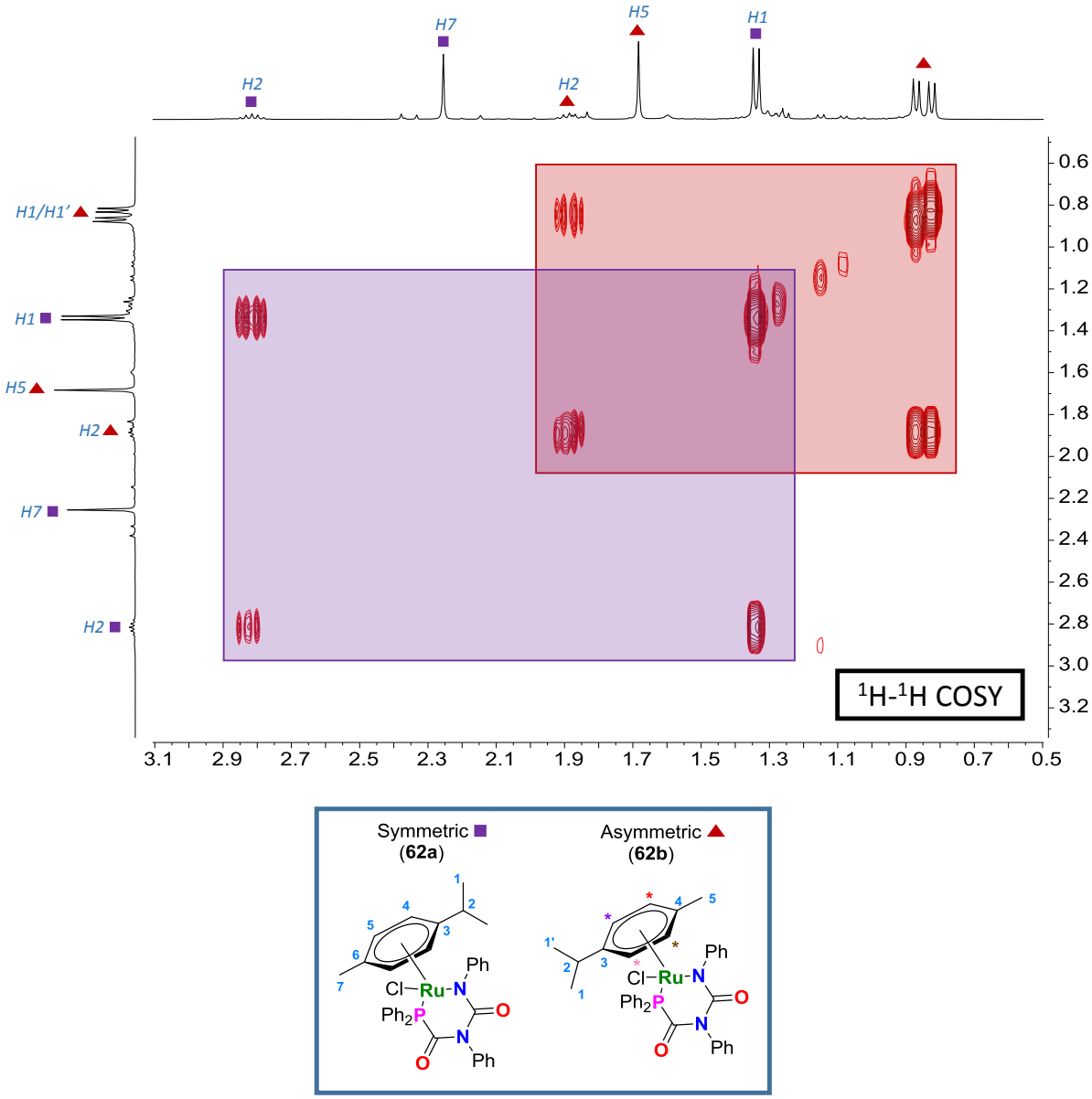


*Figure 6.4.4 Selected region of the ^{1}H-^{1}H COSY NMR spectrum of cyclised products **62a**/**62b** in CD_2Cl_2, with the two separate p-cymene moieties highlighted for the symmetric (purple) and asymmetric (red) product.*

Similar to compounds **57**-**61**, clear evidence of scalar spin-spin coupling was found, in **62** and **63**, between the *p*-cymene fragment and the phosphorus of the PDCA ($^{13}C\{^{1}H\}$) NMR).[372] With the signals for the non-quaternary aromatic carbons, in the *p*-cymene fragment, as four distinctive doublets ($^{2}J_{CP}$ = 3-6 Hz) [Figure 6.4.5].

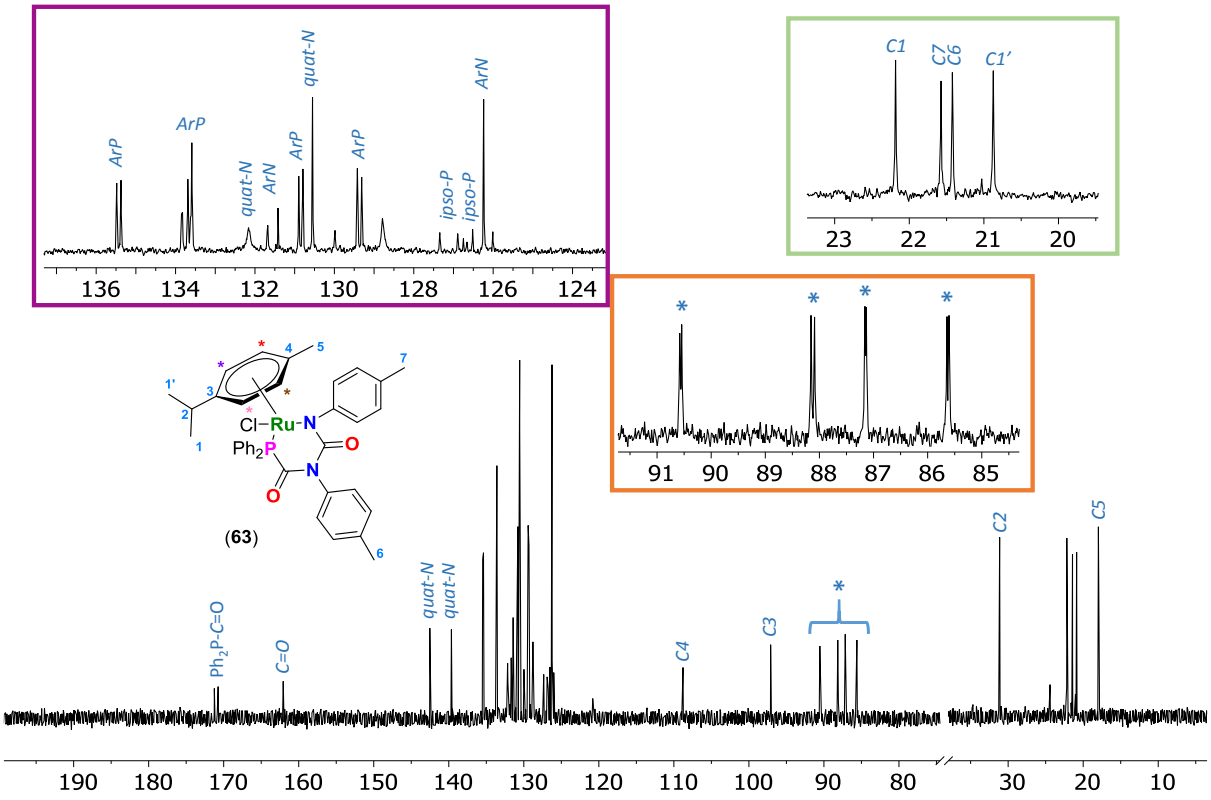


*Figure 6.4.5 $^{13}C\{^{1}H\}$ NMR spectra of **63** in CD_2Cl_2. Notice the additional multiplicity in the non-quaternary aromatic carbons (orange rectangle).*

6.4.3.1 DOSY NMR Spectroscopic Studies

The diffusion coefficients (D) of **58**, **61** and **63**, determined by DOSY NMR experiments (Table 6.4.4), allowed for calculation of the hydrodynamic radii. These values are in good agreement with the values obtained from the crystal structures of **58** and **61**, and the geometry optimised structures of **62**/**63**, in which an increase in the hydrodynamic radius is observed as a consequence of the increased length of the ligand [PCA (**58**) *vs.* PDCA (**61**)]; with only a small change in hydrodynamic radius observed upon cyclisation (**63**).

Table 6.4.4 Diffusion coefficient values obtained from DOSY NMR spectroscopy in CD_2Cl_2 (25 °C).

Substrate	Concentration	Diffusion Coefficient	Hydrodynamic Radius
58	0.014 M	1.09×10^{-9} m²/s	4.86×10^{-10} m
61	0.020 M	9.80×10^{-10} m²/s	5.43×10^{-10} m
63	0.020 M	9.15×10^{-10} m²/s	5.82×10^{-10} m

6.4.3.2 Cyclisation Mechanism and Structure Elucidation

Bidimensional NMR determinations draw a clear picture of the metallacycles formed (**62** and **63**). Upon coordination, treatment with K_2CO_3 can deprotonate the PDCA amide. However, it is not until one of the two coordinated halides is removed, by the $AgPF_6$, that formal cyclisation takes place. Although a rearrangement of a five-coordinate species cannot be ruled out, this last step is determining the ratio of **62a** and **62b**.

NOESY NMR experiments allowed to determine, in the major product (**63b**), direct correlation between the signals arising from the diphenylphosphino fragment towards the *p*-cymene moiety due to their close proximity. This can also be observed in the solid state structures of **60** and **61**. Additionally, asymmetry of the major cyclisation product **63b** could be observed in the signals from the ^{i}Pr substituent, which are shown in the ^{1}H NMR spectra as two distinct singlets (*H*1 and *H*1'), while the ^{1}H-^{13}C HMBC NMR spectra of **63b** shows coupling between $^{i}Pr^{CH}$ and only one of the protons from the *p*-cymene ring (^{i}Pr-C_6H_4-Me) (Figure 6.4.6). The overall loss of symmetry is most likely a consequence of the high steric hindrance generated from the diphenylphosphino and the aryl amine fragments, which limits the free rotation of the ^{i}Pr substituent, and the *p*-cymene moiety. Variable temperature NMR studies of **6a** and **6b**, in CD_2Cl_2 (^{1}H and ^{31}P NMR), revealed only negligible changes in proportion and chemical shift to those of the parent compounds, evidencing the impossibility of interconversion between these two species.

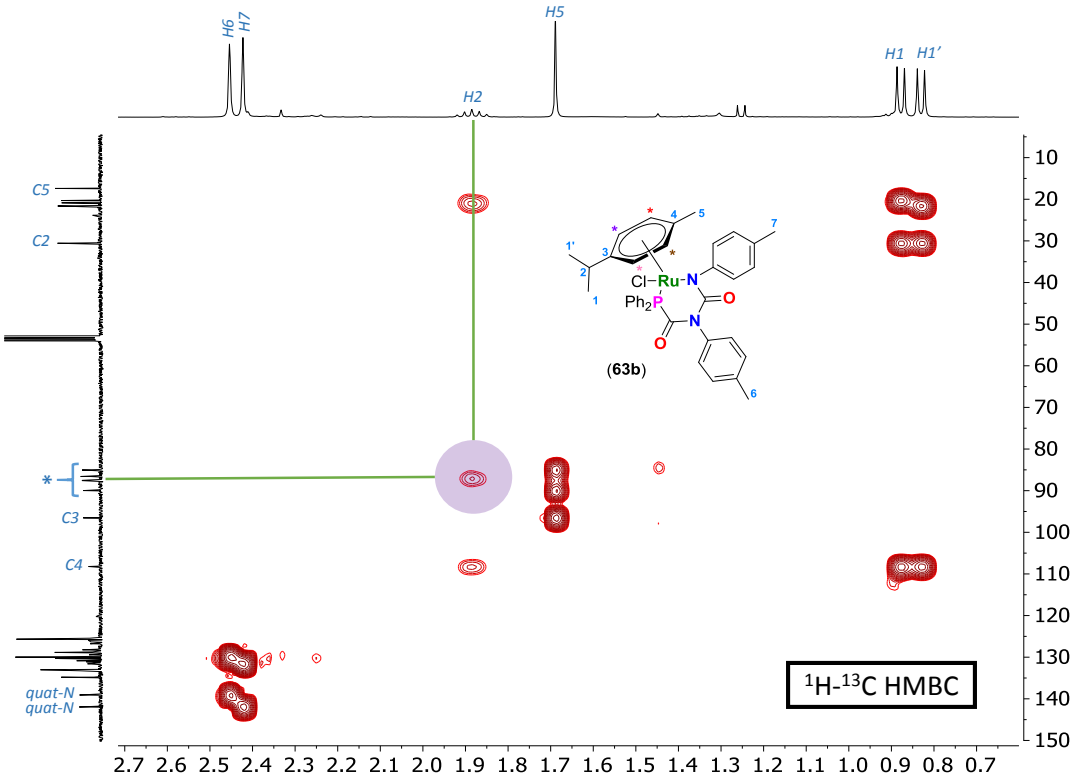


*Figure 6.4.6 ^{1}H-^{13}C HMBC NMR spectrum of cyclisation product **63b** in CD_2Cl_2.*

6.4.3.3 DFT and Geometry Optimisations

To probe further the structures of **62** and **63**, DFT calculations were performed (Figure 6.4.7). The coordination around the metal centre, includes a η^6 interaction with the *p*-cymene, a chloride and the PDCA fragment as a bidentate ligand with the ruthenium centre residing above the best mean plane generated by the six-membered metallacyle (1.045 Å). The phosphorus-ruthenium distance is in line with previously reported six-membered metallacyles containing these elements.[355–357,366–369] Thus, this ring lies almost perpendicular to the *p*-cymene moiety (best mean plane angles generated between the *p*-cymene ring and the six-membered metallacyle = 96.34°). Additionally, the phenyl rings from the phosphine moiety and the equivalent for the amine fragment, create a cavity in which the *p*-cymene is too sterically hindered to be able to rotate. As such, two possible conformers can be identified; one in which the ^{i}Pr (**62a'** and **63a'**) substituent lies directly above of the chloride and another one in which the methyl (**62b'** and **63b'**) occupies said position (Figure 6.4.7). Comparative geometry optimisation calculations for the two forms, denote only minimal energy differences between these two conformers (ΔG = –0.4 kcal mol^{-1} in **62** and –0.2 kcal mol^{-1} in **63**); ruling out a thermodynamic preference for either isomer. This is in line with the almost equal proportion of isomers for **62** by ^{1}H NMR

spectroscopy. Additionally, it is suspected that the different ratios of cyclised products (**62**-**63**), correlate to the nature of the preferred conformers of the parent coordination compounds **60**-**61**, in solution. Suggesting that under such conditions, **60** has a weaker conformational preference when compared to **61**.

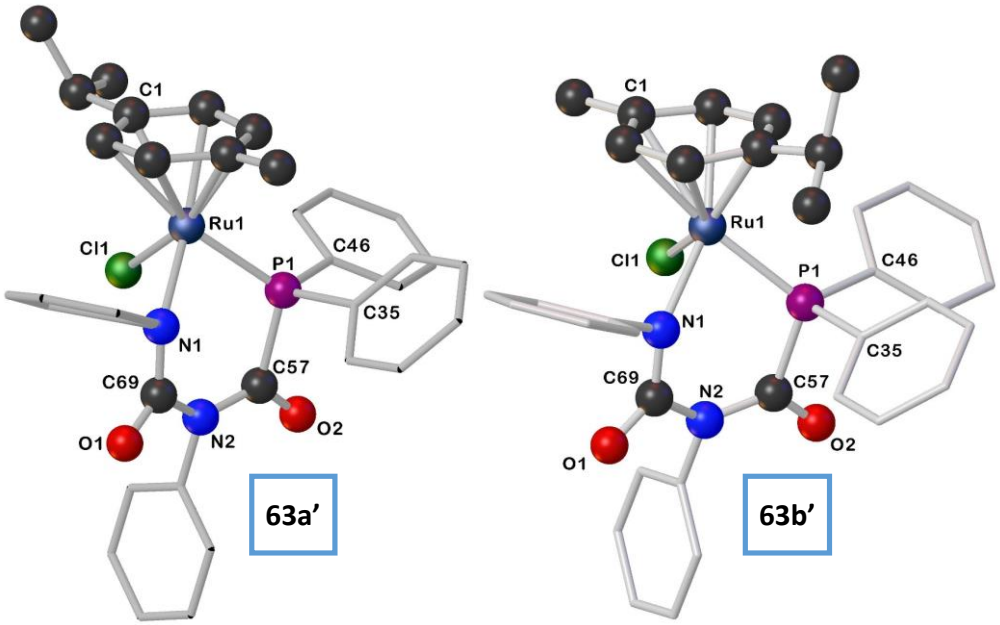
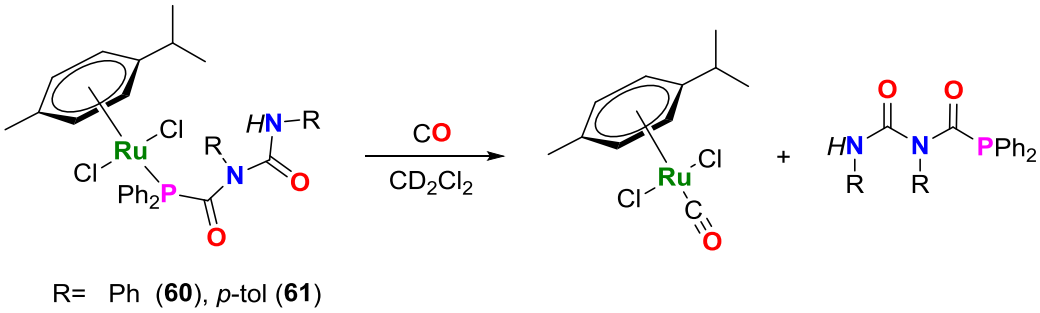


*Figure 6.4.7 Illustrations for the geometry optimised structures for **63a'** and **63b'**.*

6.4.3.4 Ligand Displacement Studies



R= Ph (**60**), *p*-tol (**61**)

*Scheme 6.4.4 Ligand replacement reaction upon exposure to $CO_{(g)}$, with formation of [{p-cymene}$RuCl_2(CO)$] and **L-60**–**L-61**, respectively.*

In order to test the stability of the Ru-P bond in these coordination complexes, solutions of **60** and **61** in CD_2Cl_2 were exposed to an atmosphere of dry $CO_{(g)}$ (Scheme 6.4.4). Reaction monitoring by NMR spectroscopy evidenced decoordination of the PDCA ligands and formation of [{*p*-cymene}$RuCl_2(CO)$][373] (Figure 6.4.8). Similar behaviour has been previously exploited using a rhodium(II) system capable of reversible coordination of CO,

$[Rh(\eta^3\text{-TMPP})_2][BF_4]_2$ (TMPP = *tris*(2,4,6-trimethoxyphenyl)phosphine), which has been used for chemosensing applications.[374,375] Contrastingly, when a solution of **62** was treated under similar conditions, no liberation of the coordinated PDCA was observed. In agreement with an increase in binding energy, when the PDCA forms a bidentate chelate, being more robust to ligand replacement by CO.

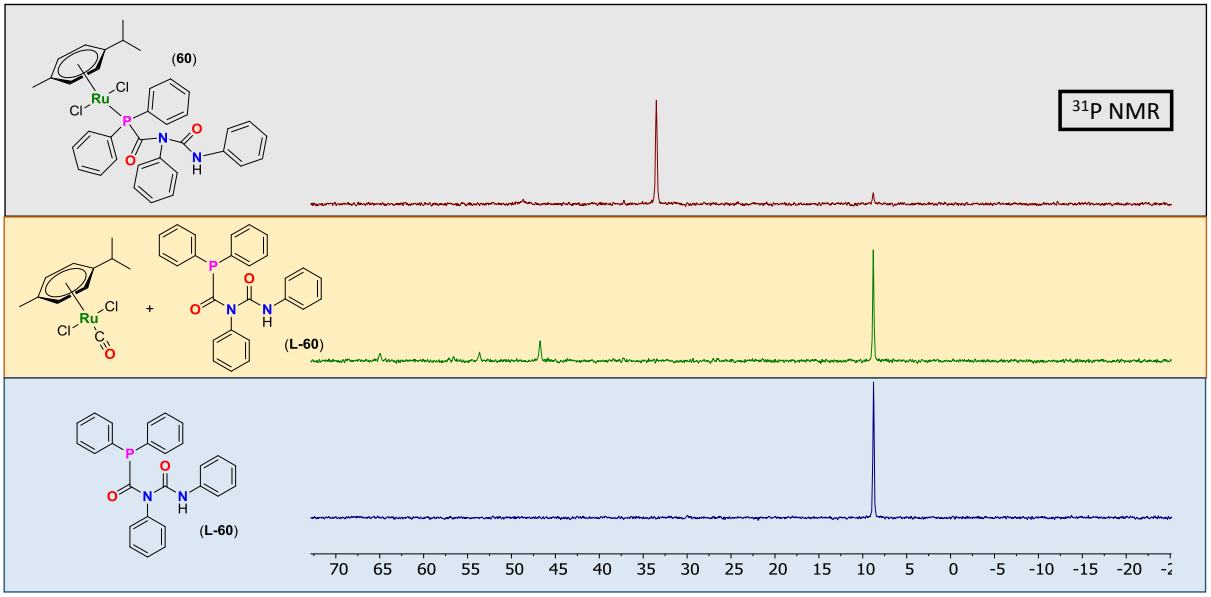


*Figure 6.4.8 Comparative ^{31}P NMR spectra of **60**, after exposure to $CO_{(g)}$ and the corresponding free PDCA **L-60** (CD_2Cl_2).*

6.5 Conclusions

Neutral complexes of general formula [Ru(*p*-cym){$PPh_2C(=O)NHR\}Cl_2$; R= ^{i}Pr (**57**), Ph (**58**) and *p*-tolyl (**59**)] and [Ru(*p*-cym){$PPh_2C(=O)N(R)C(=O)N(H)R\}Cl_2$; R = Ph (**60**) and *p*-tolyl (**61**)], have been synthesised through coordination to $[(p\text{-cym})RuCl_2]_2$ by phosphinocarboxamides (**L-57**–**L-59**) or phosphinodicarboxamides (**L-60**–**L-61**). Compounds **57**-**61** have been analysed by spectroscopic and analytical methods, including X-ray determinations. The chemical shifts of the phosphorus-bound PCA/PDCA complexes **57**-**61**, have been found in all cases to be downfield shifter with respect to their corresponding free ligand (**L-57**–**L-61**); indicative that electron density is being withrawn from the phosphorus centre. Attempts at forming intramolecular five-membered metallacycles by deprotonation/halide abstraction reactions using **57**-**59** were unsuccessful, presumably due to steric factors. While analogous procedures using **60** and **61**, allowed the formation of six-membered metallacyles, [Ru(p-cym){κ^2-*P,N*-$PPh_2C(=O)N(R)C(=O)NR\}Cl$] ([R = Ph (**62**), *p*-tol (**63**)], with two positional isomers observed for each of these. The single resonance peak found in the ^{31}P NMR of the metallacycles formed is shifted downfield with respect to their corresponding free phosphines, which is in line with similar six-membered metallacycles. Additionally, the ^{1}H NMR of these compounds evidences the formation of at least two main isomers. Formally rotameres, these compounds differ from each other due to steric hindrance upon formation of the six-membered metallacylces, which restricts the rotation of the *p*-cymene substituent, furtherly assymmetrising the metal complex. Geometry optimisation calculations were carried out for the cyclised products and are in full agreement with their spectroscopic characterisation.

6.6 Experimental Section

6.6.1 Synthesis and Characterisation

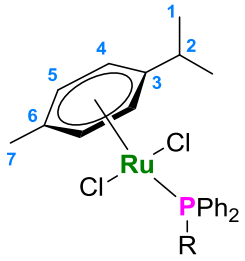


*Figure 6.6.1 General numbering scheme for the p-cymene fragment, in the coordination compounds **57-61**.*

[Ru(*p*-cym){$PPh_2C(=O)N(H)^iPr$}Cl_2] (**57**):[342]

To a mixture of **L-57** (12 mg, 0.05 mmol, 2 eq.) and [Ru(*p*-cymene)Cl_2]$_2$ (13.5 mg, 0.02 mmol) was added dichloromethane (10 mL), the resulting red solution was stirred at room temperature for 16 hours. Volatiles were removed under vacuum and the resulting red solid was extracted into toluene (5 mL) and stored at –30 °C for 1 week, resulting in the precipitation of a red crystalline solid (5 mg, 39%). Crystals suitable for X-ray diffraction were grown from a concentrated solution in C_6D_6, at room temperature.[342]

^{1}H NMR (400 MHz, C_6D_6, 25 °C): δ (ppm) 8.63 (d, $^3J_{HP}$ = 7.4 Hz, 1H, N*H*), 8.20-8.02 (m, 4H, PPh_2^o), 7.14-6.94 (m, 6H, PPh_2^{m+p}), 4.75 (d, $^3J_{HH}$ = 6.1 Hz, 2H, *H*-5), 4.70 (dd, $^3J_{HH}$ = 6.1 Hz, $^3J_{HP}$ = 1.3 Hz, 2H, *H*-4), 4.05 (m, 1H, N^{i}Pr$^{\underline{CH}}$), 2.56 (sept, $^3J_{HH}$ = 7.0 Hz, 1H, *H*-2), 1.51 (s, 3H, *H*-7), 1.04 (d, $^1J_{HH}$ = 6.6 Hz, 6H, *H*-2), 0.82 (d, $^3J_{HH}$ = 7.0 Hz, 6H, *H*-1).

^{13}C{^{1}H} (400 MHz, C_6D_6, 25 °C): δ (ppm) 167.4 (d, $^1J_{CP}$ = 55 Hz, C=O), 134.8 (d, $^2J_{CP}$ = 9 Hz, PPh_2^o), 133.7 (d, $^1J_{CP}$ = 43 Hz, PPh_2^i), 130.7 (d, $^4J_{CP}$ = 2 Hz, PPh_2^p), 128.2 (d, $^3J_{CP}$ = 10 Hz, PPh_2^m), 109.7 (C-6), 95.2 (C-3), 89.7 (d, $^2J_{CP}$ = 4 Hz, C-4), 86.0 (d, $^2J_{CP}$ = 6 Hz, C-5), 43.6 (d, *J* = 6 Hz, N^{i}Pr$^{\underline{CH}}$), 30.3 (C-2), 22.2 (C-1), 21.7 (N^{i}Pr$^{\underline{CH}}_3$), 17.3 (C-7).

^{31}P NMR (162 MHz, C_6D_6, 25 °C): δ (ppm) 29.8 (s, 1P, Ru*P*Ph_2).

HRMS (ESI)$^+$ *m/z*: $[M+H]^+$ calculated 578.0715; found 578.0712 formula $C_{26}H_{32}Cl_2NOPRu$.

IR ν/cm^{-1} (ATR): 3237 (N-H) w, 1654 (C=O) s.

[Ru(*p*-cym){$PPh_2C(=O)N(H)Ph$}Cl_2] (**58**):

L-58 (52.2 mg, 0.17 mmol, 2 eq.) was dissolved in a mixture of toluene (30 mL) and THF (20 mL), affording a light yellow solution, and added dropwise to a bright red solution of [Ru(*p*-cymene)Cl_2]$_2$ (52.4 mg, 0.08 mmol) in toluene/THF (50 mL/20mL), affording a dark orange solution. The reaction mixture was left stirring at room temperature for 16 hours. Volatiles were removed under vacuum, followed by extraction in hot toluene. Dark red crystalline material could be observed growing, over a few days (53 mg, 51%). Crystals suitable for X-ray diffraction were grown from a saturated solution in toluene, at room temperature.

^{1}H NMR (400 MHz, CD_2Cl_2, 25 °C): δ (ppm) 10.11 (s, 1H, N*H*), 7.88 (ddd, $^3J_{HH}$ = 10.0 Hz, $^3J_{HH}$ = 8.2 Hz, $^3J_{HH}$ = 1.4 Hz, 4H, PPh_2^m), 7.58 – 7.47 (m, 4H, PPh_2^o), 7.44 (d, $^3J_{HH}$ = 8.4 Hz, 2H, NPh^o), 7.42 – 7.38 (m, 2H, PPh_2^p), 7.21 (t, *J* = 7.6 Hz, 2H, NPh^m), 7.02 (t, $^3J_{HH}$ = 7.4 Hz, 1H, NPh^p), 5.29 (d, $^3J_{HH}$ = 6.4 Hz, 2H, *H*-5), 5.27 (d, $^3J_{HH}$ = 6.3 Hz, 2H, *H*-4), 2.55 (sept, $^3J_{HH}$ = 7.0 Hz, 1H, *H*-2), 1.84 (s, 3H, *H*-7), 1.04 (d, $^3J_{HH}$ = 7.0 Hz, 6H, *H*-1).

$^{13}C\{^1H\}$ NMR (100 MHz, CD_2Cl_2, 25 °C): δ (ppm) 167.8 (d, $^1J_{CP}$ = 55 Hz, C=O), 137.0 (NPh^i), 134.7(d, $^3J_{CP}$ = 9 Hz, PPh_2^m), 131.8 (d, $^3J_{CP}$ = 2 Hz, PPh_2^o), 129.9 (PPh_2^i), 129.3 (NPh^m), 129.1(d, $^2J_{CP}$ = 7 Hz, PPh_2^p), 124.9 (NPh^p), 120.3 (NPh^o), 111.0 (C-6), 97.3 (C-3), 90.1 (d, $^2J_{CP}$ = 4 Hz, C-4), 86.9 (d, $^2J_{CP}$ = 5 Hz, C-5), 30.9 (C-2), 22.1 (C-1), 17.9 (C-7).

^{31}P NMR (162 MHz, CD_2Cl_2, 25 °C): δ (ppm) 37.2 (s, 1P, Ru*P*Ph_2).

HRMS/ESI$^+$ *m/z*: $[M+Na]^+$ calculated 634.0383; found 634.0387 formula $C_{29}H_{30}Cl_2NNaOPRu$.

IR *v*/cm^{-1} (ATR): 3227 (N-H) w, 1655 (C=O) s.

[Ru(*p*-cym){$PPh_2C(=O)N(H)p$-tolyl}Cl_2] (**59**):

A solution of **L-59**, (5.2 mg, 0.016 mmol, 2 eq.) in CD_2Cl_2 (0.4 mL) was added dropwise to a solution of [Ru(*p*-cymene)Cl_2]$_2$ (5 mg, 0.008 mmol) in CD_2Cl_2 (0.4 mL) with stirring. The dark orange reaction mixture was transferred to a J. Young's tap NMR tube, whereupon NMR spectroscopy showed full disappearance of the starting materials, and conversion to **59**. Following this, volatiles were removed under vacuum, affording a dark red powder (11 mg, Quantitative yield). Crystals suitable for X-ray diffraction were grown from a concentrated toluene solution at room temperature.[342]

^{1}H NMR (400 MHz, CD_2Cl_2, 25 °C): δ (ppm) 10.03 (s, 1H, N*H*), 7.90-7.84 (m, 4H, PPh_2^{o}), 7.57-7.47 (m, 6H, PPh_2^{m+p}), 7.32 (d, $^{3}J_{HH}$ = 8.4 Hz, 2H, NPh^{m}), 7.01 (d, $^{3}J_{HH}$ = 8.2 Hz, 2H, NPh^{o}), 5.28 (d, $^{3}J_{HH}$ = 6.9 Hz, 2H, *H*-5), 5.26 (d, $^{3}J_{HH}$ = 6.7 Hz, 2H, *H*-4), 2.53 (sept, $^{3}J_{HH}$ = 6.9 Hz, 1H, *H*-2), 2.24 (s, 3H, NPh^{CH_3}), 1.83 (s, 3H, *H*-7), 1.03 (d, $^{3}J_{HH}$ = 7.0 Hz, 6H, *H*-1).

$^{13}C\{^{1}H\}$ NMR (100 MHz, CD_2Cl_2, 25 °C): δ (ppm) 167.5 (C=O), 136.2 ($NPh^{CH_3 i}$), 134.7 (PPh_2^{o}), 134.6 (NPh^{i}), 131.8 (d, $^{4}J_{CP}$ = 2 Hz, PPh_2^{p}), 129.7 (NPh^{o}), 128.9 (d, $^{3}J_{CP}$ = 10 Hz, PPh_2^{m}), 120.2 (NPh^{m}), 110.9 (C-6), 97.2 (C-3), 90.1 (d, $^{2}J_{CP}$ = 4 Hz, C-4), 86.9 (d, $^{2}J_{CP}$ = 5 Hz, C-5), 81.4 (d, $^{1}J_{CP}$ = 70 Hz, PPh_2^{i}), 30.8 (C-2), 22.1 (C-1), 21.1 (NPh^{CH_3}), 17.9 (C-7).

^{31}P NMR (162 MHz, CD_2Cl_2, 25 °C): δ (ppm) 36.6 (s, 1P, Ru*P*Ph_2).

HRMS/ESI^{+} *m/z*: $[M\text{-}Cl]^{+}$ calculated 590.0948, found 590.0961 formula $C_{30}H_{32}ClNOPRu$.

IR *v*/cm^{-1} (ATR): 3180 (N-H) w, 1665 (C=O) s.

[Ru(*p*-cym){PPh_2C(=O)N(Ph)C(=O)N(*H*)Ph}Cl_2] (**60**):

In the glovebox, **L-60** (6.9 mg, 0.016 mmol, 2 eq.) and $[Ru(p\text{-cymene})Cl_2]_2$ (5 mg, 0.008 mmol) were weighed, into two separate vials. To each vial were added equal amounts of CD_2Cl_2 (0.4 mL). The resulting solution of **L-60**, was dropwise added, while stirring to the dark red solution of ruthenium. The dark orange reaction mixture, was transferred to a Young's tap NMR tube, showing full disappearance of the starting materials; and quantitative conversion (TMS as internal standard). Crystals suitable for X-ray diffraction were grown from a concentrated toluene solution at room temperature.

^{1}H NMR (400 MHz, CD_2Cl_2, 25 °C): δ (ppm) 9.25 (s, 1H, N*H*), 7.71 (t, 3H, *J* = 9.0 Hz , *H*-ArP), 7.54 – 7.49 (dd, *J* = 11.8, 7.1 Hz, 2H, *H*-ArN), 7.42 – 7.37 (m, 3H, *H*-ArN), 7.33 – 7.30 (m, 2H, *H*-ArP), 7.26 – 7.05 (m, 9H, *H*-ArN/*H*-ArP), 6.98 (d, *J* = 7.4 Hz, 1H, *H*-ArN), 5.45 (d, $^{3}J_{HH}$ = 6.0 Hz, 2H, *H*-4), 5.15 (d, $^{3}J_{HH}$ = 6.0 Hz, 2H, *H*-5), 2.69 (sept, $^{3}J_{HH}$ = 6.7 Hz, 1H, *H*-2), 1.91 (s, 1H, *H*-7), 1.11 (d, $^{3}J_{HH}$ = 6.9 Hz, 2H, *H*-1).

$^{13}C\{^{1}H\}$ NMR (100 MHz, CD_2Cl_2, 25 °C): δ (ppm) 178.1 (C=O), 177.7 (C=O), 138.2 (d, $^{1}J_{CP}$ = 9 Hz, PPh_2^{i}), 134.9 (d, *J* = 9 Hz, ArP), 131.3 (d, *J* = 2.5 Hz, ArP), 129.9 (ArN), 129.8 (ArN), 129.1, 128.7 (NPh^{i} *x2*), 128.6 (ArN), 128.3 (d, *J* = 10.1 Hz, ArP), 124.7 (ArN), 120.7 (ArN), 120.1 ArN), 110.2 (C-6), 96.9 (C-3), 92.1 (d, $^{2}J_{CP}$ = 4 Hz, C-4), 86.5 (d, $^{2}J_{CP}$ = 5 Hz, C-5), 30.7 (C-2), 22.3 (C-1), 17.5 (C-7).

^{31}P NMR (162 MHz, CD_2Cl_2, 25 °C): δ (ppm) 33.50 (s, 1P, Ru*P*Ph$_2$).

HRMS/ESI$^+$ *m/z*: [M-Cl]$^+$ calculated 695.1168, found 695.1158; formula $C_{36}H_{35}ClN_2O_2PRu$.

IR *v*/cm^{-1} (ATR): 3228 (N-H) w, 1655 (C=O) s.

[Ru(*p*-cym){PPh$_2$C(=O)N(*p*-tolyl)C(=O)N(*H*)*p*-tolyl}Cl$_2$] (**61**):

In the glovebox, **L-61** (7.4 mg, 0.016 mmol, 2 eq.) and [Ru(*p*-cymene)Cl$_2$]$_2$ (5 mg, 0.008 mmol) were weighed, into two separate vials. To each vial were added equal amounts of CD_2Cl_2 (0.4 mL). The resulting solution of **L-61**, was dropwise added, while stirring to the dark red solution of ruthenium. The dark orange reaction mixture, was transferred to a Young's tap NMR tube, showing full disappearance of the starting materials; and quantitative conversion (TMS as internal standard). Crystals suitable for X-ray diffraction were grown from a concentrated toluene solution, layered with hexane, at room temperature.[342]

^{1}H NMR (400 MHz, CD_2Cl_2, 25 °C): δ (ppm) 9.20 (s, 1H, NH), 7.68 (t, $^3J_{HH}$ = 9.2 Hz, 4H, PPh$_2^m$), 7.34 – 7.30 (m, 4H, PPh$_2^p$), 7.25 (d, $^3J_{HH}$ = 8.5 Hz, 2H, N*H*Ph^m), 7.19 (td, $^3J_{HH}$ = 7.8, $^3J_{HH}$ = 2.0 Hz, 4H, PPh$_2^o$), 7.05 (d, $^3J_{HH}$ = 8.3 Hz, 2H, N*H*Ph^o), 6.88 (d, $^3J_{HH}$ = 8.2 Hz, 2H, NPh^o), 6.83 (d, $^3J_{HH}$ = 8.4 Hz, 2H, NPh^m), 5.44 (d, $^3J_{HH}$ = 5.4 Hz, 2H, H-4), 5.17 (d, $^3J_{HH}$ = 6.2 Hz, 2H, H-5), 2.70 (sept, $^3J_{HH}$ = 7.0 Hz, 1H, H-2), 2.29 (s, 3H, N*H*Ph^{CH_3}), 2.24 (s, 3H, NPh^{CH_3}), 1.90 (s, 3H, H-7), 1.11 (d, $^3J_{HH}$ = 7.0 Hz, 6H, H-1).

^{13}C{^{1}H} NMR (100 MHz, CD_2Cl_2, 25 °C): δ (ppm) 177.9 (C=O), 177.5 (C=O), 151.8 (PPh$_2^i$), 138.9 (NPh^i), 135.7 (N*H*Ph$^{CH_3 i}$), 135.2 (NPh$^{CH_3 i}$), 135.0 (d, $^3J_{CP}$ = 9 Hz, PPh$_2^m$), 134.5 (N*H*Ph^i), 131.1 (d, $^4J_{CP}$ = 3 Hz, PPh$_2^p$), 130.4 (NPh^o) 129.7 (N*H*Ph^o), 128.6 (NPh^m), 128.2 (d, $^2J_{CP}$ = 10 Hz, PPh$_2^o$), 120.0 (N*H*Ph^m), 110.1 (C-6), 96.9 (C-3), 92.1 (d, $^2J_{CP}$ = 4 Hz, C-4), 86.5 (d, $^2J_{CP}$ = 6 Hz, C-5), 30.8 (C-2), 22.3 (C-1), 21.3 (NPh^{CH_3}), 21.1 (N*H*Ph^{CH_3}), 17.45 (C-7).

^{31}P NMR (162 MHz, CD_2Cl_2, 25 °C): δ (ppm) 33.76 (s, 1P, Ru*P*Ph$_2$).

HRMS/ESI$^+$ *m/z*: [M-Cl]$^+$ calculated 723.1476, found 723.1489; formula $C_{38}H_{39}ClN_2O_2PRu$.

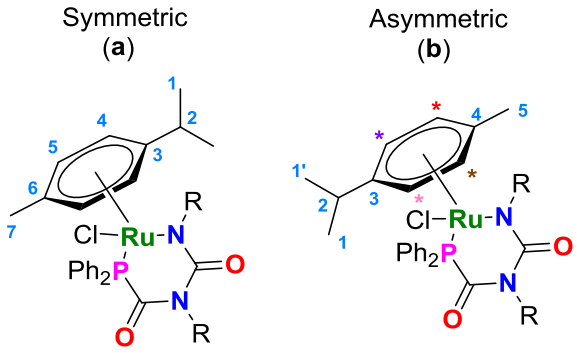


*Figure 6.6.2 General numbering scheme for cyclisation compounds **62a-b** – **63a-b**.*

[Ru(*p*-cym){κ^2-*P,N*-$PPh_2C(=O)N(Ph)C(=O)NPh$}Cl] (**62**):

A solution containing **60** (0.016 mmol, 1 eq.) was added to a mixture of K_2CO_3 (6.8 mg, 0.048 mmol, 3 eq.) and $AgPF_6$ (5.4 mg, 0.02 mmol, 1.3 eq.). The heterogeneous mixture was agitated *via* sonication at room temperature for 10 minutes, and filtered, affording an orange-red solution. Removal of volatiles *in vacuo* afforded full conversion to the cyclised products **62a**/**62b** (Quantitative conversion by NMR using TMS as internal standard). Removal of volatiles allowed isolation of a dark orange powder (10 mg, 88%).

Mixture of 2 products, ratio 60:40. (**62b** as main product) Characterisation for **62a** and **62b**:

^{1}H NMR (400 MHz, CD_2Cl_2, 25 °C): δ (ppm) 7.81-7.71 (m, Ph), 7.66-7.63 (m, 2H, Ph), 7.58-7.53 (m, Ph), 7.51 (d, *J* = 7.7 Hz, 6H, NPh), 7.47-7.37 (m, Ph), 7.23 (d, *J* = 7.6 Hz, 4H, NPh), 7.03 (s, 2H, Ph), 5.69-5.62 (m, 4H, **62b**-^{i}Pr-C$_6$*H*$_4$-Me), 5.64 (d, $^3J_{HH}$ = 6.1 Hz, 2H, **62a**-H5), 5.46 (d, $^3J_{HH}$ = 6.1 Hz, 2H, **62a**-H4), 2.78 (sept, *J* = 6.8 Hz, 1H, **62a**-H2), 2.21 (s, 3H, **62a-**H7), 1.85 (sept, *J* = 6.86 Hz, 1H, **62b**-H2), 1.64 (s, 3H, **62b**-H5), 1.30 (d, *J* = 6.9 Hz, 6H, **62a**-H1), 0.83 (d, $^3J_{HH}$ = 6.9 Hz, 3H, **62b**-H1), 0.78 (d, $^3J_{HH}$ = 6.9 Hz, 3H, **62b**-H1').

^{13}C{^{1}H} NMR (100 MHz, CD_2Cl_2, 25 °C): δ (ppm) 135.4 (d, *J* = 11 Hz, Ph), 134.3 (d, *J* = 36 Hz, Ph), 133.9 (d, *J* = 2 Hz, Ph), 133.7 (d, *J* = 10.1 Hz, Ph), 131.7 (d, *J* = 20 Hz, Ph), 130.9 (d, *J* = 10 Hz, Ph), 130.1 (NPh), 129.4 (d, *J* = 11 Hz, Ph), 129.2 (d, *J* = 11 Hz, Ph), 126.5 (NPh), 108.8 (**62b**-C4), 102.4 (**62a**-C6), 97.7 (**62a**-C3), 97.3 (**62b**-C3), 90.5 (d, $^2J_{CP}$ = 3 Hz, **62b**-^{i}Pr-C$_6$H$_4$-Me), 88.3 (d, $^2J_{CP}$ = 6 Hz, **62b**-^{i}Pr-C$_6$H$_4$-Me), 87.2 (d, $^2J_{CP}$ = 3 Hz, **62b**-^{i}Pr-C$_6$H$_4$-Me), 85.6 (d, $^2J_{CP}$ = 4 Hz, **62b**-^{i}Pr-C$_6$H$_4$-Me), 79.4 (**62a**-C5), 78.6 (**62a**-C4), 31.9 (**62a**/**62b**-C2), 22.2 (**62b**-C1), 21.4 (**62a**-C1), 20.9 (**62b-**C1'), 19.3 (**62a**-C7), 17.9 (**62b**-C5).

^{31}P NMR (162 MHz, CD_2Cl_2, 25 °C): δ (ppm) 52.59 (s, 1P, Ru*P*Ph$_2$).

HRMS/ESI$^+$ *m/z*: $[M+H]^+$ calculated 695.1168, found 695.1175; formula $C_{36}H_{35}ClN_2O_2PRu$.

IR *v*/cm^{-1} (ATR): 1616 (C=O) s, 1584 (C=O) s.

[Ru(*p*-cym){κ^2-*P,N* PPh$_2$C(=O)N(*p*-tolyl)C(=O)N*p*-tolyl}Cl] (**63**):

A solution containing **61** (0.016 mmol, 1 eq.) was added to a mixture of K_2CO_3 (6.8 mg, 0.048 mmol, 3 eq.) and $AgPF_6$ (5.4 mg, 0.02 mmol, 1.3 eq.). The heterogeneous mixture was sonicated at room temperature for 10 minutes, and filtered, affording an orange-red solution. Removal of volatiles *in vacuo* afforded full conversion to the cyclised products **63a**/**63b** (Quantitative conversion by NMR using TMS as internal standard). Removal of volatiles allowed isolation of a dark orange powder (10 mg, 85%).

Mixture of 2 products, ratio 87:13. (**63b** as main product). Characterisation for **63b**:

^{1}H NMR (400 MHz, CD_2Cl_2, 25 °C): δ (ppm) 7.80-7.70 (m, 7H, *H*-ArP), 7.64 (tq, *J* = 7.5, 2.04 Hz, 1H, *H*-ArP), 7.53 (td, *J* = 7.6, 3.0 Hz, 2H, *H*-ArP), 7.33 (t, $^3J_{HH}$ = 8.1 Hz, 5H, *H*-ArN), 7.10 (d, $^3J_{HH}$ = 8.3 Hz, 3H, *H*-ArN), 5.64-5.69 (m, 3H, ^{i}Pr-C$_6$*H*$_4$-Me), 5.62 (d, $^3J_{HH}$ = 6.3 Hz, 1H, ^{i}Pr-C$_6$*H*$_4$-Me), 2.42 (s, 3H, *H*6), 2.39 (s, 3H, *H*7), 1.85 (sept, $^3J_{HH}$ = 6.9 Hz, 1H, *H*2), 1.65 (s, 3H, *H*5), 0.84 (d, $^3J_{HH}$ = 7.0 Hz, 3H, *H*1), 0.79 (d, $^3J_{HH}$ = 7.0 Hz, 3H, *H*1').

^{13}C{^{1}H} NMR (100 MHz, CD_2Cl_2, 25 °C): δ (ppm) 170.9 (d, $^1J_{CP}$ = 51 Hz, Ph$_2$P-C=O), 162.1 (d, $^3J_{CP}$ = 3 Hz, C=O), 142.5 (quat-N), 139.6 (quat-N), 135.4 (d, *J* = 11 Hz, ArP), 133.8 (d, *J* = 3 Hz, ArP), 133.6 (d, *J* = 10 Hz, ArP), 132.2 (quat-N), 131.4 (ArN), 130.8 (d, *J* = 10 Hz, ArP), 130.5 (quat-N), 129.4 (d, *J* = 11 Hz, ArP), 127.1 (d, *J* = 45 Hz, ipso-P), 126.3 (d, *J* = 51 Hz, ipso-P), 126.2 (ArN), 108.8 (d, $^2J_{CP}$ = 2 Hz, C4), 97.1 (C3), 90.6 (d, $^2J_{CP}$ = 4 Hz, ^{i}Pr-*C*$_6$H$_4$-Me), 88.1 (d, $^2J_{CP}$ = 6 Hz, ^{i}Pr-*C*$_6$H$_4$-Me), 87.1 (d, $^2J_{CP}$ = 2 Hz, ^{i}Pr-*C*$_6$H$_4$-Me), 85.6 (d, $^2J_{CP}$ = 4 Hz, ^{i}Pr-*C*$_6$H$_4$-Me), 31.1 (C2), 22.1 (C1), 21.5 (C7), 21.4 (C-6), 20.8 (C1'), 17.9 (C5).

^{31}P NMR (162 MHz, CD_2Cl_2, 25 °C): δ (ppm) 52.34 (s, 1P, Ru*P*Ph$_2$).

HRMS/ESI$^+$ *m/z*: $[M+H]^+$ calculated 723.1476, found 723.1477; formula $C_{38}H_{39}ClN_2O_2PRu$.

IR *v*/cm^{-1} (ATR): 1594 (C=O) s, 1509 (C=O) s.

Typical procedure for reactivity with $CO_{(g)}$: A Young's tap NMR tube, containing a solution of **60** in 0.6 mL of CD_2Cl_2, was charged with an atmosphere of $CO_{(g)}$, *via* three freeze-thaw cycles. The data obtained *via* ^{1}H and ^{31}P NMR spectroscopies, was consistent with the reported characterisation for [{*p*-cymene}$RuCl_2(CO)$] and **L-60**.[373,270]

Chapter VII. Global Conclusions

To conclude, this thesis has sought to expand the methodologies involved in the stabilisation of unusual coordination motives. To this effect and aiming towards the study of low-coordinate transition metal complexes, initial work involved the preparation of two new families of carbazolido-based pincer proligands. On one hand, these studies have made use of known procedures to access the preparation of tridentate monoanionic *N*-based ligand systems, from which the naphthyl substituent has been proposed as an adequate flanking group, capable of enabling sufficient steric crowding around the central carbazolido-nitrogen (**6**). Similarly, a novel methodology has been introduced, allowing the substitution of tetrahydrocarbazole cores, from which assymetric bidentate monoanionic *N*-based ligands could be formed, employing similarly bulky flanking groups, such as -Ar* and -Dipp (**9** and **10**).

The Group 1 salts of these ligands (**12**-**17**), and more importantly their thorough characterisation, both in solution and in the solid state, have in turn allowed for systematic structural comparisons among their group. But also in terms of their differing reactivity, and ability to catalytically favour the dehydrogenation of dimethylamine-boranes. The diverging reactivity, found among these salts, highlights the potential for affecting the outcome of the reaction by varying the metal complex employed or by changing the solvent medium. A key feature that has allowed, in some cases, selective preparation of dehydrogenation products (**19**-**22**).

In addition to their effective use in catalysis, the tridentate carbazolido ligand **6**, has been successfully employed as a way of accessing metal-bearing compounds *via* metathesis reactions with the corresponding potassium salt **14**, or following an organoelimination methodology. The catalogue of new complexes synthesised through these methods, includes members of a wide range of elements in the periodic table, furtherly supporting the capabilities of the chosen scaffold, and the inherent stabilising characteristics of multidentate ligand systems. Members of these new family of compounds include Hauser base complexes (**24**), open and closed-shell first row transition-metal species (**26**-**34**), Group 12 compounds (**35**-**37**), hypervalent Group 13 metal centres (**38**-**40**) and heteroleptic tetrylenes (**41**-**43**). With a similar study being carried out using the assymetric bidentate ligand **9**, from which three/four coordinate species have been characterised, including a Group 2 halide-bridged dimer (**44**) and a monomeric three-coordinate zinc complex (**45**).

Following their structural characterisation, heteroleptic compounds **24** and **27** were thoroughly studied in terms of the space-availability of the metal centre to coordinate further substrates; an essential feature in small molecule activation and catalysis. A family of each parent compound could be prepared, following addition of substrates containing

electron rich nitrogen/oxygen functional groups, to the metal centres, from which five coordinate compounds **24b-e** and **27a-d** could be prepared.

Additionally, compounds **26**-**30** were identified as catalytically active in the hydrophosphination of acrylonitrile. The library of heteroleptic compounds prepared, allowed for further optimisation studies. Finding the novel cobalt(I)-carbonyl complex **29**, as the most selective/reactive of the series, solely yielding the anti-Markovnikov product. With this protocol being the first of its kind involving a cobalt(I) species capable of achieving such transformation on unsaturated substrates. The scope of the reaction was studied, managing to exted this protocol to a range of activated alkenes, accesing an array of hydrophosphination products, both in good yields and high selectivity (**46a**-**56a**).

Finally, investigations on the formation of ruthenium metal complexes coordinated by hemilable N/P-based ligand systems, allowed for preparation and characterisation of a family of PCA and PDCA derived ruthenium metallocenes (**57**-**61**). In all cases, the ruthenium centre is bound to the PCA/PDCA fragment *via* the phosphorus lone pair. The presence of intramolecular hydrogen bonding between the N*H* moiety and the pendant chlorides, encouraged further studies on the formation of five and six-membered metallacycles following deprotonation and halide scavenging. By doing so, it was possible to identify that the shorter PCAs are not suitable for such transformation, most likely due to steric restrictions. While the longer PDCAs allowing for such modification to take place and adopting structures in which the PDCA fragments work as an N/P bidentate chelate. Following this work, six-membered metallacylces **62** and **63**, could be isolated. With NMR determinations, indicating that upon cyclisation each compound yields a mixture of two isomers (**62a**-**b** and **63a**-**b**), as a consequence of the formation of distinctive rotationally restricted species.

General Experimental Procedures

8.1 Inert Atmosphere Techniques

Unless otherwise stated all products hereby described were treated with rigorous exclusion of air and water. This was achieved following standard air-sensitive-handling techniques[376] which included bench-top operations (Schlenk techniques) and glove box techniques in which conventional manipulations were performed in an inert-atmosphere box. Detailed descriptions of inert atmosphere methods and apparatus can be found in the literature.[377] Due to the high sensitivity towards air and moisture of the compounds, solvents and reagents were thoroughly dried and purified.[376]

8.2 Solvents Employed

Standard laboratory solvents were pre-dried by putting them in contact with meticulous drying and deoxygenating agents such as sodium wire, and subsequently dried *via* reflux over potassium (toluene) or sodium-benzophenone (tetrahydrofuran). *Iso*-hexane was passed through a drying column fitted with 4 Å molecular sieves, and stored over a potassium mirror. Freshly distilled solvents were stored in ampoules over a potassium mirror (toluene), or 4 Å molecular sieves (tetrahydrofuran); and degassed before use. C_6D_6 was dried over potassium in a sealed tube at 90°C for 4 days, before vacuum-transferring it to an ampoule containing a potassium mirror and subsequently stored in the glove box prior to use. $CDCl_3$ was dried over CaH_2 in a sealed tube at 90°C for 4 days, before vacuum-transferring it to an ampoule. Both deuterated solvents were stored in the glove box prior to use. Dry/degassed CD_2Cl_2 (0.03% $^{v}/_{v}$ TMS) was purchased from Sigma-Aldrich and stored over molecular sieves, in the glovebox.

8.3 Starting Materials and Reagents

Anhydrous $FeCl_2{\cdot}THF_{1.5}$, $CoBr_2{\cdot}DME$, $CdCl_2$, $CuCl_2{\cdot}THF_{0.8}$, $Li[N(SiMe_3)_2]$, $Na[N(SiMe_3)_2]$ and $K[N(SiMe_3)_2]$ were synthesised according to standard literature methods.[378–380] All other metal dihalides/salts were used as purchased.

$Me_2NH{\cdot}BH_3$ and $Me_3N{\cdot}BH_3$ were purchased from Sigma-Aldrich and used as received. ^{t}BuLi and MeMgI were purchased from Sigma-Aldrich as a 1.7 M solution in pentane and a 3.0 M solution in Et_2O, respectively. These solutions were transferred to Schlenk flasks and the volatiles were removed under vacuum, the resulting powders were stored in the glovebox. NaH and KH were washed with hexane and filtered, the resulting filtrate was

dried under vacuum and transferred to the glovebox, prior to use. Li[$BHEt_3$] was purchased from Sigma-Aldrich as a 1M solution in THF and stored in an air-tight ampoule. Carbon monoxide was obtained from BOC (CP Grade N3.0, minimum purity of 99.9%) and used as received. The aldiminic substrates employed in Entries 16-18, Table 5.3.3, Chapter 5 and the phosphinocarboxamides (PCAs) [**L57**-**L59**] / phosphinodicarboxamides (PDCAs) [**L60**-**L61**], used in Chapter 6, were prepared according to reported procedures.[270,381]

Safety warnings: 1-Naphthylamine is highly toxic and is suspected to be a carcinogen; great care must be taken during synthesis and adequate handling of waste should be procured. Carbon monoxide is an extremely toxic and flammable gas, good ventilation within a fumehood should be procured when running a Schlenk line with this gas as source, away from open flames and with a carbon monoxide detector operating at all times. Dehydrocoupling of $Me_2NH{\cdot}BH_3$ with precatalysts **12**-**14** evolves $H_{2(g)}$. Solutions containing Li[$BHEt_3$] (Super-Hydride®), ^{t}BuLi, MeMgI, $ZnMe_2$, Li[$N(SiMe_3)_2$], Na[$N(SiMe_3)_2$] and K[$N(SiMe_3)_2$] are extremely pyrophoric and flammable upon exposure to air, ensuring handling of these compounds under inert conditions is paramount.

CAUTION! Organo-cadmium, -mercury, -germanium, -tin and -lead compounds and their salts are known for their high toxicity, great care must be taken during their manipulation and adequate handling of heavy-metal containing waste should be procured.

8.4 NMR Spectroscopy

Samples of air and moisture sensitive compounds were prepared either using glove box techniques and contained in J. Young´s tap modified borosilicate glass NMR tubes. All NMR data was collected on Bruker DPX300, DPX400, AV400, AV(III)400 AV(III)400HD or AV(III)600 NMR spectrometers. Chemical shifts are quoted in ppm relative to TMS (^{1}H, ^{13}C, ^{13}C{^{1}H}, ^{29}Si{^{1}H}), LiCl/D_2O solution (^{7}Li{^{1}H}), $BF_3{\cdot}Et_2O$ (^{11}B, ^{11}B{^{1}H}), H_3PO_4 (^{31}P, ^{31}P{^{1}H}), $CdMe_2$ (^{113}Cd{^{1}H}), Me_4Sn 90%/C_6D_6 (^{119}Sn{^{1}H}), $HgMe_2$ (^{199}Hg{^{1}H}) and Me_4Pb/5% C_6D_6 (^{207}Pb{^{1}H}).

8.5 DOSY NMR and Hydrodynamic Radii Calculations

DOSY experiments were carried out using the PFGSE (Pulsed-Field Gradient Spin-Echo) NMR Diffusion methods and analysed with the software implemented by Bruker on an AV(III)600 or an AV(III)400HD NMR spectrometer. The variation of the intensity (integral) of one selected signal in the ^{1}H NMR spectrum (I) is related to the strength of the gradient

(G) by the following equation: $Ln(I/Io) = -\gamma^2\delta^2Gi^2(\Delta-\delta/3)D$, where γ = gyromagnetic ratio of the proton, δ = length of the gradient pulse, Gi = gradient strength, Δ = delay between the midpoints of the gradients, and D = diffusion coefficient. Before recording the DOSY experiment, the values of δ (small delta) and Δ (big delta) were optimised for each complex. The selected values provided a considerable reduction of the intensity of the signal, but it remained strong enough to be integrated. Next, the bidimensional DOSY experiment (stebpgp1s sequence) was recorded with the optimised δ and Δ values, varying G along 16-32 spectra. The data were analysed with the Bruker's software, which provided directly the diffusion coefficient (D). The quality of the data were tested by representation Ln(I) versus G2, which gave an excellent fit to a straight line in all the cases. Hydrodynamic radii (r_H) were calculated from the Stokes–Einstein equation: $r_H = (k*T)/(6*\pi*\eta*D)$ (where T is absolute temperature, k is the Boltzmann constant, η is the solvent viscosity and D is the coefficient of diffusion). Averaged molecular radii were estimated from the calculated molecular volume defined as the volume inside a contour of 0.001 electrons/Bohr^3.

8.6 Evans Method

Magnetic moments were calculated through the Evans method at 298 K, employing C_6D_6 as solvent. Diamagnetic corrections were calculated according to Pascal's constants.[382]

8.7 Mass Spectrometry

Air-sensitive mass spectrometry samples were prepared under an Argon atmosphere by placing the sample inside glass capillaries. The spectra for the air-sensitive complexes described were recorded by the EPSRC NMSF (Swansea University) using perfluorotributylamine as high resolution MS reference, on a Finnigan MAT 95 XP (Thermo Fisher Scientific, Bremen, Germany) double focussing mass spectrometer. Air-stable samples were prepared by careful dilution of the sample in methanol and run through the departmental service at the School of Chemistry, University of Nottingham using a Bruker MicroToF (ESI^+/ESI^-), with sodium formate as mass calibrant.

8.8 Elemental Analysis

Elemental Analyses of air-stable samples were run by Dr Tong Liu at the University of Nottingham, in an Exeter Analytical CE-440 Elemental Analyzer.

8.9 Infrared Spectroscopy

Infrared spectroscopy samples of air-sensitive samples were prepared as Nujol mulls between two KBr discs, using glove box techniques. In the case of non-air-sensitive samples, the infrared spectra were obtained in chloroform solution or as ATR samples. In both cases the spectra were recorded on a Bruker Tensor 27 IR spectrometer over a frequency range of 4000-400cm^{-1}.

8.10 UV/vis Absorption Spectroscopy

UV/vis spectroscopy samples were prepared as solutions of known concentration in a J. Young's tap modified 10 mm quartz cell. UV/vis spectra were recorded on a Perkin Elmer Lamda 750 UV/vis spectrophotometer, over a wavelength range of 350-1100 nm.

8.11 Cyclic Voltammetry

Cyclic voltammetric (CV) studies were performed by Dr E. Stephen Davies at the University of Nottingham, using an Autolab PGSTAT20 potentiostat. Standard cyclic voltammetry was carried out under an atmosphere of dinitrogen using a single compartment air-tight cell. A glassy carbon working electrode, a glassy carbon secondary electrode and a saturated calomel reference electrode, chemically isolated from the test solution *via* a bridge tube containing electrolyte solution and fitted with a porous ceramic frit, were used in the cell. The THF solutions were 10^{-3} M in test compound and 0.5 M in [NBu_4][BF_4] as supporting electrolyte. The test solutions were loaded into the cell in a glovebox and solutions were stirred between scans using a magnetic stirrer bar. Redox potentials are quoted *versus* the ferrocenium-ferrocene couple used as an internal reference.[383] Compensation for internal resistance was not applied.

8.12 DFT Methodologies

Restricted geometry optimisations were performed for models of [**62a'**, **62b'**, **63a'** and **63b'**], using coordinates derived from the X-ray crystal structures of [**60** and **61**]. The models were geometry optimised without constraints and the energy minima were confirmed by frequency calculations, which showed the absence of imaginary frequencies. The calculations were performed using the Amsterdam Density Functional (ADF) suite

version 2014.01.[384,385] The DFT geometry optimisations employed all-electron Slater type orbital (STO) triple-ζ-plus polarisation basis sets (from the ZORA/TZP database of the ADF suite) for the Ru, Cl, P, C, N, O, and H atoms. Scalar relativistic approaches were used within the ZORA Hamiltonian for the inclusion of relativistic effects and the local density approximation (LDA) with the correlation potential due to Vosko *et al*. was used in all of the calculations.[386] Gradient corrections were performed using the functionals of Becke and Perdew.[387,388]

8.13 Crystallographic Methods

Under a flow of N_2, crystals suitable for X-ray diffraction were quickly removed from the crystallisation vessel and covered with "fomblin" (YR-1800 perfluoropolyether oil). A suitable crystal was then mounted on a polymer-tipped MicroMount™ and cooled rapidly to 120K in a stream of cold N_2 using an Oxford Cryosystems open flow cryostat.[389] Single crystal X-ray diffraction data were collected either using an Agilent SuperNova diffractometer, Atlas CCD area detector (mirror-monochromated Cu-*Ka* radiation source; λ = 1.54184 Å or graphite-monochromated Mo-*Ka* radiation source; λ = 0.7103 Å; ω scans), an Agilent SuperNovaII diffractometer, Atlas S2 CCD area detector, an Agilent SuperNovaII diffractometer Titan S2 CCD area detector (mirror monochromated Cu-*Ka* radiation source; λ = 1.54184 Å; ω scans) or a Rigaku MM007 rotating anode X-ray source. Absorption corrections were applied using an analytical numerical method (CrysAlis Pro).[390] All non-H atoms were located using direct methods[391] and difference Fourier syntheses. Hydrogen atoms were placed and refined using a geometric riding model. All fully occupied non-H atoms were refined with anisotropic displacement parameters, unless otherwise specified. Crystal structures were solved and refined using the Olex2 software package.[392,393] Programs used include CrysAlisPro[394] (control of Supernova, data integration and absorption correction), SHELXL[395] (structure refinement), SHELXS[391] (structure solution), SHELXT[396] (structure solution), OLEX2[393] (molecular graphics). CIF files were checked using checkCIF[397] and by Dr William Lewis at the University of Nottingham Crystal Structure Service.

Appendices

Crystallographic Data

3,6-di(*tert*-butyl)-9*H*-carbazole (**1**):

[^{t}Bu$_2$carbazole]

ORNALP

$C_{20}H_{25}N$ (M =279.41 g/mol): triclinic, space group P-1 (no. 2), a = 6.0629(12) Å, b = 22.871(3) Å, c = 26.385(5) Å, α = 111.618(15)°, β = 90.127(16)°, γ = 97.542(14)°, V = 3366.7(10) Å^3, Z = 8, T = 120(2) K, μ(CuKα) = 0.472 mm^{-1}, D_{calc} = 1.102 g/cm^3, 25237 reflections measured (6.476° ≤ 2Θ ≤ 150.16°), 11977 unique (R_{int} = 0.1890, R_{sigma} = 0.3127) which were used in all calculations. The final R_1 was 0.1619 (I > 2σ(I)) and wR_2 was 0.5264 (all data).

1,8-dibromo-3,6-di(*tert*-butyl)-9*H*-carbazole (**2**):

[^{t}Bu$_2$Br$_2$carbazole]

ORNALN

$C_{20}H_{21.5}Br_2N$ (M =435.70 g/mol): triclinic, space group P-1 (no. 2), a = 9.7158(5) Å, b = 11.6319(7) Å, c = 17.3413(8) Å, α = 88.164(5)°, β = 81.495(4)°, γ = 74.127(5)°, V = 1864.28(18) Å^3, Z = 4, T = 120(2) K, μ(CuKα) = 5.490 mm^{-1}, D_{calc} = 1.552 g/cm^3, 26545 reflections measured (7.902° ≤ 2Θ ≤ 147.698°), 7403 unique (R_{int} = 0.0630, R_{sigma} = 0.0445) which were used in all calculations. The final R_1 was 0.0477 (I > 2σ(I)) and wR_2 was 0.1352 (all data).

1,8-diformyl-3,6-di(*tert*-butyl)-9*H*-carbazole (**3**):

[^{t}Bu$_2$CHO$_2$carbazole]

ORNALK

$C_{23}H_{26}Cl_3NO_2$ (M =454.80 g/mol): monoclinic, space group $P2_1/c$ (no. 14), a = 11.21228(16) Å, b = 18.54264(15) Å, c = 11.76540(14) Å, β = 114.1469(15)°, V = 2232.06(5) Å^3, Z = 4, T = 120(2) K, μ(CuKα) = 3.868 mm^{-1}, D_{calc} = 1.353 g/cm^3, 21403 reflections measured (8.642° ≤ 2Θ ≤ 147.32°), 4448 unique (R_{int} = 0.0385, R_{sigma} = 0.0228) which were used in all calculations. The final R_1 was 0.0461 (I > 2σ(I)) and wR_2 was 0.1262 (all data).

2,6-bis(diphenylmethyl)-4-methylaniline (**4**):

[Ar*NH$_2$]

MGRNLNA (MRes.)

$C_{33}H_{29}N$ (M =439.57 g/mol): monoclinic, space group $P2_1/n$ (no. 14), a = 9.5800(3) Å, b = 11.3581(3) Å, c = 22.2143(5) Å, β = 93.143(2)°, V = 2413.52(11) Å^3, Z = 4, T = 120(2) K, μ(CuKα) = 0.524 mm^{-1}, D_{calc} = 1.210 g/cm^3, 9488 reflections measured (7.972° ≤ 2Θ ≤ 148.676°), 4766 unique (R_{int} = 0.0176, R_{sigma} = 0.0224) which were used in all calculations. The final R_1 was 0.0400 (I > 2σ(I)) and wR_2 was 0.1061 (all data).

1,8-di(Ar*)imino-3,6-di(*tert*-butyl)-9*H*-carbazole (**5**):

[Ar$_2$*carbH]

ORNALG

$C_{94}H_{87}N_3$ (*M* =1258.66 g/mol): monoclinic, space group *I*2/*a* (no. 15), *a* = 19.1810(9) Å, *b* = 19.2723(8) Å, *c* = 22.1260(8) Å, *β* = 100.681(4)°, *V* = 8037.4(6) Å^3, *Z* = 4, *T* = 120(2) K, μ(CuKα) = 0.449 mm^{-1}, D_{calc} = 1.040 g/cm^3, 30127 reflections measured (6.128° ≤ 2Θ ≤ 148.408°), 8023 unique (R_{int} = 0.0487, R_{sigma} = 0.0404) which were used in all calculations. The final R_1 was 0.0932 (I > 2σ(I)) and wR_2 was 0.2962 (all data).

1,8-dinaphthylimino-3,6-di(*tert*-butyl)-9*H*-carbazole (**6**):

[$Naph_2$carbH]

CCDC 1581977

ORNALL

$C_{42}H_{39}N_3$ (*M* =585.76 g/mol): monoclinic, space group $P2_1/c$ (no. 14), *a* = 28.8139(16) Å, *b* = 8.5704(4) Å, *c* = 13.5865(7) Å, *β* = 102.756(5)°, *V* = 3272.3(3) Å^3, *Z* = 4, *T* = 120(2) K, μ(CuKα) = 0.528 mm^{-1}, D_{calc} = 1.189 g/cm^3, 24982 reflections measured (9.442° ≤ 2Θ ≤ 148.76°), 6597 unique (R_{int} = 0.0651, R_{sigma} = 0.0477) which were used in all calculations. The final R_1 was 0.0565 (I > 2σ(I)) and wR_2 was 0.1609 (all data).

8-Formyl-1,2,3,4-Tetrahydro-9*H*-carbazole (**8**):

[CHO-THCarbH]

ORNALR

$C_{13}H_{13}NO$ (*M* =199.24 g/mol): monoclinic, space group $P2_1/c$ (no. 14), *a* = 5.08255(14) Å, *b* = 22.6542(6) Å, *c* = 17.8081(4) Å, *β* = 92.427(3)°, *V* = 2048.61(10) Å^3, *Z* = 8, *T* = 120(2) K, μ(CuKα) = 0.646 mm^{-1}, D_{calc} = 1.292 g/cm^3, 8091 reflections measured (7.806° ≤ 2Θ ≤ 147.122°), 3996 unique (R_{int} = 0.0258, R_{sigma} = 0.0367) which were used in all calculations. The final R_1 was 0.0421 (I > 2σ(I)) and wR_2 was 0.1150 (all data).

8-(Ar*)imino-1,2,3,4-Tetrahydro-9*H*-carbazole (**9**):

[Ar*THCarbH]

ORNAMB

$C_{46}H_{40}N_2$ (*M* =620.80 g/mol): triclinic, space group *P*-1 (no. 2), *a* = 9.3642(5) Å, *b* = 14.1119(8) Å, *c* = 14.3239(6) Å, *α* = 112.619(5)°, *β* = 94.267(4)°, *γ* = 101.306(5)°, *V* = 1689.73(16) Å^3, *Z* = 2, *T* = 120(2) K, μ(CuKα) = 0.534 mm^{-1}, D_{calc} = 1.220 g/cm^3, 12491 reflections measured (6.998° ≤ 2Θ ≤ 149.976°), 6728 unique (R_{int} = 0.0344, R_{sigma} = 0.0486) which were used in all calculations. The final R_1 was 0.0450 (I > 2σ(I)) and wR_2 was 0.1168 (all data).

1,8-di(Ar*)imino-3,6-di(*tert*-butyl)-9-lithium-carbazole (**11**):

[Ar_2*carbLi]

LIRNLL

$C_{114}H_{122}LiN_3$ (*M* =1541.08 g/mol): trigonal, space group *P*3*c*1 (no. 158), *a* = 28.014(6) Å, *c* = 19.4138(19) Å, *V* = 13194(6) Å^3, *Z* = 6, *T* = 119.97(12) K, μ(CuKα) = 0.494 mm^{-1}, D_{calc} = 1.164 g/cm^3, 33267 reflections measured (6.31° ≤ 2Θ ≤ 149.624°), 10939 unique (R_{int} = 0.1860,

R_{sigma} = 0.1857) which were used in all calculations. The final R_1 was 0.1604 (I > 2σ(I)) and wR_2 was 0.4462 (all data).

1,8-dinaphthylimino-3,6-di(*tert*-butyl)-9-lithium-carbazole(THF) (**12**):

[$Naph_2carbLi(thf)$]

CCDC 1581978

LIRNLN

$C_{46}H_{46}LiN_3O$ (M =663.80 g/mol): triclinic, space group P-1 (no. 2), a = 12.023(8) Å, b = 12.802(10) Å, c = 13.927(7) Å, α = 66.18(6)°, β = 76.98(5)°, γ = 73.37(6)°, V = 1864(2) Å^3, Z = 2, T = 120(2) K, μ(CuKα) = 0.536 mm^{-1}, D_{calc} = 1.182 g/cm^3, 1794 reflections measured (6.992° ≤ 2Θ ≤ 61.838°), 1150 unique (R_{int} = 0.0884, R_{sigma} = 0.2702) which were used in all calculations. The final R_1 was 0.0967 (I > 2σ(I)) and wR_2 was 0.2415 (all data).

1-naphthylimino-3,6-di(^{t}Butyl)-8-methilene(*N*-^{n}butyl-*N*-1-naphthalene)-9-lithium-carbazole(THF) (**12a**):

[$Naph_2$-(^{n}Butyl)carbLi(thf)]

CCDC 1581979

LIRNLJ

$C_{50}H_{55}LiN_3O$ (M =720.91 g/mol): monoclinic, space group $P2_1/n$ (no. 14), a = 13.65773(16) Å, b = 21.7068(3) Å, c = 14.23975(17) Å, β = 105.0737(12)°, V = 4076.34(8) Å^3, Z = 4, T = 120(2) K, μ(CuKα) = 0.526 mm^{-1}, D_{calc} = 1.175 g/cm^3, 46635 reflections measured (7.61° ≤ 2Θ ≤ 147.678°), 8151 unique (R_{int} = 0.0352, R_{sigma} = 0.0202) which were used in all calculations. The final R_1 was 0.0479 (I > 2σ(I)) and wR_2 was 0.1304 (all data).

1,8-dinaphthylimino-3,6-di(*tert*-butyl)-9-sodium-carbazole(THF) (**13**):

[$Naph_2carbNa(thf)$]

CCDC 1581980

NARNLB

$C_{52}H_{60}N_3NaO$ (M =766.02 g/mol): triclinic, space group P-1 (no. 2), a = 12.1323(9) Å, b = 13.7056(11) Å, c = 14.2286(11) Å, α = 90.659(7)°, β = 106.001(7)°, γ = 103.336(7)°, V = 2205.8(3) Å^3, Z = 2, T = 120(2) K, μ(CuKα) = 0.605 mm^{-1}, D_{calc} = 1.153 g/cm^3, 16325 reflections measured (7.816° ≤ 2Θ ≤ 149.182°), 8049 unique (R_{int} = 0.0593, R_{sigma} = 0.0767) which were used in all calculations. The final R_1 was 0.0808 (I > 2σ(I)) and wR_2 was 0.2593 (all data).

1,8-dinaphthylimino-3,6-di(*tert*-butyl)-9-potassium-carbazole (**14**):

[$Naph_2carbK]_2$

CCDC 1581981

KRNALG

$C_{84}H_{76}K_2N_6$ (M =1247.70 g/mol): triclinic, space group P-1 (no. 2), a = 11.670(3) Å, b = 11.773(2) Å, c = 12.928(4) Å, α = 80.79(2)°, β = 85.14(2)°, γ = 78.098(18)°, V =

1713.1(8) Å^3, Z = 1, T = 120.02(10) K, μ(CuKα) = 1.602 mm^{-1}, D_{calc} = 1.209 g/cm^3, 10407 reflections measured (7.754° ≤ 2Θ ≤ 133.182°), 5952 unique (R_{int} = 0.1123, R_{sigma} = 0.1518) which were used in all calculations. The final R_1 was 0.1335 (I > 2σ(I)) and wR_2 was 0.3859 (all data).

8-(Ar*)imino-1,2,3,4-Tetrahydro-9-lithium-carbazole(Ar*-NH_2) (**15a**):

[Ar*THCarbLi(Ar*-NH_2)]

LIRNLS

$C_{85}H_{73}LiN_3$ (M =1143.40 g/mol): monoclinic, space group $P2_1/c$ (no. 14), a = 11.0062(5) Å, b = 37.546(2) Å, c = 17.8586(6) Å, β = 106.708(5)°, V = 7068.3(6) Å^3, Z = 4, T = 120(2) K, μ(CuKα) = 0.465 mm^{-1}, D_{calc} = 1.074 g/cm^3, 39739 reflections measured (4.708° ≤ 2Θ ≤ 146.936°), 13933 unique (R_{int} = 0.0470, R_{sigma} = 0.0491) which were used in all calculations. The final R_1 was 0.1237 (I > 2σ(I)) and wR_2 was 0.3735 (all data).

8-(Ar*)imino-1,2,3,4-Tetrahydro-9-sodium-carbazole (**16**):

[Ar*THCarbNa]

NARNLC

$C_{52}H_{45}N_2Na$ (M =720.89 g/mol): triclinic, space group P-1 (no. 2), a = 10.7541(4) Å, b = 10.9919(6) Å, c = 17.3807(8) Å, α = 105.056(5)°, β = 95.316(3)°, γ = 98.084(4)°, V = 1946.28(16) Å^3, Z = 2, T = 120(2) K, μ(CuKα) = 0.636 mm^{-1}, D_{calc} = 1.230 g/cm^3, 16699 reflections measured (8.382° ≤ 2Θ ≤ 151.516°), 7630 unique (R_{int} = 0.0422, R_{sigma} = 0.0468) which were used in all calculations. The final R_1 was 0.0650 (I > 2σ(I)) and wR_2 was 0.2093 (all data).

K[H_3B-NMe_2-BH_3] (**21a**):

CCDC 1581982

BRNALH

$C_2H_{12}B_2KN$ (M =110.85 g/mol): monoclinic, space group $P2_1/n$ (no. 14), a = 9.6343(3) Å, b = 22.8460(8) Å, c = 13.1641(4) Å, β = 91.402(3)°, V = 2896.63(17) Å^3, Z = 16, T = 120(2) K, μ(CuKα) = 5.437 mm^{-1}, D_{calc} = 1.017 g/cm^3, 16081 reflections measured (7.74° ≤ 2Θ ≤ 147.702°), 5696 unique (R_{int} = 0.0558, R_{sigma} = 0.0528) which were used in all calculations. The final R_1 was 0.0867 (I > 2σ(I)) and wR_2 was 0.2395 (all data).

1,8-dinaphthylimino-3,6-di(*tert*-butyl)-9-magnesium-iodide-carbazole(OEt_2) (**24**):

[$Naph_2$carbMg(OEt_2)I]

MGRNLL

$C_{58}H_{60}IMgN_3O$ (M =966.30 g/mol): monoclinic, space group $P2_1/n$ (no. 14), a = 30.5557(7) Å, b = 11.2340(2) Å, c = 32.1030(8) Å, β = 114.197(3)°, V = 10051.6(4) Å^3, Z = 8, T = 120(2) K, μ(CuKα) = 5.443 mm^{-1}, D_{calc} = 1.277 g/cm^3, 42834 reflections measured (5.196° ≤ 2Θ ≤ 147.96°), 19805 unique (R_{int} = 0.0364, R_{sigma} = 0.0394) which were used in all calculations. The final R_1 was 0.0365 (I > 2σ(I)) and wR_2 was 0.0977 (all data).

[1,8-dinaphthylimino-3,6-di(*tert*-butyl)-carbazole]$_2$-9-magnesium (**24a**):

[(Naph$_2$carb)$_2$Mg]

MGRNLJ

$C_{84}H_{77}MgN_6$ (M =1194.82 g/mol): triclinic, space group P-1 (no. 2), a = 13.329(2) Å, b = 15.799(3) Å, c = 19.806(2) Å, α = 73.407(14)°, β = 80.950(12)°, γ = 83.455(14)°, V = 3936.6(11) Å^3, Z = 2, T = 132(17) K, μ(CuKα) = 0.521 mm^{-1}, D_{calc} = 1.008 g/cm^3, 61442 reflections measured (7.69° ≤ 2Θ ≤ 176.958°), 16127 unique (R_{int} = 0.5365, R_{sigma} = 0.3716) which were used in all calculations. The final R_1 was 0.2353 (I > 2σ(I)) and wR_2 was 0.5906 (all data).

1,8-dinaphthylimino-3,6-di(*tert*-butyl)-9-magnesium-iodide-carbazole(acrylonitrile) (**24b**):

[Naph$_2$carbMg(acrylonitrile)I]

MGRNLX

$C_{54}H_{48}IMgN_4$ (M =904.17 g/mol): triclinic, space group P-1 (no. 2), a = 12.4515(4) Å, b = 14.0506(6) Å, c = 16.7514(7) Å, α = 106.328(4)°, β = 100.960(3)°, γ = 106.690(3)°, V = 2574.38(19) Å^3, Z = 2, T = 120(2) K, μ(CuKα) = 5.274 mm^{-1}, D_{calc} = 1.166 g/cm^3, 18572 reflections measured (7.326° ≤ 2Θ ≤ 148.7°), 10159 unique (R_{int} = 0.0406, R_{sigma} = 0.0521) which were used in all calculations. The final R_1 was 0.0414 (I > 2σ(I)) and wR_2 was 0.1129 (all data).

1,8-dinaphthylimino-3,6-di(*tert*-butyl)-9-magnesium-iodide-carbazole(dimethylfumarate) (**24c**):

[Naph$_2$carbMg(dimethylfumarate)I]

MGRNLR

$C_{102}H_{98}I_2Mg_2N_6O_8$ (M =1838.28 g/mol): triclinic, space group P-1 (no. 2), a = 10.8438(13) Å, b = 14.5471(14) Å, c = 29.569(2) Å, α = 90.051(7)°, β = 90.015(9)°, γ = 109.492(10)°, V = 4397.0(8) Å^3, Z = 2, T = 120.15 K, μ(CuKα) = 6.246 mm^{-1}, D_{calc} = 1.388 g/cm^3, 19165 reflections measured (7.102° ≤ 2Θ ≤ 147.49°), 13931 unique (R_{int} = 0.2987, R_{sigma} = 0.3696) which were used in all calculations. The final R_1 was 0.1676 (I > 2σ(I)) and wR_2 was 0.4717 (all data).

1,8-dinaphthylimino-3,6-di(*tert*-butyl)-9-magnesium-iodide-carbazole(methylpropiolate) (**24d**):

[Naph$_2$carbMg(methylpropiolate)I]

MGRNLN

$C_{58}H_{54}IMgN_3O_2$ (M =976.25 g/mol): triclinic, space group P-1 (no. 2), a = 12.4045(15) Å, b = 14.1159(17) Å, c = 16.837(2) Å, α = 71.696(11)°, β = 83.869(10)°, γ = 74.395(10)°, V = 2695.0(6) Å^3, Z = 2, T = 120(2) K, μ(CuKα) = 5.097 mm^{-1}, D_{calc} = 1.203 g/cm^3, 21781 reflections measured (7.386° ≤ 2Θ ≤ 150.246°), 10743 unique (R_{int} = 0.0888, R_{sigma} = 0.1108) which were used in all calculations. The final R_1 was 0.1155 (I > 2σ(I)) and wR_2 was 0.3234 (all data).

1,8-dinaphthylimino-3,6-di(*tert*-butyl)-9-magnesium-iodide-carbazole(dimethyladipate) (**24e**):

[Naph$_2$carbMg(dimethyladipate)I]

MGRNMA

$C_{50}H_{52}IMgN_3O_4$ (M =910.15 g/mol): monoclinic, space group $P2_1$ (no. 4), a = 11.51541(19) Å, b = 11.23458(18) Å, c = 17.3429(3) Å, β = 94.0270(15)°, V = 2238.13(6) Å^3, Z = 2, T = 120(2) K, μ(CuKα) = 6.128 mm^{-1}, D_{calc} = 1.351 g/cm^3, 16135 reflections measured (7.696° ≤ 2Θ ≤ 178.856°), 8056 unique (R_{int} = 0.2707, R_{sigma} = 0.1536) which were used in all calculations. The final R_1 was 0.5521 (I > 2σ(I)) and wR_2 was 0.8531 (all data).

1,8-dinaphthylimino-3,6-di(*tert*-butyl)-9-iron-chloride-carbazole(THF) (**26**):

[Naph$_2$carbFe(thf)Cl]

CCDC 1874664

FERNSA

$C_{52}H_{60}ClFeN_3O$ (M =834.33 g/mol): monoclinic, space group $P2_1/c$ (no. 14), a = 14.1874(17) Å, b = 13.759(5) Å, c = 23.107(5) Å, β = 91.524(16)°, V = 4509(2) Å^3, Z = 4, T = 120(2) K, μ(CuKα) = 3.529 mm^{-1}, D_{calc} = 1.229 g/cm^3, 21983 reflections measured (7.478° ≤ 2Θ ≤ 155.636°), 8906 unique (R_{int} = 0.1982, R_{sigma} = 0.2955) which were used in all calculations. The final R_1 was 0.1244 (I > 2σ(I)) and wR_2 was 0.3723 (all data).

1,8-dinaphthylimino-3,6-di(*tert*-butyl)-9-cobalt-bromide-carbazole (**27**):

[Naph$_2$carbCoBr]

CCDC 1874665

CORNLJ

$C_{55.5}H_{47}BrCoD_{4.5}N_3$ (M =903.86 g/mol): triclinic, space group P-1 (no. 2), a = 12.6392(3) Å, b = 15.3752(3) Å, c = 25.5154(4) Å, α = 73.4778(15)°, β = 77.8385(16)°, γ = 77.1765(16)°, V = 4577.00(15) Å^3, Z = 4, T = 120(2) K, μ(CuKα) = 4.260 mm^{-1}, D_{calc} = 1.312 g/cm^3, 62413 reflections measured (7.264° ≤ 2Θ ≤ 154.076°), 18632 unique (R_{int} = 0.0283, R_{sigma} = 0.0276) which were used in all calculations. The final R_1 was 0.0353 (I > 2σ(I)) and wR_2 was 0.0965 (all data).

1,8-dinaphthylimino-3,6-di(*tert*-butyl)-9-cobalt-bromide-carbazole(acrylonitrile) (**27a**):

[Naph$_2$carbCo(acrylonitrile)Br]

CCDC 1874668

CORNLB

$C_{63}H_{59}BrCoN_4$ (M =1010.98 g/mol): triclinic, space group P-1 (no. 2), a = 12.3318(4) Å, b = 13.9553(5) Å, c = 16.2879(5) Å, α = 74.231(3)°, β = 75.360(3)°, γ = 75.607(3)°, V = 2560.81(16) Å^3, Z = 2, T = 120(2) K, μ(CuKα) = 3.873 mm^{-1}, D_{calc} = 1.311 g/cm^3, 19364 reflections measured (5.752° ≤ 2Θ ≤ 147.482°), 10037 unique (R_{int} = 0.0363, R_{sigma} = 0.0485) which were used in all calculations. The final R_1 was 0.0347 (I > 2σ(I)) and wR_2 was 0.0830 (all data).

[1,8-dinaphthylimino-3,6-di(*tert*-butyl)-9-cobalt-bromide-carbazole]$_2$(dimethyladipate) (**27b**):

[Naph$_2$carbCoBr]-dimethyladipate-[Naph$_2$carbCoBr]

CCDC 1874669

CORNLC (double metallation)

$C_{110}H_{104}Br_2Co_2D_{12}N_6O_4$ (M =1875.83 g/mol): monoclinic, space group $I2/a$ (no. 15), a = 23.5352(4) Å, b = 12.5589(2) Å, c = 34.4463(7) Å, β = 107.853(2)°, V = 9691.2(3) Å^3, Z = 4, T = 120(2) K, μ(CuKα) = 4.070 mm^{-1}, D_{calc} = 1.286 g/cm^3, 19270 reflections measured (7.538° ≤ 2Θ ≤ 147.33°), 9451 unique (R_{int} = 0.0210, R_{sigma} = 0.0276) which were used in all calculations. The final R_1 was 0.0370 (I > 2σ(I)) and wR_2 was 0.1014 (all data).

1,8-dinaphthylimino-3,6-di(*tert*-butyl)-9-cobalt-bromide-carbazole(dimethyladipate) (**27b'**):

[Naph$_2$carbCo(dimethyladipate)Br]

CORNLK (mono metallation)

$C_{56}H_{49}BrCoN_3O_4$ (M =966.82 g/mol): monoclinic, space group $P2_1/c$ (no. 14), a = 12.2471(16) Å, b = 32.090(9) Å, c = 13.5926(16) Å, β = 99.803(13)°, V = 5264.0(18) Å^3, Z = 4, T = 120(2) K, μ(CuKα) = 3.800 mm^{-1}, D_{calc} = 1.220 g/cm^3, 31504 reflections measured (7.326° ≤ 2Θ ≤ 156.684°), 10437 unique (R_{int} = 0.4207, R_{sigma} = 0.3170) which were used in all calculations. The final R_1 was 0.3358 (I > 2σ(I)) and wR_2 was 0.6828 (all data).

1,8-dinaphthylimino-3,6-di(*tert*-butyl)-9-cobalt-bromide-carbazole(dimethylfumarate) (**27c**):

[Naph$_2$carbCo(dimethylfumarate)Br]

CCDC 1874670

CORNLN

$C_{60}H_{58}BrCoN_3O_4$ (M =1023.93 g/mol): triclinic, space group P-1 (no. 2), a = 12.3851(3) Å, b = 13.8980(3) Å, c = 16.8621(4) Å, α = 95.8200(19)°, β = 110.705(2)°, γ = 105.102(2)°, V = 2560.34(11) Å^3, Z = 2, T = 120(2) K, μ(CuKα) = 3.934 mm^{-1}, D_{calc} = 1.328 g/cm^3, 57475 reflections measured (6.744° ≤ 2Θ ≤ 150.222°), 10349 unique (R_{int} = 0.0443, R_{sigma} = 0.0270) which were used in all calculations. The final R_1 was 0.0363 (I > 2σ(I)) and wR_2 was 0.0959 (all data).

1,8-dinaphthylimino-3,6-di(*tert*-butyl)-9-cobalt-bromide-carbazole(methylacrylate) (**27d**):

[Naph$_2$carbCo(methylacrylate)Br]

CCDC 1874671

CORNMD

$C_{52}H_{50}BrCoN_3O_2$ (M =887.79 g/mol): triclinic, space group P-1 (no. 2), a = 12.0956(2) Å, b = 13.6818(3) Å, c = 14.8797(3) Å, α = 110.196(2)°, β = 105.042(2)°, γ = 97.660(2)°, V = 2163.31(8) Å^3, Z = 2, T = 120(2) K, μ(CuKα) = 4.533 mm^{-1}, D_{calc} = 1.363 g/cm^3, 56537 reflections

measured (6.702° ≤ 2Θ ≤ 146.93°), 8624 unique (R_{int} = 0.0316, R_{sigma} = 0.0180) which were used in all calculations. The final R_1 was 0.0257 (I > 2σ(I)) and wR_2 was 0.0659 (all data).

1,8-dinaphthylimino-3,6-di(*tert*-butyl)-9-manganese-bromide-carbazole(THF) (**28**):

[$Naph_2carbMn(thf)Br$]

CCDC 1874666

MNRNLA

$C_{49}H_{53}BrMnN_3O$ (M =834.79 g/mol): monoclinic, space group $I2/a$ (no. 15), a = 24.0057(14) Å, b = 12.6793(15) Å, c = 28.0232(18) Å, β = 96.136(6)°, V = 8480.7(12) Å^3, Z = 8, T = 120(2) K, μ(CuKα) = 3.930 mm^{-1}, D_{calc} = 1.308 g/cm^3, 28055 reflections measured (7.408° ≤ 2Θ ≤ 133.196°), 7472 unique (R_{int} = 0.1119, R_{sigma} = 0.0787) which were used in all calculations. The final R_1 was 0.1234 (I > 2σ(I)) and wR_2 was 0.3659 (all data).

1,8-dinaphthylimino-3,6-di(*tert*-butyl)-9-cobalt-carbonmonoxide-carbazole (**29**):

[$Naph_2carbCo(CO)$]

CCDC 1874667

CORNLR

$C_{49}H_{52}CoN_3O$ (M =757.86 g/mol): monoclinic, space group $P2_1/c$ (no. 14), a = 10.13986(6) Å, b = 13.11950(8) Å, c = 30.38978(19) Å, β = 99.1752(6)°, V = 3991.03(4) Å^3, Z = 4, T = 120(2) K, μ(CuKα) = 3.674 mm^{-1}, D_{calc} = 1.261 g/cm^3, 86377 reflections measured (7.354° ≤ 2Θ ≤ 155.308°), 8452 unique (R_{int} = 0.0333, R_{sigma} = 0.0178) which were used in all calculations. The final R_1 was 0.0520 (I > 2σ(I)) and wR_2 was 0.1483 (all data).

[1,8-dinaphthylimino-3,6-di(*tert*-butyl)-carbazole]$_2$-9-vanadium (**31**):

[$(Naph_2carb)_2V$]

VRNALA

$C_{84}H_{76}N_6V$ (M =1220.44 g/mol): monoclinic, space group $P2/n$ (no. 13), a = 22.044(5) Å, b = 14.2039(16) Å, c = 23.815(6) Å, β = 102.68(3)°, V = 7275(3) Å^3, Z = 4, T = 120(2) K, μ(CuKα) = 1.492 mm^{-1}, D_{calc} = 1.114 g/cm^3, 34006 reflections measured (7.294° ≤ 2Θ ≤ 155.114°), 14270 unique (R_{int} = 0.3090, R_{sigma} = 0.3906) which were used in all calculations. The final R_1 was 0.2283 (I > 2σ(I)) and wR_2 was 0.6076 (all data).

[1,8-dinaphthylimino-3,6-di(*tert*-butyl)-carbazole]$_2$-9-chromium (**32**):

[$(Naph_2carb)_2Cr$]

CRRNLA

$C_{84}H_{76}CrN_6$ (M =1221.50 g/mol): monoclinic, space group $P2/n$ (no. 13), a = 21.987(4) Å, b = 14.196(3) Å, c = 23.757(6) Å, β = 102.80(2)°, V = 7231(3) Å^3, Z = 4, T = 120.00(13) K,

μ(CuKα) = 1.656 mm^{-1}, D_{calc} = 1.122 g/cm^3, 33741 reflections measured (7.304° ≤ 2Θ ≤ 147.632°), 14219 unique (R_{int} = 0.2474, R_{sigma} = 0.3144) which were used in all calculations. The final R_1 was 0.2262 (I > 2σ(I)) and wR_2 was 0.5909 (all data).

[1,8-dinaphthylimino-3,6-di(*tert*-butyl)-carbazole]$_2$-9-nickel (**33**):

$[(Naph_2carb)_2Ni]$

NIRNLB

$C_{88}H_{84}N_6NiO$ (M =1300.32 g/mol): monoclinic, space group $P2/n$ (no. 13), a = 22.3483(4) Å, b = 14.1740(2) Å, c = 23.7363(4) Å, β = 102.7479(19)°, V = 7333.5(2) $Å^3$, Z = 4, T = 120(2) K, μ(CuKα) = 0.767 mm^{-1}, D_{calc} = 1.178 g/cm^3, 37631 reflections measured (7.312° ≤ 2Θ ≤ 147.776°), 14522 unique (R_{int} = 0.0252, R_{sigma} = 0.0243) which were used in all calculations. The final R_1 was 0.0556 (I > 2σ(I)) and wR_2 was 0.1575 (all data).

[1,8-dinaphthylimino-3,6-di(*tert*-butyl)-carbazole]$_2$-9-copper (**34**):

$[(Naph_2carb)_2Cu]$

CURNLA

$C_{96}H_{102}CuN_6$ (M =1403.37 g/mol): monoclinic, space group $P2_1/c$ (no. 14), a = 16.749(2) Å, b = 25.9637(15) Å, c = 18.3387(18) Å, β = 102.581(11)°, V = 7783.2(15) $Å^3$, Z = 4, T = 120(2) K, μ(CuKα) = 0.781 mm^{-1}, D_{calc} = 1.198 g/cm^3, 44211 reflections measured (6.808° ≤ 2Θ ≤ 147.804°), 15363 unique (R_{int} = 0.2920, R_{sigma} = 0.2885) which were used in all calculations. The final R_1 was 0.1539 (I > 2σ(I)) and wR_2 was 0.4823 (all data).

[1,8-dinaphthylimino-3,6-di(*tert*-butyl)-carbazole]$_2$-9-zinc (**35**):

$[(Naph_2carb)_2Zn]$

ZNRNLF

$C_{84}H_{76}N_6Zn$ (M =1234.87 g/mol): orthorhombic, space group $Pccn$ (no. 56), a = 18.4274(10) Å, b = 24.3811(8) Å, c = 18.8328(6) Å, V = 8461.2(6) $Å^3$, Z = 4, T = 120(2) K, μ(CuKα) = 0.706 mm^{-1}, D_{calc} = 0.969 g/cm^3, 33586 reflections measured (6.012° ≤ 2Θ ≤ 147.218°), 8140 unique (R_{int} = 0.1307, R_{sigma} = 0.0819) which were used in all calculations. The final R_1 was 0.2475 (I > 2σ(I)) and wR_2 was 0.6311 (all data).

[1,8-dinaphthylimino-3,6-di(*tert*-butyl)-carbazole]$_2$-9-cadmium (**36**):

$[(Naph_2carb)_2Cd]$

CDRNLB

$C_{90}H_{90}CdN_6$ (M =1368.07 g/mol): triclinic, space group P-1 (no. 2), a = 13.4138(5) Å, b = 15.8847(11) Å, c = 19.2562(14) Å, α = 75.526(6)°, β = 83.510(4)°, γ = 83.277(4)°, V = 3930.5(4) $Å^3$, Z = 2, T = 120(2) K, μ(CuKα) = 2.579 mm^{-1}, D_{calc} = 1.156 g/cm^3, 33010 reflections

measured (4.758° ≤ 2Θ ≤ 149.368°), 15429 unique (R_{int} = 0.0500, R_{sigma} = 0.0668) which were used in all calculations. The final R_1 was 0.0533 (I > 2σ(I)) and wR_2 was 0.1424 (all data).

1,8-dinaphthylimino-3,6-di(*tert*-butyl)-9-mercury-bromide-carbazole (**37**):

[$Naph_2carbHgBr$]

HGRNLB

$C_{41.5}H_{37}BrHgN_3$ (M =858.24 g/mol): orthorhombic, space group *Pbca* (no. 61), a = 12.4040(10) Å, b = 22.9171(11) Å, c = 54.568(3) Å, V = 15511.8(17) Å^3, Z = 16, T = 120(2) K, μ(CuKα) = 8.548 mm^{-1}, D_{calc} = 1.470 g/cm^3, 95574 reflections measured (7.716° ≤ 2Θ ≤ 164.174°), 16447 unique (R_{int} = 0.3298, R_{sigma} = 0.2071) which were used in all calculations. The final R_1 was 0.1920 (I > 2σ(I)) and wR_2 was 0.4484 (all data).

1,8-dinaphthylimino-3,6-di(*tert*-butyl)-9-aluminium-dichloride-carbazole (**38**):

[$Naph_2carbAlCl_2$]

ARNLA2

$C_{42}H_{38}AlCl_2N_3$ (M =682.63 g/mol): monoclinic, space group $P2_1/c$ (no. 14), a = 15.5657(5) Å, b = 10.9412(3) Å, c = 26.0401(10) Å, β = 103.801(3)°, V = 4306.8(2) Å^3, Z = 4, T = 120(2) K, μ(CuKα) = 1.766 mm^{-1}, D_{calc} = 1.053 g/cm^3, 73352 reflections measured (7.974° ≤ 2Θ ≤ 156.414°), 9068 unique (R_{int} = 0.0778, R_{sigma} = 0.0337) which were used in all calculations. The final R_1 was 0.1140 (I > 2σ(I)) and wR_2 was 0.4037 (all data).

1,8-dinaphthylimino-3,6-di(*tert*-butyl)-9-gallium-dichloride-carbazole (**39**):

[$Naph_2carbGaCl_2$]

GARNLB2

$C_{42}H_{38}Cl_2GaN_3$ (M =725.37 g/mol): monoclinic, space group $P2_1/c$ (no. 14), a = 15.2658(3) Å, b = 10.9949(2) Å, c = 25.6823(5) Å, β = 102.755(2)°, V = 4204.29(15) Å^3, Z = 4, T = 120(2) K, μ(CuKα) = 2.282 mm^{-1}, D_{calc} = 1.146 g/cm^3, 46927 reflections measured (5.936° ≤ 2Θ ≤ 148.354°), 8461 unique (R_{int} = 0.0668, R_{sigma} = 0.0372) which were used in all calculations. The final R_1 was 0.0765 (I > 2σ(I)) and wR_2 was 0.2423 (all data).

{[1,8-dinaphthylimino-3,6-di(*tert*-butyl)-carbazole]$_2$-9-indium}chloride (**40**):

[$(Naph_2carb)_2In$]Cl

IRNLA2

$C_{82}H_{54}Cl_2InN_6$ (M =1397.81 g/mol): orthorhombic, space group *Pccn* (no. 56), a = 18.4997(11) Å, b = 18.6653(15) Å, c = 25.124(3) Å, V = 8675.5(12) Å^3, Z = 4, T = 120(2) K, μ(CuKα) = 3.638 mm^{-1}, D_{calc} = 1.070 g/cm^3, 68355 reflections measured (7.036° ≤ 2Θ ≤ 177.742°), 7625 unique

(R_{int} = 0.1989, R_{sigma} = 0.0948) which were used in all calculations. The final R_1 was 0.3182 (I > 2σ(I)) and wR_2 was 0.6558 (all data).

1,8-dinaphthylimino-3,6-di(*tert*-butyl)-9-germanium-chloride-carbazole (**41**):

[$Naph_2$carbGeCl]

GERNLC

$C_{48}H_{52}ClGeN_3$ (M =778.96 g/mol): monoclinic, space group $C2/c$ (no. 15), a = 24.0416(4) Å, b = 16.9146(3) Å, c = 21.2300(4) Å, β = 109.327(2)°, V = 8146.8(2) Å^3, Z = 8, T = 120(2) K, μ(CuKα) = 1.895 mm^{-1}, D_{calc} = 1.270 g/cm^3, 40338 reflections measured (6.518° ≤ 2Θ ≤ 147.128°), 8095 unique (R_{int} = 0.0310, R_{sigma} = 0.0165) which were used in all calculations. The final R_1 was 0.0561 (I > 2σ(I)) and wR_2 was 0.1551 (all data).

1,8-dinaphthylimino-3,6-di(*tert*-butyl)-9-germanium-iodide-carbazole (**41a**):

[$Naph_2$carbGeI]

GERNLE

$C_{48}H_{44}GeIN_3$ (M =862.35 g/mol): monoclinic, space group $C2/c$ (no. 15), a = 23.8278(4) Å, b = 17.2823(3) Å, c = 21.2367(4) Å, β = 110.438(2)°, V = 8194.8(3) Å^3, Z = 8, T = 120(2) K, μ(CuKα) = 7.200 mm^{-1}, D_{calc} = 1.398 g/cm^3, 50135 reflections measured (7.02° ≤ 2Θ ≤ 147.394°), 8204 unique (R_{int} = 0.0408, R_{sigma} = 0.0207) which were used in all calculations. The final R_1 was 0.0501 (I > 2σ(I)) and wR_2 was 0.1360 (all data).

1-naphthylimino-3,6-di(*tert*-butyl)-8-naphthyl-p-tolyl-amidine-9-germanium-chloride-carbazole (**41c**):

[$Naph_2$-*p*-tolylcarbGeCl]$_2$

GERNLD

$C_{55}H_{52}ClGeN_4$ (M =877.04 g/mol): triclinic, space group P-1 (no. 2), a = 12.751(4) Å, b = 15.192(5) Å, c = 15.486(5) Å, α = 97.60(3)°, β = 111.19(3)°, γ = 109.28(3)°, V = 2530.0(16) Å^3, Z = 2, T = 120(2) K, μ(CuKα) = 1.589 mm^{-1}, D_{calc} = 1.151 g/cm^3, 12167 reflections measured (7.662° ≤ 2Θ ≤ 148.548°), 8387 unique (R_{int} = 0.2776, R_{sigma} = 0.4816) which were used in all calculations. The final R_1 was 0.2305 (I > 2σ(I)) and wR_2 was 0.6156 (all data).

1,8-dinaphthylimino-3,6-di(*tert*-butyl)-9-germanium-hexamethyldisilazide-carbazole (**41d**):

[$Naph_2$carbGeHMDS]

GERNLI

$C_{48}H_{56}GeN_4Si_2$ (M =817.73 g/mol): monoclinic, space group $P2_1/n$ (no. 14), a = 18.563(2) Å, b = 11.8830(9) Å, c = 22.442(2) Å, β = 109.420(12)°, V = 4668.7(9) Å^3, Z = 4, T = 120(2) K, μ(CuKα) = 1.643 mm^{-1}, D_{calc} = 1.163 g/cm^3, 23356 reflections measured (7.548° ≤ 2Θ ≤ 147.586°),

9183 unique (R_{int} = 0.1237, R_{sigma} = 0.1653) which were used in all calculations. The final R_1 was 0.0940 (I > 2σ(I)) and wR_2 was 0.2538 (all data).

1,8-dinaphthylimino-3,6-di(*tert*-butyl)-9-tin-chloride-carbazole (**42**):

[$Naph_2carbSnCl$]

SNRNLC

$C_{48}H_{52}ClN_3Sn$ (M =825.06 g/mol): monoclinic, space group $C2/c$ (no. 15), a = 24.2095(4) Å, b = 16.7154(3) Å, c = 21.5861(4) Å, β = 108.871(2)°, V = 8265.7(3) Å^3, Z = 8, T = 120(2) K, μ(CuKα) = 5.779 mm^{-1}, D_{calc} = 1.326 g/cm^3, 18722 reflections measured (6.546° ≤ 2Θ ≤ 147.452°), 8162 unique (R_{int} = 0.0236, R_{sigma} = 0.0273) which were used in all calculations. The final R_1 was 0.0382 (I > 2σ(I)) and wR_2 was 0.0986 (all data).

1,8-dinaphthylimino-3,6-di(*tert*-butyl)-9-lead-bromide-carbazole (**43**):

[$Naph_2carbPbBr$]

PBRNLA (coordination polymer)

$C_{49}H_{46}BrN_3Pb$ (M =963.99 g/mol): monoclinic, space group $P2_1/n$ (no. 14), a = 11.90588(17) Å, b = 11.9122(2) Å, c = 28.5346(4) Å, β = 100.6768(14)°, V = 3976.86(11) Å^3, Z = 4, T = 120(2) K, μ(CuKα) = 9.712 mm^{-1}, D_{calc} = 1.610 g/cm^3, 31235 reflections measured (6.304° ≤ 2Θ ≤ 147.228°), 7912 unique (R_{int} = 0.0551, R_{sigma} = 0.0460) which were used in all calculations. The final R_1 was 0.0290 (I > 2σ(I)) and wR_2 was 0.0646 (all data).

PBRNLC (monomeric)

$C_{57}H_{53}BrN_3Pb$ (M =1067.12 g/mol): monoclinic, space group $I2/m$ (no. 12), a = 13.88064(8) Å, b = 13.88089(13) Å, c = 24.57540(13) Å, β = 92.6017(5)°, V = 4730.20(6) Å^3, Z = 4, T = 120(2) K, μ(CuKα) = 8.226 mm^{-1}, D_{calc} = 1.498 g/cm^3, 81682 reflections measured (7.178° ≤ 2Θ ≤ 147.404°), 4961 unique (R_{int} = 0.0348, R_{sigma} = 0.0112) which were used in all calculations. The final R_1 was 0.0176 (I > 2σ(I)) and wR_2 was 0.0445 (all data).

8-(Ar*)imino-1,2,3,4-Tetrahydro-9-magnesium-iodide-carbazole (**44**):

[Ar*THCarbMgI]$_2$

MGRNLP

$C_{70}H_{63}IMgN_2$ (M =1083.43 g/mol): triclinic, space group P-1 (no. 2), a = 11.2908(4) Å, b = 15.1945(8) Å, c = 16.4624(9) Å, α = 94.376(4)°, β = 97.132(4)°, γ = 90.566(4)°, V = 2793.7(2) Å^3, Z = 2, T = 120(2) K, μ(CuKα) = 4.939 mm^{-1}, D_{calc} = 1.288 g/cm^3, 23851 reflections measured (5.426° ≤ 2Θ ≤ 148.032°), 11000 unique (R_{int} = 0.0871, R_{sigma} = 0.1023) which were used in all calculations. The final R_1 was 0.1472 (I > 2σ(I)) and wR_2 was 0.4013 (all data).

8-(Ar*)imino-1,2,3,4-Tetrahydro-9-zinc-methyl-carbazole (**45**):

[Ar*THCarbZnMe]

ZNRNLH

$C_{47}H_{42}N_2Zn$ (M =700.19 g/mol): triclinic, space group P-1 (no. 2), a = 10.8707(5) Å, b = 11.1400(4) Å, c = 15.4029(4) Å, α = 84.028(3)°, β = 78.719(3)°, γ = 80.456(4)°, V = 1798.99(12) Å^3, Z = 2, T = 120(2) K, μ(CuKα) = 1.211 mm^{-1}, D_{calc} = 1.293 g/cm^3, 28447 reflections measured (8.07° ≤ 2Θ ≤ 148.824°), 7016 unique (R_{int} = 0.0330, R_{sigma} = 0.0265) which were used in all calculations. The final R_1 was 0.0430 (I > 2σ(I)) and wR_2 was 0.1275 (all data).

α-(Diphenylphosphinyl)-Benzenemethanol (**56a**):

CCDC 1874672

ORNAMF

$C_{19}H_{17}O_2P$ (M =308.29 g/mol): monoclinic, space group $P2_1/n$ (no. 14), a = 11.1904(3) Å, b = 6.27332(19) Å, c = 21.7667(6) Å, β = 92.093(3)°, V = 1527.03(8) Å^3, Z = 4, T = 120(2) K, μ(CuKα) = 1.626 mm^{-1}, D_{calc} = 1.341 g/cm^3, 11530 reflections measured (8.13° ≤ 2Θ ≤ 146.418°), 3009 unique (R_{int} = 0.0409, R_{sigma} = 0.0237) which were used in all calculations. The final R_1 was 0.0389 (I > 2σ(I)) and wR_2 was 0.1047 (all data).

[Ru(*p*-cym){$Ph_2PC(=O)N(H)^iPr$}Cl_2] (**57**):

RUHRSB

$C_{32}H_{38}Cl_2NOPRu$ (M =655.57 g/mol): triclinic, space group P-1 (no. 2), a = 10.6269(9) Å, b = 12.5033(13) Å, c = 12.5086(9) Å, α = 88.346(7)°, β = 89.950(6)°, γ = 66.060(9)°, V = 1518.3(2) Å^3, Z = 2, T = 120(2) K, μ(Cu$K\alpha$) = 6.486 mm^{-1}, D_{calc} = 1.434 g/cm^3, 10786 reflections measured (7.07° ≤ 2Θ ≤ 147.608°), 5905 unique (R_{int} = 0.0274, R_{sigma} = 0.0369) which were used in all calculations. The final R_1 was 0.0248 (I > 2σ(I)) and wR_2 was 0.0634 (all data).

[Ru(*p*-cym){$Ph_2PC(=O)N(H)$Ph}Cl_2] (**58**):

TLWDKB

$C_{29}H_{30}Cl_2NOPRu$ (M =611.48 g/mol): monoclinic, space group $P2_1/n$ (no. 14), a = 11.40808(12) Å, b = 12.68260(10) Å, c = 18.88149(19) Å, β = 106.7865(11)°, V = 2615.44(5) Å^3, Z = 4, T = 120(2) K, μ(Cu$K\alpha$) = 7.488 mm^{-1}, D_{calc} = 1.553 g/cm^3, 25745 reflections measured (8.16° ≤ 2Θ ≤ 154.218°), 5403 unique (R_{int} = 0.0348, R_{sigma} = 0.0164) which were used in all calculations. The final R_1 was 0.0321 (I > 2σ(I)) and wR_2 was 0.0895 (all data).

[Ru(*p*-cym){$Ph_2PC(=O)N(H)$*p*-tolyl}Cl_2] (**59**):

RUHRSA

$C_{30}H_{32}Cl_2NOPRu$ (M =625.50 g/mol): monoclinic, space group $P2_1/n$ (no. 14), a = 9.83232(16) Å, b = 16.1381(2) Å, c = 17.4667(2) Å, β = 102.2783(14)°, V = 2708.14(7) Å^3, Z = 4, T = 120(2) K, μ(Cu$K\alpha$) = 7.246 mm^{-1}, D_{calc} = 1.534 g/cm^3, 20656 reflections measured (7.54° ≤ 2Θ ≤ 147.554°), 5362 unique (R_{int} = 0.0289, R_{sigma} = 0.0216) which were used in all calculations. The final R_1 was 0.0204 ($I > 2\sigma(I)$) and wR_2 was 0.0510 (all data).

[Ru(*p*-cym){Ph_2PC(=O)N(Ph)C(=O)N(*H*)Ph}Cl_2] (**60**):

TLWDKA

$C_{36}H_{35}Cl_2N_2O_2PRu$ (M =730.60 g/mol): triclinic, space group P-1 (no. 2), a = 10.3423(2) Å, b = 13.3792(3) Å, c = 15.2168(3) Å, α = 103.818(2)°, β = 90.321(2)°, γ = 100.687(2)°, V = 2006.42(7) Å^3, Z = 2, T = 120(2) K, μ(Cu$K\alpha$) = 4.991 mm^{-1}, D_{calc} = 1.209 g/cm^3, 23223 reflections measured (6.934° ≤ 2Θ ≤ 147.79°), 7894 unique (R_{int} = 0.0288, R_{sigma} = 0.0269) which were used in all calculations. The final R_1 was 0.0322 ($I > 2\sigma(I)$) and wR_2 was 0.0812 (all data).

[Ru(*p*-cym){Ph_2PC(=O)N(*p*-tolyl)C(=O)N(*H*)*p*-tolyl}Cl_2] (**61**):

RUHRSC

$C_{45}H_{47}Cl_2N_2O_2PRu$ (M =850.78 g/mol): monoclinic, space group $P2_1/c$ (no. 14), a = 13.7569(4) Å, b = 11.3299(3) Å, c = 25.8146(10) Å, β = 96.096(3)°, V = 4000.8(2) Å^3, Z = 4, T = 120(2) K, μ(Cu$K\alpha$) = 5.088 mm^{-1}, D_{calc} = 1.412 g/cm^3, 18329 reflections measured (6.462° ≤ 2Θ ≤ 147.096°), 7855 unique (R_{int} = 0.0422, R_{sigma} = 0.0457) which were used in all calculations. The final R_1 was 0.0516 ($I > 2\sigma(I)$) and wR_2 was 0.1219 (all data).

DFT-Geometry Optimisation Structures

Geometry Optimised Coordinates for 62a'

Ru	1.66459135	6.11988229	2.74180261
Cl	3.54302003	6.49741122	4.25646446
C	0.08363036	2.58218396	2.66461630
P	0.35909660	7.05615155	4.37469351
O	0.46294987	7.09081510	7.07634153
O	1.41656334	2.89771277	5.66258181
N	1.22196307	5.09909923	6.22831957
N	1.27371912	4.35688340	3.89600596
H	-0.85922739	3.02852040	2.98293387
C	3.09257972	6.82601709	1.00220398
C	2.02744737	7.75010282	1.15656985
H	2.23452948	8.80010106	1.34793729
C	0.67676828	7.29222983	1.15087382
H	-0.12530415	8.01450348	1.30855656
C	0.33720357	5.93273942	0.85182958
C	1.42617807	5.03214762	0.70446240
H	1.21114040	3.97321593	0.56034034
C	2.77332911	5.45230395	0.77269777
H	3.57107662	4.71638474	0.68710232
C	4.55325355	7.24050140	1.00815250
H	5.07126537	6.51560038	1.65684832
C	5.11630700	7.10592728	-0.42456924
H	4.97792445	6.09453624	-0.82872616
H	6.19237627	7.32904128	-0.42556448
H	4.62217200	7.81360237	-1.10640219
C	4.82101558	8.64000445	1.56834391
H	4.36697227	9.42428243	0.94404950
H	5.90338130	8.82667514	1.58834002
H	4.44873027	8.72876519	2.59668310
C	-1.08304042	5.49609571	0.63943896
H	-1.37644991	5.67315822	-0.40822829
H	-1.77820693	6.05273405	1.28026603
H	-1.19890162	4.42484396	0.84350573
C	-1.45174065	6.76212738	4.18284123
C	-2.26255692	7.68283757	3.49541697
H	-1.84118115	8.62747693	3.14919054
C	-3.61569414	7.41174429	3.27716433
H	-4.23400075	8.14068594	2.75108060
C	-4.17643509	6.21765374	3.73888399
H	-5.23392303	6.00804064	3.57220698
C	-3.37723027	5.29654524	4.42175371
H	-3.80898517	4.36562844	4.79233985
C	-2.02420911	5.56376447	4.64199555
H	-1.41511925	4.83440564	5.17590512
C	0.49835035	8.85925782	4.70371706
C	-0.47411763	9.54098767	5.45607854
H	-1.35174167	9.01231559	5.82348326
C	-0.30842020	10.89523792	5.74922525
H	-1.06575975	11.41577765	6.33697555
C	0.82873511	11.57781402	5.30626508
H	0.95642155	12.63573644	5.54120489
C	1.80744190	10.89937183	4.57646197
H	2.70717000	11.42154985	4.24857176
C	1.64585793	9.54370119	4.27932041
H	2.42643513	8.99526829	3.75240482
C	0.70211508	6.36209830	6.12045832
C	1.61074643	4.68851314	7.57080818
C	2.92458356	4.91969981	7.97738094
H	3.62265639	5.38561153	7.28177107
C	3.31878856	4.54579693	9.26491396
H	4.34605180	4.72100771	9.58742132
C	2.40173212	3.94953164	10.13441153
H	2.71171452	3.65737610	11.13920997
C	1.08547998	3.72746293	9.71668465
H	0.36799380	3.25974386	10.39215018
C	0.68605029	4.09786199	8.43171911
H	-0.33372315	3.92142664	8.09151522
C	1.32998793	4.04754081	5.21749025
C	1.28549092	3.15740708	3.09588778
C	2.50098975	2.56487378	2.72370761
H	3.43063860	3.00046737	3.09159461
C	2.51143371	1.43484643	1.90479454
H	3.46272891	0.97794300	1.62602216
C	1.30915449	0.87548708	1.45470979
H	1.31937738	-0.00967980	0.81736330
C	0.09558442	1.44943970	1.84432220
H	-0.84734769	1.00860201	1.51583715

Geometry Optimised Coordinates for 62b'

Ru	1.57603423	5.89635135	2.73652462
Cl	3.42517089	6.51644187	4.20372521
C	0.01889774	2.38113994	2.87477297
P	0.26307591	6.87086694	4.34228409
O	0.56512094	7.11895188	7.01963156
O	1.51160845	2.84795044	5.85594641
N	1.31437473	5.08324877	6.27496059
N	1.26286727	4.18897419	4.00356407
H	-0.90977341	2.88398892	3.14679638
C	3.14785203	5.92043752	0.92623550
C	2.48593769	7.18523016	1.14046885
H	3.09041221	8.06929165	1.34049247
C	1.07960641	7.29630467	1.06181139
H	0.61387508	8.27518821	1.18260111
C	0.25289476	6.14078379	0.83890348
C	0.90980457	4.88993771	0.79589047
H	0.32547957	3.97505426	0.72220755
C	2.34330683	4.78723249	0.77241482
H	2.80003438	3.80131397	0.70188144
C	4.64273517	5.84331146	0.98218835
H	5.09074958	6.52169317	0.24114621
C	1.18678501	0.53590695	1.82183629
C	-0.00638159	1.18608788	2.14796369
H	1.16808550	-0.39897839	1.26015853
H	-0.96324435	0.75680313	1.84548650
C	2.40545600	1.08482378	2.23826393
H	3.34127920	0.57160321	2.00900442
H	3.37466488	2.70360272	3.30615948
C	2.43137331	2.27847808	2.96128324
C	-1.22570952	6.31543220	0.55743889
C	1.23690010	2.94286527	3.27733642
C	1.38637978	3.96254152	5.33765562
H	-1.58664675	7.12955947	1.20597861
C	-1.54320779	6.48560046	4.32373651
C	-2.46520660	7.35634304	3.71726524
H	-2.12634872	8.30685312	3.30419190
C	-3.82325549	7.03196986	3.67075845
H	-4.52727709	7.72319681	3.20486908
C	-4.27907422	5.83433265	4.22749756
H	-5.34075737	5.58489880	4.19705903
C	-3.36948228	4.96220236	4.83242092
H	-3.71756449	4.02932112	5.27809944
C	-2.01082465	5.28153464	4.87931641
H	-1.31617611	4.59087581	5.35679745
C	0.32375654	8.70064050	4.52782520
C	-0.59907452	9.37908036	5.34341075
H	-1.37648759	8.82538102	5.86670444
C	-0.51355378	10.76352353	5.49635525
H	-1.23299054	11.27988255	6.13341738
C	0.49471120	11.48313449	4.84794356
H	0.55841824	12.56567890	4.96995574
C	1.43014227	10.81085108	4.05806630
H	2.23430412	11.36409491	3.57065753
C	1.34918701	9.42447818	3.90294844
H	2.10424236	8.88995279	3.32793531
C	0.75679345	6.32332148	6.10764334
C	1.82243612	4.79577108	7.60883502
C	3.15355448	5.10602480	7.88652349
H	3.77262335	5.53992654	7.10104366
C	3.66465933	4.85301364	9.16190044
H	4.70628601	5.09089634	9.38292833
C	2.84555246	4.29845450	10.14889484
H	3.24619240	4.10113130	11.14424874
C	1.51104068	3.99600211	9.85955355
H	0.86978818	3.55988090	10.62675871
C	0.99484261	4.24555637	8.58704846
H	-0.04082212	4.00639135	8.34731802
C	-1.39233693	6.77674987	-0.90793021
C	-2.07865225	5.07644866	0.84078942
H	-1.83153606	4.24899813	0.15994367
H	-3.14032995	5.31478878	0.69353612
H	-1.94952307	4.72881212	1.87320725
H	4.99888816	4.82482645	0.78883967
H	4.98806213	6.15650959	1.98111379
H	-0.81854385	7.69037583	-1.11629308
H	-2.45072619	6.98184102	-1.12209210
H	-1.04900602	5.99544882	-1.60185748

Geometry Optimised Coordinates for 63a'

Ru	2.52821822	11.60552066	2.79354076
H	-0.65091377	9.96995533	-0.54103749
Cl	0.51799563	12.50273940	3.85262706
P	2.94864637	10.71686396	4.87256925
O	4.06943196	15.01611127	5.04950896
O	2.27658915	11.55711258	7.35270022
N	3.61866856	13.23520102	3.66765909
H	-0.14957112	11.31667356	-1.58861135
N	2.87528165	13.30960989	5.99209819
C	4.44620324	13.93348572	2.71690794
C	5.79959703	13.60990373	2.57295805
H	6.23281561	12.84363201	3.21726415
C	6.58777821	14.26224755	1.61908800
H	7.64349385	13.99692143	1.52374192
C	6.05268567	15.25782599	0.79042011
C	4.69496501	15.58377865	0.95401659
H	4.25373672	16.36866284	0.33483994
C	3.90397513	14.93776906	1.90269232
H	2.85658061	15.21168051	2.03388652
C	6.90761590	15.98419396	-0.21962129
H	6.40862947	16.05060481	-1.19744355
H	7.87303914	15.48116258	-0.36346856
H	7.11541294	17.01488662	0.10781063
C	3.55434299	13.91189869	4.84219406
C	2.47858581	14.25235588	7.02682713
C	1.22220420	14.84645689	6.93479871
H	0.57471822	14.59529311	6.09423118
C	0.81488547	15.75104357	7.91863039
H	-0.16952360	16.21752909	7.84127504
C	1.64526436	16.06787565	9.00158012
C	2.90410464	15.44805319	9.07466392
H	3.56964911	15.67825774	9.90960300
C	3.32260239	14.54710944	8.09769062
H	4.30406195	14.07760793	8.15926562
C	1.20737782	17.04708336	10.06407525
H	1.22093735	16.58366354	11.06215365
H	0.18994002	17.41267251	9.87496859
H	1.87783047	17.91904038	10.10200841
C	2.66229663	11.98518279	6.27121390
C	0.65123456	9.10389672	4.84740045
H	0.32787330	9.76407349	4.04303748
C	-0.18516639	8.08228950	5.30419716
H	-1.15359663	7.92263408	4.82765004
C	0.20886752	7.28013774	6.37773544
H	-0.44437263	6.48191677	6.73407890
C	1.43576582	7.51325122	7.00604848
H	1.73890982	6.90597538	7.86004788
C	2.27364927	8.53407365	6.55505750
H	3.21772592	8.72070541	7.06435720
C	1.89469426	9.32560327	5.45699793
C	4.67019298	10.13710114	5.19377139
C	5.03413263	8.80057905	4.94993373
H	4.27988703	8.08015149	4.63046438
C	6.35011320	8.37567110	5.14706664
H	6.61351535	7.33250698	4.96495791
C	7.32207186	9.27981172	5.58454574
H	8.34825138	8.94635072	5.74456018
C	6.97041422	10.61091853	5.82408357
H	7.72079523	11.32175484	6.17357997
C	5.65522550	11.03978297	5.62927993
H	5.39912346	12.08064275	5.82733005
C	3.90284105	10.41622028	1.35042537
C	3.66045816	11.69498088	0.79483448
H	4.51267251	12.33733929	0.57312156
C	2.35036434	12.17539613	0.50369482
H	2.23400419	13.17022608	0.08148029
C	1.21908293	11.39674586	0.83425747
C	1.43054809	10.12781159	1.45991926
H	0.57261623	9.52554510	1.75463862
C	2.74312211	9.66580638	1.74417746
H	2.87026930	8.69875687	2.23284408
C	5.29326124	9.86601568	1.47787256
H	6.03387419	10.67477312	1.50788013
H	5.52413083	9.22878509	0.60881900
H	5.40983057	9.25488825	2.38163597
C	-0.20090922	11.83856057	0.53954066
H	-0.79887158	11.54981384	1.41857118
C	-0.36435611	13.34962264	0.34695764

H	0.01004051	13.89737221	1.22115385
H	0.15571567	13.70631375	-0.55463981
H	-1.42882320	13.59186333	0.22513654
C	-0.72242048	11.05661331	-0.68640906
H	-1.77659812	11.30743364	-0.86898042

Geometry Optimised Coordinates for 63b'

Ru	2.77430556	11.36081923	2.73076179
C	0.35109195	12.06500956	0.26169715
Cl	0.73238653	12.25075959	3.72737961
P	3.20597728	10.57320404	4.84239118
O	4.15335950	14.93037345	4.83496440
O	2.50263362	11.49926651	7.28365442
N	3.79238233	13.07566619	3.52565022
H	0.57121305	12.97067292	-0.31585759
N	3.05366248	13.20931359	5.85432061
C	4.53975308	13.80809093	2.53267536
C	5.90521155	13.57370610	2.34525117
H	6.41031003	12.84708997	2.98249223
C	6.61978672	14.27041666	1.36490003
H	7.68697474	14.07295939	1.23819255
C	5.99617101	15.22596304	0.55207127
C	4.62674675	15.46673127	0.76088371
H	4.11731233	16.22224257	0.15750076
C	3.90859591	14.77290053	1.73328086
H	2.85099353	14.98206040	1.89954501
C	6.76791392	15.99590165	-0.49217434
H	6.26699758	15.96102073	-1.47103958
H	7.78236186	15.59492007	-0.61631653
H	6.85992829	17.05736745	-0.21474339
C	3.69540536	13.79369768	4.67448762
C	2.63974779	14.17855859	6.85824346
C	1.37779044	14.75642190	6.74017491
H	0.73891297	14.47399578	5.90299465
C	0.95254273	15.68276310	7.69544661
H	-0.03697721	16.13445367	7.59800924
C	1.77046183	16.03803615	8.77632930
C	3.03389455	15.43222391	8.87762253
H	3.68808480	15.68926091	9.71372625
C	3.47049739	14.50970021	7.92857794
H	4.45465387	14.04950459	8.01395399
C	1.31868825	17.05292109	9.79914671
H	1.48249412	16.68854214	10.82356152
H	0.25182402	17.28568583	9.68639197
H	1.87926238	17.99519496	9.69588017
C	2.87546374	11.89199195	6.18414577
C	0.99150872	8.84826503	4.81827981
H	0.68774135	9.42467443	3.94539021
C	0.17830844	7.82182302	5.30564200
H	-0.74873329	7.57326759	4.78683889
C	0.54331640	7.12809180	6.46168909
H	-0.09116988	6.32589895	6.84214342
C	1.71483198	7.47590716	7.14098417
H	1.99247734	6.95406320	8.05784058
C	2.52928908	8.50139954	6.65893000
H	3.42832585	8.77830153	7.20647826
C	2.18227256	9.18257895	5.47907752
C	4.93983886	10.06807376	5.22690155
C	5.33842932	8.72230859	5.14507260
H	4.60376673	7.94952692	4.91717579
C	6.66504764	8.35912460	5.38937779
H	6.95576478	7.30898489	5.33102921
C	7.61166196	9.33326480	5.71668445
H	8.64630165	9.04800871	5.91282233
C	7.22440167	10.67371519	5.80097349
H	7.95427585	11.44039421	6.06501969
C	5.89964137	11.04158159	5.55603966
H	5.61606458	12.09130590	5.62964367
C	3.99795564	9.88392266	1.40944709
C	4.05824091	11.17979937	0.84837309
H	5.02421907	11.65587983	0.69159471
C	2.87883408	11.87309053	0.41044536
H	2.98334339	12.85636253	-0.04543361
C	1.60579283	11.33937058	0.64106309
C	1.52225094	10.09137878	1.35706705
H	0.54095613	9.69200834	1.60985072
C	2.68796365	9.37137998	1.70648082

H	2.58922461	8.41065496	2.21365478
C	5.21475885	9.00039641	1.59860700
H	5.05029449	8.41072184	2.51490423
C	6.53452365	9.75870396	1.76231263
C	5.28742140	8.01232165	0.41317966
H	6.12060741	7.30988320	0.55588237
H	5.45286039	8.55054642	-0.53170363
H	4.36219120	7.42843427	0.31251879
H	-0.30379713	11.41336002	-0.33558328
H	-0.19563302	12.35101081	1.17521593
H	7.34733131	9.04918746	1.96678392
H	6.48608219	10.46826668	2.59737018
H	6.80364677	10.31070330	0.85034673

References

(1) Nguyen, T.; Sutton, A. D.; Brynda, M.; Fettinger, J. C.; Long, G. J.; Power, P. P. Synthesis of a Stable Compound with Fivefold Bonding between Two Chromium(I) Centers. *Science* **2005**, *310*, 844–847.

(2) Blake, M.; Kaltsoyannis, N.; Mountford, P. Heterobimetallic Complexes Containing Ca-Fe or Yb-Fe Bonds: Synthesis and Molecular and Electronic Structures of $[M\{CpFe(CO)_2\}(_2)(THF)_3]_2$ (M = Ca or Yb). *J. Am. Chem. Soc.* **2011**, *133*, 15358–15361.

(3) Blake, M. P.; Kaltsoyannis, N.; Mountford, P. Synthesis and Reactions of β-Diketiminate-Supported Complexes with Mg-Fe or Yb-Fe Bonds. *Chem. Commun.* **2013**, *49*, 3315–3317.

(4) Green, S. P.; Jones, C.; Stasch, A. Stable Magnesium(I) Compounds with Mg-Mg Bonds. *Science* **2007**, *318*, 1754–1757.

(5) Morgan, G. T.; Keith Drew, H. D. Researches on Residual Affinity and Co-Ordination. Acetylacetones of Selenium and Tellurium. *J. Chem. Soc., Trans.* **1920**, 1456–1465.

(6) *Nomenclature of Inorganic Chemistry: IUPAC Recomendations*; 2005.

(7) McNaught, A. D.; Wilkinson, A.; Scientific, B. IUPAC. Compendium of Chemical Terminology, 2nd Ed. *Compend. Chem. Terminol. 2nd ed. (the "Gold Book")* **2014**, 1670.

(8) Portnoy, M.; Milstein, D. Chelate Effect on the Structure and Reactivity of Electron-Rich Palladium Complexes and Its Relevance to Catalysis. *Organometallics* **1993**, *12*, 1655–1664.

(9) Lawrance, G. A. *Introduction to Coordination Chemistry*; Wiley, 2009.

(10) Wilkinson, G.; Gillard, R. D.; McClevery, J. A. *Comprehensive Coordination Chemistry*; Pergamon Press, 1987.

(11) Bauer, G.; Hu, X. Recent Developments of Iron Pincer Complexes for Catalytic Applications. *Inorg. Chem. Front.* **2016**, *3*, 741–765.

(12) van Koten, G.; Jastrzebski, J. T. B. H.; Noltes, J. G.; Spek, A. L.; Schoone, J. C. Triorganotin Cations Stabilized by Intramolecular Sn-N Coordination; Synthesis and Characterisation of {C,N,N'-2,6-Bis[(Dimethylamino)Methyl]Phenyl}diorganotin Bromides. *J. Organomet.* **1978**, 233–245.

(13) Moulton, B. C. J.; Shaw, B. L. Transition Metal-Carbon Bonds. Part XLII. Complexes of Nickel, Palladium, Platinum, Rhodium and Iridium with the Tridentate Ligand 2,6-Bis[(Di-*t*-Butylphophino)Methyl]Phenyl. *J. Chem. Soc. Dalton Trans.* **1976**, 1020–1024.

(14) Creaser, C. S.; Kaska, W. C. Complexes of 1,3-Bis(Dimethylphosphinomethyl)Benzene with Nickel(II), Paladium(II) and Iron(II) Halides. *Inorganica Chim. Acta* **1978**, *30*, L325–L326.

(15) Koten, G. Van. Tuning the Reactivity of Metals Held in a Rigid Ligand Environment. *Pure Appl. Chem.* **1989**, *61*, 1681–1694.

(16) Lu, Z.; White, C.; Rheingold, A. L.; Crabtree, R. H. Deprotonated Thioamides as Thiolate S-Donor Ligands with a High Tendency to Avoid M-S-M Bridge Formation: Crystal and Molecular Structure of $[Ni(TmtssA)]_2$. *Inorg. Chem.* **1993**, *32*, 3991–3994.

(17) Vila, J. M.; Pereira, M. T.; Ortigueira, J. M.; Grana, M.; Lata, D.; Suárez, A.; Fernández, J. J.; Fernández, A.; López-torres, M.; Adams, H. Formation, Characterization, and Structural Studies of Novel Thiosemicarbazone Palladium(II) Complexes. *J. Chem. Soc. Dalton Trans.* **1999**, 4193–4201.

(18) Wang, L.; Pan, H. R.; Yang, Q.; Fu, H. Y.; Chen, H.; Li, R. X. A Family of Novel Cationic Ruthenium Pincer Complexes: Synthesis, Characterization and Catalytic Activity in the Transfer Hydrogenation of Ketones. *Inorg. Chem. Commun.* **2011**, *14*, 1422–1427.

(19) Lawrence, M. A. W.; Jackson, Y. A.; Mulder, W. H.; Björemark, P. M.; Håkansson, M. Synthesis and Structure of a Novel Substituted Benzothiazolyl-N-Phenyl-2-Pyridinecarbothioamide; Kinetics of Formation and Electrochemistry of Two of Its Palladium Pincer Complexes. *Aust. J. Chem.* **2015**, *68*, 731–741.

(20) Bakir, M.; Lawrence, M. A. W.; Singh-Wilmot, M. Synthesis and Characterization of a Cadmium-Dichloro Compound of N,N,O-Di-2-Pyridyl Ketone Thiophene-2-Carboxylic Acid Hydrazone (η^3-Dpktch). The Structure of $[CdCl_2(\eta^3\text{-Dpktch})]$. *J. Coord. Chem.* **2007**, *60*, 2385–2399.

(21) Arashiba, K.; Miyake, Y.; Nishibayashi, Y. A Molybdenum Complex Bearing PNP-Type Pincer Ligands Leads to the Catalytic Reduction of Dinitrogen into Ammonia. *Nat. Chem.* **2011**, *3*, 120–125.

(22) Peris, E.; Loch, J. A.; Mata, J.; Crabtree, R. H. A Pd Complex of a Tridentate Pincer CNC Bis-Carbene Ligand as a Robust Homogenous Heck Catalyst. *Chem. Commun.* **2001**, 201–202.

(23) Teratani, T.; Koizumi, T.; Yamamoto, T.; Tanaka, K.; Kanbara, T. Deprotonation/Protonation of Coordinated Secondary Thioamide Aunits of Pincer Ruthenium Complexes: Modulation of Voltammetric and Spectroscopic Characterisationof the Pincer Complexes. *Dalton Trans.*

2011, *40*, 8879–8886.
(24) Charette, B. J.; Ritch, J. S. A Selenium-Containing Diarylamido Pincer Ligand: Synthesis and Coordination Chemistry with Group 10 Metals. *Inorg. Chem.* **2016**, *55*, 6344–6350.
(25) Lawrence, M. A. W.; Green, K.-A.; Nelson, P. N.; Lorraine, S. C. Review: Pincer Ligands—Tunable, Versatile and Applicable. *Polyhedron* **2018**, *143*, 11–27.
(26) Gosiewska, S.; Veld, M. H. in t.; de Pater, J. J. M.; Bruijnincx, P. C. A.; Lutz, M.; Spek, A. L.; van Koten, G.; Klein Gebbink, R. J. M. Novel Enantiopure Non-C_2-Symmetric NCN-Pincer Palladium Complexes with L-Proline Chiral Auxiliaries: *mer* η^3-N,C,N versus Square Planar η^4-N,C,N,O Coordination. *Tetrahedron Asymmetry* **2006**, *17*, 674–686.
(27) Yang, M. J.; Liu, Y. J.; Gong, J. F.; Song, M. P. Unsymmetrical Chiral PCN Pincer Palladium(II) and Nickel(II) Complexes with Aryl-Based Aminophosphine-Imidazoline Ligands: Synthesis via Aryl C-H Activation and Asymmetric Addition of Diarylphosphines to Enones. *Organometallics* **2011**, *30*, 3793–3803.
(28) Bourget-Merle, L.; Lappert, M. F.; Severn, J. R. The Chemistry of SS-Diketiminatometal Complexes. *Chem. Rev.* **2002**, *102*, 3031–3065.
(29) Schulz, S.; Spielmann, J.; Bläser, D.; Wölper, C. X-Ray Crystal Structure of a Heterobimetallic Al-Zn-Oxide Complex. *Chem. Commun.* **2011**, *47*, 2676–2678.
(30) Yow, S.; Gates, S. J.; White, A. J. P.; Crimmin, M. R. Zirconocene Dichloride Catalyzed Hydrodefluorination of C-sp^2-F Bonds. *Angew. Chemie - Int. Ed.* **2012**, *51*, 12559–12563.
(31) Aguila, M. J. B.; Badiei, Y. M.; Warren, T. H. Mechanistic Insights into C−H Amination *via* Dicopper Nitrenes. *J. Am. Chem. Soc.* **2013**, *135*, 9399–9406.
(32) Sunatsuki, Y.; Motoda, Y.; Matsumoto, N. Copper(II) Complexes with Multidentate Schiff-Base Ligands Containing Imidazole Groups: Ligand-Complex or Self-Complementary Molecule? *Coord. Chem. Rev.* **2002**, *226*, 199–209.
(33) Sadimenko, A. P.; Basson, S. S. Organometallic Complexes of Heterocycles II. Complexes of Pyrazoles. *Coord. Chem. Rev.* **1996**, *147*, 247–297.
(34) Poyatos, M.; Maisse-François, A.; Bellemin-Laponnaz, S.; Gade, L. H. Coordination Chemistry of a Modular N,C-Chelating Oxazole-Carbene Ligand and Its Applications in Hydrosilylation Catalysis. *Organometallics* **2006**, *25*, 2634–2641.
(35) Janiak, C. A Critical Account on π-π Stacking in Metal Complexes with Aromatic Nitrogen-Containing Ligands. *J. Chem. Soc. Dalton Trans.* **2000**, 3885–3896.
(36) Sadinenko, A. P.; Gamovskii, A. D.; Retta, N. Organometallic Complexes of Heterocycles. I. σ,π-Complexes of Five-Membered Monoheterocycles. *Coord. Chem. Rev.* **1993**, *126*, 237–318.
(37) Graebe, C.; Glazer, C. Ueber Synthesen des Carbazols. *Ber. Dtsch. Chem. Ges.* **1872**, *5*, 376-378.
(38) Yaqub, G.; Hussain, E. A.; Rehman, M. A.; Mateen, B. Advancements in Syntheses of Carbazole and Its Dervatives. *Asian J. Chem.* **2009**, *21*, 2485–2520.
(39) Murphy, J. J.; Bastida, D.; Paria, S.; Fagnoni, M.; Melchiorre, P. Asymmetric Catalytic Formation of Quaternary Carbons by Iminium Ion Trapping of Radicals. *Nature* **2016**, *532*, 218–222.
(40) Cheng, C.; Kim, B. G.; Guironnet, D.; Brookhart, M.; Guan, C.; Wang, D. Y.; Krogh-Jespersen, K.; Goldman, A. S. Synthesis and Characterization of Carbazolide-Based Iridium PNP Pincer Complexes. Mechanistic and Computational Investigation of Alkene Hydrogenation: Evidence for an Ir(III)/Ir(V)/Ir(III) Catalytic Cycle. *J. Am. Chem. Soc.* **2014**, *136*, 6672–6683.
(41) Moser, M.; Wucher, B.; Kunz, D.; Rominger, F. 1,8-Bis(Imidazolin-2-yliden-1-yl)Carbazolide (Bimca): A New CNC Pincer-Type Ligand with Strong Electron-Donating Properties. Facile Oxidative Addition of Methyl Iodide to Rh(Bimca)(CO). *Organometallics* **2007**, *26*, 1024–1030.
(42) Johnson, K. R. D.; Hayes, P. G. Synthesis and Reactivity of Dialkyl Lutetium Complexes Supported by a Novel Bis(Phosphinimine)Carbazole Pincer Ligand. *Organometallics* **2009**, *28*, 6352–6361.
(43) Barbe, J. M.; Habermeyer, B.; Khoury, T.; Gros, C. P.; Richard, P.; Chen, P.; Kadish, K. M. Three-Metal Coordination by Novel Bisporphyrin Architectures. *Inorg. Chem.* **2010**, *49*, 8929–8940.
(44) Gaunt, J. A.; Gibson, V. C.; Haynes, A.; Spitzmesser, S. K.; White, A. J. P.; Williams, D. J. Bis(Imino)Carbazolide Complexes of Rhodium: Highly Nucleophilic Ligands Exerting a Dramatic Accelerating Effect on MeI Oxidative Addition. *Organometallics* **2004**, *23*, 1015–1023.
(45) Ashley, A. E.; Cowley, A. R.; Green, J. C.; Johnston, D. R.; Watkin, D. J.; Kays, D. L. Synthesis and Characterisation of Low-Coordinate Transition-Metal Complexes Stabilised by Sterically Demanding Carbazolido Ligands. *Eur. J. Inorg. Chem.* **2009**, 2547–2552.

(46) Blake, A. J.; Lewis, W.; McMaster, J.; Moorhouse, R. S.; Moxey, G. J.; Kays, D. L. Amido Analogues of Zincocenes and Cadmocenes. *Dalton Trans.* **2011**, *40*, 1641–1645.
(47) Moorhouse, R. S.; Moxey, G. J.; Ortu, F.; Reade, T. J.; Lewis, W.; Blake, A. J.; Kays, D. L. Structural Diversity in Alkali Metal Complexes of Sterically Demanding Carbazol-9-yl Ligands. *Inorg Chem* **2013**, *52*, 2678–2683.
(48) Ortu, F.; Moxey, G. J.; Blake, A. J.; Lewis, W.; Kays, D. L. Tuning Coordination in s-Block Carbazol-9-yl Complexes. *Chem. - A Eur. J.* **2015**, *21*, 6949–6956.
(49) DeMott, J. C.; Dekarske, J. R.; McCulloch, B. J.; Ozerov, O. V. Cyclometallation of the NNN Pincer Ligand in Complexes of Platinum. *Inorg. Chem. Front.* **2015**, *2*, 912–916.
(50) Niwa, T.; Nakada, M. A Non-Heme Iron(III) Complex with Porphyrin-like Properties That Catalyzes Asymmetric Epoxidation. *J. Am. Chem. Soc.* **2012**, *134*, 13538–13541.
(51) Gibson, V. C.; Spitzmesser, S. K.; White, A. J. P.; Williams, D. J. Synthesis and Reactivity of 1,8-Bis(Imino)Carbazolide Complexes of Iron, Cobalt and Manganese. *Dalton Trans.* **2003**, 2718–2727.
(52) Britovsek, G. J. P.; Gibson, V. C.; Hoarau, O. D.; Spitzmesser, S. K.; White, A. J. P.; Williams, D. J. Iron and Cobalt Ethylene Polymerization Catalysts: Variations on the Central Donor. *Inorg. Chem.* **2003**, *42*, 3454–3465.
(53) Gee, H.-C.; Lee, C.-H.; Jeong, Y.-H.; Jang, W.-D. Highly Sensitive and Selective Cyanide Detection via Cu^{2+} Complex Ligand Exchange. *Chem. Commun.* **2011**, *47*, 11963–11965.
(54) Bézier, D.; Guan, C.; Krogh-Jespersen, K.; Goldman, A. S.; Brookhart, M. Experimental and Computational Study of Alkane Dehydrogenation Catalyzed by a Carbazolide-Based Rhodium PNP Pincer Complex. *Chem. Sci.* **2016**, *7*, 2579–2586.
(55) Inoue, M.; Suzuki, T.; Nakada, M. Asymmetric Catalysis of Nozaki-Hiyama Allylation and Methallylation with a New Tridentate Bis(Oxazolinyl)Carbazole Ligand. *J. Am. Chem. Soc.* **2003**, *125*, 1140–1141.
(56) Spitzmesser, S. K.; Gibson, V. C. Dialkylaluminium Complexes Derived from 1,8-Diphenyl-3,6-Dimethylcarbazole: A New Sterically Hindered Monodentate Ligand System. *J. Organomet. Chem.* **2003**, *673*, 95–101.
(57) Johnson, K. R. D.; Kamenz, B. L.; Hayes, P. G. Bis(Pyrazolyl)Carbazole as a Versatile Ligand for Supporting Lutetium Alkyl and Hydride Complexes. *Organometallics* **2014**, *33*, 3005–3011.
(58) Neugebauer, F. A.; Fischer, H. Tert-Butyl-Substituierte Carbazole. *Eur. J. Inorg. Chem.* **1972**, *105*, 2686–2693.
(59) Ortu, F.; Moxey, G. J.; Blake, A. J.; Lewis, W.; Kays, D. L. Alkaline Earth Complexes of Silylated Aminopyridinato Ligands: Homoleptic Compounds and Heterobimetallic Coordination Polymers. *Inorg. Chem.* **2013**, *52*, 12429–12439.
(60) Arthur, C. C. Preparation of Dialkylmagnesium Compounds from Grignard Reagents. *J. Am. Chem. Soc.* **1935**, *57*, 2238–2240.
(61) Buchanan, W. D.; Allis, D. G.; Ruhlandt-Senge, K. Synthesis and Stabilization-Advances in Organoalkaline Earth Metal Chemistry. *Chem. Commun.* **2010**, *46*, 4449–4465.
(62) Alexander, J. S.; Ruhlandt-Senge, K. ChemInform Abstract: Not Just Heavy "Grignards": Recent Advances in the Organometallic Chemistry of the Alkaline Earth Metals Calcium, Strontium and Barium. *Eur. J. Inorg. Chem.* **2002**, 2761-2774.
(63) Harder, S.; Müller, S.; Hübner, E. Syntheses and Crystal Structures of Simple Dibenzylcalcium Complexes: Useful Reagents in the Preparation of Calcium Compounds. *Organometallics* **2004**, *23*, 178–183.
(64) Westerhausen, M.; Gärtner, M.; Fischer, R.; Langer, J.; Yu, L.; Reiher, M. Heavy Grignard Reagents: Challenges and Possibilities of Aryl Alkaline Earth Metal Compounds. *Chem. - A Eur. J.* **2007**, *13*, 6292–6306.
(65) Mulvey, R. E.; Robertson, S. D. Synthetically Important Alkali-Metal Utility Amides: Lithium, Sodium, and Potassium Hexamethyldisilazides, Diisopropylamides, and Tetramethylpiperidides. *Angew. Chemie - Int. Ed.* **2013**, *52*, 11470–11487.
(66) Westerhausen, M. Synthesis and Spectroscopic Properties of Bis(Trimethylsilyl)Amides of the Alkaline-Earth Metals Magnesium, Calcium, Strontium, and Barium. *Inorg. Chem.* **1991**, *30*, 96–101.
(67) Chadwick, S.; Englich, U.; Ruhlandt-Senge, K. A Novel Beryllium Thiolate Resulting from N-Si Bond Cleavage. *Angew. Chem. Int. Ed. Engl.* **1998**, 3007–3009.
(68) Barrios, L. A.; Bartual-Murgui, C.; Peyrecave-Lleixà, E.; Le Guennic, B.; Teat, S. J.; Roubeau, O.; Aromí, G. Homoleptic versus Heteroleptic Formation of Mononuclear Fe(II) Complexes with Tris-Imine Ligands. *Inorg. Chem.* **2016**, *55*, 4110–4116.
(69) Carter, P. H.; Plant, S. G. P.; Tomlinson, M. Formyl Derivatives of Carbazole and 1,2,3,4-Tetrahydrocarbazole. *J. Am. Chem. Soc.* **1957**, 2210–2215.
(70) Katrizky, A. R.; Rewcastle, G. W.; Vazques de Miguel, L. M. Improved Syntheses of

Substitutetd Carbazoles and Benzocarbazoles via Lithiation of the (Dialkylamino)Methyl (Aminal) Derivatives. *J. Org. Chem.* **1988**, *53*, 794–799.
(71) https://scifinder.cas.org/scifinder/login
(72) Hicks, J.; Jones, C. Extremely Bulky Amido First Row Transition Metal(II) Halide Complexes: Potential Precursors to Low Coordinate Metal-Metal Bonded Systems. *Inorg. Chem.* **2013**, *52*, 3900–3907.
(73) Li, J.; Stasch, A.; Schenk, C.; Jones, C. Extremely Bulky Amido-Group 14 Element Chloride Complexes: Potential Synthons for Low Oxidation State Main Group Chemistry. *Dalton Trans.* **2011**, *40*, 10448–10456.
(74) Li, J.; Schenk, C.; Winter, F.; Scherer, H.; Trapp, N.; Higelin, A.; Keller, S.; Pöttgen, R.; Krossing, I.; Jones, C. Weak Arene Stabilization of Bulky Amido-Germanium(II) and Tin(II) Monocations. *Angew. Chemie - Int. Ed.* **2012**, *51*, 9557–9561.
(75) Hicks, J.; Hadlington, T. J.; Schenk, C.; Li, J.; Jones, C. Utilizing Steric Bulk to Stabilize Molybdenum Aminogermylyne and Aminogermylene Complexes. *Organometallics* **2013**, *32*, 323–329.
(76) Dange, D.; Choong, S. L.; Schenk, C.; Stasch, A.; Jones, C. Synthesis and Characterisation of Anionic and Neutral Gallium(I) N-Heterocyclic Carbene Analogues. *Dalton Trans.* **2012**, *41*, 9304.
(77) Berthon-Gelloz, G.; Siegler, M. a; Spek, A. L.; Tinant, B.; Reek, J. N. H.; Markó, I. E. IPr* an Easily Accessible Highly Hindered N-Heterocyclic Carbene. *Dalton Trans.* **2010**, *39*, 1444–1446.
(78) Kays, D. L. Extremely Bulky Amide Ligands in Main Group Chemistry. *Chem. Soc. Rev.* **2016**, *45*, 1004–1018.
(79) Moxey, G. J.; Ortu, F.; Goldney Sidley, L.; Strandberg, H. N.; Blake, A. J.; Lewis, W.; Kays, D. L. Synthesis and Characterisation of Magnesium Complexes Containing Sterically Demanding N,N'-Bis(Aryl)Amidinate Ligands. *Dalton Trans.* **2014**, *43*, 4838–4846.
(80) Bradley, M. The Synthesis of Alkaline Earth Complexes Using Sterically-Demanding Multidentate Amido Ligands, University of Nottingham, 2014.
(81) Gower, A. L. Group 13 and 14 Complexes Bearing Multidentate Monoanionic Ligands, University of Nottingham, 2014.
(82) Nolla-Saltiel, R.; Geer, A. M. M.; Lewis, W.; Blake, A. J.; Kays, D. L. Dehydrogenation of Dimethylamine-Borane Mediated by Group 1 Pincer Complexes. *Chem. Commun.* **2018**, *54*, 1825–1828.
(83) Martinez, C. R.; Iverson, B. L. Rethinking the Term "Pi-Stacking." *Chem. Sci.* **2012**, *3*, 2191–2201.
(84) Harinath, A.; Bhattacharjee, J.; Nayek, H. P.; Panda, T. K. Alkali Metal Complexes as Efficient Catalysts for Hydroboration and Cyanosilylation of Carbonyl Compounds. *Dalton Trans.* **2018**, *47*, 12613–12622.
(85) Sharpe, H. R.; Geer, A. M.; Taylor, L. J.; Gridley, B. M.; Blundell, T. J.; Blake, A. J.; Davies, E. S.; Lewis, W.; McMaster, J.; Robinson, D.; *et al*. Selective Reduction and Homologation of Carbon Monoxide by Organometallic Iron Complexes. *Nat. Commun.* **2018**, *9*, 3757.
(86) Gridley, B. M.; Blake, A. J.; Davis, A. L.; Lewis, W.; Moxey, G. J.; Kays, D. L. Low-Coordinate Cobalt(II) Terphenyl Complexes: Precursors to Sterically Encumbered Ketones. *Chem. Commun.* **2012**, *48*, 8910–8912.
(87) Blundell, T. J. Transition Metal Complexes of Sterically Demanding *m*-Terphenyl Ligands: Synthesis and Small Molecule Reactivity, University of Nottingham, 2015.
(88) Ramirez, A.; Sun, X.; Collum, D. B. Lithium Diisopropylamide-Mediated Enolization: Catalysis by Hemilabile Ligands. *J. Am. Chem. Soc.* **2006**, *128*, 10326–10336.
(89) Minnaard, A. J.; Wijnberg, J. B. P. a.; de Groot, A. Synthesis of (E,E)-Germacrane Sesquiterpene Alcohols via Enolate-Assisted 1,4-Fragmentation. *J. Org. Chem.* **1997**, *62*, 7336–7345.
(90) Xiao, X.; Li, S.; Yan, X.; Liu, X.; Xu, R.; Bai, D. Synthesis of a Sec-Precursor and Analogues of Macrolactin A. *Chem. Lett.* **2005**, *34*, 906–907.
(91) Anga, S.; Sarazin, Y.; Carpentier, J. F.; Panda, T. K. Alkali-Metal-Catalyzed Cross-Dehydrogenative Couplings of Hydrosilanes with Amines. *ChemCatChem* **2016**, *8*, 1373–1378.
(92) Harinath, A.; Anga, S.; Panda, T. K. Alkali Metal Catalyzed Dehydro-Coupling of Boranes and Amines Leading to the Formation of a B-N Bond. *RSC Adv.* **2016**, *6*, 35648–35653.
(93) Bellham, P.; Hill, M. S.; Kociok-Köhn, G. Alkali Metal-Mediated Dehydrocoupling of $Me_2NH{\cdot}BH_3$. *Dalton Trans.* **2015**, *44*, 12078–12081.
(94) Melen, R. L. Dehydrocoupling Routes to Element-Element Bonds Catalysed by Main Group Compounds. *Chem. Soc. Rev.* **2016**, *45*, 775–788.
(95) Bhunya, S.; Malakar, T.; Ganguly, G.; Paul, A. Combining Protons and Hydrides by

Homogeneous Catalysis for Controlling the Release of Hydrogen from Ammonia-Borane: Present Status and Challenges. *ACS Catal.* **2016**, *6*, 7907–7934.
(96) Leitao, E. M.; Jurca, T.; Manners, I. Catalysis in Service of Main Group Chemistry Offers a Versatile Approach to p-Block Molecules and Materials. *Nat. Chem.* **2013**, *5*, 817–829.
(97) Staubitz, A.; Robertson, A. P. M.; Manners, I. Ammonia-Borane and Related Compounds as Dihydrogen Sources. *Chem. Rev.* **2010**, *110*, 4079–4124.
(98) Staubitz, A.; Robertson, A. P. M.; Sloan, M. E.; Manners, I. Amine– and Phosphine– Borane Adducts: New Interest in Old Molecules. *Chem. Rev.* **2010**, 4023–4078.
(99) Jiang, Y.; Blacque, O.; Fox, T.; Frech, C. M.; Berke, H. Development of Rhenium Catalysts for Amine Borane Dehydrocoupling and Transfer Hydrogenation of Olefins. *Organometallics* **2009**, *28*, 5493–5504.
(100) Leitao, E. M.; Stubbs, N. E.; Robertson, A. P. M.; Helten, H.; Cox, R. J.; Lloyd-Jones, G. C.; Manners, I. Mechanism of Metal-Free Hydrogen Transfer between Amine-Boranes and Aminoboranes. *J. Am. Chem. Soc.* **2012**, *134*, 16805–16816.
(101) Frueh, S.; Kellett, R.; Mallery, C.; Molter, T.; Willis, W. S.; King'Ondu, C.; Suib, S. L. Pyrolytic Decomposition of Ammonia Borane to Boron Nitride. *Inorg. Chem.* **2011**, *50*, 783–792.
(102) Johnson, H. C.; Leitao, E. M.; Whittell, G. R.; Manners, I.; Lloyd-Jones, G. C.; Weller, A. S. Mechanistic Studies of the Dehydrocoupling and Dehydropolymerization of Amine-Boranes Using a $[Rh(Xantphos)]^+$ catalyst. *J. Am. Chem. Soc.* **2014**, *136*, 9078–9093.
(103) Koepke, J. C.; Wood, J. D.; Chen, Y.; Schmucker, S. W.; Liu, X.; Chang, N. N.; Nienhaus, L.; Do, J. W.; Carrion, E. A.; Hewaparakrama, J.; *et al*. Role of Pressure in the Growth of Hexagonal Boron Nitride Thin Films from Ammonia-Borane. *Chem. Mater.* **2016**, *28*, 4169–4179.
(104) Spielmann, J.; Bolte, M.; Harder, S. Synthesis and Structure of a Magnesium-Amidoborane Complex and Its Role in Catalytic Formation of a New Bis-Aminoborane Ligand. *Chem. Commun.* **2009**, 6934–6936.
(105) Liptrot, D. J.; Hill, M. S.; Mahon, M. F.; MacDougall, D. J. Group 2 Promoted Hydrogen Release from NMe_2H-BH_3: Intermediates and Catalysis. *Chem. - A Eur. J.* **2010**, *16*, 8508–8515.
(106) Spielmann, J.; Piesik, D. E. J.; Harder, S. Thermal Decomposition of Mono- and Bimetallic Magnesium Amidoborane Complexes. *Chem. - A Eur. J.* **2010**, *16*, 8307–8318.
(107) Chua, Y. S.; Wu, H.; Zhou, W.; Udovic, T. J.; Wu, G.; Xiong, Z.; Wong, M. W.; Chen, P. Monoammoniate of Calcium Amidoborane: Synthesis, Structure, and Hydrogen-Storage Properties. *Inorg. Chem.* **2012**, *51*, 1599–1603.
(108) Bellham, P.; Anker, M. D.; Hill, M. S.; Kociok-Köhn, G.; Mahon, M. F. The Significance of Secondary Interactions during Alkaline Earth-Promoted Dehydrogenation of Dialkylamine-Boranes. *Dalton Trans.* **2016**, *45*, 13969–13978.
(109) Cowley, H. J.; Holt, M. S.; Melen, R. L.; Rawson, J. M.; Wright, D. S. Catalytic Dehydrocoupling of Me_2NHBH_3 with $Al(NMe_2)_3$. *Chem. Commun.* **2011**, *47*, 2682–2684.
(110) Hansmann, M. M.; Melen, R. L.; Wright, D. S. Group 13 BN Dehydrocoupling Reagents, Similar to Transition Metal Catalysts but with Unique Reactivity. *Chem. Sci.* **2011**, *2*, 1554–1559.
(111) Less, R. J.; Simmonds, H. R.; Dane, S. B. J.; Wright, D. S. Stoichiometric and Catalytic Reactions of $LiAlH_4$ with Me_2NHBH_3. *Dalton Trans.* **2013**, *42*, 6337–6343.
(112) Erickson, J. D.; Lai, T. Y.; Liptrot, D. J.; Olmstead, M. M.; Power, P. P. Catalytic Dehydrocoupling of Amines and Boranes by an Incipient Tin(II) Hydride. *Chem. Commun.* **2016**, *52*, 13656–13659.
(113) Mo, Z.; Rit, A.; Campos, J.; Kolychev, E. L.; Aldridge, S. Catalytic B-N Dehydrogenation Using Frustrated Lewis Pairs: Evidence for a Chain-Growth Coupling Mechanism. *J. Am. Chem. Soc.* **2016**, *138*, 3306–3309.
(114) Blaquiere, N.; Diallo-Garcia, S.; Gorelsky, S. I.; Black, D. A.; Fagnou, K. Ruthenium-Catalyzed Dehydrogenation of Ammonia Boranes. *J. Am. Chem. Soc.* **2008**, *130*, 14034–14035.
(115) Jaska, C. A.; Temple, K.; Lough, A. J.; Manners, I. Catalytic Dehydrocoupling of Amine-Borane Adducts to Form Aminoboranes and Borazines. *Phosphorus, Sulfur Silicon Relat. Elem.* **2004**, *179*, 733–736.
(116) Zhang, X.; Lu, Z.; Foellmer, L. K.; Williams, T. J. Nitrogen-Based Ligands Accelerate Ammonia Borane Dehydrogenation with the Shvo Catalyst. *Organometallics* **2015**, *34*, 3732–3738.
(117) Kim, S. K.; Han, W. S.; Kim, T. J.; Kim, T. Y.; Nam, S. W.; Mitoraj, M.; Piekoś, L.; Michalak, A.; Hwang, S. J.; Kang, S. O. Palladium Catalysts for Dehydrogenation of Ammonia Borane with Preferential B-H Activation. *J. Am. Chem. Soc.* **2010**, *132*, 9954–9955.
(118) Cui, P.; Spaniol, T. P.; Maron, L.; Okuda, J. Dehydrogenation of Amine-Borane $Me_2NH{\cdot}BH_3$ Catalyzed by a Lanthanum-Hydride Complex. *Chem. - A Eur. J.* **2013**, *19*, 13437–13444.
(119) Metters, O. J.; Flynn, S. R.; Dowds, C. K.; Sparkes, H. A.; Manners, I.; Wass, D. F. Catalytic

Dehydrocoupling of Amine-Boranes Using Cationic Zirconium(IV)-Phosphine Frustrated Lewis Pairs. *ACS Catal.* **2016**, *6*, 6601–6611.
(120) Bellham, P.; Hill, M. S.; Kociok-Köhn, G. Alkali Metal-Mediated Dehydrocoupling of $Me_2NH{\cdot}BH_3$. *Dalton Trans.* **2015**, *44*, 12078–12081.
(121) McLellan, R.; Kennedy, A. R.; Orr, S. A.; Robertson, S. D.; Mulvey, R. E. Lithium Dihydropyridine Dehydrogenation Catalysis: A Group 1 Approach to the Cyclization of Diamine Boranes. *Angew. Chemie - Int. Ed.* **2017**, *56*, 1036–1041.
(122) Reddy, T. J.; Iwama, T.; Halpern, H. J.; Rawal, V. H. General Synthesis of Persistent Trityl Radicals for EPR Imaging of Biological Systems. *J. Org. Chem.* **2002**, *67*, 4635–4639.
(123) Berben, L. A.; de Bruin, B.; Heyduk, A. F. Non-Innocent Ligands. *Chem. Commun.* **2015**, *51*, 1553–1554.
(124) Lyaskovskyy, V.; De Bruin, B. Redox Non-Innocent Ligands: Versatile New Tools to Control Catalytic Reactions. *ACS Catal.* **2012**, *2*, 270–279.
(125) Zou, J.; Berg, D. J.; Oliver, A.; Twamley, B. Unusual Redox Chemistry of Ytterbium Carbazole-Bis(Oxazoline) Compounds: Oxidative Coupling of Primary Phosphines by an Ytterbium Carbazole- Bis(Oxazoline) Dialkyl. *Organometallics* **2013**, *32*, 6532–6540.
(126) Nygren, C. L.; Bragg, M. E. T.; Turner, J. F. C. (Tetrahydrofuran)potassium *mer-trans*-tris(carbazolyl)dichloro(tetrahydrofuran)-zirconate. *Acta Crystallogr. Sect. C* **2003**, *59*, m275–m276.
(127) Langer, J.; Krieck, S.; Görls, H.; Kriesel, G.; Siedel, W.; Westerhausen, M. Organic heterobimetallic complexes of the alkaline earth metals (Ae= Ca, Sr, Ba) with tetrahedral metallate anions of three-valent metals (M= B, Al, Ga and V). *New J. Chem.* **2010**, *34*, 1667–1677.
(128) Coombs, N. D.; Stasch, A.; Cowley, A.; Thompson, A. L.; Aldridge, S. Bulky Aryl Functionalized Carbazolyl Ligands: Amido Alternatives to the 2,6-Diarylphenyl Ligand Class? *Dalton Trans.* **2008**, 332–337.
(129) Mansaray, H. B.; Kelly, M.; Vidovic, D.; Aldridge, S. Tuning Main Group Redox Chemistry through Steric Loading: Subvalent Group 13 Metal Complexes of Carbazolyl Ligands. *Chem. - A Eur. J.* **2011**, *17*, 5381–5386.
(130) Gregory, B. K.; Bremer, M.; Schleyer, P. V. R.; Klusener, P. A. A.; Brandsma, L. N-Cesiocarbazole-Pmdta and N-Potassiocarbazole-Pmdta (PMDTA = N,N,N′,N″,N″-Pentamethyldiethylenetriamine). Cation Size and Multihapto Bonding. *Angew. Chem. Int. Ed. Engl.* **1989**, *28*, 1224–1226.
(131) Esbak, H.; Behrens, U. Strukturen Der Alkalimetallsalze Aromatischer, Heterocyclischer Amide: Synthese Und Struktur von Kronenether-Addukten Der Alkalimetall-Carbazolide. *Zeitschrift fur Anorg. und Allg. Chemie* **2005**, *631*, 1581–1587.
(132) Glock, C.; Görls, H.; Westerhausen, M. Electronic, Steric, and Ligand Influence on the Solid-State Structures of Substituted Sodium and Potassium Anilides. *Eur. J. Inorg. Chem.* **2011**, 5288–5298.
(133) Dinnebier, R.; Esbak, H.; Olbrich, F.; Behrens, U. Structure Determination of Unsolvated Potassium, Rubidium, and Cesium Carbazolates. *Organometallics* **2007**, *26*, 2604–2608.
(134) Sutton, A. D.; Davis, B. L.; Bhattacharyya, K. X.; Ellis, B. D.; Gordon, J. C.; Power, P. P. Recycle of Tin Thiolate Compounds Relevant to Ammonia-Borane Regeneration. *Chem. Commun.* **2010**, *46*, 148–149.
(135) McLellan, R.; Kennedy, A. R.; Orr, S. A.; Robertson, S. D.; Mulvey, R. E. Lithium Dihydropyridine Dehydrogenation Catalysis: A Group 1 Approach to the Cyclization of Diamine Boranes. *Angew. Chemie - Int. Ed.* **2017**, *56*, 1036–1041.
(136) Cheng, C.; Kim, B. G.; Guironnet, D.; Brookhart, M.; Guan, C.; Wang, D. Y.; Krogh-Jespersen, K.; Goldman, A. S. Synthesis and Characterization of Carbazolide-Based Iridium PNP Pincer Complexes. Mechanistic and Computational Investigation of Alkene Hydrogenation: Evidence for an Ir(III)/Ir(V)/Ir(III) Catalytic Cycle. *J. Am. Chem. Soc.* **2014**, *136*, 6672–6683.
(137) Kumar, A.; Bhatti, T. M.; Goldman, A. S. Dehydrogenation of Alkanes and Aliphatic Groups by Pincer-Ligated Metal Complexes. *Chem. Rev.* **2017**, *117*, 12357–12384.
(138) Nöth, H.; Thomas, S. Metal Tetrahydridoborates and Tetrahydroborato Metallates, Solvates of Sodium Bis(Borane)Dimethylamide. *Eur. J. Inorg. Chem.* **1999**, 1373–1379.
(139) Chen, X.; Zhao, J. C.; Shore, S. G. Facile Synthesis of Aminodiborane and Inorganic Butane Analogue $NH_3BH_2NH_2BH_3$. *J. Am. Chem. Soc.* **2010**, *132*, 10658–10659.
(140) Veeraraghavan Ramachandran, P.; Kulkarni, A. S. Nucleophilic Displacement of Ammonia from Ammonia Borane for the Preparation of Alkylamine-, Pyridine- and Phosphine-Boranes. *RSC Adv.* **2014**, *4*, 26207–26210.
(141) Stevens, C. J.; Dallanegra, R.; Chaplin, A. B.; Weller, A. S.; MacGregor, S. A.; Ward, B.; McKay, D.; Alcaraz, G.; Sabo-Etienne, S. $[Ir(PCy_3)_2(H)_2(H_2B\text{-}NMe_2)]^+$ as a Latent Source of

Aminoborane: Probing the Role of Metal in the Dehydrocoupling of H_3B-NMe_2H and Retrodimerisation of $[H_2BNMe_2]_2$. *Chem. - A Eur. J.* **2011**, *17*, 3011–3020.
(142) Robertson, A. P. M.; Suter, R.; Chabanne, L.; Whittell, G. R.; Manners, I. Heterogeneous Dehydrocoupling of Amine-Borane Adducts by Skeletal Nickel Catalysts. *Inorg. Chem.* **2011**, *50*, 12680–12691.
(143) McLellan, R.; Kennedy, A. R.; Mulvey, R. E.; Orr, S. A.; Robertson, S. D. 1-Alkali-Metal-2-Alkyl-1,2-Dihydropyridines: Soluble Hydride Surrogates for Catalytic Dehydrogenative Coupling and Hydroboration Applications. *Chem. - A Eur. J.* **2017**, *23*, 16853–16861.
(144) Rossin, A.; Peruzzini, M. Ammonia-Borane and Amine-Borane Dehydrogenation Mediated by Complex Metal Hydrides. *Chem. Rev.* **2016**, *116*, 8848–8872.
(145) Titova, E. M.; Osipova, E. S.; Pavlov, A. A.; Filippov, O. A.; Safronov, S. V.; Shubina, E. S.; Belkova, N. V. Mechanism of Dimethylamine-Borane Dehydrogenation Catalyzed by an Iridium(III) PCP-Pincer Complex. *ACS Catal.* **2017**, *7*, 2325–2333.
(146) Erickson, K. A.; Kiplinger, J. L. Catalytic Dehydrogenation of Dimethylamine Borane by Highly Active Thorium and Uranium Metallocene Complexes. *ACS Catal.* **2017**, *7*, 4276–4280.
(147) Fisher, G. B.; Fuller, J. C.; Harrison, J.; Alvarez, S. G.; Burkhardt, E. R.; Goralski, C. T.; Singaram, B. Aminoborohydrides. 4. The Synthesis and Characterization of Lithium Aminoborohydrides: A New Class of Powerful, Selective, Air-Stable Reducing Agents. *J. Org. Chem.* **1994**, *59*, 6378–6385.
(148) Byung, T. C.; Sang, K. K. Direct and Indirect Reductive Amination of Aldehydes and Ketones with Solid Acid-Activated Sodium Borohydride under Solvent-Free Conditions. *Tetrahedron* **2005**, *61*, 5725–5734.
(149) Less, R. J.; García-Rodríguez, R.; Simmonds, H. R.; Allen, L. K.; Bond, A. D.; Wright, D. S. Use of Crown Ethers to Isolate Intermediates in Ammonia-Borane Dehydrocoupling Reactions. *Chem. Commun.* **2016**, *52*, 3650–3652.
(150) Ortu, F. Synthesis of s-Block Complexes Supported by Sterically Demanding *N*-Based Ligands, University of Nottingham, 2014.
(151) Arrowsmith, M.; Maitland, B.; Kociok-Kohn, G.; Stasch, A.; Jones, C.; Hill, M. S. Mononuclear Three-Coordinate Magnesium Complexes of a Highly Sterically Encumbered B-Diketiminate Ligand. *Inorg. Chem.* **2014**, *53*, 10543–10552.
(152) Addison, A. W.; Rao, T. N.; Reedijk, J.; van Rijn, J.; Verschoor, G. C. Synthesis, Structure, and Spectroscopic Properties of Copper(II) Compounds Containing Nitrogen-Sulphur Donor Ligands ; the Crystal and Molecular Structure of Aqua[l,7-Bis(N-Methylbenzimidazol-2'-yl)-2,6-Dithiaheptane]Copper(II) Perchlorate. *J. Chem. Soc. Dalton Trans.* **1984**, 1349–1356.
(153) Alexander, J. S.; Ruhlandt-Senge, K. Not Just Heavy "Grignards": Recent Advances in the Organometallic Chemistry of the Alkaline Earth Metals Calcium, Strontium and Barium. *Eur. J. Inorg. Chem.* **2002**, 2761–2774.
(154) Westerhausen, M.; Gärtner, M.; Fischer, R.; Langer, J. Aryl Calcium Compounds: Syntheses, Structures, Physical Properties, and Chemical Behavior. *Angew. Chem. Int. Ed. Engl.* **2007**, *46*, 1950–1956.
(155) Barrett, A. G. M.; Crimmin, M. R.; Hill, M. S.; Procopiou, P. A. Heterofunctionalization Catalysis with Organometallic Complexes of Calcium, Strontium and Barium. *Proc. R. Soc. A* **2010**, 927–963.
(156) Yang, L.; Powell, D. R.; Houser, R. P. Structural Variation in Copper(I) Complexes with Pyridylmethylamide Ligands: Structural Analysis with a New Four-Coordinate Geometry Index, Tau4. *Dalton Trans.* **2007**, 955–964.
(157) Beswick, M. A.; Harmer, C. N.; Raithby, P. R.; Steiner, A.; Verhorevoort, K. L; Wright, D. S. Nucleophilic Substitution *vs.* Acid–base Reactions of $[Mn\{N(SiMe_3)_2\}_2]\cdot 2thf$; Syntheses and Structures of $2[Li(thf)_4]^+[Mn(C_{12}H_8N)_4]^{2-}\cdot C_6H_5Me$ and $[Mn(C_{12}H_8N)_2]\cdot 3thf$ (Thf= Tetrahydrofuran, C12H8N= Carbazol-9-yl) Michael. *J. Chem. Soc. Dalton Trans.* **1997**, 2029–2032.
(158) Putz, M. V.; Russo, N.; Sicilia, E. Atomic Radii Scale and Related Size Properties from Density Functional Electronegativity Formulation. *J. Phys. Chem. A* **2003**, *107*, 5461–5465.
(159) Guard, L. M.; Hebden, T. J.; Linn, D. E.; Heinekey, D. M. Pincer-Supported Carbonyl Complexes of Cobalt(I). *Organometallics* **2017**, *36*, 3104–3109.
(160) Chakraborty, S.; Bhattacharya, P.; Dai, H.; Guan, H. Nickel and Iron Pincer Complexes as Catalysts for the Reduction of Carbonyl Compounds. *Acc. Chem. Res.* **2015**, *48*, 1995–2003.
(161) Jackson, C. S.; Schmitt, S.; Dou, Q. P.; Kodanko, J. J. Synthesis, Characterization, and Reactivity of the Stable Iron Carbonyl Complex $[Fe(CO)(N_4Py)](ClO_4)_2$: Photoactivated Carbon Monoxide Release, Growth Inhibitory Activity, and Peptide Ligation. *Inorg. Chem.* **2011**, *50*, 5336–5338.
(162) Papa, V.; Junge, K.; Beller, M. Cobalt Pincer Complexes in Catalysis. *Chem. - A Eur. J.* **2019**, *25*, 122-143.

(163) Halpern, J.; Pribanić, M. The Hydrogenation of Pentacyanocobaltate(II) at High Pressures. *Inorg. Chem.* **1970**, *9*, 2616–2618.
(164) Wu, L.; Liu, Q.; Jackstell, R.; Beller, M. Carbonylations of Alkenes with CO Surrogates. *Angew. Chemie - Int. Ed.* **2014**, *53*, 6310–6320.
(165) Hazari, N.; Heimann, J. E. Carbon Dioxide Insertion into Group 9 and 10 Metal-Element σ-Bonds. *Inorg. Chem.* **2017**, *56*, 13655–13678.
(166) Sun, J.; Deng, L. Cobalt Complex-Catalyzed Hydrosilylation of Alkenes and Alkynes. *ACS Catal.* **2016**, *6*, 290–300.
(167) Scheuermann, M. L.; Semproni, S. P.; Pappas, I.; Chirik, P. J. Carbon Dioxide Hydrosilylation Promoted by Cobalt Pincer Complexes. *Inorg. Chem.* **2014**, *53*, 9463–9465.
(168) Hu, X.; Castro-Rodriguez, I.; Meyer, K. Dioxygen Activation by a Low-Valent Cobalt Complex Employing a Flexible Tripodal N-Heterocyclic Carbene Ligand. *J. Am. Chem. Soc.* **2004**, *126*, 13464–13473.
(169) Kent, M. A.; Woodall, C. H.; Haddow, M. F.; McMullin, C. L.; Pringle, P. G.; Wass, D. F. Cobalt PCP Pincer Complexes *via* an Unexpected Sequence of Ortho Metalations. *Organometallics* **2014**, *33*, 5686–5692.
(170) Spentzos, A. Z.; Barnes, C. L.; Bernskoetter, W. H. Effective Pincer Cobalt Precatalysts for Lewis Acid Assisted CO_2 Hydrogenation. *Inorg. Chem.* **2016**, *55*, 8225–8233.
(171) Halpern, J. The Reaction of Hydridopentacyanocobaltate(III) with Ferricyanide. *Inorg Chem* **1972**, *11*, 658–660.
(172) Bhattacharya, P.; Krause, J. A.; Guan, H. Iron Hydride Complexes Bearing Phosphinite-Based Pincer Ligands: Synthesis, Reactivity, and Catalytic Application in Hydrosilylation Reactions. *Organometallics* **2011**, *30*, 4720–4729.
(173) Bibler, J. P.; Wojcicki, A. Reactions of Cyclopentadienyl(Methyl)Iron Dicarbonyl with Various Ligands. Cyclopentadienyl(Acetyl)Iron Carbonyl Phosphine and Phosphite Complexes. *Inorg. Chem.* **1966**, *5*, 889–892.
(174) Smith, N. E.; Bernskoetter, W. H.; Hazari, N.; Mercado, B. Q. Synthesis and Catalytic Activity of PNP-Supported Iron Complexes with Ancillary Isonitrile Ligands. *Organometallics* **2017**, *36*, 3995–4004.
(175) Carrington, S. J.; Chakraborty, I.; Mascharak, P. K. Rapid CO Release from a Mn(I) Carbonyl Complex Derived from Azopyridine upon Exposure to Visible Light and Its Phototoxicity toward Malignant Cells. *Chem. Commun.* **2013**, *49*, 11254–11256.
(176) Ward, J. S.; Morgan, R.; Lynam, J. M.; Fairlamb, I. J. S.; Moir, J. W. B. Toxicity of Tryptophan Manganese(I) Carbonyl (Trypto-CORM), against Neisseria Gonorrhoeae. *Med. Chem. Commun.* **2017**, *8*, 346–352.
(177) Pierri, A. E.; Pallaoro, A.; Wu, G.; Ford, P. C. A Luminescent and Biocompatible PhotoCORM. *J. Am. Chem. Soc.* **2012**, *134*, 18197–18200.
(178) Koike, K.; Okoshi, N.; Hori, H.; Takeuchi, K.; Ishitani, O.; Tsubaki, H.; Clark, I. P.; George, M. W.; Johnson, F. P. A.; Turner, J. J. Mechanism of the Photochemical Ligand Substitution Reactions of Fac-$[Re(Bpy)(CO)_3(PR_3)]^+$ complexes and the Properties of Their Triplet Ligand-Field Excited States. *J. Am. Chem. Soc.* **2002**, *124*, 11448–11455.
(179) Gridley, B. M.; Moxey, G. J.; Lewis, W.; Blake, A. J.; Kays, D. L. Conformational Isomerism in Monomeric, Low-Coordinate Group 12 Complexes Stabilized by a Naphthyl-Substituted *m*-Terphenyl Ligand. *Chem. - A Eur. J.* **2013**, *19*, 11446–11453.
(180) Lorber, C.; Choukroun, R.; Vendier, L. Hydroamination of Alkynes Catalyzed by Imido Complexes of Titanium and Vanadium. *Organometallics* **2004**, *23*, 1845–1850.
(181) Döhring, A.; Göhre, J.; Jolly, P. W.; Kryger, B.; Rust, J.; Verhovnik, G. P. J. Donor-Ligand-Substituted Cyclopentadienylchromium(III) Complexes: A New Class of Alkene Polymerization Catalyst. 1. Amino-Substituted Systems. *Organometallics* **2000**, *19*, 388–402.
(182) Segnitz, O.; Winter, M.; Fischer, R. A. Novel Complexes of Nickel with N-Heterocyclic Ligands and the Hemilabile [2-(Dimethylamino)Ethyl]Cyclopentadienyl Group. *J. Organomet. Chem.* **2006**, *691*, 4733–4739.
(183) Grüger, N.; Rodríguez, L. I.; Wadepohl, H.; Gade, L. H. Achiral and Chiral PNP-Pincer Ligands with a Carbazole Backbone: Coordination Chemistry with d^8 Transition Metals. *Inorg. Chem.* **2013**, *52*, 2050–2059.
(184) Chang, C. K.; Barkigia, K. M.; Hanson, L. K.; Fajer, J. Models of Heme d_1. Structure and Redox Chemistry of Dioxoisobacteriochlorins. *J. Am. Chem. Soc.* **1986**, *108*, 1352–1354.
(185) Veidis, M. V.; Schreiber, G. H.; Gough, T. E.; Palenik, G. J. Jahn-Teller Distortions in Octahedral Copper(II) Complexes. *J. Am. Chem. Soc.* **1969**, *91*, 1859–1860.
(186) Wood, J. S.; Keijzers, C. P.; de Boer, E.; Buttafava, A. Dynamic and Cooperative Jahn-Teller Distortions in Copper Pyridine N-Oxide Complexes, $Cu(PyO)_6X_2$ (X = Tetrafluoroborate(1-), Perchlorate(1-), and Nitrate(1-): Structural and EPR Studies of Pure and Zinc-Doped

Systems. *Inorg. Chem.* **1980**, *19*, 2213–2225.
(187) Layfield, R. A. Manganese(II): The Black Sheep of the Organometallic Family. *Chem. Soc. Rev.* **2008**, *37*, 1098–1107.
(188) Shannon, R. D. Revised Effective Ionic Radii and Systematic Studies of Interatomie Distances in Halides and Chaleogenides. *Acta Cryst.* **1976**, *A32*, 751–767.
(189) Allen, T. L. Bond Energies of Transition Metal Halides. *J. Chem. Phys.* **1957**, *26*, 1644–1647.
(190) Noltes, J. G.; Boersma, J. Investigations on Organozinc Compounds. Coordination Chemistry of Organozinc Compounds RZnX: Organozinc-Nitrogen Compounds of the Type EtZnNPhCOZ. *J. Organometalic Chem.* **1969**, *16*, 345–355.
(191) Henriques, A. M.; Barbosa, A. G. H. Chemical Bonding and the Equilibrium Composition of Grignard Reagents in Ethereal Solutions. *J. Phys. Chem. A* **2011**, *115*, 12259–12270.
(192) Coles, M. P.; Hitchcock, P. B. Zinc Guanidinate Complexes and Their Application in Ring-Opening Polymerisation Catalysis. *Eur. J. Inorg. Chem.* **2004**, 2662–2672.
(193) Fisher, K. J.; Alyea, E. C. New Two- and Three-Coordinate Cadmium(II) Dialkylamides. *Polyhedron* **1984**, *3*, 509–512.
(194) Rodesiler, P. F.; Griffith, E. H.; Ellis, P. D.; Amma, E. L. X-Ray Crystal Structure and ^{113}Cd N.M.R. Spectrum of Tetraphenyl-Porphinatocadmium(II)-Bis(Dioxane) Solvate. *J. Chem. Soc., Chem. Commun.* **1980**, 492–493.
(195) Wrackmeyer, B.; Contreras, R. ^{199}Hg NMR Parameters. *Annu. Reports NMR Spectrosc.* **1992**, *24*, 267–329.
(196) Al-Showiman, S. S. ^{1}H ^{13}C and ^{199}Hg NMR Characteristics of New Amine-Mercuric Chloride Complexes. *Inorganica Chim. Acta* **1988**, *141*, 263–274.
(197) Drew, M. G. B.; McFall, Stephen, G.; Nelson, S. M. Pentagonal-Pyramidal Cadmium(II) and Mercury(II) Complexes of the Quinquedentate Macrocyclic Ligand 2,15-Dimethyl-3,7,10,14,20-Penta-Azabicyclo[14.3.1]Eicosa-1(20),2,14,16,18,-Pentaene. *J. Chem. Soc. Dalton Trans.* **1979**, 575–581.
(198) Perkins, C. W.; Martin, J. C.; Arduengo, A. J.; Lau, W.; Alegría, A.; Kochi, J. K. An Electrically Neutral σ-Sulfuranyl Radical from the Homolysis of a Perester with Neighboring Sulfenyl Sulfur: 9-S-3 Species. *J. Am. Chem. Soc.* **1980**, *102*, 7753–7759.
(199) Akiba, K. Y. *Chemistry of Hypervalent Compounds*; 1998.
(200) Holmes, R. R. Comparison of Phosphorus and Silicon: Hypervalency, Stereochemistry, and Reactivity. *Chem. Rev.* **1996**, *96*, 927–950.
(201) Oae, S.; Uchida, Y. Ligand-Coupling Reactions of Hypervalent Species. *Acc. Chem. Res.* **1991**, *24*, 202–208.
(202) Yamashita, M.; Yamamoto, Y.; Akiba, K. Y.; Nagase, S. Synthesis of a Versatile Tridentate Anthracene Ligand and Its Application for the Synthesis of Hypervalent Pentacoordinate Boron Compounds (10-B-5). *Angew. Chemie - Int. Ed.* **2000**, *39*, 4055–4058.
(203) Dou, C.; Saito, S.; Yamaguchi, S. A Pentacoordinate Boron-Containing π-Electron System with Cl-B-Cl Three-Center Four-Electron Bonds. *J. Am. Chem. Soc.* **2013**, *135*, 9346–9349.
(204) Nakatsuji, J. Y.; Moriyama, Y.; Matsukawa, S.; Yamamoto, Y.; Akiba, K. Y. Synthesis and Structure of Hypervalent Boron (10-B-5) Compounds Bearing a 2,6-(p-Tolyloxymethyl)Benzene Tridentate Ligand. *Main Gr. Chem.* **2006**, *5*, 277–285.
(205) Yamashita, M.; Yamamoto, Y.; Akiba, K. Y.; Hashizume, D.; Iwasaki, F.; Takagi, N.; Nagase, S. Syntheses and Structures of Hypervalent Pentacoordinate Carbon and Boron Compounds Bearing an Anthracene Skeleton - Elucidation of Hypervalent Interaction Based on X-Ray Analysis and DFT Calculation. *J. Am. Chem. Soc.* **2005**, *127*, 4354–4371.
(206) Yano, T.; Yamaguchi, T.; Yamamoto, Y. Synthesis and Structure of Pentacoordinate Hypervalent Boron Compounds Bearing a 1,8-Dimethoxy-10-Methylacridinium Skeleton. *Chem. Lett.* **2009**, *38*, 794–795.
(207) McGovern, G. P.; Zhu, D.; Aquino, A. J. A.; Vidović, D.; Findlater, M. Synthesis and Characterization of Terpyridine-Supported Boron Cations: Evidence for Pentacoordination at Boron. *Inorg. Chem.* **2013**, *52*, 13865–13868.
(208) Hirano, Y.; Kojima, S.; Yamamoto, Y. A Hypervalent Pentacoordinate Boron Compound with an N-B-N Three-Center Four-Electron Bond. *J. Org. Chem.* **2011**, *76*, 2123–2131.
(209) https://www.ccdc.cam.ac.uk/.
(210) Emig, N.; Nguyen, H.; Krautscheid, H.; Réau, R.; Cazaux, J.-B.; Bertrand, G. Neutral and Cationic Tetracoordinated Aluminum Complexes Featuring Tridentate Nitrogen Donors: Synthesis, Structure, and Catalytic Activity for the Ring-Opening Polymerization of Propylene Oxide and (D,L)-Lactide. *Organometallics* **1998**, *17*, 3599–3608.
(211) Sangokoya, S. A.; Moise, F.; Pennington, W. T.; Self, M. F.; Robinson, G. H. Reaction of Organoaluminum Species with Macrocyclic and Open-Chain Tetradentate Amines: Synthesis and Molecular Structure of $[Cl_2Al\text{-}C_8H_{20}N_4][Al(C_2H_5)_2]$ and $[Al(CH_3)_2][ClAl\text{-}C_{10}H_{21}N_4\text{-}OCH_3][ClAl(CH_3)]$. An Examination of Aminoalanes Containing Six-Coordinate Aluminium Atoms.

Organometallics **1989**, *8*, 2584–2589.
(212) Moise, F.; Sangokoya, S. A.; Pennington, W. T.; Robinson, G. H. Reaction of Diisobutylaluminum Chloride with N,N′ -Bis(3-Aminopropyl)Ethylenediamine. Synthesis and Molecular Structure of $[C_{12}Al\text{-}C_8H_2ON_4][A1(C_4H_9)_2]$. *J. Coord. Chem.* **1990**, *21*, 129–135.
(213) Qian, B.; Ward, D. L.; Smith, M. R. Synthesis, Structure, and Reactivity of *β*-Diketiminato Aluminum Complexes. *Organometallics* **1998**, *17*, 3070–3076.
(214) Cui, C.; Roesky, H. W.; Noltemeyer, M.; Lappert, M. F.; Schmidt, H.-G.; Hao, H. Synthesis and Structures of Mono(1-Aza-Allyl) Complexes of Aluminum. *Organometallics* **1999**, *18*, 2256–2261.
(215) Nagendran, S.; Roesky, H. W. The Chemistry of Aluminum(I), Silicon(II), and Germanium(II). *Organometallics* **2008**, *27*, 457–492.
(216) Dang, J. D.; Bender, T. P. Boron, Aluminum, Gallium, and Indium Complexes of 1,3-Bis(2-Pyridylimino) Isoindoline (BPI). *Inorg. Chem. Commun.* **2013**, *30*, 147–151.
(217) Leman, J. T.; Roman, H. A.; Barron, A. R. Indium Complexes of 1,3-Diphenyltriazene. *J. Chem. Soc. Dalton Trans.* **1992**, *1*, 2183–2191.
(218) Regitz, B. M. Stable Carbenes-Illusion or Reality? *Angew. Chemie - Int. Ed.* **1991**, *30*, 674–676.
(219) Herrmann, W. A.; Kocher, C. N-Heterocyclic Carbenes. *Angew. Chem. Int. Ed.* **1997**, *3*, 2162–2187.
(220) Arduengo, A. J.; Harlow, R. L.; Kline, M. A Stable Crystalline Carbene. *J. Am. Chem. Soc.* **1991**, *113*, 361–363.
(221) Hopkinson, M. N.; Richter, C.; Schedler, M.; Glorius, F. An Overview of N-Heterocyclic Carbenes. *Nature* **2014**, *510*, 485–496.
(222) Denk, M.; Lennon, R.; Hayashi, R. Synthesis and Structure of a Stable Silylene. *J. Am. Chem. Soc.* **1994**, *6*, 2691–2692.
(223) Herrmann, W. A.; Denk, M.; Behm, J.; Scherer, W.; Klingan, F. -R; Bock, H.; Solouki, B.; Wagner, M. Stable Cyclic Germanediyls ("Cyclogermylenes"): Synthesis, Structure, Metal Complexes, and Thermolyses. *Angew. Chemie Int. Ed.* **1992**, *31*, 1485–1488.
(224) Gans-Eichler, T.; Gudat, D.; Nieger, M. Tin Analogues of "Arduengo Carbenes": Synthesis of 1,3,2λ^2-Diazastannoles and Transfer of Sn Atoms between a 1,3,2λ^2-Diazastannole and a Diazadiene. *Angew. Chemie - Int. Ed.* **2002**, *41*, 1888–1891.
(225) Charmant, J. P. H.; Haddow, M. F.; Hahn, F. E.; Heitmann, D.; Fröhlich, R.; Mansell, S. M.; Russell, C. A.; Wass, D. F. Syntheses and Molecular Structures of Some Saturated N-Heterocyclic Plumbylenes. *Dalton Trans.* **2008**, 6055–6059.
(226) Davidson, P. J.; Lappert, M. F. Stabilisation of Metals in a Low Co-Ordinative Environment Using the Bis(Trimethylsilyl)Methyl Ligand; Coloured Sn(II) and Pb(II) Alkyls, $M[CH(SiMe_3)_2]_2$. *J. Chem. Soc. Chem. Commun.* **1973**, 317a.
(227) Davidson, P. J.; Harris, D. H.; Lappert, M. F. Subvalent Group 4B Metal Alkyls and Amides . Part I. The Synthesis and Physical Properties of Kinetically Stable Bis[Bis(Trimethylsilyl)Methyl]-Germanium(II), -Tin(II) and Lead(II). *J. Chem. Soc. Dalton Trans.* **1976**, 2268–2274.
(228) Veith, M. Cyclic Nitrogen Derivatives. *Angew. Chem. Int. Ed.* **1975**, *14*, 263–264.
(229) Harris, D. H.; Lappert, M. F. Monomeric, Volatile Bivalent Amides of Group IV Elements, $M(NR^1_2)_2$ and $M(NR^1R^2)_2$ (M=Ge, Sn, or Pb; R^1=Me_3Si, R^2=Me_3C). *J. Chem. Soc., Chem. Commun.* **1974**, 895–896.
(230) Schaeffer, C. D.; Zuckerman, J. J. Tin(II) Organosilylamine. *J. Am. Chem. Soc.* **1974**, *96*, 7160–7162.
(231) Zabula, A. V.; Hahn, F. E. Mono- and Bidentate Benzannulated N-Heterocyclic Germylenes, Stannylenes and Plumbylenes. *Eur. J. Inorg. Chem.* **2008**, 5165–5179.
(232) Mizuhata, Y.; Sasamori, T.; Tokitoh, N. Stable Heavier Carbene Analogues. *Chem. Rev.* **2009**, *109*, 3479–3511.
(233) Asay, M.; Jones, C.; Driess, M. N-Heterocyclic Carbene Analogues with Low-Valent Group 13 and Group 14 Elements: Syntheses, Structures, and Reactivities of a New Generation of Multitalented Ligands. *Chem. Rev.* **2011**, *111*, 354–396.
(234) Fischer, R. C.; Power, P. P. π-Bonding and the Lone Pair Effect in Multiple Bonds Involving Heavier Main Group Elements: Developments in the New Millennium. *Chem. Rev.* **2010**, *110*, 3877–3923.
(235) Paul, D.; Heins, F.; Krupski, S.; Hepp, A.; Daniliuc, C. G.; Klahr, K.; Neugebauer, J.; Glorius, F.; Hahn, F. E. Synthesis and Reactivity of Intramolecularly NHC-Stabilized Germylenes and Stannylenes. *Organometallics* **2017**, *36*, 1001–1008.
(236) Hitchcock, P. B.; Hu, J.; Lappert, M. F.; Severn, J. R. Synthesis and Structure of B-Diketiminatotin(II) Halides, an Amide and of $Sn(=E)[\{N(R)C(Ph)\}_2CH](NR_2)$ (E = S or Se, R = $SiMe_3$). *Dalton Trans.* **2004**, 4193–4201.

(237) Smith, P. J.; Tupčiauskas, A. P. Chemical Shifts of ^{119}Sn Nuclei in Organotin Compounds. *Annu. Reports NMR Spectrosc.* **1978**, *8*, 291–370.
(238) Schmidbaur, H.; Schier, A. π-Complexation of Post-Transition Metals by Neutral Aromatic Hydrocarbons: The Road from Observations in the 19th Century to New Aspects of Supramolecular Chemistry. *Organometallics* **2008**, *27*, 2361–2395.
(239) Gash, A. G.; Rodesiler, P. F.; Amma, E. L. Metal Ion-Aromatic Complexes. XV. Synthesis, Structure, and Bonding of Bis(Tetrachloroaluminato)-π-Benzene Lead(II)-Benzene. *Inorg. Chem.* **1974**, *13*, 2429–2434.
(240) Avent, A. G.; Drost, C.; Gehrhus, B.; Hitchcock, P. B.; Lappert, M. F. Synthetic and Structural Studies on the Cyclic Bis(Amino)Stannylenes Sn[$(NR)_2$-$C_{10}H_6$-1,8] and Their Reactions with $SnCl_2$ or Si[$(NCH_2But)_2$-C_6H_4-1,2] (R = $SiMe_3$ or CH_2But). *Zeitschrift fur Anorg. und Allg. Chemie* **2004**, *630*, 2090–2096.
(241) Bellini, C.; Carpentier, J.-F.; Dorcet, V.; Silvestru, A.; Sarazin, Y. Heteroleptic Lead(II)-Halide Complexes Supported by a Bulky Iminoanilide Ligand. *Main Group Met. Chem.* **2017**, *40*, 73–80.
(242) Jana, A.; Pillai Sarish, S.; Herbert, R. W.; Schulzke, C.; Döring, A.; John, M. Facile Access of Well-Defined Stable Divalent Lead Compounds with Small Organic Substituents. *Organometallics* **2009**, *28*, 2563–2567.
(243) Tam, E. C. Y.; Coles, M. P.; Smith, J. D.; Fulton, J. R. The Steric Influence of β-Diketiminato Ligands on the Coordination Chemistry of Lead(II). *Polyhedron* **2015**, *85*, 284–294.
(244) Vaňkátová, H.; Broeckaert, L.; De Proft, F.; Olejník, R.; Turek, J.; Padělková, Z.; Růžička, A. Tetrylenes Chelated by Hybrid Amido-Amino Ligand: Derivatives of 2-[(N,N-Dimethylamino)Methyl]Aniline. *Inorg. Chem.* **2011**, *50*, 9454–9464.
(245) Briand, G. G.; Smith, A. D.; Schatte, G.; Rossini, A. J.; Schurko, R. W. Probing Lead(II) Bonding Environments in 4-Substituted Pyridine Adducts of (2,6-$Me_2C_6H_3S$)2Pb: An X-Ray Structural and Solid-State ^{207}Pb NMR Study. *Inorg. Chem.* **2007**, *46*, 8625–8637.
(246) Taylor, M. J.; Saunders, A. J.; Coles, M. P.; Fulton, J. R. Low-Coordinate Tin and Lead Cations. *Organometallics* **2011**, *30*, 1334–1339.
(247) Dmitrenko, O.; Bai, S.; Beckmann, P. a; van Bramer, S.; Vega, A. J.; Dybowski, C. The Relationship between ^{207}Pb NMR Chemical Shift and Solid-State Structure in Pb(II) Compounds. *J. Phys. Chem. A* **2008**, *112*, 3046–3052.
(248) Clegg, W.; Little, I. R.; Straughan, B. P. The Chain Polymeric Structure of Lead(II) Crotonate. *Acta Crystallogr.* **1986**, *C42*, 1319–1322.
(249) Akhbari, K.; Morsali, A. Reversible Solid State Structural Transformation of a Polyhapto Lead(II) Polymeric Chain to a Tetrahapto Lead(II) Two-Dimensional Network by Thermal Dehydration with No Change in Nanoplate Morphology. *CrystEngComm* **2011**, *13*, 2047.
(250) Zhu, H. G.; Xu, Y.; Yu, Z.; Wu, Q. J.; Fun, H. K.; You, X. Z. The Synthesis, Structure of 1-D Lead Halide Adducts: PbI_2(L) (L=2,2′-Bipyridine, 1,10-Phenanthroline). *Polyhedron* **1999**, *18*, 3491–3495.
(251) Hahn, F. E.; Heitmann, D.; Pape, T. Synthesis and Characterization of Stable N-Heterocyclic Plumbylenes. *Eur. J. Inorg. Chem.* **2008**, 1039–1041.
(252) Stephan, D. W. Frustrated Lewis Pairs. *J. Am. Chem. Soc.* **2015**, *137*, 10018–10032.
(253) Stephan, D. W. "Frustrated Lewis Pairs": A Concept for New Reactivity and Catalysis. *Org. Biomol. Chem.* **2008**, *6*, 1535–1539.
(254) Pearson, R. G. Hard and Soft Acids and Bases. *J. Am. Chem. Soc.* **1963**, *85*, 3533–3539.
(255) Pearson, R. G. Hard and Soft Acids and Bases, HSAB, Part I: Fundamental Principles. *J. Chem. Educ.* **1968**, *45*, 581–586.
(256) Pearson, R. G. Hard and Soft Acids and Bases, HSAB, Part II: Underlying Theories. *J. Chem. Educ.* **1968**, *45*, 643–648.
(257) Neumann, W. P.; Obloh, R. C. Linear Dispiro Decanes and Tetrazolines from Organic Azides and Heavy Diamino Carbene Analogues R_2M, M = Ge, Sn. *Bull. des Sociétés Chim. Belges* **1991**, *100*, 145–152.
(258) Hill, N. J.; Moser, D. F.; Guzei, I. A.; West, R. Reactions of Stable Silylenes with Organic Azides. *Organometallics* **2005**, *24*, 3346–3349.
(259) Evans, D. G.; Boeyens, J. C. A. Mapping the Conformation of Eight-Membered Rings. *Acta Crystallogr. Sect. B Struct. Sci.* **1988**, *44*, 663–671.
(260) Cabeza, J. A.; Fernández-Colinas, J. M.; García-Álvarez, P.; Polo, D. Diaminogermylene and Diaminostannylene Derivatives of Gold(I): Novel AuM and AuM_2 (M=Ge, Sn) Complexes. *Inorg. Chem.* **2012**, *51*, 3896–3903.
(261) Cabeza, J. A.; García-Álvarez, P.; Pérez-Carreño, E.; Polo, D. Ring Opening and Bidentate Coordination of Amidinate Germylenes and Silylenes on Carbonyl Dicobalt Complexes: The Importance of a Slight Difference in Ligand Volume. *Chem. - A Eur. J.* **2014**, *20*, 8654–8663.
(262) Veith, M.; Frank, W.; Tollner, F.; Lange, H. Stickstoffverbindungen von Elementen Der Dritten

Hauptgruppe Mit Intra- Und Intermolekularen Donor-Akzeptor-Bindungen. *J. Organomet. Chem.* **1987**, *326*, 315–333.
(263) Veith, M.; Spaniol, A.; Pohlmann, J.; Gross, F.; Huch, V. Homo- Und Hetero-Metall-Amide Des Tris (Tert-Butyamino)Methylsilans Polycyclen Und Cluster Mit Li, Na, Mg, Al Und Tl. *Chem. Ber.* **1993**, *126*, 2625–2635.
(264) Hannant, M. D.; Schormann, M.; Bochmann, M. Synthesis and Catalytic Activity of Three-Coordinate Zinc Cations. *J. Chem. Soc. Dalton Trans.* **2002**, 4071–4073.
(265) Schmidt, S.; Schulz, S.; Bläser, D.; Boese, R.; Bolte, M. Synthesis and Structural Characterization of New Zinc Amidinate Complexes. *Organometallics* **2010**, *29*, 6097–6103.
(266) Chisholm, M.; Eilerts, N. W.; Huffman, J. C.; Iyer, S. S.; Pacold, M.; Phomphrai, K. Molecular Design of Single-Site Metal Alkoxide Catalyst Precursors for Ring-Opening Polymerization Reactions Leading to Polyoxygenates. 1. Polylactide Formation by Achiral and Chiral Magnesium and Zinc Alkoxides, (η^3-L)MOR, Where L = Trispyrazolyl- and Trisindazolylborate Ligands. *J. Am. Chem. Soc.* **2000**, *122*, 11845–11854.
(267) Methot, J. L.; Roush, W. R. Nucleophilic Phosphine Organocatalysis. *Adv. Synth. Catal.* **2004**, *346*, 1035–1050.
(268) Pellissier, H.; Clavier, H. Enantioselective Cobalt-Catalyzed Transformations. *Chem. Rev.* **2014**, *114*, 2775–2823.
(269) Allen, D. W. Phosphines and Related C-P Bonded Compounds. *Organophosphorus Chem.* **2016**, *45*, 1–50.
(270) Sharpe, H. R.; Geer, A. M.; Lewis, W.; Blake, A. J.; Kays, D. L. Iron(II)-Catalyzed Hydrophosphination of Isocyanates. *Angew. Chemie - Int. Ed.* **2017**, *56*, 4845–4848.
(271) Espinal-Viguri, M.; King, A. K.; Lowe, J. P.; Mahon, M. F.; Webster, R. L. Hydrophosphination of Unactivated Alkenes and Alkynes Using Iron(II): Catalysis and Mechanistic Insight. *ACS Catal.* **2016**, *6*, 7892–7897.
(272) Itazaki, M.; Katsube, S.; Kamitani, M.; Nakazawa, H. Synthesis of Vinylphosphines and Unsymmetric Diphosphines: Iron-Catalyzed Selective Hydrophosphination Reaction of Alkynes and Vinylphosphines with Secondary Phosphines. *Chem. Commun.* **2016**, *52*, 3163–3166.
(273) Di Giuseppe, A.; De Luca, R.; Castarlenas, R.; Pérez-Torrente, J. J.; Crucianelli, M.; Oro, L. A. Double Hydrophosphination of Alkynes Promoted by Rhodium: The Key Role of an N-Heterocyclic Carbene Ligand. *Chem. Commun.* **2016**, *52*, 5554–5557.
(274) Bange, C. A.; Waterman, R. Zirconium-Catalyzed Intermolecular Double Hydrophosphination of Alkynes with a Primary Phosphine. *ACS Catal.* **2016**, *6*, 6413–6416.
(275) Routaboul, L.; Toulgoat, F.; Gatignol, J.; Lohier, J. F.; Norah, B.; Delacroix, O.; Alayrac, C.; Taillefer, M.; Gaumont, A. C. Iron-Salt-Promoted Highly Regioselective α- and β-Hydrophosphination of Alkenyl Arenes. *Chem. - A Eur. J.* **2013**, *19*, 8760–8764.
(276) Geer, A. M.; Serrano, A. L.; De Bruin, B.; Ciriano, M. A.; Tejel, C. Terminal Phosphanido Rhodium Complexes Mediating Catalytic P-P and P-C Bond Formation. *Angew. Chemie - Int. Ed.* **2015**, *54*, 472–475.
(277) Sues, P. E.; Lough, A. J.; Morris, R. H. Reactivity of Ruthenium Phosphido Species Generated through the Deprotonation of a Tripodal Phosphine Ligand and Implications for Hydrophosphination. *J. Am. Chem. Soc.* **2014**, *136*, 4746–4760.
(278) Gallagher, K. J.; Webster, R. L. Room Temperature Hydrophosphination Using a Simple Iron Salen Pre-Catalyst. *Chem. Commun.* **2014**, *50*, 12109–12111.
(279) Brown, C. A.; Nile, T. A.; Mahon, M. F.; Webster, R. L. Iron Catalysed Negishi Cross-Coupling Using Simple Ethyl-Monophosphines. *Dalton Trans.* **2015**, *44*, 12189–12195.
(280) Gallagher, K. J.; Espinal-Viguri, M.; Mahon, M. F.; Webster, R. L. A Study of Two Highly Active, Air-Stable Iron(III)-μ-Oxo Precatalysts: Synthetic Scope of Hydrophosphination Using Phenyl- and Diphenylphosphine. *Adv. Synth. Catal.* **2016**, *358*, 2460–2468.
(281) King, A. K.; Gallagher, K. J.; Mahon, M. F.; Webster, R. L. Markovnikov versus Anti-Markovnikov Hydrophosphination: Divergent Reactivity Using an Iron(II) β-Diketiminate Pre-Catalyst. *Chem. - A Eur. J.* **2017**, *23*, 9039–9043.
(282) Pritzwald-Stegmann, J. R. F.; Lönnecke, P.; Hey-Hawkins, E. Hydrophosphination Reactions with Transition Metal Ferrocenylphosphine Complexes. *Dalton Trans.* **2016**, *45*, 2208–2217.
(283) Kamitani, M.; Itazaki, M.; Tamiya, C.; Nakazawa, H. Regioselective Double Hydrophosphination of Terminal Arylacetylenes Catalyzed by an Iron Complex. *J. Am. Chem. Soc.* **2012**, *134*, 11932–11935.
(284) Sugiura, J.; Kakizawa, T.; Hashimoto, H.; Tobita, H.; Ogino, H. Synthesis of μ-Phosphide Diiron Complexes Having a P-H Bond: Hydrophosphination of Phenylacetylene and Methyl Acrylate with the Cationic μ-Phosphide Diiron Complex. *Organometallics* **2005**, *24*, 1099–1104.
(285) Price, A. J.; Edwards, P. G. A New Template for the Synthesis of Triphosphorus Macrocycles.

Chem. Commun. **2000**, *3*, 899–900.
(286) King, A. K.; Buchard, A.; Mahon, M. F.; Webster, R. L. Facile, Catalytic Dehydrocoupling of Phosphines Using B-Diketiminate Iron(II) Complexes. *Chem. - A Eur. J.* **2015**, *21*, 15960–15963.
(287) Huang, J. S.; Yu, G. A.; Xie, J.; Wong, K. M.; Zhu, N.; Che, C. M. Primary and Secondary Phosphine Complexes of Iron Porphyrins and Ruthenium Phthalocyanine: Synthesis, Structure, and P-H Bond Functionalization. *Inorg. Chem.* **2008**, *47*, 9166–9181.
(288) Rajpurohit, J.; Kumar, P.; Shukla, P.; Shanmugam, M.; Shanmugam, M. Mechanistic Investigation of Well-Defined Cobalt Catalyzed Formal E-Selective Hydrophosphination of Alkynes. *Organometallics* **2018**, *37*, 2297-2304.
(289) Ohmiya, H.; Yorimitsu, H.; Oshima, K. Cobalt-Catalyzed Syn Hydrophosphination of Alkynes. *Angew. Chemie - Int. Ed.* **2005**, *44*, 2368–2370.
(290) Teo, W. J.; Wang, C.; Tan, Y. W.; Ge, S. Cobalt-Catalyzed Z-Selective Hydrosilylation of Terminal Alkynes. *Angew. Chem. Int. Ed.* **2017**, *56*, 4328–4332.
(291) Guo, J.; Shen, X.; Lu, Z. Regio- and Enantioselective Cobalt-Catalyzed Sequential Hydrosilylation/Hydrogenation of Terminal Alkynes. *Angew. Chemie Int. Ed.* **2017**, *56*, 615–618.
(292) Guo, J.; Lu, Z. Highly Chemo-, Regio-, and Stereoselective Cobalt-Catalyzed Markovnikov Hydrosilylation of Alkynes. *Angew. Chemie - Int. Ed.* **2016**, *55*, 10835–10838.
(293) Leyva-Pérez, A.; Vidal-Moya, J. A.; Cabrero-Antonino, J. R.; Al-Deyab, S. S.; Al-Resayes, S. I.; Corma, A. Copper(I)-Catalyzed Hydrophosphination of Styrenes. *J. Organomet. Chem.* **2011**, *696*, 362–367.
(294) Baker, R.; Onions, A.; Popplestone, R. J.; Smith, T. N. Reactions of Amines and Active Methylene Compounds with Buta-1,3-Diene and Isoprene : Catalysis by Nickel, Cobalt, Rhodium, and Iridium Complexes. *J. Chem. Soc., Perkin Trans.* **1975**, 1133–1138.
(295) Girijavallabhan, V.; Alvarez, C.; Njoroge, F. G. Regioselective Cobalt-Catalyzed Addition of Sulfides to Unactivated Alkenes. *J. Org. Chem.* **2011**, *76*, 6442–6446.
(296) Halbritter, G.; Knoch, F.; Wolski, A.; Kisch, H. Functionalization of Aromatic Azo Compounds by the Cobalt-Catalyzed, Regioselective Double Addition of Tolane: 2,6-Distilbenylazobenzenes and 2,3-Dihydrocinnolines. *Angew. Chem. Int. Ed.* **1994**, *33*, 1603–1605.
(297) Scheuermann, M. L.; Johnson, E. J.; Chirik, P. J. Alkene Isomerization-Hydroboration Promoted by Phosphine-Ligated Cobalt Catalysts. *Org. Lett.* **2015**, *17*, 2716–2719.
(298) Lenges, C. P.; Brookhart, M. Co(I)-Catalyzed Inter- and Intramolecular Hydroacylation of Olefins with Aromatic Aldehydes. *J. Am. Chem. Soc.* **1997**, *119*, 3165–3166.
(299) Lenges, C. P.; White, P. S.; Brookhart, M. Mechanistic and Synthetic Studies of the Addition of Alkyl Aldehydes to Vinylsilanes Catalyzed by Co(I) Complexes. *J. Am. Chem. Soc.* **1998**, *120*, 6965–6979.
(300) Bolig, A. D.; Brookhart, M. Activation of sp^3 C-H Bonds with Cobalt(I): Catalytic Synthesis of Enamines. *J. Am. Chem. Soc.* **2007**, *129*, 14544–14545.
(301) Ibrahim, A. D.; Entsminger, S. W.; Fout, A. R. Insights into a Chemoselective Cobalt Catalyst for the Hydroboration of Alkenes and Nitriles. *ACS Catal.* **2017**, *7*, 3730–3734.
(302) Gao, K.; Yoshikai, N. Low-Valent Cobalt Catalysis: New Opportunities for C-H Functionalization. *Acc. Chem. Res.* **2014**, *47*, 1208–1219.
(303) Guo, J.; Shen, X.; Lu, Z. Regio- and Enantioselective Cobalt-Catalyzed Sequential Hydrosilylation/Hydrogenation of Terminal Alkynes. *Angew. Chemie - Int. Ed.* **2017**, *56*, 615–618.
(304) Whitesides, G. M.; Hackett, M.; Brainard, R. L.; Lavalleye, J.-P. P. M.; Sowinski, A. F.; Izumi, A. N.; Moore, S. S.; Brown, D. W.; Staudt, E. M. Heterogeneous Platinum(0)-Catalyzed Reactions By Poisoning With Mercury(0) in Systems Involving Competing Homogeneous Reactions of Soluble Organoplatinum. *Organometallics* **1985**, *4*, 1819.
(305) Hornstein, B. J.; Aiken, J. D.; Finke, R. G. Nanoclusters in Catalysis: A Comparison of CS_2 Catalyst Poisoning of Polyoxoanion- and Tetrabutylammonium-Stabilized 40 ± 6 Å Rh(0) Nanoclusters to 5% Rh/Al_2O_3, Including an Analysis of the Literature Related to the CS_2 to Metal Stoichiometry Issue. *Inorg. Chem.* **2002**, *41*, 1625–1638.
(306) Malekafzali, A.; Malinovska, K.; Patureau, F. W. The Cumene/O_2 System: A Very Simple Tool for the Radical Chain Oxidation of Some Functional Groups. *New J. Chem.* **2017**, *41*, 6981–6985.
(307) Moglie, Y.; González-Soria, M. J.; Martín-García, I.; Radivoy, G.; Alonso, F. Catalyst- and Solvent-Free Hydrophosphination and Multicomponent Hydrothiophosphination of Alkenes and Alkynes. *Green Chem.* **2016**, *18*, 4896–4907.
(308) Miller, Y.; Miao, L.; Hosseini, A. S.; Chemler, S. R. Copper-Catalyzed Intramolecular Alkene Carboetherification: Synthesis of Fused-Ring and Bridged-Ring Tetrahydrofurans. *J. Am.*

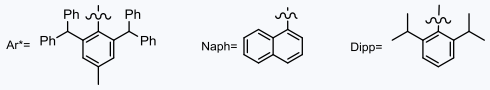
Chem. Soc. **2012**, *134*, 12149–12156.
(309) Hawari, J. A.; Engel, P. S.; Griller, D. Rate Constants for the Reactions of Alkyl Radicals with 1,4-Cyclohexadiene. *Int. J. Chem. Kinet.* **1985**, *17*, 1215–1219.
(310) Priya, S.; Balakrishna, M. S.; Mague, J. T.; Mobin, S. M. Insertion of Carbon Fragments into P(III)-N Bonds in Aminophosphines and Aminobis(Phosphines): Synthesis, Reactivity, and Coordination Chemistry of Resulting Phosphine Oxide Derivatives. *Inorg. Chem.* **2003**, *42*, 1272–1281.
(311) Priya, S.; Balakrishna, M. S.; Mobin, S. M. Reactions of Aminophosphines and Aminobis(Phosphines) with Aldehydes and Ketones: Coordination Complexes of the Resultant Aminobis(Alkylphosphineoxides) with Cobalt, Uranium, Thorium and Gadolinium Salts: Crystal and Molecular Structures of $Ph_2P(O)CH(C_6H_4)$. *Polyhedron* **2005**, *24*, 1641–1650.
(312) Costa, E.; Pringle, P. G.; Smith, M. B.; Worboys, K. Self-Replication of Tris(Cyanoethyl)Phosphine Catalysed by Platinum Group Metal Complexes. *J. Chem. Soc. Dalton Trans.* **1997**, 4277–4282.
(313) Pringle, P. G.; Smith, M. B. Platinum(0)-Catalysed Hydrophosphination of Acrylonitrile. *Chem. Commun.* **1990**, 1701–1702.
(314) Wicht, D. K.; Kourkine, I. V.; Lew, B. M.; Nthenge, J. M.; Glueck, D. S. Platinum-Catalyzed Acrylonitrile Hydrophosphination *via* Olefin Insertion into a Pt−P Bond. *J. Am. Chem. Soc.* **1997**, *119*, 5039–5040.
(315) Wicht, D. K.; Kourkine, I. V.; Kovacik, I.; Glueck, D. S. Platinum-Catalyzed Acrylonitrile Hydrophosphination. P-C Bond Formation via Olefin Insertion into a Pt-P Bond. *Organometallics* **1999**, *18*, 5381–5394.
(316) Kovacik, I.; Wicht, D. K.; Grewal, N. S.; Glueck, D. S.; Incarvito, C. D.; Guzei, I. A.; Rheingold, A. L. Pt(Me-Duphos)-Catalyzed Asymmetric Hydrophosphination of Activated Olefins: Enantioselective Synthesis of Chiral Phosphines. *Organometallics* **2000**, *19*, 950–953.
(317) Rosenberg, L. Mechanisms of Metal-Catalyzed Hydrophosphination of Alkenes and Alkynes. *ACS Catal.* **2013**, *3*, 2845–2855.
(318) Douglass, M. R.; Ogasawara, M.; Hong, S.; Metz, M. V.; Marks, T. J. "Widening the Roof": Synthesis and Characterization of New Chiral C_1-Symmetric Octahydrofluorenyl Organolanthanide Catalysts and Their Implementation in the Stereoselective Cyclizations of Aminoalkenes and Phosphinoalkenes. *Organometallics* **2002**, *21*, 283–292.
(319) Kawaoka, A. M.; Douglass, M. R.; Marks, T. J. Homoleptic Lanthanide Alkyl and Amide Precatalysts Efficiently Mediate Intramolecular Hydrophosphination/Cyclization. Observations on Scope and Mechanism. *Organometallics* **2003**, *22*, 4630–4632.
(320) Kawaoka, A. M.; Marks, T. J. Organolanthanide-Catalyzed Synthesis of Phosphine-Terminated Polyethylenes. *J. Am. Chem. Soc.* **2004**, *126*, 12764–12765.
(321) Kawaoka, A. M.; Marks, T. J. Organolanthanide-Catalyzed Synthesis of Phosphine-Terminated Polyethylenes. Scope and Mechanism. *J. Am. Chem. Soc.* **2005**, *127*, 6311–6324.
(322) Sadow, A. D.; Togni, A. Enantioselective Addition of Secondary Phosphines to Methacrylonitrile: Catalysis and Mechanism. *J. Am. Chem. Soc.* **2005**, *127*, 17012–17024.
(323) Kazankova, M. A.; Shulyupin, M. O.; Beletskaya, I. P. Catalytic Hydrophosphination of Alkenylalkyl Ethers. *Synlett* **2003**, *2*, 2155–2158.
(324) Jerome, F.; Monnier, F.; Lawicka, H.; Derien, S.; Dixneuf, P. H. Ruthenium Catalyzed Regioselective Hydrophosphination of Propargyl Alcohols. *Chem. Commun.* **2003**, *6*, 696–697.
(325) Couce-Rios, A.; Lledós, A.; Ujaque, G. The Origin of Anti-Markovnikov Regioselectivity in Alkene Hydroamination Reactions Catalyzed by $[Rh(DPEphos)]^+$. *Chem. - A Eur. J.* **2016**, *22*, 9311–9320.
(326) Eisenstein, O.; Hoffmann, R. Activation of a Coordinated Olefin toward Nucleophilic Attack. *J. Am. Chem. Soc.* **1980**, *102*, 6148–6149.
(327) Eisenstein, O.; Hoffmann, R. Transition-Metal Complexed Olefins: How Their Reactivity toward a Nucleophile Relates to Their Electronic Structure. *J. Am. Chem. Soc.* **1981**, *103*, 4308–4320.
(328) Belli, R. G.; Burton, K. M. E.; Rufh, S. A.; McDonald, R.; Rosenberg, L. Inner- and Outer-Sphere Roles of Ruthenium Phosphido Complexes in the Hydrophosphination of Alkenes. *Organometallics* **2015**, *34*, 5637–5646.
(329) Riondato, M.; Camporese, D.; Martin, D.; Suades, J.; Alvarez-Larena, A.; Mazzi, U. Synthesis and Characterisation of $[Re(CO)_3(SS)(P)]$ Complexes: A [2+1] Concept for $^{99m}Tc^-$ and $^{188}Re^-$ Radiopharmaceutical Applications. *Eur. J. Inorg. Chem.* **2005**, 4048–4055.
(330) Stockland, R. A.; Taylor, R. I.; Thompson, L. E.; Patel, P. B. Microwave-Assisted Regioselective Addition of P(O)-H Bonds to Alkenes without Added Solvent or Catalyst. *Org. Lett.* **2005**, *7*, 851–853.

(331) Heesche-Wagner, K.; Mitchell, T. N. Approaches to Water-Soluble Phosphines. II. Free Radical Addition Reactions of Phenylphosphines. *J. Organomet. Chem.* **1994**, *468*, 99–106.
(332) Hayashi, M.; Matsuura, Y.; Watanabe, Y. Fluoride-Mediated Phosphination of Alkenes and Alkynes by Silylphosphines. *Tetrahedron Lett.* **2004**, *45*, 9167–9169.
(333) Shulyupin, M. O.; Kazankova, M. A.; Beletskaya, I. P. Catalytic Hydrophosphination of Styrenes. *Org. Lett.* **2002**, *4*, 761–763.
(334) Patent Number CN101805375B
(335) Ben-Aroya, B. B.-N.; Portnoy, M. Preparation of α-Aminophosphines on Solid Support: Model Studies and Parallel Synthesis. *Tetrahedron* **2002**, *58*, 5147–5158.
(336) Andrieu, J.; Dietz, J.; Poli, R.; Richard, P. Reversible P – C Bond Formation for Saturated α-Aminophosphine Ligands in Solution : Stabilization by Coordination to Cu(I). *New J. Chem.* **1999**, *23*, 581–583.
(337) Gusarova, N. K.; Ivanova, N. I.; Volkov, P. A.; Khrapova, K. O.; Larina, L. I.; Smirnov, V. I.; Borodina, T. N.; Trofimov, B. A. Catalyst- and Solvent-Free Rapid Addition of Secondary Phosphine Chalcogenides to Aldehydes: Another Click Chemistry. *Synthesis* **2015**, *47*, 1611–1622.
(338) Greenberg, S.; Stephan, D. W. Stoichiometric and Catalytic Activation of P-H and P-P Bonds. *Chem. Soc. Rev.* **2008**, *37*, 1482–1489.
(339) Wauters, I.; Debrouwer, W.; Stevens, C. V. Preparation of Phosphines through C-P Bond Formation. *Beilstein J. Org. Chem.* **2014**, *10*, 1064–1096.
(340) Bange, C. A.; Waterman, R. Challenges in Catalytic Hydrophosphination. *Chem. - A Eur. J.* **2016**, *22*, 12598–12605.
(341) Koshti, V.; Gaikwad, S.; Chikkali, S. H. Contemporary Avenues in Catalytic PH Bond Addition Reaction: A Case Study of Hydrophosphination. *Coord. Chem. Rev.* **2014**, *265*, 52–73.
(342) Sharpe, H. R. *m*-Terphenyl Transition Metal Complexes: Catalysis and Small Molecule Activation, University of Nottingham, 2017.
(343) Štěpnika, P. Phosphino-Carboxamides: The Inconspicuous Gems. *Chem. Soc. Rev.* **2012**, *41*, 4273–4305.
(344) Jupp, A. R.; Trott, G.; Payen De La Garanderie, É.; Holl, J. D. G.; Carmichael, D.; Goicoechea, J. M. Exploiting the Brønsted Acidity of Phosphinecarboxamides for the Synthesis of New Phosphides and Phosphines. *Chem. - A Eur. J.* **2015**, *21*, 8015–8018.
(345) Jupp, A. R.; Goicoechea, J. M. Phosphinecarboxamide: A Phosphorus-Containing Analogue of Urea and Stable Primary Phosphine. *J. Am. Chem. Soc.* **2013**, *135*, 19131–19134.
(346) Fernandes, C.; Correia, J. D. G.; Gano, L.; Santos, I.; Seifert, S.; Syhre, R.; Bergmann, R.; Spies, H. Dramatic Effect of the Tridentate Ligand on the Stability of ^{99m}Tc "3 + 1" Oxo Complexes Bearing Arylpiperazine Derivatives. *Bioconjug. Chem.* **2005**, *16*, 660–668.
(347) Meléndez-Alafort, L.; Nadali, A.; Pasut, G.; Zangoni, E.; De Caro, R.; Cariolato, L.; Giron, M. C.; Castagliuolo, I.; Veronese, F. M.; Mazzi, U. Detection of Sites of Infection in Mice Using ^{99m}Tc-Labeled PN_2S-PEG Conjugated to UBI and ^{99m}Tc-UBI: A Comparative Biodistribution Study. *Nucl. Med. Biol.* **2009**, *36*, 57–64.
(348) Léautey, M.; Jubault, P.; Pannecoucke, X.; Quirion, J. C. Synthesis and Evaluation of a Broad Range of New Chiral (Aminoalkyl)Phosphane Ligands for Asymmetric Hydrogen-Transfer Reduction of Prochiral Ketones. *Eur. J. Org. Chem.* **2003**, 3761–3768.
(349) Sladojevich, F.; Trabocchi, A.; Guarna, A.; Dixon, D. J. A New Family of Cinchona-Derived Amino Phosphine Precatalysts: Application to the Highly Enantio- and Diastereoselective Silver-Catalyzed Isocyanoacetate Aldol Reaction. *J. Am. Chem. Soc.* **2011**, *133*, 1710–1713.
(350) Seidenkranz, D. T.; McGrath, J. M.; Zakharov, L. N.; Pluth, M. D. Supramolecular Bidentate Phosphine Ligand Scaffolds from Deconstructed Hamilton Receptors. *Chem. Commun.* **2017**, *53*, 561–564.
(351) Braunstein, P.; Naud, F. Hemilability of Hybrid Ligands and the Coordination Chemistry of Oxazoline-Based Systems. *Angew. Chemie - Int. Ed.* **2001**, *40*, 680–699.
(352) Geeson, M. B.; Jupp, A. R.; McGrady, J. E.; Goicoechea, J. M. On the Coordination Chemistry of Phosphinecarboxamide: Assessing Ligand Basicity. *Chem. Commun.* **2014**, *50*, 12281–12284.
(353) Sun, Y.; Zhang, Z.; Wang, X.; Li, X.; Weng, L.; Zhou, X. Isocyanate Diinsertion into the N-H Bond of the 2-Pyridylamino Ligand of Organolanthanides. *Dalton Trans.* **2010**, *39*, 221–226.
(354) Ito, M.; Iseki, M.; Itazaki, M.; Nakazawa, H. Tetrahedral Cage Complex with Planar Vertices: Selective Synthesis of Pt_4L_6 Cage Complexes Involving Hydrogen Bonds Driven by Halide Binding. *Chem. Commun.* **2016**, *52*, 7205–7208.
(355) Ding, F.; Sun, Y.; Verpoort, F. O,N-Bidentate Ruthenium Azo Complexes as Catalysts for Olefin Isomerization Reactions. *Eur. J. Inorg. Chem.* **2010**, 1536–1543.
(356) Rath, R. K.; Nethaji, M.; Chakravarty, A. R. Synthesis, Crystal Structure and Catalytic Properties of (*p*-Cymene)Ruthenium(II) Azophenol Complexes: Azophenyl to Azophenol

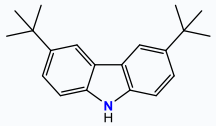
Conversion by Oxygen Insertion to a Ruthenium-Carbon Bond. *J. Organomet. Chem.* **2001**, *633*, 79–84.
(357) Rath, R. K.; Nethaji, M.; Chakravarty, A. R. Transfer Hydrogenation of Acetophenone Promoted by (Arene)Ruthenium(II) Reduced Schiff Base Complexes: An X-Ray Structure of [(η^6-*p*-Cymene)RuCl(OC_6H_4-2-$CH_2NHC_6H_4$-*p*-Me)]. *Polyhedron* **2001**, *20*, 2735–2739.
(358) Bozec, H. Le; Touchard, D.; Dixneuf, P. H. Organometallic Chemistry of Arene Ruthenium and Osmium Complexes. *Adv. Organomet. Chem.* **1989**, *29*, 163–247.
(359) Noyori, R.; Hashiguchi, S. Asymmetric Transfer Hydrogenation Catalyzed by Chiral Ruthenium Complexes. *Acc. Chem. Res.* **1997**, *30*, 97–102.
(360) Naota, T.; Takaya, H.; Murahashi, S. I. Ruthenium-Catalyzed Reactions for Organic Synthesis. *Chem. Rev.* **1998**, *98*, 2599–2660.
(361) Bruneau, C.; Dixneuf, P. H. Metal Vinylidenes in Catalysis. *Acc. Chem. Res.* **1999**, *32*, 311–323.
(362) Cadierno, V.; Gamasa, M. P.; Gimeno, J. Recent Developments in the Reactivity of Allenylidene and Cumulenylidene Complexes. *Eur. J. Inorg. Chem.* **2001**, 571–591.
(363) Bruce, M. I. Transition Metal Complexes Containing Allenylidene, Cumulenylidene, and Related Ligands. *Chem. Rev.* **1998**, *98*, 2797–2858.
(364) Touchard, D.; Dixneuf, P. H. A New Class of Carbon-Rich Organometallics. The C_3, C_4 and C_5 Metallacumulenes Ru=(C=)NCR_2. *Coord. Chem. Rev.* **1998**, *178–180*, 409–429.
(365) Berenguer, J. R.; Bernechea, M.; Forniés, J.; García, A.; Lalinde, E. (*p*-Cymene) Ruthenium (II) (Diphenylphosphino) Alkyne Complexes: Preparation of (μ-Cl) (μ-$PPh_2C{\equiv}CR$)-Bridged Ru/Pt Heterobimetallic Complexes. *Organometallics* **2004**, *23*, 4288–4300.
(366) Çalık, H. S.; Ispir, E.; Karabuga, Ş.; Aslantas, M. Ruthenium(II) Complexes of NO Ligands: Synthesis, Characterization and Application in Transfer Hydrogenation of Carbonyl Compounds. *J. Organomet. Chem.* **2016**, *801*, 122–129.
(367) Cabrero-Antonino, J. R.; Alberico, E.; Drexler, H. J.; Baumann, W.; Junge, K.; Junge, H.; Beller, M. Efficient Base-Free Hydrogenation of Amides to Alcohols and Amines Catalyzed by Well-Defined Pincer Imidazolyl-Ruthenium Complexes. *ACS Catal.* **2016**, *6*, 47–54.
(368) Adam, R.; Alberico, E.; Baumann, W.; Drexler, H. J.; Jackstell, R.; Junge, H.; Beller, M. NNP-Type Pincer Imidazolylphosphine Ruthenium Complexes: Efficient Base-Free Hydrogenation of Aromatic and Aliphatic Nitriles under Mild Conditions. *Chem. - A Eur. J.* **2016**, *22*, 4991–5002.
(369) Lee, C. C.; Huang, H. C.; Liu, S. T.; Liu, Y. H.; Peng, S. M.; Chen, J. T. Coordination Chemistry and Catalytic Activity of Ruthenium(II) Complexes Containing a Phospha-Macrocyclic Ligand. *Polyhedron* **2013**, *52*, 1024–1029.
(370) Batsanov, S. S. Van Der Waals Radii of Elements. *Inorg. Mater.* **2001**, *37*, 871–885.
(371) García de la Arada, I.; Díez, J.; Gamasa, P.; Lastra, E. Isomerization Processes on Organoruthenium Complexes Bearing κ^2(P,C)- Bidentate Ligands Generated Through Nucleophilic Addition To Coordinated Alkenyl Phosphanes. *Eur. J. Inorg. Chem.* **2018**, 4875–4886.
(372) Hierso, J. C. Indirect Nonbonded Nuclear Spin-Spin Coupling: A Guide for the Recognition and Understanding of "through-Space" NMR J Constants in Small Organic, Organometallic, and Coordination Compounds. *Chem. Rev.* **2014**, *114*, 4838–4867.
(373) Hodson, E.; Simpson, S. J. Synthesis and Characterisation of [(η^6-Cymene)Ru(L)X_2] Compounds: Single Crystal X-Ray Structure of [(η^6-Cymene)Ru(P{OPh}$_3$)Cl_2] at 203 K. *Polyhedron* **2004**, *23*, 2695–2707.
(374) Dulebohn, J. I.; Berglund, K. A.; Haefner, S. C.; Dunbar, K. R. Reversible Carbon Monoxide Addition to Sol-Gel Derived Composite Films Containing a Cationic Rhodium(I) Complex: Towards the Development of a New Class of Molecule-Basedcarbon Monoxide Sensors. *Chem. Mater.* **1992**, *4*, 506–508.
(375) Dunbar, K. R. New Applications of Weak Donor Atoms to Coordination, Organometallic and Materials Chemistry. *Comments Inorg. Chem.* **1992**, *13*, 313–357.
(376) Shriver, D. A.; Drezden, M. A. *The Manipulation of Air-Sensitive Compounds*; Wiley-Interscience, New York, 2nd Ed., 1986.
(377) Dodd, R. E.; Robinson, P. L. *Experimental Inorganic Chemistry*; 1954.
(378) Liu, H. Y.; Scharbert, B.; Holm, R. H. An Initial Approach To Biologically Related Bridged Assemblies - Pyridinethiolate-Linked Fe_4S_4-Fe Complex-Systems. *J. Am. Chem. Soc.* **1991**, *113*, 9529–9539.
(379) Grimes, R. N.; Boudjouk, P.; So, J.-H.; Ackermann, M. N.; Hawley, S. E.; Turk, B. E. Solvated and Unsolvated Anhydrous Metal Chlorides from Metal Chloride Hydrates. *Inorg. Synth.* **2007**, *29*, 108-111.
(380) Mulvey, R. E.; Robertson, S. D. Synthetically Important Alkali-Metal Utility Amides: Lithium, Sodium, and Potassium Hexamethyldisilazides, Diisopropylamides, and

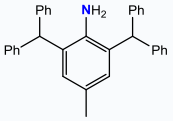
Tetramethylpiperidides. *Angew. Chemie - Int. Ed.* **2013**, *52*, 11470–11487.
(381) Hasegawa, A.; Naganawa, Y.; Fushimi, M.; Ishihara, K.; Yamamoto, H. Design of Bronsted Acid-Assisted Chiral Bronsted Acid Catalyst Bearing a Bis(Triflyl)Methyl Group for a Mannich-Type Reaction. *Org. Lett.* **2006**, *8*, 3175–3178.
(382) Evans, D. F. The Determination of the Paramagnetic Susceptibility. *J. Chem. Soc.* **1959**, 2003–2005.
(383) Gagne, R. R.; Koval, C. A.; Lisensky, G. C. Ferrocene as an Internal Standard for Electrochemical Measurements. *Inorg. Chem.* **1980**, *19*, 2854–2855.
(384) Fonseca Guerra, C.; Snijders, J. G.; Velde, G. te; Baerends, E. J. Towards an Order-N DFT Method. **1998**, *99*, 391–403.
(385) Te Velde, G.; Bickelhaupt, F. M.; Baerends, E. J.; Fonseca Guerra, C.; van Gisbergen, S. J. A.; Snidjers, J. G.; Ziegler, T. Chemistry with ADF. *J. Comput. Chem.* **2001**, *22*, 931–967.
(386) Vosko, S. H.; Wilk, L.; Nusair, M. Accurate Spin-Dependent Electron Liquid Correlation Energies for Local Spin Density Calculations: A Critical Analysis. *Can. J. Phys.* **1980**, *58*, 1200–1211.
(387) Becke, A. D. Density-Fnnctional Exchange-Energy Approximation with Correct Asymptotic Behavior. *Phys. Rev. A* **1988**, *38*, 3098–3100.
(388) Perdew, J. P. Density-Functional Approximation for the Correlation Energy of the Inhomogeneous Electron Gas. *Phys. Rev. B* **1986**, *33*, 8822–8824.
(389) Cosier, J.; Glazer, A. M. A Nitrogen-Gas-Stream Cryostat for General X-ray Diffraction Studies. *J. Appl. Crystallogr.* **1986**, *19*, 105–107.
(390) CrysalisPro. Agilent Technologies: Yarnton, U.K. 2013.
(391) Sheldrick, G. M. A Short History of SHELX. *Acta Crystallogr. Sect. A Found. Crystallogr.* **2008**, *64*, 112–122.
(392) Dolomanov, O. V.; Blake, A. J.; Champness, N. R.; Schröder, M. OLEX: New Software for Visualization and Analysis of Extended Crystal Structures. *J. Appl. Crystallogr.* **2003**, *36*, 1283–1284.
(393) Dolomanov, O. V.; Bourhis, L. J.; Gildea, R. J.; Howard, J. A. K.; Puschmann, H. OLEX2: A Complete Structure Solution, Refinement and Analysis Program. *J. Appl. Crystallogr.* **2009**, *42*, 339–341.
(394) CrysAlisPRO Oxford Diffraction/Agilent Technologies UK Ltd Yarnton England.
(395) Sheldrick, G. M. Crystal Structure Refinement with SHELXL. *Acta Crystallogr. Sect. C Struct. Chem.* **2015**, *71*, 3–8.
(396) Sheldrick, G. M. SHELXT - Integrated Space-Group and Crystal-Structure Determination. *Acta Crystallogr. Sect. A Found. Crystallogr.* **2015**, *71*, 3–8.
(397) http://checkcif.iucr.org.

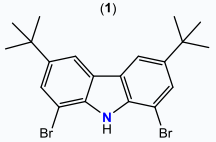
Flanking Groups

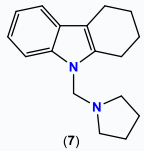


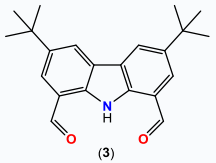
Chapter II

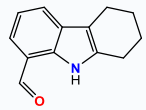

(**1**)


(**4**)

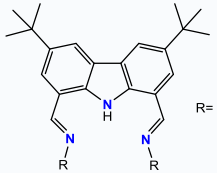

(**2**)


(**7**)


(**3**)

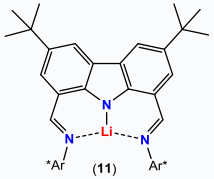

(**8**)

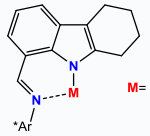
Symmetric and asymmetric ligands

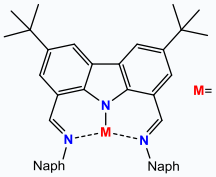

R= Ar* (**5**)
Naph (**6**)

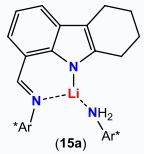

R= Ar* (**9**)
Dipp (**10**)

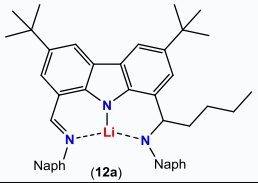
Chapter III


(**11**)


M= Li (**15**)
Na (**16**)
K (**17**)

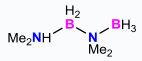

M= Li (**12**)
Na (**13**)
K (**14**)

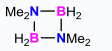

(**15a**)

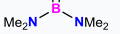

(**12a**)

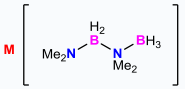
Group I salts

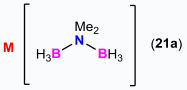
Dehydrocoupling products


(**18**)

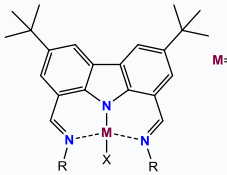

(**19**)


(**20**)


M= K (**21**), Li (**22**)

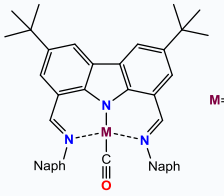

(**21a**)

Chapter IV



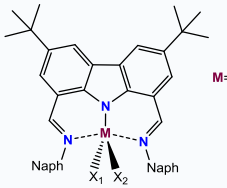
Four-coordinate

M= Mg, R=Ar*, X=I (**23**)
Ca, R=Naph, X=I (**25**)
Co, R=Naph, X=Br (**27**)
Co, R=Naph, X=H (**27-H**)
Zn, R=Naph, X=I (**35a**)
Cd, R=Naph, X=Cl (**36a**)
Hg, R=Naph, X=Br (**37**)



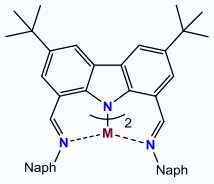
Four-coordinate

M= Co (**29**)
Fe (**30**)



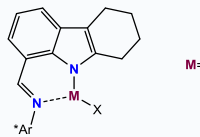
Five-coordinate

M= Mg, X_1= I, X_2=OEt_2 (**24**)
Fe, X_1=Cl, X_2=THF (**26**)
Mn, X_1=Br, X_2=THF (**28**)
Al, X_1=Cl, X_2=Cl (**38**)
Ga, X_1=Cl, X_2=Cl (**39**)
In, X_1=Cl, X_2=Cl (**40a**)



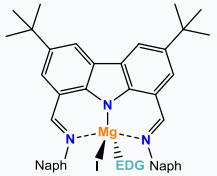
Six-coordinate

M= Mg (**24a**)
V (**31**)
Cr (**32**)
Ni (**33**)
Cu (**34**)
Zn (**35**)
Cd (**36**)
[In]Cl (**40**)



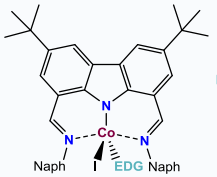
Three/Four-coordinate

M= Mg, X=I (**44**)
Zn, X=CH_3 (**45**)



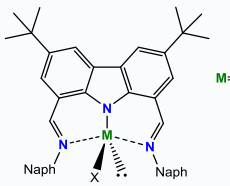
Five-coordinate

EDG= acrylonitrile (**24b**)
dimethylfumarate (**24c**)
methylpropiolate (**24d**)
dimethyladipate (**24e**)



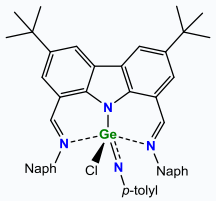
Five-coordinate

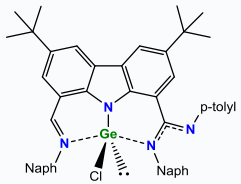
EDG= acrylonitrile (**27a**)
dimethyladipate (**27b**)
dimethylfumarate (**27c**)
methylacrylate (**27d**)



Four-coordinate

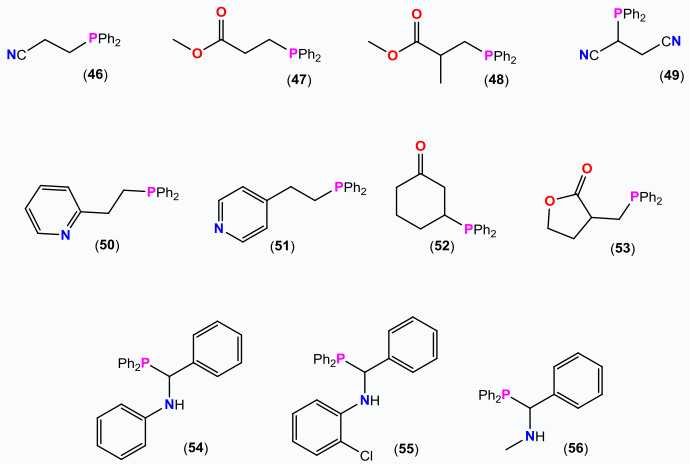
M= Ge, X=Cl (**41**)
Ge, X=I (**41a**)
Ge, X=HMDS (**41d**)
Sn, X=Cl (**42**)
Pb, X=Br (**43**)


(**41b**)

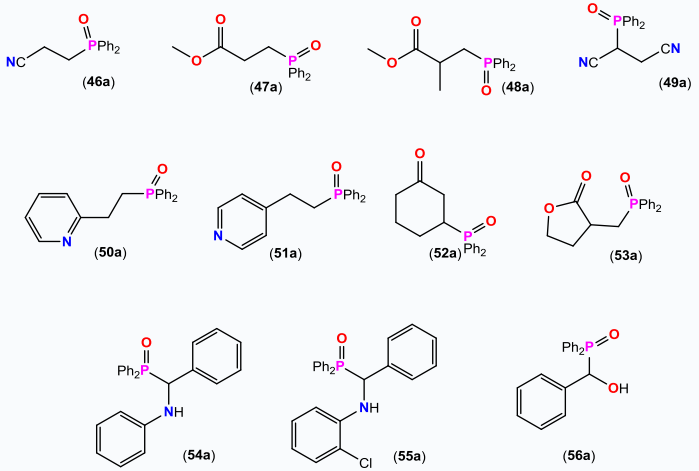

(**41c**)

Chapter V

Free phosphines

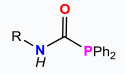


Phosphine oxides



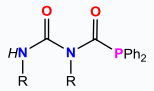
Chapter VI

PCAs



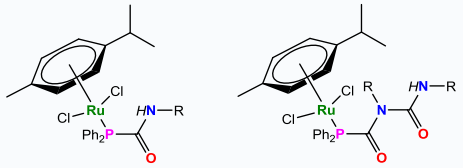
R= ^{i}Pr (**L-57**)
Ph (**L-58**)
p-tol (**L-59**)

PDCAs



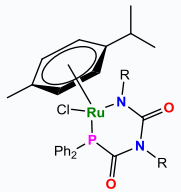
R= Ph (**L-60**)
p-tol (**L-61**)

Coordination compounds



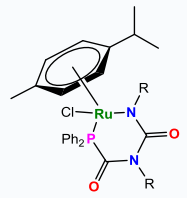
R= ^{i}Pr (**57**)
Ph (**58**)
p-tol (**59**)

R= Ph (**60**)
p-tol (**61**)



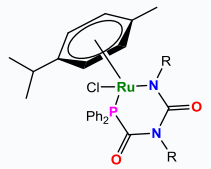
R= Ph (**62**)
p-tol (**63**)

Symmetric



R= Ph (**62a-a'**)
p-tol (**63a-a'**)

Asymmetric



R= Ph (**62b-b'**)
p-tol (**63b-b'**)

Six-membered metallacycles